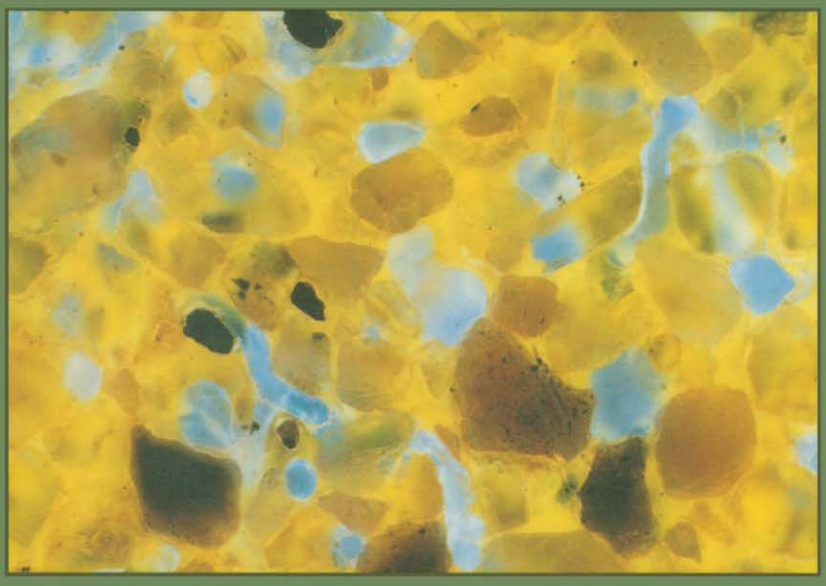
ADVANCES IN POROUS MEDIA



Volume 3

Edited by

M. Yavuz Corapcioglu

Elsevier

ADVANCES IN POROUS MEDIA

Volume 3

Further titles in this series:

1 M.Y. Corapcioglu, editor
Advances in Porous Media, volume 1

2 M.Y. Corapcioglu, editor
Advances in Porous Media, volume 2

ADVANCES IN POROUS MEDIA
Volume 3

Edited by
M. Yavuz Corapcioglu

Department of Civil Engineering, Texas A&M University
College Station, TX 77843-3136, U.S.A.



1996

ELSEVIER
AMSTERDAM–LAUSANNE–NEW YORK–OXFORD–SHANNON–TOKYO

ELSEVIER SCIENCE B.V.
Sara Burgerhartstraat 25
P.O. Box 211, 1000 AE Amsterdam, The Netherlands

ISBN 0 444 82500 2

© 1996 ELSEVIER SCIENCE B.V. All rights reserved.

No part of this publication may be reproduced, stored in a retrieval system or transmitted in any form or by any means, electronic, mechanical, photocopying, recording or otherwise, without the prior written permission of the publisher, Elsevier Science B.V., Copyright & Permissions Department, P.O. Box 521, 1000 AM Amsterdam, The Netherlands.

Special regulations for readers in the U.S.A. – This publication has been registered with the Copyright Clearance Center Inc. (CCC), 222 Rosewood Drive, Danvers, MA 01923. Information can be obtained from the CCC about conditions under which photocopies of parts of this publication may be made in the USA. All other copyright questions, including pholocopying outside thc USA, should be referred to the publisher.

No responsibility is assumed by the Publisher for any injury and/or damage to persons or property as a matter of products liability, negligence or otherwise, or from any use or operation of any methods, products, instructions or ideas contained in the material herein.

This book is printed on acid-free paper.

Printed in The Netherlands

Preface

This book is the third volume of a series: "Advances in Porous Media". Our objective is to present in-depth review papers that give comprehensive coverage to the field of transport in porous media. This series treats transport phenomena in porous media as an interdisciplinary topic. Thus, "Advances in Porous Media" will continue to promote the extension of principles and applications in one area to others, cutting across traditional boundaries. The objective of each chapter is to review the work done on a specific topic including theoretical, numerical as well as experimental studies. The contributors of this volume, as for previous ones, come from a variety of backgrounds: civil and environmental engineering, and earth and environmental sciences. The articles are aimed at all scientists and engineers in various diversified fields concerned with the fundamentals and applications of processes in porous media.

The first volume published in 1991 included five reviews: 1. Compositional multiphase flow models by M.Y. Corapcioglu; 2. Water flux in melting snow covers by P. Marsh; 3. Magnetic and dielectric fluids in porous media by M. Zahn and R. E. Rosensweig; 4. A dispersed multiphase theory and its application to filtration by M.S. Willis, I. Tosun, W. Choo, G.G. Chase and F. Desai; 5. Stochastic differential equations in the theory of solute transport through inhomogeneous porous media by G. Sposito, D.A. Barry and Z.J. Kabala.

The second volume published in 1994, included six reviews: 1. Transport of reactive solutes in soils by S.E.A.T.M. van der Zee and W.H. van Riemsdijk; 2. Propagating and stationary patterns in reaction-transport systems by P. Ortoleva, P. Foerster and J. Ross; 3. The anion exclusion phenomenon in the porous media flow by M.Y. Corapcioglu and R. Lingam; 4. Critical concentration models for porous materials by Q. Chen and A. Nur; 5. Electrokinetic flow processes in porous media and their applications by A.T. Yeung; 6. Modeling flow and contaminant transport in fractured media by B. Berkowitz.

This volume includes five chapters within the same framework we have envisioned for these series. The first chapter reviews various efforts to model physical, chemical and biological phenomena governing the subsurface biodegradation of nonaqueous liquids. It describes several models in detail to illustrate different approaches. In the past decade, groundwater modeling has increasingly became an indispensable tool within the industry, and its application will certainly continue

to grow. The authors recommend ways in which subsurface biodegradation modeling can be further developed to incorporate various important factors.

The second chapter provides a comprehensive theoretical study of single and multiphase flow of non-Newtonian fluids through porous media. Although non-Newtonian fluid flow in porous media has received significant attention since 1950s because of its importance in industrial applications, our understanding of fundamentals governing the flow is very limited in comparison to that of Newtonian fluids. This chapter brings some physical insights into this important field.

The third chapter discusses coupled hydrological, thermal and geochemical processes in large-scale porous media such as sedimentary basins. Mathematical models of these coupled processes can provide insight into the mechanisms that control the evaluation of sedimentary basins by enabling the examination of processes that may not be observed in the field or laboratory due to geological time and space scales.

The fourth chapter provides a review of an environmental containment technology of hazardous wastes. Stabilization and solidification of large quantities of soils contaminated by hazardous wastes is a relatively inexpensive and generally appropriate technology. The authors present a review of various chemical reactions and environmental interactions.

The last chapter reviews wave propagation in porous media. It presents a general survey of the literature within the contest of porous media mechanics. Wave propagation in porous media is of interest in various diversified areas of science and engineering such as soil mechanics, seismology, acoustics, earthquake engineering and geophysics. This chapter attempts to present governing equations of wave propagation in various media including unsaturated soils and fractured porous media.

We appreciate the permission of J.L. Wilson of New Mexico Tech to use the photo on the cover. It has been taken from "Laboratory investigation of residual liquid organics from spills, leaks, and the disposal of hazardous wastes in groundwater, US EPA, Ada, OK, 1990".

We hope that the third volume fulfills its objectives and provides an avenue of bringing information available in various disciplines and fields to the attention of researchers in other areas. The first two volumes received very favorable response from our readers. Again, we would like to have the readers' comments, criticisms and suggestions for future volumes.

M. YAVUZ CORAPCIOGLU (Editor)

List of contributors

B. BATCHELOR	*Department of Civil Engineering, Texas A & M University College Station, TX 77805-3136, U.S.A.*
E.R. COOK	*Department of Civil Engineering, Texas A & M University College Station, TX 77805-3136, U.S.A.*
M.Y. CORAPCIOGLU	*Department of Civil Engineering, Texas A & M University College Station, TX 77805-3136, U.S.A.*
P.C. DE BLANC	*Department of Civil Engineering, University of Texas at Austin, College of Engineering, Austin, TX 78712-1076, U.S.A.*
D.C. McKINNEY	*Department of Civil Engineering, University of Texas at Austin, College of Engineering, Austin, TX 78712-1076, U.S.A.*
K. PRUESS	*Earth Sciences Division, University of California, Lawrence Berkeley Laboratory, 1 Cyclotron Road, Berkeley, CA 94720, U.S.A.*
J.P. RAFFENSPERGER	*Department of Environmental Sciences, University of Virginia, 213 Clark Hall, Charlottesville, VA 22093, U.S.A.*
G.E. SPEITEL JR.	*Department of Civil Engineering, University of Texas at Austin, College of Engineering, Austin, TX 78712-1076, U.S.A.*
K. TUNCAY	*Department of Civil Engineering, Izmir Institute of Technology, Gaziosmanpasa Bulvari, No. 16, Cankaya, Izmir, Turkey*
YU-SHU WU	*Earth Sciences Division, University of California, Lawrence Berkeley Laboratory, 1 Cyclotron Road, Berkeley, CA 94720, U.S.A.*

This Page Intentionally Left Blank

Contents

Preface V
List of contributors VII

Chapter 1. Modeling subsurface biodegradation of non-aqueous phase liquids
by P.C. de Blanc, Daene C. McKinney, Gerald E. Speitel, Jr. . 1

Abstract 1
1. Introduction 1
2. Physical properties of NAPL compounds 2
2.1. Solubility 2
2.2. Volatility 2
2.3. Density 3
2.4. Adsorbability 3
3. NAPL environmental degradation 4
3.1. Abiotic NAPL degradation reactions 4
3.2. General principles of organic chemical biodegradation 5
3.2.1. Energetics of microbial growth 6
3.2.2. Fermentation 7
3.2.3. Respiration 9
3.2.3.1. Aerobic respiration 9
3.2.3.2. Anaerobic respiration 9
3.2.4. Cometabolism and secondary utilization 10
3.3. NAPL biodegradation 11
3.3.1. Petroleum hydrocarbons 11
3.3.1.1. Aliphatic compounds 11
3.3.1.2. Alicyclic compounds 12
3.3.1.3. Single-ring aromatic compounds 12
3.3.1.4. Polycyclic aromatic hydrocarbons 13
3.3.2. Chlorinated aliphatic compounds 13
3.3.3. PCBs 14
4. Modeling subsurface biodegradation 15
4.1. General conceptual model of biodegradation 15
4.1.1. Unsaturated zone 15
4.1.2. Saturated zone 18
4.2. Transport equations 19
4.2.1. Mass balance equations 20
4.2.2. Conservation of momentum 21
4.2.3. Constitutive relations 21
4.2.4. Simplifications for column studies 21
4.3. Physical phenomena affecting biodegradation 22
4.3.1. Hydrodynamic dispersion 22
4.3.2. Adsorption 24

4.3.3. Reaeration 26
4.3.4. Temperature 26
4.3.5. pH 27
4.3.6. Reduction potential 28
4.4. Microbial community 28
4.4.1. Number and distribution of subsurface microorganisms 29
4.4.1.1. Macroscopic scale 29
4.4.1.2. Pore scale 30
4.4.1.3. Location within phases and at interfaces 30
4.4.2. Acclimation 31
4.4.3. Microbial community composition and capabilities 32
4.5. Microorganism growth periods 33
4.6. Models of microbial growth 35
4.7. Substrate biodegradation kinetic expressions 36
4.7.1. Instantaneous reaction 37
4.7.2. Monod kinetics 38
4.7.3. First-order kinetics 40
4.7.4. Other growth kinetics 41
4.7.5. Lag period 41
4.7.6. Inhibition kinetics 42
4.7.6.1. Substrate inhibition 43
4.7.6.2. Product inhibition 43
4.7.6.3. Competitive inhibition 44
4.7.7. Cometabolism 46
4.7.8. Multiple limiting substrates and/or nutrients 48
4.7.9. Multiple electron acceptors 48
4.7.10. Incorporation of kinetic expressions into transport equations 50
4.8. Multiple microorganism populations 51
4.9. Incomplete destruction/multiple reactions 51
4.10. Diffusional resistances to mass transfer 52
4.10.1. No diffusion resistances 53
4.10.2. Diffusion resistance from a stagnant liquid layer 54
4.10.3. Diffusion resistances from the biomass and a stagnant liquid layer 55
4.10.4. Biofilms in biodegradation modeling 57
4.11. Biomass conceptualization and mass balance equations 58
4.11.1. Strictly macroscopic viewpoint—no biomass configuration assumptions 58
4.11.2. Microcolony viewpoint 60
4.11.3. Biofilm viewpoint 61
4.11.4. Summary of biomass configuration conceptualization 62
4.12. Biomass growth Limitations 62
4.12.1. Mass transfer resistances 63
4.12.2. Biomass inhibition functions 63
4.12.3. Sloughing and shearing losses 64
4.13. Importance of boundary conditions on biomass growth 64
4.14. Microorganism transport and effect on porous media 65
4.14.1. Important considerations and mechanisms 65
4.14.2. Methods of modeling bacterial transport and Attachment 66
4.14.2.1. Adsorption models 67
4.14.2.2. Filtration and combined adsorption/filtration models 68
4.15. Effect of microorganism growth on porous media 70
5. Discussion of representative models 72
5.1. Widdowson et al., 1988 76
5.1.1. Important assumptions 76
5.1.2. Validation 76

5.1.3. Comments 76
5.2. Semprini and McCarty, 1992 77
5.2.1. Important assumptions 77
5.2.2. Validation 77
5.2.3. Comments 78
5.3. Chen et al., 1992 78
5.3.1. Important assumptions 78
5.3.2. Validation 78
5.3.3. Comments 79
5.4. Taylor and Jaff, 1990b 79
5.4.1. Important assumptions 80
5.4.2. Validation 80
5.4.3. Comments 80
5.5. Sarkar et al., 1994 80
5.5.1. Important assumptions 81
5.5.2. Validation 81
5.5.3. Comments 81
6. Conclusions and recommended modeling approach 81
Acknowledgment 82
References 82

Chapter 2. Flow of non-Newtonian fluids in porous media
by Yu-Shu Wu and Karsten Pruess 87

Abstract 87
1. Introduction 87
1.1. Background 87
1.2. Non-Newtonian fluids 89
1.3. Laboratory experiment and rheological models 96
1.4. Analysis of flow through porous media 101
1.5. Summary 104
2. Rheological model 106
3. Mathematical model 109
3.1. Introduction 109
3.2. Governing equations for non-Newtonian and Newtonian fluid flow 110
3.3. Constitutive equations 112
3.4. Numerical model 112
3.5. Treatment of non-Newtonian behavior 115
3.5.1. Power-law fluid 115
3.5.2. Bingham fluid 116
3.5.3. General pseudoplastic fluid 118
4. Single-phase flow of power-law non-Newtonian fluids 118
4.1. Introduction 118
4.2. Well testing analysis of power-law fluid injection 119
4.3. Transient flow of a power-law fluid through a fractured medium 122
4.4. Flow behavior of a general pseudoplastic non-Newtonian fluid 128
4.5. Summary 134
5. Transient flow of a single-phase Bingham non-Newtonian fluid 137
5.1. Introduction 137
5.2. Governing equation and integral solution 138
5.3. Verification of integral solutions 139
5.4. Flow behavior of a Bingham fluid in porous media 140
5.5. Well testing analysis of Bingham fluid flow 142
5.6. Summary 151

6. Multiphase immiscible flow involving non-Newtonian fluids 152
6.1. Introduction 152
6.2. Analytical solution for non-Newtonian and Newtonian fluid displacement 153
6.3. Displacement of a Newtonian fluid by a power-law non-Newtonian fluid 158
6.4. Displacement of a Bingham non-Newtonian fluid by a Newtonian fluid 163
6.5. Summary 170
7. Concluding remarks 172
Acknowledgment 175
Appendix 1: List of symbols 176
References 179

Chapter 3. Numerical simulation of sedimentary basin-scale hydrochemical processes
by Jeff P. Raffensperger 185

Abstract 185
1. Introduction 186
1.1. Conceptual models of groundwater flow in sedimentary basins 188
2. Governing equations 193
2.1. Groundwater flow 193
2.1.1. Fluid mass conservation in a nondeformable porous medium 193
2.1.2. Darcy's law 194
2.1.3. Boundary conditions 197
2.1.4. Equations of state 198
2.1.5. Stream function 199
2.2. Solute transport 205
2.2.1. Mass conservation of a conservative species in solution 205
2.2.2. Boundary conditions 208
2.2.3. Mass conservation of a reactive species in solution 209
2.2.4. Chemical equilibrium 211
2.2.5. Chemical kinetics 213
2.2.6. Local equilibrium 213
2.2.7. Permeability and feedback coupling 219
2.3. Heat transport 221
2.3.1. Conservation of thermal energy in a porous medium 222
2.3.2. Boundary conditions 225
3. Numerical solution 226
3.1. Groundwater flow 226
3.1.1. Formulation of finite element equations 228
3.1.2. Element basis functions 230
3.1.3. Evaluating the integrals 231
3.1.4. Transient and steady-state equations 231
3.1.5. Rotation of the hydraulic conductivity tensor 232
3.1.6. Solution of the matrix equations 233
3.1.7. Stream function 233
3.2. Solute transport 235
3.2.1. Formulation of finite element equations 236
3.2.2. Evaluating the integrals 237
3.2.3. Determination of average linear velocities 238
3.2.4. Transient equations 238
3.2.5. On the numerical solution of the advection-dispersion equation 239
3.2.6. Finite element equations for reactive solute transport 240
3.2.7. Numerical algorithm 246

3.3. Chemical equilibrium 246
3.3.1. Equilibrium without solids 248
3.3.2. Equilibrium with solids 251
3.3.3. Equilibrium with activity coefficients 254
3.3.4. Direct search optimization 256
3.3.5. Newton-Raphson iteration 256
3.4. Heat transport 257
3.4.1. Formulation of finite element equations 258
3.4.2. Evaluating the integrals 259
3.4.3. Transient and steady-state equations 260
4. Applications 261
4.1. One-dimensional simulations of reaction-front propagation 261
4.1.1. Supergene copper enrichment 267
4.2. Two-dimensional simulations 270
4.2.1. Dispersion and two-dimensional reaction fronts 270
4.2.2. Unconformity-type uranium ores 273
4.2.3. Sediment diagenesis 281
5. Summary 285
Appendix 1: Notation list 290
Acknowledgment 292
References 292

Chapter 4. Stabilization/solidification of hazardous wastes in soil matrices
by Evan R. Cook and Bill Batchelor 307

Abstract 307
1. Introduction 307
2. Soil stabilization/solidification applications 309
3. Cement hydration reactions 313
4. Soil/cement reactions 317
4.1. Pozzolanic reactions 318
4.1.1. Soil reactivity 320
4.1.1.1. Particle size distribution 321
4.1.1.2. Clay mineralogy 322
4.1.1.3. Organic matter content 324
4.1.1.4. Iron (III) content 324
4.1.2. Calcium hydroxide availability 325
4.2. Alkali metal reactions 328
4.3. Alkali-silica reactions 330
4.4. Soil interference 331
4.4.1. Clay particles 331
4.4.2. 332
5. Environmental interactions 334
5.1. Intermedia transport 334
5.2. Acid reactions 339
5.3. Carbonation 342
5.4. Sulfate Soil organic matter 345
5.5. Magnesium reactions 349
6. Long Term performance assessment 359
6.1. SOLTEQ 350
6.2. SOLDIF 352
7. Conclusions and recommendations 354
References 355

Chapter 5. Propagation of waves in porous media
by M. Yavuz Corapcioglu and Kagan Tuncay 361

Abstract 361
1. Introduction 361
2. Biot's theory 363
2.1. Stress-strain relationships for a fluid saturated elastic porous medium 363
2.2. Equations of motion 365
2.3. Derivation of dilatational wave propagation equations 368
2.4. Derivation of rotational wave propagation equations 371
2.5. Modification of Biot's theory 373
2.6. Elaboration of Biot's work by other researchers 376
2.7. Applicability of Biot's theory 379
3. Solutions of Biot's formulation 380
3.1. Analytical solutions of Biot's formulation 381
3.2. Numerical solutions 384
3.3. Solutions by the method of characteristics 388
4. Liquefaction of soils 391
5. Wave propagation in unsaturated porous medium 395
6. Use of wave propagation equation to estimate permeability 402
7. Wave propagation in marine environments 406
7.1. Response of porous beds to water waves 406
7.2. Mei and Foda's boundary layer theory 407
7.3. Modifications of boundary layer theory 412
7.4. Wave attenuation in marine sediments 412
8. Application of mixture theory 414
9. The use of macroscopic balance equations to obtain wave propagation equations in saturated porous media 418
9.1. Mass balance equations for the fluid and the solid matrix 418
9.2. Momentum balance equations for the fluid and solid phases 419
9.3. Complete set of equations 422
10. Wave propagation in fractured porous media saturated by two immiscible fluids 422
10.1. Compressional waves 426
10.2. Rotational waves 427
10.3. Results 427
References 428

Chapter 1

Modeling subsurface biodegradation of non-aqueous phase liquids

PHILLIP C. DE BLANC, DAENE C. McKINNEY and GERALD E. SPEITEL, JR.

Abstract

Subsurface biodegradation of non-aqueous phase liquid (NAPL) compounds is extremely complex. Understanding of the interaction of physical, chemical and biological phenomena is still primitive, and much experimental and investigative work is needed in order to elucidate the important factors. Mathematical modeling of subsurface biodegradation can help us to understand the factors that are likely to be most important in harnessing the restorative power of this technology. The literature contains many mathematical models that describe subsurface biodegradation. These models approach the subject from many different perspectives, and each contribute something to our understanding of the phenomena. This report describes the methods by which researchers have modeled subsurface NAPL biodegradation, describes several models in detail to illustrate different approaches, and recommends how subsurface biodegradation modeling can be further developed.

1. Introduction

Mathematical modeling of in-situ non-aqueous phase liquid (NAPL) biodegradation is potentially useful in the assessment of the transport and fate of contaminants, in the optimization and design of cleanup operations, and in the estimation of the duration of such restoration operations (Chen et al., 1992). Over the past several years, numerous biodegradation models have been proposed. These models take many different approaches to biodegradation modeling and often emphasize a particular aspect of the biodegradation and/or transport problem. The purpose of this report is to summarize the methods by which different researchers model subsurface biodegradation and provide examples of several complete models that represent the variety of approaches.

This chapter begins by briefly reviewing the physical properties of NAPLs that are important to modeling their transport and biodegradation. In Section 3, an overview of microbiological metabolism is provided for those unfamiliar with the concepts, followed by a summary of NAPL biodegradation. Section 4 describes

the factors important in subsurface NAPL biodegradation modeling and describes how different researchers have incorporated these factors into biodegradation models. The application of these methods is demonstrated in Section 5, where five biodegradation models are described and discussed. The report concludes in Section 6 with a discussion of possible approaches to biodegradation modeling.

2. Physical properties of NAPL compounds

This section provides a brief overview of NAPL compound physical properties, since these properties are important in establishing a conceptual and mathematical model of NAPL biodegradation. Emphasis is placed on petroleum hydrocarbons and chlorinated solvents, since these compounds are the most ubiquitous NAPL contaminants. A thorough discussion of DNAPL physical properties and a bibliography can be found in Cohen and Mercer (1993).

2.1. Solubility

NAPL compounds vary widely in their solubility. In many cases, NAPL contaminant plumes consist of a mixture of tens or even hundreds of compounds, some of which are very soluble and others that are practically insoluble. Crude oil is an example of this type of mixture. However, a few generalizations about NAPL solubility can be made.

For petroleum mixtures, the most soluble compounds are typically aromatic hydrocarbons such as benzene, toluene, xylenes and ethylbenzene (Fetter, 1993). These compounds will typically leach out of a contaminant plume faster than the less soluble compounds, which tend to stay within the NAPL phase. Solubilities of these aromatics range from 150 mg/L for ethylbenzene to 1,780 mg/L for benzene (Fetter, 1993). Polychlorinated biphenyls (PCBs) and polynuclear aromatic hydrocarbons (PAHs) are much less soluble than aromatic hydrocarbons. Solubilities of PCBs range from 0.05 mg/L for PCB-1254 to 1.5 mg/L for PCB-1232 (Cohen and Mercer, 1993). PAH solubilities range from 0.00026 mg/L for benzo(g,h,i)perylene to 31.7 mg/L for naphthalene (Fetter, 1993).

Chlorinated solvents are typically much more soluble than hydrocarbons. Solubilities of representative chlorinated solvents at 20°C are shown in Table 1 (Fetter, 1993).

Solubility is important to biodegradation because microorganisms typically exist in the aqueous phase (Brock et al., 1984). Compounds with greater solubilities may be more available to microorganisms, and, all other factors being equal, may be more biodegradable than similar compounds of lesser solubility.

2.2. Volatility

Volatility is an important factor in determining a compound's potential to migrate in the vadose zone. The combination of a NAPL compound's solubility and vapor pressure will determine its air/water partitioning coefficient (Henry's

TABLE 1

Chlorinated organic solvent solubilities (Fetter, 1993)

Compound	Water solubility (mg/L)
Dichloromethane	20,000
Chloroform	8,000
1,1-dichloroethane	5,500
1,1,1-trichloroethene	4,400
Vinyl chloride	1
Trichloroethene	1,100
Tetrachloroethene	150

constant). Henry's constants of NAPL compounds vary widely. For aromatic hydrocarbons, Henry's law constants (in atm-m^3/mol) range from 5.6×10^{-3} for benzene to 8.7×10^{-3} for ethylbenzene (Brown, 1993). PAHs have much lower Henry's constants, from 4.1×10^{-4} for naphthalene to 2.5×10^{-5} for phenanthrene (Brown, 1993). Henry's law constants for PCBs range from 3.24×10^{-4} for PCB-1221 to 3.5×10^{-3} for PCB-1248 (Cohen and Mercer, 1993). Chlorinated hydrocarbons generally have much higher Henry's law constants, ranging from 1.31×10^{-3} for dichloromethane to 2.1×10^{-2} for carbon tetrachloride (Fetter, 1993). Most other chlorinated hydrocarbons have Henry's law constants in the range of 10^{-2} to 10^{-3} (Fetter, 1993).

2.3. Density

NAPL density determines whether the compound tends to float or sink when it encounters a water bearing zone. Petroleum hydrocarbons are mostly lighter than water and tend to float on the surface. Although PCBs are more dense than water, they are typically mixed with carrier fluids that may be more or less dense than water. Typical carrying fluids include chlorinated benzenes (which are heavier than water) and petroleum mixtures (Cohen and Mercer, 1993). PAHs are also typically mixed with a petroleum-derived carrier oil, although some mixtures may be heavier than water. Nearly all of the chlorinated solvents have a greater density than water.

2.4. Adsorbability

Adsorption of NAPL compounds could be important in limiting their bioavailability. A relative measure of a compound's adsorbability can be gained by examining its organic carbon partition coefficient (K_{oc} or log K_{oc}). The higher a compound's log K_{oc}, the greater is its tendency to adsorb onto organic matter in the subsurface. For aromatic hydrocarbons, log K_{oc} values range from approximately 2 mL/g for benzene to approximately 3 mL/g for ethylbenzene (Fetter, 1993). PCBs are much more adsorbable than aromatic hydrocarbons, with log K_{oc} values ranging from 2.44 mL/g for PCB-1221 to 5.64 mL/g for PCB-1248 (Cohen and

Mercer, 1993). PAHs are also highly adsorbable. Log K_{oc} values for PAHs range from approximately 3 mL/g for naphthalene to approximately 5 mL/g for pyrene (Fetter, 1993). Chlorinated solvents do not adsorb as strongly, with representative log K_{oc} values ranging from approximately 1.2 mL/g for 1,2-dichloroethane to 2.4 mL/g for tetrachloroethene (Cohen and Mercer, 1993).

3. NAPL environmental degradation

NAPLs undergo both biotic (biologically mediated) and abiotic (non-biologically mediated) reactions in the subsurface (Vogel et al., 1987). Most abiotic transformations are slow compared to biotic reactions, but they can still be significant on the time scale of groundwater movement (Vogel et al., 1987). Although this report is concerned with modeling biodegradation of NAPLs in the subsurface, ignoring relatively fast abiotic reactions could lead to underestimates of NAPL compound destruction rates. Therefore, the most important abiotic reactions are discussed briefly, followed by a more thorough discussion of biodegradation reactions. A brief review of basic microbial metabolism applicable to NAPL biodegradation is also provided.

3.1. Abiotic NAPL degradation reactions

Abiotic reactions may occur independently or as a result of microorganism growth. In addition, microbial reactions may alter the environment's pH and *Eh* and produce agents that can lead to abiotic reactions (Bouwer and McCarty, 1984). Abiotic reactions are most important for chlorinated solvents since abiotic transformations of petroleum hydrocarbons are not expected to be significant in the time scales encountered in biodegradation modeling. Vogel et al. (1987) provide a summary of the current understanding of both abiotic and biotic reactions that these compounds undergo.

The two abiotic reactions of primary concern in biodegradation modeling are substitution reactions and dehydrohalogenation reactions (Vogel, 1993). Hydrolysis reactions, in which water reacts with the halogenated compound to substitute an OH^- for an X^-, create an alcohol (Vogel, 1993) which can then be biodegraded. Hydrolysis reactions occur most rapidly for monohalogenated compounds. As the number of halogen atoms on the molecule increases, the rate of hydrolysis reactions decreases (Vogel, 1993).

Dehydrohalogenation reactions occur when an alkane loses a halide ion from one carbon atom and then a hydrogen ion from an adjacent carbon (Vogel, 1993). A double bond then forms between the carbon atoms to create an alkene. The rate of dehalogenation increases with increasing numbers of halogen atoms on the molecule (Vogel, 1993).

The importance of these reactions is evident from the abiotic hydrolysis or dehydrohalogenation half-lives of some common chlorinated NAPL compounds

TABLE 2

Environmental half-lives from abiotic reactions of selected chlorinated aliphatic compounds (Vogel et al., 1987)

Compound	Half-life (year)	Products
Dichloromethane	1.5 to 704	
Trichloromethane	1.3–3,500	
1,2-dichloroethane	50	
1,1,1-trichloroethene	0.5 to 2.5	Acetic acid, 1,1-dichloroethylene
1,1,2,2-tetrachloroethene	0.8	Trichloroethene
Trichloroethene	0.9 to 2.5	
Tetrachloroethene	0.7 to 6	

listed in Table 2 (Vogel et al., 1987). Models that fail to consider these reactions could considerably overestimate contaminant concentrations if the model is attempting to predict contaminant concentrations over a number of years.

3.2. General principles of organic chemical biodegradation

To survive, microorganisms must have (1) a source of energy, (2) carbon for the synthesis of new cellular material, and (3) inorganic elements (nutrients) such as nitrogen, phosphorous, sulfur, potassium, calcium, magnesium and other inorganic micronutrients (Metcalf and Eddy, 1991; Chapelle, 1993). Electron acceptors are needed to allow the chemical energy contained in biodegradable compounds to be released. Organic nutrients (growth factors) may also be required for cell synthesis (Metcalf and Eddy, 1991).

The process of breaking down compounds to provide energy is called catabolism. The utilization of this energy to synthesize compounds necessary for a microorganism's survival is called anabolism. Collectively, the chemical reactions involved in these two processes are called metabolism (Brock et al., 1984). As shown in Table 3, microorganisms are often classified according to the sources of carbon and energy. In the degradation of NAPLs, chemoheterotrophs are of greatest interest because they utilize organic carbon for both energy and cell growth (Metcalf and Eddy, 1991).

TABLE 3

Classification of microorganisms based on carbon and energy sources (Metcalf and Eddy, 1991)

Classification	Energy source	Carbon source
Autotrophic:		
Photoautotrophic	Light	CO_2
Chemoautotrophic	Inorganic redox reactions	CO_2
Heterotrophic:		
Photoheterotrophic	Light	Organic carbon
Chemoheterotrophic	Organic redox reactions	Organic carbon

3.2.1. Energetics of microbial growth

All reactions involved in the day-to-day processes within microorganisms can be described with established principles of chemistry and thermodynamics (Brock et al., 1984). Therefore, the reactions from which microorganisms obtain energy can be modeled using the same equations used for chemical reactions. Microorganisms obtain energy from oxidation/reduction (redox) reactions in which electrons are transferred from an electron donor to an electron acceptor. The electron donor is oxidized and the electron acceptor is reduced. In biological reactions, the electron donor is often called the energy source or substrate (Brock et al., 1984). Electron acceptors are organic or inorganic compounds that are relatively oxidized compared to the electron donor and are capable of accepting electrons from the electron donor in energetically favorable redox reactions.

The tendency of a substance to give up electrons is expressed as the substance's reduction potential. The more negative the reduction potential of a substance, the greater the tendency of the substance to donate electrons. The amount of energy released in any redox reaction depends on both the electron donor and the electron acceptor. The greater the difference between the reduction potentials of the donor and acceptor half reactions, the greater the amount of energy released. Redox pairs can be written in an "electron tower" to graphically illustrate the potential energy release for coupling of the two redox half reactions (Fig. 1; Brock et al., 1984).

The transfer of electrons from the substrate to the electron acceptor usually proceeds in a number of steps, with intermediate electron acceptors and donors carrying electrons to the final or terminal electron acceptor. The total energy available from the substrate oxidation is the energy released when only the original substrate and ultimate electron acceptor are considered. Some of the energy released by the oxidation of substrates is stored as chemical energy (usually in the high-energy phosphate bonds of molecules such as adenosine triphosphate or ATP) so that it can be used to carry out synthesis and other reactions necessary for cell growth and maintenance (Brock et al., 1984).

NAPL compounds are biodegraded because they are substrates (electron donors) for microorganisms. NAPL compounds are oxidized by microorganisms to provide them with energy. Microorganisms also use some fraction of the carbon in NAPL compounds for synthesis of new cells.

Microorganisms utilize substrates for energy through a number of different biochemical pathways. These pathways are defined by the chemical reactions they involve and the terminal electron acceptor. If no *external* electron acceptor (a compound other than the substrate) is utilized in the redox reactions to generate energy, then the process is called fermentation. If an external electron acceptor is used by the microorganism, the process is called respiration. Aerobic respiration utilizes oxygen as the terminal electron acceptor. In anaerobic respiration, microorganisms utilize an external electron acceptor other than oxygen (Brock et al., 1984).

Both respiration and fermentation are potentially important in subsurface biodegradation of NAPL compounds. Although aerobic respiration reactions typically occur much faster than anaerobic respiration and fermentation reactions, oxygen

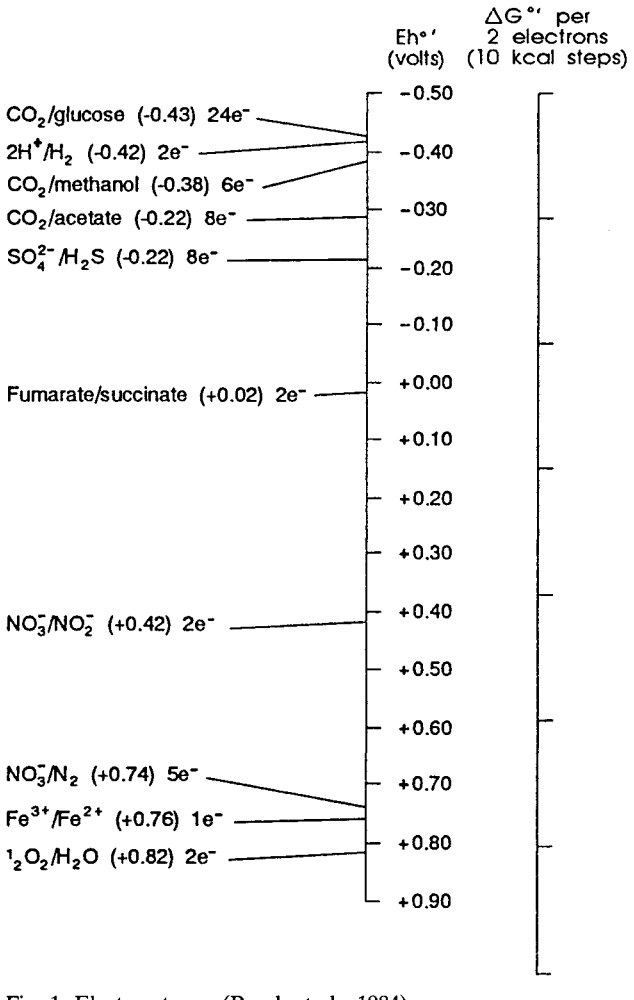


Fig. 1. Electron tower (Brock et al., 1984).

may often be absent in the contaminant plume so that these reactions may be the only significant biotic reactions occurring.

3.2.2. Fermentation

In fermentation, substrates are only partially oxidized. Electrons are "internally recycled," generally yielding at least one product that is more oxidized and one that is more reduced than the original substrate. As a result, only part of the compound can be used to generate energy, and the energy released is less than that released by respiration. An example of a fermentation reaction is the catabolism of glucose by yeast (Brock et al., 1984)

$$C_6H_{12}O \rightarrow 2CH_3CH_2OH + 2CO_2 \qquad \Delta G^{\circ\prime} = -57 \text{ kcal/mol}$$

Note that there is no external electron acceptor in this reaction. The fer-

mentation of glucose actually proceeds in a number of intermediate steps. The collective steps in which glucose is fermented to pyruvate is called glycolysis or the Embden–Meyerhof pathway (Brock et al., 1984). Many compounds other than glucose can be fermented, including sugars, amino acids, organic acids, alcohols, purines, and pyrimidines (Brock et al., 1984). To be fermented, compounds must not be too reduced or too oxidized because part of the compound must transfer electrons to the other part of the compound for energy to be released.

The end products of complete fermentation depend on the initial electron donor and the type of microorganism(s) carrying out the reactions. Typical fermentation end products include (Chapelle, 1993):

- acetic acid
- lactic acid
- formic acid, H_2 and CO_2
- ethanol and CO_2
- 2,3-butanediol and CO_2
- propionic acid and CO_2
- butyric acid
- acetone, butanol, isopropanol and CO_2
- CH_4 and CO_2

Methanogens (methane-producing bacteria) and fermentative bacteria often live together in a symbiotic association (Chapelle, 1993). The fermentative organisms degrade complex sedimentary organic matter to produce CO_2 or acetate and H_2 required by methanogens. In turn, the methanogens use these fermentative products for metabolism, thereby preventing them from accumulating to concentrations inhibitory to the fermentative organisms. There are two common methanogenesis pathways: the CO_2 reduction pathway and the acetate reduction pathway. The overall reactions for these two pathways may be written (Chapelle, 1993)

$$4H_2 + CO_2 \rightarrow CH_4 + 2H_2O$$

$$CH_3COOH \rightarrow CH_4 + CO_2$$

As an example, the overall reaction for toluene destruction by methanogenesis can be written (Reinhard, 1993)

$$C_7H_8 + 5H_2O \rightarrow 4.5CH_4 + 2.5CO_2$$

The CO_2 reduction pathway is actually an anaerobic respiration reaction with CO_2 as the electron acceptor. However, because the methanogens live in such a mutually dependent relationship with the fermentative bacteria producing these substances, the processes are usually discussed together. Other anaerobic bacteria also exist with fermentative bacteria in similar associations (Chapelle, 1993).

In addition to acetate and CO_2, methanogens can also convert methanol, formate, methyl mercaptan, and methylamines to methane. The end products of methanogenisis are either methane and water for CO_2 reduction, or methane and CO_2 for organic acid reduction. Methanogens are strict anaerobes so that they cannot function when significant levels of oxygen are present in their environment.

Methanogens are also inhibited by sulfate (Brock et al., 1984). Methanogenic reactions are often the predominant metabolic processes in environments lacking other electron acceptors (Chapelle, 1993).

Fermentation to pyruvate or other simple organic compounds is often the first step in the biodegradation of more complex natural organic molecules (Chapelle, 1993). If external electron acceptors are present, the simple products produced from fermentation are channeled into established respiration pathways where the fermentation products can be used to generate far more energy than would be available from fermentation alone.

3.2.3. Respiration

Unlike fermentation, in which substances are only partially oxidized, respiration oxidizes compounds completely to CO_2 and water by using an external electron acceptor. Respiration yields much more energy per mass of substrate metabolized because: (1) compounds are completely oxidized and, (2) the difference in reduction potentials between the initial electron donor and terminal electron acceptor is much higher than in fermentation (Brock et al., 1984).

3.2.3.1. Aerobic respiration. Conversion of compounds to pyruvate or other central intermediates is often the first step in aerobic respiration. Following generation of pyruvate in glycolysis, pyruvate is completely oxidized to CO_2 through the tricarboxylic acid (TCA) cycle. The TCA cycle is also sometimes called the citric acid or Krebs cycle. As the starting point in the TCA cycle, pyruvate is oxidized to CO_2 in a number of oxidation/reduction reactions in which the electrons from pyruvate are ultimately transferred to oxygen (Brock et al., 1984).

Aerobic respiration is much more efficient than glycolysis. For example, the amount of energy released from the aerobic metabolism of glucose is 686 kcal/mol compared to the 57 kcal/mol released by fermentation (Bailey and Ollis, 1986). Of course, not all of this energy is recovered by microorganisms. Glycolysis actually generates 7.4 kcal/mol of glucose while aerobic respiration generates 266 kcal. Aerobic respiration is both more efficient and more energy-yielding than glycolysis alone. Aerobic respiration yields the most energy per mol of substrate because oxygen has the most positive reduction potential of the common electron acceptors. This can be seen by examining Fig. 1. The O_2/H_2O redox pair is further down the "electron tower" from the CO_2/glucose redox pair than any other electron acceptor redox pair. The end products of aerobic respiration are CO_2 and water.

3.2.3.2. Anaerobic respiration. Anaerobic respiration involves a terminal electron acceptor other than oxygen. Anaerobic respiration is less efficient than aerobic respiration because the reduction potential of these alternate electron acceptors is less positive than that of oxygen. Therefore, as seen in Fig. 1, less energy is released in the oxidation of the substrate (Brock et al., 1984). The most important alternate electron acceptors in groundwater environments are nitrate, sulfate, iron(III), and carbon dioxide.

Microorganisms can use nitrate as a terminal electron acceptor in the degra-

dation of many organic compounds in a process called denitrification. Nitrate is first converted to nitrite, and then to either nitrous oxide or nitrogen gas. The overall reaction, with toluene as the substrate and elemental nitrogen as the final product, is (Reinhard, 1993)

$$C_7H_8 + 7.2NO_3^- + 7.2H^+ \rightarrow 7CO_2 + 3.6N_2 + 7.6H_2O$$

The end products of denitrification are CO_2, N_2 or N_2O, and water. Nitrate reducing organisms are facultative organisms. They use oxygen as a terminal electron acceptor when it is available and switch to nitrate when oxygen levels become low (Brock et al., 1984).

Like methanogens, sulfate reducing bacteria usually depend on fermentative bacteria to supply them with the principal substrates on which they depend. These substrates are formate, lactate, acetate and hydrogen. The overall process for toluene biodegradation by sulfate reducing bacteria is (Reinhard, 1993)

$$C_7H_8 + 4.5SO_4^{2-} + 3H_2O \rightarrow 2.25H_2S + 2.25HS^- + 7HCO_3^- + 0.25H^+$$

The end products of sulfate reduction are CO_2, H_2 and sulfide. Like methanogens, sulfate reducing organisms are strict anaerobes, i.e., they cannot function when oxygen is present and can even be killed by high oxygen levels.

Ferric iron can also be used as an electron acceptor by many organisms. Ferric iron is reduced to ferrous iron in a process that probably involves the TCA cycle (Chapelle, 1993). The reaction for toluene oxidation by ferric iron reducing bacteria is (Reinhard, 1993)

$$C_7H_8 + 36Fe^{3+} + 21H_2O \rightarrow 7HCO_3^- + 36Fe^{2+} + 43H^+$$

The relative amount of energy released with these different anaerobic electron acceptors, in decreasing order, is $Fe^{3+} > NO_3^- \gg SO_4^{2-} > CO_2$ (Brock et al., 1984).

3.2.4. Cometabolism and secondary utilization

Cometabolism is the fortuitous biodegradation of a compound during the biodegradation of another compound that supports microbial growth (Brock et al., 1984). A more rigorous definition is provided by Criddle (1993) as

> . . . the transformation of a non-growth substrate by growing cells in the presence of a growth substrate, by resting cells in the absence of a growth substrate, or by resting cells in the presence of an energy substrate. A growth substrate is defined as an electron donor that provides reducing power and energy for cell growth and maintenance . . . . An energy substrate is defined as an electron donor that provides reducing power and energy, but does not by itself support growth.

Cometabolism is an important biodegradation mechanism for many compounds that normally cannot be biodegraded, especially chlorinated aliphatic compounds. Cometabolism usually occurs when enzymes generated by microorganisms to degrade a substrate also act on the cometabolite.

Often confused with cometabolism is a process called secondary utilization. Secondary utilization is the metabolism of a compound in the presence of other substrates that supply the microorganism's primary growth needs (Bouwer and McCarty, 1984). The secondary metabolite is typically present at a concentration

too low to support growth alone, but is metabolized when other substrates are present. The secondary metabolite may or may not supply the microorganism with energy or carbon needed for growth. Secondary metabolism may be an important biodegradation mechanism for biodegradable NAPL compounds present at concentrations too low to support microbial growth.

The difference between secondary metabolism and cometabolism is that a cometabolite is not inherently biodegradable but is degraded fortuitously by an operating enzyme system, whereas a secondary substrate could be degraded if its concentration were sufficient to support growth.

3.3. NAPL biodegradation

Most man-made compounds tend to be more resistant to biodegradation than natural compounds. However, most man-made compounds can be biodegraded under the right conditions by microorganisms (Kobayashi and Rittmann, 1982). Extensive literature is available on the biodegradation of particular compounds. References that include good bibliographies are Fetter (1993), Kobayashi and Rittmann (1982), Chapelle (1993), and Environmental Protection Agency (1993). The main pathways of NAPL biodegradation likely to be encountered in groundwater systems are summarized in Table 4.

3.3.1. Petroleum hydrocarbons

Chapelle (1993) provides a comprehensive discussion of petroleum hydrocarbon biodegradation, and the following discussion is taken largely from this work.

3.3.1.1. Aliphatic compounds. Aliphatic (non-aromatic, non-cyclic) compounds are primarily biodegraded aerobically. Although anaerobic degradation of hydrocarbons has been demonstrated, biodegradation rates are orders of magnitude less than aerobic rates, so that anaerobic degradation is not considered to be a significant process of removal (Atlas, 1981).

With the exception of methane, aliphatic hydrocarbons are usually degraded by converting the compounds to fatty acids. The fatty acids are then broken down primarily by a process called beta-oxidation. In beta-oxidation, straight-chain hydrocarbons are progressively reduced in size by the successive cleavage of terminal ethyl groups. The ethyl groups are removed as acetyl-coenzyme A, which is fed directly into the TCA cycle. Alkenes are degraded by mechanisms similar to alkanes, although some anaerobic pathways may be important. Branched-chain aliphatics are also likely to be degraded by beta-oxidation after being transformed into straight-chain fatty acids. Three generalizations with regard to aliphatic organic degradation can be made (Chapelle, 1993; Borden, 1993):

1. Moderate to lower weight hydrocarbons (C_{10} to C_{14}) are most easily biodegraded. As the molecular weight increases, resistance to biodegradation increases.
2. Biodegradability increases with decreasing number of double bonds.
3. Biodegradability increases with decreasing carbon chain branching.

TABLE 4

Biodegradation pathways for representative NAPL compounds or classes of compounds (Chapelle, 1993; Borden, 1993; McCarty and Semprini, 1993; Atlas, 1981)

		Biodegradation potential			
		Primary substrate[a]		Cometabolism[b]	
Compound	Formula	Aerobic	Anaerobic	Aerobic	Anaerobic
Carbon tetrachloride	CCl_4			0	4
Methylene chloride	CH_2Cl_2	Yes	Yes	3	
1,1,1-trichloroethene	CH_3CCl_3			1	4
1,1-dichloroethane	CH_3CHCl_2			1	2
1,2-dichloroethane	CH_2ClCH_2Cl	Yes		1	1
Chloroethane	CH_3CH_2Cl	Yes		2	[c]
Tetrachloroethene	$CCl_2{=}CCl_2$			0	3
Trichloroethene	$CHCl{=}CCl_2$			2	3
cis-1,2-dichloroethene	$CHCl{=}CHCl$			3	2
1,1-Dichloroethene	$CH_2{=}CCl_2$			1	2
Vinyl chloride	$CH_2{=}CHCl$	Yes		4	1
Benzene	C_6H_6	Yes	Yes		
Toluene	C_7H_8	Yes	Yes		
Xylene	C_8H_{10}	Yes	Yes		
Ethylbenzene	C_8H_{11}	Yes	Yes		
Aliphatic hydrocarbons	N/A	Yes	No		
Alicyclic hydrocarbons	N/A	Yes	No		
Polynuclear aromatics	N/A	Yes	Yes		
PCBs	N/A	Yes	Yes		

[a]No entry means there is not sufficient information available.
[b]Increasing numbers indicate increasing potential for degradation.
[c]Readily oxidized abiotically, with half-life on order of one month.

3.3.1.2. Alicyclic compounds. Alicyclic (non-aromatic cyclic) petroleum hydrocarbons are generally more resistant to biodegradation than non-cyclic compounds (Atlas, 1981), but they are still relatively easily biodegraded. Studies on the biodegradation of cyclohexane indicate that alicyclic hydrocarbons are degraded by two or more organisms working in concert (Chapelle, 1993). Alicyclic hydrocarbons may also be degraded by anaerobic pathways, although this process has received little attention in the literature.

3.3.1.3. Single-ring aromatic compounds. Single-ring aromatic hydrocarbons such as benzene, toluene and xylene are readily degraded aerobically. Aromatic compounds with complex side groups are less easily degraded than benzene or simple alkyl substitutions. Biodegradation of these compounds generally proceeds by the formation of catechol (a benzene molecule with two hydroxyl groups attached at adjacent carbon atoms). The aromatic ring is then broken, and further degradation occurs by beta-oxidation or other mechanisms.

Anaerobic degradation of benzene, toluene and xylene has also been documented (Reinhard, 1993). In biodegradation of benzene by methanogenic bacteria (fermentation), phenol appears to be an intermediate. The oxygen forming the

hydroxy group is thought to come from water. Toluene and xylene are also degraded by methanogenic bacteria (Reinhard, 1993).

Studies indicate that toluene, ethylbenzene and xylene can be degraded anaerobically with nitrate as the terminal electron acceptor (Reinhard, 1993). Evidence of benzene biodegradation under denitrifying conditions is not conclusive (Reinhard, 1993). Toluene and xylene have also been biodegraded with sulfate as the electron acceptor, although benzene and ethylbenzene were not degraded (Reinhard, 1993).

Biodegradation of toluene by iron reducing bacteria has been demonstrated (Reinhard, 1993). This finding is especially important since many shallow sand aquifers that are particularly susceptible to contamination from surface spills lack nitrate but contain significant concentrations of iron(III) hydroxides. As a result, biodegradation by iron reducing bacteria may be the first anaerobic process to degrade the hydrocarbons (Chapelle, 1993).

3.3.1.4. Polycyclic aromatic hydrocarbons. Polycyclic compounds can be degraded aerobically by mechanisms similar to those used by microorganisms to degrade single-ring aromatic compounds. Resistance to biodegradation generally increases with the number of additional aromatic rings. An increase in branched substitutions may increase biodegradation resistance (Chapelle, 1993).

3.3.2. Chlorinated aliphatic compounds

Chlorinated compounds are relatively oxidized, because the chlorine atom withdraws electrons from the carbon-chlorine bond. As a result, chlorinated compounds release less energy than their unchlorinated counterparts in oxidation reactions. This property makes chlorinated compounds less easily degraded than non-chlorinated compounds (Chapelle, 1993). However, chlorinated aliphatic compounds (CAHs) can be degraded either aerobically or anaerobically, although the mechanisms for these two processes differ considerably (Chapelle, 1993).

Only a few chlorinated compounds have been shown to serve as primary energy and growth substrates (McCarty and Semprini, 1993). These compounds include dichloromethane, 1,2-dichloroethane, chloroethane, and vinyl chloride. Dichloromethane has been shown to degrade under aerobic or anaerobic conditions, while the other three compounds have been shown to degrade only under aerobic conditions (McCarty and Semprini, 1993). These few studies indicate that the less-halogenated one- and two-carbon CAHs may be used as primary substrates, but that organisms capable of utilizing them are rare (McCarty and Semprini, 1993).

Cometabolism is the predominant method of transformation of most CAHs (McCarty and Semprini, 1993). In early studies, trichloroethene (TCE) was shown to be degraded to CO_2 by soil microorganisms growing on methane (Chapelle, 1993). The degradation is catalyzed by a methane monooxygenase (MMO), an enzyme that catalyzes the incorporation of molecular oxygen into methane to form methanol (Chapelle, 1993). Current evidence indicates that the process is self-limiting and is inhibited by high methane concentrations (Chapelle, 1993). Microorganisms that oxidize propane, ethylene, toluene, phenol cresol, ammonia, isoprene and vinyl chloride have also been shown to transform CAHs through comet-

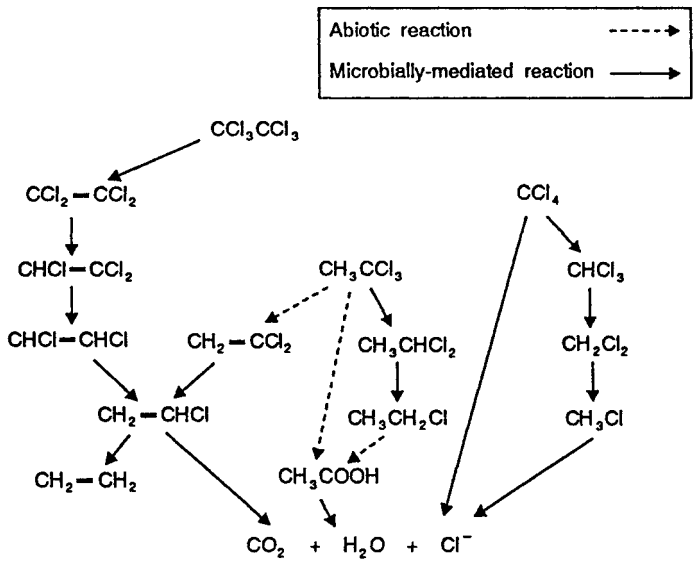


Fig. 2. Anaerobic transformation of CAHs (McCarty and Semprini, 1993).

abolism (McCarty and Semprini, 1993). Under aerobic conditions in mixed cultures typical of natural conditions, TCE is mineralized completely to CO_2, water and chloride through cooperation between the TCE oxidizers and other bacteria (McCarty and Semprini, 1993).

CAHs can be cometabolized anaerobically under a variety of environmental conditions (McCarty and Semprini, 1993). The first step in the process is reductive dechlorination. In reductive dechlorination, the CAH is reduced by substituting a hydrogen atom for chlorine or by forming a double bond between two carbon atoms, one or both of which contained a chlorine substitution (Vogel et al., 1987; Kobayashi and Rittmann, 1982). As shown in Fig. 2, successive reductive dechlorination can transform CAHs into a series of byproducts containing fewer chlorine atoms, and all of these products may be found with the parent CAH (McCarty and Semprini, 1993). In general, the highly chlorinated compounds are degraded more easily than less-chlorinated compounds so that less-chlorinated compounds are more persistent in the environment (McCarty and Semprini, 1993). Biodegradation rates tend to be highest under highly reducing conditions (McCarty and Semprini, 1993).

3.3.3. PCBs

Chapelle (1993) summarizes current knowledge on PCB degradation. PCBs can be degraded aerobically if the molecules contain relatively few chlorine atoms. PCBs with a larger number of chlorine atoms are degraded anaerobically by reductive dechlorination. Thus, a sequence of anaerobic degradation followed by aerobic degradation can degrade PCBs completely to CO_2.

4. Modeling subsurface biodegradation

Modeling biodegradation in the subsurface is extremely complex. Many of the biological and physical phenomena involved are only partially understood. The difficulty of modeling is compounded by our inability to actually see what is going on in the subsurface. Although we know that the subsurface is generally heterogeneous, we typically do not know the locations and extent of the heterogeneities. We also cannot see the microorganisms in the subsurface and must make assumptions about their distribution and metabolic capabilities. Our lack of knowledge is demonstrated by the relative lack of successful field-scale biodegradation modeling. However, many models have been quite successful at describing biodegradation on a smaller scale in one-dimensional column experiments. In this section, the important factors affecting biodegradation of NAPLs are discussed, and the methods used by other modelers to describe these factors are described.

4.1. General conceptual model of biodegradation

Before attempting to model a complex phenomenon such as subsurface biodegradation, it is often helpful to develop a conceptual model. The conceptual model should include all of the factors affecting the phenomenon. These factors can then be described mathematically and their relative importance assessed. Those factors that do not have a significant effect can be neglected or estimated while those that significantly affect the results of the simulation can be retained.

A conceptual model of the transport and biodegradation of a hypothetical NAPL spill is described below to illustrate the factors that need to be considered in modeling and the complexity of subsurface biodegradation. The conceptual model is derived from a compilation of literature on the subject, and the particular phenomena will be described in greater detail and referenced later.

To begin simply, suppose a spill of LNAPL occurs at the ground surface above a shallow water table. The LNAPL could contain dissolved chlorinated species that may be difficult to biodegrade. What will be the fate of the NAPL? Many of the more volatile components will vaporize before seeping downward into the soil. The fraction of NAPL that remains is the subject of the conceptual model.

4.1.1. Unsaturated zone

The LNAPL will follow the basic physical laws of any other fluid and will begin to flow downward through the soil under the force of gravity. Being the non-wetting fluid compared to water, NAPL will tend to occupy the medium-sized pores, while water occupies the smaller pores and air the largest. Assuming the spill is large enough, NAPL will travel downward until it reaches the water table, where it will spread over the surface of the water and form a lens because it is lighter than water. When the spill stops, the lens will continue to spread until the NAPL in the vadose zone has reached residual saturation. Residual saturation is the NAPL saturation at which the NAPL is no longer able to flow as a continuous phase. Fluctuations in the water table elevation can cause the NAPL to smear into the capillary fringe and below the original lens surface.

In the vadose zone, a four-phase system will be established, consisting of NAPL, air, water, and solid (soil). The different components of the NAPL will partition among the different phases. If local equilibrium is established, the partitioning can be described with partition coefficients. If the transfer of constituents from one phase to another is rate-limited, then kinetic expressions must be used to predict the change in concentrations of constituents in the different phases. Volatile NAPL components will vaporize into the air phase, more soluble NAPL components will dissolve into the pore water, and highly adsorbable components will adsorb onto organic material in the soil. NAPL will also dissolve from the lens into the groundwater. The composition of the NAPL changes as its components are removed by leaching, dissolution into the groundwater, volatilization, and biodegradation, since the chemical and physical properties of each component are affected by these different phenomena at different rates.

Until it reaches residual saturation, the NAPL does not remain static; it moves through the vadose zone under the influence of capillary pressure and gravity. If advection in the vadose zone is neglected, diffusion is the primary transport mechanism once the NAPL reaches residual saturation. NAPL constituent vapors evolve principally from the NAPL phase and diffuse through the air phase. The mobilized vapors dissolve into pore water as they move and also adsorb onto the soil so that the NAPL constituents tend to spread. NAPL constituent vapors establish equilibrium with the capillary fringe outside of the residual NAPL area. Dissolved NAPL constituents also diffuse through the pore water, which is interconnected throughout the vadose zone. Volatile and soluble NAPL components move through the NAPL phase under induced concentration gradients caused by their loss across the NAPL/air and NAPL/water phase boundaries. As the NAPL constituents spread, some may be lost to the atmosphere by diffusion upward to the ground surface.

The soil contains microorganisms, most of which are attached to small particles and others that are free floating in the pore water. However, even the microorganisms attached to particles are surrounded by water because microorganisms must be in aqueous solutions to be active. Microorganisms are present within pore cavities and at the throats of pores. Most of the bacterial species are adapted to the aquifer conditions, but they have a tremendous variety of metabolic capabilities and nutrient requirements. The microorganism population is in a constant state of flux, with organisms detaching and becoming free-floating, other microorganisms attaching to colloidal particles and moving with the pore water, and other organisms moving along particle surfaces by processes of bacterial motion.

As soon as NAPL is introduced to the ground, the environment experienced by the microorganisms changes. The NAPL components dissolve into the pore water, becoming accessible to microorganisms. Whereas before contamination existed the environment was likely to be substrate-limited, it suddenly becomes limited by electron acceptors or nutrients. Microorganisms immediately begin to adapt to the new environment and begin the processes necessary to biodegrade the NAPL components. If microorganisms possess the necessary metabolic machinery, they may begin to degrade some of the more easily degradable dissolved components of the NAPL. The microorganisms will also begin acclimating to the

new conditions created by the NAPL constituents. Because the NAPL components are likely to be different from the substrate the microorganisms normally metabolize, they must begin synthesizing new enzymes capable of acting on the dissolved NAPL constituents. In addition to being chemically different substrates, the NAPL constituents may affect other environmental conditions such as pH, redox potential, and ionic strength. The NAPL may also contain toxic compounds that cannot be tolerated by the microorganisms present. Microorganisms must adapt to these new conditions to survive.

The microorganisms may accumulate near the NAPL/water interfaces where concentrations of the new substrate are highest. If the NAPL components are not too toxic, the microorganisms will first accumulate directly on the water/NAPL interface. If the NAPL components are toxic, the microorganisms will not be present at the interface, but will metabolize diluted NAPL constituents that diffuse out of the NAPL some distance from the interface. Aerobic bacteria will first utilize the NAPL constituents and will quickly deplete the oxygen in the pore water. In sandy or gravelly strata, diffusion of oxygen and infiltration of oxygenated precipitation from the surface may supply microorganisms with enough oxygen to maintain aerobic conditions. More likely, reaeration will not be fast enough to supply aerobic organisms with oxygen, and microorganisms adapted to anaerobic conditions will begin to metabolize the NAPL constituents. The anaerobic zone will grow as the NAPL constituents migrate with the concomitant switching from aerobic to anaerobic conditions. If the microbial community is relatively diverse and alternate electron acceptors are present, the NAPL constituents may be degraded by successive microbial communities utilizing different electron acceptors, based on their relative availability and energy yield.

The utilization of NAPL components will not be uniform. Larger aliphatic NAPL components will be degraded by aerobic bacteria but not by anaerobic bacteria, so that they will be present in the soil for a very long time. Other NAPL components are degraded only anaerobically as primary substrates. Other NAPL components are degraded both aerobically and anaerobically. Some NAPL components are degraded by cometabolism, while still others are degraded by a complex sequence which may involve aerobic, anaerobic, and cometabolic steps as well as abiotic reactions such as hydrolysis. The NAPL components are not degraded independently of each other, even if cometabolism is not a significant process. Microorganisms may compete for the most easily degraded compounds. One compound may interfere with the degradation of another compound due to its toxicity or binding of a key enzyme site. The products of biodegradation may be toxic and inhibit further degradation of the compound or of other compounds. These compounds may be biodegraded until their concentration is sufficiently low that it becomes energetically favorable to biodegrade a less easily biodegradable compound. Two compounds may be degraded by the same enzyme so that they are degraded more slowly than if they were present alone.

Individual bacteria may not be capable of completing all of the steps in the biodegradation. One bacteria may dechlorinate a molecule, another may add a hydroxyl group, while another may convert the molecule into a form that can be utilized in one of the many metabolic pathways present in most bacteria. The

products from one biochemical reaction may be required by another microorganism so that the two can only exist together. Biodegradation rates of the same organism may differ depending upon whether the organisms are attached to soil surfaces or are free-floating in the pore water.

As the bacteria act on the NAPL constituents, nutrients will be depleted near the interface since they must be supplied by diffusion through the pore water. Microbiological activity may decrease if nutrients cannot be supplied to the interface as fast as they are being consumed, and very little activity may be observed near the interface where nutrient conditions are most limiting due to the high NAPL concentrations. As the NAPL constituents spread in the vadose zone, additional microbial communities begin acclimating to the changing conditions so that the biodegradation processes occurring are constantly changing both with time and position throughout the vadose zone.

4.1.2. Saturated zone

The biodegradation phenomena occurring in the saturated zone are similar to those in the vadose zone. However, only three phases are present in the saturated zone, air being absent. Transport in the saturated zone also differs from that in the vadose zone. Advection is the dominant transport mechanism in the saturated zone, and physical factors such as dispersion and adsorption play a much larger role.

As in the vadose zone, aerobic microorganisms in the saturated zone will first tend to accumulate at the NAPL/water interface where substrate concentrations are highest. However, oxygen will become rapidly depleted and is not renewed as fast as it is in the vadose zone so that anaerobic conditions are likely to develop quickly. Although flowing groundwater will resupply oxygen to the microorganisms, this type of transport may be slow relative to the oxygen depletion rate. Therefore, as in the vadose zone, a fringe of aerobic activity develops at the edge of the contaminant plume. In the interior of the plume, anaerobic conditions predominate and electron acceptors other than oxygen must be used by the microorganisms.

Microorganisms in the saturated zone are likely to exist as small colonies. These colonies may be the result of cell division and agglomeration due to extracellular polymers or may be communities of synergistic organisms. Because of the sparing solubility of most typical NAPL contaminants, the colonies are likely to be relatively thin, so that the contaminant concentrations within the colony are the same throughout and perhaps the same as the substrate concentrations dissolved in the bulk aqueous phase. However, if the NAPL constituents, nutrient and electron acceptor fluxes into the colonies are sufficiently high, a thicker biofilm may form so that NAPL constituents must diffuse across not only a liquid boundary layer but also within the biofilm in order to be utilized by microorganisms throughout the biofilm interior. Even if no thick biofilm forms, NAPL constituents may have to diffuse across a stagnant liquid layer to the biomass before they can be biodegraded. If the bacteria are supplied with sufficient substrate and electron acceptor, they may form a continuous film and alter the porosity, permeability and dispersion properties of the aquifer.

As NAPL components dissolve out of the NAPL residual, the NAPL phase shrinks, and the dissolved constituents move with the groundwater flow. Because of dispersion, the dissolved constituents at the front edge of the plume are diluted so that more oxygen is available for aerobic respiration. Mixing also occurs along the edges of the plume, promoting higher rates of aerobic respiration there. The more adsorbable components of the NAPL will move through the aquifer at a rate slower than the average groundwater flow. Dissolved oxygen in the groundwater entering the rear edge of the plume will promote aerobic respiration at this edge also, so that adsorption may increase the rate of aerobic respiration there. However, adsorption may decrease biodegradation in other parts of the aquifer by making the adsorbed compounds less available to microorganisms. Reaeration of the aquifer from the vadose zone, if it is significant, will favor aerobic conditions at the water table surface.

As the plume moves through the aquifer, microorganisms first encountering the plume must acclimate to the dissolved NAPL. Since this takes some time, the leading edge of the dissolved NAPL plume may not be biodegraded and a pulse of contamination may move through the aquifer. This effect may be partly mitigated through detachment of microorganisms from acclimated communities within the plume. The detached microorganisms may move as free floating bacteria or move attached to colloid particles at a rate faster than the average groundwater movement. They may become attached to soil ahead of the plume and be able to begin degrading the plume as soon as it reaches them.

On the pore scale, biodegradation may be limited by microorganisms' inability to diffuse into small or dead-end pores so that NAPL contaminants remain separated from microorganisms until the decrease in bulk concentration causes them to diffuse out. If microorganisms can reach these small pore spaces, biodegradation may be limited by the rate of electron acceptor diffusion into these areas. Depending on the pore geometry and location of microorganisms within the pores, biodegradation may be diffusion limited, kinetically limited, diffusion limited in some areas and kinetically limited in others, or limited by both processes to varying degrees throughout the medium.

This conceptual description is obviously very complex, and includes just a few of the many physical, chemical and biological processes that we know are important in subsurface biodegradation. In the next section, these factors are described in more detail and the methods other researchers have used to account for them are presented.

4.2. Transport equations

This section briefly describes the main equations for multi-phase, multi-component NAPL transport. More complete descriptions of the governing equations and solution methods can be found in other sources (Abriola, 1989; Pinder and Abriola, 1986; Corapcioglu and Baehr, 1987).

Although multi-phase flow and solute transport equations may be written in innumerable ways, most developments begin with basic mass balance equations, supplemented by constitutive relationships to solve the system for all of the

variables. This discussion of the flow equations follows the development by Abriola (1989).

4.2.1. Mass balance equations

One mass balance equation can be written for each constituent in each phase. The basic form of the mass balance equation is

$$\frac{\partial}{\partial t}(\theta_\alpha \rho^\alpha \omega_i^\alpha) + \nabla\cdot(\theta_\alpha \rho^\alpha \omega_i^\alpha \mathbf{v}^\alpha) - \nabla\cdot\mathbf{J}_i^\alpha = R_i^\alpha + r_i^\alpha \tag{1}$$

where α is the phase; i is the component; θ_α is the volumetric content of phase alpha (volume of phase α/total volume); ρ_α is the density of phase alpha (M/L^3); ω_i^α is the mass fraction of species i in phase alpha; $\mathbf{v}^\alpha$ is the average linear velocity of phase alpha relative to the solid phase (L/T); $\mathbf{J}_i^\alpha$ is the non-advective flux of species i in the α phase (M/L^{2}T); R_i^α is the rate of exchange of mass of species i due to interphase diffusion and/or phase change (M/L^{3}T); r_i^α is the rate of creation of species i in phase α (M/L^{3}T).

In this equation, the product $\theta_\alpha \rho^\alpha \omega_i^\alpha$ has units of mass of i per unit volume of porous media (the concentration of species i). The overall dimensions of the equation are M/L^{3}T.

The four phases typically modeled are the solid, aqueous, NAPL and air phases. The mass balance equations can be summed over all phases to give a mass balance equation for each species in all phases. When the mass balance equations are summed in this manner so that individual chemical species can be tracked, the approach is often termed compositional. The summation yields an equation of the following form for each chemical species

$$\sum_\alpha^{\text{np}} \left\{ \frac{\partial}{\partial t}(\rho^\alpha \theta_\alpha \omega_i^\alpha) + \nabla\cdot(\rho^\alpha \theta_\alpha \mathbf{v}^\alpha \omega_i^\alpha) - \nabla\cdot\mathbf{J}_i^\alpha \right\} = \sum_\alpha^{\text{np}} r_i^\alpha \tag{2}$$

where np is the number of phases. The first term in the above equation represents the accumulation of component i. The second term accounts for component i advective flux. The third term represents component i transport by diffusion and mechanical dispersion. The last term represents the rate of production or destruction of component i. Note that the R_i terms drop out of the above equation since all chemical species are conserved across phase boundaries. The non-advective flux term is represented by (Abriola, 1989)

$$\mathbf{J}_i^\alpha = \rho^\alpha \theta_\alpha D^\alpha \cdot \nabla \omega_i^\alpha \tag{3}$$

where D^α is the hydrodynamic dispersion tensor (L^2/T).

The mass balance equations are constrained by the following requirements (Pinder and Abriola, 1986)

$$\sum_i^{\text{nc}} \omega_i^\alpha = 1 \qquad \sum_\alpha^{\text{np}} \theta_\alpha = 1 \tag{4}$$

A mass balance equation is written for each NAPL constituent, electron acceptor, growth nutrient, and microbial population being modeled. The reaction

term (r_i^α) is the part of the mass balance equation of primary interest in this report. Microbial degradation of the NAPL constituents of interest are accounted for through this term by substitution of the appropriate biodegradation kinetic expression. Separate reaction terms can be included to account for non-biological reactions such as rate-limited adsorption and abiotic degradation.

4.2.2. Conservation of momentum

In order to be solved, the average linear phase velocity must be determined for each phase. The velocities are found through the conservation of momentum equation in the form of Darcy's Law

$$\mathbf{v}^\alpha = \frac{q}{\theta_\alpha} = -\frac{\mathbf{k}k_{r\alpha}}{\mu_\alpha \theta_\alpha}\cdot(\nabla P^\alpha + \rho^\alpha g \nabla z) \tag{5}$$

where $\mathbf{v}^\alpha$ is the average linear velocity of phase alpha relative to the solid phase (L/T); q is the specific discharge (Darcy velocity, L/T); $\mathbf{k}$ is the intrinsic permeability (L^2); $k_{r\alpha}$ is the relative permeability for phase alpha; μ_α is the viscosity of phase alpha (M/LT); P^α is the pressure of phase alpha (M/LT^2); g is the acceleration of gravity (L/T^2); z is the elevation (L).

Relative permeabilities are a function of phase saturations (volume of phase/volume of pore space) and can be predicted from laboratory data or semi-empirical models.

4.2.3. Constitutive relations

In addition to the constraints on mass fractions and volumetric contents, the mass balance equations are coupled by other constitutive relations. These constitutive relations include:

- capillary pressures = f (P^α, P^β)
- saturations = f (capillary pressures)
- densities = f (phase pressure, composition of phase)
- viscosity = f (pressure, phase composition)
- equilibrium partition coefficients or kinetic expressions for interphase mass transfer.

The above constitutive relationships make the system of equations highly nonlinear so that they must be solved using numerical methods.

4.2.4. Simplifications for column studies

Many of the models reviewed in this report describe biodegradation in only one dimension and only account for a single phase—the aqueous phase. In addition, density, viscosity, and permeability are often considered constant and capillary effects do not apply. In this case, the mass balance equations for each constituent reduce to

$$\frac{\partial C_i}{\partial t} = D_i \frac{\partial^2 C_i}{\partial x^2} - v_x \frac{\partial C_i}{\partial x} - r_i \tag{6}$$

where C_i is the concentration of the chemical species of interest.

4.3. Physical phenomena affecting biodegradation

The transport equations presented above include terms to account for adsorption and dispersion, two phenomena that are very important in modeling biodegradation. In addition to these phenomena, other physical factors must be considered in biodegradation modeling. These factors can either be explicitly incorporated into the model equations or need to be considered in evaluating the parameters used in the model. Physical factors affecting biodegradation are discussed below. Where appropriate, methods used by other researchers to include these factors are described.

4.3.1. Hydrodynamic dispersion

Diffusion and mechanical dispersion cause a spreading of the solute front as the front travels through the subsurface in the saturated zone. Diffusion is the movement of a solute from an area of high concentration to an area of less concentration and occurs whenever there is a concentration gradient, regardless of whether or not the fluid is in motion (Fetter, 1993). Mechanical dispersion is mixing caused by differing fluid velocities along the flow path due to three different phenomena (Fetter, 1993):

- solutes travel faster through large pores than through small ones;
- solutes travel over different path lengths for the same displacements because of the tortuous nature of the subsurface matrix;
- frictional forces cause solute velocities in the center of pores to be higher than velocities along the pore walls.

Longitudinal dispersion causes spreading along the direction of flow, while transverse dispersion causes spreading in a direction normal to the flow. In solute transport modeling, diffusion and mechanical dispersion are usually combined into a parameter called the hydrodynamic dispersion tensor, D_{ij}. D_{ij} is defined for longitudinal and transverse dispersion of component β and phase α as follows (Sleep and Sykes, 1993)

$$D^{\alpha}_{\beta ij} = a_{\mathrm{T}} |v_{\alpha}| \delta_{ij} + (a_{\mathrm{L}} - a_{\mathrm{T}}) \frac{v_{\alpha i} v_{\alpha j}}{|v_{\alpha}|} + \delta_{ij} D^{\alpha}_{\beta m,ij} \tau_{\alpha} \tag{7}$$

where: $v_{\alpha i}$, $v_{\alpha j}$ are the longitudinal and transverse components of the average linear velocity of phase α (L/T); a_{L}, a_{T} is the longitudinal and transverse dispersivities (L); δ_{ij} is the Kronecker delta function; $D^{\alpha}_{\beta m,ij}$ is the molecular diffusion coefficient (L^2/T); τ_{α} is the tortuosity.

At the laboratory scale, dispersion is well understood and can be readily quantified for a given experiment. In the field, however, dispersivity is scale dependent and is not a characteristic constant for the aquifer (Fetter, 1993). In general, dispersivities tend to increase as solute travel distances increase. The variability in dispersivity causes complications in solute transport modeling. All of the solute transport models reviewed in this study used a constant hydrodynamic dispersion coefficient to account for diffusion and dispersion.

Diffusion of solutes is practically negligible for most saturated aquifers, and

mechanical dispersion is usually the dominant cause of solute front spreading. However, diffusion can be important at low flow velocities. The relative importance of these two phenomena can be determined from the Peclet number, defined as

$$\mathrm{Pe} = \frac{vd}{D_m} \tag{8}$$

where: Pe is the dimensionless Peclet number; v is the average linear velocity (L/T); d is the average aquifer grain diameter (L); D_m is the molecular diffusion coefficient of the solute (L^2/T).

The Peclet number is the ratio of the rate of transport by advection to the rate of transport by diffusion. Longitudinal diffusion is usually not important for $\mathrm{Pe} > 6$, and transverse diffusion is usually not important for $\mathrm{Pe} > 100$ (Fetter, 1993). However, if solutes diffuse into dead-end pores or small pores where the velocity is much slower than the average velocity, intra-particle diffusion can cause extensive tailing of solute fronts. Intra-particle diffusion is discussed briefly by Valocchi (1985). The effects of intra-particle diffusion on biodegradation are discussed by Chung et al., (1993). At the pore scale, intra-particle diffusion may cause solutes to be unavailable to microorganisms if the microorganisms are too large to penetrate deep into the pores. Solutes diffusing into the pores can only be degraded when they diffuse back out under induced concentration gradients caused by biodegradation in the bulk liquid phase (Chung et al., 1993).

As pointed out by Lee et al. (1988), intra-particle diffusion can also have important effects on mixing, especially during high flow rates induced by pumping. Solutes may become trapped in dead-end pores or other areas of low permeability during the relatively slow movement of groundwater before remediation begins. When water carrying nutrients for in-situ bioremediation is pumped through the aquifer, the water will tend to flow through the large pores and may not mix with the trapped solute. Models that assume complete mixing of substrates and nutrients without taking diffusion effects into account could substantially overpredict biodegradation.

Although intra-particle diffusion has not been explicitly incorporated into any transport models reviewed for this report, it may be possible to model it as dispersion (Valocchi, 1985). In this case, intra-particle diffusion could be accounted for as an increase in dispersivity. It may also be possible to model intra-particle diffusion as a rate-limited adsorption process (Fetter, 1993). Fetter (1993) identifies work potentially applicable to biodegradation modeling done by Raven et al. (1988) in which diffusion into an immobile fluid zone along fractures is considered. More theoretical work is necessary to determine how to best account for intra-particle diffusion and determine whether or not it is an important process for biodegradation modeling.

On a macroscopic scale, dispersion can be very important to biodegradation modeling. As a result of hydraulic conductivity differences between vertical aquifer layers, flow velocities within different aquifer layers will not be equal. Dissolved NAPL constituents will move with different velocities in these different layers. At

any given point, the groundwater may contain contaminants or it may not, depending on the layer's hydraulic conductivity and distance from the source of contamination (Freeze and Cherry, 1979). These aquifer heterogeneities are typically modeled by including areas of high and low permeability in the modeling grid and including a term for dispersion. Since we are often interested in the average concentration of contaminants in the aquifer at a particular point, this treatment of dispersion adequately accounts for the observed spreading of the contaminant front.

In biodegradation modeling, however, the actual local concentrations of the contaminants are important because the rates of degradation depend on the local concentrations, not vertically averaged concentrations. Models based on spatially averaged concentrations could either over- or under-estimate biodegradation rates depending on whether nutrients, electron acceptors, or substrate were limiting the biodegradation reactions. For example, the extent of biodegradation could be overestimated significantly if a substrate is toxic. In this case, the vertically averaged concentration might indicate that the contaminant concentration in some locations is below some threshold toxicity and that biodegradation will proceed, when the actual concentration is much more than the vertically averaged concentration, and no biodegradation occurs at all. True three-dimensional modeling may be necessary to adequately describe biodegradation, especially when distinct, continuous vertical heterogeneities exist.

Since most of the models reviewed in this report are one-dimensional, the effect of dispersion on biodegradation is not readily apparent. The effect of dispersion on biodegradation was investigated by Borden and Bedient (1986) using their two-dimensional model. They concluded that transverse dispersion was the dominant source of oxygen for biodegradation as a result of mixing of hydrocarbon plumes with oxygenated formation water. Longitudinal dispersion had little effect. Since aerobic biodegradation can be the dominant biodegradation mechanism in some aquifers, the increased mixing caused by dispersion is very important. If a constant dispersion coefficient is used to describe dispersion, however, the mixing can be considerably overestimated with a corresponding overestimation of biodegradation rates. Borden and Bedient (1986) reported that transverse dispersion causes greater aerobic biodegradation at a hydrocarbon plume's sides and causes the plume to appear much narrower than expected.

4.3.2. Adsorption

Adsorption is "the process in which matter is extracted from the solution phase and concentrated on the surface of the solid material" (Weber, 1972). Adsorption results in the distribution or partitioning of solutes between the solid and fluid phases. Adsorption can be modeled as an equilibrium process or as a kinetic process. If the rate of adsorption and desorption is fast relative to other processes occurring in the aquifer, the solute(s) can be assumed to be at equilibrium between the fluid and solid phases. This assumption is called the local equilibrium assumption (LEA). The applicability of the LEA has been studied for some time by a number of researchers (Valocchi, 1985; Bahr and Rubin, 1987; Harmon et al., 1992).

If the LEA is applicable, then the equilibrium partitioning of solutes between the solid and liquid phases can be described by an isotherm in which the solid phase concentration is some function of the solute concentration in the bulk liquid. The most common isotherm relationships are the linear isotherm, Freundlich isotherm and Langmuir isotherm (see Fetter, 1993). The simplest partitioning relationship is the linear isotherm where the solute concentration on the solid is a linear function of the bulk fluid solute concentration. In this case, the mass of solute adsorbed onto the solid is (Fetter, 1993)

$$C^* = K_d C \tag{9}$$

where C^* is the mass of solute sorbed per mass of solid; (M solute/M solid); C is the fluid phase solute concentration (M/L^3); K_d is the distribution coefficient (L^3/M solid).

This description of adsorption is used in most of the transport models reviewed in this report. It is usually valid at low solute concentrations. At higher substrate concentrations, the equilibrium partitioning between solute and solid phase is often non-linear. In this case, the Freundlich and Langmuir non-linear equilibrium adsorption isotherms could be more accurate than the linear adsorption isotherm.

For situations where the LEA is not applicable, kinetic expressions must be used. The reversible linear kinetic sorption model describes the rates of sorption and desorption as first-order according to (Fetter, 1993)

$$\frac{dC^*}{dt} = k_f C - k_r C^* \tag{10}$$

where k_f is the forward (sorption) rate constant; k_r is the backward (desorption) rate constant.

This expression was used by Semprini and McCarty (1992) to model biodegradation of dissolved chlorinated organics at the Moffet Naval Air Station field site. Semprini and McCarty (1992) reported that their model did not accurately predict the observed concentrations with a simple linear equilibrium model, but predicted the data well when adsorption was treated as a first-order reversible reaction.

The first-order reversible adsorption model reduces to the linear equilibrium sorption expression if equilibrium is assumed ($dC^*/dt = 0$). Similar rate expressions can be developed from the Freundlich or Langmuir isotherm equations. If adsorption is assumed to be controlled by diffusion, then a diffusion-controlled rate expression can be used to described adsorption as described by Fetter (1993).

Surface diffusion (movement of a sorbed compound over the solid surface) can also affect adsorption. If surface diffusion occurs slowly relative to liquid diffusion, it may dominate the adsorption process.

Adsorption is important in modeling biodegradation, and could either increase or decrease the biodegradation rate (McCarty, 1988). Adsorption could increase biodegradation by concentrating nutrients in the subsurface, by immobilizing substrates so that microorganisms have more time to degrade them, or by immobilizing nutrients so that water-borne nutrients flow into the area (Borden and Bedient, 1986; Lee et al., 1988). Conversely, adsorbed solutes may reduce biodegradation

by making the solute unavailable to microorganisms in the water phase, or by reducing the rate of biodegradation in the water phase by reducing the fluid phase concentration (Lee et al., 1988; McCarty, 1988).

Speitel and DiGiano (1987) modeled the regeneration of activated carbon by biofilms and determined that the substrate flux into the biomass from the sorbed phase was greater than the substrate flux from the liquid phase. This suggests that contaminants adsorbed on particles before significant biomass growth occurs can be substantially biodegraded by biomass growing on the particles at later times. Lee et al. (1988) reported studies in which adsorption increased or decreased biodegradation and postulated that sorption may increase biodegradation under oligotrophic (nutrient poor) conditions by concentrating nutrients, but may decrease biodegradation under nutrient-rich conditions by competing with microorganisms for substrate. Simulations of BTEX degradation performed by Borden and Bedient (1986) indicated that adsorption may enhance biodegradation by allowing oxygen to continuously move into the retarded contaminant plume. This would supply more oxygen and increase biodegradation under oxygen limited conditions. From these and other studies it is apparent that the effects of adsorption are complex and could increase or decrease the biodegradation rate. More research on the effects of adsorption on biodegradation is needed.

Adsorption could also have important implications for both microorganism and NAPL movement. Migration of highly sorbed compounds has been observed to exceed the expected migration rates as predicted by the compounds' retardation factor (Corapcioglu and Jiang, 1993). The unexpectedly high migration rate may be due to the compounds' adsorption onto colloidal particles (including bacteria) that travel through the aquifer much faster than the average groundwater velocity (Corapcioglu and Jiang, 1993). Column studies have verified this effect (Lindqvist and Enfield, 1992; Jenkins and Lion, 1993).

4.3.3. Reaeration

Reaeration from the ground surface could be a major oxygen source for aerobic microorganisms and could be important in modeling biodegradation. A significant mass of NAPL vapors can vaporize from contaminated pore water and groundwater, entering the air phase of the vadose zone where they can dissolve into pore water near the surface. The oxygen-rich conditions near the surface could accelerate removal by biodegradation. Oxygenation of the groundwater from reaeration could provide substantial oxygen to oxygen-poor groundwater when the vapor pressures of the NAPL components are low. Borden and Bedient (1986) reported that vertical exchange of oxygen and hydrocarbon with the unsaturated zone may significantly enhance the rate of biodegradation. In multi-phase, multi-component models, reaeration should be accounted for as an additional mass transfer process.

4.3.4. Temperature

The biochemical reactions that microorganisms carry out are affected by temperature just like non-biological reactions. Growth of *pseudomonad* bacteria, a genus known to degrade a variety of organic compounds, is usually optimal at

temperatures between 25 and 30°C (Focht, 1988), whereas groundwater temperatures can be significantly lower. Dibble and Bartha (1979) found that biodegradation of oil sludge in soil was negligible at 5°C, occurred only after a two-week lag period at 13°C, but was significant above 20°C. Focht (1988) reports that the Q_{10} (difference in reaction rate for a 10°C difference in temperature) for most biological systems is 1.5 to 3. In a review, Atlas (1981) reported that the rate of oil biodegradation was affected by temperature, although the ultimate extent of transformation of petroleum compounds was not. In some cases, Atlas (1981) reported a greater extent of biodegradation at low temperatures than at high temperatures. Atlas (1981) points out that temperature affects the composition of petroleum mixtures through volatilization and dissolution as well as the rates of biodegradation.

Since biodegradation modeling is still in an early stage of development, many models attempt only to describe biodegradation in simple laboratory column studies so that temperature effects are not relevant. In simulations of biodegradation in actual aquifers, the incorporation of temperature effects is not always clear. For example, Borden and Bedient (1986) modeled the migration of a creosote plume using data from rate studies conducted with actual aquifer material. However, the temperature of the test conditions and in-situ groundwater were not explicitly given, and some parameters were taken from the literature. Sykes et al. (1982) used a maximum growth rate value of $\frac{1}{2}$ the measured value to account for lower temperatures in the aquifer being modeled. MacQuarrie et al. (1990) assumed that the biodegradation kinetic parameters were independent of temperature and used values determined from laboratory experiments.

Two points regarding temperature for biodegradation modeling in the subsurface are important. First, because the rates of biodegradation are dependent on temperature, caution must be used in extrapolating results of biodegradation experiments carried out at typical laboratory temperatures to actual biodegradation in the subsurface. Not only are reaction rates slower at lower temperatures, but the Arrehenius relation may not hold below temperatures of 10°C, making predictions of reaction rates at lower temperatures difficult (Focht, 1988). Second, the effects of temperature on biodegradation are complex, since temperature affects not only biochemical reactions but also NAPL phase transfer and transport (Atlas, 1981). These points must be considered when modeling NAPL biodegradation.

4.3.5. pH

Bacteria live in subsurface environments under a wide pH range. Bacteria have been reported in environments ranging from <3 to >10 pH (Chapelle, 1993). However, bacteria living in these pH extremes are usually adapted to the environment. Most bacteria prefer a pH in the neutral range (Chapelle, 1993). Natural waters tend to buffer the pH so that it remains around neutral. However, the pH in contaminated environments can be drastically altered by contaminants (Chapelle, 1993).

The pH of an aquifer has at least two important effects on subsurface biodegradation. First, the pH affects the type of microorganisms present and will

select for those most adapted to the pH environment. Second, the pH, together with the reduction potential, will determine the ionic form of ionizable species in the groundwater. Both of these factors affect the type of biodegradation that can occur. For example, nitrification is inhibited at values of <6 pH (Lee et al., 1988). Biodegradation reactions can change the pH of aquifers if the amount of oxidized material is large enough (Bouwer and McCarty, 1984). Generally, biodegradation is optimum at a pH of neutral to slightly alkaline (Lee et al., 1988; Focht, 1988).

The pH can be controlled in laboratory experiments so that biodegradation modeling is relatively unaffected by pH. As a consequence, most models of biodegradation do not explicitly consider pH. In field systems, the pH should be determined before modeling begins. If biodegradation reactions are expected to significantly alter pH, then pH shifts should be included in the model, especially if electron acceptors other than oxygen are involved.

4.3.6. Reduction potential

The reduction potential (*Eh*) is an indication of the degree of oxidation of dissolved constituents in an aqueous solution. Positive *Eh* values indicate that most NAPL constituents are oxidized and are typical of aerobic aquifers. Negative *Eh* values indicate that most constituents are in reduced form so that there is a high potential for redox reactions to occur. Another way of thinking about *Eh* is that at very positive *Eh* values, there are many chemical species present which can accept electrons and few donors, while at low values of *Eh* there are many electron donors but few acceptors. Low *Eh* values also indicate that the electron acceptors present will yield less energy in redox reactions than the electron acceptors present at high *Eh* values.

The *Eh* value of an aquifer is important because it reflects the thermodynamic potential for different redox reactions to occur. As each electron acceptor, beginning with oxygen, is consumed in biodegradation reactions, the *Eh* decreases. As the *Eh* decreases, redox reactions in which other electron acceptors participate become thermodynamically favored (Freeze and Cherry, 1979). This process results in a sequential utilization of electron acceptors (see Section 4.4.3).

Eh is an important variable when modeling anaerobic biodegradation with multiple electron acceptors because it is an indicator of when anaerobic biodegradation reactions are thermodynamically favored. None of the models reviewed in this report account for changes in *Eh*, although researchers did consider *Eh* when determining the potential for denitrification or desulfurization reactions to occur (Frind et al., 1990). The *Eh* value of the aquifer can be modeled by tracking the concentrations of all dissolved species that could participate in redox reactions.

4.4. Microbial community

Most models of subsurface biodegradation assume that a population of microorganisms exists that can degrade the contaminants under study. These microorganisms are implicitly assumed to occur in subsurface locations where the contaminant is accessible. While studies have shown that bacteria in shallow aquifers are capable of degrading a variety of organic compounds (Chapelle, 1993), the distribution and

composition of the subsurface microbial community can have a significant effect on the rates at which biodegradation occurs. This section describes the occurrence of microorganisms in the subsurface and explains the importance of the microbial community on modeling biodegradation. The methods by which some of these factors have been incorporated into biodegradation models are contained in the next section.

4.4.1. Number and distribution of subsurface microorganisms

4.4.1.1. Macroscopic scale. The vast majority of microorganisms in subsurface soils are bacteria, and their numbers decrease with increasing depth (Chapelle, 1993). The upper 1 to 2 m of the vadose zone, called the soil zone, is the most biologically active and varied subsurface microbial habitat due to its proximity to vegetation at the ground surface. Fewer microbiological studies of deeper soil zones have been made, but the few studies completed indicate that microorganisms exist at appreciable numbers down to the water table. Total bacterial counts of 10^6 to 10^7 cells/g of dry sediment were measured in one study (Chapelle, 1993). Very deep soils in dry environments may contain less than 10^5 cells/g, and these cells may contain less than 100 viable cells/g (Chapelle, 1993). The low viable cell counts in these relatively dry environments could be due to a lack of moisture, which all microorganisms require to survive.

The total number of microorganisms in the saturated zone usually depends on the type of flow system being studied. Three types of flow systems can be defined (Chapelle, 1993). A local flow system has its recharge area at a topographic high and its discharge area at a topographic low located adjacent to the topographic high. Local flow systems are typically water table aerobic aquifers with short hydraulic residence times. Because of their proximity to the surface, local flow systems may contain most of the cases of water pollution. In intermediate flow systems, recharge and discharge areas are separated by one or more topographic highs. Intermediate flow systems are typically anaerobic and often consist of confined aquifers less than 300 m in depth (Chapelle, 1993). Regional flow systems are characterized by a recharge area at a water divide and a discharge area at the bottom of the basin. Regional aquifers are characterized by very low groundwater flow rates, anaerobic conditions, and very high dissolved mineral concentrations (Chapelle, 1993).

The three different flow systems tend to support different types and numbers of microorganisms. Microorganism concentrations of 10^6 to 10^7 cells/g have been reported in local flow systems (Lee et al., 1988), and these bacteria are typically aerobic (Chapelle, 1993). In intermediate flow systems, microbial counts are typically lower, and concentrations of 10^5 to 10^6 cells/g have been reported. Little data are available on the numbers of microorganisms in regional flow systems, probably because of their relative unimportance as drinking water sources and their distance from surface contamination sources.

The concentration of bacteria is an important parameter in biodegradation modeling because substrate utilization rates depend on the biomass concentration (see Section 4.5). In the saturated zone, most modelers assume that microorgan-

isms are present at a concentration of around 10^6 cells/g of aquifer material (Chen et al., 1992; Wood et al., 1994). However, the concentration of microorganisms varies tremendously between the soil zone and the saturated zone, so that a distribution of microorganism concentrations must be used to accurately model biodegradation in all portions of an aquifer. A realistic model would account for both the lateral and vertical initial distribution of biomass.

4.4.1.2. Pore scale Little data are available on the distribution of microorganisms at the pore scale. Studies have indicated that most bacteria tend to be attached to solid particles, and that a majority of the attached bacteria are associated with particles less than 20 μm in diameter (Harvey et al., 1984). The data by Harvey et al. (1984) also indicate that bacteria tend to be present as small colonies rather than as continuous films. The lack of continuous films is most likely due to the oligotrophic environment; there are not enough nutrients and growth substrates present to support continuous biofilms. However, when contaminants enter the subsurface, the environment is changed drastically. Continuous films could develop where there is a sufficient concentration of substrate, electron acceptor and nutrients, such as at injection wells. Whether microorganisms are attached as continuous and potentially thick biofilms or as microcolonies has important implications for biodegradation modeling. The methods by which the microorganism configuration is accounted for in various models are discussed in Section 4.11.

The location of attached microorganisms at the pore scale could also be important for reasons of transport (see Section 4.13) and biodegradation rates. If many bacteria are free-floating, then they may be more easily transported than attached bacteria. For attached bacteria, the location of attachment could have important effects on biodegradation rates. If most bacteria are attached at pore throats, then they would have greater accessibility to substrates and nutrients flowing through the aquifer than bacteria attached at the walls of pore cavities. In pore cavities, substrates and nutrients would have to diffuse from pore centers to the pore walls before they could be utilized by bacteria growing there. This phenomenon could be described with equations similar to those used to describe diffusion-controlled adsorption (Fetter, 1993). Theoretical analyses could indicate whether the physical location of microorganisms has an appreciable effect on subsurface biodegradation rates.

4.4.1.3. Location within phases and at interfaces Microscopic evidence indicates that microorganisms grow only in the water phase (Brock et al., 1984; Atlas, 1981). Therefore, biodegradation can occur only where water is present: in the water phase of the vadose zone and in the saturated zone. Although biodegradation can only occur in the water phase, this does not mean that attached bacteria cannot biodegrade contaminants. On the contrary, since most bacteria are attached to surfaces, biodegradation by attached bacteria may be significant. However, microorganisms' requirement for water does preclude their growth when attached to particles in direct contact with the air or NAPL.

When pure-phase NAPL that can be degraded by microorganisms is introduced in the subsurface, microorganisms will accumulate in the water phase at the

NAPL/water interface where substrate concentrations are highest (Atlas, 1981). Thus, the higher the available surface area, the faster biodegradation will proceed (Atlas, 1981). Microorganisms may increase the available surface area and increase NAPL dissolution by releasing emulsifying agents (Atlas, 1981).

Biodegradation at NAPL/water interfaces is typically limited by nutrient availability (Atlas, 1981). If the NAPL constituents are toxic, then microorganisms may not exist at the interface, but may accumulate at a distance at which the toxic constituent concentration is low enough that they can survive.

Biodegradation activity at NAPL/water interfaces may have at least three important implications for modeling. First, if the NAPL is toxic to microorganisms, modeling could overpredict NAPL biodegradation if biodegradation is assumed to occur everywhere within the water phase. Second, NAPL toxicity or nutrient limitations could cause sharp concentration gradients near NAPL phases, which could require very fine spatial grids in computer simulations, resulting in long computer run times. Third, if the NAPL is not toxic, bacteria may release emulsifying agents that could break the NAPL up into small droplets, creating a high NAPL/water interfacial area (Atlas, 1981). This could cause biodegradation rates to be much higher than would be predicted if the total surface area available to microorganisms is assumed to be the surface area of a single continuous interface, such as in an oil slick floating on a water surface.

It is not clear how these implications would actually affect predicted biodegradation rates. Further research in this area is needed.

4.4.2. Acclimation

When placed in a new environment, bacteria usually take time to adjust or acclimate to the new environmental conditions. Acclimation is characterized by a lag time during which microorganisms do not grow significantly. The length of the lag period depends on many factors, including the type of organism, the organism's growth rate, the magnitude of the changing conditions, and the nature of the environmental change (Bailey and Ollis, 1986). When the lag period is over, bacteria begin to grow and reproduce normally. Acclimation mechanisms are discussed briefly below. Modeling of the lag period is discussed in more detail in Section 4.7.5.

Microorganisms adjust to changing conditions by three mechanisms (Chapelle, 1993):

1. Induction of specific enzymes not present (or present at low levels) before exposure to the new conditions;
2. Selection of new metabolic capabilities produced by genetic changes; and,
3. Increase in the number of organisms able to metabolize newly available substrates.

All of these mechanisms are important in subsurface biodegradation, where environmental changes can be dramatic with the introduction of contamination to the subsurface environment. Aerobic organisms typically consume nearly all available oxygen very quickly, so that surviving organisms must adapt to the use of other electron acceptors as well as to the changing environmental conditions (Chapelle, 1993). Acclimation is affected by the kinds of organic compounds and

their relative concentrations, the time of exposure to the compounds, and the similarity of the compounds to those the microorganisms are accustomed to using as substrates (Chapelle, 1993). Some xenobiotics typically are metabolized without any lag time at all, while others are metabolized only after a significant lag time (Lee et al., 1988).

Acclimation can have important effects on biodegradation modeling. When a spill occurs and contamination is introduced to the subsurface, it will take time for the microorganisms present to begin biodegradation. As the contaminant plume moves in the saturated zone, the edge of the contaminant front may move past microorganisms before they have time to acclimate to the contaminants as substrates. Thus, a pulse of contamination may spread out from the spill source even though microorganisms are capable of using the contaminants as substrates (Wood et al., 1994). Models that do not take acclimation into account may not accurately predict the spatial distribution of the plume concentration. Dispersion may help to mitigate this effect. Additional research is needed to quantify the effects of acclimation on contaminant plume movement in biodegradation models.

Of the models reviewed in this report, only the model of Wood et al. (1994) accounted for acclimation. The method by which a lag period was accounted for by this model is discussed in Section 4.7.5.

4.4.3. Microbial community composition and capabilities

Studies indicate that the subsurface microbial community is metabolically active, nutritionally diverse, and usually oligotrophic because of the low substrate concentrations and refractory nature of substrates in the subsurface environment (Lee et al., 1988). As a result, subsurface microorganisms are capable of utilizing a variety of substrates, including xenobiotic compounds. Some strains of microorganisms are capable of degrading NAPL compounds alone, while other biodegradation reactions can only be completed by microorganisms with the aid of other microbial strains.

The interdependence of some strains of bacteria that carry out biodegradation reactions is important for biodegradation modeling, particularly when conditions are anaerobic. Under anaerobic conditions, microorganisms utilize alternate electron acceptors in an order of those yielding the most energy from redox reactions to those yielding the least. Thus, in groundwater systems, electron acceptors will usually be used in the following order: nitrate, iron(III), sulfate, CO_2, and conditions become increasingly reducing (Lee et al., 1988; Freeze and Cherry, 1979). As the contaminant plume travels, different electron acceptors and redox conditions may prevail downstream from the initial point, and each particular environment may tend to favor the transformations of different constituents of the NAPL plume (Bouwer and McCarty, 1984). This phenomenon, depicted graphically in Fig. 3, was shown to exist in studies of the Middendorf aquifer in South Carolina (Chapelle, 1993). In order to model these successive reactions successfully, the aquifer *Eh*, pH and electron acceptor concentrations must be known so that the appropriate biodegradation reactions can be modeled (Bouwer and McCarty, 1984).

Although no models reviewed in this report model *Eh*, pH and electron acceptor

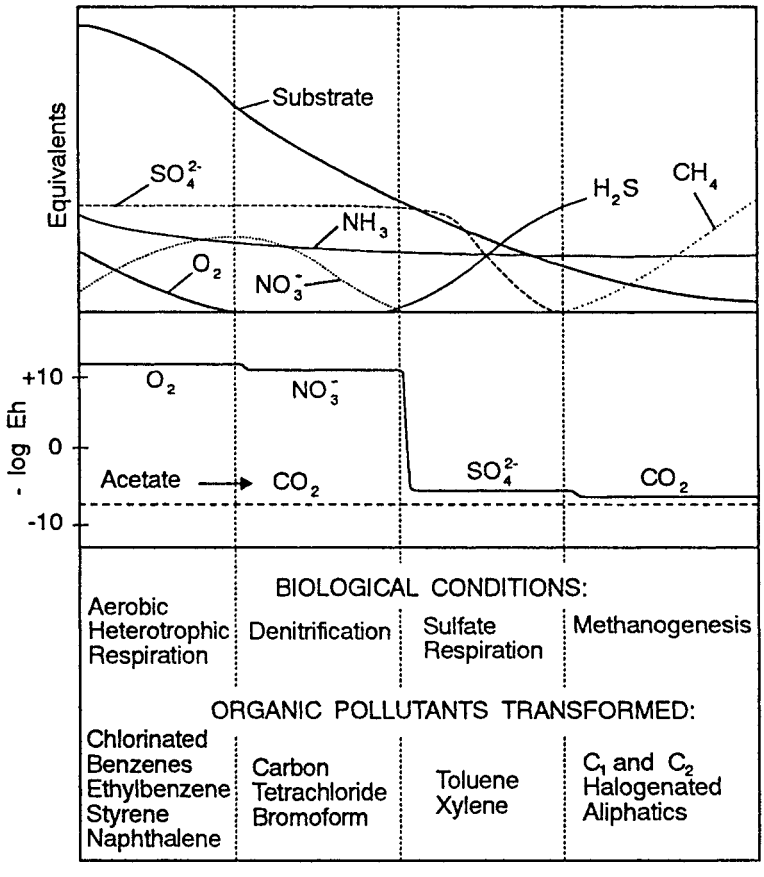


Fig. 3. Potential microbially mediated reactions in a aquifer (Bouwer and McCarty, 1984).

concentrations, several models account for multiple electron acceptors (Frind et al., 1990; Widdowson et al., 1988; Kindred and Celia, 1989; Kinzelbach and Schafer, 1991; Chen et al., 1992). The way in which the multiple electron acceptors are accounted for is discussed in the Section 4.7.9.

4.5. Microorganism growth periods

Since microorganisms in the subsurface experience varying concentrations of substrate and electron acceptor, their growth rate and stages may be constantly changing. Therefore, the growth cycles of subsurface microorganisms may show some similarity to microbial growth in batch cultures. Microorganisms in batch culture experience four distinct growth periods (Bailey and Ollis, 1986). These periods, shown graphically in Figure 4, are the lag period, exponential growth period, stationary period and death period.

In the lag period, microorganisms adapt to changing environmental conditions while growing little or none at all. The lag period is thought to be due to the microorganisms' synthesis of new enzymes and other necessary chemicals used in

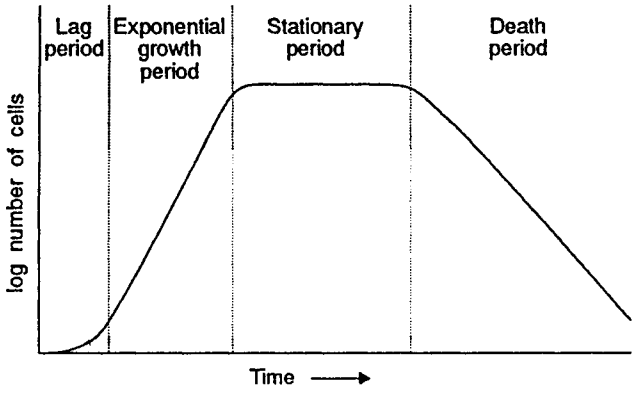


Fig. 4. Microorganism growth periods (Baily and Ollis, 1986).

the metabolic pathways necessary to survive in the new conditions. A lag in growth may also occur when microorganisms are transferred into an environment of different ionic strength. Multiple lag periods are sometimes observed when a culture is fed two substrates, one of which is preferentially utilized. A lag occurs when the organism switches from the exhausted preferred substrate to the second substrate. This phenomenon is called diauxic growth. The length of the lag period depends on many factors, including the type of organism, the organism's growth rate, the magnitude of the changing conditions, and the nature of the environmental change (Bailey and Ollis, 1986).

At the end of the lag period, the population of microorganisms is well adapted to its new environment. During this exponential period, microorganisms reproduce rapidly according to the expression (Bailey and Ollis, 1986)

$$\mu = \frac{1}{X}\frac{dX}{dt} = \mu_{max} \tag{11}$$

where X is the concentration of cells (M/L^3); μ is the specific growth rate of cells (T^{-1}); μ_{max} is the maximum specific growth rate (T^{-1}); t is the time (T).

Exponential (first-order) growth continues until some nutrient necessary for growth becomes limiting, at which time the population enters the stationary period, where the cell concentration reaches its maximum. In the stationary period, nutrient limitations prevent further increase of the microbial concentration. Some cells die and lyse, and other cells utilize the nutrients released by the lysed cell for growth. Eventually, due to severe nutrient depletion or toxic buildup, the population begins to decline and the death period begins (Bailey and Ollis, 1986). The death period is usually described as an exponential decay, where the number of cells that die at any time is a constant fraction of those living.

In the subsurface, microorganisms can go through each of these periods. In the saturated zone in front of a contaminant plume, for example, the indigenous microflora are probably in the stationary period or simply dormant since substrates are in scarce supply. When the contaminant plume encounters the microorganisms, the microorganisms must adapt to the new conditions and substrates so that there

is a lag before they begin growing. When they are adapted to the new conditions, the microorganisms begin growing exponentially until some nutrient limits their growth. The exponential period may be quite short or non-existent in most aquifers, where electron acceptors are likely to severely limit growth regardless of substrate concentrations. After the plume has passed, the microorganisms enter the stationary period, where there is no longer a supply of substrate for growth. After a time, the population begins to die off once nutrients are completely exhausted.

All of these growth periods are important in biodegradation modeling. The lag period is typically called acclimation and is discussed further in Section 4.7.5. The growth and death periods are central to biodegradation modeling and are discussed further in Section 4.7 in the context of microbial growth kinetics.

4.6. Models of microbial growth

A given microbial population consists of individual cells, each carrying out a complex array of chemical reactions necessary to survive. However, a description of all of the processes occurring in the microbial population is not practical, so models have been developed to describe how the average population behaves. Microorganism population growth can be described in several ways, depending on the assumptions made about the population as a whole. The descriptions of the different growth models given below are based on the treatment by Bailey and Ollis (1986).

Microbial growth can be described by unstructured or structured models. Unstructured models assume that the microbial population can be characterized by a single variable; for example, cell number or mass concentration. In structured models, cells are recognized to consist of multiple interacting components that can be described separately, e.g., DNA, ATP, or some key enzyme (Bailey and Ollis, 1986).

The collection of cells that make up a microbial population can also be viewed as either single entities, which they are, or as a single "average" cell. If the population is modeled as individual cells, the model is called segregated. If the population is viewed as a collection of cells with the same average characteristics, the model is called unsegregated. Unsegregated models can be applied when growth is balanced, i.e., when cell components are constant with time as in exponential growth. During the lag and stationary periods of batch growth, balanced growth generally does not occur, and different cells in the population may have very different characteristics, depending on their age, location, or other factors. As a result, unsegregated models may not be a good approximation to bacterial growth during these periods.

Unstructured and unsegregated models have the advantage of simplicity over structured models. In unstructured, unsegregated models, only one variable need be considered. This variable can be treated similar to a solute in a solution, and no consideration of different cell components is necessary. The unstructured, unsegregated assumption is common in the environmental field. In wastewater treatment, for example, the cells are typically represented by an average mass

concentration. All of the biodegradation models reviewed in this study are unstructured, unsegregated models. Therefore, in all of these models, biomass is described as a single component, although it may exist in more than one phase.

Structured models may be able to describe batch microbial growth more effectively than unstructured models, but at the expense of considerable added complexity. Three types of structured models are briefly discussed below.

In compartmental models, the microbial population is assumed to be unsegregated, but the biomass is compartmentalized into a small number of components. The components can be cellular components important to the cells' growth, such as the concentration of DNA or a particular protein of interest. The model is justified on the basis of system dynamics. All of the processes occurring within a cell have a characteristic relaxation time, or time to reach equilibrium after a perturbation. The relaxation time can be used to determine the rate at which cellular processes occur with respect to environmental changes. Components depending on processes that have very long relaxation times can be taken as constant. Components depending on processes that have very fast relaxation times can be assumed to be at quasi-steady state. However, components that depend on processes that occur at the same time scale as environmental changes are included in the model. Since relaxation times vary by many orders of magnitude, the number of compartments is typically only two or three in these models. Compartmental models have potential application in biodegradation modeling.

Metabolic models describe growth based on the metabolic processes cells undergo. These models typically require a fairly detailed knowledge of the important metabolic processes in order to describe experimental data accurately. The models are both structured and segregated, since different cellular components and the change of these components with time are both modeled. Metabolic models are most useful when a single metabolic pathway controls metabolic rates, or when the interaction of all metabolic rates is well understood. The complexity of metabolic models probably makes their application to subsurface biodegradation modeling impractical.

Cybernetic growth models describe the effects of cellular regulatory processes as the outcome of an optimization strategy (Bailey and Ollis, 1986). These models can be used to describe the growth dynamics of a population on multiple substrates. The advantage of these models is that kinetic parameters can be determined based on kinetic studies on single substrates, since the interaction of multiple substrates is accounted for in the optimization modeling. Cybernetic models are potentially useful in subsurface biodegradation modeling, but much more research is needed before they can be applied.

4.7. Substrate biodegradation kinetic expressions

Expressions for microorganism growth and substrate utilization, together with the transport equations described in Section 4.2, form the basis for biodegradation models. A number of kinetic expressions exist to describe decrease in substrate concentration. The particular kinetic expressions used depend on assumptions about the microbial population and growth, since in most cases substrate utilization

is assumed to result in a biomass increase. The form and complexity of these expressions depend on the type of growth model (unstructured/structured; segregated/unsegregated) and factors specifically included in the model such as inhibition. Three basic types of substrate utilization kinetics are typically used in the biodegradation models reviewed in this report: (1) instantaneous reaction, (2) Monod kinetics, and (3) first-order kinetics.

4.7.1. Instantaneous reaction

The assumption of an instantaneous reaction is equivalent to assuming that the reaction rate is infinitely fast so that kinetics can be ignored altogether. In this case, sufficient biomass is assumed to be present so that substrate and electron acceptor react stoichiometrically. If the electron acceptor is in excess, then all of the substrate in contact with the electron acceptor is assumed to react, and the electron acceptor concentration is reduced by the stoichiometric amount required to oxidize the substrate to CO_2. If substrate is in excess, then all of the electron acceptor is assumed to react and the substrate concentration is reduced by the stoichiometric amount that can be oxidized by the available electron acceptor. The reaction is assumed to occur in each gridblock where substrate and electron acceptor are both present. This treatment of biodegradation reactions is used by Borden and Bedient (1986) and was adopted by Corapcioglu and Baehr (1987) for the case where biodegradation is limited by oxygen transport into the contaminant plume.

The instantaneous reaction model has two important advantages over models in which biodegradation kinetics are explicitly considered. First, no estimate of kinetic parameters is needed. Since kinetic parameters are difficult to estimate accurately, especially for field modeling, this is a significant advantage. Second, biomass is assumed to be constant. As a result, the equations governing the transport and biodegradation of contaminants are much easier to solve because the equation for microbial growth is eliminated and there are no non-linear kinetic expressions.

The instantaneous reaction model may be applicable when biodegradation kinetics are fast relative to the transport of oxygen into the contaminant plume (Rifai and Bedient, 1990). In cases where groundwater velocities are fast or biodegradation reaction rates are slow, the assumption of an instantaneous reaction is not a good approximation of the physical situation. To help determine when the instantaneous reaction model is appropriate, Rifai and Bedient (1990) compare model results from two runs of the same model in which instantaneous reaction kinetics is used in one run and biodegradation kinetics in the other. For the example problem, Rifai and Bedient provide quantitative data on when the instantaneous reaction assumption approximates the more rigorous kinetic approach in terms of a Damköhler number, Da_1, and a dimensionless concentration product, π_2. The Damköhler number is the ratio of a chemical reaction rate to the rate of advective transport. Rifai and Bedient defined Da_1 as

$$Da_1 = \frac{kL}{v} \tag{12}$$

where k is the maximum specific rate of substrate utilization (T^{-1}); L is the length of the modeling domain (L); v is the average velocity (L/T).

The dimensionless concentration product was defined as

$$\pi_2 = \left(\frac{C_o}{K_c + C_o}\right)\left(\frac{O_o}{K_o + O_o}\right) \tag{13}$$

where C_o and O_o are the initial substrate and oxygen concentrations (M/L^3); K_c and K_o are the substrate and oxygen half-saturation constants (M/L^3).

For the particular situation that they examined, the instantaneous reaction model approached the kinetic model as Da_1 increased and as π_2 approached 1. The differences in the results of the two approaches were also a function of the half-saturation constants of the substrate and oxygen, and of the initial oxygen concentration. For $Da_1 > 2{,}500$, the instantaneous reaction model differed from the kinetic model by approximately 20%.

Although the instantaneous reaction model may be applicable in some situations, Rifai and Bedient (1990) make the important observation that its applicability varies with time and space in the modeling domain. Because biodegradation reaction rates are generally a function of both microorganism concentration and limiting nutrient concentrations (including substrate, electron acceptor, or other nutrients) and because these concentrations vary spatially, different biodegradation reaction rates will typically be observed at different points in the modeling domain and at different times. Therefore, the instantaneous reaction rate model may apply only to part of the domain only part of the time. If the instantaneous reaction rate model is used, constant checks on its applicability would have to be made to ensure that the assumption was valid where it was being used. The kinetic biodegradation model would have to be used at locations where the instantaneous model was not valid. The mixing of the two kinetics could add complexity to a biodegradation model. This is an important disadvantage of the instantaneous reaction model.

4.7.2. Monod kinetics

The Monod equation is the most popular kinetic expression applied to modeling groundwater biodegradation. This discussion is based on the treatment by Bailey and Ollis (1986).

The Monod equation expresses the microbial growth rate as a function of the nutrient that limits growth. The expression is of the same form as the Michaelis–Menton equation for enzyme kinetics but was derived empirically. The limiting nutrient can be a substrate, electron acceptor, or any other nutrient such as nitrogen or phosphorous that prevents the cells from growing at their maximum (exponential) rate. The nutrient limitation is expressed in the form of a Monod term multiplying the maximum growth rate. The Monod equation is

$$\mu = \mu_{max}\left(\frac{S}{K_S + S}\right) \tag{14}$$

where μ is the specific growth rate (T^{-1}); S is the substrate concentration (M/L^3);

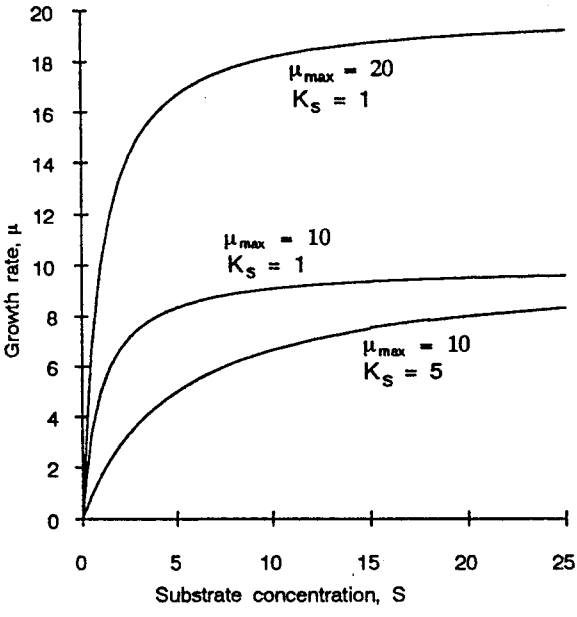


Fig. 5. Functional form of Monod kinetics and effects of K_s and μ_{max} on reaction rates.

μ_{max} is the maximum specific growth rate (T^{-1}); K_s is the half saturation constant (value of S at which μ is $\frac{1}{2}\mu_{max}$, M/L^3).

The term in parentheses is the Monod term. Note that equation (14) is simply the expression for exponential cell growth multiplied by a Monod or growth limiting term. The functional form of this expression for batch growth, and the effects of the Monod parameters K_s and μ_{max}, are shown in Fig. 5. The maximum specific growth rate (μ_{max}) and K_s must be determined experimentally for each substrate and microbial culture.

Studies have shown that the Monod expression overpredicts the cell concentrations in continuous flow reactors at low dilution rates (long hydraulic residence times) (Bailey and Ollis, 1986). This phenomenon can be explained considering endogenous decay. Endogenous decay consists of internal cellular reactions that consume cell substance. The endogenous decay term is also sometimes conceived of as a cell death rate or maintenance energy rate and represents cells in the death period of the microbial growth cycle. Endogenous decay is accounted for by adding a decay term to the Monod expression

$$\mu = \mu_{max}\left(\frac{S}{K_s + S}\right) - b \tag{15}$$

where b is the endogenous decay rate constant (T^{-1}).

Under oxygen or other electron acceptor limited conditions, the endogenous decay term can be multiplied by a Monod term for the limiting electron acceptor. This approach is taken by Molz et al. (1986), Widdowson et al. (1988), and Semprini and McCarty (1991).

Substrate utilization is determined by dividing the Monod expression by a yield coefficient, $Y_{x/s}$. The yield coefficient must also be determined experimentally. Substitution of the yield coefficient into the Monod expression for microbial growth results in the following expression for substrate utilization

$$r_s = \frac{dS}{dt} = -\frac{r_x}{Y_{x/s}} = -\frac{\mu_{max} X}{Y_{x/s}}\left(\frac{S}{K_s + S}\right) \tag{16}$$

where X is the biomass concentration (M/L^3); r_s is the rate of substrate utilization (M/L^3T); r_x is the rate of biomass growth (M/L^3T); S is the substrate concentration (M/L^3); $Y_{x/s}$ is the biomass yield coefficient (mass of cells formed/mass of substrate consumed).

The constant quotient $\mu_{max}/Y_{x/s}$ is often called k, the maximum specific substrate utilization rate, so that the Monod equation for substrate utilization becomes

$$r_s = -kX\left(\frac{S}{K_s + S}\right) \tag{17}$$

Two limiting conditions of the Monod equation should be noted. First, when the substrate concentration is sufficiently low that $K_s \gg S$, then the Monod equation becomes $dS/dt = -k'XS$ where $k' = k/K_s$. In this situation, the Monod equation predicts that the substrate utilization is linearly dependent on S (first-order with respect to S). When all nutrients are present in great excess so that $K_s \ll S$, the substrate utilization rate is independent of S and equal to $-kX$ (zero order with respect to S). It is important to note that the substrate utilization is first-order with respect to the biomass concentration, X, regardless of the substrate concentration.

Most of the models reviewed in this report use Monod kinetics to describe subsurface biodegradation. Monod kinetics may not be applicable to all biodegradation reactions, however, and use of the Monod expression should be justified based on some other information before it is used. In particular, Monod kinetics may not be applicable when substrate concentrations are very low (Bailey and Ollis, 1986).

4.7.3. First-order kinetics

Some substrate biodegradation rates follow reaction kinetics in which the biodegradation rate is first-order with respect to the substrate concentration

$$r_s = -kXS \tag{18}$$

Note that the biodegradation rate in this expression is also first-order with respect to biomass concentration so that the reaction is second-order overall. Wood et al. (1994) found that this type of first-order kinetic expression best described the disappearance of quinoline from a groundwater system, although they modified the first-order kinetics with a Monod term for oxygen limitation. In this case, first-order kinetics were justified by experiments.

Brusseau et al. (1992) used pseudo first-order kinetics in which the biodegradation rate is first-order with respect to substrate concentration only to describe the disappearance of an arbitrary substrate, and applied the equations to the

disappearance of 2,4,5-T in soil columns. They justified the use of pseudo first-order kinetics by assuming that microbial growth was negligible and that no nutrient, substrate or electron acceptor limitations existed. Under these assumptions, X can be treated as a constant in equation (17), and the growth rate is $r_s = -k'S$ where $k' = kX/K_s$. Brusseau et al. (1992) determined the parameters for their simulations independently of the data being simulated. Their simulations matched data obtained from the literature quite well.

As discussed above, Monod substrate utilization kinetics reduce to pseudo first-order kinetics in S for very low substrate concentrations if X is assumed to be constant. The advantage of using pseudo first-order kinetics is that the kinetic expressions are linear and can be solved more easily than the non-linear equations that Monod kinetics produces. When data indicate that pseudo first-order kinetics are applicable throughout the range of expected concentrations, pseudo first-order kinetics should be used. If pseudo first-order kinetics cannot be justified throughout the entire range of expected concentrations, then Monod kinetics or some other kinetic expression should be used. Use of first-order or pseudo first-order kinetics as an approximation to Monod kinetics when Monod kinetics are applicable would tend to over-predict substrate destruction.

4.7.4. Other growth kinetics

Many other forms of growth kinetics are provided in the literature. Three of the most common alternative expressions include (Bailey and Ollis, 1986)

Tessier

$$\mu = \mu_{max}(1 - e^{-s/K_s}) \tag{19}$$

Moser

$$\mu = \mu_{max}(1 + K_s S^{-\lambda})^{-1} \tag{20}$$

Contois

$$\mu = \mu_{max}\left(\frac{S}{BX + S}\right) \tag{21}$$

The Tessier equation is based on the assumption of a diffusion-controlled substrate supply (Luong, 1987). The Moser expression is similar to the Monod equation except that the substrate concentration is raised to the power λ. The Contois expression contains an apparent Michaelis constant that is proportional to biomass concentration (X). The maximum growth rate diminishes as X increases, eventually leading to $\mu \propto 1/X$ (Bailey and Ollis, 1986). Sarkar et al. (1994) used Contois kinetics to describe the anaerobic degradation of glucose by *B. licheniformis* JF-2 in a multi-phase microbial transport model.

4.7.5. Lag period

Most researchers ignore the lag period in biodegradation modeling either because the systems being modeled are acclimated to the contaminants in advance

(in column studies, for example) or because the phenomenon is not well understood (Borden and Bedient, 1986). However, as discussed in Section 4.4.2, the lag period can be important in modeling biodegradation. Wood et al. (1994) modeled the lag period with a metabolic potential function given by

$$\begin{aligned} \lambda &= 0 && t < \tau_L \\ \lambda &= \frac{\tau - \tau_L}{\tau_E - \tau_L} && \tau_L \leq t \leq \tau_E \\ \lambda &= 1 && t > \tau_E \end{aligned} \tag{22}$$

where λ is the metabolic potential function (dimensionless); τ is the time that microorganisms in a given volume have been in contact with the inducing substrates (T); τ_L is the lag time (length of time for significant growth to begin (T)); τ_E = length of time required to reach exponential growth (T).

The function λ multiplies the biomass growth and substrate utilization terms that depend on electron acceptors. λ increases from 0 to 1 over the acclimation period τ_L to τ_E. After the acclimation period is over, λ no longer limits biomass growth or substrate utilization.

Wood et al. (1994) determined the lag time parameters τ_L and τ_E in separate experiments. Inclusion of this expression for lag time in the simulations of quinoline degradation in soil columns indicated that a pulse of quinoline would travel through the column before the microorganisms became acclimated to the substrate and began degrading it. The pulse predicted by the model matched the experimental data well. The authors noted that dispersion had a significant effect on this pulse. Because dispersion causes spreading of the substrate, the trailing edge of the substrate pulse was in contact with the microorganisms longer than the front edge. Because of the longer contact time, microorganisms in contact with the trailing edge of the pulse acclimated to the substrate and began biodegrading it. This caused a sharpening of the trailing edge of the pulse.

Incorporation of lag into biodegradation models is likely to be important when groundwater contaminants move fast relative to their rate of disappearance from the bulk liquid phase. This might occur when contaminants are very slowly biodegrading or when groundwater velocities are very high. High dispersivities should tend to decrease the effects of acclimation by increasing contact time for the trailing edge of the leading edge of the plume and by decreasing the concentration of the leading edge of the plume, reducing the concentration of any pulse that may develop. The need for including acclimation is therefore dependent on both the flow conditions and factors affecting biodegradation rates.

4.7.6. Inhibition kinetics

Many xenobiotic compounds are toxic to microorganisms at higher concentrations. Other organic compounds degrade into toxic intermediates or final products. Kinetic expressions have been developed to incorporate this toxicity, and some of these kinetic expressions have been used by researchers to model subsurface biodegradation. The kinetic parameters for these expressions can be determined from laboratory experiments.

4.7.6.1. Substrate inhibition A simple method of accounting for substrate inhibition is to assume that no biodegradation occurs when the substrate concentration is above some critical level. This method was used by Corapcioglu et al. (1991) in modeling the cometabolism of tetrachloroethene (PCE) and TCE in laboratory columns under methanogenic conditions.

A popular kinetic expression for substrate utilization with substrate inhibition is (Grady, 1990)

$$r_s = -kX\left(\frac{S}{K_s + S + S^2/K_i}\right) \tag{23}$$

where K_s is the substrate half saturation constant (M/L^3); K_i is the inhibition coefficient (M^2/L^6).

This expression is similar to the expression for Haldane enzyme inhibition kinetics (Luong, 1987) and can be derived from enzyme kinetics considerations (Bailey and Ollis, 1986). As the substrate concentration increases, this equation predicts Monod behavior until the substrate concentration reaches a maximum. The rate then decreases because of the S^2 term in the denominator. When K_i is very large, the equation predicts Monod behavior for the entire range of substrate concentration. The expression has been used to successfully model substrate inhibition by other researchers (Bailey and Ollis, 1986).

The above equation predicts that some growth occurs for inhibitory substrates even at very high concentrations. However, it has been observed that growth ceases altogether at sufficiently high concentrations of inhibitory substrates (Grady, 1990). Grady (1990) identifies equations proposed by Luong (1987) and Han and Levenspiel (1988) that account for the cessation of growth at high inhibitory substrate concentrations

$$r_s = -kX\left(1 - \frac{S}{S^*}\right)^n \frac{S}{S + K_s(1 - S/S^*)^m} \tag{24}$$

where S^* is the critical substrate concentration above which growth stops (M/L^3); m is the exponent depicting the impact of the substrate on K_s (M/L^3); n is the exponent depicting the impact of the substrate of μ_{max}.

Luong's equation is the same, except that $m = 0$ (Grady, 1990). Other expressions for substrate inhibition are given by Luong (1987). The Luong (1987) model represented the inhibition of a batch culture growing on butanol better than three other models tested.

4.7.6.2. Product inhibition Product inhibition occurs when biodegradation end products inhibit biodegradation of the original substrate. An equation for modeling product inhibition substrate utilization is

$$r_s = -kX\left(\frac{S}{K_s + S}\right)\left(\frac{K_p}{K_p + P}\right) \tag{25}$$

where P is the product concentration and K_p is a product inhibition coefficient

(Bailey and Ollis, 1986). Sarkar et al. (1994) used a product inhibition term of this form to model anaerobic growth on glucose when lactic acid and 2,3-butanediol were expected to accumulate. This expression could also be used to account for substrate inhibition.

Luong (1987) identifies the following equation for product inhibition

$$r_s = -kX\left(\frac{S}{K_s + S}\right)e^{-p/K_i} \tag{26}$$

where the terms have the same meaning as in equation (25). Many of the expressions for substrate inhibition may also be used for product inhibition as discussed by Luong (1987).

Kindred and Celia (1989) present a method of accounting for any type of inhibition, including product inhibition, through an inhibition factor $I(i)$ defined as

$$I(i) = 1 + \frac{Q_i}{k_i} \tag{27}$$

where i is the subscript indicating the inhibiting substance; Q_i is the concentration of inhibiting substance (M/L^3); k_i is the inhibition constant (M/L^3).

If the product or substrate is inhibiting, then the biodegradation rate is divided by this expression. In this case, the expression is identical to the inhibition term in equation (25). The biodegradation rate of an inhibiting substrate could then be expressed as

$$r_s = -\frac{kX}{I(s)}\left(\frac{S}{K_s + S}\right) = -\frac{kX}{(1 + S/k_s)}\left(\frac{S}{K_s + S}\right) \tag{28}$$

where S is the substrate concentration. At low substrate concentrations, $I(s)$ ($=1 + S/k_s$) is approximately equal to 1, and no inhibition is observed. At high substrate concentrations, $I(s)$ becomes larger and larger, and the biodegradation rate approaches 0 as S grows large.

4.7.6.3. Competitive inhibition When two or more compounds serve as substrates for a microbial population, the compounds can be degraded simultaneously, sequentially, or simultaneously with competition (Chang et al., 1993). Competitive inhibition may be observed in this situation if the same enzymes are required for degradation of more than one compound. Competitive inhibition may also be observed in cometabolic processes where the cometabolites compete with the primary growth substrate for enzyme sites (Semprini and McCarty, 1992). Grady (1990) points out that a different fraction of biomass could be responsible for degradation of the different compounds so that experiments may be necessary to accurately predict substrate utilization.

The most popular kinetic expression for competitive inhibition in the groundwater modeling literature is of the general form (Bailey and Ollis, 1986)

$$r_{s_1} = \frac{ds_1}{dt} = -\frac{k_1 X S_1}{K_{s_1} + S_1 + K_{s_1} S_2 / K_{s_2}} \tag{29}$$

$$r_{s_2} = \frac{ds_2}{dt} = -\frac{k_2 X S_2}{K_{s_2} + S_2 + K_{s_2} S_1 / K_{s_1}} \tag{30}$$

where r_{s_1}, r_{s_2} are the utilization rates of substrates 1 and 2 (M/L^3T); k_1, k_2 are the maximum specific substrate utilization rates of substrates 1 and 2 (T^{-1}); S_1, S_2 are the concentrations of substrates 1 and 2 (M/L^3); K_1, K_2 are the half-saturation constants of substrates 1 and 2 (M/L^3).

An alternative way of writing equation (29) is (Alvarez-Cohen and McCarty, 1991)

$$r_{s_1} = \frac{ds_i}{dt} = -\frac{k_i X S_i}{K_{s_i}(1 + S_j / K_{s_j}) + S_i} \tag{31}$$

This expression has been used by a number of researchers to describe competitive inhibition in cometabolism of multiple substrates (Chang et al., 1993; Alvarez-Cohen and McCarty, 1991; Semprini and McCarty, 1992); and by Kindred and Celia (1989) to model competitive inhibition for aerobic biodegradation of multiple substrates. An expression of this type was used by Chang et al. (1993) to accurately describe competitive inhibition and cometabolism of benzene, toluene, and p-xylene biodegradation by two *pseudomonas* isolates in batch laboratory cultures. Alvarez-Cohen and McCarty (1991) found that this expression accurately predicted TCE and chloroform (CF) biodegradation by methanogenic resting cells in batch cultures when the expression was coupled to a more complex cometabolism model.

A modified form of the expression given above was used by Semprini and McCarty (1992) to model transport and cometabolic biodegradation of VC, t-DCE, c-DCE and TCE at the Moffett Naval Air Station field site. The expression was modified by multiplying by a Monod term to account for oxygen limitations as the electron acceptor. The inhibiting compound for the model was methane, as the concentrations of the chlorinated compounds were negligible in comparison to the methane concentration. The model was able to accurately predict the breakthrough curves of the substrates only when competitive inhibition was included, which demonstrates the importance of competitive inhibition in some systems.

Malone et al. (1993) modeled the transport and biodegradation of benzene, toluene and xylene in a gasoline mixture with a competitive inhibition expression similar to the one above. The substrate utilization expression in their model was

$$r_{s_i} = -\left[\frac{k_i X S}{\left(K_i + p_{\text{int}} S_{\text{int}}^a + \sum_{j=1}^{M} p_{ij} S_i^a\right)}\right]\left(\frac{O}{K_o + O}\right) \tag{32}$$

where S_i is the concentration of substrate i; k_i is the maximum specific substrate

utilization rate of component i (T^{-1}); p_{ij} is the Yoon's inhibition constant ($p_{ii} = 1$); K_i, K_{int} are the half-saturation constant for compounds i and intermediate (M/L^3); O is the oxygen concentration (M/L^3); K_o is the oxygen half-saturation coefficient (M/L^3).

In this model, the substrates are first converted to intermediate compounds (S^a_{int}). The intermediates are then biodegraded to CO_2. Malone et al. (1993) were able to accurately simulate the laboratory column biodegradation of a benzene, toluene and xylene mixture using the full model.

4.7.7. Cometabolism

The kinetics of cometabolism have been addressed by a number of researchers (Anderson and McCarty, 1994; Criddle, 1993; Chang et al., 1993; Corapcioglu et al., 1991; Alvarez-Cohen and McCarty, 1991; Bae et al., 1990; Bouwer and McCarty, 1984; Semprini and McCarty, 1992; Kindred and Celia, 1989). The simplest method to account for cometabolism is to model the disappearance of the cometabolite as a first-order process with respect to the cometabolite. Such a method can be viewed as a simplification of the Monod equation for low substrate concentrations. The disappearance of the cometabolite is modeled by the expression (Bouwer and McCarty, 1984)

$$\frac{dS}{dt} = -\frac{kX}{K_s} S \tag{33}$$

where S is the concentration of secondary substrate undergoing cometabolism (M/L^3); X is the biomass concentration (M/L^3); k is the specific secondary substrate utilization rate (T^{-1}); K_s is the half-saturation constant of secondary substrate (M/L^3).

Bouwer and McCarty (1984) used this expression to model the steady-state cometabolism of chlorobenzene and 1,4-dichlorobenzene in laboratory columns under methanogenic conditions where the biomass was assumed to exist as a biofilm. The model correctly predicted the disappearance of these compounds and correlated the disappearance of acetate with the disappearance of the chlorinated compounds. Bouwer and McCarty (1984) concluded that a first-order expression was adequate when the cometabolite concentration is very low. Corapcioglu et al. (1991) also used first-order kinetics to model the successive cometabolic conversion of PCE to TCE, DCE and finally VC by a methanogenic culture in laboratory columns. Corapcioglu et al. (1991) assumed that first-order kinetics were adequate because the influent PCE and TCE concentrations were very low. The data of Vogel and McCarty (1985) were used to test the model. The model parameters were determined by fitting the experimental data to a linear plot. The model did an adequate job of matching the experimental data from Vogel and McCarty's (1985) experiments.

Other researchers have used an unmodified Monod expression to model cometabolism. Bae et al. (1990) used a Monod expression to model the steady-state utilization of several halogenated compounds in laboratory columns by denitrifying biofilms. Bae et al. (1990) conducted the experiments at three different flow rates.

The kinetic parameters were determined from one run at one flow rate, and these same parameters were used to predict cometabolic removal of the chlorinated compounds at the other two flow rates. The model slightly overestimated the chlorinated organics substrate profiles but successfully predicted the decrease in substrate concentration to a steady-state concentration. A general Monod expression modified by the incorporation of competitive inhibition was used by Anderson and McCarty (1994) to model the cometabolic degradation of TCE by methanogenic biofilms. No verification studies were performed, but the simulation results were consistent with published data.

Semprini and McCarty (1992) used a modified form of the Monod expression to model methanotrophic cometabolism of TCE, DCE and VC in groundwater at the Moffet Naval Air Station field site. In this study, methane and oxygen were pulsed into the aquifer to prevent excessive biofilm growth at the injection well and to ensure that the biomass in the entire aquifer was stimulated. Semprini and McCarty (1992) included a deactivation process in their model because studies have shown that cometabolic transformations of these compounds stop when methane injection stops, and that MMO enzyme activity is deactivated when methane is absent. Biodegradation would be overestimated without accounting for deactivation because the total amount of biomass is not capable of cometabolizing the substrates when methane is not present. The pulsing creates such zones where methane is not present. The kinetic expression used by Semprini and McCarty (1992) in this model is

$$\frac{dC_2}{dt} = -F_a X k_2 \left(\frac{C_2}{K_{S2} + C_2 + C_D/K_i}\right)\left(\frac{C_A}{K_{SA} + C_A}\right) \tag{34}$$

where C_2 is the concentration of substrate undergoing cometabolism (M/L^3); C_D is the methane concentration (M/L^3); C_A is the concentration of electron acceptor (M/L^3); K_{SA} is the half-saturation constant of electron acceptor (M/L^3); K_{SD} is the half-saturation constant of methane (M/L^3); K_{S2} is the half-saturation constant for substrate undergoing cometabolism (M/L^3); K_i is the an inhibition constant = K_{SD}/K_{S2}; F_a is the fraction of the total microbial population active towards the cometabolic transformation.

The above expression includes inhibition in the C_D/K_i term and the limitations of the electron acceptor in a Monod term. This type of inhibition expression is identical to the type in equation (31). The deactivation process is embodied in F_a. When biomass is growing (because methane is present at sufficient amounts to promote growth), $F_a = 1$, and all of the biomass is capable of cometabolizing the substrates. When the biomass is decaying ($dS/dt < 0$), F_a decreases with time according to

$$\frac{dF_a}{dt} = -b_d F_a \tag{35}$$

where b_d is the rate constant for a first-order deactivation process. Semprini and McCarty were able to accurately model biodegradation of TCE, DCE and VC using this kinetic expression.

A thorough discussion of even more advanced methods of accounting for deactivation is provided by Criddle (1993). These methods incorporate a transformation capacity that serves to limit the capacity of biomass to cometabolize substrates. These more advanced methods have not generally been incorporated into biodegradation models, although they have been used successfully to predict batch biodegradation reactions (Chang et al., 1993).

4.7.8. Multiple limiting substrates and/or nutrients

It is possible and perhaps even likely that microorganisms in the subsurface are growth limited by more than a single substrate, nutrient, or electron acceptor. In this case, substrate utilization rate limitations can be accounted for by adding additional Monod terms to the expression for substrate utilization (Bailey and Ollis, 1986)

$$r_s = -kX\left(\frac{S_1}{K_{s_1} + S_1}\right)\left(\frac{S_2}{K_{s_2} + S_2}\right)\cdots\left(\frac{S_n}{K_{s_n} + S_n}\right) \tag{36}$$

where S_1, S_2, ... S_n are the concentrations of limiting substrates, electron acceptors or other nutrients. This expression is the most common method of accounting for multiple nutrient limitations in the groundwater modeling literature, and nearly all of the models reviewed in this report rely on it.

An alternate method of accounting for multiple nutrient limitations is to assume that the most limiting nutrient controls the growth rate so that the rate of substrate utilization is (Widdowson et al., 1988)

$$r_s = -kX\left[\min\left\{\left(\frac{S_1}{K_{s_1} + S_1}\right); \left(\frac{S_2}{K_{s_2} + S_2}\right); \cdots\right\}\right] \tag{37}$$

Use of the latter expression requires that the identity of the limiting nutrient in the single Monod term incorporating the nutrient limitation be changed as the limiting nutrient changes, and could be different in different areas of the modeling domain. This approach was used by Kindred and Celia (1989) to model biodegradation of arbitrary substrates. The advantage of this method is that numerical computations may be easier because the transport equations are less strongly coupled. However, a method of determining which nutrient is limiting in each model grid must be added and the switching could add considerable complexity to the model.

Other kinetic expressions exist to account for multiple substrate utilization (Roels, 1983). There is no consensus on which kinetic expression for modeling multiple limiting substrates is most accurate (Widdowson el al., 1988), and more research is needed in this area.

4.7.9. Multiple electron acceptors

As discussed in Section 4.4.3, some microorganisms are capable of using more than one electron acceptor to oxidize groundwater contaminants. Often, many different strains of microorganisms are present, each with its own particular ability

to use one or more electron acceptors. Therefore, as suggested by Bouwer and McCarty (1984), the most sophisticated models should account not only for growth limitations due to one particular electron acceptor, but also for the presence and changes of multiple electron acceptors.

The substrate utilization rate dependence on electron acceptor concentration is usually accounted for by multiplying the substrate utilization rate expression by a Monod term for the electron acceptor concentration as discussed in equation (36). This is the approach taken by all of the biodegradation models reviewed in this report.

The loss of the electron acceptor is commonly accounted for through the use of a yield coefficient defined as E = (*mass of electron acceptor consumed/mass of substrate consumed*). The yield coefficient can be determined by considering the stoichiometric requirement for conversion of the substrate being modeled to its end products by the electron acceptor in question. Some electron acceptors are used only for catabolism (e.g., SO_4^{2-}) while other electron acceptors are also used in building biomass (e.g., O_2). Therefore, the energy and growth reactions must both be taken into account in calculating E. The rate of electron acceptor use is then calculated as (Chen et al., 1992)

$$r_i = E_j^i r_{sj}^i \tag{38}$$

where r_i is the utilization rate of electron acceptor i (M/L^3T); E_j^i is the use coefficient of electron acceptor i under j-based respiration; r_{sj}^i is the substrate utilization rate under j-based respiration (M/L^3T).

This approach is taken by, for example, Borden and Bedient (1986), Kindred and Celia (1989), and Chen et al. (1992). Widdowson et al. (1988) also include the loss of oxygen from endogenous decay using the expression

$$r_o = \gamma Y_o r_{so} + \alpha_o k_o \left[\frac{o}{K_o' + o}\right] \tag{39}$$

where r_o is the specific oxygen utilization rate (M/L^3T); γ is the oxygen use coefficient for synthesis of biomass; Y_o is the cell yield coefficient under oxygen-based respiration; r_{so} is the substrate utilization rate under oxygen-based respiration (M/L^3T); α_o is the oxygen use coefficient for endogenous metabolism; k_o is the endogenous decay rate constant for aerobic decomposition (T^{-1}); o is the microorganism colony/stagnant liquid layer interfacial oxygen concentration (M/L^3); K_o' is the oxygen half-saturation coefficient for endogenous decay (M/L^3).

When multiple electron acceptors may be used by the same population of microorganisms, one electron acceptor usually inhibits respiration using the other available electron acceptor. This type of inhibition is called non-competitive inhibition. For example, some facultative microorganisms are capable of utilizing either oxygen under aerobic conditions or nitrate under anaerobic conditions. The presence of a significant oxygen concentration inhibits denitrification (use of nitrate as an electron acceptor). When the microorganisms exhaust the available oxygen, they switch to nitrate. The inhibition of nitrate respiration can be modeled with

an inhibition function such as that in equation (27) as follows (Widdowson et al., 1988)

$$r_n = \eta Y_n r_{sn} + \alpha_n k_n \left[\frac{n}{K'_n + n}\right] I(o) \tag{40}$$

where r_n is the specific nitrate utilization rate (M/L^3T); Y_n is the cell yield coefficient under nitrate-based respiration; r_{sn} is the substrate utilization rate under nitrate-based respiration (M/L^3T); η is the nitrate use coefficient for biomass synthesis; α_n is the oxygen use coefficient for endogenous metabolism; k_n is the endogenous decay rate constant for aerobic decomposition (T^{-1}); n is the microorganism colony/stagnant liquid layer interfacial oxygen concentration; K'_n is the oxygen half-saturation coefficient for endogenous decay (M/L^3); $I(o)$ is the inhibition function ($=1 + O/k_o$; k_o is the oxygen inhibition constant).

This approach can be extended to multiple electron acceptors by specifying an inhibition function for each type of respiration based on the concentration of any other electron acceptors that inhibit that type of respiration. This approach is used by Chen et al. (1992) and Kindred and Celia (1989). The inhibition function approach can be used to model the biodegradation of many different compounds, each of which degrade only under certain conditions. The inhibition functions "switch on" the ability of the biomass in any local model grid section to degrade the particular compound, based on the concentration of other compounds that inhibit its respiration.

4.7.10. Incorporation of kinetic expressions into transport equations

Regardless of the form of the kinetic expressions, they are incorporated into the mass balance equations in a sink term. If no mass transfer resistances are modeled, then the kinetic expressions can be directly substituted into the mass balance equations. For Monod kinetics, the biomass mass balance equation (in one dimension for saturated conditions and ignoring adsorption) is written (Baveye and Valocchi, 1989)

$$\frac{\partial X}{\partial t} = \mu_{max} X \left(\frac{S}{K_s + S}\right) - bX \tag{41}$$

Examination of this mass balance equation for biomass reveals an important point. The biomass will continue to grow until the substrate concentration drops below some threshold concentration for which the decay of biomass due to endogenous decay equals growth due to substrate utilization (Rittmann and McCarty, 1980). In some cases, the amount of biomass predicted by this equation could exceed the porosity because there is no upper bound on the concentration of biomass. Furthermore, since biomass is expressed as a concentration (dimensions = M/L^3) and not as a volume fraction multiplied by a density, it may not be obvious from the model output whether or not realistic biomass concentrations are being predicted. Since substrate utilization is proportional to biomass concentration, unrealistic biomass concentrations also result in unrealistic substrate utilization rates. In column studies, for example, a model might predict that all of the

substrate was utilized at the column inlet if the simulation were run long enough for the biomass to get unrealistically high. Methods of establishing limits on biomass growth are discussed in Section 4.12.

4.8. Multiple microorganism populations

Often a single microbial population may not be able to use more than one electron acceptor, but several electron acceptors are available for respiration. In this case, since substrate utilization is a function of both biomass and substrate concentration, multiple microorganism populations must be accounted for to accurately model biodegradation. Multiple populations are handled by writing a separate mass balance equation for each microbial population. The different populations can only grow under the particular type of respiration of which they are capable. Their growth is controlled in the model by using inhibition functions similar to those used to control electron acceptor utilization. This method of modeling multiple microbial populations was used by Chen et al. (1992) and Kindred and Celia (1989). It is usually assumed that growth of each microbial population occurs independently of the others.

4.9. Incomplete destruction/multiple reactions

In most biodegradation models, it is implicitly assumed that the substrate is completely mineralized in a single reaction, even though the actual process consists of a complex sequence of multiple reactions. Electron acceptor utilization and nutrient requirements are then calculated based on this assumption. In some cases, however, the initial substrate may be only partially degraded, either because further degradation requires different electron acceptors or because the product of initial biodegradation is resistant to further microbial attack. If complete mineralization is assumed in model development while only partial degradation physically occurs, then the model will underestimate the degree of disappearance of the primary substrate and overestimate electron acceptor and nutrient requirements. For example, if oxygen is limiting in an aerobic aquifer, then most of the oxygen may be used in the initial stages of biodegradation but may be depleted before the intermediates formed are biodegraded (Malone et al., 1993). In other cases, a sequence of reactions is required to model the conversion of an initial substrate to its intermediate products, some of which may be of particular interest due to their persistence or toxicity. An example would be the sequential transformation of PCE to TCE, DCE and finally VC. Sequential reactions may also be required if the initial substrate produces intermediates that biodegrade further under different types of kinetics, or if the intermediate compounds differ in adsorbability from the initial substrate.

Partial biodegradation is accounted for by adjusting the electron acceptor and other nutrient utilization rates to account for only partial degradation of the primary substrate. Experiments can be performed to measure the rate of disappearance of the primary substrate with time to determine the kinetic parameters. Utilization of electron acceptors and other nutrients can be calculated from the

reaction stoichiometry. Multiple reactions, whether they result in one or more intermediates, are handled in the same general way. A mass balance equation is written for the initial substrate and each intermediate of interest. The mass balance equation for the initial substrate includes only a sink term, while the mass balance equations for the intermediates include a sink term as well as a generation term from the generating reactions. These reaction rates can be multiplied by an inhibition function to control the conditions under which they occur. In this way, multiple reactions can be modeled even if they require different electron acceptors.

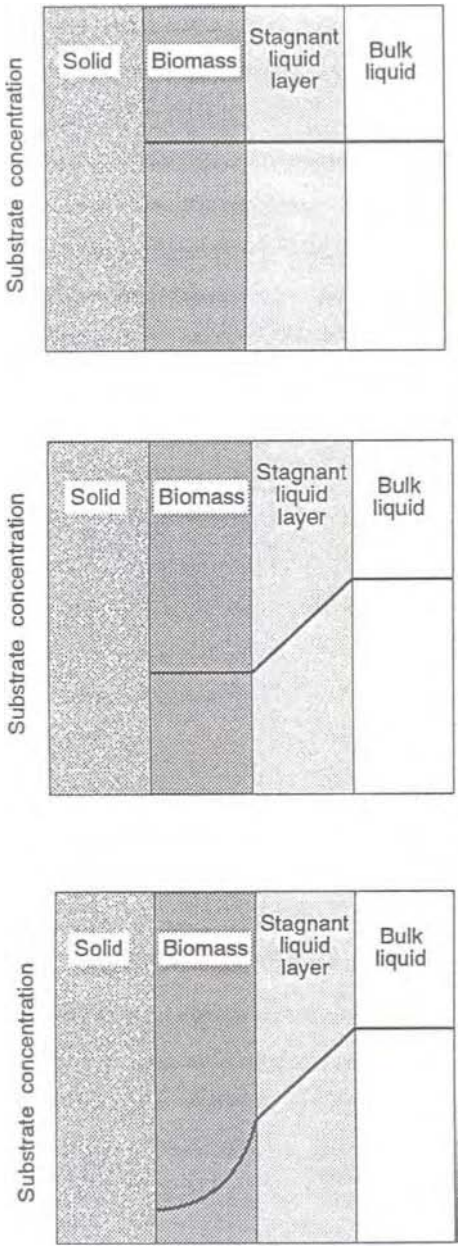
Malone el al. (1993) modeled the biodegradation of benzene, toluene and xylene under the assumption that biodegradation occurred in two steps, with the formation of a general intermediate. The system was described by writing one mass balance equation for the partial degradation of the initial substrate and a second mass balance equation for the degradation of the intermediate to carbon dioxide. The model accurately predicted the disappearance of benzene, toluene and xylene from laboratory columns in the high concentration range and captured the general trend of disappearance in the low concentration range.

Wood et al. (1994) used a two-step reaction model to describe the aerobic biodegradation of quinoline in a layered porous media. Laboratory studies indicated that the biodegradation of quinoline to 2-hydroxy-quinoline (2HQ) was first-order, while the biodegradation of 2HQ to CO_2 was assumed to follow Monod kinetics. Model parameters were determined independently of the simulation runs in other laboratory studies. The model successfully predicted breakthrough curves of quinoline, 2HQ and oxygen.

Corapcioglu et al. (1991) modeled the sequential transformation of PCE to TCE, DCE and VC in methanogenic columns using first-order kinetics for all of the reactions. They justified first-order kinetics based on the low substrate concentrations and assumed constant biomass. The model results were fit to the data of Vogel and McCarty (1985) from a separate study and successfully predicted column profiles of these compounds.

4.10. Diffusional resistances to mass transfer

Under some conditions, diffusion resistances to mass transfer can be important in modeling biodegradation. In order to become available to microorganisms, substrates, electron acceptors and other nutrients may first have to diffuse across stagnant liquid layers at the bulk liquid/biomass interface or diffuse deep into the biomass. These diffusion resistances can reduce the chemical concentrations experienced by microorganisms to below the bulk fluid concentration, affecting the rate of biodegradation reactions and biomass growth. In general, biodegradation models have been developed that include either: (1) no diffusional resistances, (2) diffusional resistance across a stagnant liquid layer adjacent to the biomass, or (3) diffusional resistance in both a stagnant liquid layer and within the biomass itself. Concentration profiles that result from each of these three assumptions are shown in Fig. 6. The effect of these different assumptions on the biodegradation model mass balance equations are discussed in the following sections.



a) No diffusion resistance.

b) Stagnant liquid layer diffusion resistance only.

c) Intra-biomass and stagnant liquid layer diffusion resistances.

Fig. 6. Substrate concentration profiles for different diffusion resistance assumptions.

4.10.1. No diffusion resistances

If no diffusion resistances exist, then the concentration of substrates, electron acceptors and nutrients within the biomass is the same as the concentration of these substances in the bulk fluid (Fig. 6a). In this case, the loss of substrate from

the bulk liquid is equal to its rate of biodegradation. The biodegradation kinetic expression can then be substituted directly into the bulk liquid substrate mass balance equation (Baveye and Valocchi, 1989). Assuming a one-dimensional, single-phase, saturated porous media with one limiting nutrient (the substrate) for illustrative purposes, the transport and biodegradation of the substrate and microbial growth can be represented by the following system of equations

$$\frac{\partial S_m}{\partial t} = \frac{\partial}{\partial x}\left(\frac{D\partial S_m}{\partial x} - vS_m\right) - \frac{\mu_{max}X}{Y_{x/s}}\left(\frac{S_m}{K_s + S_m}\right) \tag{42}$$

$$\frac{\partial X}{\partial t} = \mu_{max}X\left(\frac{S_j}{K_{s_i} + S_j}\right) - bX \tag{43}$$

where S_m is the substrate concentration in the bulk (mobile) fluid (M/L^3); D is the dispersion coefficient (L^2/T); v is the average linear groundwater velocity (L/T); X is the biomass concentration (M/L^3); b is the endogenous decay coefficient (T^{-1}).

Substrate biodegradation is therefore described with two equations in two unknowns (S_m and X). This approach is taken by Borden and Bedient (1986), Corapcioglu and Haridas (1984), and Kindred and Celia (1989). In effect, the pore volume in each modeling cell is assumed to be equivalent to a completely mixed reactor containing a homogeneous mixture of substrate, electron acceptor, nutrients and biomass.

4.10.2. Diffusion resistance from a stagnant liquid layer

In the second approach, chemicals must diffuse from the bulk liquid to the biomass across a stagnant liquid layer that offers resistance to mass transfer. This approach is commonly used in the chemical engineering field and is generally referred to as the "stagnant film model" of mass transfer resistance (Bailey and Ollis, 1986). With this assumption, the system of equations describing substrate biodegradation and biomass growth becomes (Baveye and Valocchi, 1989)

$$\frac{\partial S_m}{\partial t} = \frac{\partial}{\partial x}\left(\frac{D\partial S_m}{\partial x} - vS_m\right) - C(S_m - S_{im}) \tag{44}$$

$$\frac{\partial S_{im}}{\partial t} = C(S_m - S_{im}) - \frac{\mu_{max}X}{Y_{x/s}}\left(\frac{S_{im}}{K_s + S_{im}}\right) \tag{45}$$

$$\frac{\partial X}{\partial t} = \mu_{max}X\left(\frac{S_j}{K_{s_i} + S_j}\right) - bX \tag{46}$$

where C is the a mass transfer rate coefficient expression ($1/T$); S_{im} is the substrate concentration at the stagnant liquid layer/biomass interface (M/L^3).

In these equations, diffusion within the biomass is neglected so that all of the biomass experiences the same local substrate concentration S_{im}. Unless there are no biological reactions occurring, S_{im} will be less than S_m. As a result, the substrate

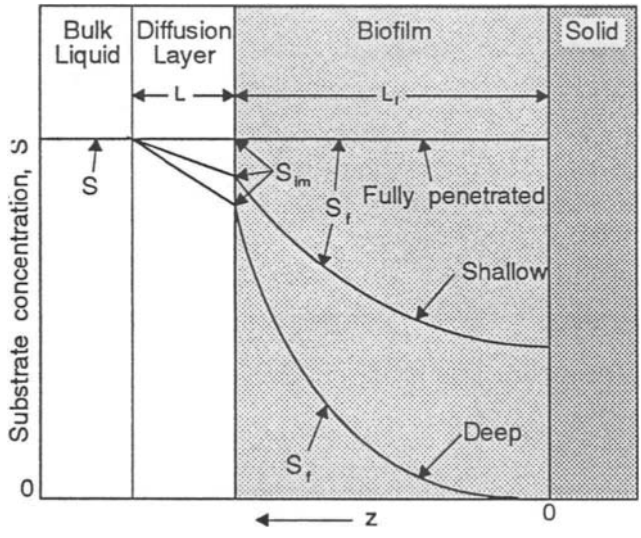


Fig. 7. Biofilm substrate concentration for different assumptions (Rittmann and McCarty, 1980).

concentration in the biomass will then be less than the bulk liquid substrate concentration (Fig. 6b). The last term in equation (44) is the substrate flux through the stagnant liquid layer. If no diffusional resistances are accounted for, then $S_{im} = S_m$, and the system reduces to the two equations shown in Section 4.10.1.

The magnitude of the mass transfer resistance depends on the mass transfer coefficient expression C. The mass transfer coefficient expression C is a function of the biomass/bulk fluid interfacial area, the substrate diffusion coefficient, and the boundary layer thickness. The value of C can be constant or variable, depending on the conceptualization of the biomass configuration (see Section 4.11).

4.10.3. Diffusion resistances from the biomass and a stagnant liquid layer

If the biomass becomes sufficiently thick, there may be diffusion resistances within the biomass itself as well as in a stagnant liquid layer. In this case, the outer layers of the biomass will experience higher substrate concentrations than the inner layers because substrate is degraded before it can diffuse deep into the biomass. The substrate profile that develops is shown in Fig. 6c.

Consideration of biomass diffusion resistances results in a system of equations much more complicated than those that consider only a stagnant liquid layer diffusion resistance. These equations are described below in the context of the biomass as a continuous film.

Rittmann and McCarty (1980) presented a model of steady-state biofilm kinetics, which defined many important biofilm concepts. Figure 7 shows the concentration profiles that result under different assumptions about biofilm mass transfer. In a "fully penetrated biofilm," the concentration of a constituent within the biofilm is the same as the concentration at the interface between the biofilm and the stagnant liquid layer. This case corresponds to the case where all mass transfer

resistance is contained in the stagnant liquid layer. If no stagnant liquid layer is assumed to exist, then the concentration within the biofilm is equal to the bulk liquid concentration. This corresponds to the assumption of no mass transfer resistance.

If the concentration of the rate limiting chemical reaches 0 at or before the biofilm/solid surface interface is reached, the biofilm is termed "deep". The substrate concentration profile is non-linear because the substrate is being biodegraded in the biofilm, resulting in a continuously changing concentration gradient with distance into the biofilm. In the case of a deep biofilm, the steady-state substrate flux into the biofilm is at its maximum, and the steady-state substrate flux into the biofilm can be calculated (Rittmann and McCarty, 1980).

Biofilms of intermediate thickness between deep and fully penetrated are termed "shallow." To calculate the substrate flux into a shallow biofilm, a mass balance is performed on a differential volume element within the biofilm. The mass balance results in a second order, non-linear differential equation for the substrate concentration within the biofilm (Rittmann and McCarty, 1980)

$$\frac{\partial S_f}{\partial t} = D_f \frac{d^2 S_f}{dz^2} - kX_f\left(\frac{S_f}{K_s + S_f}\right) \qquad 0 \leqslant z \leqslant L_f \tag{47}$$

where D_f is the diffusion coefficient of substrate within the biofilm (L^2/T); S_f is the substrate concentration within the biofilm (M/L^3); X_f is the biofilm density (M/L^3); L_f is the biofilm thickness (L); $z = 0$ at the biofilm/solid surface interface.

The biofilm substrate profile is usually assumed to be at steady-state because the concentration profile within the biofilm changes rapidly with respect to the biofilm thickness (Rittmann and McCarty, 1981). Therefore, the $\partial S_f/\partial t$ term is usually taken to equal 0. The boundary conditions used to solve this equation are (Sáez and Rittmann, 1988)

$$S_f = S_{im} \qquad \text{at } z = L_f; \quad t \geqslant 0 \tag{48}$$

$$\frac{\partial S_f}{\partial z} = 0 \qquad \text{at } z = 0; \quad t \geqslant 0 \tag{49}$$

The substrate flux through the stagnant liquid layer is assumed to be equal to the substrate flux into the biofilm. This is expressed mathematically as

$$\mathbf{J}_{im} = \mathbf{J}_f \tag{50}$$

The stagnant liquid film substrate flux is given by

$$\mathbf{J}_{im} = k_m(S_m - S_{im}) \tag{51}$$

where k_m is a mass transfer coefficient (L/T). The flux into the biofilm is given by

$$\mathbf{J}_f = D_f \frac{\partial S_f}{\partial z} \qquad \text{at } z = L_f \tag{52}$$

where $\mathbf{J}_f$ is the substrate flux into the biofilm (M/L^2T). The system of equations is augmented by an additional equation for the change in biofilm thickness

$$\frac{dL_f}{dt} = \int_0^{L_f} \left(\frac{YkS_f}{K_s + S_f} - b' \right) dz \tag{53}$$

where dz is the local biofilm thickness (L_f, L); b' is the total mass loss coefficient (including decay and shear, T^{-1}).

This is a system of five equations (47, 50–53) and five unknowns (S_f, S_{im}, $\mathbf{J}_{im}$, $\mathbf{J}_f$ and L_f). If the biofilm thickness is assumed to be at steady-state (the biofilm thickness remains constant), the term on the left-hand side of (53) is 0, and L_f can be calculated directly

$$L_f = \frac{\mathrm{J}_f Y}{b' Y_f} \tag{54}$$

The solution to the steady-state model is typically found by putting the equations in dimensionless form and solving them by iterative methods (Rittmann and McCarty, 1980). Pseudo-analytical solutions to steady-state biofilms are also available (Sáez and Rittmann, 1988, 1992) in which the numerical solutions to the differential equations are accurately approximated with algebraic equations.

In modeling substrate utilization with intra-biomass diffusional resistances, the substrate flux expression is the sink term in the substrate transport equation. Additional complexity is added because the intra-biomass mass balance equation must be solved simultaneously with the expression for mass flux into the biomass. Additionally, the substrate may not be the limiting nutrient for microbial growth. In the case of two potentially limiting nutrients, diffusion of one may limit growth in the outer portion of the biomass, and the diffusion of the other may limit growth in the inner portion, or either may limit growth in the entire thickness of the biomass. These limitations may change with time and space in the modeling domain. For additional limiting nutrients, the situation becomes even more complicated.

4.10.4. Biofilms in biodegradation modeling

Because of the complexity of intra-biomass diffusion, a key question is: when is it necessary to consider intra-biomass mass transport resistance when modeling contaminant transport and biodegradation? This question has been addressed by a number of researchers, including Rittmann (1993).

Rittmann (1993) presents the following equation for utilization of substrate by biofilms

$$r_f = -(X_f L_f a)\eta k \left(\frac{S_f}{K_s + S_f} \right) \tag{55}$$

where S_f is the substrate concentration within the biofilm (M/L^3); r_f is the rate of substrate utilization in the biofilm (M/L^3T); X_f is the biofilm density (M/L^3); L_f is the biofilm thickness (L); a is the specific surface area of the biofilm (area of biofilm/volume of porous media, L^{-1}); η is the effectiveness factor, defined as the substrate flux into the biofilm divided by the substrate flux into a fully pen-

etrated biofilm of equal thickness; k is the maximum specific rate of substrate utilization (T^{-1}).

When $\eta = 1$, the biofilm is fully penetrated and $S_f = S_{im}$, the substrate concentration at the biofilm/stagnant liquid layer interface. As the biofilm thickness increases, S_f becomes $<S_{im}$ and η becomes <1. The question then becomes: when is $\eta = 1$ so that the biofilm can be assumed to be fully penetrated? This question was investigated by Odencrantz et al. (1990), who found that $\eta = 1$ for all reasonable values of groundwater flow velocity and substrate utilization (Rittmann, 1993). In experiments to determine how permeability was affected by biofilm growth, Taylor and Jaffé (1990b) determined that η was only slightly less than 1, even though the permeability of the porous media in their experiments was reduced by three orders of magnitude because of microbial growth.

From these sources, it appears that intra-biomass diffusion is probably not important for modeling transport and biodegradation of contaminants under natural conditions. However, near injection wells where both substrate and electron acceptor are being injected, intra-biomass diffusion could have a more noticeable effect on biodegradation rates if the pore sizes were large enough for thick biofilms to form. Suidan et al. (1987) give rigorous criteria of when biofilms can be assumed to be fully penetrated in terms of a dimensionless biofilm thickness. Suidan et al. (1987) also provide quantitative criteria of when external mass transfer is important. Rittmann (1993) suggests that if biofilms are assumed to be fully penetrated, then the assumption should be checked in areas of the modeling domain where formation of shallow biofilms is possible.

4.11. Biomass conceptualization and mass balance equations

In an evaluation of subsurface biodegradation and transport models, Baveye and Valocchi (1989) describe three schools of thought regarding the configuration of biomass in the subsurface. The three configurations are depicted in Fig. 8. In the first school, no particular assumption about the configuration of the microorganisms is made. The biomass could exist as either a continuous biofilm or as scattered, small microbial colonies of arbitrary shape. This is referred to as the "strictly macroscopic" viewpoint. In the second school, biomass is assumed to exist as small, discontinuous, geometrically defined colonies. This viewpoint is called the "microcolony" concept. The third school assumes that biomass exists as a continuous film over all of the particles in the subsurface (the "biofilm" concept). The choice of the biomass configuration conceptual model affects the interpretation of the parameters used in the models to account for diffusional limitations and affect the models' ability to incorporate these diffusional effects (Baveye and Valocchi, 1989).

4.11.1. Strictly macroscopic viewpoint—no biomass configuration assumptions

In the models of Borden and Bedient (1986), Corapcioglu and Haridas (1984), and Kindred and Celia (1989), biomass is conceptualized as being attached to subsurface particles in some unspecified configuration (see Fig. 8a). The chemical concentrations experienced by the biomass are assumed to be the same as the

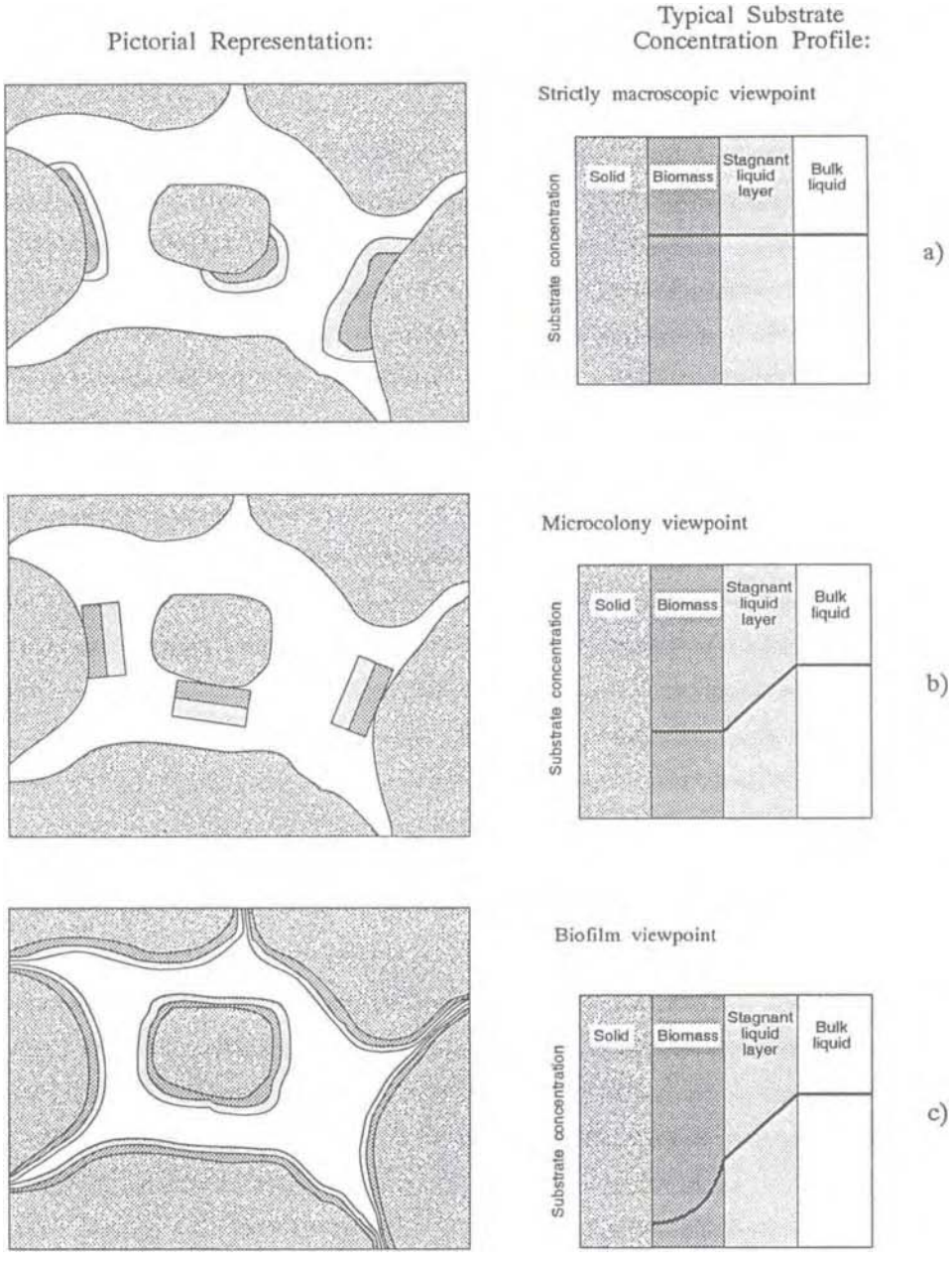


Fig. 8. Three conceptualizations of biomas configuration in porous media (Baveye and Valocchi, 1989; Odencrantz et al., 1990).

average bulk fluid concentrations, and the biomass is represented by a concentration similar to another chemical component. No diffusional resistances are explicitly assumed to exist. This is the simplest conceptual model because bulk fluid concentrations can be used directly in the kinetic expressions for substrate utilization. The kinetic expressions can then be substituted directly into the mass balance equations, resulting in the set of two equations (42) and (43).

As Baveye and Valocchi (1989) point out, the lack of a conceptual depiction of biomass does not have to eliminate any possibility of diffusional limitations. Equations (44)–(46) can be used to describe diffusion through a stagnant liquid layer into attached and immobile biomass, or equations (47)–(53) can be used (with some modifications) to describe both stagnant liquid layer diffusion and intra-biomass diffusion resistances. However, the assumption of no diffusional resistance is typically invoked with this biomass configuration. If diffusion is considered with this biomass conceptualization, the mass transfer coefficient expression C is usually an empirical constant used to match experimental data. If the substrate diffusion coefficient and stagnant liquid layer thickness are known or calculated from literature correlations, then the true fitting parameter is the biomass/bulk liquid interfacial area. This area is constant for all times and positions in the modeling domain.

4.11.2. Microcolony viewpoint

The microcolony concept was introduced by Molz et al. (1986) and is incorporated into the models of Widdowson et al. (1988) and Chen et al. (1992). In this conceptual model, the biomass is assumed to exist in disk-shaped microcolonies of thickness τ and radius r_c, with a stagnant liquid (diffusion) layer of thickness δ on the flat face facing the bulk fluid (see Figs. 8b and 9). Biomass growth is modeled as an increase in the *number* of microcolonies; the *size* of each microcolony remains constant. This conceptualization is typically coupled with the assumption that all mass transfer resistance occurs across the stagnant liquid layer so that the concentration of substrate and electron acceptor within the colony is equal to the concentration at the colony/stagnant layer interface. However, as in the strictly macroscopic viewpoint, either no diffusion resistance or intra-biomass diffusion resistances can be considered.

Conceptualization of the biomass as microcolonies results in a different mass

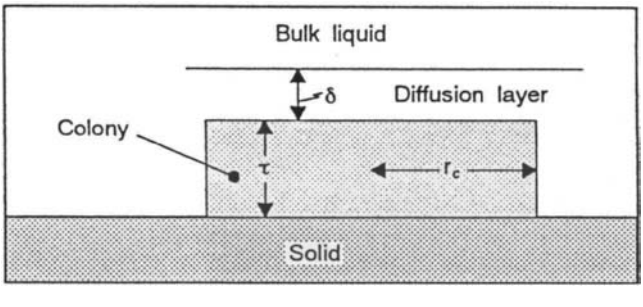


Fig. 9. Microcolony dimensions (Molz et al., 1986).

transfer expression than the empirical constant in the strictly macroscopic model. Under substrate-limiting conditions, the microcolony conceptual model equations describing substrate utilization and biomass growth in one dimension are (Molz et al., 1986)

$$\frac{\partial S_m}{\partial t} = \frac{\partial}{\partial x}\left(\frac{D\partial S_m}{\partial x} - vS_m\right) - \frac{D_{im}}{\theta}\left(\frac{S_m - S_{im}}{\delta}\right) N_c \pi r_c^2 \tag{56}$$

$$\pi r_c^2 \tau \frac{\partial S_{im}}{\partial t} = D_{im}\left(\frac{S_m - S_{im}}{\delta}\right) \pi r_c^2 - \frac{\mu_{max} m_c}{Y_{x/s}}\left(\frac{S_{im}}{K_s + S_{im}}\right) \tag{57}$$

$$\frac{1}{N_c}\frac{\partial N_c}{\partial t} = \mu_{max}\left(\frac{S_{im}}{K_s + S_{im}}\right) - b \tag{58}$$

where D_{im} is the molecular diffusion coefficient of substrate in the stagnant liquid layer (L^2/T); m_c is the mass of a single microorganism colony (M); N_c is the number of bacterial colonies per volume of porous media (L^{-3}).

Note that the mass transfer rate coefficient expression and biomass concentration are (Baveye and Valocchi, 1989)

$$C = D_{im} N_c \pi r_c^2 / \delta$$

$$X = N_c \rho_c \pi r_c^2 \tau = N_c m_c$$

The mass transfer coefficient expression is no longer a constant, but depends on the biomass concentration. This is a consequence of the assumption that microcolonies of fixed size increase in number; the interfacial area available for mass transfer into the biomass increases with an increasing number of microcolonies. Since the colonies are assumed to have a fixed mass, the interfacial area increase is proportional to the biomass increase. As a result, substrate is removed at an increasing rate as biomass grows.

Although the microcolony concept has the advantage of a physical basis, it requires that the biomass exist in a predetermined configuration, which is obviously a great simplification, whereas the strictly macroscopic viewpoint does not. However, in the model of Widdowson et al. (1988), an alternative approach is used that precludes this restriction. Instead of defining a definite shape with an accompanying interfacial area to each microcolony, an interfacial area is assigned to each microcolony or unit of biomass. Although the choice of what interfacial area to assign must still be made, the microcolonies are no longer envisioned as geometrically simple structures. This approach retains the advantage of a changing interfacial area with biomass growth while eliminating the application of a definite shape to the biomass (Widdowson, 1991).

4.11.3. Biofilm viewpoint

In the biofilm conceptual model, biomass is assumed to cover the entire surface of the solid in a continuous biofilm. As in the strictly macroscopic and microcolony viewpoints, mass transfer resistances can be ignored, assumed to exist across a stagnant liquid layer, or assumed to exist both within the biofilm as well as across

a stagnant liquid layer. However, the biofilm viewpoint is most useful when intra-biomass mass transfer is assumed to exist.

If mass transfer resistance is assumed to occur only across a stagnant liquid layer for purposes of comparison with the other two conceptual models, then the equations for substrate utilization and biomass growth for the biofilm model are

$$\frac{\partial S_m}{\partial t} = \frac{\partial}{\partial x}\left(\frac{D\partial S_m}{\partial x} - vS_m\right) - \frac{D_{im}}{\theta}\left(\frac{S_m - S_{im}}{\delta}\right)A \tag{59}$$

$$\frac{\partial S_{im}}{\partial t} = \frac{D_{im}}{L_f}\left(\frac{S_m - S_{im}}{\delta}\right) - \frac{\mu_{max}\rho_f}{Y_{x/s}}\left(\frac{S_{im}}{K_s + S_{im}}\right) \tag{60}$$

$$\frac{\partial L_f}{\partial t} = \mu_{max}\left(\frac{S_{im}}{K_s + S_{im}}\right)L_f - bL_f \tag{61}$$

where X_f is the biomass density (M/L^3); A is the specific surface area of porous medium (L^{-1}); L_f is the thickness of continuous biofilm (L), and ρ_f is the biomass density (M/L^3).

These equations are formally the same as those for the strictly macroscopic viewpoint. In this system of equations, the specific surface area A must be known, and the change in biomass is reflected by changes in the biofilm thickness L_f. The advantage of this model is that the specific surface area A can usually be measured so that no assumption about the interfacial area must be made. The disadvantage of this viewpoint is that studies have shown that the biomass is not usually uniformly distributed on the porous media so that the assumption of a continuous biofilm may be unrealistic. In addition, the assumption of a continuous biofilm leads to excessive mass transfer into the biomass if the diffusion coefficient and stagnant liquid layer thickness are obtained independently.

4.11.4. Summary of biomass configuration conceptualization

Since biomass has generally been observed to exist as scattered colonies in oligotrophic environments (Harvey et al., 1984), the microcolony conceptualization appears to be the most realistic model. However, in some cases, the choice of conceptual model does not make any difference because the governing equations are identical. For example, if no diffusion resistance is assumed to exist, or if mass transfer is assumed to be rapid relative to biodegradation rates, then all three models collapse into a system of two equations and will yield the same results. The only difference is in how biomass is defined; as a concentration, number of microcolonies, or biofilm thickness.

4.12. Biomass growth limitations

As discussed in Section 4.7.10, the biomass mass balance equation does not have a built-in mechanism for limiting the amount of biomass that can exist to physically possible quantities. When substrates or other nutrients are low, biomass growth can be limited by the low concentrations of these chemicals through Monod

terms. However, at locations where there are no substrate, electron acceptor, or other nutrient limitations, most models predict continued growth of biomass, even beyond the volume of biomass equal to the pore volume of the porous media. Therefore, methods are required to limit the growth of biomass independent of nutrient concentrations. In general, biodegradation models have controlled the growth of biomass by one of three methods: (1) explicit consideration of mass transfer through stagnant liquid layers and within the biomass itself; (2) biomass inhibition functions, and (3) consideration of biomass as a separate phase with losses from the biofilms due to sloughing and shearing. Each of these methods is discussed below.

4.12.1. Mass transfer resistances

As discussed in Section 4.10, diffusion resistances across a stagnant liquid layer reduce the substrate concentration within the biomass. The biomass grows at a rate slower than it would grow if the substrate concentration within the biomass were the same as the bulk liquid concentration. Although the stagnant liquid layer diffusive resistances reduce the substrate concentration available to the biomass, these resistances to mass transfer may not limit biomass growth sufficiently. Additional biomass growth limitations are imposed when intra-biomass diffusion is considered. If the biomass grows so thick that the substrate concentration becomes 0 at or before the biomass/solid interface (a deep biofilm), the biomass cannot continue to grow (or at least become thicker) because it is already receiving the maximum flux of substrate possible from the bulk liquid.

Intra-biomass diffusional limitations may be sufficient to limit the ultimate biomass concentration if the pore volume is large enough for a deep biofilm to form. However, the pores in some media may be too small for deep biofilms to form. In these media, the predicted biomass volume could exceed the porosity even with intra-biomass diffusional resistances.

4.12.2. Biomass inhibition functions

Kindred and Celia (1989) used a biomass inhibition function of the following form to limit biomass growth and model intra-biomass diffusional resistances

$$I_b = (1 + X/k_b) \tag{62}$$

where I_b is the biomass inhibition factor; X is the biomass concentration (M/L^3); k_b is the biomass inhibition constant (M/L^3).

This biomass inhibition term is identical to the product inhibition term (equation (25)) if the numerator and denominator of the product inhibition term are divided by K_p. The inhibition function is incorporated into the Monod expression for biomass growth

$$\frac{dX}{dt} = \mu_{max} X \left(\frac{S}{(K_s + S)(1 + X/k_b)} \right) - bX \tag{63}$$

If $X \ll k_b$, then $1 + X/k_b \cong 1$ and the basic Monod equation results. If $X \gg k_b$, then $1 + X/k_b \cong X/k_b$ and the expression for biomass growth becomes

$$\frac{dX}{dt} = \mu_{max} k_b \left(\frac{S}{K_s + S} \right) - bX \tag{64}$$

This expression is the same as the Monod equation except that X is replaced by k_b. The result is that biomass growth is no longer first-order with respect to X and depends only on the substrate concentration. As the biomass continues to utilize substrate, X will continue to increase. However, equation (64) predicts that the growth rate will tend to 0 as X continues to increase because of the second term for endogenous decay, which depends on the increasingly large X. As a result, biomass concentration will reach a maximum for some given substrate concentration. Kindred and Celia (1989) point out that the above expression corresponds to a situation where a biofilm is fully penetrated and the total thickness of the biofilm is irrelevant since only the outer layer degrades the substrate.

Two points about this approach should be emphasized. First, the inhibition function is empirical. Experiments would be necessary to determine a realistic value of k_b. Since porous media are usually not homogeneous, this value would have to be an average or effective value for the media as a whole. Second, depending on the value of the inhibition constant, the inhibition function could limit biomass growth even at biomass concentrations far below the concentrations that would significantly restrict pores. For small pore volumes, this limitation may be realistic. However, for media with large pore sizes, biomass growth could be unjustifiably restricted.

4.12.3. Sloughing and shearing losses

Sloughing is the detachment of biomass sections caused by the death of cells at the biomass/solid interface. The cell death is in turn caused by lack of sufficient nutrients at the interface due to their complete utilization in the outer portion of the biomass. Sloughing is difficult to predict quantitatively and is not well understood.

Biomass shearing is more amenable to quantitative treatment. As pores become restricted from biomass growth, the groundwater velocity through the pore openings increases. These increased velocities could cause shearing of biomass from the pore walls. Since the shearing loss is a function of the velocity, biomass losses could increase with increasing biomass growth until a steady state is reached between biomass growth and shearing loss. Equations for biomass shearing losses are shown in Section 4.14 from the work of Taylor and Jaffé (1990b).

3. ortance of boundary conditions on biomass growth

Under most natural settings, the substrate and electron acceptor concentrations in an aquifer are probably not sufficient to support growth of biomass in quantities that would cause its volume to comprise a significant fraction of the pore space. This is not true when injection wells inject substrate and electron acceptor into aquifers in large quantities, or when substrate and electron acceptor are continuously injected at a column inlet in the laboratory. Under these conditions, the selection of the inlet boundary conditions can have a large impact on the model

predictions of biomass growth at the column inlet (or adjacent to the well screen for injection wells).

The two most common inlet boundary conditions for laboratory column studies are (Fetter, 1993)

$$S = S_o \qquad x = 0, t \geq 0 \qquad \text{first type}$$
$$-D\frac{\partial S}{\partial x} + vS = vS_o \qquad x = 0, t \geq 0 \qquad \text{third type} \tag{65}$$

The first-type boundary condition provides the biomass with an unlimited supply of substrate and electron acceptor by holding the concentration of these species constant at the column inlet (Chen et al., 1992). Thus, the biomass can continue to grow unbounded according to equation (41) because no substrate limitations exist (Chen et al., 1992). Models that use this boundary condition will, therefore, predict excessive biomass growth at the column inlet. However, if the third-type boundary condition is used, then the flux of substrate and electron acceptor is limited at the column inlet, a much more realistic situation (Chen et al., 1992). Under this boundary condition, the concentration at the inlet can be reduced by the biomass growing there so that much more realistic estimates of biomass growth will be simulated. Chen et al. (1992) demonstrated this boundary condition effect in simulations of biodegradation in laboratory columns.

4.14. Microorganism transport and effect on porous media

Microorganism transport is important to biodegradation modeling for a number of reasons. First, contaminants have been shown to migrate when adsorbed on colloidal-sized bacteria (Lindqvist and Enfield, 1992; Jenkins and Lion, 1993). Second, bacteria themselves may be transported when attached to colloidal particles. If this type of transport occurs, then an acclimated population of microorganisms could develop in advance of a contaminant plume and significantly reduce the acclimation period. Finally, it may be desirable to introduce microorganisms acclimated to a particular contaminant or genetically engineered to degrade a contaminant into a subsurface environment to enhance bioremediation (Lindqvist and Enfield, 1992). The transport and attachment of bacteria to subsurface particles is also important in estimating permeability reductions.

4.14.1. Important considerations and mechanisms

The movement of bacteria in the subsurface is governed by transport processes, attachment phenomenon, and detachment phenomenon. Transport is generally assumed to occur by advection, diffusion (for small bacteria), and chemotaxis (Corapcioglu and Haridas, 1984). Chemotaxis is the directed movement of bacteria in response to chemical gradients (Corapcioglu and Haridas, 1984). Through chemotaxis, bacteria move toward areas of higher nutrient concentrations (Corapcioglu and Haridas, 1984).

Many interacting factors govern the transport and attachment of bacteria to surfaces. These factors include physical, chemical and biological properties of both

TABLE 5

Factors affecting bacterial attachment and transport

Factor	Effect on transport or attachment
pH	Low pHs favor attachment (Yates and Yates, 1988).
Ionic strength	High ionic strength increases attachment by reducing the size of the particle double layer (Yates and Yates, 1988; Fontes et al., 1991).
Clay content	Increasing clay content favors increasing attachment due to a greater specific area for adsorption (Teutsch et al., 1991) and possible filtering effects (Yates and Yates, 1988; Fontes et al., 1991).
Oxygen limitations	Oxygen-limited biofilms exhibit lower shear removal rates but higher sloughing possibly due to high extracellular polymer production (Applegate and Bryers, 1991).
Charge on media	Positive charges on media tend to increase attachment by negatively-charged bacteria (Lindqvist and Bengtsson, 1991).
Flowrate	Higher flowrates reduce attachment of bacteria (Yates and Yates, 1988).
Nutrient concentrations	Higher nutrient concentrations reduce bacterial size (Camper et al., 1993).
Bacterial size	May decrease or increase attachment. Smaller bacteria may interact with the media less and may not be removed by filtration as easily as large bacteria (Camper et al., 1993). On the other hand, larger bacteria have been shown to move faster than small bacteria, possibly due to size exclusion (Fontes et al., 1991; Yates and Yates, 1988).
Cell concentration	Attachment is favored when the cell density (mass concentration) in the liquid is decreased (Lindqvist and Enfield, 1992). Also, bacteria tend to move from areas of high concentration to areas of low concentration by a tumbling diffusive flux (Sarkar et al., 1994).
Bacterial motility	Motile bacteria may migrate faster than non-motile bacteria through chemotaxis.
Water content	Bacteria move faster through unsaturated soils at higher water contents (Yates and Yates, 1988).

the bacteria and surfaces and are summarized in Table 5. Removal of bacteria from the flowing liquid phase generally occurs by filtration (Yates and Yates, 1988), adsorption (Lindqvist and Bengtsson, 1991) and cell death (Camper et al., 1993). Detachment in subsurface environments is most likely to occur by desorption, erosion, or sloughing (Stewart, 1993). The various attachment and detachment mechanisms are affected by one or more of the factors listed in Table 5, among others.

4.14.2. Methods of modeling bacterial transport and attachment

Bacterial transport and elucidation of the methods by which bacteria attach to porous media is a very large area of active research. This section provides only a brief summary of a few of the factors known to affect bacterial transport and several relatively simple methods of modeling the phenomenon.

All of the models of bacterial transport reviewed in this report are based on the advection-dispersion equation. Some models account for chemotaxis by lumping a chemotactic dispersion coefficient into the overall dispersion coefficient (Corapcioglu and Haridas, 1985), while other models include a separate chemotactic disper-

sion coefficient (Sarkar et al., 1994). The major differences in the models are in the method by which bacterial attachment and detachment are modeled. Removal of bacteria from the liquid phase is generally modeled as an adsorption process, a filtration process, or a combination of both. Two methods of modeling detachment are desorption and removal by shearing.

4.14.2.1. Adsorption models. The simplest method of modeling bacterial transport is to assume that bacteria are adsorbed according to the linear equilibrium model. This approach is taken by Borden and Bedient (1986) and MacQuarrie et al. (1990). In fact, these researchers were the only ones to account for bacterial transport in models whose primary objective was to model contaminant transport. All of the other methods of accounting for bacterial transport discussed below are incorporated into models specifically designed to describe bacterial transport, although some also describe contaminant transport since they include terms for growth and decay of the biomass.

The next level of complexity is to model bacterial detachment as a reversible, first-order adsorption process. The equations used are the same as the equations used to model first-order reversible adsorption of a chemical constituent (equation (10)). This method was adopted by Corapcioglu and Haridas (1984, 1985) in a model to describe bacterial transport. Hornberger et al. (1992) used a modified version of Corapcioglu and Haridas's model to describe the data obtained by Fontes et al. (1991) in laboratory columns. The growth term was eliminated from the model since experiments were conducted by resting cells. The model was compared to two other models, one ignoring detachment and one ignoring dispersion. The model of Corapcioglu and Haridas (1985) best predicted the data, as the effects of both detachment and dispersion were important. The model performed reasonably well and captured the general shape of the bacterial breakthrough curves. The model seemed to perform best for the larger bacteria and finer grained soils.

Lindqvist and Bengtsson (1991) described the transport of bacteria through sand columns with both a linear equilibrium isotherm adsorption model and a two-site model. The two-site model assumes that a fraction of the adsorbing solute adsorbs to soil instantaneously while the adsorption of the remaining fraction is kinetically limited. The two-site model is also used to describe adsorption of chemical constituents. Lindqvist and Bengtsson (1991) accounted for both growth and decay of biomass where growth was described with a Monod term and decay was described as first-order. The equations used for the two-site model were

$$\left(1 + \frac{f\rho_b K_d}{\theta}\right)\frac{\partial C_a}{\partial t} + \frac{\rho_b}{\theta}\frac{\partial C_s^{II}}{\partial t} = D\frac{\partial^2 C_a}{\partial x^2} - v\frac{\partial C_a}{\partial x} - bC_a + \mu C_a \tag{66}$$

$$\frac{\partial C_s^{II}}{\partial t} = k_m[(1-f)K_d C_a - C_s^{II}] \tag{67}$$

where f is the fraction of instantaneous adsorption sites; ρ_b is the bulk soil density (M/L^3); C_a is the concentration of bacteria in the bulk liquid (M/L^3); θ is the

porosity; b is the first-order rate coefficient for bacterial loss by all mechanisms (T^{-1}); μ is the Monod growth rate (T^{-1}); C_s^{II} is the mass fraction of bacteria adsorbed onto kinetically limited adsorption sites (M/M solid); k_m is the mass transfer coefficient (T^{-1}); K_d is the adsorption partition coefficient (L^3/M).

Lindqvist and Bengtsson (1991) determined that the two-site model described the breakthrough of bacteria better than a linear equilibrium model.

4.14.2.2. Filtration and combined adsorption/filtration models. Harvey and Garabedian (1991) investigated bacterial transport in an organically contaminated groundwater plume in Cape Cod, Massachusetts. Harvey and Garabedian (1991) used filtration theory coupled with either linear equilibrium adsorption or first-order reversible kinetic adsorption to describe bacterial removal from the bulk liquid. Their version of the advection-dispersion equation was

$$\theta\frac{\partial C}{\partial t} + \rho_b\frac{\partial C^*}{\partial t} = D\theta\frac{\partial^2 C}{\partial x^2} - v\theta\frac{\partial C}{\partial x} - k_p C \tag{68}$$

where C^* is the adsorbed bacterial concentration and k_p (T^{-1}), the irreversible adsorption constant, is

$$k_p = \frac{3}{2}\frac{(1-\theta)}{d}\alpha\eta \tag{69}$$

where α is the collision efficiency factor and η is the single-collector efficiency. $\partial C^*/\partial t$ is equal to $K_d\partial C/\partial t$ for linear adsorption and to $k_f C - k_r C^*$ for first-order reversible kinetic adsorption. Harvey and Garabedian (1991) fitted the model parameters to the elution curves and concluded that their model fit the data reasonably well. Because adsorption was not a major factor in their studies, the linear equilibrium model and first-order reversible kinetic adsorption models performed equally well.

Lindqvist and Enfield (1992) compared the two-site adsorption model to a filter model in which the concentration of bacteria were described as

$$\frac{dC}{dx} = -\lambda C \tag{70}$$

where C is the aqueous bacterial concentration and λ is a filter coefficient (T^{-1}). The filter coefficient is essentially the same as the irreversible adsorption constant k_p used by Harvey and Garabedian (1991). However, if an empirical fit to the data is desired and if the filtration parameters are assumed to remain constant, the function can be lumped into the filter coefficient. Lindqvist and Enfield (1992) determined that this description of bacterial attachment did not perform as well as the two-site adsorption model.

Sarkar et al. (1994) present a model for bacterial transport and growth using a different approach to filtration. This multi-phase, multi-component model uses an empirical fractional flow curve to simulate the data from column experiments. The fractional flow curve is represented by

$$C_{fD} = \frac{AC_{TD}}{1 + BC_{TD}} \tag{71}$$

where

$$C_{fD} = \frac{C_f}{C_T} \quad \text{and} \quad C_{TD} = \frac{C_T - C^*}{C_T} \tag{72}$$

and C_f is the flowing bacterial concentration (M/L^3); C_T is the total bacterial concentration (M/L^3); C_{fD}, C_{TD} are the dimensionless flowing bacterial and total bacterial concentrations; A, B, C^* are the retention parameters determined experimentally.

The trapped bacterial concentration is $\hat{C}_k = C_T - C_f$. This filtration model was successful in simulating the bacterial elution curves and in describing reductions in permeability of the experimental columns.

Taylor and Jaffé (1990b) use a first-order model for bacterial deposition that differs slightly from the other filtration models discussed above. They assume that the biomass exists as a continuous film and model bacterial removal from the water phase as

$$R_d = (c_1\theta^f + c_2)\theta^w C_b^w \tag{73}$$

where R_d is the rate of removal of bacteria (M/L^{3}T); θ^f is the volume fraction of biomass phase (volume biomass/volume of porous medium); θ^w is the volume fraction of water phase (volume water/volume of porous medium); C_b^w is the concentration of bacteria in water phase (M/L^3); c_1, c_2 are experimentally determined constants.

The simplest method of modeling biomass detachment is to assume that it is first-order with respect to adsorbed biomass concentration (Taylor and Jaffé, 1990b). The first-order rate constant may be a function of the shear stress, which is itself a function of fluid viscosity, seepage velocity, and permeability (Taylor and Jaffé, 1990b).

Taylor and Jaffé (1990b) modeled biomass detachment with a biofilm shearing model based on the work of Speitel and DiGiano (1987). Incorporating the effectiveness factor concept into the biofilm shearing model, Taylor and Jaffé (1990b) expressed the loss of biomass from the biofilm as

$$R_s = b_s\theta^f\rho^f + b_s'\left(\frac{Y\eta k C_s^w}{K_s + C_s^w}\right) AL_f\rho^f \tag{74}$$

where L_f is the biofilm thickness (L); A is the specific surface area of the water/biofilm interface (L^{-1}); θ^f is the volume fraction of biofilm phase (volume biofilm/total volume of porous media); η is the biofilm effectiveness factor; b_s is the specific shear loss coefficient (a function of shear stress and L_f); b_s' is the dimensionless parameter describing biological aspects of shearing; C_s^w is the concentration of substrate in the bulk phase (M/L^3); ρ^f is the biomass density (M/L^3).

Taylor and Jaffé (1990b) incorporate the expressions for biomass deposition and detachment into a comprehensive model that accounts for bacterial transport

and substrate utilization in both the biomass and in the bulk fluid where free-floating bacteria are assumed to contribute to substrate biodegradation.

4.15. Effect of microorganism growth on porous media

In many realistic field situations, substrate and electron acceptor are not present in sufficiently high concentrations or for sufficient time for growing biomass to occupy a significant fraction of the pore space. In these cases, biomass growth may have an insignificant effect on the porous medium properties. However, in column studies and in bioremediation projects where high concentrations of substrate and electron acceptor coexist for long periods, biomass growth may cause changes in the porosity, permeability and dispersivity of the porous medium, and these changes must be considered.

Only four models reviewed in this study addressed the effects of biomass growth on properties of the porous media (Corapcioglu and Haridas, 1985; Taylor and Jaffé, 1990b; Sarkar, 1992; and Sarkar et al., 1994). Sarkar (1992) and Sarkar et al. (1994) used effective medium theory (EMT) to estimate permeability losses due to the retention of bacteria. A complete description of the theory can be found in other sources (Sharma and Yortsos, 1987), and only a summary of the important relationships are provided here.

The basic premise of EMT is that as bacteria are retained by the porous media, the pore size distribution is changed (Sarkar, 1992). Some pores become plugged and cannot transmit fluid while others remain unaffected. The initial undamaged mean conductance is defined as (Sarkar, 1992)

$$g_{mi} = \frac{\int_0^\infty \frac{r^n f(r)}{r^n + \alpha g_m} dr}{\int_0^\infty \frac{f(r)}{r^n + \alpha g_m} dr} \tag{75}$$

where g_{mi} is the initial undamaged mean conductance (L^3); r is the pore throat radius (L); $f(r)$ is the pore throat radius distribution function; g_m is the effective hydraulic conductance (L^3); n is the exponent between 3 and 4; $\alpha = z/2 - 1$; z is the coordination number (of pore throats that join at each interior pore body).

The damaged mean conductance is calculated from (Sarkar, 1992)

$$g_{mD} = \frac{(1-y)\int_0^\infty \frac{r^n f_D(r)}{r^n + \alpha g_{mD}} dr}{\frac{y}{\alpha g_m} + (1-y)\int_0^\infty \frac{f_D(r)}{r^n + \alpha g_{mD}} dr} \tag{76}$$

where y is the fraction of non-conductive pores (a function of the effective particle radius); $f(r)$ is the damaged medium pore size distribution function; g_{mD} is the mean conductance for the damaged medium (L^3).

The permeability of the damaged medium is then found from

$$\frac{k_D}{k_i} = \left(\frac{g_{mD}}{g_{mi}}\right)^{2/n} = \sqrt{\frac{g_{mD}}{g_{mi}}} \tag{77}$$

where k_i is the intrinsic permeability of the medium. The EMT model in this form assumes zero permeability for the non-conductive pores, but in actuality the permeability will have some very low value (Sarkar, 1992). In this case, the damaged permeability is expressed by the empirical relation

$$\frac{k_D}{k_{D_c}} = e^{d(a-a_c)}$$

where a_c is the percolation threshold; k_{D_c} is the permeability at a_c; d is the critical damage parameter.

Sarkar (1992) and Sarkar et al. (1994) used the model to simulate the permeability reduction and bacteria breakthrough curves for saturated water flow and NAPL/water flow. In the experiments, permeability was reduced to 70 to 80 percent of the initial permeability. The simulation matched the experimental data reasonably well. The model underpredicted permeability reduction at early times but matched the leveling of permeability reduction.

The experiments conducted by Sarkar (1992) and Sarkar et al. (1994) were for relatively high flow velocities: 25 and 100 ft/day. Taylor and Jaffé (1990a) conducted experiments of aerobic methanol biodegradation in laboratory columns with lower flow rates of approximately 10 and 33 ft/day. They found that permeability was reduced by three orders of magnitude over the initial permeability, but that the permeability was not reduced below a threshold of about three orders of magnitude. The experimental permeability data were found to be a function of the biomass volume fraction

$$\frac{k}{k_o} = \exp\left(a[\mathrm{BOC}] + b[\mathrm{BOC}]^2\right) \qquad [\mathrm{BOC}] \leq 0.4\ \mathrm{mg/cm^3}$$

$$\frac{k}{k_o} = c \qquad [\mathrm{BOC}] > 0.4\ \mathrm{mg/cm^3} \tag{79}$$

where k is the permeability at the end of the experiment (L^2); k_o is the initial permeability (L^2); [BOC] is the bacterial organic carbon (M/L^3).

Taylor and Jaffé (1990b) used a cut-and-random-rejoin type of model to simulate the porosity and permeability reduction observed in their experiments

$$n^w = \beta\left(\frac{L_f}{R}\right)^{\lambda}\left[I_2\left(\frac{R}{L_f} - 1, \lambda\right) - I_2\left(\frac{r_o}{L_f} - 1, \lambda\right)\right] \tag{80}$$

$$k = \frac{\kappa\sqrt{n^w}\beta^2 L_f^2}{8}\left(\frac{L_f}{R}\right)^{2\lambda}\left[I_3\left(\frac{R}{L_f} - 1, \lambda\right) - I_3\left(\frac{r_o}{L_f} - 1, \lambda\right)\right]^2 \tag{81}$$

$$I_n(u, \lambda) = \int_0^u \frac{x^n}{(x+1)^{3-\lambda}}\,dx \tag{82}$$

$$a_L = \frac{(n^w)^2\langle L_b\rangle\langle T_b^*\rangle^2\beta}{k}\left(\frac{L_f}{R}\right)^{\lambda}\left(\frac{L_f^2}{8}\right)^2\left\{\left[I_6\left(\frac{R}{L_f}-1,\lambda\right)-I_6\left(\frac{r_o}{L_f}-1,\lambda\right)\right]\right.$$
$$\left.-\beta\left(\frac{L_f}{R}\right)^{\lambda}\left[I_6\left(\frac{R}{L_f}-1,\lambda\right)^2-I_4\left(\frac{r_o}{L_f}-1,\lambda\right)^2\right]\right\} \quad (83)$$

where R is the maximum pore radius (L); κ, β are dimensionless constants; L_f is the biofilm thickness (L); λ is the pore size distribution index; a_L is the longitudinal dispersivity (L); $\langle L_b\rangle$ is the average length of an elemental pore channel (L); $\langle T_b^*\rangle$ is the tortuosity; k is the permeability (L^2).

Taylor and Jaffé (1990b) were successful in predicting biofilm thicknesses on a laboratory column. Taylor and Jaffé (1990b) also compared the effect of three test cases to determine whether such a complex model is justified. In case 1, dispersivity, porosity and permeability were allowed to change with biomass growth (the most complex case for which the above model applies). In case 2, these parameters were considered constant and equal to their values when no biomass is present. Case 3 was the same as case 2 except that interphase biomass transfer were not allowed, i.e., there was no exchange of biomass from the biofilm and bulk liquid.

At low substrate loadings, cases 1 and 2 predicted an increase in biomass concentration with distance through the column followed by a decrease and gradual decline with distance. This prediction matched the observed experimental results. The case 3 scenario predicted excessive biomass growth at the column inlet since no biomass shearing was taken into account. This effect is the same effect seen with other models which do not establish an upper limit on biomass growth. At high substrate loading, case 1 still predicted realistic biomass distributions. However, the higher substrate loadings caused the case 2 simulation to overpredict biomass accumulation at the column inlet because aquifer properties were not taken into account. In fact, the case 2 solution became unstable because of very high predicted advective fluxes, whereas in case 1, where dispersivity was allowed to vary with biomass growth, the solution remained stable. Thus, accounting for changes in the porous media may not only lead to more realistic predictions of biomass distributions, but also assist in the stability of the numerical solutions (Taylor and Jaffé, 1990b).

5. Discussion of representative models

Table 6 summarizes the features of the biodegradation models reviewed in this literature review. The objective of this section is to describe the performance of representative models reviewed. To accomplish this objective, the following information is provide for each model:

- brief general description
- key model features
- important assumptions

TABLE 6

Features of selected biodegradation models included in this review

Author(s):	Sykes et al.	Bouwer & McCarty	Borden & Bedient	Molz et al.	Baehr & Corapcioglu	Rifai et al.	Widdowson et al.	Chiang et al.
Year published	1982	1984	1986	1986	1987	1988	1988	1989
General:								
Maximum dimensions	2	1	2	1	1	2	1	2
Maximum phases (excluding the solid phase)	1	1	1	1	3	1	1	1
Numerical solution method	FE	IT	FD/MOC	FD	I D	FD, MOC	FD	FD/MOC
Multiple substrates?	N	N	N	N	Y	N	N	N
Multiple electron acceptors?	N	N	N	N	N	N	Y	N
Multiple reactions?	N	N	N	N	N	N	N	N
Growth kinetics:								
Microbial growth included?	Y	Y	Y	Y	N	N	Y	Y
Kinetics: Monod (M), first-order (FO), other (O)	M FO	FO	M/O	M	O	M	M	FO/O
Aerobic (AR), anaerobic (AN), or both (B)	AN	B	AR	AR	AR	AR	B	AR
Cometabolism?	N	Y	N	N	N	N	N	N
Inhibition included?	N	N	N	N	N	N	N	N
Acclimation included?	N	N	N	N	N	N	N	N
Biofilm/diffusion limitations:								
Stagnant liquid layer diffusion limitation?	N	Y	N	Y	N	N	Y	N
Intra-biofilm diffusion limitation?	N	Y	N	N	N	N	N	N
Adsorption:								
Included?	N	N	Y	Y	Y	Y	Y	N
Linear (LN) or non-linear (NL)	N/A	N/A	LN	LN	LN	LN	LN	N/A
Equilibrium (E) or kinetic (K)	N/A	N/A	E	E	E	E	E	N/A
Microorganism concept:								
Biofilm (BF), microcolony (MC), not specified (NS)	NS	BF	NS	MC	NS	NS	MC	NS
Microbial transport included?	N	N	Y	N	N	N	N	N
Multiple microorganism populations?	N	N	N	N	N	N	N	N
Upper limit on biomass volume?	N	N	N	N	N	N	N	N
Growth effects on porous media included?	Y	N	N	N	N	N	N	N
Testing/verification:								
Compared to analytical solution?	N	N	Y	Y	N	Y	Y	N
Laboratory tested?	N	Y	N	N	N	N	N	N
Field tested?	Y	N	Y	N	N	Y	N	Y

TABLE 6 *Continued*

Author(s):	Kindred & Celia	MacQuarrie et al.	Odencrantz et al.	Taylor & Jaffé	Corapcioglu et al.	Kinzelbach et al.	Taylor & Jaffé	Angley et al.
Year published	1989	1990	1990	199Oa	1991	1991	1991	1992%
General:								
Maximum dimensions	1	2	2	1	1	2	1	1
Maximum phases (excluding the solid phase)	1	1	1	2	1	3	2	1
Numerical solution method	FE	FE	FD	FE	FD	?	FE	FD
Multiple substrates?	Y	N	N	N	Y	N	N	N
Multiple electron acceptors?	Y	N	N	N	N	Y	N	N
Multiple reactions?	N	N	N	N	Y	N	N	N
Growth kinetics:								
Microbial growth included?	Y	Y	Y	Y	N	Y	Y	N
Kinetics: Monod (M), first-order (FO), other (O)	M	M	M	M	M	M	M	FO
Aerobic (AR), anaerobic (AN), or both (B)	B	AR	AN	N/A	AN	B	AR	AR
Cometabolism?	Y	N	N	N	Y	N	N	N
Inhibition included?	Y	N	N	N	N	N	Y	N
Acclimation included?	N	N	N	N	N	N	N	N
Biofilm/diffusion limitations:								
Stagnant liquid layer diffusion limitation?	N	N	Y	N	N	Y	N	N
Intra-biofilm diffusion limitation?	N	N	Y	N	N	N	N	N
Adsorption:								
Included?	Y	Y	N	N	Y	?	N	Y
Linear(LN) or non-linear(NL)	LN	LN	N/A	N/A	LN	?	N/A	LN
Equilibrium (E) or kinetic (K)	E	E	N/A	N/A	E	?	N/A	K
Microorganism concept:								
Biofilm (BF), microcolony (MC), not specified (NS)	NS	NS	NS/BF	BF	NS	NS	BF	NS
Microbial transport included?	N	Y	N	Y	N	N	Y	N
Multiple microorganism populations?	Y	N	N	N	N	N	N	N
Upper limit on biomass volume?	N	N	N	Y	N	N	Y	N
Growth effects on porous media included?	N	N	N	Y	N	N	Y	N
Testing/verification:								
Compared to analytical solution?	N	Y	N	N	N	?	N	N
Laboratory tested?	N	Y	Y	Y	Y	?	N	Y
Field tested?	N	N	N	N	N	?	N	N

TABLE 6 *Continued*

Author(s):	Brusseau et al.	Chen et al.	Semprini & McCarty	Malone et al.	Wood et al.
Year published	1992	1992	1992	1993	1994
General:					
Maximum dimensions	1	1	1	1	2
Maximum phases (excluding the solid phase)	1	3	1	1	1
Numerical solution method	FD	FE	FD	FD	FE/MOC
Multiple substrates?	N	Y	Y	Y	N
Multiple electron acceptors?	N	Y	N	N	N
Multiple reactions?	N	N	N	Y	Y
Growth kinetics:					
Microbial growth included?	N	Y	Y	Y	Y
Kinetics: Monod (M), first-order (FO), other (O)	FO	M	M	M	FO/M
Aerobic (AR), anaerobic (AN), or both (B)	N/A	B	AR	AR	AR
Cometabolism?	N	N	Y	N	N
Inhibition included?	N	Y	Y	Y	N
Acclimation included?	N	N	Y	N	Y
Biofilm/diffusion limitations:					
Stagnant liquid layer discussion limitation?	Y	Y	N	N	N
Intra-biofilm diffusion limitation?	N	N	N	N	N
Adsorption:					
Included?	Y	Y	Y	Y	N
Linear (LN) or non-linear (NL)	LN	LN	LN	LN	N/A
Equilibrium (E) or kinetic (K)	K	E	K	E	N/A
Microorganism concept:					
Biofilm (BF), microcolony (MC), not specified (NS)	NS	MC	NS	NS	NS
Microbial transport Included?	N	N	N	N	N
Multiple microorganism populations?	N	Y	N	N	N
Upper limit on biomass volume?	N	N	N	N	N
Growth effects on porous media included?	N	N	N	N	N
Testing/verification:					
Compared to analytical solution?	Y	Y	Y	N	Y
Laboratory tested?	Y	Y	N	Y	Y
Field tested?	N	N	Y	N	N

- method of validation
- comments on the model's advantages and disadvantages.

5.1. Widdowson et al. (1988)

The Widdowson et al. (1988) model simulates the biodegradation of generic organic carbon in laboratory columns. This is one of the first models to incorporate multiple electron acceptors. The concentration of two electron acceptors and one additional nutrient are simulated. Distinguishing features of the model include:
- Conceptualization of the microorganisms as microcolonies.
- Inhibition functions to "switch" from oxygen to nitrate metabolism.
- Consideration of a stagnant liquid film diffusion layer.

5.1.1. Important assumptions
- Adsorption is described as a linear equilibrium process.
- Monod kinetics apply.
- Bacterial transport is not significant.
- Microbial community consists of a single bacterial species.

5.1.2. Validation
The model solution for a conservative tracer was compared to the one-dimensional analytical solution of the advection-dispersion equation (van Genutchten and Alves, 1982) for a conservative tracer. The numerical solution matched the analytical solution extremely well for Peclet numbers of 1 and 100.

5.1.3. Comments
Widdowson et al. (1988) ran a number of simulations designed to mimic conditions expected to develop in laboratory columns. Substrate, oxygen, nitrate and biomass concentration profiles in the column were shown for several different times under different limiting conditions.

The lack of any experimental validation of this model is an important drawback. However, the model demonstrates several important simulation methods. First, the model simulates biodegradation under any combination of limiting conditions. Substrate, oxygen, nitrate, a fourth limiting nutrient or a combination of these can control the rate of biodegradation. The biodegradation rates in each modeling grid are controlled by the local concentration of these nutrients. This multiple limitation model is probably physically realistic in that multiple zones, each characterized by its own chemical conditions, are expected to develop in a contaminant plume.

Second, the model illustrates how inhibition functions can be used to switch between oxygen and nitrate limiting conditions. The inhibition factor multiplies the rate expressions for substrate utilization and microbial growth under nitrate metabolism. At high oxygen concentrations, this factor is nearly zero. As oxygen is depleted, the function approaches 1 and nitrate metabolism steadily increases. These type of inhibition functions can be used to model multiple microbial populations under multiple types of respiration or fermentation.

A key part of the model is the modeling of a stagnant liquid layer between the microcolony and the bulk fluid. A linear concentration profile across the diffusion layer is assumed and a mass transfer coefficient controls the chemical flux. The concentration of nutrients experienced by the microorganisms is less than the concentration of nutrients in the bulk fluid. The lower concentration tends to reduce the growth rate of biomass at the column inlet. However, the simulations were not run long enough to determine whether or not the reduced concentrations of nutrients in the microcolonies were sufficient to reach a steady-state biomass concentration below the maximum physically possible. The structure of the model does not limit unbridled growth of biomass.

5.2. Semprini and McCarty (1992)

The model of Semprini and McCarty (1992) demonstrates how a relatively simple model can accurately simulate a real contaminant plume. The one-dimensional model simulates the pulsing of methane and oxygen into an aquifer at the Moffet Field Naval Air Station to stimulate a methanotrophic culture into biodegrading chlorinated hydrocarbons by cometabolism. Key features of the model include:

- Biomass is modeled as a concentration.
- Biodegradation is inhibited by high primary substrate (methane) concentrations.
- First-order deactivation of the methanotrophic culture's biodegradation ability is simulated when it is decaying due to lack of oxygen or methane or both.
- Adsorption is modeled as a first-order non-equilibrium process.

5.2.1. Important assumptions

- Monod kinetics apply.
- Bacterial transport is not significant.
- A single bacterial species is present.
- Biodegradation is aerobic only.
- Cometabolism is assumed to follow Monod kinetics.
- Biodegradation rates are limited by either oxygen, methane, or both.

5.2.2. Validation

The model was used to simulate the cometabolism of vinyl chloride, *trans*-dichloroethylene, *cis*-dichloroethylene, and trichloroethylene between an injection well and two downgradient sampling wells. The solution containing these compounds was injected continuously into the aquifer until the concentrations at the sampling well were nearly equal to the concentrations at the injection well. Methane and oxygen were then pulsed into the aquifer to stimulate the methanotrophic population to begin biodegrading the contaminants. The main fitting parameter for the model was k_2, the TCE transformation rate constant. The model successfully simulated the oscillating concentrations of methane and the chlorinated contaminants at the sampling well.

5.2.3. Comments

This model illustrates the importance of accounting for inhibition when the primary substrate, products, or other substrates interfere with biodegradation of the compound of primary interest. Simulations of inhibition kinetics were compared to simulations where Monod kinetics without inhibition were used. Semprini and McCarty (1992) found that inhibition kinetics were necessary to accurately represent the methane and contaminant concentrations seen at the sampling wells.

This model is also one of only a few models that used non-equilibrium reactions to model adsorption and illustrates how adsorption can influence biodegradation predictions. Simulations using linear equilibrium adsorption did not match the data as well as simulations where rate-limited adsorption was included. Simulations using rate-limited adsorption correctly modeled the extensive tailing observed at the sampling wells, whereas equilibrium adsorption predicted more rapid declines in contaminant concentrations.

5.3. Chen et al. (1992)

Chen et al. (1992) present a model of considerably greater complexity than the two models discussed above. Most of the complexity comes from the fact that this model is a multi-phase model, accounting for four phases: solid, water, NAPL and air. The model accounts for mass exchange between these phases, two substrates, two electron acceptors, one additional limiting nutrient, and two microbial populations. Other chemicals can be added if necessary. The two substrates modeled are benzene and toluene, and the two electron acceptors are oxygen and nitrate. The model is applied to biodegradation of these chemicals in laboratory columns with only an aqueous phase present. Key features of the model include:

- Biomass is modeled as microcolonies with fully penetrated biofilms.
- A stagnant liquid film diffusion layer exists between the bulk fluid and the microcolonies.
- Inhibition functions switch from oxygen to nitrate respiration.

5.3.1. Important assumptions

- Local equilibrium exists for mass transfer between phases.
- Monod kinetics apply.
- Bacterial transport is insignificant.
- Biodegradation rates are limited by any substrate, electron acceptor, or nutrient.
- The air phase is immobile.
- Biodegradation occurs only in the aqueous phase.
- No adsorption occurs on particles exposed only to the air phase.
- One microbial population degrades only benzene, only aerobically.
- The second microbial population degrades only toluene either aerobically or anaerobically (with nitrate as the electron acceptor).

5.3.2. Validation

The model was validated in three ways. First, the model numerical solution for a conservative tracer was compared to the analytical solution of Ogata and Banks

(1961) for transport under steady-state flow conditions in a homogeneous, water-saturated, soil-packed column. Second, the model solutions were compared to the solutions obtained by Molz et al. (1986). Finally, simulated breakthrough curves were compared to breakthrough curves from laboratory experiments.

An attempt was made to measure all parameters independent of the experiments so that the model parameters represented physical quantities and not fitting parameters. Monod kinetic parameters were determined from aquifer slurry experiments, and other parameters were determined by experiments with the soil columns prior to the biodegradation experiments. The only parameter that was adjusted to provide a better fit to the data was the fraction of benzene and toluene degrading microorganisms in the reactor at the beginning of the experiments, since these proportions could not be determined prior to the experiment.

The columns were continuously fed a mixture containing substrate(s), electron acceptors and sufficient nutrients and the breakthrough curves of benzene and toluene were recorded. The breakthrough curves were successfully simulated by the model under substrate-limited aerobic conditions. The model successfully simulated the toluene breakthrough curve under nitrate-based respiration and oxygen-limited conditions, but did not simulate the benzene breakthrough curve well.

5.3.3. Comments

This model illustrates how multiple electron acceptors, nutrients, and microbial populations can be simulated. Although the model was not applied to a multiphase or three-dimensional modeling domain, the model equations are general so that modification of the model to account for this greater complexity is relatively straightforward. The model contains nearly all of the elements that are likely to be important in biodegradation modeling including inhibition kinetics, multiple nutrient/electron acceptor growth limitations, inhibition functions to switch between methods of substrate utilization, and diffusional resistances. This model forms a good basis on which to build for future modeling efforts.

5.4. Taylor and Jaffé (1990b)

One shortcoming of the three previous models is their inability to model bacterial transport and the effect of biomass growth on permeability, porosity and dispersivity. The model presented by Taylor and Jaffé (1990b, 1991) includes methods to account for these changes. The single-phase model is typical of models in the groundwater literature (as opposed to models in the petroleum literature) in the manner in which concentrations and phases are expressed. Taylor and Jaffé (1990b) used the model to simulate the growth and transport of bacteria in laboratory columns under conditions where only one nutrient (the substrate) was limiting. Taylor and Jaffé (1991) then used the model to investigate the effectiveness of different nutrient addition strategies during a simulation of in-situ bioremediation. Key features of the model include:

- Biomass is modeled as a separate phase (a fully penetrated biofilm).
- Biomass transport is modeled with an advection-dispersion equation.

- Biofilm removal is by shearing, and deposition is modeled as a first-order process.
- Porosity, permeability and dispersivity change with biomass growth.

5.4.1. Important assumptions
- Monod kinetics apply.
- Biodegradation rate is limited by a single substrate.
- No diffusional limitations exist.
- No adsorption of the substrate or microorganisms occurs.

5.4.2. Validation

Taylor and Jaffé compared the modeled biofilm thicknesses to observed biofilm thicknesses in an experimental reactor. Model parameters were determined from these laboratory experiments or literature sources. The model was calibrated by adjusting the dimensionless parameter describing the biological aspects of shearing appearing in the expression for biomass decay, and the depositional parameters that appear in the biomass deposition expression. The model was then used to predict substrate concentration profiles and biofilm thicknesses in a second laboratory column. The substrate profiles and biomass thicknesses were predicted well at early and late times, although the predictions at intermediate times were not as good.

5.4.3. Comments

This model is probably the most sophisticated model for predicting changes in the porous media from biomass growth. With the exception of the model of Corapcioglu and Haridas (1985), this model is the only one reviewed that treats biomass as a separate phase. It may be possible to incorporate the expressions used to model biomass growth and its effects on porous media into other models that are focused more on contaminant biodegradation.

5.5. Sarkar et al. (1994)

The model of Sarkar et al. (1994) is based on the sophisticated platform of the multi-component, multi-phase, three-dimensional model UTCHEM. The method of expressing concentration, particularly adsorbed phase concentrations, differs slightly from the models in the groundwater and soils literature. However, the results are the same. The primary purpose of the Sarkar et al. (1994) model is to simulate microbial-enhanced oil recovery (MEOR) processes. However, the flow principles are the same as those in multi-phase groundwater flow. The model is used to simulate bacteria and substrate effluent concentrations, as well as the changes in the permeability of the porous media, in laboratory columns. Bacterial growth is anaerobic with glucose as the substrate. Key features of the model include:
- Biomass is modeled as a concentration.
- Adsorption is modeled as a reversible process with a Langmuir isotherm.
- Transport and retention of bacteria are modeled with a fractional flow function.

- Permeability reduction is modeled using effective medium theory (EMT).
- Contois kinetics are used to model substrate utilization and biomass growth.
- Inhibition kinetics are used to model the effect of toxic metabolites on bacterial growth.

5.5.1. Important assumptions
- No diffusional resistances exist.
- Biodegradation rate is limited by one substrate.
- Biodegradation occurs only in the aqueous phase.
- Bacteria, nutrients and produced metabolites exist only in the aqueous phase.

5.5.2. Validation

Model simulations of effluent bacteria and glucose concentrations were compared to laboratory experiment effluent concentrations. Simulated permeability histories were also compared to laboratory experiments. Experiments were performed for both single-phase (water only--no NAPL) and multi-phase flow. Effluent bacteria concentrations were predicted by the model with good accuracy at low flow rates in single-phase flow. Predictions of effluent bacteria concentrations were not as good for higher flow rates. Effluent bacteria concentration simulations of the two-phase experiments was very good. Simulations of permeability reduction and effluent glucose concentration histories were also fairly good.

5.5.3. Comments

This model demonstrates how bacterial transport and multi-phase flow can be integrated into the same model. It also illustrates an alternative to the first-order removal process used to model bacterial deposition in the model of Taylor and Jaffé. Like the model of Chen et al. (1992), this model could also serve as a good platform for incorporation of other biodegradation processes, which could be important in predicting subsurface biodegradation.

6. Conclusions and recommended modeling approach

From the variety of approaches other researchers have taken to model subsurface biodegradation, it is apparent that much work remains before the process can be modeled with a high degree of accuracy in the field. However, our understanding of the processes has increased immeasurably over the last few years, and many models have been successful in simulating biodegradation in laboratory studies. These modeling efforts help identify the factors that are important in biodegradation modeling and suggest expanded approaches to model the phenomenon.

From the extensive review of biodegradation models and the related engineering principles completed for this report, it appears that a comprehensive model can be developed that incorporates the best aspects of the other models reviewed. A successful comprehensive model should:

1. Account for changes in porosity, permeability and dispersivity due to biomass growth.

2. Treat adsorption as a non-linear process.
3. Model multiple phases.
4. Account for reaeration from the surface through diffusion and/or infiltration.
5. Base biodegradation rates on local, not spatially averaged, concentrations.
6. Account for diffusion through a stagnant liquid layer adjacent to the biomass.
7. Model growth and decay of biomass as a separate phase.
8. Model multiple microbial populations.
9. Account for transport of microorganisms.
10. Allow different growth rates for free-floating and adsorbed bacteria.
11. Limit biomass growth to what is physically possible.
12. Include a lag phase for microorganisms to adapt to contamination.
13. Include inhibition kinetics if necessary.
14. Accommodate cometabolism.
15. Accommodate multiple substrates with substrate inhibition functions.
16. Model multiple electron acceptors.
17. Account for sequential reactions of substrates.
18. Track the concentration of all potential redox reaction participants.
19. Account for multiple nutrient limitations on biomass growth.
20. Model fermentative, anaerobic and aerobic metabolism simultaneously.

Also from the literature review, it appears that the following assumptions are reasonable:

1. The biophase is a fully penetrated biofilm (no intra-film diffusional limitations exist), except possibly at injection wells where substrate and electron acceptor concentrations are kept very high.
2. Biodegradation occurs only in the aqueous phase.
3. Diffusion across a stagnant liquid layer can be modeled by Fick's Law.
4. Biomass can be modeled with an unstructured, unsegregated approach.

Acknowledgements

Partial funding for this project was provided by the United States Environmental Protection Agency under contract number CR821897.

References

Abriola, L.M., 1989. Modeling multiphase migration of organic chemicals in groundwater systems—a review and assessment. Environ. Health Prospect., 83: 117–143.

Alvarez-Cohen, L. and McCarty, P.L., 1991. Product toxicity and cometabolic competitive inhibition modeling of chloroform and trichloroethylene transformation by methanotrophic resting cells. Appl. Environ. Microbiol., 57(4): 1031–1037.

Anderson, J.E. and McCarty, P.L., 1994. Model for treatment of trichloroethylene by methanotrophic biofilms. J. Environ. Eng., 120(2): 379–400

Angley, J.T., Brusseau, M.L., Miller, W.L., and Delfino, J.J., 1992. Nonequilibrium sorption and aerobic biodegradation of dissolved alkylbenzenes during transport in aquifer material: column experiments and evaluation of a coupled-process model. Environ. Sci. Technol., 26(7): 1404–1410.

Applegate, D.H. and Bryers, J.D., 1991. Effects of carbon and oxygen limitations and calcium concentrations on biofilm removal processes. Biotech. and Bioeng., 37: 17–25.

Atlas, R.M., 1981. Microbial degradation of petroleum hydrocarbons: an environmental perspective. Microbiol. Rev, 45(1): 180–209.

Bae, W., Odencrantz, J.E., Rittmann, B.E., and Valocchi, A.J., 1990. Transformation kinetics of trace-level halogenated organic contaminants in a biologically active zone induced by nitrate injection. J. Contam. Hydrol., 6: 53–68.

Baehr, A.L. and Corapcioglu, M.Y., 1987. A compositional multiphase model for groundwater contamination by petroleum products; 2. numerical solution. Water Resour. Res., 23(1): 201–213.

Bahr, J.M. and Rubin, J. 1987. Direct comparison of kinetic and local equilibrium formulations for solute transport affected by surface reactions. Water Resour. Res., 23(3): 438–452.

Bailey, J.E. and Ollis, D.F., 1986. Biochemical Engineering Fundamentals, 2nd ed., McGraw-Hill, New York, N.Y.

Baveye, P. and Valocchi, A., 1989. An evaluation of mathematical models of the transport of biologically reacting solutes in saturated soils and aquifers. Water Resour. Res., 25(6): 1413–1421.

Borden, R.C., 1993. Natural bioremediation of hydrocarbon-contaminated ground water. In: J.E. Mathews (Project Officer), Handbook of Bioremediation, Lewis Publishers, Boca Raton, F.L., pp. 177–199.

Borden, R.C. and Bedient, P.B., 1986. Transport of dissolved hydrocarbons influenced by oxygen-limited biodegradation; 1. theoretical development. Water Resour. Res., 22(13): 1973–1982.

Bouwer, E.J. and McCarty, P.L., 1984. Modeling of trace organics biotransformation in the subsurface. Ground Water, 22(4): 433–440.

Brock, T.D., Smith, D.W., and Madigan, M.T., 1984. Biology of Microorganisms, 4th ed., Prentice-Hall, Englewood Cliffs, N.J.

Brown, R., 1993. Treatment of petroleum hydrocarbons in ground water by air sparging. In: J.E. Mathews (Project Officer), Handbook of Bioremediation, Lewis Publishers, Boca Raton, F.L., pp. 61–85.

Brusseau, M.L., Jessup, R.E., and Rao, P.S.C. 1992. Modeling solute transport influenced by multiprocess nonequilibrium and transformation reactions. Water Resour. Res., 28(1): 175–182.

Camper, A.K., Hayes, J.T., Sturman, P.J., Jones, W.L., and Cunningham, A.B., 1993. Effects of motility and adsorption rate coefficient on transport of bacteria through saturated porous media. Appl. Environ. Microbiol., 59(10): 3455–3462.

Chang, M., Voice, T.C., and Criddle, C.S., 1993. Kinetics of competitive inhibition and cometabolism in the biodegradation of benzene, toluene and p-xylene by two pseudomonas isolates. Biotech. and Bioeng., 41: 1057–1065.

Chapelle, F.H., Ground-Water Microbiology and Geochemistry, John Wiley, New York, N.Y., 1993.

Chen, Y., Abriola, L.M., Alvarez, P.J.J., Anid, P.J., and Vogel, T.M., 1992. Modeling transport and biodegradation of benzene and toluene in sandy aquifer material: comparisons with experimental measurements. Water Resour. Res., 28(7): 1833–1847.

Chiang, C.Y., Salanitro, J.P., Chai, E.Y., Colthart, J.D., and Klein, C.L., 1989. Aerobic biodegradation of benzene, toluene, and xylene in a sandy aquifer—data analysis and computer modeling. Ground Water, 27(6): 823–834.

Chung, G., McCoy, B.J., and Scow, K.M., 1993. Criteria to assess when biodegradation is kinetically limited by intra-particle diffusion and sorption. Biotech. and Bioeng., 41: 625–632,.

Cohen, R.M. and Mercer, J.W., 1993. DNAPL Site Evaluation, CRC Press, Boca Raton, F.L.

Corapcioglu, M.Y. and Haridas, A. 1984. Transport and fate of microorganisms in porous media: a theoretical investigation. J. Hydrol., 72: 149–169.

Corapcioglu, M.Y. and Haridas, A. 1985. Microbial transport in soils and groundwater: a numerical model. Adv. Water Resour., 8: 188–200.

Corapcioglu, M.Y. and Baehr, A.L., 1987. A compositional multiphase model for groundwater contamination by petroleum products; 1. theoretical considerations. Water Resour. Res., 23(1): 191–200.

Corapcioglu, M.Y. and Hossain, M.A., 1990. Theoretical modeling of biodegradation and biotransformation of hydrocarbons in subsurface environments. J. Theor. Biol., 142: 503–516.

Corapcioglu, M.Y., Hossain, M.A., and Hossain, M.A., 1991. Methanogenic biotransformation of chlorinated hydrocarbons in ground water. J. Environ. Eng., 117(1): 47–65.

Corapcioglu, M.Y. and Jiang, S., 1993. Colloid-facilitated groundwater contaminant transport. Water Resour. Res., 29(7): 2215–2226.

Criddle, C.S., 1993. The kinetics of cometabolism. Biotech. and Bioeng., 41: 1048–1056.

Dibble, J.T. and Bartha, R., 1979. Effect of parameters on the biodegradation of oil sludge. Appl. Environ. Microbiol., 37(4): 729–739.

Environmental Protection Agency, 1993. In: J.E. Mathews (Project Officer), Handbook of Bioremediation, Lewis Publishers, Boca Raton, F.L., 1993.

Fetter, C.W., 1993. Contaminant Hydrology, MacMillan, New York, N.Y.

Focht, D.D., 1988. Performance of biodegradative microorganisms in soil: xenobiotic chemicals as unexploited metabolic niches. In: G.S. Omenn, (Editor), Environmental Biotechnology, Reducing Risks from Environmental Chemicals through Biotechnology. Plenum Press, New York, N.Y., pp. 15–29.

Fontes, D.E., Mills, A.L., Hornberger, G.M., and Herman, J.S., 1991. Physical and chemical factors influencing transport of microorganisms through porous media. Appl. Environ. Microbiol., 57(9): 2473–2481.

Freeze, R.A. and Cherry, J.A., 1979. Groundwater, Prentice-Hall, Englewood Cliffs, N.J.

Frind, E.O., Duynisveld, W.H.M., Strebel, O., and Boettcher, J., 1990. Modeling of multicomponent transport with microbial transformation in groundwater: the Fuhrberg case. Water Resour. Res., 26(8): 1707–1719.

Grady, C.P.L. Jr., 1990. Biodegradation of toxic organics: status and potential. J. Environ. Eng., 116(5): 805–829.

Han, K. and Levenspiel, O. 1988. Extended Monod kinetics for substrate, product and cell inhibition. Biotech. and Bioeng., 32(4): 430–437.

Harmon, T.C., Semprini, L., and Roberts, P.V., 1992. Simulating solute transport using laboratory-based sorption parameters. J. Environ. Eng., 118(5): 666–689.

Harvey, R.H., Smith, R.L., and George, L.H., 1984. Effect of organic contamination upon microorganism distributions and heterotrophic uptake in a Cape Cod, M.A., aquifer. Appl. Environ. Microbiol., 48(6): 1197–1202.

Harvey, R.W. and Garabedian, S.P., 1991. Use of colloid filtration theory in modeling movement of bacteria through a contaminated sandy aquifer. Environ. Sci. Technol., 25(1): 178–185.

Hornberger, G.M., Mills, A.L., and Herman, J.S., 1992. Bacterial transport in porous media: evaluation of a model using laboratory observations. Water Resour. Res., 28(3): 915–938.

Jenkins, M.B. and Lion, L.W., 1993. Mobile bacteria and transport of polynuclear aromatic hydrocarbons in porous media. Appl. Environ. Microbiol., 59(10): 3306–3313.

Kindred, J.S. and Celia, M.A., 1989. Contaminant transport and biodegradation; 2. conceptual model and test simulations. Water Resour. Res., 25(6): 1149–1159.

Kinzelbach, W. and W. Schäfer, 1991. Numerical modeling of natural and enhanced denitrification processes in aquifers. Water Resour. Res., 27(6): 1123–1135.

Kobayashi, H. and Rittmann, B.E., 1982. Microbial removal of hazardous compounds. Environ. Sci. Technol., 16(3): 170A–183A.

Lee, M.D., Thomas, J.M., Borden, R.C., Bedient, P.B., Ward, C.H., and Wilson, J.T., 1988. Biorestoration of aquifers contaminated with organic compounds. CRC Crit. Rev. Environ. Cont., 18(1): 29–89.

Lindqvist, R. and Bengtsson, G., 1991. Dispersal dynamics of groundwater bacteria. Microbial Ecol., 21: 49–72.

Lindqvist, R. and Enfield, C.G., 1992. Cell density and non-equilibrium sorption effects on bacterial dispersal in groundwater microcosms. Microbial Ecol., 24: 25–41.

Luong, J.H.T., 1987. Generalization of monod kinetics for analysis of growth data with substrate inhibition. Biotech. and Bioeng., 29: 242–248.

MacQuarrie, K.T.B., Sudicky, E.A., and Frind, E.O., 1990. Simulation of biodegradable organic contaminants in groundwater; 1. numerical formulation in principal directions. Water Resour. Res. 26(2): 207–222.

Malone, D.R., Kao, C., and Borden, R.C., 1993. Dissolution and biorestoration of nonaqueous phase

hydrocarbons: model development and laboratory evaluation. Water Resour. Res., 29(7): 2203–2213.

McCarty, P.L., 1988. Bioengineering issues related to in situ remediation of contaminated soils and groundwater. In: G.S. Omenn (Editor.), Environmental Biotechnology, Reducing Risks from Environmental Chemicals through Biotechnology Plenum Press, New York, N.Y., pp. 143–162.

McCarty, P.L. and Semprini, L., 1993. Ground-water treatment for chlorinated solvents. In: J.E. Mathews (Project Officer), Handbook of Bioremediation, Lewis Publishers, Boca Raton, F.L., pp. 87–116.

Metcalf and Eddy, Inc., 1991. Wastewater Engineering, 3rd ed., McGraw-Hill, New York, N.Y.

Molz, F.J., Widdowson, M.A., and Benefield, L.D., 1986. Simulation of microbial growth dynamics coupled to nutrient and oxygen transport in porous media. Water Resour. Res., 22(8): 1207–1216.

Odencrantz, J.E., Valocchi, A.J., and Rittmann, B.E., 1990. Modeling two-dimensional solute transport with different biodegradation kinetics. In: Proceedings of Petroleum Hydrocarbons and Organic Chemicals in Groundwater: Prevention, Detection, and Restoration, Houston, Texas, October 31–November 2, 1990.

Ogata, A. and Banks, R.B., 1961. A solution of the differential equation of longitudinal dispersion in porous media, U.S. Geological Survey Professional Paper *411*-A.

Pinder, G.F. and Abriola, L.M., 1986. On the simulation of nonaqueous phase organic compounds in the subsurface. Water Resour. Res., 22(9): 109S–119S.

Raven, K.G., Novakowski, K.S., and Papcevic, P.A., 1988. Interpretation of field tests of a single fracture using a transient solute storage model. Water Resour. Res., 24(12): 2019–2032.

Reinhard, M., 1993. In-situ bioremediation technologies for petroleum-derived hydrocarbons based on alternate electron acceptors (other than molecular oxygen). In: J.E. Mathews (Project Officer), Handbook of Bioremediation, Lewis Publishers, Boca Raton, F.L., pp. 131–147.

Rifai, H.S., Bedient, P.B., Wilson, J.T., Miller, K.M., and Armstrong, J.M., 1988. Biodegradation modeling at aviation fuel spill site. J. Environ. Eng., 114(5): 1007–1029.

Rifai, H.S., Bedient, P.B., 1990. Comparison of biodegradation kinetics with an instantaneous reaction model for groundwater. Water Resour. Res. 26(4): 637–645.

Rittmann, B.E. and McCarty, P.L., 1980. Model of steady-state-biofilm kinetics. Biotech. and Bioeng., 22: 2343–2357.

Rittmann, B.E. and McCarty, P.L., 1981. Substrate flux into biofilms of any thickness. J. Environ. Eng., 107: 831–849.

Rittmann, B.E., 1993. The significance of biofilms in porous media. Water Resour. Res., 29(7): 2195–2202.

Roels, J.A., 1983. Energetics and Kinetics in Biotechnology, Elsevier Biomedical Press, Amsterdam.

Sáez, P.B. and Rittmann, B.E., 1988. Improved pseudoanalytical solution for steady-state biofilm kinetics. Biotech. and Bioeng., 32: 379–385.

Sáez, P.B. and Rittmann, B.E., 1992. Accurate pseudoanalytical solution for steady-state biofilms. Biotech. and Bioeng. 39(7): 790–793.

Sarkar, A.K., 1992. Simulation of Microbial Enhanced Oil Recovery Processes, Ph.D. Dissertation, Univ. of Texas.

Sarkar, A.K., Georgiou, G., and Sharma, M.M., 1994. Transport of bacteria in porous media: II. a model for convective transport and growth. Biotech. and Bioeng., 44: 499–508.

Semprini, L. and McCarty, P.L., 1991. Comparison between model simulations and field results for in-situ biorestoration of chlorinated aliphatics: part 1. biostimulation of methanotrophic bacteria. Ground Water, 29(3): 365–374.

Semprini, L. and McCarty, P.L., 1992. Comparison between model simulations and field results for in-situ biorestoration of chlorinated aliphatics: part 2. cometabolic transformations. Ground Water, 30(1): 37–44.

Sharma, M.M. and Yortsos, Y.C., 1987. Transport of particulate suspensions in porous media: model formulation. AIChE J., 33(10): 1636–1643.

Sleep, B.E. and Sykes, J.F., 1993. Compositional simulation of groundwater contamination by organic compounds; 1. model development and verification. Water Resour. Res., 29(6): 1697–1708.

Speitel, G.E. Jr. and DiGiano, F.A., 1987. Mathematical modeling of bioregeneration in GAC columns. J. Environ. Eng., 113(1): 32–48.

Stewart, P.S., 1993. A model of biofilm detachment. Biotech. and Bioeng., 41: 111–117.

Suidan, M.T., Rittmann, B.E., and Traegner, U.K., 1987. Criteria establishing biofilm-kinetic types. Water Research, 21(4): 491–498.

Sykes, J.F., Soyupak, S., and Farquhar, G.J., 1982. Modeling of leachate organic migration and attenuation in groundwaters below sanitary landfills. Water Resour. Res., 18(1): 135–145.

Taylor, S.W. and Jaffé, P.R., 1990a. Biofilm growth and the related changes in the physical properties of a porous medium; 1. experimental investigation. Water Resour. Res., 26(9): 2153–2159.

Taylor, S.W. and Jaffé, P.R., 1990b. Substrate and biomass transport in a porous medium. Water Resour. Res., 26(9): 2181–2194.

Taylor, S.W. and Jaffé, P.R., 1991. Enhanced in-situ biodegradation and aquifer permeability reduction. J. Environ. Eng., 117(1): 25–46.

Teutsch, G., Herbold-Paschke, Tougianidou, D., Hahn, T., and Botzenhart, K. 1991. Transport of microorganisms in the underground—processes, experiments and simulation models. Water Sci. Technol. 24(2): 309–314.

Valocchi, A.J., 1985. Validity of the local equilibrium assumption for modeling sorbing solute transport through homogeneous soils. Water Resour. Res., 21(6): 808–820.

van Genuchten, M.T. and Alves, W.J., 1982. Analytical solution of the one-dimensional convection-dispersion solute transport equation, U.S. Depart. Agric. Tech. Bull. *1161*, 151 pp.

Vogel, T.M. and McCarty, P.L., 1985. Biotransformation of tetrachloroethylene to trichloroethylene, dichloroethylene, vinyl chloride, and carbon dioxide under methanogenic conditions. Appl. Environ. Microbiol., 49(5): 1080–1083.

Vogel, T.M., Criddle, C.S., and McCarty, P.L., 1987. Transformations of halogenated aliphatic compounds. Environ. Sci. Technol., 21(8): 722–736.

Vogel, T.M., 1993. Natural bioremediation of chlorinated solvents. In: J.E. Mathews (Project Officer), Handbook of Bioremediation, Lewis Publishers, Boca Raton, F.L., pp. 201–225.

Weber, W.J., 1972. Physiochemical Processes for Water Quality Control, John Wiley, New York, N.Y.

Widdowson, M.A., Molz, F.J., and Benefield, L.D., 1988. A numerical transport model for oxygen- and nitrate-based respiration linked to substrate and nutrient availability in porous media. Water Resour. Res., 24(9): 1553–1565.

Widdowson, M.A., 1991. Comment on "An evaluation of numerical models of the transport of biologically reacting solutes in saturated soils and aquifers," by Philippe Baveye and Albert Valocchi. Water Resour. Res., 27(6): 1375–1378.

Wood, B.D., Dawson, C.N., Szecsody, J.E., and Streile, G.P., 1994. Modeling contaminant transport and biodegradation in a layered porous media system. Water Resour. Res. 30(6): 1833–1845.

Yates, M.V. and Yates, S.R., 1988. Modeling microbial fate in the subsurface environment. CRC Crit. Rev Environ. Cont., 17(4): 307–345.

Chapter 2

Flow of non-Newtonian fluids in porous media

YU-SHU WU and KARSTEN PRUESS

Abstract

Flow of non-Newtonian fluids through porous media occurs in many subsurface systems and has found applications in certain technological areas. Previous studies of the flow of fluids through porous media were focusing for the most part on Newtonian fluids. Since the 1950s, the flow of non-Newtonian fluids through porous media has received a significant amount of attention because of its important industrial applications, and considerable progress has been made. However, our understanding of non-Newtonian flow in porous media is very limited when compared with that of Newtonian flow. This work presents a comprehensive theoretical study of single and multiple phase flow of non-Newtonian fluids through porous media. The emphasis in this study is in obtaining some physical insights into the flow of power-law and Bingham fluids. Therefore, this work is divided into three parts: (1) review of the laboratory and theoretical research on non-Newtonian flow, (2) development of new numerical and analytical solutions, (3) theoretical studies of transient flow of non-Newtonian fluids in porous media, and (4) demonstration of applying a new method of well test analysis and displacement efficiency evaluation to field problems.

1. Introduction

1.1. Background

Flow of non-Newtonian fluids through porous media occurs in many subsurface systems and has found applications in certain technological areas. Previous studies on the flow of fluids through porous media were limited for the most part to Newtonian fluids (Muskat, 1946; Collins, 1961; and Scheidegger, 1974). Since the 1950s, the flow of non-Newtonian fluids through porous media has received a significant amount of attention because of its important industrial applications. In the applications related to the petroleum industry, non-Newtonian fluids, especially polymer solutions, microemulsions, and foam, are often injected into reservoirs in various enhanced oil recovery (EOR) processes. The use of polymers in water flooding can yield significant increases in oil recovery when compared with conventional water flood methods in certain reservoirs. Therefore, polymer flood-

ing is the most commonly used EOR technique of chemical flooding in the petroleum industry (Dauben and Menzie, 1967; Mungan, et al., 1966; Gogarty, 1967; Harvey and Menzie, 1970; and van Poollen, 1980). The flow of polymer solutions through porous media generally behaves like a power-law non-Newtonian fluid (Savins, 1969; Gogarty; 1967; and Christopher and Middleman; 1965).

There is considerable evidence that the flow behavior of heavy oil is non-Newtonian and may be approximated by that of a Bingham plastic fluid. A large amount of heavy oil reservoirs have been found and developed worldwide. The non-Newtonian behavior of heavy oil flow in these oil reservoirs have been reported in the petroleum literature (Barenblatt et al., 1984; Kasraie et al., 1989). Laboratory rheological and filtration experiments and field tests in a number of oil fields have shown that flow of heavy oil often takes place only after the applied pressure or potential gradient exceeds a certain minimum value (Mirzadjanzade et al., 1971). The flow of heavy oil in porous media does not follow Darcy's law; and some authors explain this phenomenon as a lower limit of Darcy's law. The presence of a minimum pressure or potential gradient usually results in a large decrease in oil recovery. Similar phenomena have been also found in gas fields of argillaceous reservoirs with interstitial water present by Mirzadjanzade et al. (1971). There exists a threshold gas pressure gradient before gas moves, and the magnitude of the threshold pressure gradient depends on water content in pore space, decreasing as the water content decreases.

The existence of a threshold hydraulic gradient has also been observed for certain groundwater flow problems in saturated clay soils, or strongly argillized rocks. When the applied hydraulic gradient is below some minimum value, there is very little flow. This phenomenon has been attributed to the rheological non-Newtonian behavior caused by clay-water interactions (Bear, 1972). Mitchell (1976) discussed a number of mechanisms that may be responsible for the deviations of water flow through clays from that predicted by Darcy's law.

The flow of foam in porous media is a focus of current research in many fields. Foam has been shown to be one of the most promising fluids for mobility control in underground energy recovery and subsurface storage projects. When flowing through porous media, foam is a discontinuous fluid, comprised of gas bubbles separated by thin liquid lamellae. The flow and behavior of foam in permeable media involve complex gas-liquid-solid interactions on the pore level, which are not completely understood at the present time. However, considerable progress has been made in recent years, and many experimental and theoretical studies of foam flow in porous media have contributed significantly to our understanding of the physics of foam transport in porous media (Witherspoon et al. 1989; Hirasaki and Lawson, 1985; Falls et al., 1986; Ransohoff and Radke 1986). On a continuum macroscopic scale, non-Newtonian flow behavior of foam through porous materials has been referred to by all the researchers in this area. The power-law is generally used to correlate apparent viscosities of foam with other flow properties for a given porous medium and a given surfactant (Hirasaki and Lawson, 1985; Patton et al. 1983). It has also been observed experimentally that foam will start to flow in a porous medium only after the applied pressure gradient exceeds a certain threshold value (Albrecht and Marsden, 1970; and Witherspoon et al., 1989).

Drilling and hydraulic fracturing fluids used in the oil industry are usually non-Newtonian liquids. Therefore during well drilling or hydraulic fracturing operations, the non-Newtonian drilling muds or hydraulic fluids will infiltrate into permeable formations surrounding the wellbore, which may seriously damage the formation. The rheological behavior of drilling muds, cement slurries and hydraulic fracturing fluids is often described by a Bingham plastic or a power-law model (Cloud and Clark, 1985; Shah, 1982; Robertson et al., 1976; and Iyoho and Azar, 1981). The importance of flow of non-Newtonian fluids from the wellbore into the surrounding formations has been recognized in the industry. Some techniques have been developed and used to remove drilling muds or fracturing agents from the borehole and the adjacent formation (Coulter et al., 1987).

1.2. Non-Newtonian fluids

In contrast with classical fluid mechanics developed for Newtonian fluids, the theory of non-Newtonian fluid dynamics is a relatively new branch of applied sciences. The increasing importance of non-Newtonian fluids has been recognized in those fields dealing with materials, whose flow behavior of stress and shear rate can not be characterized by Newton's law of viscosity (Skelland, 1967; Bohme, 1987; Astarita and Marrucci, 1974; and Crochet et al., 1984). Therefore, non-Newtonian fluid mechanics is being developed. In a broad sense, fluids are divided into two main categories: (1) Newtonian and (2) non-Newtonian. Newtonian fluids follow Newton's law of viscous resistance and possess a constant viscosity. Non-Newtonian fluids deviate from Newton's law of viscosity, and exhibit variable viscosity. The behavior of non-Newtonian fluids is generally represented by a rheological model, or correlation of shear stress and shear rate. Examples of substances which exhibit non-Newtonian behavior include solutions and melts of high molecular weight polymers, suspensions of solids in liquids, emulsions, and materials possessing both viscous and elastic properties. There are many rheological models available for different non-Newtonian fluids in the literature (Skelland, 1967; Savins, 1969; Bird et al., 1960). Scheidegger (1974) gave a very comprehensive summary of rheological equations of various non-Newtonian fluids in porous media. The present review focuses only on those non-Newtonian fluids which are commonly encountered in porous media. The major attention here is directed to the rheological properties of flow systems of interest in studies of non-Newtonian flow through porous media.

For a Newtonian fluid, the shear stress τ is linearly related to the shear rate by *Newton's law of viscosity* (Bird et al., 1960) as,

$$\tau = -\mu\dot{\gamma} \tag{1.1}$$

where the coefficient μ is defined as dynamic viscosity of the fluid.

According to the relationships between shear stress and shear rate, non-Newtonian fluids are commonly grouped in three general classes (Skelland, 1967): (1) time-independent non-Newtonian fluids, (2) time-dependent non-Newtonian fluids, and (3) viscoelastic non-Newtonian fluids.

1. *Time-independent fluids* are those for which the rate of shear, or the velocity

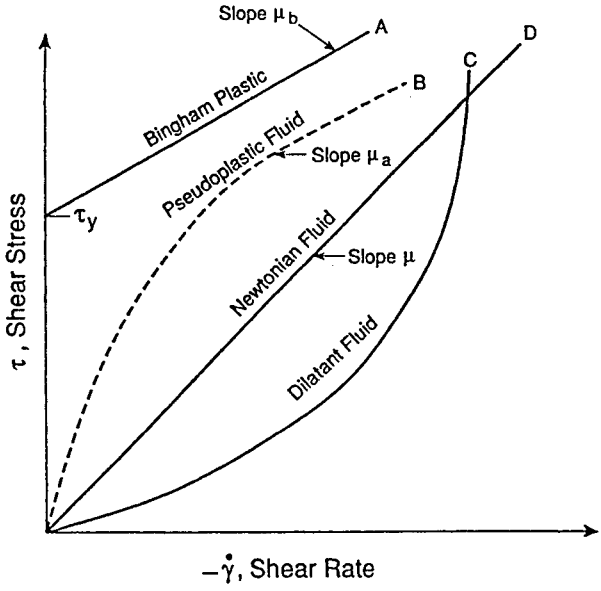


Fig. 1. Typical shear stress and shear rate relationships for non-Newtonian fluids (after Hughes and Brighton, 1967).

gradient, is a unique but non-linear function of the instantaneous shear stress τ at that point. For the time-independent fluid, the relationship is

$$\dot{\gamma} = f(\tau)$$

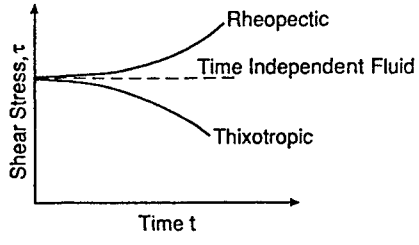
The time-independent non-Newtonian fluids can be characterized by the flow curves of τ versus $\dot{\gamma}$, as shown in Fig. 1. These are: (a) Bingham plastics, curve A, (b) pseudoplastic fluids (shear thinning), curve B, and (c) dilatant fluids (shear thickening), curve C.

2. *Time-dependent fluids* have more complex shear stress and shear rate relationships. In these fluids, the shear rate depends not only on the shear stress, but also on shearing time, or on the previous shear stress rate history of the fluid. These materials are usually classified into two groups, thixotropic fluids and rheopectic fluids, depending upon whether the shear stress decreases or increases in time at a given shear rate and under constant temperature. Typical curves of the time-dependent behavior of non-Newtonian fluids are shown in Fig. 2.

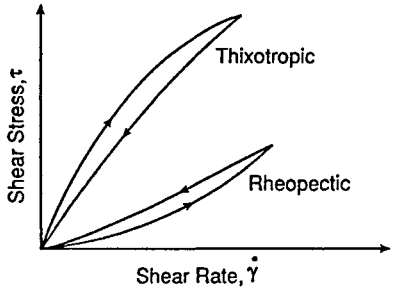
3. *A viscoelastic material* exhibits both elastic and viscous properties, and shows partial recovery upon the removal of the deformable shear stress. The rheological properties of such a substance at any instant will be a function of the recent history of the material and can not be described by relationships between shear stress and shear rate alone, but will require inclusion of the time derivative of both quantities.

One of the mechanical models, first proposed by Maxwell (Skelland, 1967) for viscoelastic fluids, is

$$\tau = \mu \frac{d\dot{\gamma}}{dt} - \frac{\mu}{\lambda} \frac{d\tau}{dt} \tag{1.2}$$



(a) Behavior of non-Newtonian fluids-under a given shear rate.



(b) Behavior of non-Newtonian fluids-shearing -history dependence.

Fig. 2. Flow curves for time-dependent thixotropic and rheopectic non-Newtonian fluids (after Bear, 1972; Skelland, 1967).

where μ is viscosity, and λ is a rigidity modulus. Liquids which obey this law are known as Maxwell liquids. Another mechanical model is referred to as the Voigt model, which characterizes the rheological performance by the relationship

$$\tau = \mu \frac{d\dot{\gamma}}{dt} + \lambda \dot{\gamma} \tag{1.3}$$

The rheological behavior of real viscoelastic fluids has been represented with some success by more or less complex combinations of generalized Maxwell and Voigt models, consisting of Maxwell or Voigt model units connected in series or in parallel.

For flow through porous media, the time-independent non-Newtonian fluids have been used almost exclusively in both experimental and theoretical studies (Savins, 1969). However, there do exist some examples for the flow of the viscoelastic non-Newtonian fluids through porous media (Sadowski, 1965; and Wissler, 1971). The effect of time-dependent non-Newtonian fluids on flow behavior in porous media have been virtually neglected in all previous investigations.

Among the most common time-independent non-Newtonian fluids (Scheidegger, 1974; Bear, 1972), Bingham plastics exhibit a finite yield stress at zero shear rate. The physical behavior of fluids with a yield stress is usually explained

in terms of an internal structure in three dimensions which is capable of preventing movement when the values of shear stress are less than the yield value, τ_y, as shown in Fig. 1. For shear stress, τ, larger than τ_y, the internal structure collapses completely, allowing shear movement to occur. The characteristics of these fluids are defined by two constants: the yield stress τ_y, which is the stress that must be exceeded for flow to begin, and the Bingham plastic viscosity μ_b, which is the slope of the straight line portion of curve A in Fig. 1. The rheological equation for a Bingham plastic is then

$$\tau = \tau_y - \mu_b \dot{\gamma} \tag{1.4}$$

The Bingham plastic concept has been found to closely approximate many real fluids existing in porous media, such as heavy tarry and paraffin oils (Barenblatt et al., 1984; Mirzadjanzade et al. 1971), and drilling muds and fracturing fluids (Hughes and Brighton, 1967), which are suspensions of finely divided solids in liquids.

To date the power-law, or the Ostwald-de Waele model (Bird et al., 1960), is the most widely used rheological model for flow problems in porous media. The power law model has been successfully applied to describe the flow behavior of polymer and foam solutions by a number of authors (Christopher and Middleman, 1965; McKinley et al., 1966; Gogarty, 1967; Harvey and Menzie, 1970, Mungan, 1972; Hirasaki and Pope, 1974; and others). Originally formulated from an empirical curve-fitting function, the power law is represented by

$$\tau = -H\dot{\gamma}^n \tag{1.5}$$

where n is the power-law index; and H is called the consistence coefficient. For $n = 1$, the fluid becomes Newtonian. A fluid which obeys equation (1.5) is called a power-law fluid. Because of its inherent simplicity, the power-law is of considerable interest in applications and is used to approximate the rheological behavior of both shear-thinning or pseudoplastic ($n < 1$) and shear-thickening or dilatant ($n > 1$) fluids over a large range of flow conditions.

Comparing equation (1.5) with Newton's law of viscosity, equation (1.1), we see that such a fluid exhibits an apparent viscosity μ_a of the form

$$\mu_a = H\dot{\gamma}^{n-1} \tag{1.6}$$

For most power-law fluids, the power-law index n is less than 1.0, and so the apparent viscosity μ_a decreases with increasing shear rate $\dot{\gamma}$. The shear-thinning behavior, which amounts to a monotonic decrease in apparent viscosity with increasing shear rate, is readily observed in the flow of polymer and foam solutions, moderately concentrated suspensions, and biological fluids.

Physically, when the fluid is at rest, fluid dispersions of asymmetric molecules or particles are probably characterized by an extensive entanglement of the particles. Progressive disentanglement should occur under the influence of shearing forces, and the particles will tend to orient themselves in the direction of shearing. This orienting effect is proportional to the shear rate and is opposed by the randomly disorienting Brownian movement. Pseudoplastic behavior should also be consistent with the existence of highly solvated molecules or particles in dispersion. Progres-

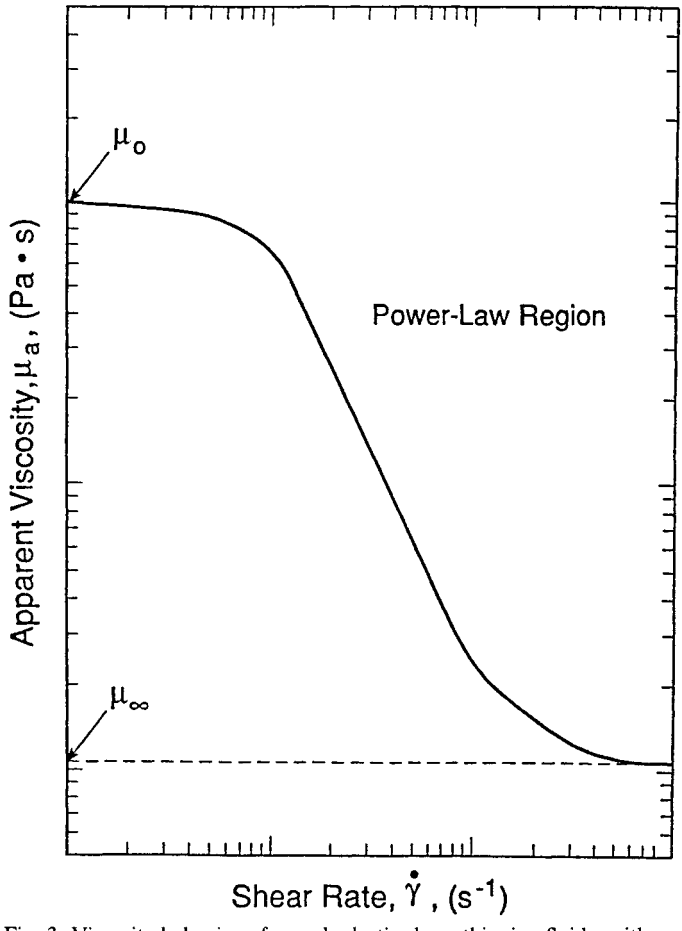


Fig. 3. Viscosity behavior of pseudoplastic shear-thinning fluids, with maximum and minimum limiting viscosities.

sive shearing away of solvated layers with increasing shear rate would result in decreasing interactions between the molecules or particles and a consequent reduction in apparent viscosity.

Although the power-law equation accurately portrays the behavior of a large number of non-Newtonian fluids over a wide range of shear rate or velocity gradients, some fluids exhibit more complex behavior. In addition, at both very low and very high velocity gradients, most fluids appear to exhibit Newtonian behavior with constant viscosities μ_0 and μ_∞, respectively, as shown in Fig. 3. Complete orientation at high shear rate and complete disorientation at very low shear rate should account for the observed Newtonian behavior in these regions. The power law predicts an infinite viscosity at vanishingly small velocity gradients.

In order to describe the entire viscosity curve, a more complex expression than the power-law model, equation (1.5), is needed. One of the numerous proposed expressions is the extended Williamson model (Fahien, 1983)

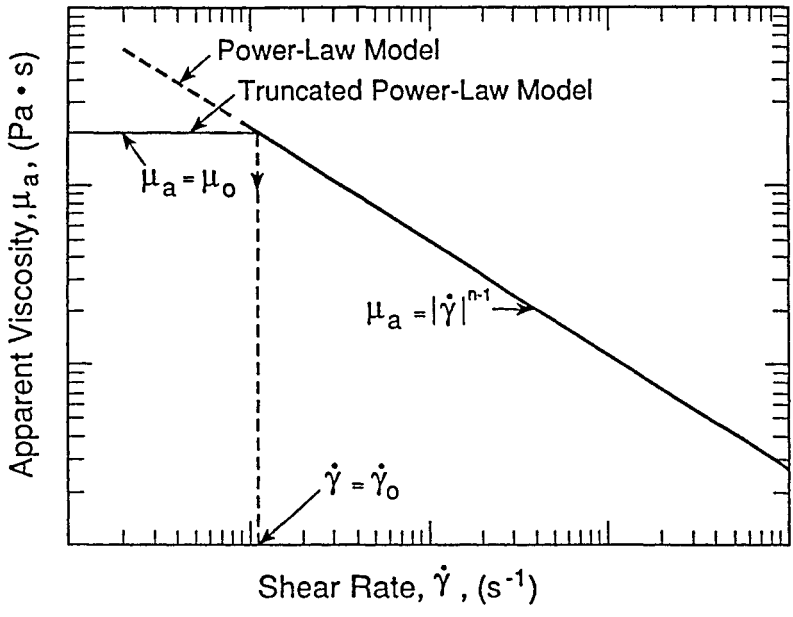


Fig. 4. Viscosity behavior of the truncated power-law model (after Vongvuthipornchai and Raghavan, 1987a).

$$\mu_a = \mu_\infty + \frac{\mu_0 - \mu_\infty}{1 + (\dot{\gamma}/\alpha_1)^{\alpha_2}} \tag{1.7}$$

where α_1 and α_2 are constants. For low and high values of shear rate $\dot{\gamma}$, equation (1.7) yields $\mu_a \to \mu_0$ and $\mu_a \to \mu_\infty$, respectively.

A similar correlation of the apparent viscosity for polymer solutions was proposed by Meter (Meter and Bird, 1964)

$$\mu_a = \mu_\infty + \frac{\mu_0 - \mu_\infty}{1 + (\tau/\tau_m)^{\alpha-1}} \tag{1.8}$$

where α and τ_m are constants. Equation (1.8) has been used to investigate flow problems of polymer solutions in porous media (Lake, 1987; and Camilleri et al., 1987).

One simple relationship for describing the viscosity of a power-law fluid is called the truncated power-law model (Bird, 1965)

$$\mu_a = \mu_0 \qquad \text{for} \qquad |\dot{\gamma}| \leq |\dot{\gamma}_0| \tag{1.9}$$

and

$$\mu_a = H|\dot{\gamma}|^{n-1} \qquad \text{for} \qquad |\dot{\gamma}| > |\dot{\gamma}_0| \tag{1.10}$$

Figure 4 presents the apparent viscosity as a function of shear rate for the truncated power-law model. This model was used by Vongvuthipornchai and Raghavan (1987a) in their numerical studies of the pressure falloff behavior of power-law fluid flow in a vertically fractured well.

The power law is also called a two parameter model (Bird et al., 1960), since it is characterized by the two parameters, H and n. In order that the power-law relationship be of engineering value, it is necessary for H and n to remain constant over considerable ranges of shear rate. In the general case, H and n may vary continuously with shear rate. Then, a logarithmic form of the power law should be used (Skelland, 1967), instead of equation (1.5). However, many published laboratory studies of polymer solution flow in porous media reveal that it is a reasonable assumption to take H and n as constants.

Shear thickening behavior has been observed with dilatant materials, although these materials are far less common than pseudoplastic fluids. Volumetric dilatancy denotes an increase in total volume under shearing, whereas rheological dilatancy refers to an increase in apparent viscosity with increasing shear rate. A number of mechanisms proposed to explain the shear thickening phenomena were summarized by Savins (1969). The shear thickening behavior is of particular interest in connection with non-Newtonian flow through porous media because certain dilute polymeric solutions exhibit a shear thickening response under appropriate conditions of flow, even though they show shear thinning behavior in viscometric flow. This general type of behavior has been reported in porous media flow experiments involving a variety of dilute to moderately concentrated solutions of high-molecular-weight polymers. In the case when the power-law model applies, the power-law index $n > 1$ generates a monotonically increasing shear thickening response. However, the shear thickening or dilatant phenomena may be the most controversial and least understood rheological behavior of non-Newtonian fluids.

The approaches available for rheological data analysis and characterization of non-Newtonian systems are: (1) the integration method, (2) the differentiation method (Savins, Wallick and Foster, 1962a; 1962b; 1962c), and (3) the dual differentiation-integration method (Savins, 1962). However, only the integration technique is of interest in porous media flow problems. The integral method consists of interpreting flow properties in terms of a particular model. The rheological parameters appear, on integrating, in an expression relating the pairs of observable quantities, such as volume flux and pressure. Many theoretical correlations of non-Newtonian fluid flow through porous media are based on capillary models. Consider steady laminar upward flow of a time-independent fluid through a vertical cylindrical tube with a radius R. The volumetric flow rate, Q, is (Skelland, 1967)

$$\frac{Q}{\pi R^3} = \frac{1}{\tau_w^3} \int_0^{\tau_w} \tau_{rx}^2 f(\tau_{rx}) d\tau_{rx} \tag{1.11}$$

where τ_w shear stress at the tube wall; and $f(\tau_{rx})$ is the rheological function, depending on the rheological model of the fluid; and τ_{rx} is the shear stress, given by

$$\tau_{rx} = \frac{r\Delta P}{2L} \tag{1.12}$$

With an appropriate rheological function $f(\tau_{rx})$, as summarized by Savins (1962),

equation (2.11) relates the volumetric flow rate through a capillary and the shear stress on the wall of many useful fluids, such as Bingham plastic and power-law fluids.

1.3. Laboratory experiment and rheological models

Many studies on the flow of non-Newtonian fluids in porous media exist in the chemical engineering, rheology, and petroleum engineering from the early 1960s. Because of the complexity of pore geometries in a porous medium, Darcy's law has to be used to obtain any meaningful insights into the physics of flow in porous media. Some equivalent or apparent viscosities for non-Newtonian fluid flow are needed in the Darcy equation. Therefore, a lot of experimental and theoretical investigations have been conducted to find rheological models, or correlations of apparent viscosities with flow properties for a given non-Newtonian fluid as well as a given porous material. The viscosity of a non-Newtonian fluid depends upon the shear rate, or the velocity gradient. However, it is impossible to determine the distribution of the shear rate in a microscopic sense in a porous medium, and the rheological models developed in fluid mechanics for non-Newtonian fluids cannot be applied directly to porous media. Hence, many laboratory studies were undertaken in an attempt to relate the rheological properties of a non-Newtonian fluid to the pore flow velocity of the fluid or the imposed pressure drop in a real core or in a packed porous medium.

The viscosity used in Darcy's equation for non-Newtonian fluids depends on, (1) rheological properties of the fluids, (2) characteristics of the porous medium, and (3) shear rate. Empirical attempts to establish correlations between the various dynamic properties of porous media need to introduce certain additional parameters. Theoretical considerations may be able to identify the physical significance of these parameters. The simplest theoretical models that can be constructed for a porous medium are those consisting of capillaries. The capillary model, in which the porous medium is represented by a bundle of straight, parallel capillaries of uniform diameters, was used to derive a flow equation, the modified Darcy's law for non-Newtonian fluid flow through porous media. Under steady-state and laminar flow conditions, the momentum flux distribution in the radial direction within the capillary is first solved from the conservation of momentum. Then, by introducing a special rheological model for the non-Newtonian fluid in the momentum distribution and integrating in the radial direction, one obtains the total flow rate through the capillary. By comparing the expression for the total flow rate with Darcy's law, one can deduce a modified Darcy's law with an apparent viscosity for the special non-Newtonian fluid. The resulting equations usually involve some coefficients that need to be determined by experiments for a given fluid in a given porous medium.

In a pioneering work, Christopher and Middleman (1965) developed a modified Blake-Kozeny equation for a power-law, non-Newtonian fluid with laminar flow through packed porous media. Their theory was based on a capillary model and the Blake-Kozeny equation of permeability, and it was tested by experiment with the flow of dilute polymer solutions through packed porous material. They claimed

that the accuracy of their correlation was probably acceptable for most engineering design purposes. The modified Blake-Kozeny equation is

$$u = \left(\frac{K}{\mu_{\text{eff}}}\frac{\Delta P}{L}\right)^{1/n} \tag{1.13}$$

where u is the Darcy's velocity; K is absolute permeability; $\Delta P/L$ is the pressure gradient; and μ_{eff} is given as

$$\mu_{\text{eff}} = \frac{H}{12}\left(9 + \frac{3}{n}\right)^{n} (150K\phi)^{(1-n)/2} \tag{1.14}$$

with ϕ being the porosity. Note that μ_{eff} does not have the units of viscosity. Christopher and Middleman also derived an expression for average shear rate for a power law fluid in porous media as

$$\dot{\gamma}_a = \frac{3n+1}{4n}\frac{12u}{(150K\phi)^{1/2}} \tag{1.15}$$

In order to use equations (1.13) and (1.15), one must measure the absolute permeability K with a Newtonian fluid, measure the porosity ϕ, and determine the rheological parameters, n and H. Bird, Stewart and Lightfoot (1960) presented a similar model to equation (1.13), except that it includes a factor of $(25/12)^{n-1}$.

Polymer solutions seem to exhibit the same general behavior with regard to the non-Newtonian apparent viscosity μ_a as a function of shear stress τ. In the limit of very small shear stress, the viscosity approaches a lower shear rate maximum value μ_0. With increasing shear stress the viscosity μ_a decreases, and if the shear stress can be increased sufficiently the viscosity reaches its upper shear rate minimum constant value, μ_∞. Hence, μ_0 and μ_∞ are measurable quantities characteristic of the fluid. A four-parameter model, equation (1.8), was proposed by Meter (Meter and Bird, 1964) to describe the more realistic shear-thinning behavior of polymer solutions. Meter and Bird (1964) presented a practical procedure to determine the four parameters in equation (1.8) by fitting experimental non-Newtonian viscosity. The curve-fitting results appeared quite satisfactory.

Sadowski and Bird (1965) conducted a systematic study on non-Newtonian flow through porous media. They used a non-Newtonian viscosity μ_a in an empirical curve-fitting Ellis function, given by

$$\frac{1}{\mu_a} = \left(\frac{1}{\mu_0}\right)\left(1 + \left[\frac{\tau}{\tau_{1/2}}\right]^{\alpha-1}\right) \tag{1.16}$$

where μ_0 is zero-shear viscosity, $\tau_{1/2}$ is the shear stress at which μ_a has dropped to $\frac{1}{2}\mu_0$, and α characterizes the slope of log μ_a vs. log $\tau_{1/2}$ in the "power-law" region. The three parameters μ_0, $\tau_{1/2}$, and α can be obtained by a graphical approach to the viscosity curve. By using the Blake-Kozeny-Carman equation of permeability and the capillary model, they were able to derive a modified Darcy's law as

$$u = \frac{K}{\mu_a}\frac{\Delta P}{L} \tag{1.17}$$

where the apparent or effective viscosity is defined by

$$\frac{1}{\mu_a} = \frac{1}{\mu_0}\left(1 + \frac{1}{\alpha + 3}\left[\frac{\tau_{Rh}}{\tau_{1/2}}\right]^{\alpha - 1}\right) \tag{1.18}$$

with $\tau_{Rh} = (\Delta P/L)[D_p\phi/6(1 - \phi)]$, and D_p is the particle diameter.

In an experimental study of flow in porous media using fourteen different polymer solutions, Sadowski (1965) found that the shear-sensitive viscosities of these fluids were characterized by the three-parameter Ellis model (2.16). The modified Darcy's law (1.17) was used successfully to correlate the constant volumetric flow rate to the rheological properties for polymer solutions with low and medium molecular weight. Sadowski also pointed out that the results depended on the experimental procedure. If the flow rate of the fluid passing through the packed bed was held constant, the observed results were both steady and reversible. If the pressure drop across the packed bed was held constant, for very small or very large polymer solution concentrations, the observed results were unsteady and irreversible. The explanation for the unsteady and irreversible flow behavior observed for constant pressure drop was that polymer adsorption and gel formation occurred throughout the bed.

Another modified form of Darcy's law for calculating non-Newtonian fluid flow in porous media was obtained by McKinley et al. (1966) as

$$\mathbf{u} = -F(\tau)\frac{K}{\mu_0}\nabla P \tag{1.19}$$

where μ_0 is the apparent viscosity at some convenient reference stress τ_0. The dimensionless viscosity ratio, $F(\tau)$, is defined as

$$F(\tau) = \frac{\mu_0}{\mu(\tau)} \tag{1.20}$$

Here the shear stress τ is given by

$$\tau = \alpha_0\left(\frac{K}{\phi}\right)^{1/2}|\nabla P| \tag{1.21}$$

The constant α_0 and the dimensionless viscosity ratio $F(\tau)$ are determined experimentally from capillary measurements for a given type of rock and a given fluid. This model was developed by direct analogy with the flow through a uniform capillary and was confirmed experimentally by the authors.

A universal equation for the prediction of the average velocity in the flow of non-Newtonian fluids through packed beds and porous media was proposed by Kozicki et al. (1967). This general average velocity-pressure gradient relationship was also based on the Blake-Kozeny equation and the capillary model, and was confirmed experimentally for various non-Newtonian fluids. The modification of

Darcy's law is expressed in terms of the flow potential gradient $\nabla\Phi$ and the apparent viscosity μ_a, as

$$\mathbf{u} = -\frac{K}{\mu_a}\nabla\Phi \tag{1.22}$$

for zero "slip" velocity on the pore wall. The apparent viscosity is defined as

$$\mu_a = \frac{\tau_w^{1+\xi}}{(1+\xi)\displaystyle\int_{\tau_y T}^{\tau_w} \frac{\tau^{\xi}}{\mu}\,d\tau} \tag{1.23}$$

where τ_w is the shear stress at the wall, ξ is a dimensionless aspect factor, τ_y is the yield stress, T is the tortuosity of the porous medium, and μ is the viscosity of the non-Newtonian fluid as a function of shear stress. In reducing the general expressions (1.22) and (1.23) to specific situations, the authors set the aspect factor $\xi = 3$ to arrive at results in agreement with the available experimental data.

An in-depth laboratory study of the rheological adsorption and oil displacement characteristics of polymer solutions was reported by Mungan et al. (1966). One of the most important contributions to the understanding of the rheological behavior of non-Newtonian fluid flow through porous media was made by Gogarty (1967a, 1967b). By using a number of real cores and consolidated porous media in experiments, he correlated the rheological and flow data to obtain a useful relationship for shear rate and pore velocity in porous material. The average shear rate $\dot{\gamma}_a$ is defined as a ratio of the pore velocity and a characteristic length for the porous medium, and it is then modified by an exponent y

$$\dot{\gamma}_a = \left(\frac{Bu}{f(K)(K/\phi)^{1/2}}\right)^{y} \tag{1.24}$$

where B is a constant determined from experiments. The exponent y accounts for the possible deviation between the slope of the apparent viscosity-shear rate curve from a capillary viscometer experiment, and the slope of the corresponding curve for the same fluid, but determined from an experiment with the porous medium. The function $f(K)$ is a linear function of the logarithm of the permeability,

$$f(K) = m\log(K/K_r) + p \tag{1.25}$$

Here the constants m and p depend on the fluid type in a given kind of rock; and K_r is some reference permeability.

Gogarty proved experimentally that the apparent viscosity for use in the Darcy's equation was a function only of the shear rate, as defined by equation (1.24)

$$\mu_a = F(\dot{\gamma}_a) \tag{1.26}$$

This rheological model was found to fit data for fluids whose character changed rapidly with shear rate from Newtonian to non-Newtonian. Flow experiments were performed with permeabilities in the range from 0.069 darcy through 0.425 darcy, and porosities in the range from 17 through 21.7%.

In contrast with the above work dealing with one-dimensional flow, Benis (1968) presented a theory to consider non-Newtonian fluid flow through two-dimensional narrow channels. The equations were solved numerically for the case of a power-law fluid. This method may be interesting for flow problems in fractured reservoirs.

Viscoelastic effects for non-Newtonian flow in porous media were observed and studied by Wissler (1971). He used a third-order perturbation technique to analyze the flow of a viscoelastic fluid in a converging-diverging channel and concluded that the actual pressure gradient would exceed the purely viscous gradient by a certain factor. The modified Darcy's law for a visco-inelastic, power-law fluid can then be used.

An important experimental study on flow of polymer solutions through porous media was reported by Dauben and Menzie (1967). They observed that the apparent viscosities of polyethylene oxide solutions under certain conditions were much higher than would be predicted from solution viscosity measurements. These polymer solutions exhibited dilatant behavior in porous media in contrast with the pseudoplastic behavior in simple flow systems. Glass bead packs were used as the porous material. The shear rate they derived is

$$\dot{\gamma} = \frac{12(2)^{1/2} v_p (L - \phi)}{D_p \phi} \tag{1.27}$$

where v_p is the pore velocity of flow, L is the spacing of the parallel plate instrument, and D_p is the diameter of the glass beads.

Harvey and Menzie (1970) developed a method for investigating the flow through unconsolidated porous media of high molecular weight polymer solutions. By introducing the "pseudo Reynolds number" and the "effective particle diameter," they successfully analyzed experimental data for three different polymer solutions. From experiments conducted over a period of years under reservoir flow conditions, Jennings et al. (1971) found that viscoelastic behavior also contributed to the mobility control activity of some polymers. Complex flow behavior of viscoelastic fluids can result in very large flow resistances at high flow rates in porous media. However, viscoelastic flow is not significant under reservoir flow conditions.

Mungan (1972) tested three partially hydrolized polyacrylamide polymers under experimental conditions and observed that the polymers exhibited pseudoplastic behavior over an eight-order-magnitude range of shear rates. The correlation for shear rate that he used is

$$\dot{\gamma} = \frac{3n' + 1}{4n'} \cdot \frac{4v_p}{R} \tag{1.28}$$

where R is the radius of the equivalent capillary of the porous medium, n' is the slope of the log-log plot of shear stress τ vs. $4v_p/R$. All of Mungan's experimental data show that the apparent viscosity of the polymers is a function solely of the shear rate defined in equation (1.28).

A detailed analysis of factors influencing mobility and adsorption in the flow

of polymer solutions through porous media was provided by Hirasaki and Pope (1974). The pseudoplastic behavior was modeled with the modified Blake-Kozeny equation for the power-law fluid, and the apparent viscosity was defined as

$$\mu_a = H\dot{\gamma}^{n-1} \tag{1.29}$$

where the shear rate is given by

$$\dot{\gamma} = \left(\frac{3n+1}{4n}\right)^{n/(n-1)} \frac{12u}{(150k\phi)^{1/2}} \tag{1.30}$$

A model to include dilatant behavior in the modified Blake-Kozeny equation was given as

$$\mu_a = \frac{\mu_{eff} u^{n-1}}{(1-\theta_f u/[(1-\phi)(150k/\phi)^{1/2}])} \tag{1.31}$$

where μ_{eff} defined in equation (1.14), and θ_f is the fluid relaxation time.

A new experimental technique was recently developed by Cohen and Christ (1986) for determining mobility reduction as a result of polymer adsorption in the flow of polymer solutions through porous media. The experimental data were analyzed by correlating mobility with fluid shear stress, τ_w, at the pore wall, under adsorbing and non-adsorbing conditions. Among many investigations conducted on the flow of polymer solutions in porous media, one of the most extensive studies was presented by Sorbie et al. (1987). They used both experimental and theoretical approaches to look at adsorption, dispersion, inaccessible-volume effects, and non-Newtonian behavior as well.

1.4. Analysis of flow through porous media

The subject of transient flow of non-Newtonian fluids in porous media is relatively new to many applications. Almost all of the analytical and numerical investigations have focused on the one-dimensional flow of single-phase power-law fluids. One of the first papers in this area was published by van Poollen and Jargon (1969), in which they derived an equation that described the flow of a power-law non-Newtonian fluid in porous media. An analytical solution for steady state flow was obtained, and the unsteady-state flow was studied by a finite difference model. They found that drawdown curves for a power-law fluid did not exhibit the semi-log straight-line relationship that exists for Newtonian fluid flow in a homogeneous medium. A number of transient well tests were used to examine the theory.

Patton et al. (1971) presented an analytical solution to the linear polymer flood problem and also a numerical model utilizing a stream tube approach that could be used to simulate linear or five-spot polymer floods. However, the effects of non-Newtonian behavior were neglected. A more comprehensive three-phase and three-dimensional finite difference numerical code for polymer flooding was developed by Bondor et al. (1972). This code represented the polymer solution as a fourth component fully miscible with the aqueous phase, in addition to the three

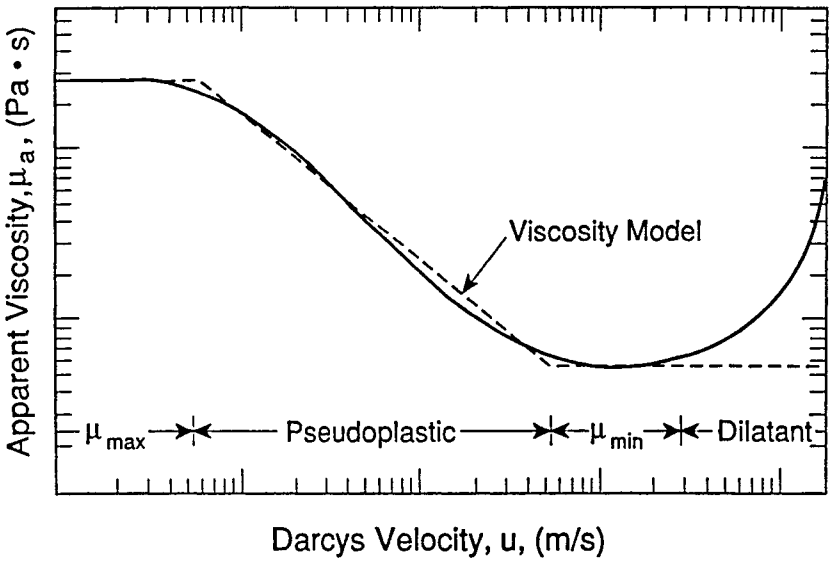


Fig. 5. Rheological behavior of polymer solution in porous media (after Bondor et. al., 1972).

other components, oil, water and gas. The rheological behavior of the polymer solution was included in the code by extending the modified Blake-Kozeny model to the multiphase flow problem. The apparent viscosity μ_a was modeled as that similar to the Meter model (1.8). As shown in Fig. 5 the formulation is

$$\mu_a = \begin{cases} \mu_{max}, & \text{low velocities} \\ \mu_{eff} u^{n-1}, & \text{pseudoplastic region} \\ \mu_{min}, & \text{high velocities} \end{cases} \tag{1.32}$$

where the coefficient μ_{eff} is also given by equation (1.14). However, to take into account the effects of multiphase flow, the permeability and porosity are replaced by an effective permeability to water phase, (Kk_{rw}), and an effective porosity (ϕS_w), respectively. Here k_{rw} is the relative permeability to water, and S_w is the saturation of the water phase. This simulator also incorporated the adsorption of polymer, the reduction of rock permeability to the aqueous phase, and the dispersion of the polymer plug. The result was shown to represent the displacement as observed in a physical experiment.

Pressure transient theory of flow of non-Newtonian power-law fluids in porous media was developed by Odeh and Yang (1979) and Ikoku and Ramey (1979). They simultaneously derived a partial differential equation for flow of power-law fluids through porous media using similar linearization procedures to the non-linear flow equation, and obtained approximate analytical solutions. Then, new well test analysis techniques were proposed for interpreting pressure data observed during injectivity and falloff tests in reservoirs. A limitation of this theory arises from the assumption used to linearize the governing equation, which requires

$$\left(-\frac{\partial P}{\partial r}\right)^{1/n} \approx \left[\frac{\mu_{\text{eff}}}{K}\right]^{1/n} \frac{Q}{2\pi rh} \tag{1.33}$$

where Q is the volumetric injection rate; and h is the thickness of formation. This is equivalent to assuming that the flow rate is constant at each radial location and that a steady-state viscosity profile exists. It has been shown numerically that this solution introduces significant errors by Vongvuthipornchai and Raghavan (1987a) when the power-law index $n < 0.6$. Generally, the linearized solution can not be used for pressure falloff test analysis when the power-law index $n < 0.5$.

In another paper, Ikoku and Ramey (1980) extended their theory to include wellbore storage and skin effects using a numerical wellbore storage simulator. Pressure responses with storage and skin effects were obtained in terms of Duhamel's integral, which was solved numerically. This work was extended by Vongvuthipornchai and Raghavan (1987b). They developed an approximate analytical solution in the Laplace domain, and a long-time asymptotic solution in the real domain for this problem. The solution in the Laplace domain was evaluated by a numerical inversion technique (Stehfest, 1970), and was used to examine pressure falloff behavior dominated by storage and skin effects.

The linearized governing equation derived by Odeh and Yang (1979) for a power-law fluid was solved by McDonald (1979) using a finite difference model. He found that very fine grids were needed for power-law flow calculations, and the coarser meshes led to unacceptable truncation errors.

Pressure transient behavior during non-Newtonian power-law fluid and Newtonian fluid displacement has also been studied using numerical methods. Lund and Ikoku (1981) applied the partial differential equation for radial flow of power-law fluids by Ikoku and Ramey (1979) to non-Newtonian and Newtonian fluids in composite reservoirs. The non-Newtonian fluid was injected to displace the Newtonian fluid under a piston-like displacement process. Polymer flooding projects are usually characterized by composite systems with moving banks of different fluids surrounding injection wells. Theory and analysis including a moving displacement front are more realistic than single-phase flow solutions. The well testing method of Ikoku and Ramey was extended to multiphase flow of non-Newtonian and Newtonian fluids by Gencer and Ikoku (1984). They used a numerical model to investigate the pressure behavior of power-law fluids during two-phase flow and gave an example for analysis of simulated injectivity and falloff test data.

A detailed numerical study of the flow of non-Newtonian power-law fluids in a vertically fractured well was reported by Vongvuthipornchai and Raghavan (1987a). They presented a new numerical analysis technique for fractured well tests, and also examined the general pressure falloff behavior in unfractured wells after the injection of non-Newtonian power-law fluids.

A more sophisticated numerical simulator of compositional micellar/polymer flow was developed by Camilleri et al. (1987a). This model took into account many important process properties, such as polymer inaccessible pore volume, permeability reduction, adsorption, residual saturations, relative permeability, phase, and non-Newtonian behavior as well. The phase behavior was modeled by

four pseudocomponents: surfactant, alcohol, oil, and brine (Camilleri et al., 1987b). The polymer apparent viscosity was calculated from the Meter model, and the shear rate equation used was equation (1.36) from the work of Hirasaki and Pope (1974). This new phase behavior code was used to match many simulated and experimental data, and satisfactory results were obtained (Camilleri et al., 1987c). The success of closely matching experimental phase concentration histories showed that this code provided a good description of the physical processes occurring during the displacement of oil by surfactant.

Compared with studies conducted on flow of non-Newtonian power-law fluids, there are not many publications dealing with flow problems in porous media involving non-Newtonian Bingham fluids (Barenblatt et al., 1984; Scheidegger, 1974). However, it has long been observed in heavy oil development and in laboratory experiments that there exists a minimum pressure gradient for heavy oil to start flow (Mirzadjanzade et al., 1971). Similar phenomena occur when groundwater flows in strongly argillized rocks and in clay soils (Bear, 1972). In such cases, the formulation of Darcy's law has been modified as

$$\mathbf{u} = -\frac{K}{\mu_b}\left(1 - \frac{G}{|\nabla P|}\right)\nabla P \qquad |\nabla P| > G \tag{1.34a}$$

$$\mathbf{u} = 0 \qquad |\nabla P| \leq G \tag{1.34b}$$

where G is the minimum pressure gradient. The physical meaning of G can be found by considering flow of a Bingham fluid through a capillary with radius R. Then, the Bingham equation was solved by Buckingham (Scheidegger, 1974; Skelland, 1967) to give the average flow velocity over the cross-section of the tube. By comparing this velocity with the result from Darcy's law, we can obtain

$$G = \frac{\tau_y}{3R/8} = \frac{\tau_y}{d} \tag{1.35}$$

where d is a characteristic pore size of a porous medium, $d = 3R/8$. Therefore, physically, the minimum pressure gradient G is the pressure gradient corresponding to the yield stress τ_y in a porous medium.

1.5. Summary

To date considerable progress has been made in understanding the flow behavior of non-Newtonian fluids through porous media. The experimental and theoretical studies performed in this field have focused on single-phase flow behavior. Solutions for single-phase non-Newtonian fluid flow are very useful in providing fundamentals for well testing analysis techniques, which are widely used in petroleum reservoir engineering and groundwater hydrology to determine reservoir and fluid properties. The main goals of the laboratory investigations are to correlate rheological properties with flow conditions for a particular non-Newtonian fluid within a given porous medium. An apparent viscosity is needed in Darcy's equation for further study of the flow behavior. The general procedure in the experimental studies is to find a relationship between the most important

physical quantities, such as shear rate, shear stress, and pressure gradient for the fluid of interest. This is normally done by using a capillary model to approximate the porous system. The remaining unknown parameters are left to be determined from flow experiments. The primary objectives of the theoretical studies are to develop well testing analysis methods for field applications. Based on theoretical pressure responses calculated from analytical or numerical solutions, the transient pressure analysis methods developed for non-Newtonian flow will permit approximate estimations of fluid and formation properties by matching observed pressure responses from wells.

Despite considerable advances over the past three decades in studying the flow of non-Newtonian fluids through porous media, it is obvious that further studies are still needed in understanding the physics of non-Newtonian flow in a complicated porous system. It has been well-documented that pseudoplastic fluids exhibit Newtonian behavior at high and low velocities. Even for single-phase non-Newtonian fluids, few theoretical investigations including such complicated phenomena have been published that are based on the more realistic rheological model of Meter, equation (1.8). The flow behavior of pseudoplastic fluids in porous media is still poorly understood. Also there are no techniques or theories available for analysis of non-Newtonian flow behavior in a fractured porous system. However, many underground formations for energy recovery or for waste storage have been found to be naturally fractured reservoirs.

At present, there are few standard approaches in the petroleum engineering or groundwater literature for analyzing well test data for Bingham-type fluids. Interpretation of transient pressure responses with Bingham flow in porous media will be very important for heavy oil development, for groundwater flow evaluation in certain clay formations, and for foam flow analysis. A thorough study of Bingham-type fluid flow in reservoir conditions is needed not only for engineering applications, but also for the physical insights of transport behavior.

Non-Newtonian and Newtonian fluid immiscible displacement occurs in many EOR processes. These operations involve the injection of non-Newtonian fluids, such as polymer and foam solutions, or heavy oil production by waterflooding. However, very little research has been published on multiple phase flow of both non-Newtonian and Newtonian fluids in porous media, and the only analytical solutions available for such flow are based on piston-like displacement assumptions (Pascal, 1984; Pascal et. al., 1988; and Chen and Liu, 1991). Even using numerical methods, very few studies have been performed to look at the physics of displacement. As a result, the mechanisms of immiscible displacement involving non-Newtonian fluids is still not well understood. Until we are able to predict how immiscible flow is affected by the properties of non-Newtonian fluids, it seems unlikely that a realistic theoretical model can be developed to describe the complex problems when such fluids are present.

It should be pointed out that non-Newtonian behavior is only one important factor that affects the flow of these fluids through porous media. There are many other factors which also have effects on the flow behavior. These include adsorption on pore surfaces of rock, dispersion, inaccessible pore volume, viscous fingering, and lithology of the formation of interest, etc. A complete understanding of

the flow behavior of non-Newtonian fluids in porous media with consideration of all these physical phenomena will be possible only after much more theoretical and experimental studies have been performed.

2. Rheological model

The *rheological model or condition* is the connection between shear stress and shear rate in the fluid (and their time derivatives). For flow in porous media, the rheological model usually refers to the correlation of apparent viscosities of a non-Newtonian fluid and flow conditions for a given porous material. For an incompressible Newtonian fluid, Newton's law defining the dynamic viscosity μ is generalized to the following form (Savins, 1962; Fahien, 1983)

$$\underline{\tau} = -2\mu \underline{D} \tag{2.1}$$

where $\underline{\tau}$ is the stress tensor and $\underline{D}$ is the "rate-of-strain" tensor, or "rate-of-deformation" tensor. It is defined as

$$\underline{D} = \frac{1}{2}(\nabla \mathbf{V} + \nabla \mathbf{V}^{\mathrm{T}}) \tag{2.2}$$

or

$$D_{ij} = \frac{1}{2}\left(\frac{\partial v_i}{\partial x_j} + \frac{\partial v_j}{\partial x_i}\right) \tag{2.3}$$

where $\nabla \mathbf{V}$ is the velocity gradient, and D_{ij} is the (i, j) component of the tensor $\underline{D}$ $(i, j = 1, 2, 3)$, $\nabla \mathbf{V}^{\mathrm{T}}$ is the transpose of $\nabla \mathbf{V}$, and v_i is the component of vector $\mathbf{V}_i$ in the x_i direction $(x_1 = x, x_2 = y, x_3 = z)$. The ijth component of tensor $\nabla \mathbf{V}$ is given by

$$(\nabla \mathbf{V})_{ij} = \frac{\partial v_i}{\partial x_j} \tag{2.4}$$

For an incompressible non-Newtonian fluid, termed as the generalized Newtonian fluid in fluid mechanics (Astarita and Marrucci; 1974), Newton's law of viscosity can be modified to read

$$\underline{\tau} = -2\mu_{\mathrm{a}}(s)\underline{D} \tag{2.5}$$

where μ_{a} is an apparent or effective viscosity which varies with the velocity gradient function s, which is defined as

$$s = 2\sum_i \sum_j D_{ij} D_{ji} \tag{2.6}$$

Several forms of the $\mu_{\mathrm{a}}(s)$ function in equation (2.5) have been proposed in the literature and are widely used in flow calculations. Among the rheological models for non-Newtonian fluids, only the power-law and Bingham models have been extensively used in research on porous media flow problems.

In this study, Darcy's law is assumed to be applicable to describe the flow of non-Newtonian fluids in porous media, in the form

$$\mathbf{u} = -\frac{K}{\mu_{nn}}\nabla\Phi \tag{2.7}$$

where the non-Newtonian behavior is taken into account by the apparent viscosity μ_{nn}, and the flow potential Φ is defined as (Narasimhan, 1982; and Hubbert, 1956)

$$\Phi = \rho_{nn}\left(\int_{P_0}^{P}\frac{dP}{\rho_{nn}(P)} - zg\right) \tag{2.8}$$

where P_0 is a reference pressure; and the positive z-direction is chosen to be downward in the Cartesian coordinates (x, y, z).

Since theoretical and experimental considerations of non-Newtonian flow are based on an analysis of the microscopic properties of flow, we need to use the concept of "pore velocity". The pore velocity is defined to represent the "real" flow velocity along flow channels. However, it is physically meaningful only in an average or statistical sense because the actual velocity of the fluid will change within one flow channel and from one flow channel to another. In practice, it is generally assumed the porous medium is isotropic as far as the distribution of the porosity over the section is concerned. A commonly accepted hypothesis for the connection between pore velocity $\boldsymbol{\nu}_p$ and Darcy's velocity $\mathbf{u}$ is the Dupuit-Forchheimer assumption (Scheidegger, 1974; Marsily, 1986)

$$\boldsymbol{\nu}_p = \frac{\mathbf{u}}{\phi} = -\frac{K}{\mu_{nn}\phi}\nabla\Phi \tag{2.9}$$

By definition, the viscosity of a non-Newtonian fluid is a function of the shear rate. For single-phase flow of non-Newtonian fluids through porous media, it has been shown experimentally that shear rate depends only on the pore velocity for a given porous material and the particular fluid used (Gogarty, 1967; Savins, 1969; Hirasaki and Pope, 1974). For simplicity in the analytical and numerical solutions, it is better to correlate the non-Newtonian viscosity directly to the flow potential gradient. For single phase flow problems through porous media, the flow potential has been traditionally used as the primary dependent variable from its easily-measurable property. If we also want to use the potential as a primary variable in study of a non-Newtonian flow problem, it is logical to express all the other dependent variables in terms of functions of the flow potential and flow potential gradient. Non-Newtonian viscosities in a flow system change with the pore velocity, and the pore velocity changes accordingly with flow potential gradient, which is described by the Dupuit-Forchheimer formulation, equation (2.9) and Darcy's law, equation (2.7). Therefore, the treatment of non-Newtonian viscosities as functions of flow potential gradient will become necessary in the development of the calculable numerical and analytical solutions of Non-Newtonian fluid flow in porous media. Specifically, it would be extremely difficult to relate viscosity of a

Bingham fluid with pore velocity in a flow study from equation (1.34). This treatment can be verified to be valid by representing the pore velocity v_p by equation (2.9) as follows

$$\mu_{nn} = f(v_p) = f\left(-\frac{K}{\mu_{nn}\phi} \nabla\Phi \right)$$

This equation implicitly states that the apparent viscosity used in Darcy's law for a non-Newtonian fluid is a function of the potential gradient only. Therefore, it is assumed in this work that the apparent viscosity μ_{nn} in the modified Darcy's equation (2.7) depends only on the potential gradient for the flow system under consideration

$$\mu_{nn} = \mu_{nn}(\nabla\Phi) \tag{2.10}$$

For flow of a power-law fluid in porous media, a comparison of equation (1.13) with equation (2.7) leads to the following explicit relationship

$$\mu_{nn} = \mu_{eff}\left(\frac{K}{\mu_{eff}}|\nabla\Phi|\right)^{(n-1)/n} \tag{2.11}$$

where μ_{eff} is defined in equation (1.14).

If the four-parameter model by Meter (Meter and Bird, 1964) is used to describe the rheological behavior of shear-thinning fluids, one may choose the shear rate in a form (Hirasaki and Pope, 1974)

$$\dot{\gamma} = \left(\frac{3n+1}{4n}\right)^{n/(n-1)} \left(\frac{4K|\nabla\Phi|}{\phi\mu_{nn}[8K/\phi]^{1/2}}\right) \tag{2.12}$$

Using equation (2.12) in the Meter model (1.8) will result in (Camilleri et al., 1987a)

$$\mu_{nn} = \mu_\infty + \frac{\mu_0 - \mu_\infty}{1 + (\dot{\gamma}/\dot{\gamma}_{1/2})^{\beta-1}} \tag{2.13}$$

where the constants μ_0, μ_∞, and $\dot{\gamma}_{1/2}$ are defined in equations (1.7) and (1.8), and the constant β may be different from α in equation (1.8). Then, equation (2.13) gives an implicit expression for the viscosity μ_{nn} as a function of the potential gradient in the Meter model.

For purposes of numerical simulation, the flow of Bingham fluids is best represented by a constant viscosity and a threshold pressure gradient, as in equation (1.34). However, formally it is also possible to treat Bingham fluids as having a $|\nabla\Phi|$ dependent viscosity, which will be used to evaluate the analytical solution for immiscible displacement in this study. From Darcy's law (1.34), we have

$$\mu_{nn} = \frac{\mu_b}{1 - G/|\nabla\Phi|}, \qquad \text{for } |\nabla\Phi| > G \tag{2.14a}$$

and

$$\mu_{nn} = \infty, \qquad \text{for } |\nabla\Phi| \leq G \tag{2.14b}$$

where G is the minimum potential gradient. Flow takes place only after the applied potential gradient exceeds the value of G.

Similarly, many viscosity functions can be derived in terms of the potential gradient from rheological models available in the literature for flow of non-Newtonian fluids in porous media, such as those given by Scheidegger (1974).

All the viscosity models discussed above for non-Newtonian fluids were obtained originally from an analysis of experimental data or from the capillary analog for a porous medium, and they are valid only for single phase flow in porous media. The interest of this work is not only in single phase flow, but also in multiple phase flow. Therefore, the previously modified versions of Darcy's law for single non-Newtonian fluids are extended to include the effects of multiple phase flow on the viscosity of non-Newtonian fluids. The permeabilities, which are constants for single phase non-Newtonian fluid flow, may become functions of other dependent variables, such as saturation, from the inherent complexities of multiple phase flow. Since the viscosity of a non-Newtonian fluid is a flow property, it depends on the shear rate among other parameters for the multiphase flow case. Physically, it is reasonable to assume that the shear rate of a non-Newtonian fluid in multiple phase flow is also a function of the pore velocity of that fluid only for a given fluid and a given porous medium, based on the results for single phase non-Newtonian flow. The average shear rate, or pore velocity, during multiple phase flow in a porous medium is determined by the local potential gradient in the direction of flow and also by the local saturation of the flowing phase. Hence, the apparent viscosity of non-Newtonian fluids for multiple phase flow is supposed to be a function of both flow potential gradient and saturation. For a given porous medium in the study, this may be expressed by

$$\mu_{nn} = \mu_{nn}(\nabla\Phi, S_{nn}) \tag{2.15}$$

This correlation should be obtained from experiments with non-Newtonian multiple phase flow where relative permeability and capillary pressure are known. A simpler way to find the dependence of viscosity on flow potential gradient and saturation may be to modify the viscosity function that is available for the single phase non-Newtonian fluid (Gencer and Ikuko, 1984; and Bondor et al., 1972). In this method, the corresponding permeability for single phase flow is replaced by the effective permeability (Kk_{rnn}), and porosity by (ϕS_{nn}) in the single phase viscosity function.

3. Mathematical model

3.1. Introduction

Conservation of mass, momentum and energy governs the behavior of fluid flow through porous media. The physical laws at the pore level in a porous medium are simple and well-known. In practice, however, only the global behavior of the

system is of interest. Due to the complexity of pore geometries, the macroscopic behavior is not easily deduced from that on the pore level. Any attempts to directly apply the Navier-Stokes equation to flow problems in porous media will face the difficulties of poorly-defined pore geometries and the complex phenomena of physical and chemical interactions between fluids or between fluids and solids, which cannot be solved at the present time. Therefore, the macroscopic continuum approach has been used prevalently both theoretically and in applications. Almost all theories on flow phenomena occurring in porous media lead to macroscopic laws applicable to a finite volume of the system under consideration whose dimensions are large compared with those of pores. Consequently, these laws lead to equations in which the medium is treated as if it were continuous and characterized by the local values of a certain number of parameters defined for all points.

The physical laws governing equilibrium and flow of several fluids in a porous medium are represented mathematically on the macroscopic level by a set of partial differential equations, which generally are non-linear when multiple phase or non-Newtonian fluids are involved. Solutions of the governing differential equations can often be obtained only by numerical methods. Under very special circumstances with appropriate idealizations, analytical solutions may be possible, such as in the case of the Buckley-Leverett solution for a linear waterflood situation.

The governing equations used for non-Newtonian and Newtonian fluid flow in this study are similar to those of multiple phase flow in porous media, and Darcy's law is assumed to be valid and modified to include the effects of the rheological properties of non-Newtonian fluids on flow behavior. In the present work, the flow system is assumed to be isothermal, so that the energy conservation equation is not required.

3.2. Governing equations for non-Newtonian and Newtonian fluid flow

Consider an arbitrary volume V_n of a porous medium with porosity ϕ, filled with a Newtonian fluid of density ρ_{ne} and a non-Newtonian fluid of density ρ_{nn}, bounded by surface S (Fig. 6). It is assumed that the non-Newtonian and Newtonian fluids are immiscible, and no mass transfer occurs between the two phases. The formal development and notations used here for the governing equations follow the work in the "TOUGH User's Guide" by Pruess (1987). The law of conservation of mass for each fluid states that the sum of the net fluxes crossing the boundary plus the generation rate of the mass of the fluid must be equal to the rate of the mass accumulated in the domain for the fluid, in an integral form

$$\frac{d}{dt}\int_{V_n}\int\int M_\beta \, dV = -\int_S\int \mathbf{F}_\beta \cdot \mathbf{n} \, dS + \int_{V_n}\int\int q_\beta \, dV \tag{3.1}$$

Where for Newtonian fluid β = ne, for non-Newtonian fluid β = nn, $\mathbf{n}$ is the unit outward normal vector on surface S, and q_β is source terms for fluid β. The mass accumulation terms M_β for Newtonian and non-Newtonian fluids (β = ne, nn) are

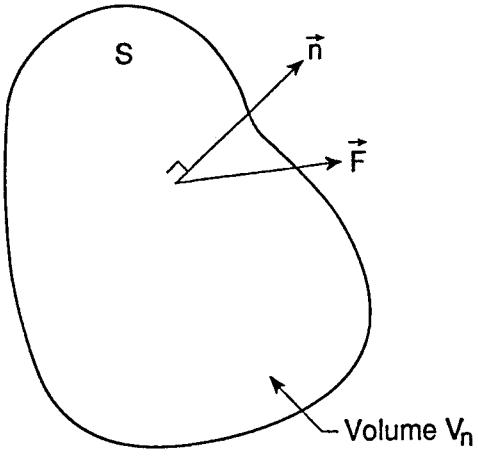


Fig. 6. Arbitrary volume of formation in a flow field bounded by surface S.

$$M_\beta = \phi S_\beta \rho_\beta \tag{3.2}$$

where S_β is the saturation of phase β (β = ne, nn), and ρ_β is density of phase β (β = ne, nn).

The mass flux terms $\mathbf{F}_\beta$ in equation (3.1) are described by Darcy's law for Newtonian and non-Newtonian fluids as

$$\mathbf{F}_\beta = -K \frac{k_{r\beta}}{\mu_\beta} \rho_\beta (\nabla P_\beta - \rho_\beta \mathbf{g}) \tag{3.3}$$

where K is absolute permeability, $k_{r\beta}$ is relative permeability to phase β, μ_β is dynamic viscosity of phase β, P_β is pressure in phase β, and $\mathbf{g}$ is gravitational acceleration.

Upon applying the Gauss theorem to equation (3.1), the surface integral on the right side of equation (4.1) can be transformed into a volume integral

$$\frac{d}{dt} \int\int\int_{V_n} M_\beta \, dV = \int\int\int_{V_n} (-\operatorname{div} \mathbf{F}_\beta + q_\beta) dV \tag{3.4}$$

Since equation (3.4) is valid for any arbitrary region in the flow system, it follows that

$$\frac{\partial M_\beta}{\partial t} = -\operatorname{div} \mathbf{F}_\beta + q_\beta \tag{3.5}$$

This is a differential form of the governing equations for mass conservation of non-Newtonian and Newtonian fluids.

From the definition of fluid phase saturations, it follows that

$$S_{ne} + S_{nn} = 1 \tag{3.6}$$

This constraint condition is always valid in a two phase flow problem.

The governing equations for flow of single-phase non-Newtonian fluids in porous media can always be considered as a special case of the multiphase equations. They are readily derived from equations (3.1) or (3.5) by setting $S_{ne} = 0$, and $S_{nn} = 1$.

3.3. Constitutive equations

The mass transport governing equations (3.1) or (3.5) need to be supplemented with constitutive equations, which express all the parameters as functions of a set of primary thermodynamic variables of interest (P_β, S_β). The following relationships will be used to complete the statement of multiple phase flow of non-Newtonian and Newtonian fluids through porous media.

Equations of state of the densities for Newtonian and non-Newtonian fluids are, respectively

$$\rho_{ne} = \rho_{ne}(P_{ne}) \tag{3.7}$$

$$\rho_{nn} = \rho_{nn}(P_{nn}) \tag{3.8}$$

The difference in pressure between the two phases may be described in terms of capillary pressure

$$P_c(S_{nn}) = P_{ne} - P_{nn} \tag{3.9}$$

and the capillary pressure P_c is determined experimentally as a function of saturation only.

The relative permeabilities are also assumed to be functions of fluid saturation only (Honarpour et al., 1986)

$$k_{rne} = k_{rne}(S_{nn}) \tag{3.10}$$

$$k_{rnn} = k_{rnn}(S_{nn}) \tag{3.11}$$

As pointed out by other workers (Bird et al., 1960), the permeability for single-phase non-Newtonian fluid flow should be obtained from core experiments with Newtonian fluids. In order to reduce the uncertainties when non-Newtonian flow is involved, the relative permeability data for multiphase flow of non-Newtonian fluids should also be determined by using Newtonian fluids in the laboratory experiment.

3.4. Numerical model

When a non-Newtonian fluid is involved in a flow problem, the apparent viscosity as used in Darcy's law depends on the pore velocity, or the potential gradient. Therefore, the governing integral or partial differential equations are highly non-linear. Solutions for such problems can only be found by numerical methods. However, under some special circumstances, analytical and approximate analytical solutions are possible. Both analytical and numerical methods have been employed in this work in order to provide a general theoretical approach to analysis of the flow behavior of non-Newtonian fluids.

The numerical technique presented in this work is the "integral finite difference" method (Narasimhan and Witherspoon, 1976). A modified version of the "MULKOM" family of multi-phase, multi-component codes (Pruess, 1983; 1988) for non-Newtonian and Newtonian fluid flow has been developed in analyzing flow problems of single and multiple phase non-Newtonian fluids in porous media. The input data and running procedures are similar to those for the code "MULKOM-GWF", which was developed to model the flow of gas, water and foam in porous media (Pruess and Wu, 1988). This simulator for Newtonian fluid flow calculations has been validated by Pruess and his co-workers at Lawrence Berkeley Laboratory. MULKOM has been used extensively for fundamental and applied research on geothermal reservoirs, oil and gas fields, nuclear waste repositories, and for the design and analysis of laboratory experiments (Pruess, 1988).

Based on the integral finite difference method, the mass balance equations for each phase are expressed in terms of the integral difference equations, which are fully implicit to provide stability and time step tolerance in highly non-linear problems (Thomas, 1982). Thermodynamic properties are represented by averages over explicitly defined finite subdomains, while fluxes of mass across surface segments are evaluated by finite difference approximations. The mass balance difference equations are solved simultaneously, using the Newton/Raphson iteration procedure.

The capillary pressures and relative permeabilities are treated as functions of saturation, and can be specified differently for different flow regions. Thermophysical properties of water and gas (methane) substance, such as density and viscosity, are represented within experimental accuracy by the steam table equations given by the International Formulation Committee (1967) and by Vargaftik (1975), respectively. The rheological properties for non-Newtonian viscosity need special treatments and depend on the rheological models used. A number of the common viscosity functions have been implemented in the codes, such as the power-law and Bingham models.

A brief description of the numerical method used in this non-Newtonian flow version of MULKOM is included in the following section for completeness. It is almost identical to that given in the TOUGH code (Pruess, 1987). The continuum equation (3.1) is discretized in space using the "integral finite difference" scheme. Introducing an appropriate volume average, it follows that

$$\int\int\int_{V_n} M dV = V_n M_n \tag{3.12}$$

where M is a volume-normalized extensive quantity, and M_n is the average value of M over the domain V_n. The surface integrals are approximated as a discrete sum of averages over surface segments A_{nm}

$$-\int\int_{S_n} \mathbf{F}\cdot\mathbf{n} dS = \sum_m A_{nm} F_{nm} \tag{3.13}$$

Here F_{nm} is the average value of the (inward) normal component of $\mathbf{F}$ over the

surface segment A_{nm} between volume elements V_n and V_m. This is expressed in terms of averages over parameters for elements V_n and V_m. For the basic Darcy flux term, equation (3.3), we have

$$F_{\beta,nm} = -K_{nm}\left[\frac{k_{r\beta}\rho_\beta}{\mu_\beta}\right]_{nm}\left[\frac{P_{\beta,n} - P_{\beta,m}}{D_{nm}} - \rho_{\beta,nm}g_{nm}\right] \tag{3.14}$$

where the subscripts (nm) denote a suitable averaging (interpolation, harmonic weighting, upstream weighting). D_{nm} is the distance between the nodal points n and m, and g_{nm} is the component of gravitational acceleration in the direction from m to n.

Substituting equations (3.12) and (3.13) into the governing equation (3.1), a set of first-order ordinary differential equations in time is obtained

$$\frac{dM_{\beta,n}}{dt} = \frac{1}{V_n}\sum_m A_{nm}F_{\beta,nm} + q_{\beta,n} \tag{3.15}$$

Time is discretized as a first order difference, and the flux and sink and source terms on the right hand side of equation (3.15) are evaluated at the new time level, $t^{k+1} = t^k + \Delta t$, to obtain the numerical stability needed for an efficient calculation of multi-phase flow. This treatment of flux terms is known as "fully implicit," because the fluxes are expressed in terms of the unknown thermodynamic parameters at time level t^{k+1}, so that these unknowns are only implicitly defined in the resulting equations. The time discretization results in the following set of coupled non-linear, algebraic equations

$$R_{\beta,n}^{k+1} = M_{\beta,n}^{k+1} - M_{\beta,n}^{k} - \frac{\Delta t}{V_n}\left\{\sum_m A_{nm}F_{\beta,nm}^{k+1} + V_n(q_{\beta,n})^{k+1}\right\} = 0 \tag{3.16}$$

Following Pruess (1987), "the entire geometric information of the space discretization in equation (3.16) is provided in the form of a list of grid block volumes V_n, interface areas A_{nm}, nodal distances D_{nm} and components g_{nm} of gravitational acceleration along nodal lines. There is no reference whatsoever to a global system of coordinates, or to the dimensionality of a particular flow problem. The discretized equations are in fact valid for arbitrary irregular discretizations in one, two or three dimensions, and for porous as well as for fractured media. This flexibility should be used with caution, however, because the accuracy of the solutions depends on the accuracy with which the various interface parameters in equations, such as in equation (3.14), can be expressed in terms of average conditions in grid blocks. A sufficient condition for this to be possible is that there exists approximate thermodynamic equilibrium in (almost) all grid blocks at (almost) all times. For systems of regular grid clocks referenced to global coordinates (such as $r - z$, $x - y - z$), equation (3.16) is identical to a conventional finite difference formulation."

For each volume element (grid block) V_n there are two equations for the primary thermodynamic variables, P_{nn} and S_{nn}, if the problem is two-phase flow of one Newtonian and one non-Newtonian fluid. For a flow system which is discretized into N grid blocks, equation (4.16) represents a set of $2N$ algebraic

equations. The unknowns are the $2N$ independent primary variables x_i ($i = 1, 2, 3, \ldots, 2N$) which completely define the state of the flow system at time level t^{k+1}. These equations are solved by Newton/Raphson iteration, which is implemented as follows. An iteration index p is used here, and the residuals are expanded in terms of the primary variables $x_{i,p}$ at iteration level p

$$R^{k+1}_{\beta,n}(x_{i,p+1}) = R^{k+1}_{\beta,n}(x_{i,p}) + \sum_i \left.\frac{\partial R^{k+1}_{\beta,n}}{\partial x_i}\right|_p (x_{i,p+1} - x_{i,p}) + \cdots = 0 \tag{3.17}$$

Retaining only terms up to first order, a set of $2N$ linear equations for the increments $(x_{i,p+1} - x_{i,p})$ is obtained

$$-\sum_i \left.\frac{\partial R^{k+1}_{\beta,n}}{\partial x_i}\right|_p (x_{i,p+1} - x_{i,p}) = R^{k+1}_{\beta,n}(x_{i,p}) \tag{3.18}$$

All terms $\partial R_n/\partial x_i$ in the Jacobian matrix are evaluated by numerical differentiation. Equation (3.18) is solved with the Harwell subroutine package "MA 28" (Duff, 1977). Iteration is continued until the residuals R^{k+1}_n are reduced below a preset convergence tolerance.

3.5. Treatment of non-Newtonian behavior

The apparent viscosity functions for non-Newtonian fluids in porous media depend on the pore velocity, or the potential gradient, in a complex way, as discussed in Sections 1 and 2. The rheological correlations for different non-Newtonian fluids are quite different. Therefore, it is impossible to develop a general numerical scheme that can be universally applied to various non-Newtonian fluids. Instead, a special treatment for the particular fluid of interest has to be worked out. However, for some fluids, such as power-law, Bingham plastic, pseudoplastic fluids, which are most often encountered in porous media, the numerical treatment developed in this work will be discussed here.

3.5.1. Power-law fluid

The power-law model, equation (2.11), is the most widely used to describe the rheological property of shear-thinning fluids, such as polymer and foam solutions. The power-law index n ranges between 0 and 1 for a shear thinning fluid, and the viscosity becomes infinite as the flow potential gradient tends to zero. Therefore, direct use of equation (2.11) in the calculation will cause numerical difficulties. A formulation incorporated in the code for a power-law fluid is to use a linear interpolation when the potential gradient is very small. As shown in Fig. 7, the viscosity for a small value of potential gradient is calculated by

$$\mu_{nn} = \mu_1 + \frac{\mu_1 - \mu_2}{\delta_1 - \delta_2}(|\nabla\Phi| - \delta_1) \tag{3.19}$$

for $|\nabla\Phi| \leq \delta_1$, where the interpolation parameters δ_1 and δ_2 are defined in Fig. 7. If the potential gradient is larger than δ_1, equation (2.11) is used in the code. In order to maintain the continuities in the viscosity and its derivative at (δ_1, μ_1),

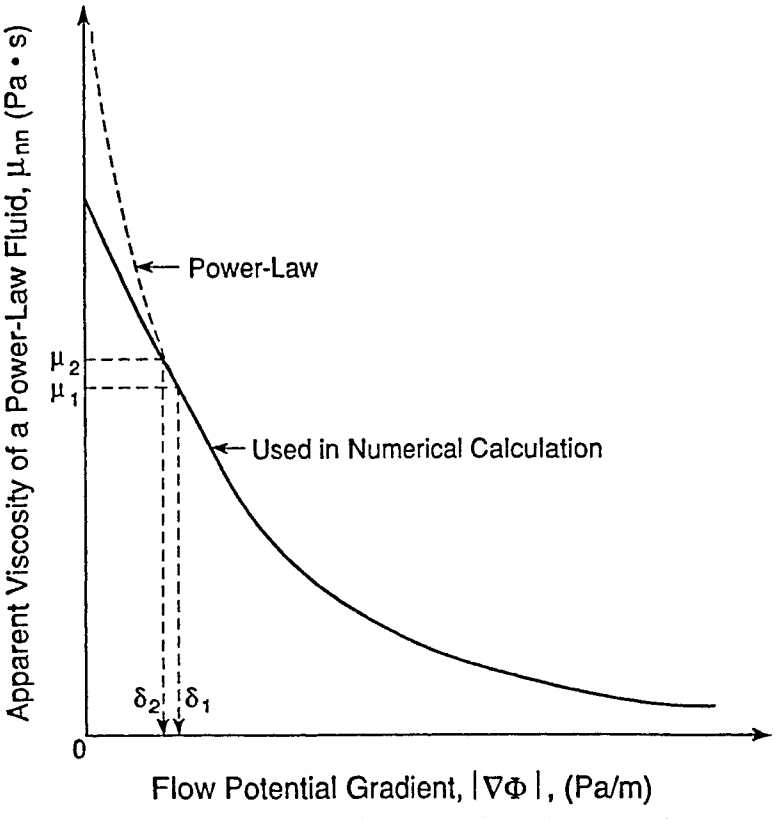


Fig. 7. Schematic of linear interpolation of viscosities of power-law fluids with small flow potential gradient.

the difference in values of δ_1 and δ_2 should be chosen sufficiently small. Then, the values for μ_1, and μ_2 may be taken as

$$\mu_j = \mu_{\text{eff}}\left(\frac{K}{\mu_{\text{eff}}}\delta_j\right)^{(n-1)/n} \qquad (j = 1, 2) \tag{3.20}$$

The numerical tests show that the treatment of power-law fluids by equation (3.19) works very well for a power-law fluid flow problem with various potential gradients. The accuracy of this scheme has been confirmed by a number of runs. Another way for the linear interpolation at small potential gradient is to use the tangential slope $\mu'_{nn}|_{\delta_1}$ in equation (3.19) instead of the chord slope. In the numerical studies of transient flow problems of power-law fluids in this work, the values of the interpolation parameters are taken as $\delta_1 = 10$ Pa/m, and $\delta_1 - \delta_2 = 10^{-7}$ Pa/m.

3.5.2. Bingham fluid

The apparent viscosity of Bingham fluids, as given by equation (2.14), has a similar behavior to that of a power-law fluid. As the potential gradient decreases

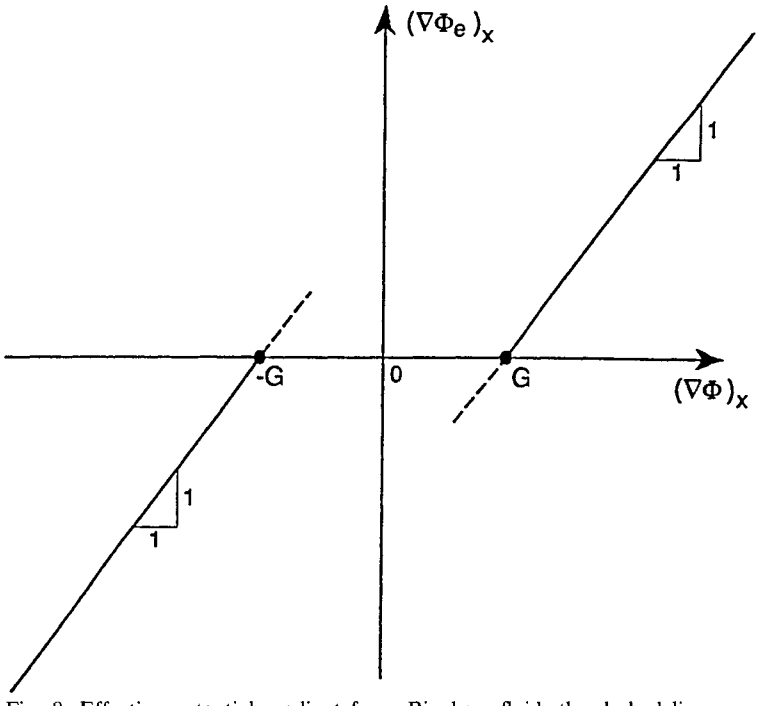


Fig. 8. Effective potential gradient for a Bingham fluid, the dashed linear extension for numerical calculation of derivatives When $(\nabla\Phi)$ is near + G or − G.

and comes close to the minimum potential gradient G, the viscosity tends to be infinite. It is possible to use a linear interpolation approximation for the viscosity when the potential gradient nears G to overcome the associated numerical difficulties. However, a much better approach is to introduce an effective potential gradient $\nabla\Phi_e$, whose scalar component in the x direction, flow direction, is defined as

$$(\nabla\Phi_e)_x = \begin{cases} (\nabla\Phi)_x - G & (\nabla\Phi)_x > G \\ (\nabla\Phi)_x + G & (\nabla\Phi)_x \leqslant -G \\ 0 & -G \leqslant (\nabla\Phi)_x \leqslant G \end{cases} \tag{3.21}$$

where $(\nabla\Phi)_x$ is the scalar component of the potential gradient $\nabla\Phi$. As shown in Fig. 8, Darcy's law as used in the code for a Bingham fluid is

$$\mathbf{u} = -\frac{K}{\mu_b}\nabla\Phi_e \tag{3.22}$$

and replaces equation (1.34) in the numerical calculations. This treatment of the code using the effective potential gradient has proven to be the most efficient when simulating Bingham fluid flow in porous media.

Modeling of Bingham fluid flow in porous media is a very difficult problem numerically because of the minimum pressure gradient phenomenon. For a single

well flow problem with a uniform initial pressure distribution in the formation, the fluid in many grids near wellbore maybe change from immobile to mobile within only one time step at early transient times after the well is put into production. With each Newton-Raphson iteration during a time step, pressure disturbance may penetrate one more grid. As a result, more Newton-Raphson iterations for convergence at each time step are then needed in the calculation. Therefore, no explicit formula can be used in the code, and we have to use some fully implicit numerical scheme to handle the non-linear convergent problem with Bingham fluids.

3.5.3. General pseudoplastic fluid

In this study, a general pseudoplastic fluid is defined as a fluid whose apparent viscosity is described by the Meter four-parameter model, equation (2.13) (Meter and Bird, 1964). The shear rate, $\dot{\gamma}$, in equation (2.13) for single phase one-dimensional flow of a power law fluid is given by equation (2.12) (Camilleri et al., 1987a; Hirasaki and Pope, 1974). For the special cases, where $\mu_0 = \mu_\infty$, or, $\beta = 1$, the fluid becomes Newtonian. For a horizontal flow problem, ignoring the effects of gravity on shear rate in equation (2.12), and introducing the resulting shear rate function into equation (2.13), one can obtain

$$\mu_{nn}^{\beta} + C_n\left(-\frac{\partial P}{\partial x}\right)^{\beta-1}\mu_{nn} - \mu_0\mu_{nn}^{\beta-1} - \mu_\infty C_n\left(-\frac{\partial P}{\partial x}\right)^{\beta-1} = 0 \tag{3.23}$$

Note that $(-\partial P/\partial x) \geq 0$ for injection and C_n is

$$C_n = \left(\frac{((3n+1)/4n)^{n/(n-1)}}{\dot{\gamma}_{1/2}}(2K/\phi)^{1/2}\right)^{\beta-1} \tag{3.24}$$

equation (3.23) implicitly defines the viscosity μ_{nn} as a function of the pressure gradient $(-\partial P/\partial x)$. For the pseudoplastic fluid in porous media, this has been implemented in the numerical code to correlate apparent viscosity of the psuedoplastic fluid with pressure gradient in the numerical study.

4. Single-phase flow of power-law non-Newtonian fluids

4.1. Introduction

Considerable progress has been made in the literature since the early 1960s in understanding the flow of a single-phase power-law non-Newtonian fluid through porous media. Among many researchers, Odeh and Yang (1979), Ikoku and Ramey (1979) made the major contributions to the analysis of flow behavior and well tests of power-law fluids in porous media. By using a linearized assumption that there exists a steady-state radial viscosity profile in the reservoir, as given by equation (1.33), they obtained approximate analytical solutions. Based on these solutions, a number of analytical and numerical methods have been developed to interpret well testing data during injectivity and falloff tests of power-law fluids.

Vongvuthipornchai and Raghavan (1987a) examined the approximate solutions

by Odeh and Yang, and Ikoku and Ramey, and found that the solutions would give large errors in analyzing pressure falloff behavior when the power-law index $n < 0.6$. It has been found from laboratory experiments and field tests that the in-situ rheological properties of polymer solutions in reservoirs may be quite different from the laboratory-measured values (Castagno et al., 1984; 1987). Changes in the non-Newtonian parameters of polymer solutions under reservoir condition may be caused by degradation in polymer concentration due to adsorption on the pore surface, or by effects of different shear rate distributions for flow through different pore geometries. In general, the two parameters, power-law index, n, and the consistency coefficient, H, are both unknowns in a well testing problem with a power-law fluid injection. Therefore, the conditions for the application of their methods may not be satisfied, and a direct use of the transient pressure analysis methods available for power-law fluid flow may result in significant errors in the predicted fluid and formation properties.

The flow of power-law fluids in fractured media is of interest in many applications, such as in EOR operations by polymer-flooding in naturally fractured petroleum reservoirs, or in the use of foam as a blocking agent in a fractured medium for underground energy and waste storage purposes. Very little research has been published on the flow of non-Newtonian fluids through fracture systems. In the petroleum literature, Luan (1981) extended the work of Ikoku and Ramey (1979) to the flow problem of power-law fluids in naturally fractured reservoirs (Warren and Root, 1963). He was able to obtain an approximate analytical solution by using the linearization assumption, equation (1.33), for the fracture system and a constant viscosity for the power-law fluid in calculating interporosity flow between matrix and fracture.

Pseudoplastic fluid flow in porous media shows more complicated behavior than that predicted by the power-law. It has been observed in many laboratory experiments that any pseudoplastic fluid exhibits Newtonian behavior at high or low shear rates (Savins, 1969; Fahien, 1983, Christopher and Middleman, 1965). Therefore, a more realistic rheological model, such as the Meter model, for general pseudoplastic fluids (Meter and Bird, 1964), should be used in further studies of power-law fluid flow through porous media. It should be possible to obtain a more comprehensive look at transport phenomena including Newtonian behavior at very high and very low shear rates during a pseudoplastic fluid flow in porous media.

This section presents the following numerical studies: (1) well testing analysis during a power-law fluid injection, (2) transient flow of a power-law fluid through a fractured medium, and (3) transient flow of a general pseudoplastic non-Newtonian fluid, described by the Meter model, through a porous medium.

4.2. Well testing analysis of power-law fluid injection

The transient pressure analysis technique applied in this work is a combination of the existing analytical method with numerical simulation. First, a log-log plot of the observed pressure increase at the wellbore versus the injection time is used to obtain an approximate value of n. The long time approximate analytical solution (Ikoku and Ramey, 1979) is

$$\log(P_{wf}(t) - P_i) = \left(\frac{1-n}{3-n}\right)\log(t)$$

$$+ \log\left(\frac{(Q/2\pi h)^{(n+1)/(3-n)}(\mu_{eff}/K)^{2/(3-n)}((3-n)^2/n\phi C_t)^{(1-n)/(3-n)}}{(1-n)\Gamma(2/(3-n))}\right) \tag{4.1}$$

where $P_{wf}(t)$ is the wellbore flowing pressure; P_i is the initial constant pressure in the formation; h is the thickness of the formation; Q is a constant volumetric injection rate; C_t is total system compressibility; and μ_{eff} is defined in equation (1.14).

Equation (4.1) indicates that at long injection times, a graph of $\log(P_{wf} - P_i)$ versus $\log(t)$ yields a straight line with a slope

$$m' = \frac{1-n}{3-n} \tag{4.2}$$

which can be used to obtain a first-order approximation for n. The intercept at $t = 1$ second, ΔP_1, can give the effective mobility λ_{eff} from

$$\lambda_{eff} = \frac{K}{\mu_{eff}} = \frac{(Q/2\pi h)^{(n+1)/2}((3-n)^2/n\phi C_t)^{(1-n)/2}}{(\Delta P_1(1-n)\Gamma(2/(3-n)))^{(3-n)/2}} \tag{4.3}$$

The modified Darcy's law for this horizontal radial flow can be obtained by substituting equation (2.11) into equation (2.7)

$$u = \left(\frac{K}{\mu_{eff}}\left(-\frac{\partial P}{\partial r}\right)\right)^{1/n} \tag{4.4}$$

Therefore, as long as the straight line occurs in the log-log plot of a well test, the power-law index n and the effective mobility λ_{eff} can be calculated from the slope and intercept of the straight line if the porosity and compressibility are known. Then, the problem is well-posed for a numerical calculation since the parameters in equation (4.4) are defined. The observed pressure data can be matched by the numerical calculation using the value of n, and λ_{eff} obtained as an initial guess.

An injection test example is given here to illustrate the approach used. The well test data used are from the published data of a field test that was performed on biopolymer injection (Odeh and Yang, 1979). The pressure transient data are plotted on Fig. 9 and formation properties are listed in Table 1. The slope of the log-log straight line part of the observed wellbore pressure increase versus injection time in Fig. 9 is determined as $m = 0.21$, and then, $n = 0.46$. The intercept, $\Delta P_1 = 6.236 \times 10^5$ Pa is found at a time of 1 sec. A tentative effective mobility can be calculated by equation (4.3) as

$$\lambda_{eff} = \left(\frac{\left(\frac{8.059 \times 10^{-4}}{2 \times \pi \times 4.419}\right)^{(1+0.46)/2}\left(\frac{(3-0.46)^2}{0.46 \times 0.22 \times 2.176 \times 10^{-9}}\right)^{(1-0.46)/2}}{\left(6.235 \times 10^5 \Gamma\left(\frac{2}{3-0.46}\right)\right)^{(3-0.46)/2}}\right)$$

$$= 1.514 \times 10^{-8}\,(m^{1.46}/\text{Pa} \cdot \text{s})$$

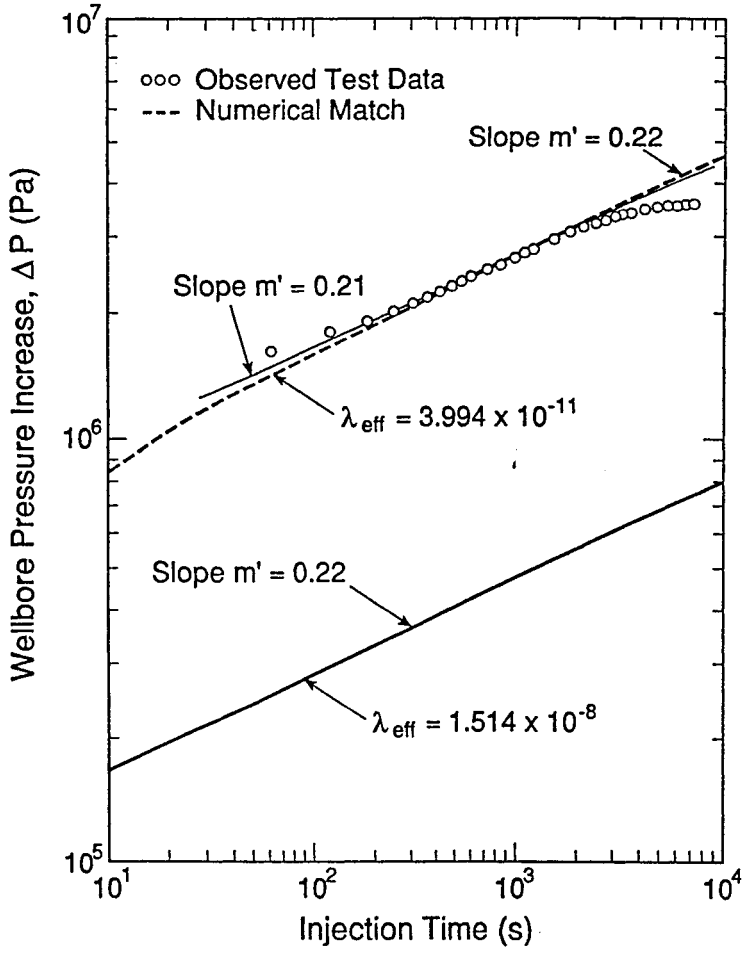


Fig. 9. Numerical matching curve of pressure increase versus injection time for a biopolymer fluid injectivity test (data from Odeh and Yang, 1979).

TABLE 1

Parameters for well testing analysis of biopolymer injection

Initial pressure	$P_i = 2.606 \times 10^3$ Pa
Initial porosity	$\phi_i = 0.22$
Formation thickness	$h = 4.419$ m
Total compressibility	$C_t = 2.176 \times 10^{-10}$ Pa^{-1}
Production rate	$Q = 8.059 \times 10^{-4}$ m^3 s^{-1}
Permeability	$K = 8.684 \times 10^{-14}$ m^2
Wellbore radius	$r_w = 0.0762$ m

Using these values of n and λ_{eff}, and the parameters in Table 1, we have the pressure responses at the wellbore as shown by the bottom solid curve of Fig. 9. Obviously, this result is unacceptable with an error in pressure increase by a factor of 5, when compared with the actual field data. However, the log-log straight line

of the pressure-time curve, with a slope $m = 0.22$ is approximately parallel with that of the observed curve where the slope $m = 0.21$. Therefore, the long time asymptotic solution by Ikoku and Ramey again gives a good approximation for the power-law index n. We shall use $n = 0.46$, and adjust λ_{eff}. In four more test runs, the result is shown by the dashed curve in Fig. 9, and this yields an effective mobility $\lambda_{\text{eff}} = 3.99 \times 10^{-11}$, and a slope $m = 0.22$. For this case, the permeability was known, $K = 88$ md, from a core analysis. Then, if the power-law model, equation (2.11), holds for flow in the reservoir, we can calculate the consistency, $H = 0.019$ Pa·s$^{0.46}$. These results further illustrate the errors that can occur in the analysis of field data using the approximate analytical solutions of Ikoku and Ramey (1979), Odeh and Yang (1979).

4.3. Transient flow of a power-law fluid through a fractured medium

A numerical study of the flow of a power-law non-Newtonian fluid in a fractured medium is performed in order to obtain some insight into its flow behavior. We shall assume the standard model of parallel smooth sides for the fractures (see Fig. 10). This is the simplest model, and is often used to approximate more complicated fracture networks in reservoirs. The rheological model for a power-law fluid, equation (2.11), is used for flow in the matrix system. However, because of the two-dimensional nature of flow through a fracture, the modified Darcy's law, such as equation (1.13) derived from the capillary model, cannot be employed directly in fracture flow. Therefore, a modified Darcy's equation for a power-law fluid in a parallel-plate fracture is presented here. The fracture model is given in Fig. 10 for a horizontal system of parallel-plate fractures. It can be shown (Wu, 1990) that the modified Darcy's law for the flow of a power-law fluid in fractures can also be described by equation (2.7), as

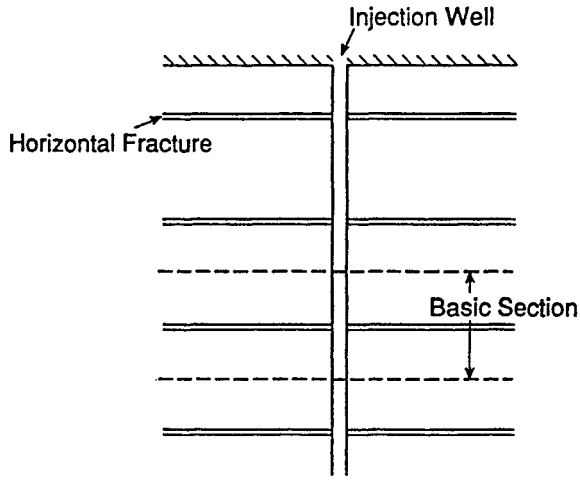
$$\mu_{\text{nn}} = \frac{H^{1/n}}{3}\frac{2n+1}{n}(b/2)^{(n-1)/n}\left(-\frac{\partial P}{\partial z}\right)^{(n-1)/n} \tag{4.5}$$

where b is aperture of the fracture. However, we may use the same form of the viscosity function as in equation (2.11). Here, μ_{eff} is replaced by

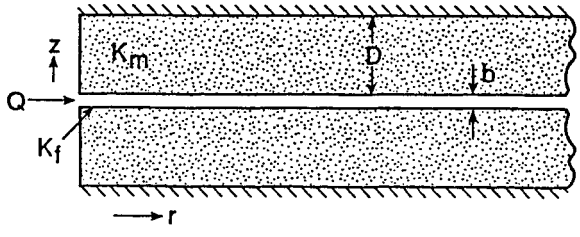
$$\mu^*_{\text{eff}} = H\left(\frac{2n+1}{3n}\right)^n\left(\frac{b}{2K_{\text{f}}}\right)^{n-1} \tag{4.6}$$

where K_{f} is the effective fracture permeability used in the Darcy's equation, calculated normally by the cubic law.

Flow through fractured media is of fundamental importance in many subsurface systems, such as the exploitation of hydrocarbon and geothermal energy, and underground waste storage in naturally fractured reservoirs. The study of fluid flow in naturally fractured reservoirs has been a challenging task, and considerable progress has been made since the 1960s (Barenblatt et al., 1960; and Warren and Root, 1963). Most studies of flow in fractured reservoirs use the double-porosity concept and consider that global flow occurs primarily through the high-permeability, low-effective-porosity fracture system surrounding blocks of rock matrix.



(a) Basic Model - Uniform horizontal fracture



(b) Basic Section

Fig. 10. Schematic of a horizontal fracture system.

The matrix blocks contain the majority of the formation storage volume and act as local source or sink terms connected to the fracture system. The fractures are interconnected and provide the main fluid flow path to injection or production wells.

A very important characteristic of a double-porosity system is the nature of the fluid exchange between the two constitutive media, the so-called interporosity flow. The conventional treatment of the interporosity flow between matrix and fractures resorts to an approximation that a quasi-steady state exists in the matrix elements at all times, with the interporosity flow rate being proportional to the difference of the average pressures in matrix and fractures. The quasi-steady assumption was originally proposed by Barenblatt et al. and Warren and Root and has been used by many subsequent authors. For isothermal single phase Newtonian fluid flow, this assumption was shown to give accurate results by Kazemi (1969) using a numerical model. However, for more complicated flow problems, such as those involving heat exchange between matrix and fractures,

and for multiple phase flow with strong mobility effects, transient interporosity flow conditions may last a long time (decades) before reaching quasi-steady state. Under these conditions, it is necessary to treat the flow inside the blocks and at the block-fracture interface as a transient process. Pruess and Narasimhan (1982, 1985) developed a "multiple interacting continua" technique (MINC), in which fully transient flow in the matrix and between matrix blocks and fractures is described by a numerical method. Using appropriate subgridding in the matrix blocks, it is possible to resolve the details of the gradients (of pressure, temperature, etc.) which drive the interporosity flow. The MINC-method has been successfully applied to a number of geothermal reservoir (Pruess, 1983a) and multiple phase flow problems (Wu and Pruess, 1986).

For the flow of a single phase power-law fluid in a fractured medium, the apparent viscosity of the fluid inside the matrix and at the matrix-fracture interfaces depends on the pore velocity, or pressure gradient, as described by equation (2.11). One should expect a strong effect of the non-linearity in non-Newtonian viscosity on flow behavior. Therefore, the MINC-method will be used in simulating the interporosity flow of a power-law fluid. Also, a comparison of the MINC-calculations with the conventional double-porosity results is given here to demonstrate that the double-porosity approximation is generally not suitable for simulating non-Newtonian fluid flow in fractured media.

Let us consider the flow of a power-law fluid in a fracture system where the matrix blocks are permeable. The same horizontal fracture model is used, as shown in Fig. 10. The matrix subgridding in this numerical simulation employs the MINC-technique and is generated by a mesh generator—GMINC (Pruess, 1983b). The basic section of the horizontal fracture system is first partitioned into "primary" volume elements (or grid blocks) such as would be employed for a porous medium. The interblock flow connections are then assigned to the fracture continuum, and each primary grid block is sub-divided into a sequence of "secondary" volume elements. Here, the secondary elements are a number of horizontal layers parallel to the fracture in each primary element. The flow inside the matrix system and between matrix blocks and fractures is assumed to be vertical.

The MINC-method contains the double-porosity approximation as a special case by defining only two continua in each primary grid block, representing fracture and matrix, respectively. Therefore, we can check the applicability of the double-porosity concept to the injection of a power-law fluid into a fractured reservoir. The fluid and formation parameters for this power-law fluid injection are given in Table 2. A comparison of wellbore injection pressures is shown in Fig. 11, and were calculated for different levels of subgridding with 2–10 continua. The matrix block was sub-divided into equal-volume subdomains in this calculation, except the element connected with the fracture, whose volume was taken as 1% of the total matrix volume. It is obvious that the double-porosity approximation (MINC-2) introduces larger errors during the early transient time and only approaches the correct solution at long injection times. As the number of subdivisions in the matrix system increases, the results become more accurate, and little improvement could be obtained after eight sub-domains were used. Therefore, meshes with eight sub-divisions are used in the following study. The reason the double-porosity

TABLE 2

Parameters for power-law fluid injection in a double-porosity system

Initial pressure	$P_i = 3 \times 10^6$ Pa
Fracture aperture	$b = 2.3 \times 10^{-4}$ m
Half fracture spacing	$D = 0.5$ m
Matrix porosity	$\phi_m = 0.20$
Fracture porosity	$\phi_f = 2.3 \times 10^{-4}$
Matrix permeability	$K_m = 9.869 \times 10^{-15}$ m^2
Effective fracture permeability	$K_f = 1.014 \times 10^{-12}$ m^2
Fluid compressibility	$C_f = 4.557 \times 10^{-10}$ Pa^{-1}
Rock compressibility	$C_r = 5.443 \times 10^{-10}$ Pa^{-1}
Initial fluid density	$\rho_i = 972.78$ kg m^{-3}
Injection rate	$Q_m = 2 \times 10^{-2}$ kg s^{-1}
Wellbore radius	$r_w = 0.10$ m
Power-law index	$n = 0.5$
Power-law coefficient	$H = 0.10$ Pa · s^n

method is inaccurate for non-Newtonian fluid flow is apparent on Fig. 12, which gives a distribution of the pressure increases in the fractures after $t = 10$ sec. When the number of subdivisions is small, the double-porosity prediction overestimates pressures in the fractures. This indicates that flow into the matrix system is underestimated by the double-porosity approximation, which treats the matrix as a single continuum with locally uniform pressure and fluid distributions. The pressure gradient and pore velocity into the matrix from this calculation are smaller than it should be, and the result is a higher viscosity for this shear-thinning fluid. This phenomenon is similar to that obtained using the double-porosity method for multiple phase flow in fractured reservoirs, as discussed by Wu and Pruess (1986). It is concluded that, in general, the double-porosity method cannot be used for the analysis of non-Newtonian fluid flow in fractured media, and some method of transient interporosity flow, such as MINC, will have to be utilized instead.

The transient flow of a Newtonian fluid in fractured reservoirs, as pointed out by Warren and Root (1963), is distinguished on semi-log plots of pressure buildup by two parallel straight lines. This enables one to determine two parameters, the storage coefficient, ω, and the interporosity flow coefficient, λ, which are sufficient to characterize a fractured medium in the double-porosity approximation. We shall use the same two parameters to discuss the flow behavior of a power-law fluid in a fractured medium. The storage coefficient is defined (Warren and Root, 1963) as,

$$\omega = \frac{\phi_f C_f}{\phi_m C_m + \phi_f C_f} \tag{4.6}$$

where C_f and C_m are total compressibilities of fracture and matrix systems, respectively. The interporosity coefficient is defined (Lai, 1985) as,

$$\lambda = \frac{r_w^2 K_m}{K_f D^2} \tag{4.7}$$

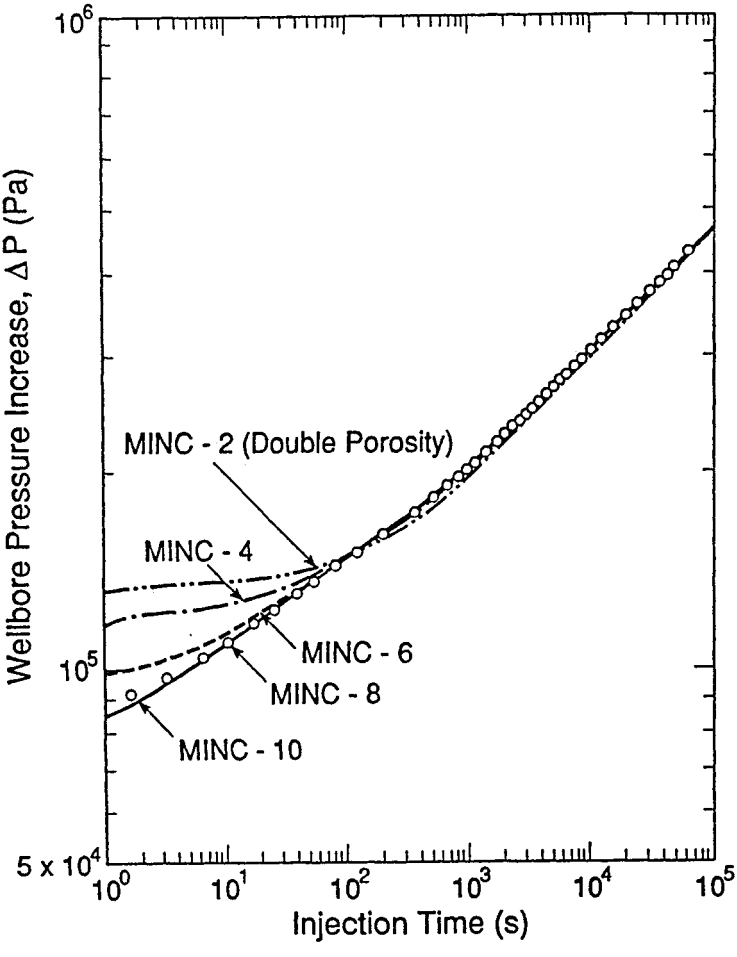


Fig. 11. Transient pressure responses in a double-porosity system during a power-law fluid injection, effects of subdivisions of the matrix system on interporosity flow.

The characteristic curves of transient pressure behavior for power-law fluid flow in this idealized fracture model, calculated with MINC-8 subgridding, are given in Figs. 13 and 14. The fluid and formation parameters in these calculations are summarized in Table 2. Figure 13 shows that the flow of a power-law fluid in a fractured medium is now characterized by two parallel log-log straight lines, instead of the semi-log straight lines obtained for Newtonian flow. Interestingly, the slopes of the straight lines of $\log(\Delta P)$ versus $\log(t)$ during the early and long injection times are also described by equation (4.2) with $m' = 0.20$. This indicates that, at very early times, the pressure responses are dominated by flow only in the fractures; and the behavior approaches that of an equivalent system of a homogeneous reservoir at long times. The results on Figs. 13 and 14 indicate that the power-law flow behavior is also controlled by the same two dimensionless parameters, ω and λ. The coefficient λ governs the interporosity flow and

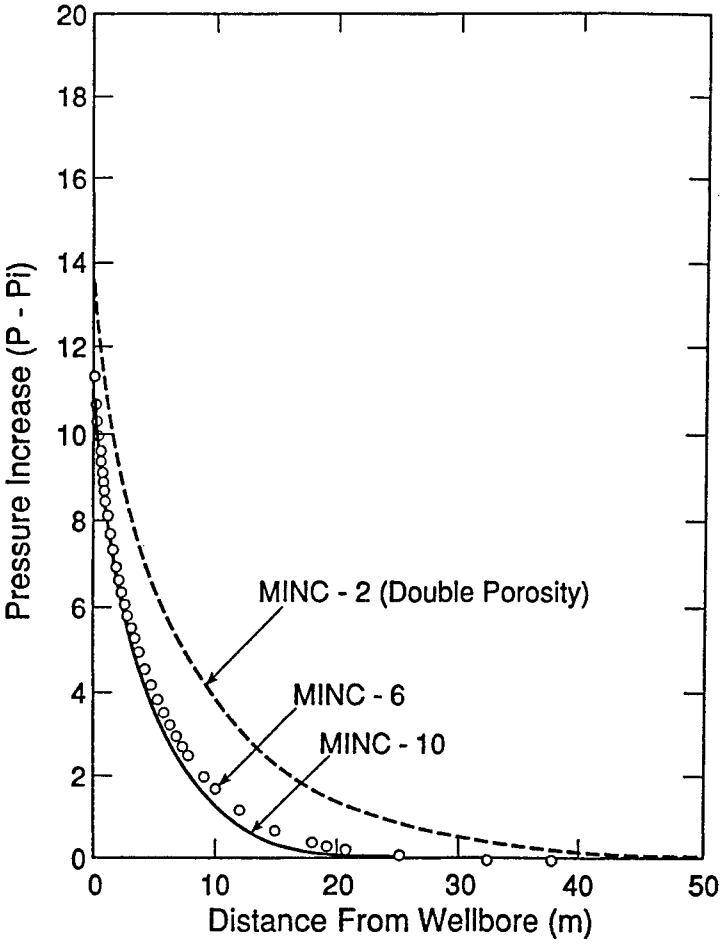


Fig. 12. Distributions of pressure increases in the fracture system for different subdivisions of the matrix system.

determines the time frame when the transitional period in the pressure plot will occur between the two log-log straight lines, as shown in Fig. 13. The other parameter ω is the ratio of the storage capacity of the fracture to the total storage capacity of the medium and is related to the vertical displacement between the parallel straight lines (see Fig. 13). In a real field test of power-law fluid flow in a fractured reservoir, there may be only one of the two straight lines that develops on the log-log plot, depending on the fluid and formation properties. At early time, the log-log straight lines may not be evident when the interporosity flow parameter λ is large, because of wellbore flow conditions, such as wellbore storage and skin effects. For a finite system with a small value of λ, the long time straight line may never form. Knowing these effects of the two dimensionless parameters, λ and ω, on pressure response helps in the analysis of well test data with power-law fluid flow in fractured reservoirs.

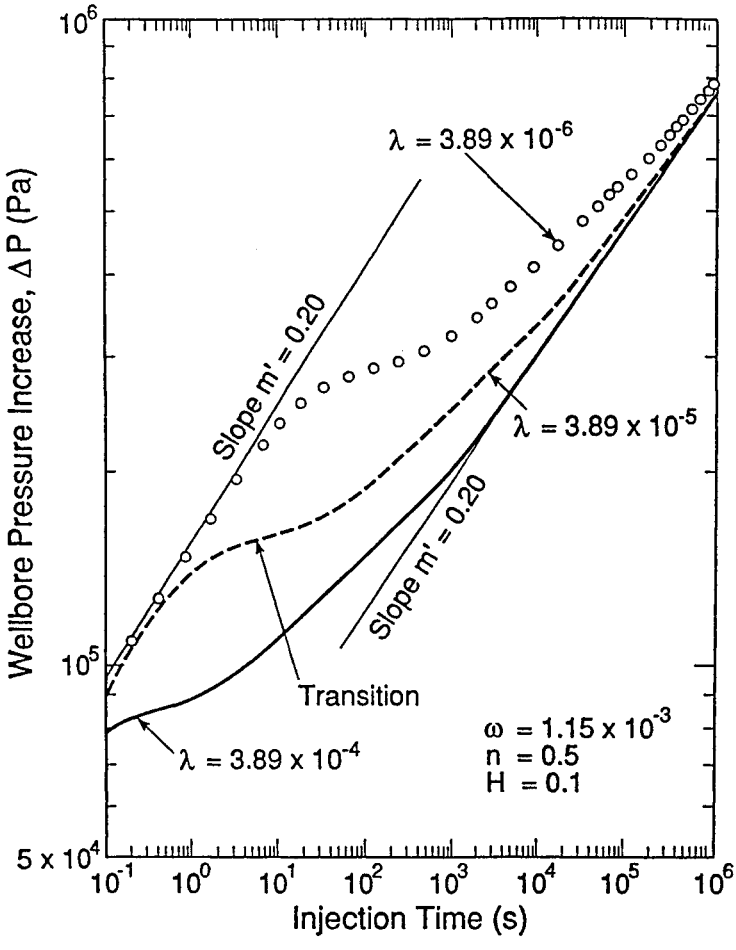


Fig. 13. Characteristic curves of flow behavior of a power-law fluid through a double-porosity medium, effects of interporosity flow coefficient λ.

There is a significant difference in the log-log plot for a Newtonian fluid. Figure 15 shows the results for pressure increases in the same fracture system with a Newtonian fluid having a constant viscosity $\mu_{ne} = 10$ cp. The difference between Newtonian and power-law non-Newtonian fluid flow is that no straight line develops on the log-log plot for Newtonian flow. For the same fracture system with a Newtonian fluid, the usual semi-log plot of pressure increase versus time will exhibit two parallel straight lines (Kazemi, 1969). It is apparent that flow resistance in the fractured medium increases more rapidly with a power-law fluid than with a Newtonian fluid.

4.4. Flow behavior of a general pseudoplastic non-Newtonian fluid

The apparent viscosity of a general pseudoplastic fluid is assumed to be described by the Meter four-parameter model, equation (2.13) (Meter and Bird,

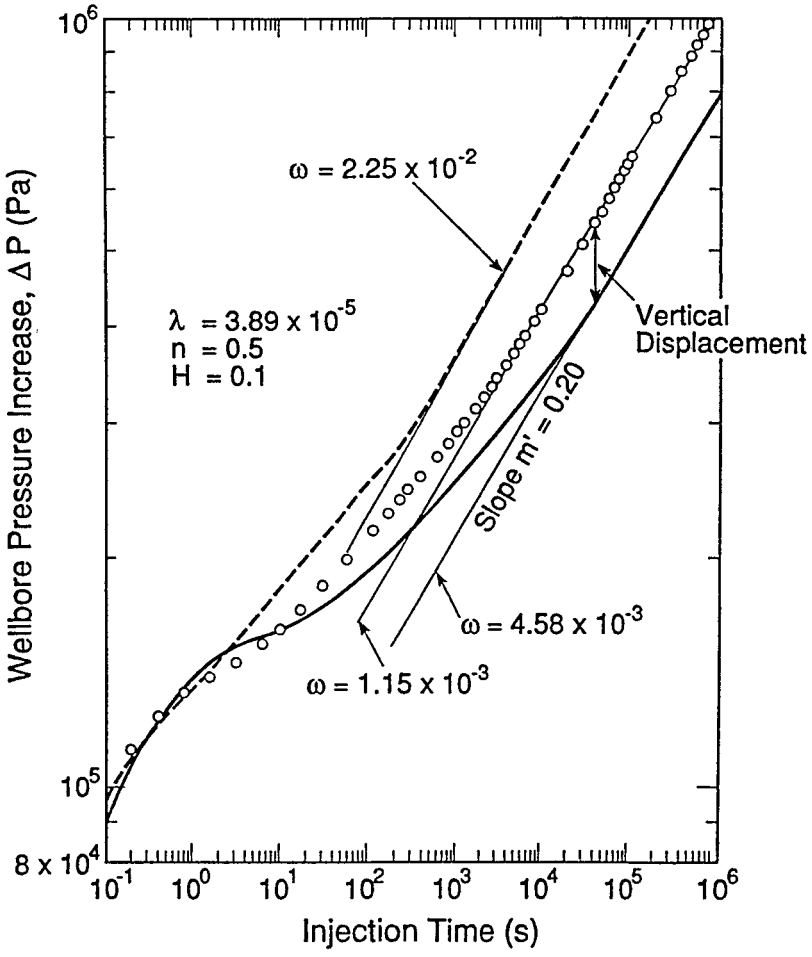


Fig. 14. Characteristic curves of flow behavior of a power-law fluid through a double-porosity medium, effects of storage coefficient ω.

1964). The shear rate function,, needed in equation (2.13) for single phase one-dimensional flow of a power law fluid is given by equation (2.12) (Camilleri et al., 1987a; Hirasaki and Pope, 1974). Then, the viscosity is determined by equation (3.23). As shown in Fig. 16, viscosities calculated from equation (3.23) for the pseudoplastic fluid depend on pressure gradients and approach constants μ_0 and μ_∞, respectively, for small and large values of pressure gradient. This is physically more realistic than the power-law model because the power law predicts an infinite viscosity in the limit of vanishing shear rate.

Let us now consider the problem of injecting a pseudoplastic fluid into a horizontal porous formation through a well. The fluid and formation properties for this study are given in Table 3. It should be mentioned that, based on the literature, the non-Newtonian parameters used here are in a reasonable range for polymer solution flow in porous media. A log-log plot of pressure increase versus

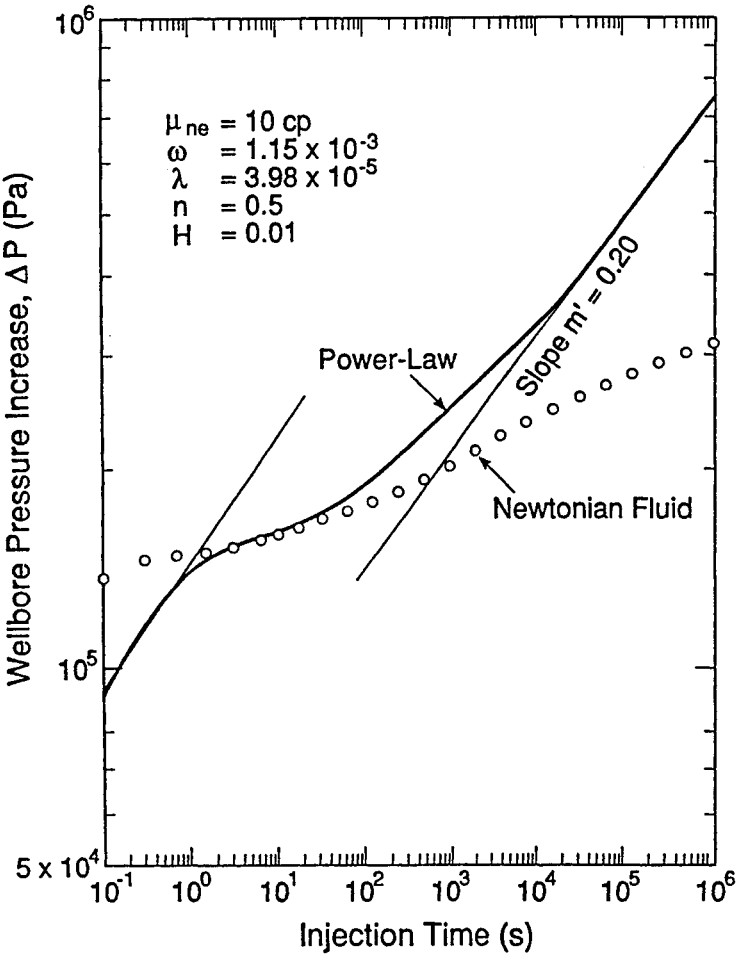


Fig. 15. Comparison of pressure responses between Newtonian and non-Newtonian power-law fluid through a double-porosity system.

injection time is given in Fig. 17, showing the effects of maximum viscosities, μ_0. It is evident that even at large injection times, no log-log straight lines develop on the curves of Fig. 17. The slopes of the pressure-time curves decrease as injection time increases. As discussed in Section 4.2, a log-log straight line develops on the transient pressure curve at late times for power-law fluids. Therefore, the flow resistance for a power-law fluid increases more rapidly than for a pseudoplastic fluid under the same flow condition. If we keep the maximum viscosity constant at $\mu_0 = 100$ cp, and change the minimum viscosities, μ_∞, a comparison of the pressure responses is given in Fig. 18. It is evident on this figure that the minimum viscosity parameter, μ_∞, has little influence on wellbore pressure as long as $\mu_\infty \ll \mu_0$. This simply means that the flow is essentially dominated by the low pore velocity (or shear rate) zone near the pressure penetration front, where the viscosity is close to the maximum viscosity μ_0 for this radial flow case.

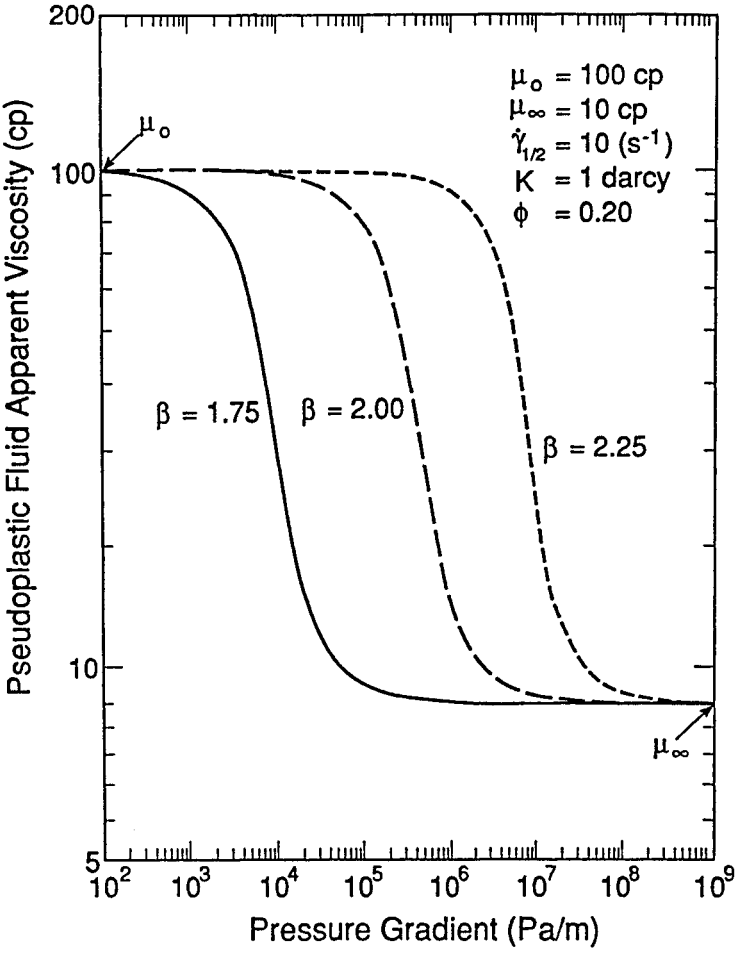


Fig. 16. Apparent viscosity curves of a general pseudoplastic fluid, by Meter's model, effects of the exponential parameter β.

TABLE 3

Parameters for Pseudoplastic fluid injection in a porous medium

Initial pressure	$P_i = 1 \times 10^7$ Pa
Initial porosity	$\phi_i = 0.20$
Formation thickness	$h = 1$ m
Permeability	$K = 9.869 \times 10^{-13}$ m^2
Fluid compressibility	$C_f = 4.557 \times 10^{-10}$ Pa^{-1}
Rock compressibility	$C_t = 2 \times 10^{-10}$ Pa^{-1}
Initial fluid density	$\rho_i = 975.92$ kg/m^3
Injection rate	$Q_m = 0.05$ kg/s
Wellbore radius	$r_w = 0.10$ m
Power-law index	$n = 0.5$

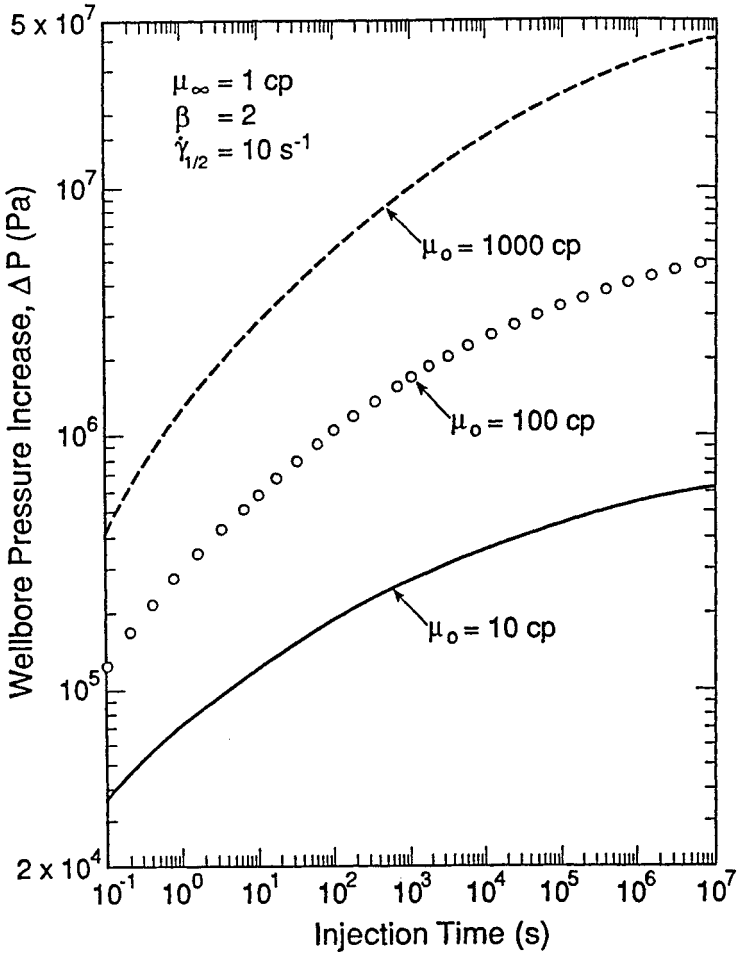


Fig. 17. Transient pressure behavior of pseudoplastic fluid flow in porous media, effects of the maximum viscosity μ_0.

The effects of the parameter, $\dot{\gamma}_{1/2}$, are shown in Figs. 19 and 20. It serves as a shift factor on these log-log curves of both viscosity versus pressure gradient and pressure increase versus injection time. The exponential parameter, β, in equation (2.13), affects the flow behavior more significantly, as shown in Fig. 21. The magnitude and shapes of the wellbore pressure-time plots both change as β changes.

Meter and Bird (1964) discussed a method for determining the parameters of the four parameter model, equation (1.8), by analyzing laboratory experiments. However, flow properties obtained from core experiments are usually quite different from those observed for a reservoir in the field. Therefore, well test techniques are used in many applications to find the in-situ flow parameters for the system of interest. As the number of physical parameters increases, analysis of well test data becomes more difficult to perform and the results may not be unique. In

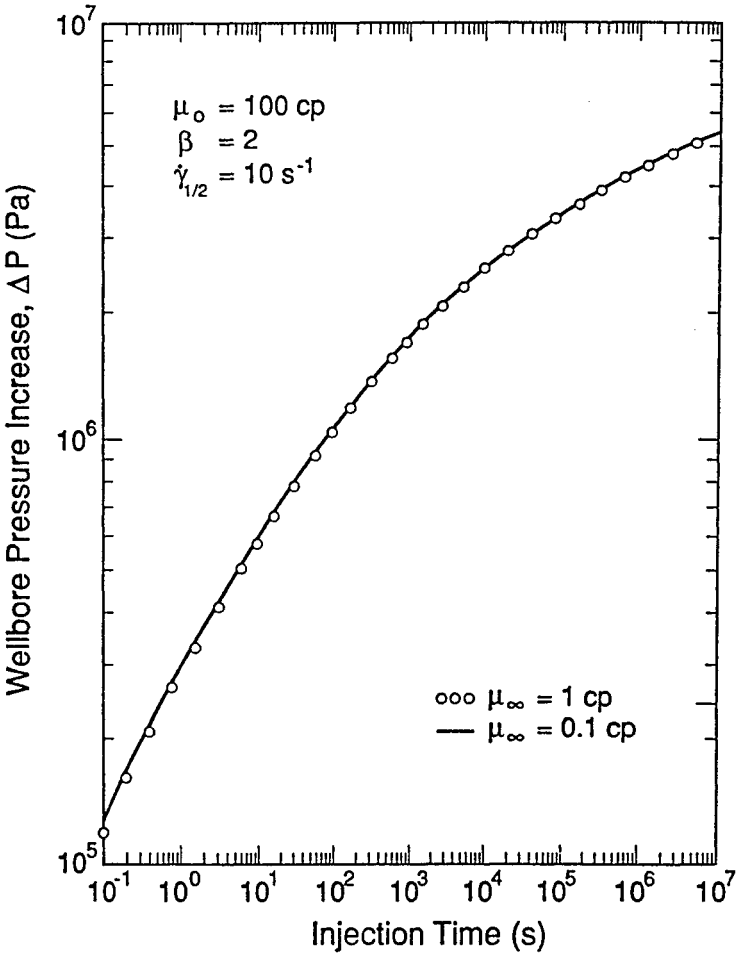


Fig. 18. Transient pressure behavior of pseudoplastic fluid flow in porous media, effects of the minimum viscosity μ_∞.

practice, it is very important to reduce the number of unknowns so that a successful well test may be obtained.

For the pseudoplastic non-Newtonian fluid flow problem, the semi-log plots of pressure increase versus time are given in Fig. 22, in which the pressure-time data are the same as those in Fig. 21. It is encouraging to note that semi-log straight lines develop at long injection times. This indicates that at long time, the behavior of pseudoplastic fluids tends toward that of a Newtonian fluid. For $\beta = 2$ and 3, the semi-log straight lines are almost parallel to each other; their slopes are measured to be $m|_{\beta=2} = 9.21 \times 10^5$ Pa and $m|_{\beta=3} = 9.51 \times 10^5$ Pa per log-cycle, respectively. By using the standard semi-log analysis method (Earlougher, 1977; Matthews and Russell, 1967), we can calculate the equivalent Newtonian viscosity μ_{eqv} at long times as,

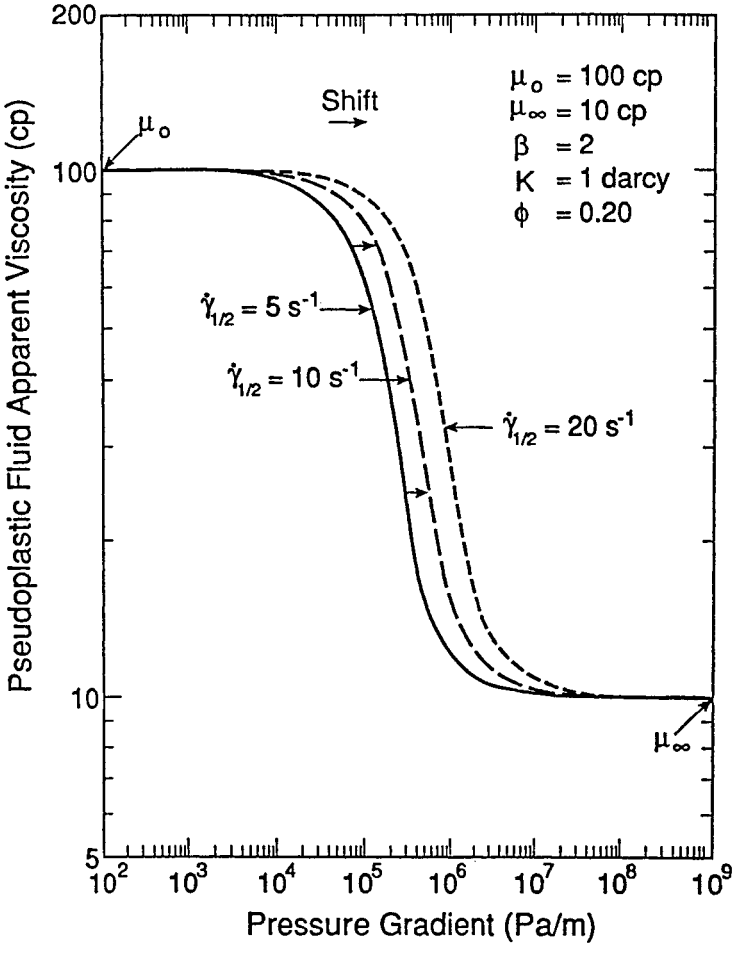


Fig. 19. Apparent viscosity curves of a general pseudoplastic fluid, by Meter's model, effects of the coefficient $\gamma_{1/2}$.

$$\mu_{eqv} = \frac{4\pi Khm}{2.303Q} = \frac{4 \times \pi \times 9.869 \times 10^{-13} \times 9.51 \times 10^5}{2.303 \times 0.05/975.92} = 99.95 \text{ (cp)} \tag{4.8}$$

where Q is the constant volumetric injection rate. This calculated equivalent viscosity value is close to μ_0, i.e., $\mu_{eqv} \approx \mu_0 = 100$ cp. Therefore, this further confirms that the long time flow behavior is controlled by the low flow velocity and high viscosity region far from the well. This indicates that the maximum viscosity parameter μ_0 for flow of a pseudoplastic fluid can be obtained approximately by a semi-log analysis of pressure drawdown tests.

4.5. Summary

A numerical study of transient flow of single-phase power-law fluids has been carried out in this Section. The semi-analytical test analysis method is discussed

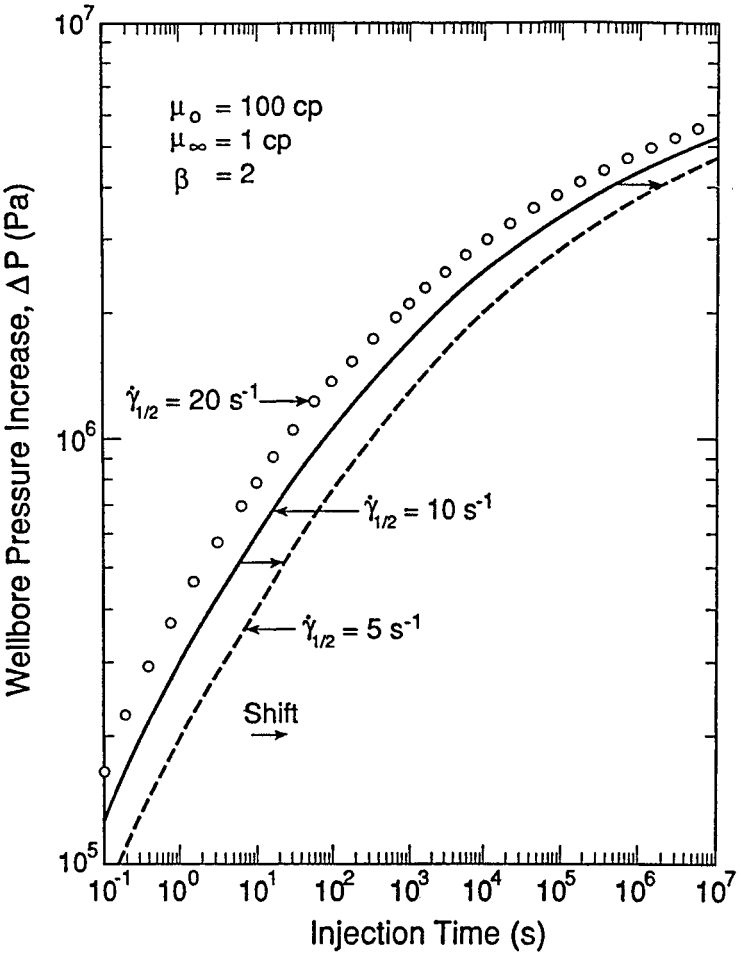


Fig. 20. Transient pressure behavior of pseudoplastic fluid flow in porous media, effects of the coefficient $\gamma_{1/2}$.

and recommended for transient pressure analysis of power-low fluid injectivity tests. This method combines the log-log analysis technique by Ikoku and Ramey with numerical simulation. One published example of well test data was analyzed by using this method to demonstrate its application to field problems. The results show that considerable improvement on the existing analysis techniques has been obtained for more accurate fluid and formation properties.

By using an idealized fracture model, this study presents the fundamentals of the behavior of power-law fluid flow in a fractured medium. Transient flow of a power-law fluid in a double-porosity system is controlled by the two dimensionless parameters, the storage coefficient ω and the interporosity parameter λ, and is characterized by the two-parallel straight lines on a log-log plot of wellbore pressure increases versus injection time. The slopes of the straight lines are related to

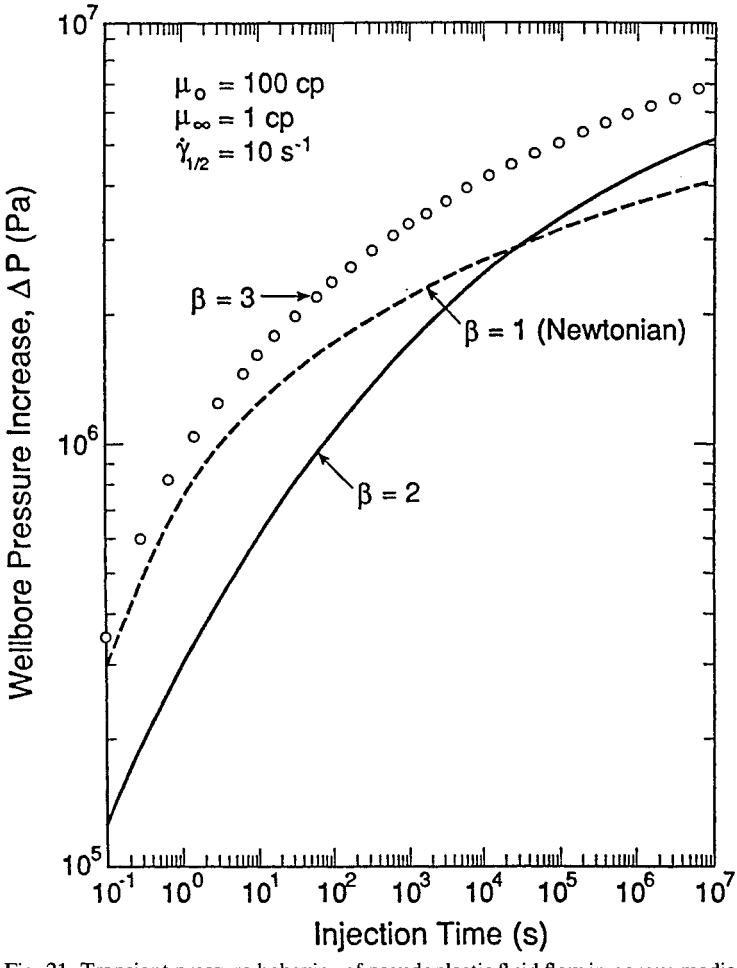


Fig. 21. Transient pressure behavior of pseudoplastic fluid flow in porous media, effects of the exponential parameter β.

the power-law index n. In general, the double-porosity approximation will result in large errors for the early time pressure prediction.

Some insights into transient flow of a general pseudoplastic non-Newtonian fluid in porous medium have also been obtained in this work. Unlike power-law fluid flow, no straight lines appear in log-log plots of pressure increase versus injection time during pseudoplastic fluid injection. Instead, semi-log straight lines on the pressure-time plots develop at late times. Therefore, the long time flow behavior of pseudoplastic fluids approaches that of an equivalent Newtonian system and is essentially determined by the low flow velocity and high viscosity zone far from the injection well.

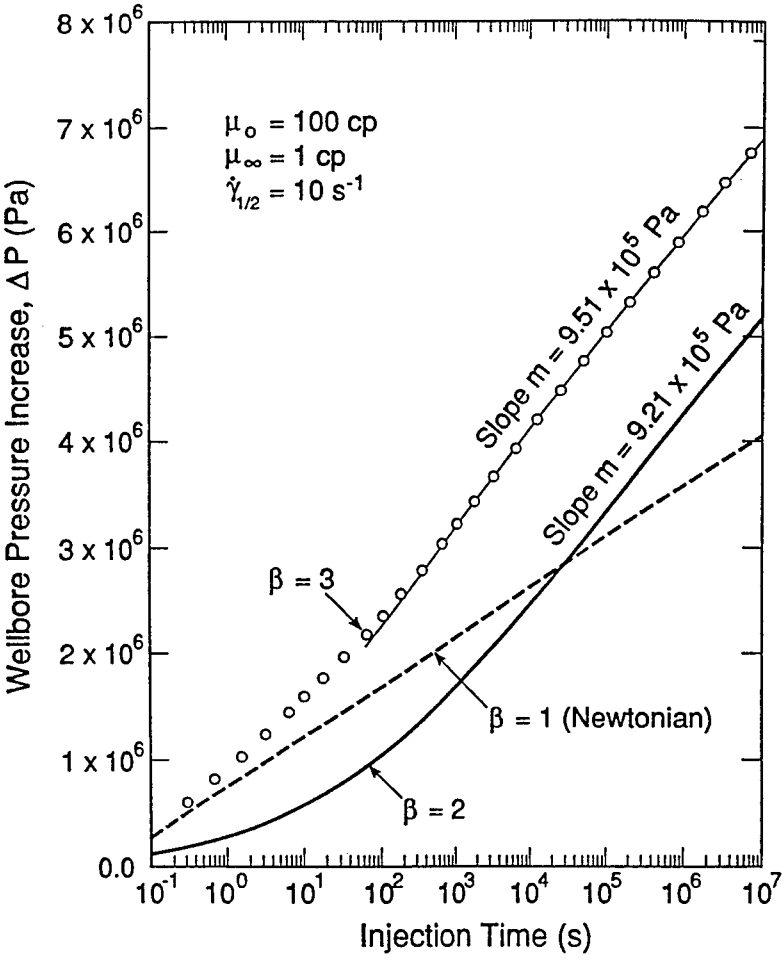


Fig. 22. Semi-log plot of transient pressure behavior of pseudoplastic fluid flow in porous media.

5. Transient flow of a single-phase Bingham non-Newtonian fluid

5.1. Introduction

This chapter presents an integral analytical method for analyzing non-linear Bingham fluid flow in porous media (Wu, Pruess, and Witherspoon, 1992). The integral method, which has been widely used in the study of unsteady heat transfer problems (Ozisik, 1980), is applied here to obtain an approximate analytical solution for Bingham fluid flow in porous media. The integral approach to heat conduction utilizes a simple parametric representation of the temperature profile, e.g., by means of a polynomial, which is based on physical concepts such as a time-dependent thermal penetration distance. An approximate solution of the heat transfer problem is then obtained from simple principles of the continuity and conservation of heat flux. This solution satisfies the governing partial differential

equation only in an average, integral sense. However, it is encouraging to note that many integral solutions to heat transfer and fluid mechanics problems have an accuracy that is generally acceptable for engineering applications (Ozisik, 1980). When applied to fluid flow problems in porous media, the integral method consists of assuming a pressure profile in the pressure disturbance zone and determining the coefficients of the profiles by making use of the integral mass balance equation.

The integral solution obtained in this section for Bingham fluid flow has been checked by comparison with solutions for a special linear case where the exact solution is available. The numerical model in Section 3 is also used to examine the analytical results from the integral solution for general non-linear problems. It is found that the accuracy of the integral solution is surprisingly good when compared with both the exact solution and the numerical results for Bingham fluid flow through an infinite radial system. In addition, a new pressure profile for integral solutions is proposed for radial flow in porous media that is better than what is typically recommended for heat conduction in radial flow systems (Lardner and Pohle, 1961). This pressure profile is able to provide very accurate results for transient fluid flow in a radial system.

The effects of non-Newtonian properties on flow behavior during a slightly-compressible Bingham fluid flow are discussed using the integral solution. The analytical results reveal the basic pressure responses in the formation during a Bingham fluid production or injection operation. Based on the analytical and numerical solutions, a new method for well test analysis of Bingham non-Newtonian fluids has been developed, which can be used to determine reservoir fluid and formation properties. In order to demonstrate the use of the new approach, two examples of pressure drawdown and buildup tests are created by the numerical and analytical simulations, and the simulated well test data are analyzed using this new technique.

5.2. Governing equation and integral solution

The problem concerned here is the flow of a Bingham fluid into a fully penetrating well in an infinite horizontal reservoir of constant thickness, in which the formation is initially saturated with the same fluid. To formulate the flow problem, the following basic assumptions are made: (1) isothermal, isotropic and homogeneous formation, (2) horizontal flow of a single-phase fluid without gravity effects, (3) Darcy's law, equation (2.7), applies with the viscosity function of equation (2.14) for the Bingham fluid, and (4) constant fluid properties.

The governing flow equation can be derived by combining the modified Darcy's law with the continuity equation, and is expressed in a radial coordinate system as

$$\frac{K}{r}\frac{\partial}{\partial r}\left\{\frac{\rho(P)}{\mu_b} r\left[\frac{\partial P}{\partial r} - G\right]\right\} = \frac{\partial}{\partial t}[\rho(P)\phi(P)] \tag{5.1}$$

The density, $\rho(P)$, of the Bingham fluid, and the porosity, $\phi(P)$, of formation, are functions of pressure only.

The initial condition is

$$P(r, t = 0) = P_i \qquad \text{(constant)} \qquad (r \geqslant r_w) \tag{5.2}$$

For the inner boundary at the wellbore, $r = r_w$, the fluid is produced at a given mass production rate $Q_m(t)$

$$\frac{2\pi r_w K h \rho(P_0)}{\mu_b}\left[\frac{\partial P}{\partial r} - G\right]_{r = r_w} = Q_m(t) \tag{5.3}$$

where $P_0 = P_0(t) = P(r_w, t)$, the unknown wellbore pressure.

The integral solution for the radial flow into a well at a specified mass production rate $Q_m(t)$ is (Wu et al., 1992)

$$P(r, t) = P_i + (r - r_w\eta)G - \frac{Q_m(t)\mu_b}{2\pi Kh}\frac{1}{\rho(P_0)}\left(\frac{1 + 2\delta(t)/r_w}{2\delta(t)/r_w}\right) \times \ln\left(\frac{2r/r_w}{\eta} - \left(\frac{r/r_w}{\eta}\right)^2\right) \tag{5.4}$$

where $\eta = 1 + \delta(t)/r_w$. The unknowns, P_0, the wellbore pressure, and $\delta(t)$, the pressure penetration distance, are determined by solving equation (5.4) by setting $r = r_w$ and the following integral equation simultaneously

$$\int_{r_w}^{r_w + \delta(t)} 2\pi h r \rho(P)\phi(P)dr = -\int_0^t Q_m(t)dt + \pi h \rho_i \phi_i [(r_w + \delta(t))^2 - r_w^2] \tag{5.5}$$

where $\rho_i = \rho(P_i)$, and $\phi_i = \phi(P_i)$. Equation (5.5) is simply a mass balance equation in the region of pressure disturbance.

For slightly compressible fluid flow, the explicit expression of the integral mass balance equation is given by

$$\int_0^t Q_m(t)dt + \rho_i \phi_i C_t r_w^t \left\{2\pi h r_w G\left(-\frac{1}{6}\eta^3 + \frac{1}{2}\eta - \frac{1}{3}\right) + \frac{Q_m(t)\mu_b}{K\rho(P_0)}\left(\frac{1 + 2\delta(t)/r_w}{2\delta(t)/r_w}\right) \times \left(-\frac{3}{2}\eta^2 + \eta + \frac{1}{2} + 2\eta \ln(\eta) - \frac{1}{2}[1 - 4\eta^2]\ln\left(\frac{2\eta - 1}{\eta^2}\right)\right)\right\} = 0 \tag{5.6}$$

Solving equations (5.4) and (5.6) with $r = r_w$ simultaneously for $\delta(t)$ and $P_0(t)$ and substituting them back into equation (5.4) give the final solution for Bingham fluid flow in a slightly compressible system.

5.3. Verification of integral solutions

The solution from the integral method is approximate and needs to be checked by comparison with an exact solution or with numerical results. In this section, the accuracy of the integral solution obtained in Section 5.2 is examined and confirmed by comparison with an exact solution for a special case and with numerical calculations in general.

TABLE 4

Parameters used for checking with exact solution

Initial pressure	$P_i = 10^7$ Pa
Initial porosity	$\phi_i = 0.20$
Initial fluid density	$\rho_i = 975.9$ kg/m^3
Formation thickness	$h = 1$ m
Fluid viscosity	$\mu_f = 0.35132 \times 10^{-3}$ Pa · s
Fluid compressibility	$C_f = 4.557 \times 10^{-10}$ Pa^{-1}
Rock compressibility	$C_r = 5 \times 10^{-9}$ Pa^{-1}
Mass injection rate	$Q_m = 1$ kg/s
Permeability	$K = 9.869 \times 10^{-13}$ m^2
Wellbore radius	$r_w = 0.1$ m

(*a*) *Comparison with exact solution*: For the special case of minimum pressure gradient $G = 0$, a Bingham fluid becomes Newtonian. Then, the Theis solution can be used to check the integral solution. A comparison of the exact Theis solution and the integral solution using parameters as given in Table 4, with $G = 0$, is presented in Figs. 23 and 24. Essentially, no differences can be observed between the wellbore pressures calculated from the two solutions in Fig. 23. There are only minor errors near the pressure penetration front of the pressure profile after 1,000 seconds of injection (Fig. 24). Many additional comparisons using different fluid and formation properties have been performed between the integral and Theis solutions, and excellent agreement has been obtained in all cases.

(*b*) *Comparison with numerical solution*: For the radial flow problem of Bingham fluid production with $G > 0$, the results from the integral solution have been examined by comparison with numerical simulations. The wellbore flowing pressures calculated from the integral and numerical solutions are shown in Fig. 25, and the parameters are summarized in Table 5. It is interesting to note that the agreement between the approximate integral and numerical results is excellent for the entire transient flow period. The pressure distribution in the formation after 1,000 sec, as shown in Fig. 26, also matches the numerical predictions extremely well.

5.4. Flow behavior of a Bingham fluid in porous media

The flow of a Bingham fluid in a porous medium is characterized by the two non-Newtonian parameters, the minimum pressure gradient G, and the Bingham plastic coefficient μ_b. The effects of the non-Newtonian rheological properties on the flow behavior in an infinite radial formation can be discussed using the integral solution of Section 5.2. The input parameters used for the fluid and formation are given in Table 6.

Pressure drawdown at the wellbore is shown in Fig. 27 while a Bingham fluid is produced at a constant mass production rate. Physically, the flow resistance increases with an increase in the minimum pressure gradient G in the reservoir.

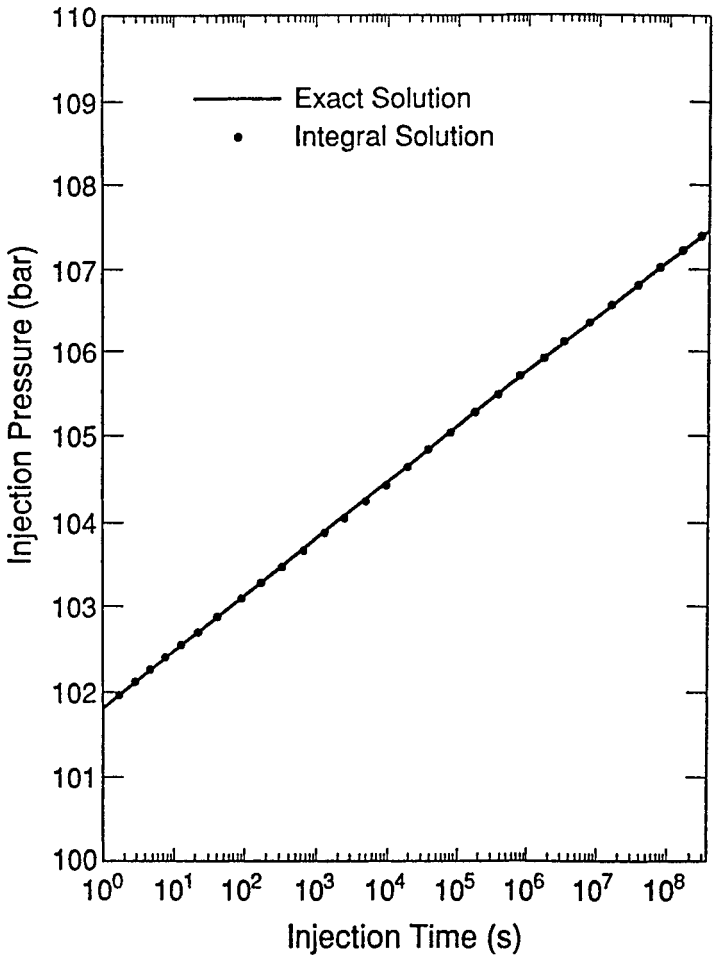


Fig. 23. Comparison of injection pressures during Newtonian fluid injection, calculated from the exact theis solution and the integral solutions with pressure profiles recommended in this work.

It can be seen from Fig. 27 that in order to maintain the same production rate, the wellbore pressures will decrease more rapidly as G increases. The pressure profiles at different values of G after continuous production of 10 hr are given on Figs. 28 and 29. The pressure drops penetrate less deeply into the formation as the minimum pressure gradient increases. It should be noted in the semi-log plot of the pressure distributions on Fig. 29 that parallel semi-log straight lines of pressure versus $\log(r)$ in the formation exist near the wellbore for various values of G. Semi-log straight lines are also developed in the pressure drawdown curves of Fig. 27. This suggests that the conventional semi-log analysis method to calculate flow and formation properties can be used.

The effects of the Bingham plastic coefficient, μ_b, are shown in Fig. 30. This coefficient becomes the viscosity of a Newtonian fluid if $G = 0$. The apparent

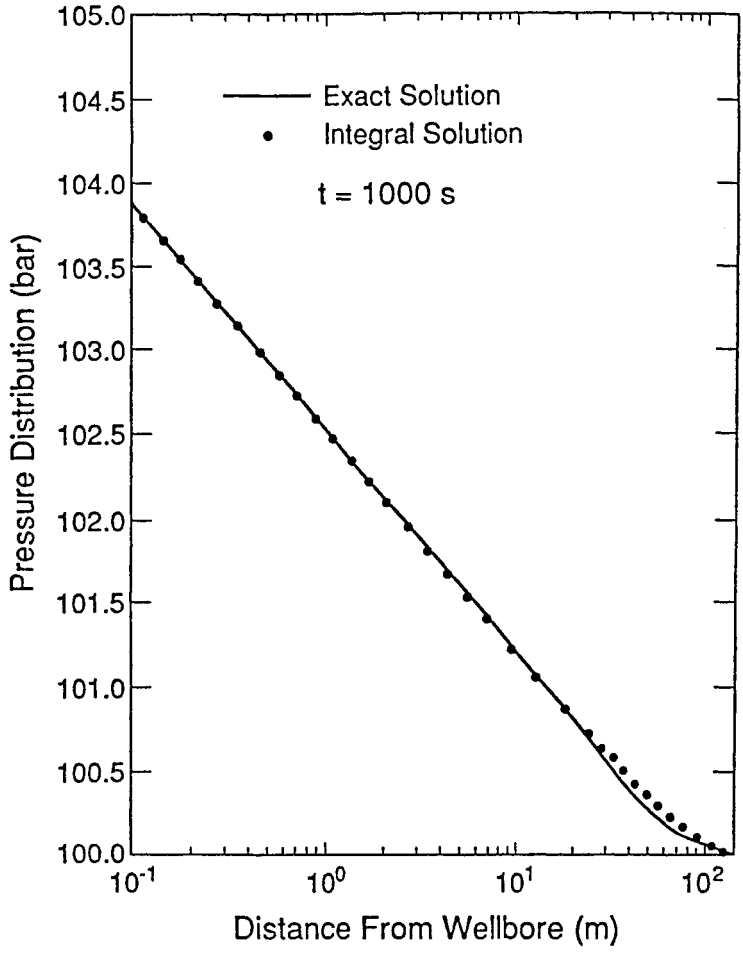


Fig. 24. Comparison of pressure distributions of Newtonian fluid injection, calculated from the exact Theis solution and the integral solutions with pressure profiles recommended in this work.

viscosity of a Bingham fluid is proportional to μ_b, as given by equation (2.14). Therefore, as μ_b increases, the flow resistance increases, and the pressure drops more rapidly to satisfy the constant production rate at the well. Fig. 30 also shows that semi-log straight lines exist during the earlier transient times which can be used to estimate the value of μ_b.

5.5. Well testing analysis of Bingham fluid flow

An analysis approach of transient pressure tests during a Bingham fluid production from and injection into a well can be developed, based on the integral and numerical solutions. The most important factors of controlling Bingham fluid flow through porous medium are the two characteristic rheological parameters: the minimum pressure gradient, G, and the coefficient, μ_b. Both of them can be

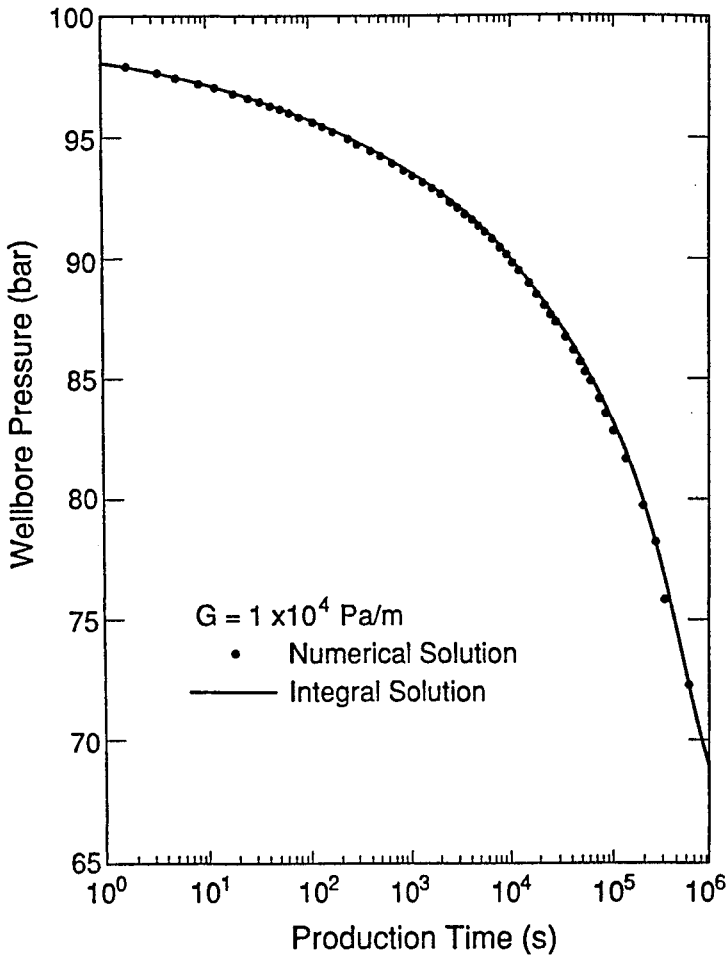


Fig. 25. Comparison of wellbore pressures during Bingham fluid production, calculated from the numerical solution and the integral solution (G = 10000 Pa/m).

TABLE 5

Parameters used for checking with numerical solution

Initial pressure	$P_i = 10^7$ Pa
Initial porosity	$\phi_i = 0.20$
Initial fluid density	$\rho_i = 975.9$ kg/m^3
Formation thickness	$h = 1$ m
Bingham plastic coefficient	$\mu_b = 5 \times 10^{-3}$ Pa · s
Total compressibility	$C_t = 3 \times 10^{-9}$ Pa^{-1}
Mass production	$Q_m = 0.1$ kg/s
Permeability	$K = 9.869 \times 10^{-13}$ m^2
Wellbore radius	$r_w = 0.1$ m
Minimum pressure gradient	$G = 10^2, 10^3, 10^4$ Pa m^{-1}

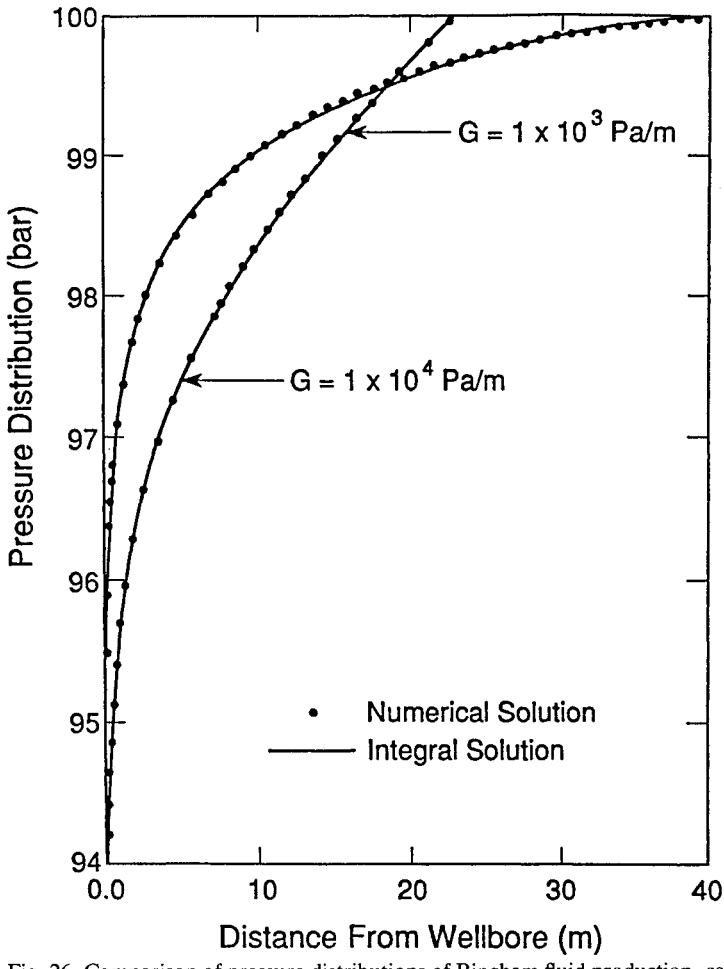


Fig. 26. Comparison of pressure distributions of Bingham fluid production, calculated from the numerical solution and the integral solution.

TABLE 6

Parameters for a Bingham fluid flow through a porous medium

Initial pressure	$P_i = 10^7$ Pa
Initial porosity	$\phi_i = 0.20$
Initial fluid density	$\rho_i = 1000.0$ kg m^{-3}
Formation thickness	$h = 1$ m
Bingham plastic coefficient	$\mu_b = 1.0 \times 10^{-3}$ Pa · s
Fluid compressibility	$C_f = 4.55575 \times 10^{-10}$ Pa^{-1}
Rock compressibility	$C_r = 2.0 \times 10^{-10}$ Pa^{-1}
Mass production rate	$Q_m = 0.5$ kg/s
Permeability	$K = 9.869 \times 10^{-13}$ m^2
Wellbore radius	$r_w = 0.1$ m
Minimum pressure gradient	$G = 10^2, 10^3, 10^4$ Pa m^{-1}

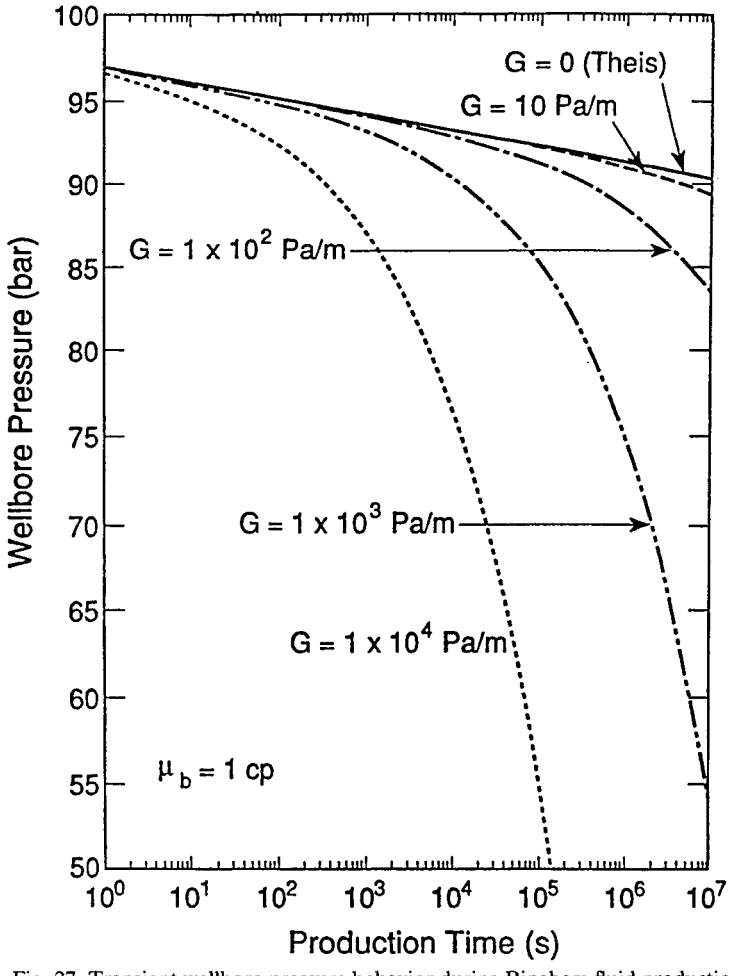


Fig. 27. Transient wellbore pressure behavior during Bingham fluid production, effects of the minimum pressure gradient.

determined by a well-designed single well pressure test, discussed below. It is always possible to obtain these parameters by trial and error, using the integral or numerical solutions to match the observed pressure data. However, the following approach is more accurate and convenient to use, and therefore is recommended for field applications.

Let us consider the pressure buildup behavior at a producing well in an infinite horizontal formation. After a period of production, the well is shut in. Physically, the pressure in the system after a long enough shut-in period will buildup until a new equilibrium is reached. Then, there is a stable pressure drop formed from wellbore to a certain pressure penetration distance, and the pressure gradient everywhere in the pressure drop zone is expected to be equal to the minimum pressure gradient. This is confirmed by a numerical study of the pressure buildup, as shown in Fig. 31, after t_p = 1,000 seconds of Bingham fluid production from a

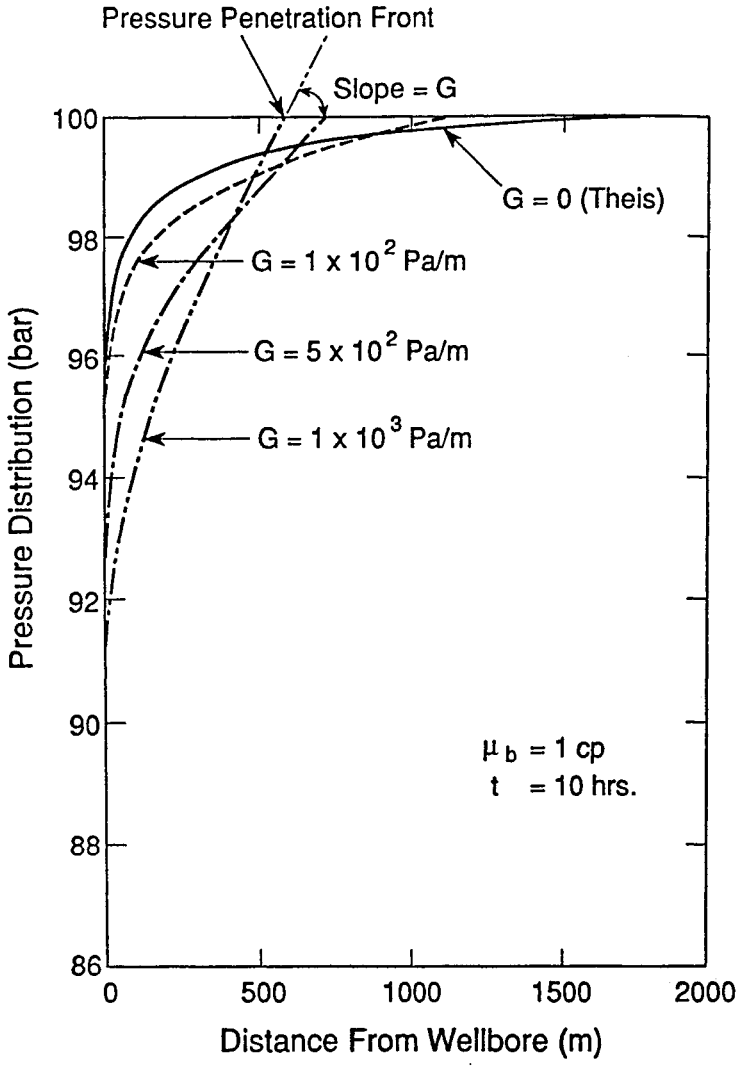


Fig. 28. Pressure distributions in a linear plot of Bingham fluid production, effects of the minimum pressure gradient.

well. The flow and formation properties used are provided in Table 7. If we know the cumulative mass production rate Q_c before the well is shut in, and measure the stable wellbore pressure P_w at a long time after stopping production from the well, the minimum pressure gradient of the system can be calculated (Wu, 1990) by

$$G = \frac{1}{2Q_c}\{\pi h r_w \rho_i \phi_i C_t (\Delta P)^2 + ([\pi h r_w \rho_i \phi_i C_t (\Delta P)^2]^2 + 4\pi h \rho_i \phi_i C_t (\Delta P)^3/3)^{1/2}\} \quad (5.7)$$

where $\Delta P = P_i - P_w$, the stable pressure drop at wellbore, measured at a long time after well shut-in. It is interesting to note that the minimum pressure gradient

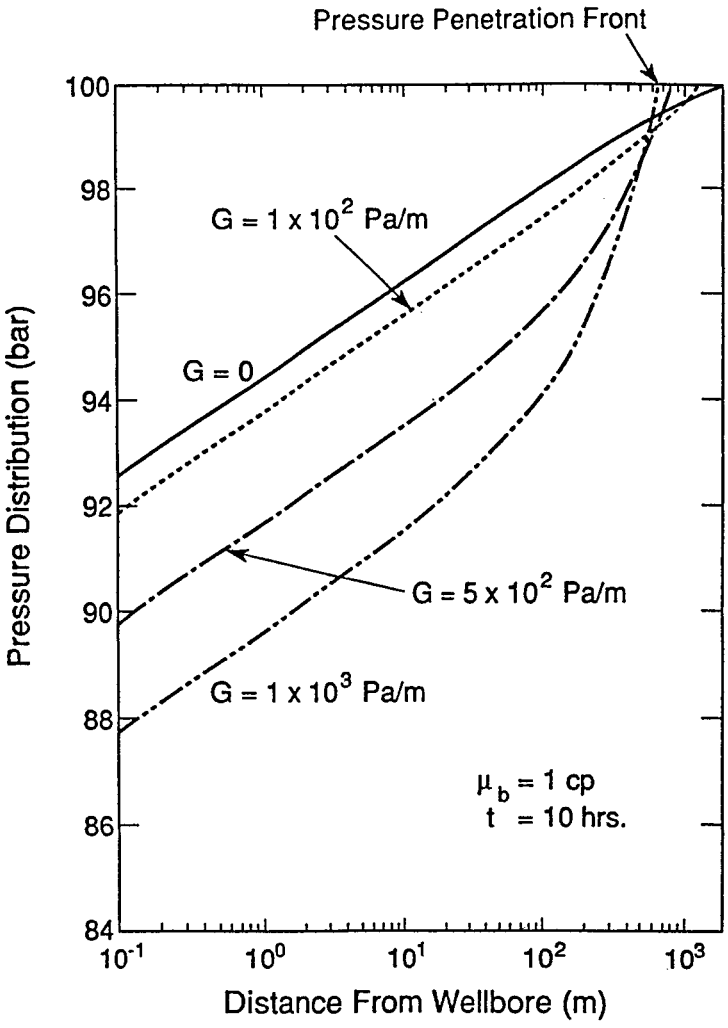


Fig. 29. Pressure distributions in a semi-log plot of Bingham fluid production, effects of the minimum pressure gradient.

determined by the pressure buildup method, equation (5.7), is independent of the flow properties, such as permeability K, and the coefficient μ_b, since the equilibrium is obtained in the system.

A test example of Bingham fluid buildup has here been created by the numerical simulator, to illustrate the procedure of calculating the value of G. The input data are from Table 6, and the stable wellbore pressure is found to be $P_w = 0.97474 \times 10^7$ Pa, at a long well shut-in time from the simulated test. A Bingham fluid is produced at a mass rate $Q_m = 0.1$ kg/s until the production time $t_p = 1{,}000$ sec, and then the well is shut in. Thus, the minimum pressure gradient can be calculated by equation (5.7)

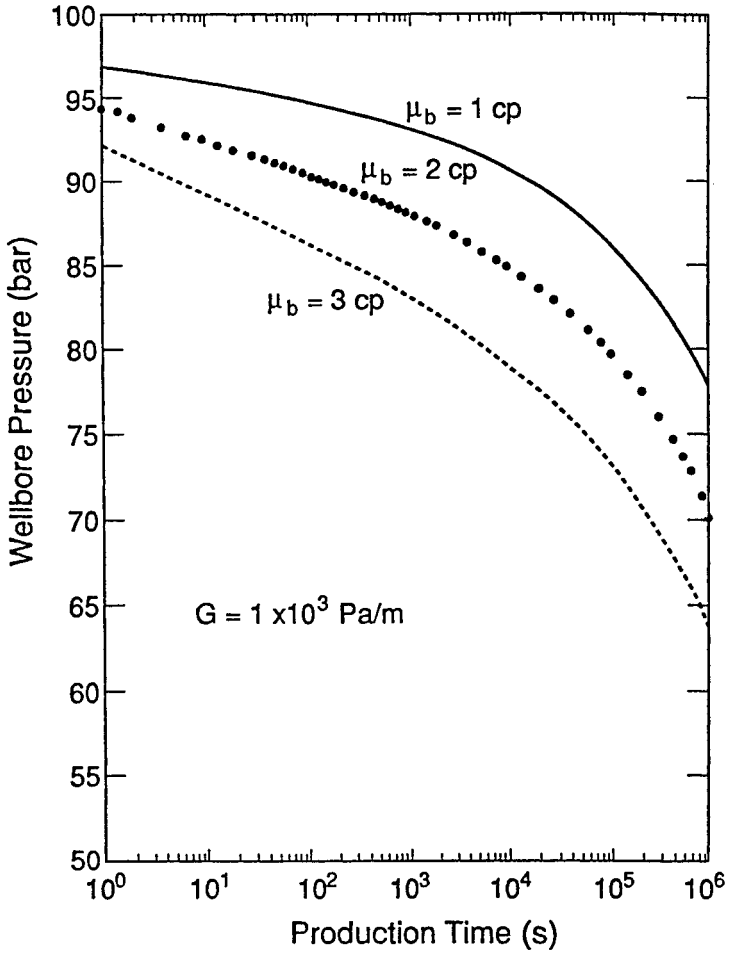


Fig. 30. Transient wellbore pressure behavior during Bingham fluid production, effects of the Bingham coefficient μ_b.

$$G = \frac{1}{200} \times (1.1737423 \times 10^5 + (1.377671 \times 10^8 + 3.953165 \times 10^{12})^{1/2})$$

$$= 10{,}000.14 \text{ (Pa/m)}$$

This is very accurate compared with the input value, $G = 10{,}000$ Pa/m, in the numerical calculation. Then, the pressure penetration distance under the equilibrium is

$$\delta(t) = \frac{\Delta P}{G} = \frac{2.526 \times 10^5}{10{,}000.14} = 25.26 \text{ (m)} \tag{5.9}$$

The pressure distribution after a long time shut-in calculated from the mass balance is also shown in Fig. 31, by the solid line curve. The analytical and numerical results are essentially identical to each other in the figure.

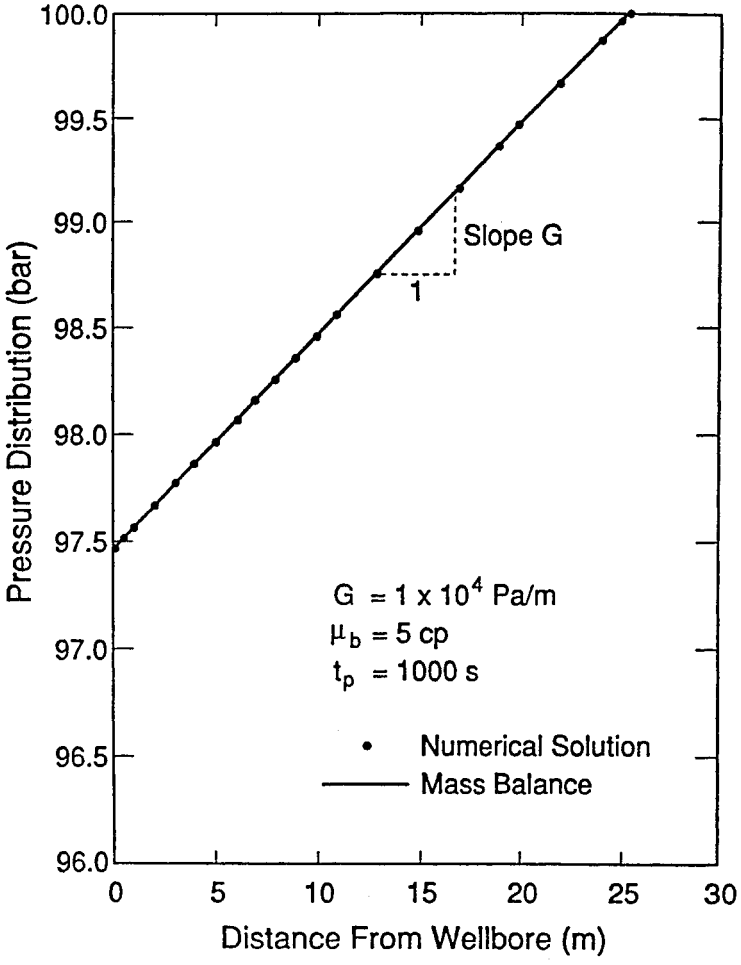


Fig. 31. Pressure distribution at long-time of well shut-in after 1000 sec of Bingham fluid production.

TABLE 7

Parameters for well testing analysis

Initial pressure	$P_i = 10^7$ Pa
Initial porosity	$\phi_i = 0.20$
Initial fluid density	$\rho_i = 975.9$ kg/m^3
Formation thickness	$h = 1$ m
Bingham plastic coefficient	$\mu_b = 5.0 \times 10^{-3}$ Pa · s
Total compressibility	$C_t = 9.0 \times 10^{-9}$ Pa^{-1}
Mass production rate	$Q_m = 0.1$ kg/s
Permeability	$K = 9.869 \times 10^{-13}$ m^2
Minimum pressure gradient	$G = 1.0 \times 10^4$ Pa/m
Wellbore radius	$r_w = 0.1$ m

The apparent mobility, (K/μ_b), is a flow property of the system, and may be determined by only the transient flow tests of pressure drawdown and buildup. As shown in Figs. 27 and 30, the semi-log straight lines occur in the pressure drawdown curves during the early transient period, when minimum pressure gradient, G, is not very large. The semi-log straight lines are almost in parallel with the straight line from the Theis solution ($G = 0$) on Fig. 27. Therefore, if the semi-log straight line is developed during the earlier flow time in the transient drawdown analysis plot, the conventional analysis technique of pressure drawdown (Earlougher, 1977; Matthews and Russell, 1967) can be used to estimate the value of (K/μ_b) for a Bingham fluid flow problem

$$\frac{K}{\mu_b} = \frac{2.303 \times Q}{4\pi hm} \tag{5.10}$$

where m is the slope of the semi-log straight line; and Q is the constant volumetric production rate.

A simulated pressure drawdown test is generated by the integral solution, and the parameters used are the same as in Table 6. The pressure drawdown curves of the test are shown in Fig. 27, and the slope m of the semi-log straight line part of the curve $G = 100$ Pa/m, is measured as 9.24×10^4 Pa/$\log_{10}$-cycle, and the slope of the curve $G = 1{,}000$ Pa/m is 9.95×10^4 Pa/$\log_{10}$-cycle. Then, K/μ_b, can be estimated as

$$\frac{k}{\mu_b} = \frac{2.303 \times 0.5/1000}{4 \times 3.1415926 \times 1 \times 9.24 \times 10^4} = 9.92 \times 10^{-10}\ (\mathrm{m^2/Pa \cdot s}) \tag{5.11}$$

In the simulated test, the actual input is

$$\frac{K}{\mu_b} = \frac{0.9869 \times 10^{-12}}{1 \times 10^{-3}} = 9.87 \times 10^{-10}\ (\mathrm{m^2/Pa \cdot s}) \tag{5.12}$$

So, the relative errors introduced into the results are only 0.5% from the calculation.

For a large value of minimum pressure gradient, G, in a system, there hardly exist semi-log straight lines in the pressure drawdown plots of Fig. 27. However, the pressure buildup curves, as shown in Fig. 32, do result in a longer straight line even for the large minimum pressure gradient, $G = 10{,}000$ Pa/, in which the pressure buildup test is conducted by the numerical code. The top curve is calculated from the integral solution, based on the superposition principle. It is obvious that the superposition technique cannot be used for the non-linear problem of Bingham fluid flow. The slope of the semi-log straight line of Fig. 32 can be measured as, $m = 9.17 \times 10^4$ $\log_{10}$-cycle. Then, we have

$$\frac{K}{\mu_b} = \frac{2.303 \times 0.1/975.9}{4 \times 3.1415926 \times 1 \times 9.17 \times 10^4} = 2.05 \times 10^{-10}\ (\mathrm{m^2/Pa \cdot s}) \tag{5.13}$$

This value introduces only 3.8% errors in the result by comparison with the input value, $K/\mu_b = 1.97 \times 10^{-10}$ $\mathrm{m^3/Pa \cdot s}$.

If no straight lines have developed in both pressure drawdown and pressure buildup curves in a well test, then the apparent mobility can be obtained using

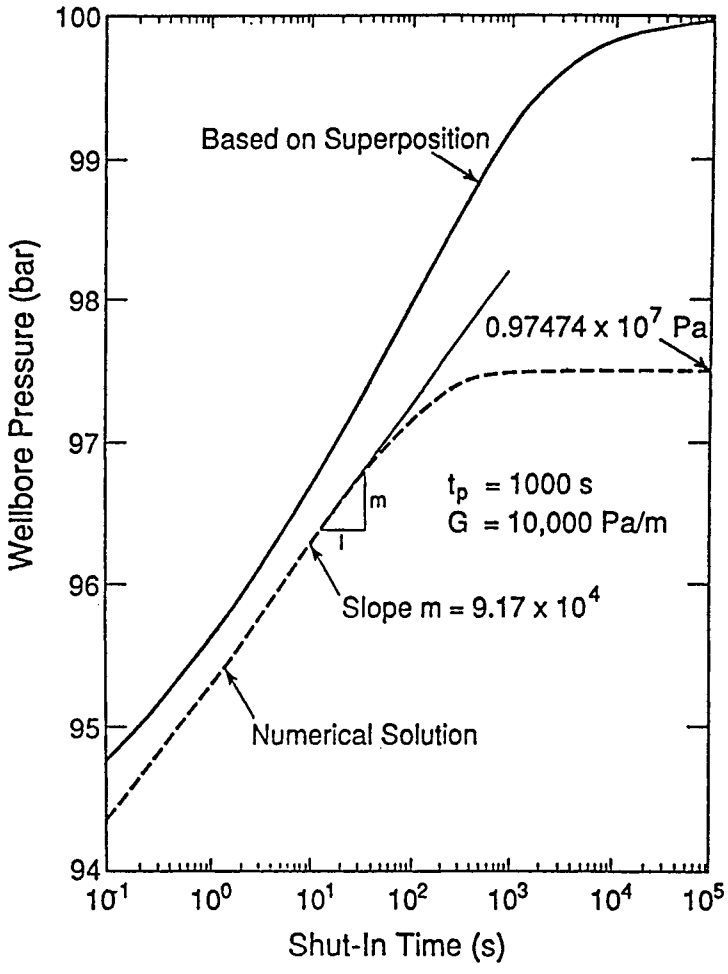


Fig. 32. Pressure buildup during well shut-in after 1000 sec of Bingham fluid production.

the integral solution to match the observed transient pressure data. In this procedure, the minimum pressure gradient, G, should be calculated first by the mass balance calculation of equation (5.7), which is always applicable. Then, the only unknown is the apparent mobility, (K/μ_b), which can be determined by trial and error using the integral solution.

5.6. Summary

An integral solution has been presented for analysis of flow behavior of Bingham fluids through a porous medium, and its accuracy is confirmed by comparison of the integral results with the exact and numerical solutions, respectively. The analytical and numerical studies show that the transient flow behavior of a slightly compressible Bingham fluid is essentially controlled by the non-Newtonian properties, the minimum pressure gradient G, and the coefficient μ_b. Therefore, the

transient pressure data will provide some important information related to the non-Newtonian fluid and formation properties. A well testing analysis technique, developed from the integral solution, uses these flow test data to estimate the non-Newtonian flow properties in the system.

The integral method with the pressure profile used in this work will find more applications for transient radial flow problems in porous medium. It is especially useful when the flow equation is non-linear and other analytical approaches cannot apply.

6. Multiphase immiscible flow involving non-Newtonian fluids

6.1. Introduction

Immiscible flow of multiphase fluids through porous media occurs in many subsurface systems. The behavior of multiphase flow, as compared with single-phase flow, is much more complicated and is not well understood in many areas due to the complex interactions of different fluid phases and heterogeneous nature of porous materials. A fundamental understanding of immiscible displacement of Newtonian fluids in porous media was contributed by Buckley and Leverett (1942) in their classical study of the fractional flow theory. The Buckley-Leverett solution gave a saturation profile with a sharp displacement front by ignoring the capillary pressure and gravity effects. A frequently encountered property of the Buckley-Leverett method is that the saturation becomes a multiple-valued function of the distance coordinate, x. This difficulty can be overcome by consideration of a material balance. Following the work of Buckley and Leverett (1942), a simple graphic approach was invented by Welge (1952), which can easily determine the sharp saturation front without the difficulty of the multiple-valued saturation problem for a uniform initial saturation distribution. More recently, some special analytical solutions for immiscible displacement including the effects of capillary pressure were obtained by Yortsos and Fokas (1983), Chen (1988), and McWhorter and Sunada (1990).

The Buckley-Leverett fractional flow theory has been applied and generalized by various authors to study the enhanced oil recovery (EOR) problems (Pope 1980), surfactant flooding (Larson and Hirasaki, 1978), polymer flooding (Patton, Coats and Colegrone, 1971), mechanism of chemical methods (Larson, Davis and Scriven, 1982), detergent flooding (Fayers and Perrine, 1959), displacement of oil and water by alcohol (Wachmann, 1964; Taber, Kamath and Reed, 1961), displacement of viscous oil by hot water and chemical additive (Karakas, Saneie, and Yortsos, 1986), and alkaline flooding (deZabala, Vislocky, Rubin and Radke, 1982). An extension to more than two immiscible phases dubbed "coherence theory" was described by Helfferich (1981). However, no non-Newtonian behavior has been considered in any of these works.

Non-Newtonian and Newtonian fluid immiscible displacement occurs in many EOR processes involving the injection of non-Newtonian fluids, such as polymer solutions, microemulsions, macroemulsions, and foam solutions. Almost all the

theoretical and experimental studies performed on non-Newtonian fluid flow in porous media have focused on single non-Newtonian phase flow. Very little research has been published in the English literature on multiphase flow of non-Newtonian and Newtonian fluids through porous media (Bernadiner, 1991). To the best of our knowledge, not many analytical solutions are available on this subject. Even using numerical methods, very few studies have been conducted (Gencer and Ikoku, 1984). Therefore, the mechanism of immiscible displacement involving non-Newtonian fluids in porous media is still not well understood, as compared with Newtonian fluid flow.

In this Section, an analytical solution describing the displacement mechanism of non-Newtonian/Newtonian fluid flow in porous media will be presented for one-dimensional linear flow (Wu, Pruess, and Witherspoon, 1991). Our approach follows the classical work of Buckley and Leverett (1942) for immiscible displacement of Newtonian fluids. The major difference due to non-Newtonian behavior is in the fractional flow curve, which because of the velocity-dependent effective viscosity of a non-Newtonian fluid now becomes dependent on injection rate, or fluid velocity. A practical procedure for evaluating the behavior of non-Newtonian and Newtonian displacement is also provided, based on the analytical solution, which is similar to the graphic method by Welge (1952). The resulting procedure can be regarded as an extension of the Buckley-Leverett theory to the flow problem of non-Newtonian fluids in porous media. The analytical results reveal how the saturation profile and the displacement efficiency are controlled not only by the relative permeabilities, as in the Buckley-Leverett solution, but also by the inherent complexities of non-Newtonian fluids.

The analytical solution will find application in two areas: (1) it can be employed to study the displacement mechanisms of non-Newtonian and Newtonian fluid in porous media, and (2) it may be used to check numerical solutions from a simulator of non-Newtonian flow.

In addition, a numerical method has been used to simulate non-Newtonian and Newtonian multiple phase flow using the integral finite difference approach (Pruess and Wu, 1988). The numerical model can take into account all the important factors which affect the flow behavior of non-Newtonian and Newtonian fluids, such as capillary pressure, complicated flow geometry and operation conditions. The different rheological models for non-Newtonian fluid flow in porous media can easily be incorporated in the code. The validity of the numerical method has been checked by comparing the numerical results with those of the analytical solution, and excellent agreement has been obtained using power-law and Bingham non-Newtonian fluids.

6.2. Analytical solution for non-Newtonian and Newtonian fluid displacement

Two-phase flow of non-Newtonian and Newtonian fluids is considered in a homogeneous and isotropic porous medium. There is no mass transfer between non-Newtonian and Newtonian fluids, and dispersion and adsorption on the rock are ignored. Then, the governing equations are given by equation (3.5)

$$-\nabla \cdot (\rho_{ne}\mathbf{u}_{ne}) = \frac{\partial}{\partial t}(\rho_{ne}S_{ne}\phi) \tag{6.1}$$

for the Newtonian fluid

$$-\nabla \cdot (\rho_{nn}\mathbf{u}_{nn}) = \frac{\partial}{\partial t}(\rho_{nn}S_{nn}\phi) \tag{6.2}$$

for the non-Newtonian fluid. The flow for Newtonian and non-Newtonian phases is described by a multiple phase extension of Darcy's law, equation (2.7)

$$\mathbf{u}_{ne} = -K\frac{k_{ne}}{\mu_{ne}}(\nabla P_{ne} - \rho_{ne}\mathbf{g}) \tag{6.3}$$

and

$$\mathbf{u}_{nn} = -K\frac{k_{rnn}}{\mu_{nn}}(\nabla P_{nn} - \rho_{nn}\mathbf{g}) \tag{6.4}$$

The pressures in the two phases depend on the capillary pressure

$$P_c(S_{nn}) = P_{ne} - P_{nn} \tag{6.5}$$

k_{ne}, k_{nn} and P_c are assumed to be functions of saturation only. Also, from the definition of saturation, we have

$$S_{ne} + S_{nn} = 1 \tag{6.6}$$

For the derivation of the analytical solution, the following additional assumptions are made (Wu, Pruess and Witherspoon, 1991): (1) the two fluids and the porous medium are incompressible, (2) the capillary pressure gradient is negligible, (3) the viscosity of non-Newtonian fluids is a function of pressure gradient and saturation only, as described in equation (2.15), and (4) one-dimensional linear flow.

The flow system is a semi-infinite linear reservoir with a constant cross-sectional area A, as shown in Fig. 33. The system is initially saturated with both Newtonian and non-Newtonian fluids, and a non-Newtonian fluid is injected at the inlet. It is further assumed that gravity segregation is negligible and stable displacement exists near the displacement front. Equations (6.1) and (6.2) can then be changed to read

$$-\frac{\partial u_{ne}}{\partial x} = \phi\frac{\partial S_{ne}}{\partial t} \tag{6.7}$$

and

$$-\frac{\partial u_{nn}}{\partial x} = \phi\frac{\partial S_{nn}}{\partial t} \tag{6.8}$$

where u_{ne} and u_{nn} are the volumetric flow velocities of Newtonian and Newtonian fluids, respectively. For the Newtonian phase, the flow velocity is

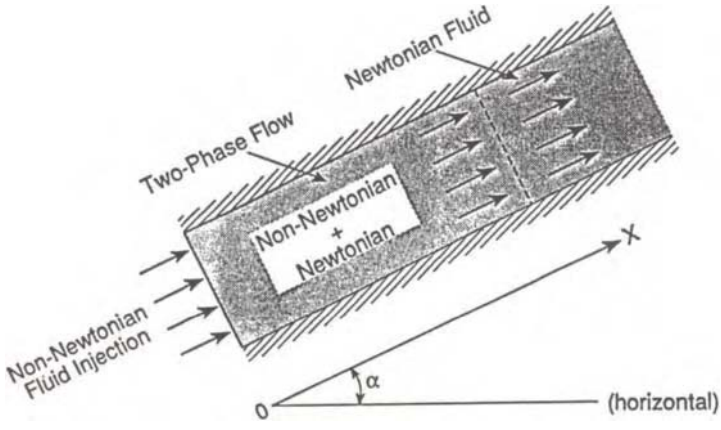


Fig. 33. Schematic of displacement of a Newtonian fluid by a non-Newtonian fluid.

$$u_{ne} = -K\frac{k_{rne}}{\mu_{ne}}\left(\frac{\partial P}{\partial x} + \rho_{ne}g\sin\alpha\right) \tag{6.9}$$

and for the non-Newtonian phase

$$u_{nn} = -K\frac{k_{nn}}{\mu_{nn}}\left(\frac{\partial P}{\partial x} + \rho_{nn}g\sin\alpha\right) \tag{6.10}$$

Here α is the angle between the horizontal plane and the flow direction of the x coordinate. To complete the mathematical description of the physical problem, the initial and boundary conditions must be specified. Initially, the Newtonian fluid is at its maximum saturation in the system.

$$S_{ne}(x, 0) = 1 - S_{nnir}(x) \tag{6.11}$$

where S_{nnir} is the initial immobile non-Newtonian fluid saturation. For most practical field problems, S_{nnir} is usually zero, which can be treated as a special case.

In this problem, we are concerned with continuously injecting a non-Newtonian fluid at a known rate $q(t)$, which is generally a function of injection time t. The boundary conditions at $x = 0$ are

$$u_{nn}(0, t) = \frac{q(t)}{A} \tag{6.12}$$

$$u_{ne}(0, t) = 0 \tag{6.13}$$

In this semi-infinite system, the following condition must be imposed as $x \to \infty$

$$S_{ne} \to 1 - S_{nnir} \tag{6.14}$$

and

$$S_{nn} \to S_{nnir} \tag{6.15}$$

The solution procedure follows the work by Buckley and Leverett (1942), as outlined by Willhite (1986). The fractional flow concept is also used to simplify the governing equations in terms of saturation only in this study. The fractional flow of a phase is defined as a volume fraction of the phase flowing at x and t to the total volume of the flowing phases (Willhite, 1986). For the Newtonian phase, this can be written

$$f_{ne} = \frac{u_{ne}}{u_{ne} + u_{nn}} = \frac{u_{ne}}{u(t)} \tag{6.16}$$

and for the non-Newtonian phase

$$f_{nn} = \frac{u_{nn}}{u_{ne} + u_{nn}} = \frac{u_{nn}}{u(t)} \tag{6.17}$$

where $u(t) = u_{ne} + u_{nn}$. From a volume balance, the sum of equations (5.16) and (5.17) yields

$$f_{ne} + f_{nn} = 1 \tag{6.18}$$

The fractional flow function for the non-Newtonian phase may be written in the following form (Willhite, 1986)

$$f_{nn} = \frac{1}{1 + \left[\frac{k_{rne}(S_{nn})}{k_{rnn}(S_{nn})}\right]\left[\frac{\mu_{nn}(\partial\Phi/\partial x, S_{nn})}{\mu_{ne}}\right]} + \frac{[AKk_{rne}(S_{nn})/\mu_{ne}q(t)]/(\rho_{ne} - \rho_{nn})g\sin(\alpha)}{1 + \left[\frac{k_{rne}(S_{nn})}{k_{rnn}(S_{nn})}\right]\left[\frac{\mu_{nn}(\partial\Phi/\partial x, S_{nn})}{\mu_{ne}}\right]} \tag{6.19}$$

where the component of the potential gradient $\nabla\Phi$ along the x coordinate for the non-Newtonian fluid is

$$\frac{\partial\Phi}{\partial x} = \frac{\partial P}{\partial x} + \rho_{nn} g \sin\alpha \tag{20}$$

Equation (6.19) indicates that the fractional flow f_{nn} for the non-Newtonian phase is generally a function of both saturation and potential gradient. However, for a given injection rate, and fluid and rock properties, the potential gradient at a given time can be shown to be a function of saturation only under the Buckley-Leverett flow condition

$$q(t) + AK\left[\frac{k_{rne}(S_{nn})}{\mu_{ne}} + \frac{k_{rnn}(S_{nn})}{\mu_{nn}(\partial\Phi/\partial x, S_{nn})}\right]\frac{\partial P}{\partial x} + K\left[\frac{\rho_{ne}k_{rne}(S_{nn})}{\mu_{ne}} + \frac{\rho_{nn}k_{rnn}(S_{nn})}{\mu_{nn}(\partial\Phi/\partial x, S_{nn})}\right]g\sin(\alpha) = 0 \tag{6.21}$$

Equation (6.21) shows that the flow potential gradient and the saturation are

dependent on each other for this particular displacement system, and defines the potential gradient in the system as a function of saturation implicitly.

The governing equations (6.7) and (6.8) subject to the boundary and initial conditions (6.11)–(6.15) can be solved to obtain the following solution (Wu, Pruess and Witherspoon, 1991)

$$\left(\frac{dx}{dt}\right)_{S_{nn}} = \frac{q(t)}{\phi A}\left(\frac{\partial f_{nn}}{\partial S_{nn}}\right)_t \tag{6.22}$$

This is the frontal advance equation for the non-Newtonian displacement, and interestingly it is in the same form as the Buckley-Leverett equation. However, the dependence of the fractional flow f_{nn} for the non-Newtonian displacement on saturation is not only through the relative permeability, but also through the non-Newtonian phase viscosity, as described by equation (6.19). Equation (6.22) shows that, for a given time and a given injection rate, a particular non-Newtonian fluid saturation profile propagates through the porous medium at a constant velocity. As in the Buckley-Leverett theory, the saturation for a vanishing capillary pressure gradient will in general become a triple-valued function of distance near the displacement front (Cardwell,1959). Equation (6.22) will then fail to describe the velocity of the shock saturation front, since $\partial f_{nn}/\partial S_{nn}$ does not exist on the front because of the discontinuity in S_{nn} at that point. Consideration of material balance across the shock front (Sheldon, et al., 1959) provides the velocity of the front

$$\left(\frac{dx}{dt}\right)_{S_f} = \frac{q(t)}{A\phi}\left(\frac{f_{nn}^{+} - f_{nn}^{-}}{S_{nn}^{+} - S_{nn}^{-}}\right) \tag{6.23}$$

where S_f is the front saturation of the displacing non-Newtonian phase. The superscripts " + " and " − " refer to values ahead of and behind the front, respectively.

The location $x_{S_{nn}}$ of any saturation S_{nn} traveling from the inlet at time t can be determined by integrating equation (6.22) with respect to time, which yields

$$x_{S_{nn}} = \frac{Q(t)}{A\phi}\left(\frac{\partial f_{nn}}{\partial S_{nn}}\right)_{S_{nn}} \tag{6.24}$$

where $Q(t)$ is the cumulative volume of the injected fluid

$$Q(t) = \int_0^t q(\lambda)d\lambda \tag{6.25}$$

A direct use of equation (6.24), given x and t, will result in a multiple-valued saturation distribution, which can be handled by a mass balance calculation, as in the Buckley-Leverett solution. An alternative Welge (1952) graphic method of evaluating the above solution has been shown (Wu, Pruess and Witherspoon, 1991) to apply to a non-Newtonian fluid displacement by integration of the mass balance of the fluid injected into the system and incorporating the result of equation (6.24). The additional work in applying this method is to take into account the contribution of a velocity-dependent apparent viscosity of the non-

Newtonian fluid on the fractional flow curve. Therefore, the non-Newtonian fluid saturation at the moving saturation front is determined by

$$\left(\frac{\partial f_{nn}}{\partial S_{nn}}\right)_{S_f} = \frac{f_{nn}|_{S_f} - f_{nn}|_{S_{nnir}}}{S_f - S_{nnir}} \tag{6.26}$$

and the average saturation in the displaced zone is given by

$$\left(\frac{\partial f_{nn}}{\partial S_{nn}}\right)_{S_f} = \frac{1}{\bar{S}_{nn} - S_{nnir}} \tag{6.27}$$

where $\bar{S}_{nn}$ is the average saturation of the non-Newtonian phase in the swept zone. Then, the complete saturation profile can be determined using equation ((6.24) for a given problem.

6.3. Displacement of a Newtonian fluid by a power-law non-Newtonian fluid

In this section, the analytical solution presented above is used to look at displacement phenomena of a Newtonian fluid by a power-law, non-Newtonian fluid. The physical flow model is a one-dimensional linear porous medium, which is initially saturated only with a Newtonian Fluid. A constant volumetric injection rate of a power-law fluid is imposed at the inlet, $x = 0$, from $t = 0$. The relative permeability curves used for all the calculations in this chapter are shown in Fig. 34, and the properties of rock and fluids are given in Table 8. The solution (6.24) is evaluated to obtain the saturation profiles with the sharp-front saturation determined by equation (6.26). The apparent viscosity for a power-law fluid is represented by equation (2.11) for single-phase flow, and it may be extended to the two-phase flow by replacing permeability K by phase permeability Kk_{rnn} and porosity ϕ by $\phi(S_{nn} - S_{nnir})$. Then, we can obtain the following relationship for the pressure gradient corresponding to a particular value of S_{nn} using equation (6.21)

$$\frac{Kk_{rne}(S_{nn})}{\mu_{ne}}\left(-\frac{\partial P}{\partial x}\right)_{S_{nn}} + \left(\frac{Kk_{rnn}(S_{nn})}{\mu_{eff}}\right)^{1/n}\left(\left(-\frac{\partial P}{\partial x}\right)_{S_{nn}} - \rho_{nn} g \sin(\alpha)\right)^{1/n} - \left(\frac{q}{A} + \frac{Kk_{rne}(S_{nn})}{\mu_{ne}}\rho_{ne} g \sin(\alpha)\right) = 0 \tag{6.28}$$

where μ_{eff} is defined as

$$\mu_{eff} = \frac{H}{12}\left(9 + \frac{3}{n}\right)^n [150 Kk_{rnn}(S_{nn})\phi(S_{nn} - S_{nnir})]^{(1-n)/2} \tag{6.29}$$

Equation (6.28) is incorporated in the calculation of the fractional flow to solve potential gradients corresponding to saturations under different flow conditions.

For a given operating condition, non-Newtonian fluid displacement in porous media is controlled not only by relative permeability data, as in Newtonian fluid displacement, but also by the rheological properties of the non-Newtonian fluid.

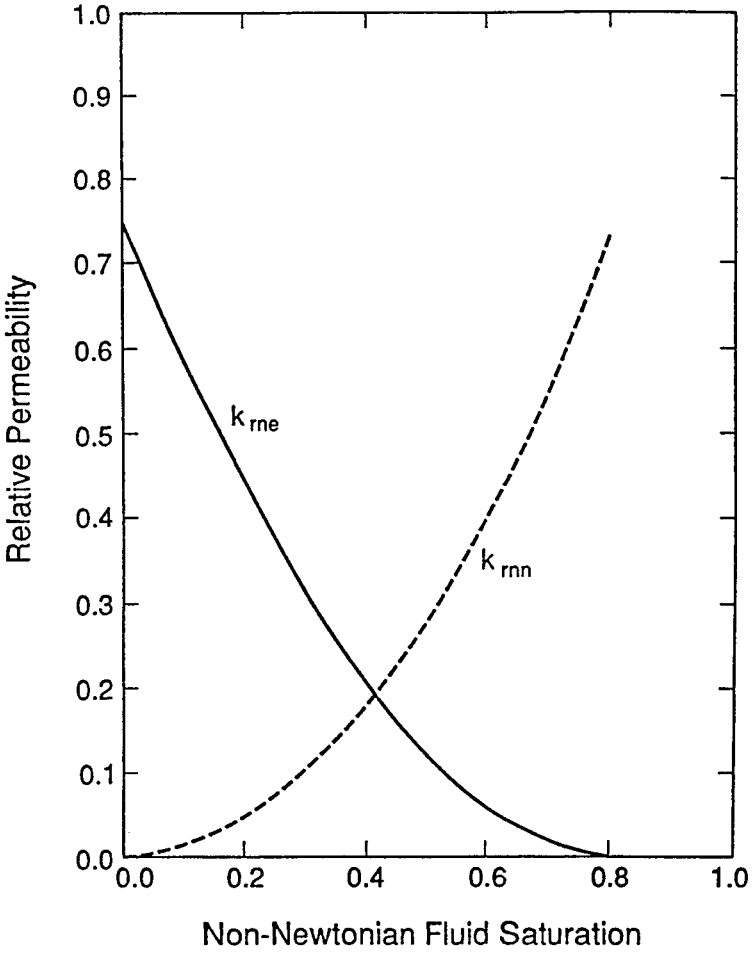


Fig. 34. Relative permeability functions used for evaluation of displacement by a non-Newtonian fluid.

TABLE 8

Parameters for linear power-law fluid displacement

Porosity	$\phi = 0.20$
Permeability	$K = 1$ darcy
Cross-sectional area	$1\ m^2$
injection rate	$q = 0.8233 \times 10^{-5}\ m^3\ s^{-1}$
Injection time	$T = 10$ hr
Displaced phase viscosity	$\mu_{ne} = 5$ cp
Irreducible Newtonian saturation	$S_{neir} = 0.20$
Initial non-Newtonian saturation	$S_{nnir} = 0.00$
Power = law index	$n = 0.5$
Power-law coefficient	$H = 0.01\ Pa \cdot s^n$

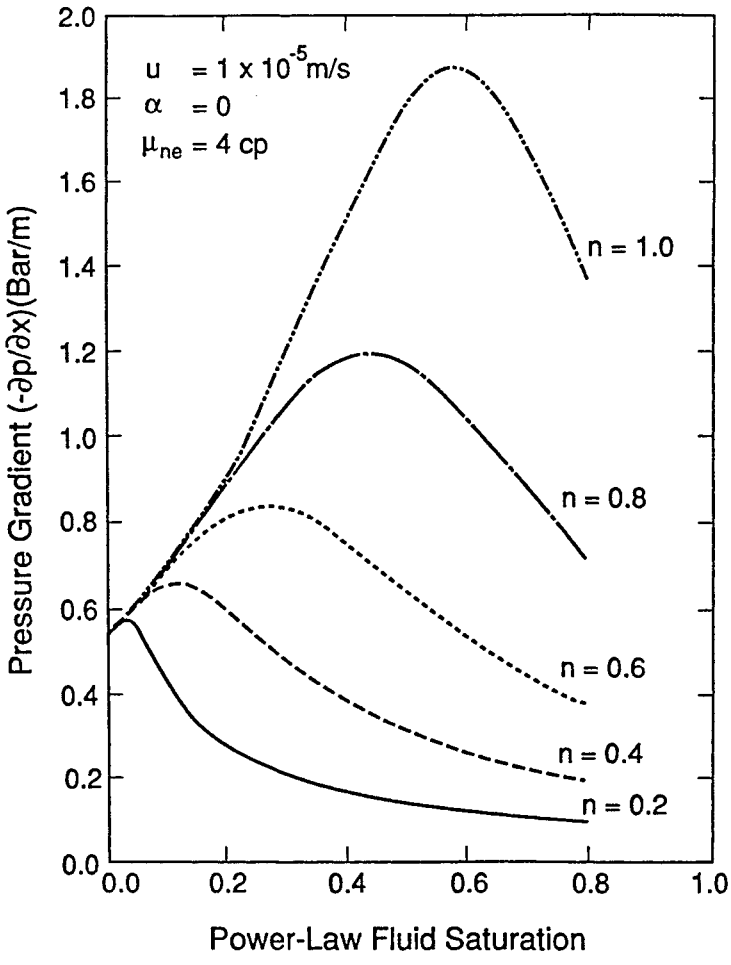


Fig. 35. Effects of the power-law index on pressure gradients.

Some fundamental aspects of power-law non-Newtonian fluid displacement will be discussed using the results from the analytical solution. There are two parameters that characterize the flow behavior of a power-law fluid, which are the exponential index, n, and the coefficient, H. For a pseudoplastic shear-thinning fluid, $0 < n < 1$. If $n = 1$, the fluid is Newtonian. The effect of the power-law index, n, on linear horizontal displacement can be quite significant. Fig. 35 shows that pressure gradients are changed significantly as a function of saturation for different values of n under the same flow condition. At both high and low values for the non-Newtonian phase saturation, the pressure gradients become smaller because the flow resistance decreases as the flow tends to single phase flow. The apparent viscosities of several power-law fluids with different power-law indices n are given in Fig. 36, and the resulting fractional flow curves are shown in Fig. 37. Figure 38 presents the derivatives of the fractional flow function with respect to saturation for different values of n. Saturation profiles after a 10-hr injection

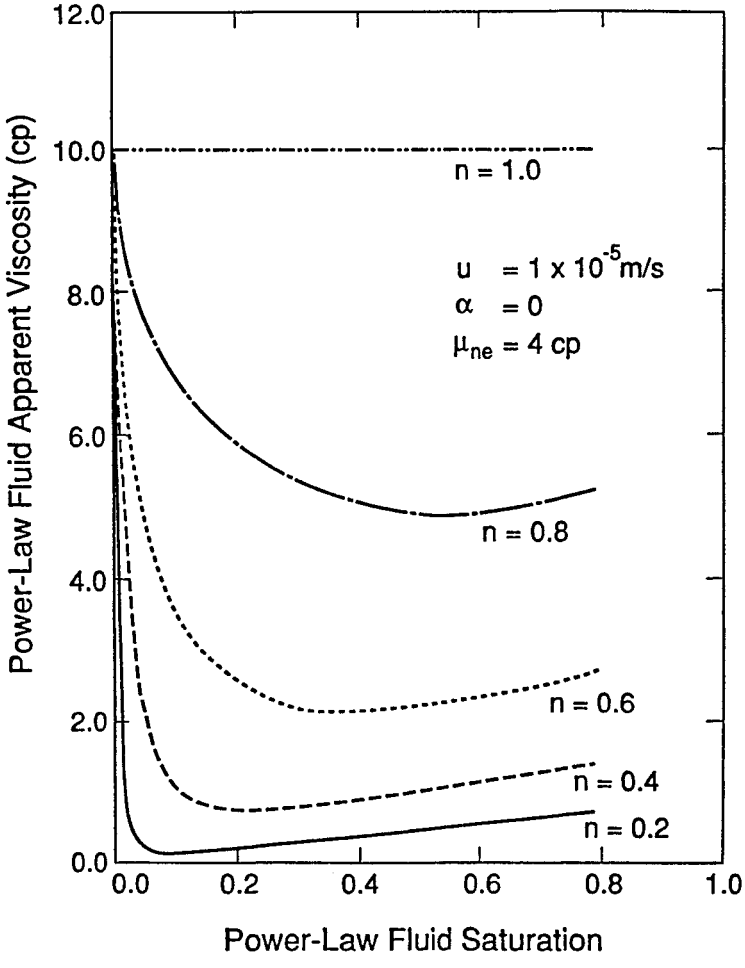


Fig. 36. Effects of the power-law index on non-Newtonian phase apparent viscosity.

period in the system are plotted in Fig. 39. Note the significant decreases in terms of sweeping efficiency as the power-law index n is reduced.

Since the power-law index, n, is usually determined by experiment or from well test analysis, some errors cannot be avoided in determining the values of n. These results show how difficult it will be to use a numerical code to match experimental data from non-Newtonian displacement investigations in the laboratory, because of the extreme sensitivity of the core saturation distribution to the value of n. The sensitivity of the displacement behavior to the power-index suggests that in determining the index for flow through porous media, it may be helpful to match experimental saturation profiles using the analytical solution.

The effects of the consistence coefficient, H, are also examined. As described by equation (6.29), H acts as a scaling factor of the viscosity for a given power-law index, n. The pressure gradients and the viscosities as functions of saturation will change with changes in H. Using the parameters of Table 8, Fig. 40 exhibits

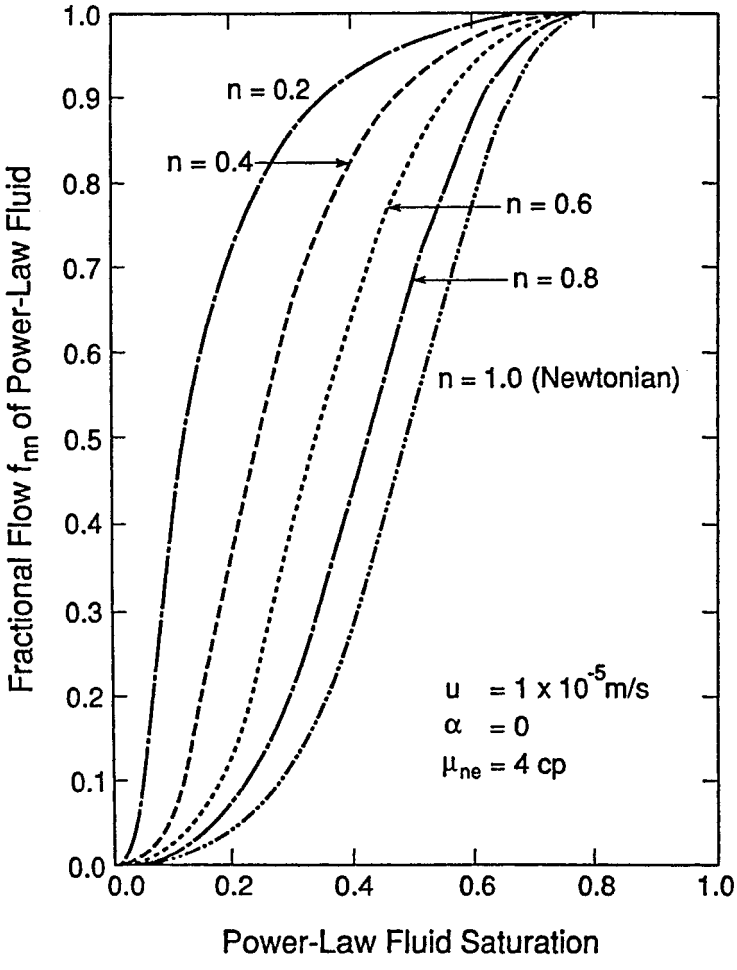


Fig. 37. Effects of the power-law index on non-Newtonian phase fractional flow.

the linear-scaling effect of H on the fractional flow curves for three values of H. The resulting saturation profiles after 10 hr of injection are shown in Fig. 41. The horizontal lines in this figure stands for the average saturations in the swept zone, which reflect the sweep efficiency. The results indicate that the effects of H on the displacement process are also significant.

For a stable Newtonian displacement in porous media, the injection rate has no effect on displacement efficiency or sweep efficiency by the Buckley-Leverett theory. However, the displacement is quite different when a non-Newtonian fluid is involved. Changes in the injection rate will result in changes in the pore velocity, or in the shear rate, in turn affect the viscosity of the non-Newtonian phase and therefore alter the fractional flow curve. Using the fluid and rock parameters in Table 8 (differences will be indicated on the figures), Fig. 42 gives non-Newtonian viscosity versus saturation curves for three different injection rates in a semi-infinite linear horizontal system. The calculated saturation profiles corresponding

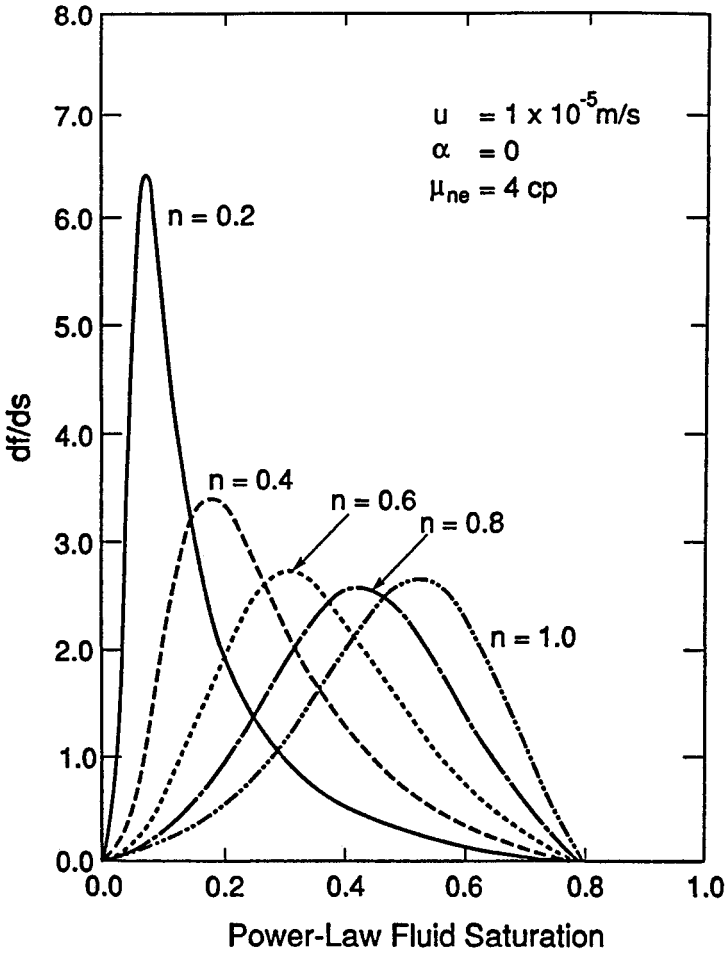


Fig. 38. Effects of the power-law index on derivative of fractional flow with respect to non-Newtonian phase saturation.

to the injection rates are shown in Fig. 43. Since the only varying parameter in this calculation is the injection rate, the saturation distributions in Fig. 43 indicate that the injection rate has a significant effect on displacement. For a displacement process with this type of shear thinning fluid, the lower the injection rate, the larger the viscosity of the displacing phase, and the higher the displacement efficiency will be.

6.4. Displacement of a Bingham non-Newtonian fluid by a Newtonian fluid

In this section, the analytical solution of Section 6.2 is used to obtain some insights into the physics behind the displacement of a Bingham fluid by a Newtonian fluid under isothermal condition. One application of this study is to look at the production process of heavy oil from oil reservoirs by waterflooding when

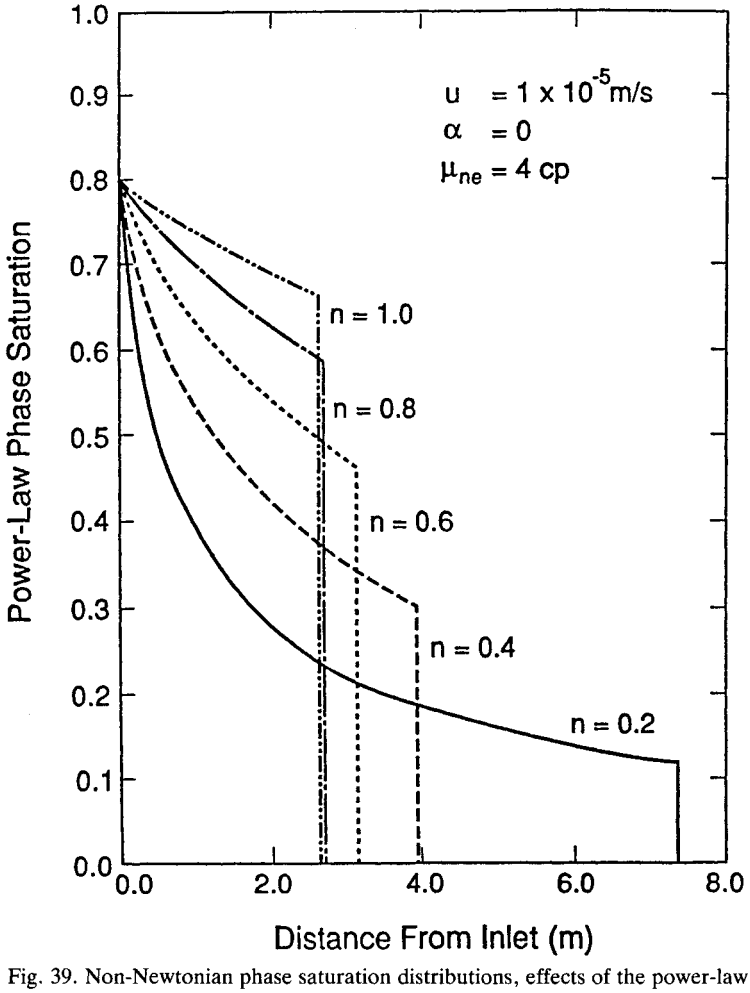


Fig. 39. Non-Newtonian phase saturation distributions, effects of the power-law index on displacement efficiency.

heavy oil flow through porous media can be approximated by a Bingham fluid (Mirzadjanzade et al., 1971; Kasraie et al., 1989).

The flow physical model is a one-dimensional linear porous system with a constant cross-sectional area, A. Initially, the system is saturated with only a Bingham fluid, and a Newtonian fluid is injected at a constant volumetric rate at the inlet, $x = 0$, from $t = 0$. The relative permeabilities used are given as functions of saturation of the displacing Newtonian fluid by Fig. 34. The fluid and rock properties are summarized in Table 9, and the effects of capillary pressure gradient are ignored. The rheological model for the flow of a single-phase Bingham plastic fluid in porous media, equation (2.14), is extended to this two-phase case,

$$\mu_{nn} = \frac{\mu_b}{1 - G/|\partial\Phi/\partial x|} \tag{6.30a}$$

for $|\partial\Phi/\partial x| > G$, and

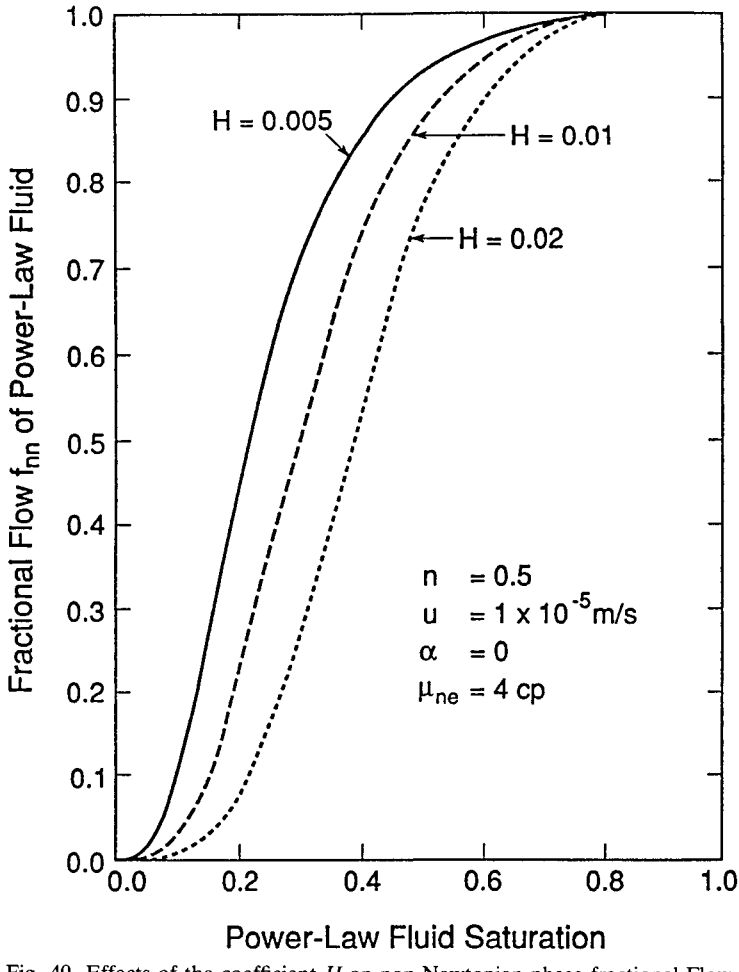


Fig. 40. Effects of the coefficient H on non-Newtonian phase fractional Flow.

$$\mu_{nn} = \infty \tag{6.30b}$$

for $|\partial\Phi/\partial x| \leqslant G$. For a particular saturation S_{ne} of the Newtonian phase, the corresponding flow potential gradient for the non-Newtonian phase can be derived by introducing equation (6.30a) in equation (6.21) as

$$-\left(\frac{\partial\Phi}{\partial x}\right)_{S_{ne}} = -\rho_{nn} g \sin(\alpha) + \frac{\dfrac{q}{AK} + \dfrac{k_{rnn}(S_{ne})}{\mu_b} G + \dfrac{k_{rne}(S_{ne})}{\mu_{ne}} \rho_{ne} g \sin(\alpha) + \dfrac{k_{rnn}(S_{ne})}{\mu_b} \rho_{nn} g \sin(\alpha)}{\dfrac{k_{rne}(S_{ne})}{\mu_{ne}} + \dfrac{k_{rnn}(S_{ne})}{\mu_b}} \tag{6.31}$$

The apparent viscosity for the Bingham fluid is determined by using equation

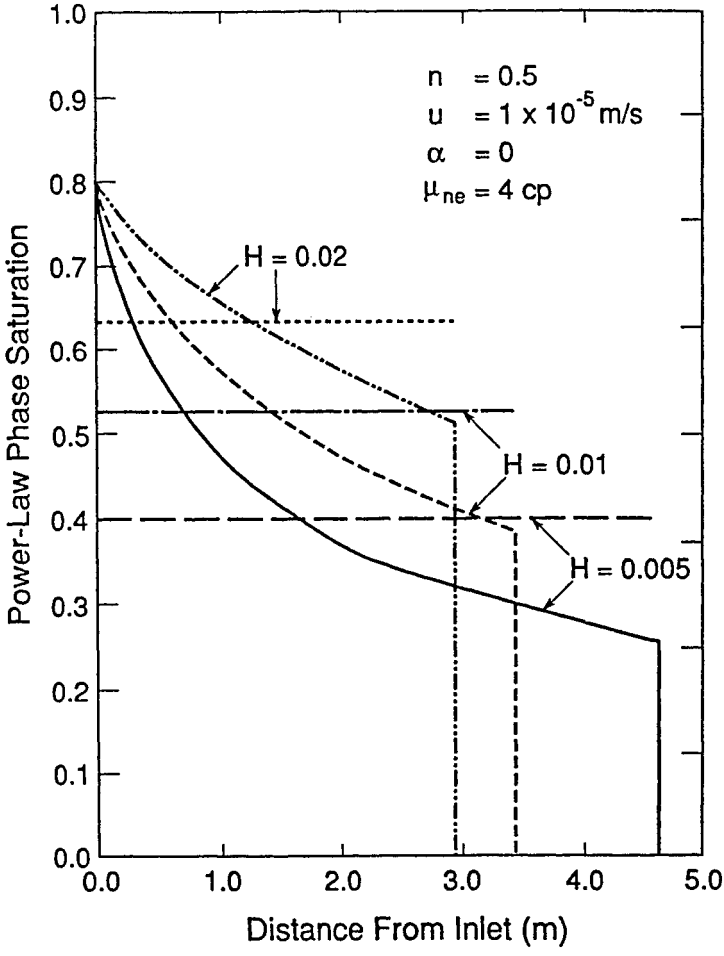


Fig. 41. Non-Newtonian phase saturation distributions, effects of the coefficient H on displacement efficiency.

(6.31) in equation (6.30), and then the fractional flow curves are calculated from equation (6.19), in which S_{nn} is replaced by S_{ne} for this problem.

For the given operating conditions similar to those used in the Buckley-Leverett theory, the non-Newtonian fluid displacement is described by the analytical solution in Section 6.2. The displacement involving a Bingham fluid is also determined only by the fractional flow function, which is controlled not only by relative permeability effects, as in Newtonian fluid displacement, but also by the non-Newtonian rheological properties of Bingham fluids.

A basic feature of the displacement process of a Bingham fluid in porous media is the existence of an ultimate or maximum displacement saturation, S_{max}, for the displacing Newtonian phase (see Figs. 44 and 45). The maximum displacement saturation occurs at the point of the fractional flow curve where $f_{ne} = 1.0$. For this particular displacement system, initially saturated only with the Bingham fluid,

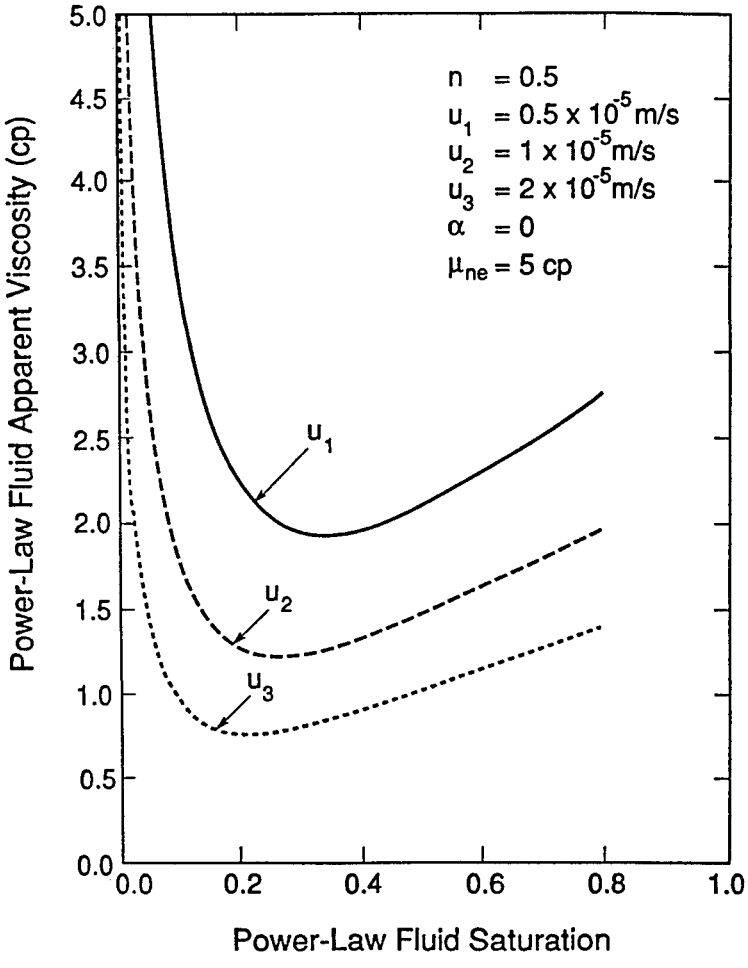


Fig. 42. Effects of injection rates on non-Newtonian phase apparent viscosities.

the displacing saturation cannot exceed the maximum value S_{max}. The resulted saturation distributions are given in Fig. 45 for the different minimum pressure gradients G. It is obvious that the sweep efficiency decreases rapidly as G increases. In contrast, for Newtonian displacement, the ultimate saturation of the displacing fluid is equal to the total mobile saturation of the displaced fluid, as shown by the curve for $G = 0$ in Fig. 45.

Physically, the phenomenon of ultimate displacement saturation occurs as the flow potential gradient approaches the minimum threshold pressure gradient G, at which the apparent viscosity is infinite. Then the only flowing phase is the displacing Newtonian fluid. Consequently, once the maximum saturation has been reached in a flow system, no improvement of sweep efficiency can be obtained no matter how long the displacement process continues. The flow condition in reservoirs is more complicated than in this linear semi-infinite system. Since oil wells are usually drilled according to certain patterns, there always exist some regions

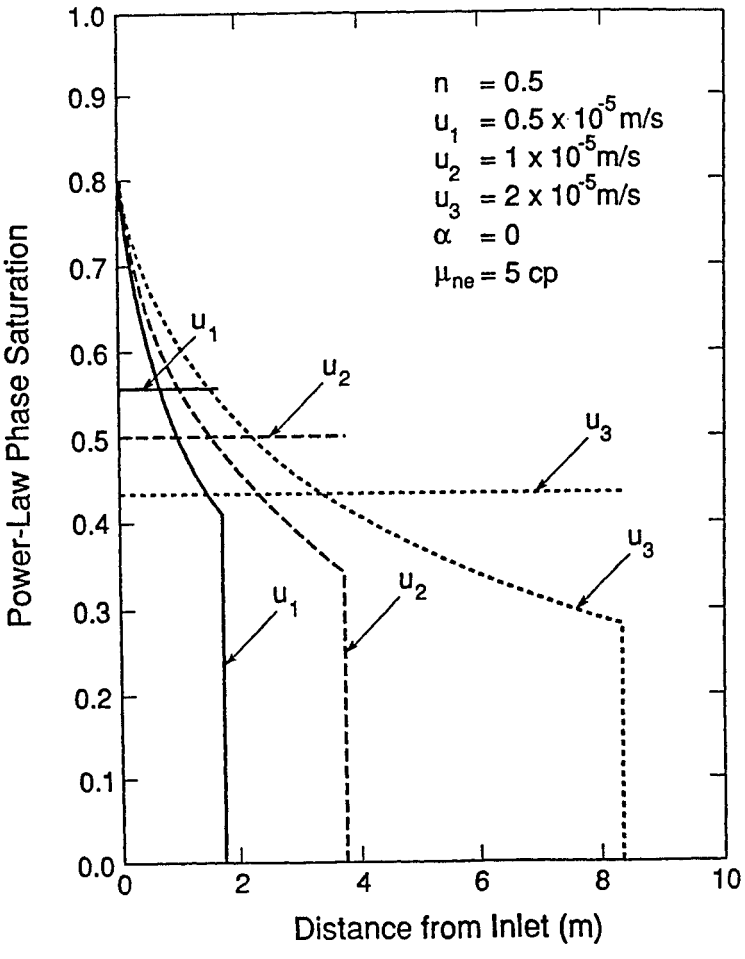


Fig. 43. Non-Newtonian phase saturation distributions, effects of injection rates on displacement efficiency.

TABLE 9

Parameters for linear Bingham fluid displacement

Porosity	$\phi = 0.20$
Permeability	$K = 1$ darcy
Cross-sectional area	$1\ m^2$
Injection rate	$q = 1.0 \times 10^{-6}\ m^3\ s^{-1}$
Injection time	$T = 10$ hr
Displacing Newtonian viscosity	$\mu_{ne} = 1$ cp
Irreducible saturation	$S_{nnir} = 0.20$
Bingham plastic coefficient	$\mu_b = 4.0$ cp
Minimum pressure gradient	$G = 10{,}000\ Pa\ m^{-1}$

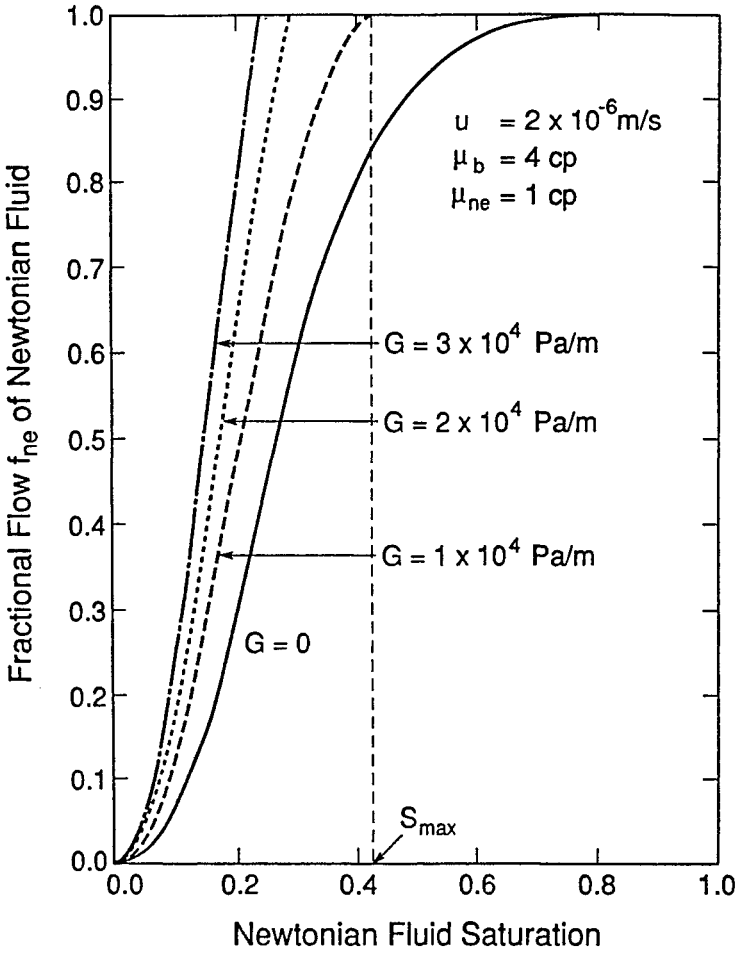


Fig. 44. Fractional flow curves for a Bingham fluid displaced by a Newtonian fluid, effects of the minimum pressure gradient.

with low potential gradients between production and injection wells. The presence of the ultimate displacement saturation for a Bingham fluid displacement indicates that no oil can be driven out of these regions. Therefore, the ultimate displacement saturation phenomenon will contribute to the low oil recovery observed in heavy oil reservoirs developed by water-flooding, in addition to effects from the high oil viscosity.

The effects of the other rheological parameter, the Bingham plastic coefficient μ_b, are shown in Fig. 46. It is interesting to note that the ultimate displacement saturations hardly change with μ_b, since ultimate displacement saturation is essentially determined by the minimum pressure gradient G. However, the average saturations in the swept zones are quite different for different values of μ_b.

Effects of injection rates can also be revealed by the analytical solution. If water injection rate at the inlet is increased, the pressure gradient in the system will increase, and the apparent viscosity for the displaced Bingham fluid will be

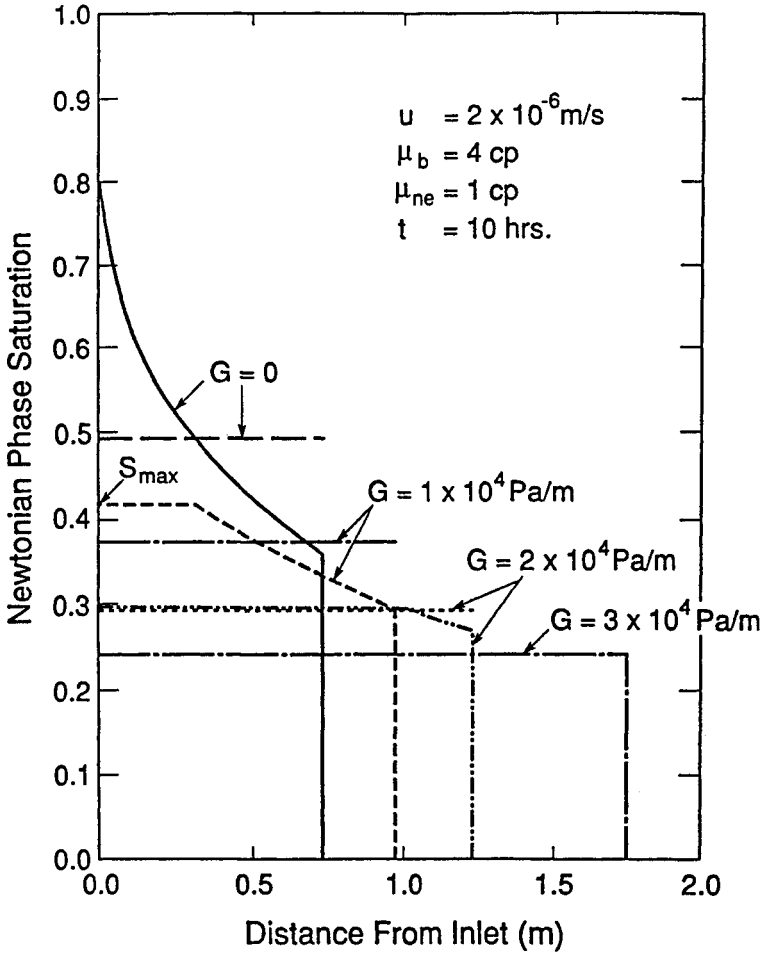


Fig. 45. Newtonian phase saturation distributions, effects of the minimum pressure gradient on displacement efficiency of a Bingham fluid by a Newtonian fluid.

reduced. Therefore, a better sweep efficiency will result. Figure 47 presents the saturation profiles after injection of 10 hr with the different rates. It is interesting to note that both the sweep efficiency and the ultimate displacement saturation can be greatly increased by increasing the injection rate alone.

6.5. Summary

A Buckley-Leveret type analytical solution for describing the displacement of a Newtonian fluid and a non-Newtonian fluid through porous media has been presented. A general viscosity function for non-Newtonian fluids is proposed and used in the solution, which defines non-Newtonian phase viscosity as a function of the local fluid potential gradient and saturation, and is suitable for different rheological models of non-Newtonian fluids. The analytical solution is applicable

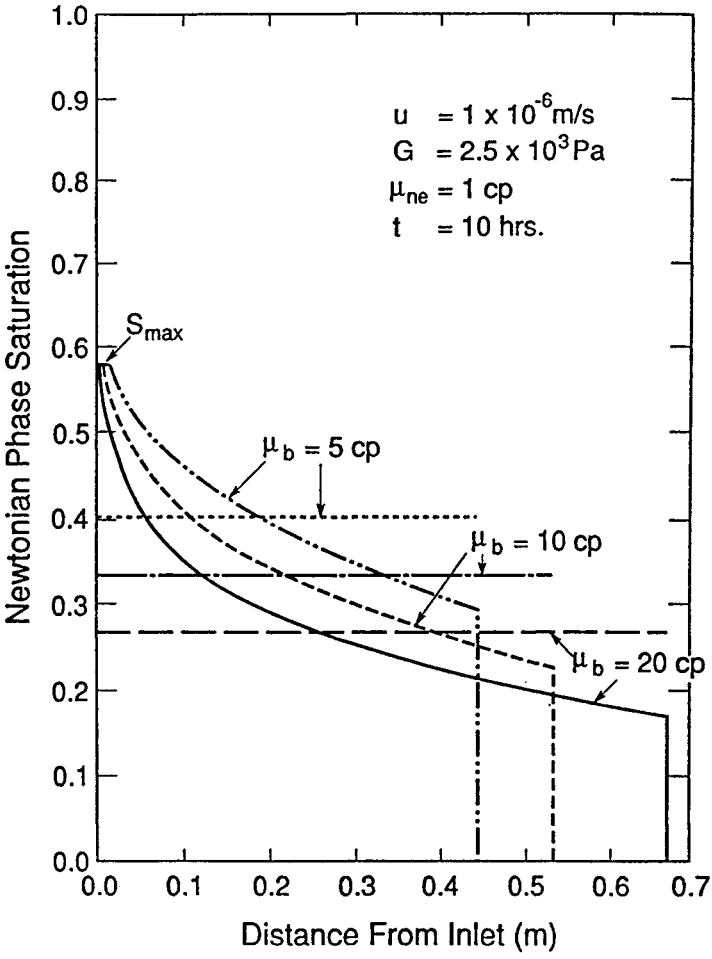


Fig. 46. Newtonian phase saturation distributions, effects of Bingham's coefficient μ_b on displacement efficiency of a Bingham fluid by a Newtonian fluid.

to displacement of a non-Newtonian fluid by a Newtonian fluid or to displacement of a non-Newtonian fluid by another non-Newtonian fluid.

The analytical solution has been used to obtain some insight into the physics of displacement involving power-law, and Bingham fluids in porous media. The calculated model results reveal that non-Newtonian displacement is a complicated process, controlled by the rheological properties of non-Newtonian fluids used, and the injection condition, in addition to relative permeability curves as in Newtonian fluid displacement.

The fundamental feature of immiscible displacement involving a Bingham plastic fluid is that there exists an ultimate displacement saturation, which is essentially determined by the minimum pressure gradient G. Once the saturation approaches the ultimate saturation in the formation, no further displacement can be obtained regardless of how long the displacement lasts for a given operating condition.

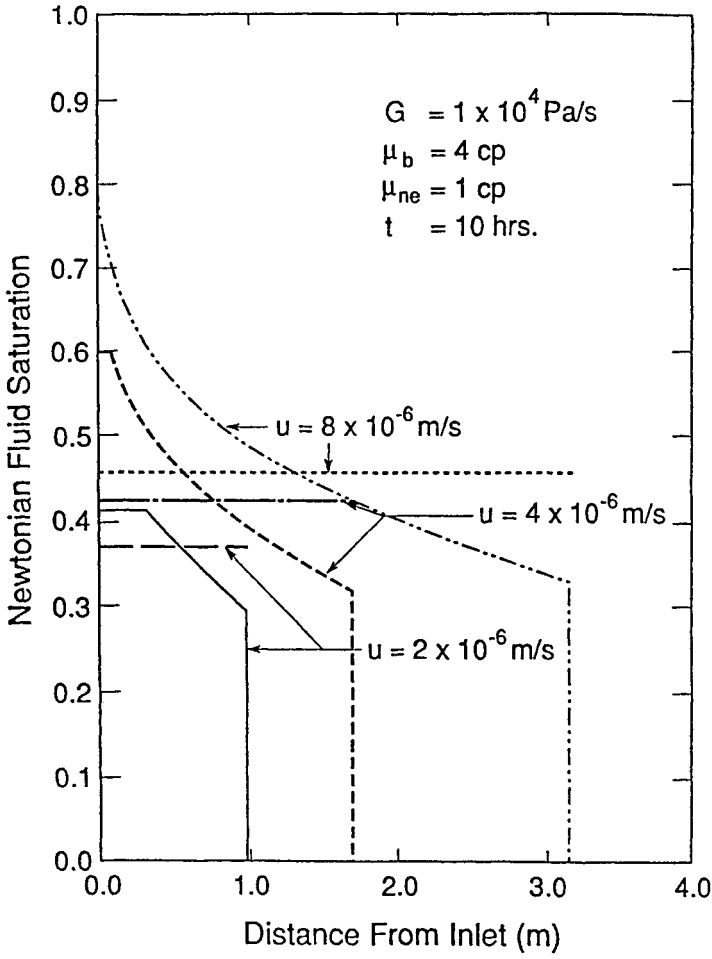


Fig. 47. Newtonian phase saturation distributions, effects of injection rates on displacement efficiency of a Bingham fluid by a Newtonian fluid.

7. Concluding remarks

The primary objective of the present work was to present a methodology to investigate transport phenomena of non-Newtonian fluids through porous media. Whenever non-Newtonian fluids are involved in porous media, the flow problem will become non-linear because the apparent viscosity used in the Darcy equation is a function of shear rate. The viscosity function for a non-Newtonian fluid depends on shear rate, or pore velocity in a porous medium in a complex way. The non-Newtonian rheological behavior is quite different for different fluids and/or for different porous materials. Therefore, it is impossible to develop a universal approach for handling all flow problems invoving various non-Newtonian fluis in porous media. However, under some special circumstances, analytical solutions have been proven here to be possible to be obtained for describing non-

Newtonian flow in porous media. In this work both analytical and numerical methods have been employed, and major attention has been paid to power-law and Bingham plastic fluids, since they are the most likely to be encountered in reservoirs.

Among the theoretical methods contributed from this work, a fully implicit three-dimensional integral finite difference model has been developed by modifying the general numerical code "MULKOM" to include the effects of non-Newtonian viscosity. This new simulator is capable of modeling both single and multiple phase non-Newtonian fluid flow through porous or fractured media. The numerical model can take account of all the important factors which affect the flow behavior of non-Newtonian and Newtonian fluids, such as capillary pressure, complicated flow domains, inhomogeneous porous media, and various well operation conditions. Different non-Newtonian rheological models have been incorporated in the code. The validity of the numerical method has been checked by comparing the numerical results with analytical solutions for displacement of a Newtonian fluid by a power-law fluid. In this study, this code has been successfully applied to numerical investigations of transient flow of power-law fluids and to verification of the integral solution for Bingham fluid flow.

Along with the numerical technique, an analytical solution for one-dimensional immiscible displacement of non-Newtonian and Newtonian fluids in porous media has been obtained, in analogy with the Buckley-Leverett theory for Newtonian fluid displacement. The non-Newtonian fluid viscosity is assumed to be a function of the local flow potential gradient and saturation. Therefore, this solution is generally applicable to various non-Newtonian and Newtonian fluid displacement. To apply this theory to a field problem, a graphic procedure for evaluating displacement of non-Newtonian and Newtonian fluids has also been developed from the analytical solution. The resulting method can be regarded as an extension of the Buckley-Leverett-Welge theory to the flow problem of non-Newtonian fluids in porous media. This solution has been used: (i) to study the physical mechanisms of immiscible flow with power-law and Bingham fluids, and (ii) to verify the numerical code in this work.

An integral method has also been presented for analysis of non-linear single phase Bingham fluid flow through porous media. The integral method, widely used in the study of unsteady heat transfer problems, is applied to derive an approximate analytical solution for radial flow of a Bingham fluid. Using a newly-proposed pressure profile, the integral solution has been examined numerically to give very accurate results for the Bingham fluid flow. Based on the integral solution, a well test analysis method for Bingham fluid flow is constructed to determine the rheological and formation properties.

A further theoretical study has been performed for transient flow problems of power-law fluids by using the numerical code. First, this numerical investigation has improved the existing well test analysis technique of power-law fluid injectivity tests for general applicability. Second, an idealized fracture model has been used to study the transient flow of a power-law fluid through a double-porosity medium. The non-Newtonian behavior is found to generate two parallel log-log straight lines on a wellbore pressure-time plot, instead of two parallel semi-log straight

lines for Newtonian fluid flow. The third problem is to obtain some insights into pseudoplastic fluid flow through porous media. The Meter four-parameter rheological model was used for calculating apparent viscosity of the pseudoplastic fluid. The finding is that the transient pressure responses in the flow system tend to an equivalent Newtonian system at long times, which is quite different from a power-law flow problem.

A new theory for analyzing single phase Bingham fluid flow in porous media has been developed, based on the integral analytical and numerical solutions. The transient flow of a slightly-compressible Bingham fluid has been shown to be determined essentially by the Bingham rheological properties. Application of the theory has been demonstrated for analysis of two simulated pressure drawdown and buildup tests.

The physical mechanisms of non-capillary displacement with non-Newtonian fluids in porous media are revealed by the Buckley-Leverett type analytical solution. The non-Newtonian immiscible displacement is a complicated process, which is controlled by the rheological properties of the non-Newtonian fluids and the flow condition, in addition to relative permeability. It has been known from Buckley-Leverett theory that injection rate has no effects on displacement efficiency for Newtonian fluids under the stabilized condition. As discussed in this work, a fundamental difference between Newtonian and Non-Newtonian displacement is that the non-Newtonian displacement is flow rate dependent because of changes in non-Newtonian viscosity with pore flow velocity.

Power-law and Bingham plastic fluids are the most commonly encountered non-Newtonian fluids in porous media flow problems. Therefore, a detailed study has been made on the displacement behavior of these two fluids in order to obtain an understanding of the physics behind the immiscible flow process. For displacement of a Newtonian fluid by a shearing-thinning power-law fluid, such as in oil production by polymer flooding, the sweep efficiency can be improved by reducing injection rates of the power-law fluid. As to a Bingham fluid displaced by a Newtonian one, with a practical example of heavy oil recovery by water flooding, the displacement is characterized by an ultimate sweep saturation, and no further improvement can be achieved when the saturation approaches the ultimate saturation under the same flow operation.

This work has focused on the theoretical aspects of non-Newtonian fluid transport through porous media, and its emphasis is on the physical insights in "non-Newtonian" behavior of porous media flow. As a result of this, many of the results in the theoretical development depend on the assumptions on rheological properties, which are based on the previous experimental research. Since most of the laboratory studies of non-Newtonian flow in the literature were conducted using only single-phase non-Newtonian fluids, there certainly is a need for further experiments under multiphase flow condition. Such experimental studies should be designed to provide us with rheological models for the non-Newtonian fluid and porous materials of interest. In the present study, the apparent viscosity for multiphase flow of non-Newtonian fluids is taken as a function of flow potential gradient and saturation. Physically, this is a natural extension of the single phase flow theory to a multiple phase flow problem. However, this assumption needs to be confirmed experimentally. Just as in multiple phase Newtonian fluid flow, the

extension of Darcy's law to multiple phase flow is, in fact, a heuristic procedure suggested by the analogy with single phase flow. Then, experimental work is required to verify this speculation.

Effects of capillary pressure on immiscible non-Newtonian fluid flow have been ignored in the analytical analysis, which is necessary to develop the Buckley-Leverett type solution. For Newtonian displacement, various investigators have concluded that for high flow rates the Buckley-leverett non-capillary theory gives a good approximation of the actual saturation distribution. At low flow rates, the influence of capillary pressure becomes important. For non-Newtonian displacement, similar experimental studies should also be carried out to look at capillary effects. This can be done by using the numerical code since it has the ability to include capillary effects, as long as the capillarity data are obtained from experiments.

In order to verify applicability of the well testing analysis approach on the transient flow of Bingham type non-Newtonian fluids in porous media, transient pressure tests are needed in certain heavy oil reservoirs. Since no well test data can be found for Bingham oil flow in the literature, the new analysis method proposed for analyzing Bingham fluid flow was here used to interpret only the simulated well testing examples. Currently, there is few quantitative approaches in the petroleum engineering and groundwater literature for well test analysis on Bingham fluid production or injection operations in reservoirs. Further efforts should be made to obtain flow properties of Bingham fluid in porous media, which are very important for heavy oil development and numerous other applications.

Non-Newtonian fluid flow in porous media usually is affected by the chemical concentration in the fluid. Such as for a polymer solution, changes in polymer concentration will result in changes in its viscosity. The chemical composition effect is not included in this work. It is obvious that the study of non-Newtonian flow coupled with chemical transport is a whole new area for further research efforts in this field. Among other factors, phenomena of adsorption and dispersion of chemicals in non-Newtonian fluids during flow through porous media must be understood first before a realistic theoretical model can be developed. Such an investigation will depend heavily on experimental and numerical approaches. Even though many results of chemical adsorption during polymer solution flow in porous media can be found in the petroleum literature, very few studies have been reported on dispersion of non-Newtonian fluids in porous media (Payne and Parker, 1973; Wen and Yim, 1971). Many mechanisms which govern non-Newtonian fluid flow coupling with chemical transport process are very poorly understood. Therefore, a beter understanding of the physics of non-Newtonian fluid flow and chemical transport in porous media needs many more experimental and theoretical studies.

Acknowledgements

This work was supported by the director, Office of Energy Research, Office of Basic Energy Sciences, U.S. Department of Energy, under Contract No. DE-AC03–76SF0098, and by HydroGeoLogic, Inc., Herndon, Virginia. Yu-Shu Wu

acknowledges guidance from Paul Witherspoon for the research conducted at Lawrence Berkeley Laboratory, California. The authors are grateful to Suzann Heinrich for her help in preparing the manuscript.

Glossary

A	cross-sectional area (m^2)
A_{nm}	surface element between V_n and V_m (m^2)
b	fracture aperture (m)
B	Gogarty's constant ($s^{(y-1)/y}$)
C_f	fluid compressibility Pa^{-1}
C_f	total compressibility of fracture (Pa^{-1})
C_m	total compressibility of matrix (Pa^{-1})
C_r	formation compressibility (Pa^{-1})
C_t	total compressibility (Pa^{-1})
D	half fracture spacing (m)
D_p	particle diameter of porous material (m)
$\underline{D}$	rate-of-deformation tensor (s^{-1})
D_{ij}	ijth component of $\underline{D}$ (s^{-1})
D_{nm}	distance between V_n and V_m (m)
f_{ne}	fractional flow of Newtonian phase
f_{nn}	fractional flow of non-Newtonian phase
$f(K)$	permeability function
$\mathbf{F}_\beta$	mass flux for fluid β (m/s)
$F_{\beta,nm}$	flux term of fluid β between V_n and V_m (m/s)
g	magnitude of the gravitational acceleration (m/s^2)
$\mathbf{g}$	gravitational acceleration vector (m/s^2)
G	minimum pressure gradient (Pa/m)
h	formation thickness (m)
H	power-law consistence ($Pa \cdot s^n$)
K	absolute permeability (m^2)
K_f	fracture permeability (m^2)
K_m	matrix permeability (m^2)
k_{ne}	relative permeability to Newtonian phase
k_{nn}	relative permeability to non-Newtonian phase
k_{rw}	relative permeability to water phase
L	length of a system or a core (m)
m	Gogarty's permeability constant
m	slope of semi-log curves (Pa)
M	mass of fluid (kg)
m'	slope of log-log curves
M_n	average value of mass in V_n (kg/m^3)
M_β	mass accumulation for fluid β (kg/m^3)
$M_{\beta,n}$	mass of fluid β in V_n (kg)
n	power-law exponential index
N_p	cumulative displaced fluid (m^3)
n'	Mungan's coefficient
$\mathbf{n}$	unit outward normal vector
P_c	capillary pressure (Pa)
$P_{fw}(t)$	wellbore flowing pressure (Pa)
P_i	initial formation pressure (Pa)
P_{ne}	pressure of Newtonian phase (Pa)

P_{nn} pressure of non-Newtonian phase (Pa)
ΔP pressure difference (Pa)
∇P pressure gradient (Pa/m)
q_β source for fluid β (kg/(m^{3}s))
$q_{\beta,n}$ source for fluid β in V_n (kg/(m^{3}s))
Q volumetric injection (m^3/s)
$Q(t)$ cumulative fluid of injection (m^3)
Q_c cumulative mass production (kg)
$Q_m(t)$ mass injection/production rate (kg/s)
r radial distance, coordinate (m)
R radius of a tube (m)
r_w wellbore radius (m)
s velocity gradient function (s^{-1})
S saturation
S surface of a volume
S_f saturation at displacement front
S_{max} ultimate displacement saturation
S_{ne} Newtonian phase saturation
S_{neir} irreducible Newtonian fluid saturation
S_{nn} non-Newtonian fluid saturation
S_{nnir} Connate non-Newtonian phase saturation
S_w water saturation
$\bar{S}_{nn}$ average non-Newtonian saturation
t time (s)
T tortuosity of porous media
t^k time at level k (s)
Δt time step (s)
u Darcy velocity (m/s)
$\mathbf{u}$ Darcy velocity vector (m/s)
u_{ne} Darcy velocity of Newtonian phase (m/s)
u_{nn} Darcy velocity of non-Newtonian phase (m/s)
$\mathbf{u}_{ne}$ Darcy flux of Newtonian phase (m/s)
$\mathbf{u}_{nn}$ Darcy flux of non-Newtonian phase (m/s)
$\mathbf{V}$ velocity vector (m/s)
v_i component of $\mathbf{V}$ in the x_1 (m/s)
V_n volume of a system (m^3)
v_p pore velocity (m/s)
$\mathbf{v}_p$ pore velocity vector (m/s)
$\nabla\mathbf{V}$ velocity gradient (s^{-1})
W width of fracture (m)
x distance from inlet, coordinate (m)
x_f distance to shock saturation front (m)
x_i $x_1 = x$, $x_2 = y$, and $x_3 = z$ (m)
$x_{i,p}$ primary variable of numerical equations
$x_{S_{nn}}$ distance to saturation S_{nn} (m)
y Gogarty's exponential
y coordinate (m)
z coordinate (m)

Greek symbols
α angle with horizontal plane
α exponential coefficient
α_1 Williamson model coefficient (s^{-1})
α_2 Williamson model exponential
α_2 exponential coefficient

$\Gamma(x)$	gamma function or factorial function
$\dot{\gamma}$	shear rate (s^{-1})
$\dot{\gamma}_a$	average shear rate (s^{-1})
$\dot{\gamma}_0$	low limiting shear rate (s^{-1})
$\delta(t)$	pressure penetration distance (m)
θ_f	fluid relaxation time (s)
δ_1	interpolated value of $\nabla\Phi$ (Pa/m)
δ_2	interpolated value of $\nabla\Phi$ (Pa/m)
λ	rigidity modulus (Pa)
λ	interporosity coefficient
λ_{eff}	effective mobility ($m^{1+n}/Pa \cdot s$)
μ	viscosity (Pa · s)
μ_a	apparent viscosity (Pa · s)
μ_b	Bingham plastic coefficient (Pa · s)
μ_{eff}	power-law coefficient ($Pa \cdot s^n \cdot m^{1-n}$)
μ_{eqv}	equivalent viscosity (Pa · s)
μ_f	fluid viscosity (Pa · s)
μ_∞	viscosity at infinite shear (Pa · s)
μ_{max}	higher limit viscosity (Pa · s)
μ_{min}	lower limit viscosity (Pa · s)
μ_{nn}	non-Newtonian apparent viscosity (Pa · s)
μ_0	viscosity at zero shear (Pa · s)
μ_1	viscosity at $\lvert\nabla\Phi\rvert = \delta_1$ (Pa · s)
μ_2	viscosity at $\lvert\nabla\Phi\rvert = \delta_2$ (Pa · s)
η	$\eta = 1 + \delta(t)/r_w$
ξ	dimensionless aspect factor
ρ_i	initial fluid density (kg/m^3)
ρ_{ne}	density of Newtonian fluid (kg/m^3)
ρ_{nn}	density of non-Newtonian fluid (kg/m^3)
τ	shear stress (Pa)
τ_m	meter model coefficient (Pa)
τ_{rx}	shear stress function of r (Pa)
τ_w	shear stress at wall (Pa)
τ_y	yield stress (Pa)
$\tau_{1/2}$	shear stress for $\mu = 1/2\mu_0$ (Pa)
τ	stress tensor (Pa)
ϕ	porosity
Φ	flow potential (Pa)
ϕ_f	porosity of fracture
ϕ_i	initial formation porosity
ϕ_m	porosity of matrix
$\nabla\Phi$	flow potential gradient (Pa/m)
$\nabla\Phi_e$	effective flow potential gradient (Pa/m)
ω	storage coefficient

Subscripts

a	apparent
a	average
b	Bingham fluid
e	equivalent
eff	effective
eqv	equivalent
f	fluid
f	fracture
f	displacement front

i	initial
m	mass
m	matrix
m	volume V_m
n	nth degree
n	volume V_n
ne	Newtonian fluid
nm	between V_n and V_m
nn	non-Newtonian fluid
p	production
rne	relative to Newtonian fluid
rnn	relative to non-Newtonian fluid
t	time
t	total
w	wall
w	wellbore
x	x direction
y	yield
z	z direction
0	zero shear stress
1/2	half shear stress
∞	infinite shear stress
β	fluid index

References

Albrecht, R.A. and Marsden, S.S., 1970. Foams as blocking agents in porous media. Soc. Pet. Eng. J., 51.

Astarita, G. and Marrucci, G., 1974. Principles of Non-Newtonian Fluid Mechanics. McGraw-Hill Book Company (UK) Limited, Maidenhead, Berkshire, England.

Aziz, K. and Settari, A., 1979. Petroleum Reservoir Simulation. Applied Science, London.

Barenblatt, G.E., Entov, B.M., and Rizhik, B.M., 1984. Flow of Liquids and Gases in Natural Formations. Nedra, Moscow.

Barenblatt, G.E., Zheltov, I.P., and Kochina, I.N., 1960. Basic concepts in the theory of seepage of homogeneous liquids in fissured rocks. J. Appl. Math., USSR, 24(5): 1286–1303.

Bear, J., 1972. Dynamics of Fluids in Porous Media. American Elsevier, New York, N.Y..

Benis, A.M., 1968. Theory of non-Newtonian flow through porous media in narrow three-dimensional channels. Int. J. Non-Linear Mechanics, 3: 31–46.

Bensten, R.G., 1985. A new approach to instability theory in porous media. Soc. Pet. Eng. J., 765–779.

Bernadiner, M., 1991. Private communication.

Bird, R.B., 1965. Polymer fluid dynamics, Selected Topics in Transport Phenomena, Chemical Engineering Progress Symposium Series 65, No. 58, Vol. 61, AIChE, New York, N.Y.

Bird, R.B., Stewart, W.E., and Lightfoot, E.N., 1960. Transport Phenomena. Wiley, New York, N.Y.

Bohme, G., 1987. Non-Newtonian Fluid Mechanics, Vol. 31, North-Holland, Amsterdam/New York.

Bondor, P.L., Hirasaki, G.J., and Tham, M.J., 1972. Mathematical simulation of polymer flooding in complex reservoirs. Soc. Pet. Eng. J., 369–382.

Buckley, S.E. and Leverett, M.C., 1942. Mechanism of fluid displacement in sands. Trans., AIME 146: 107–116.

Camilleri, D., Engelsen, S., Lake, L.W., Lin, E.T., Pope, G.A., and Sepehrnoori, K., 1987a. Description of an improved compositional micellar/polymer simulator. SPE Reservoir Engineering, 427–432.

Camilleri, D., Fil, A., Pope, G.A., Rouse, B.A., and Sepehrnoori, K., 1987b. Improvements in physical-property models used in micellar/polymer flooding. SPE Reservoir Engineering, 433–440.

Camilleri, D., Fil, A., Pope, G.A., Rouse, B.A., and Sepehrnoori, K., 1987c. Comparison of an improved compositional micellar/polymer simulator with laboratory corefloods. SPE Reservoir Engineering, 441–451.

Cardwell, W.T. Jr., 1959. The Meaning of the triple value in noncapillary Buckley-Leverett theory. Trans., AIME, 216: 271–276.

Castagno, R.E., Shupe, R.D., Gregory, M.D., and Lescarboura, J.A., 1984. A method for laboratory and field evaluation of a proposed polymer flood. SPE Paper 13124, presented at the 59th Annual Technical Conference and Exhibition Held in Houston, T.X.

Castagno, R.E., Shupe, R.D., Gregory, M.D., and Lescarboura, J.A., 1987. Method for laboratory and field evaluation of a proposed polymer flood. SPE Reservoir Engineering, 452–460.

Chen, Z.X., 1988. Some invariant solutions to two-phase fluid displacement problems including capillary effect, SPE Reservoir Engineering, 691–700.

Chen Z.X. and Liu, C.Q., 1991. Self-similar solutions for displacement of non-Newtonian fluids through porous media. Transport in Porous Media, 6, 13–33.

Chen, Z.X. and Whitson, C.H., 1987. Generalized Buckley-Leverett theory of two-phase flow through porous media. Division of Petroleum Engineering and Applied Geophysics, Norwegian Institute of Technology, University of Trondheim.

Christopher, R.H. and Middleman, S., 1965. Power-law flow through a packed tube. I & EC Fundamentals, 4(4): 422–426.

Chu, C., 1987. Thermal recovery. Petroleum Engineering Handbook, SPE., Richardson, T.X., pp. 46.1–46.46.

Cloud, J.E. and Clark, P.E., 1985. Alternatives to the power-law fluid model for crosslinked fluids. Soc. Pet. Eng. J., 935–942.

Coats, K.H., 1978. A highly implicit steamflooding model. Soc. Pet. Eng. J., 369–383.

Coats, K.H., 1980. In-situ combustion model. Soc. Pet. Eng. J., 533–553.

Coats, K.H., 1987. Reservoir simulation. Petroleum Engineering Handbook, SPE., Richardson, T.X., pp. 48.1–48.13.

Coats, K.H., George, W.D., Chu, C., and Marcum, B.E., 1974. Three-dimensional simulation of steamflooding. Soc. Pet. Eng. J., 573–592.

Cohen, Y. and Christ, F.R., 1986. Polymer retention and adsorption in the flow of polymer solutions through porous media. SPE Reservoir Engineering, 113–118.

Collins, R.E., 1961. Flow of Fluids through Porous Materials. Reinhold, New York, N.Y.

Coulter, A.W. Jr., Martinez, S.J., and Fischer, K.F., 1987. Remedial cleanup, sand control, and other stimulation treatments. Petroleum Engineering Handbook, Society of Petroleum Engineers, Richardson, T.X., pp. 56.1–56.9.

Crochet, M.J., Davies, A.R., and Walters, K., 1984. Numerical Simulation of Non-Newtonian Flow. Rheology Series Vol. 1, Elsevier, Amsterdam/Oxford.

Dauben, D.L. and Menzie, D.E., 1967. Flow of polymer solutions through porous media. J. Pet. Tech., 1065–1073.

deZabala, E.F., Vislocky, J.M., Rubin, E., and Radke, C.J., 1982. A chemical theory for linear alkaline flooding. Soc. Pet. Eng. J., 245–258.

Douglas, J. Jr., Peaceman, D.W., and Rachford, H.H. Jr., 1959. A method for calculating multidimensional immiscible displacement. Trans., AIME 216: 147–155.

Duff, I.S., 1977. A Set of FORTRAN Subroutines for Sparse Unsymmetric Linear Equations.

Earlougher, R.C. Jr., 1977. Advances in Well Test Analysis. SPE Monograph Series, Vol. 5, New York and Dallas.

Fahien, R.W., 1983. Fundamentals of Transport Phenomena. McGraw-Hill, New York, N.Y.

Falls, A.H., Gauglitz, P.A., Hirasaki, G.J., Miller, D.D., Patzek, T.W., and Ratulowski, J., 1986. Development of a mechanistic foam simulator: The population balance and generation by snap-off. Paper SPE-14961, presented at SPE/DOE Enhanced Oil Recovery Symposium, Tulsa, O.K.

Falls, A.H., Musters, J.J., and Ratulowski, J., 1986. The apparent viscosity of foams in homogeneous bead packs. submitted to Soc. Pet. Eng. J. for publication.

Fayers, F.J. and Perrine, R.L., 1959. Mathematical description of detergent flooding in oil reservoirs. Trans., AIME., 277–283.

Fayers, F.J. and Sheldon, J.W., 1959. The effect of capillary pressure and gravity on two-phase fluid flow in a porous medium. Trans., AIME 216: 147–155.

Frisch, U., Hasslacher, B., and Pomeau, Y., 1986. Lattice gas automata for the Navier-Stokes equation. Phys. Rev. Lett., 56(14): 1505–1507.

Gencer, C.S. and Ikoku, C.U., 1984. Well test analysis for two-phase flow of non-Newtonian power-law and Newtonian fluids. ASME J. Energy Resour. Technol., 106: 295–304.

Gogarty, W.B., 1967a. Rheological properties of pseudoplastic fluids in porous media. Soc. Pet. Eng. J., 149–159.

Gogarty, W.B., 1967b. Mobility control with polymer solutions. Soc. Pet. Eng. J., 161–173.

Harvey, A.H. and Menzie, D.E., 1970. Polymer solution flow in porous media. Soc. Pet. Eng. J., 111–118.

Helfferich, F.G., 1981. Theory of multicomponent, multiphase displacement in porous media. Soc. Pet. Eng. J., 51–62.

Hirasaki, G.J., 1981. Application of the theory of multicomponent, multiphase displacement to three-component, two-phase surfactant flooding. Soc. Pet. Eng. J., 191–204.

Hirasaki, G.J. and Lawson, J.B., 1985. Mechanisms of foam flow in porous media apparent viscosity in smooth capillaries. Soc. Pet. Eng. J., 176–190.

Hirasaki, G.J. and Pope, G.A., 1974. Analysis of factors influencing mobility and adsorption in the flow of polymer solution through porous media. Soc. Pet. Eng. J., 337–346.

Honarpour, M., Koederitz, L., and Harvey, A.H., 1986. Relative Permeability of Petroleum Reservoirs. CRC Press, Boca Raton, F.L.

Hovanessian, S.A. and Fayers, F.J., 1961. Linear waterflood with gravity and capillary effects. Trans., AIME 222: 32–36.

Hubbert, M.K., 1956. Darcy's law and field equations of flow of underground fluids. Trans., AIME 207: 222–239.

Hughes, W.F. and Brighton, J.A., 1967. Theory and Problems of Fluid Dynamics. Schaum's Outline Series, McGraw-Hill, N.Y., pp. 230–241.

Ikoku, C.U. and Ramey, H.J. Jr., 1979. Transient flow of non-Newtonian power-law fluids in porous media. Soc. Pet. Eng. J., 164–174.

Ikoku, C.U. and Ramey, H.J. Jr., 1980. Wellbore storage and skin effects during the transient flow of non-Newtonian power-law fluids in porous media. Soc. Pet. Eng. J., 25–38.

International Formulation Committee, 1967. A Formulation of the Thermodynamic Properties of Ordinary Water Substance. IFC Secretariat, Duesseldorf, Germany.

Iyoho, A.W. and Azar, J.J., 1981. An accurate slot-flow model for non-Newtonian fluid flow through eccentric annuli. Soc. Pet. Eng. J., 565–572.

Jennings, R.R., Rogers, J.H., and West, Y.J., 1971. Factor influencing mobility control by polymer solutions. J. Pet. Tech., 391–401.

Karakas, N., Saneie, S., and Yortsos, Y., 1986. Displacement of a viscous oil by the combined injection of hot water and chemical additive. SPE Reservoir Engineering, 391–402.

Kasraie, M. and Farouq Ali, S.M., 1989. Role of foam, non-Newtonian flow, and thermal upgrading in steam injection. Paper SPE 18784, presented at the 1989 California Regional Meeting of SPE, Bakersfield, C.A.

Kazemi, H., 1969. Pressure transient analysis of naturally fractured reservoirs with uniform fractured distribution. Soc. Pet. Eng. J., Trans., AIME 246: 451–462.

Kozicki, W., Hsu, C.J., and Tiu, C., 1967. Non-Newtonian flow through packed beds and porous media. Chem. Eng. Sci., 22: 487–502.

Lai, C.-H., 1985. Mathematical models of thermal and chemical transport in geologic media. Ph.D. thesis, Report LBL-21171, Earth Sciences Division, Lawrence Berkeley Laboratory, Berkeley, C.A.

Lake, L.W., 1987. Chemical flooding. Petroleum Engineering Handbook, SPE, Richardson, T.X., pp. 47.1–47.26.

Lardner, T.J. and Pohle, F.V., 1961. Application of the heat balance integral to problems of cylindrical geometry. J. Appl. Mech., Trans., ASME, 310–312.

Larson, R.G., Davis, H.T., and Scriven, L.E., 1982. Elementary mechanisms of oil recovery by chemical methods. Soc. Pet. Eng. J., 243–258.

Larson, R.G. and Hirasaki, G.J., 1978. Analysis of the physical mechanisms in surfactant flooding. Soc. Pet. Eng. J., 42–58.

Luan, Z.-A., 1981. Analytical solution for transient flow of non-Newtonian fluids in naturally fractured reservoirs. Acta Petrolei Sinica 2(4): 75–79 (in Chinese).

Lund, O. and Ikoku, C.U., 1981. Pressure transient behavior of non-Newtonian/Newtonian fluid composite reservoirs. Soc. Pet. Eng. J., 271–280.

Mandl, G. and Volek, C.W., 1969. Heat and mass transport in steam-drive processes. Soc. Pet. Eng. J., 59–79.

Marle, C.M., 1981. Multiphase Flow in Porous Media. Technip, Paris.

Marsily, G. de., 1986. Quantitative Hydrogeology—Groundwater Hydrology for Engineers. Translated by G. de Marsily, Academic Press, London.

Matthews, C.S. and Russell, D.G., 1967. Pressure Buildup and Flow Tests in Wells. Monograph Series, Vol. 1, Society of Petroleum Engineers AIME, Dallas, T.X.

Marx, J.W. and Langenheim, R.N., 1959. Reservoir heating by hot fluid injection. Trans., AIME 216: 312–315.

McDonald, A.E., 1979. Approximate solutions for flow on non-Newtonian power-law fluids through porous media. Paper SPE 7690, presented at the SPE-AIME Fifth Symposium on Reservoir Simulation, Denver, C.O.

McKinley, R.M., Jahns, H.O., Harris, W.W., and Greenkorn, R.A., 1966. Non-Newtonian flow in porous media. AIChE J., 12(1): 17–20.

McWhorter, D.B. and Sunada, D.K., 1990. Exact integral solutions for two-phase flow. Water Resour. Res., 26(3): 399–413.

Meter, D.M. and Bird, R.B., 1964. Tube flow of non-Newtonian polymer solutions: Part I. Laminar flow and rheological models. AIChE J., 10(6): 878–881.

Mirzadjanzade, A.KH., Amirov, A.D., Akhmedov, Z.M., Barenblatt, G.I., Gurbanov, R.S., Entov, V.M., and Zaitsev, Y.U.V., 1971. On the special features of oil and gas field development due to effects of initial pressure gradient. Preprints of Proceedings of 8th World Petroleum Congress, Special Papers, Elsevier, London.

Mitchell, J.K., 1976. Fundamentals of Soil Behavior. Wiley, New York, N.Y.

Mungan, N., 1972. Shear viscosities of ionic polyacrylamide solutions. Soc. Pet. Eng. J., 469–473.

Mungan, N., Smith, F.W., and Thompson, J.L., 1966. Some aspects of polymer floods. J. Pet. Tech., 1143–1150.

Muskat, M., 1946. The Flow of Homogeneous Fluids through Porous Media. McGraw-Hill, New York, N.Y.

Narasimhan, T.N., 1982. Recent Trends in Hydrogeology. Special Paper 189, the Geological Society of America, P.O. Box 9140. 3300 Penrose Place, Boulder, C.O.

Narasimhan, T.N. and Witherspoon, P.A., 1976. An integrated finite difference method for analyzing fluid flow in porous media. Water Resourc. Res., 12(1): 57–64.

Odeh, A.S. and Yang, H.T., 1979. Flow of non-Newtonian power-law fluids through porous media. Soc. Pet. Eng. J., 155–163.

Ozisik, M.N., 1980. Heat Conduction. Wiley, New York, N.Y.

Pascal, H., 1984. Dynamics of moving interface in a porous medium for power law fluids with yield stress. Int. J. Engng Sci., 22(5): 577–590.

Pascal, H. and Pascal, F., 1988. Dynamics of non-Newtonian fluid interfaces in a porous medium: Compressible fluids. Journal of Non-Newtonian Fluid Mechanics, 28, 227–238.

Patton, J.T., Coats, K.H. Colegrove, G.T., 1971. Prediction of polymer flood performance. Soc. Pet. Eng. J., Trans., AIME 251: 72–84.

Patton, J.T., Holbrook, S.T., and Hsu, W., 1983. Rheology of mobility-control foams. Soc. Pet. Eng. J., 456–460.

Payne, L.W. and Parker, H.W., 1973. Axial dispersion of non-Newtonian fluids in porous media. AIChE J., 19(1): 202–204.

Peaceman, D.W., 1977. Fundamentals of Numerical Reservoir Simulation. Elsevier, Amsterdam.

Peaceman, D.W. and Rachford, H.H. Jr., 1962. Numerical calculation of multidimesional miscible displacement. Soc. Pet. Eng. J., Trans., AIME 225: 327–339.

Pope, G.A., 1980. The application of fractional flow theory to enhanced oil recovery. Soc. Pet. Eng. J., 191–205.

Pruess, K., 1983a. Heat transfer in fractured geothermal reservoirs with boiling. Water Resourc. Res., 19(1): 201–208.

Pruess, K., 1983b. GMINC—A Mesh Generator for Flow Simulation in Fractured Reservoirs. Lawrence Berkeley Laboratory LBL-15227, Berkeley, C.A.

Pruess, K., 1983c. Development of the General Purpose Simulator MULKOM. Annual Report, Earth Sciences Division, Lawrence Berkeley Laboratory, Berkeley, C.A.

Pruess, K., 1987. TOUGH User's Guide Report LBL-20700. Earth Sciences Division, Lawrence Berkeley Laboratory, Berkeley, C.A.

Pruess, K., 1988. SHAFT, MULKOM, TOUGH a set of numerical simulators for multiphase fluid and heat flow. Report LBL-24430, Earth Sciences Division, Lawrence Berkeley Laboratory, Berkeley, C.A.

Pruess, K. and Narasimhan, T.N., 1982. On fluid reserves and the production of superheated steam from fractured, vapor-dominated geothermal reservoirs. J. Geo. Res., 87(B11): 9329–9339.

Pruess, K. and Narasimhan, T.N., 1985. A practical method for modeling fluid and heat flow in fractured porous media. Soc. Pet. Eng. J., 25(1): 14–26.

Pruess, K. and Wu, Y.-S., 1988. On PVT-data, well treatment, and preparation of input data for an isothermal gas-water-foam version of MULKOM. Report LBL-25783, UC-403, Earth Sciences Division, Lawrence Berkeley Laboratory, Berkeley, C.A.

Ramey, H.J. Jr., 1959. Discussion of reservoir heating of hot fluid injection. Trans., AIME 216: 364–365.

Ransohoff, T.C. and Radke, C.J., 1986. Mechanisms of foam generation in glass bead packs. Paper SPE-15441, presented at the 61st Annual Meeting of SPE, New Orleans, L.A.

Robertson, R.E. and Stiff, H.A. Jr., 1976. An improved mathematical model for relating shear stress to shear rate in drilling fluids and cement slurries. Soc. Pet. Eng. J., 31–36.

Rothman, D.H., 1988. Lattice-gas automata for immiscible two-phase flow. MIT Porous Flow Project, Report No. 1, pp. 11–26.

Rothman, D.H. and Keller, J.M., 1988. Immiscible cellular-automaton fluids. MIT Porous Flow Project, Report No. 1, pp. 1–10.

Sadowski, T.J., 1965 Non-Newtonian flow through porous media, II: Experimental. Trans. Society of Rheology, 9(2): 251–271.

Sadowski, T.J. and Bird, R.B., 1965. Non-Newtonian flow through porous media. I: Theoretical. Trans. Society of Rheology, 9(2): 243–250.

Savins, J.G., 1962. The characterization of non-Newtonian systems by a dual differentiation-integration method. Soc. Pet. Eng. J., 111–119.

Savins, J.G., 1969. Non-Newtonian flow through porous media. Ind. Eng. Chem., 61(10): 18–47.

Savins, J.G., Wallick, G.C., and Foster, W.R., 1962a. The differentiation method in rheology, I: Poiseuille-type flow. Soc. Pet. Eng. J., 211–215.

Savins, J.G., Wallick, G.C., and Foster, W.R., 1962b. The differentiation method in rheology, II: Characteristic derivatives of ideal models in Poiseuille flow. Soc. Pet. Eng. J., 309–316.

Savins, J.G., Wallick, G.C., and Foster, W.R., 1962c. The differentiation method in rheology, III: Couette flow. Soc. Pet. Eng. J., 14–18.

Scheidegger, A.E., 1974. The Physics of Flow through Porous Media. University of Toronto Press, Toronto, Canada.

Shah, S.N., 1982. Propant settling correlations for non-Newtonian fluids under static and dynamic conditions. Soc. Pet. Eng. J., 164–170.

Sheldon, J.W., Zondek, B., and Cardwell, W.T. Jr., 1959. One-dimensional, incompressible, noncapillary, two-phase fluid flow in a porous medium. Trans., AIME 216: 290–296.

Skelland, A.H.P., 1967. Non-Newtonian Flow and Heat Transfer, Wiley, New York, N.Y.

Sorbie, K.S., Parker, A., and Clifford, P.J., 1987. Experimental and theoretical study of polymer flow in porous media. SPE Reservoir Engineering, 281–304.

Stalkup, F.I. Jr., 1983. Miscible Displacement. SPE Monograph Series, Dallas, T.X.

Stehfest, H., 1970. Numerical inversion of Laplace transform. Communication, ACM 13(1): 47–48.
Taber, J.J., Kamath, I.S.K., and Reed, R.L., 1961. Mechanism of alcohol displacement of oil from porous media. Soc. Pet. Eng. J., 195–212.
Thomas, G.W., 1982. Principles of Hydrocarbon Reservoir Simulation. International Human Resources Development Co., Boston, M.A.
van Poollen, H.K. and Associates, Inc., 1980. Fundamentals of Enhanced Oil Recovery. PennWell Books, Tulsa, O.K.
van Poollen, H.K. and Jargon, J.R., 1969. Steady-state and unsteady-state flow of non-Newtonian fluids through porous media. Soc. Pet. Eng. J., Trans., AIME 246: 80–88.
Vargaftik, N.B., 1975. Tables on the Thermophysical Properties of Liquids and Gases. 2nd edn., Wiley, New York, N.Y.
Vongvuthipornchai, S. and Raghavan, R., 1987a. Pressure falloff behavior in vertically fractured wells: Non-Newtonian power-law fluids. SPE Formation Evaluation, 573–589.
Vongvuthipornchai, S. and Raghavan, R., 1987b. Well test analysis of data dominated by storage and skin non-Newtonian power-law fluids. SPE Formation Evaluation, 618–628.
Wachmann, C., 1964. A mathematical theory for the displacement of oil and water by alcohol. Soc. Pet. Eng. J., 250–266.
Warren, J.E. and Root, P.J., 1963. The behavior of naturally fractured reservoirs. Soc. Pet. Eng. J., Trans., AIME 228: 245–255.
Welge, H.J., 1952. A simplified method for computing oil recovery by gas or water drive. Trans., AIME 195: 91–98.
Wen, C.Y. and Yim, J., 1971. Axial dispersion of a non-Newtonian liquid in a packed bed. AIChE J., 17(6): 1503–1504.
Willhite, G.P., 1986. Waterflooding. SPE Textbook Series, Society of Petroleum Engineers, Richardson, T.X.
Wissler, E.H., 1971. Viscoelastic effects in the flow of non-Newtonian fluids though a porous medium. Ind. Eng. Chem. Fundam., 10(3): 411–417.
Witherspoon, P.A., Benson, S., Persoff, P., Pruess, K., Radke, C.J., and Y.-S. Wu., 1989 Feasibility Analysis and Development of Foam Protected Underground Natural Gas Storage Facilities. Final Report, Earth Sciences Division, Lawrence Berkeley Laboratory, C.A.
Wu, Y.-S., 1990. Theoretical studies of non-Newtonian and Newtonian fluid flow through porous media. Ph.D. thesis, Earth Sciences Division, Lawrence Berkeley Laboratory, LBL-28642, University of California, Berkeley, C.A.
Wu, Y.-S. and Pruess, K., 1986. A multiple-porosity method for simulation of naturally fractured petroleum reservoirs. SPE Paper 15129, presented at the 56th California Regional Meeting of SPE, Oakland, C.A. SPE Reservoir Engineering, 1988, 327–336.
Wu, Y.-S., Pruess, K., and Witherspoon, P.A., 1991. Displacement of a Newtonian fluid by a non-Newtonian fluid in a porous medium. Transport in Porous Media 6: 115–142, Report LBL-27412, Earth Sciences Division, Lawrence Berkeley Laboratory, C.A.
Wu, Y.-S., Pruess, K., and Witherspoon, P.A., 1992. Flow and displacement of Bingham non-Newtonian fluids in porous media. SPE Reservoir Engineering, 369–376.
Yortsos, Y.C. and Fokas, A.S., 1983. An analytical solution for linear waterflood including the effects of capillary pressure. Sec. Pet. Eng. J., 115–124.
Yortsos, Y.C. and Huang, A.B., 1986. Linear-stability analysis of immiscible displacement, Part 1: Simple basic flow profiles. SPE Reservoir Engineering, 378–390.

Chapter 3

Numerical simulation of sedimentary basin-scale hydrochemical processes

JEFF P. RAFFENSPERGER

Abstract

Sedimentary basins represent large-scale porous media, are important hosts to a significant portion of the world's economic energy and mineral resources. Processes occurring in sedimentary basins include groundwater flow, heat transport, and reactive mass transport. Quantitative models of flow and transport in these settings can provide insight into the processes that control the evolution of sedimentary basins by enabling the examination of processes that may occur too slowly to be observed in the field or laboratory. In many cases, such models may be the only available tool for studying processes occurring over geological time and space scales. In addition, it is important to consider the behavior of the processes occurring in sedimentary basins simultaneously, since they are generally coupled. Groundwater flow is controlled by the boundary conditions and the distribution of hydraulic conductivity; as a result, flow velocities vary spatially and temporally. This circulation is capable of transporting thermal energy and dissolved mass. In general, flow rates will be sufficiently small that the water will reach approximate equilibrium with each lithology along the flow path at the ambient temperature and pressure. These successive equilibria produce changes in the chemical composition of the fluid, resulting in reactions with the medium (i.e., precipitation, dissolution), which in turn modify the porosity and permeability. This modification may be insignificant at a human time scale, but very significant at the geological time scale.

The hydrogeological flow field then is a coupled hydrological-thermal-geochemical system, requiring solution to three sets of coupled partial differential equations. This paper reviews developments over the past several years in numerical simulation of these coupled processes. The governing conservation equations are presented, and solution procedures discussed; the finite element equations are developed for the case where local chemical equilibrium is assumed. Application of coupled models to a variety of geological problems is discussed, such as the propagation of mineral reaction fronts in one spatial dimension. These studies have noted the importance of hydrodynamic dispersion and its control on the spatial distribution of reaction rates and products. Relatively few two-dimensional simulations are available in the literature, but these few are reviewed, including the formation of uranium ore deposits, mixing-zone reactions in carbonate aquifers, and sandstone diagenesis. These studies note the importance of transport-controlled reaction-front propagation, fluid mixing, and gradient reactions, which all occur to varying degrees in a heterogeneous sedimentary basin. Future developments will require greater computer capability, and are likely to focus on application to well-documented field problems and greater inclusion of natural geological heterogeneity, but results presented to date show promise of enabling quantitative study of coupled hydrological, geochemical, and thermal processes in evolving sedimentary basins.

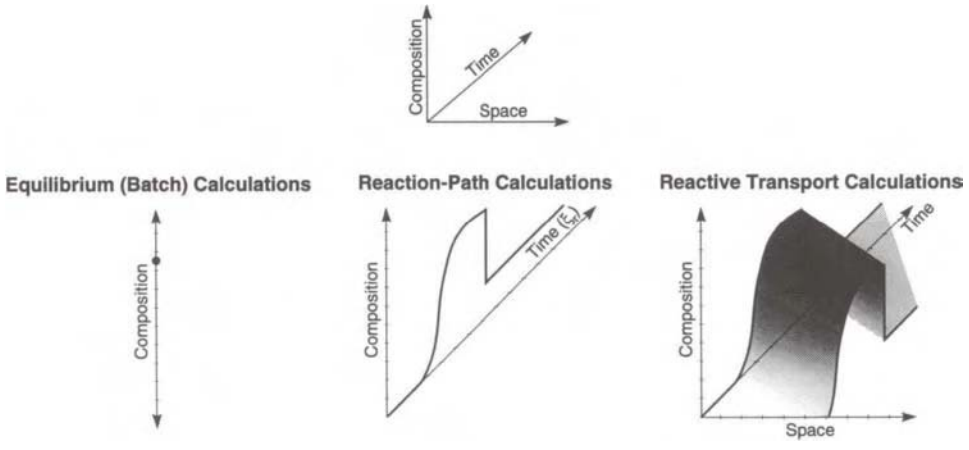


Fig. 1. Depiction of three levels of complexity in geochemical models.

1. Introduction

Sedimentary basins are areas of prolonged crustal subsidence, in which sediments accumulate to considerable thickness, typically several kilometers. They represent essentially massive geological porous media, tens to hundreds of kilometers in lateral extent. Processes occurring within sedimentary basins include groundwater flow, thermal energy (heat) transport, and reactive multicomponent mass transport, which evolve through geological time as a basin subsides, compacts, and is modified by tectonic forces. These processes interact, are "coupled", and produce significant economic mineral and hydrocarbon accumulations (Bethke et al., 1988).

The interpretation and understanding of chemical processes in sedimentary basins has benefited from the development of geochemical models, which, as their complexity and sophistication have increased, often require the use of computers for their solution (Nordstrom et al., 1979). Early models assumed equilibrium and ignored any changes due to mass transport. Many of these codes, such as WATEQ (Truesdell and Jones, 1973), REDEQL (Morel and Morgan, 1972), EQUIL (I and Nancollas, 1972), EQ3 (Wolery, 1978), and their descendants, are still in use today. For many geological systems, the assumption of thermodynamic equilibrium may not be valid, especially when reactions involving solids (Helgeson, 1969) or oxidation/reduction reactions (Stumm and Morgan, 1981) are important. Therefore, disequilibrium processes must often be included in any meaningful analysis of the particular geochemical system under study. Helgeson (1968) described a mathematical procedure for incorporating these processes and calculating the state of a geochemical system as a function of reaction progress (ξ_r). Computer codes such as PATHI (Helgeson et al., 1970), EQ6 (Wolery, 1978), and PHREEQE (Parkhurst et al., 1980) have been constructed which enable the calculation of reaction paths (Fig. 1).

Both of these approaches (equilibrium and reaction path) make the assumption

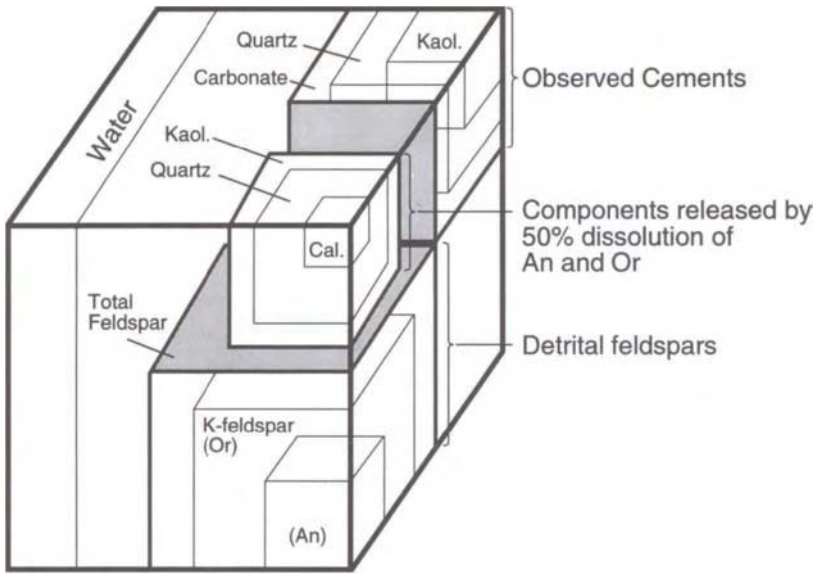


Fig. 2. Schematic representation of volumes of abundant reactive phases in Gulf Coast sandstones, assuming 20% porosity. If one-half of the detrital feldspars (lower front right) dissolve, and components derived from them re-precipitate as calcite, kaolinite, and quartz, then the volume those phases would occupy are depicted on the top right front corner of the cube. Observed volumes (top back right corner), except for Si, are very different, indicating the importance of transport in geochemical reactions (after Land and Macpherson, 1992, reprinted by permission).

that no mass is added to or removed from the system. (Reaction path codes, such as EQ6, may allow the user to simulate a "flow-through" system by removing intermediate phases. However, this approach neglects the important transport processes of diffusion and dispersion (Steefel and Lasaga, 1992) and can not be used to calculate the state of a chemical system as a function of space.) However, in most sedimentary basins, major fluxes of energy and matter have a significant impact (Gluyas and Coleman, 1992). In the Gulf of Mexico Basin (Fig. 2), for example, physical, chemical, and lithological evidence demonstrates that large-scale circulation of pore fluids has a significant impact on the diagenesis of basin sediments (Sharp et al., 1988). Dolomitization of limestone in the subsurface is common, and most theories of dolomitization involve the addition of magnesium by circulating groundwater (Hardie, 1987). Finally, many sediment-hosted ore deposits, by virtue of their high concentration, can not be considered the product of static geochemical processes (Garven and Freeze, 1984a, 1984b). In order to examine these and other geological phenomena, models are required which incorporate fluid flow and mass transport (National Research Council, 1990).

The study of reactive multicomponent chemical transport has been undertaken by researchers in a variety of fields, such as chemical engineering, petroleum engineering, soil science, geochemistry, and hydrogeology. Due to the complexity of the problem, mathematical models are generally solved numerically, and are often custom-designed for a specific use. As a result, the majority of these efforts

do not consider the full range of physical phenomena. One of the greatest limitations with existing models of reactive solute transport is the almost universal lack of direct coupling between transport and fluid flow. The majority of published studies rely on the assumption of steady uniform flow, and never actually solve a groundwater flow equation. Studies which incorporate flow dynamics are relatively rare (White et al., 1984; Liu and Narasimhan, 1989a, 1989b).

Although the effects of heterogeneous reactions on porosity and permeability have been studied quantitatively (Lund and Fogler, 1976), these results have not been incorporated in flow calculations in order to assess the resultant effect of mass transport on flow rates. Ortoleva et al. (1987) describe the development of a fully coupled model. They have applied their model to a variety of small-scale phenomena, such as porous fingering in sandstones and cement banding, as well as to the formation of uranium roll-front ores. More recently, Steefel and Lasaga (1992) describe a two-dimensional model which includes heat transport and is fully coupled.

Phillips (1990) classifies flow-controlled reactions as either isothermal reaction fronts, gradient reactions, or mixing zone reactions. Included in the second class are reactions which occur as fluids transport species across temperature gradients. Such reactions are ubiquitous in the earth's crust, which, while recognized by some geologists (Hewett, 1986; Ferry, 1987), constitutes another shortcoming of existing modeling efforts. Few studies consider the effects of temperature (Carnahan, 1987), and few consider coupling between fluid flow, heat transport, and chemical reactions (Garven and Freeze, 1984a).

The current state of hydrochemical transport modeling is limited to a few application-specific models, which generally involve several simplifications or are limited in consideration of the physical and chemical processes occurring in sedimentary basins. Despite progress in modeling the chemistry of static fluid-rock systems using speciation and reaction path calculations, and parallel progress in numerical modeling of groundwater flow and conservative solute transport (Anderson, 1979; Abriola, 1987), only recently have models been developed which integrate these two approaches.

This review will focus on recent efforts to quantify the coupled processes of groundwater flow, heat transport, and chemical transport with reactions in sedimentary basins, using numerical simulation. In addition to reviewing these developments, this paper will present the governing equations (Section 2) and outline in detail their solution by the finite element method (Section 3). Several applications will also be presented (Section 4), which will serve to illustrate the strengths and limitations of existing methods. Recent advances in coupled hydrochemical modeling including mechanical processes (compaction, deformation, faulting and fracturing, pressure solution) are beyond the scope of this review; see Ortoleva (1994) and Person et al. (1996) for recent reviews.

1.1. Conceptual models of groundwater flow in sedimentary basins

Numerical simulation provides a means of studying processes which may occur too slowly to be directly observed (Bethke, 1989). In this regard, it is important

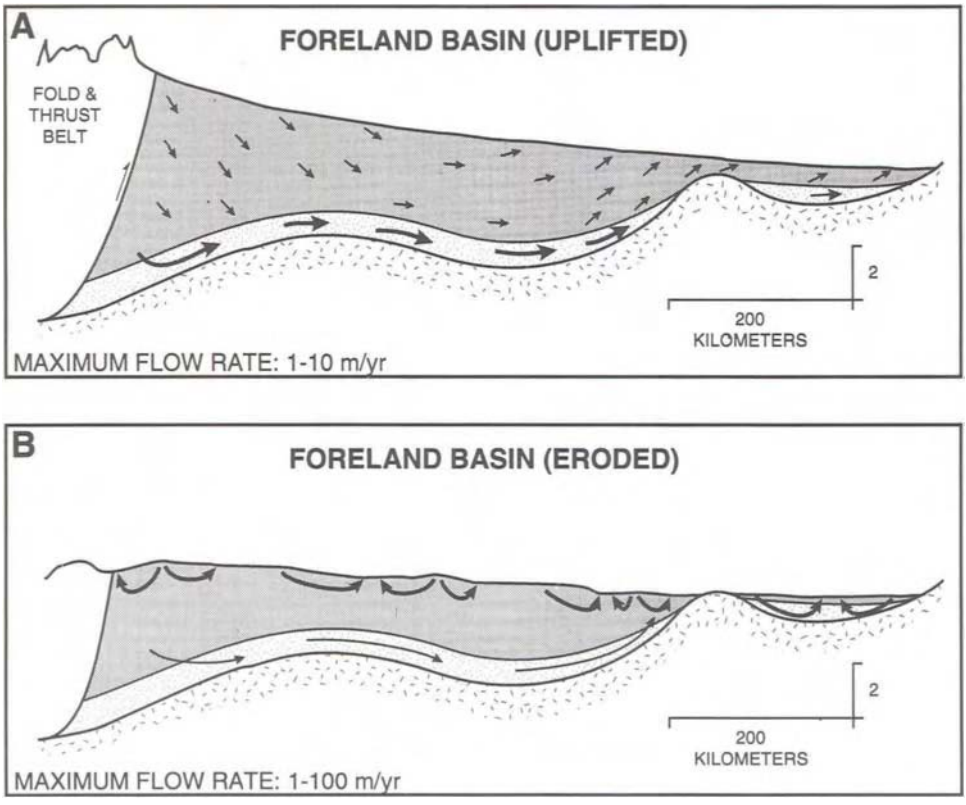


Fig. 3. Patterns of topographically-driven flow in a sedimentary basin (after Garven and Raffensperger, in press, used with permission of the authors).

to recognize that the results of the dynamic processes of basin hydrogeology (patterns of diagenesis, isotopic variations, ore mineral and hydrocarbon accumulations) provide evidence of the possible patterns of groundwater flow. Several driving mechanisms for large-scale fluid flow in sedimentary basins have been proposed, including: (i) topography- or gravity-driven flow (Garven and Freeze, 1984a; Deming and Nunn, 1991); (ii) buoyancy-driven flow or free convection (Cathles, 1981; Bjorlykke et al., 1988); (iii) compaction-driven flow during basin subsidence (Cathles and Smith, 1983; Bethke, 1985; Ge and Garven, 1989; Deming et al., 1990); and (iv) seismic pumping and tectonically-driven flow (Sibson et al., 1975; Oliver, 1986).

Water table topography is the dominant mechanism driving groundwater flow in the subsurface (Hubbert, 1940), and the important controls on resulting flow patterns (water table slope and relief, permeability distribution, and basin aspect ratio) are well-established (Tóth, 1962, 1963; Freeze and Witherspoon, 1967; Hitchon, 1969a, 1969b). At the scale of a large sedimentary basin, Garven and Freeze (1984a, 1984b) called upon gravity- or topographically-driven flow produced by tectonic uplift in a foreland basin (Fig. 3A) to explain the formation of

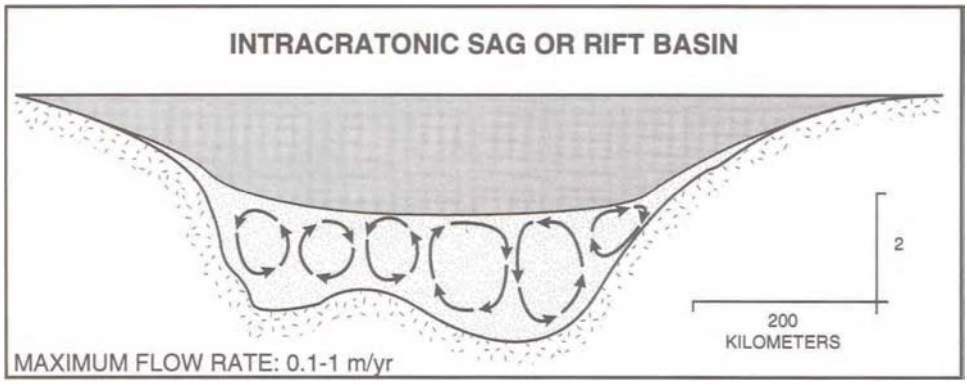


Fig. 4. Free convection in a thick sandstone aquifer (after Garven and Raffensperger, in press, used with permission of the authors).

Mississippi-Valley type lead-zinc deposits. Finite element simulations determined that flow rates would approach 10 m/yr in deep aquifers. Garven (1989) further explored regional gravity-driven flow to explain the formation of the Alberta oil sands.

Regional gravity-driven systems will persist while large regional water table gradients exist; subsequent erosion and dissection by rivers will tend to produce small shallow local flow systems (Fig. 3B; Senger et al., 1987; Garven, 1989). Several basins appear to be experiencing regional gravity-driven flow at the present (Hitchon, 1969a, 1969b; Bredehoeft et al., 1983; Senger and Fogg, 1987; Belitz and Bredehoeft, 1988). Musgrove and Banner (1993) provide geochemical evidence for deep regional groundwater flow in the Western Interior Plains aquifer system.

Free convection, or buoyancy-driven flow, has been postulated for a variety of geological settings, including shallow oceanic crust (Anderson et al., 1979) and deep continental crust (Norton and Knight, 1977; Nunn, 1994). However, relatively few studies present direct evidence of the occurrence of free convection in sedimentary basins (Blanchard and Sharp, 1985; Hanor, 1987). Raffensperger and Garven (1995a, 1995b) hypothesized that free convection in thick sandstone aquifers in Proterozoic sedimentary basins (Fig. 4) formed massive unconformity-type uranium deposits. Other modeling studies have examined buoyancy-driven flows in evolving continental rift basins (Person and Garven, 1994) and around salt domes (Evans and Nunn, 1989; Evans et al., 1991). This mechanism requires large density gradients and thick permeable sedimentary sequences, but provides a valid mechanism for significant groundwater flow rates under these conditions. Free convection is characterized by cellular flow patterns (Combarnous and Bories, 1975) which may give rise to recognizable diagenetic patterns (see Section 4.2.3).

Sedimentation and basin subsidence lead to compaction, which may also drive large-scale groundwater flow (Bethke, 1985). If sedimentation is rapid, overpressuring at depth may result, driving fluids upward and toward basin margins (Fig. 5A). Overpressured zones are common in young sedimentary basins characterized by rapid infilling of fine-grained sediments (Bethke, 1986; Harrison and Summa,

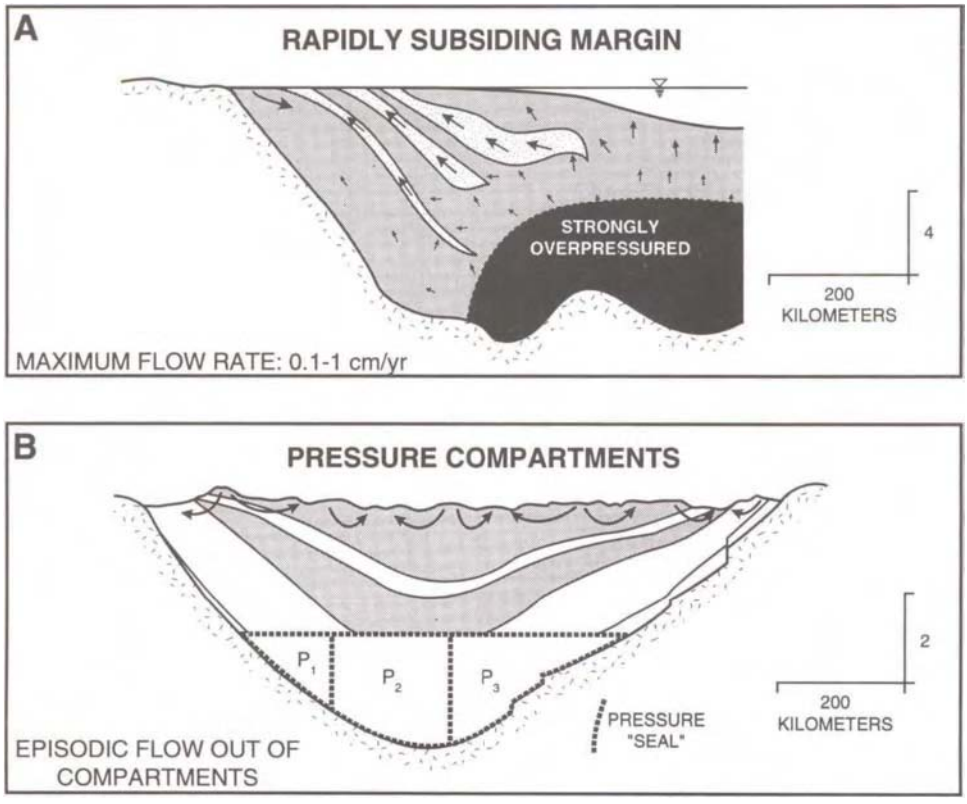


Fig. 5. Patterns of groundwater flow in subsiding sedimentary basins (after Garven and Raffensperger, in press, used with permission of the authors).

1991). Calculated flow velocities are generally small, unless faulting produces periodic rupturing and fluid expulsion (Cathles and Smith, 1983).

The formation of pressure "compartments" (Fig. 5B), regions of fluid pressure much greater than hydrostatic bounded by impermeable "seals", has been suggested to explain observations from petroleum-bearing basins (Hunt, 1990; Powley, 1990). According to this theory, sedimentological or diagenetic seals separate deep basin compartments from the normal hydrodynamic regime. Oscillatory fracturing, fluid expulsion, and re-sealing is postulated (Dewers and Ortoleva, 1994).

The connection between tectonics and basinal fluid migration has been the subject of several studies. Sibson, Moore, and Rankin (1975) noted that significant fluid volumes could be produced by dilatancy following seismic faulting ("seismic pumping"; Fig. 6A). A variety of crustal fluid sources and mechanism have been proposed to contribute to the movement of basin groundwater, such as magma intrusion at depth (Skinner and Barton, 1973) and metamorphic dehydration or rehydration following thrusting. Oliver (1986) proposed a "squeegee" mechanism for flow in foreland basins in which compression and thrusting drive fluids away

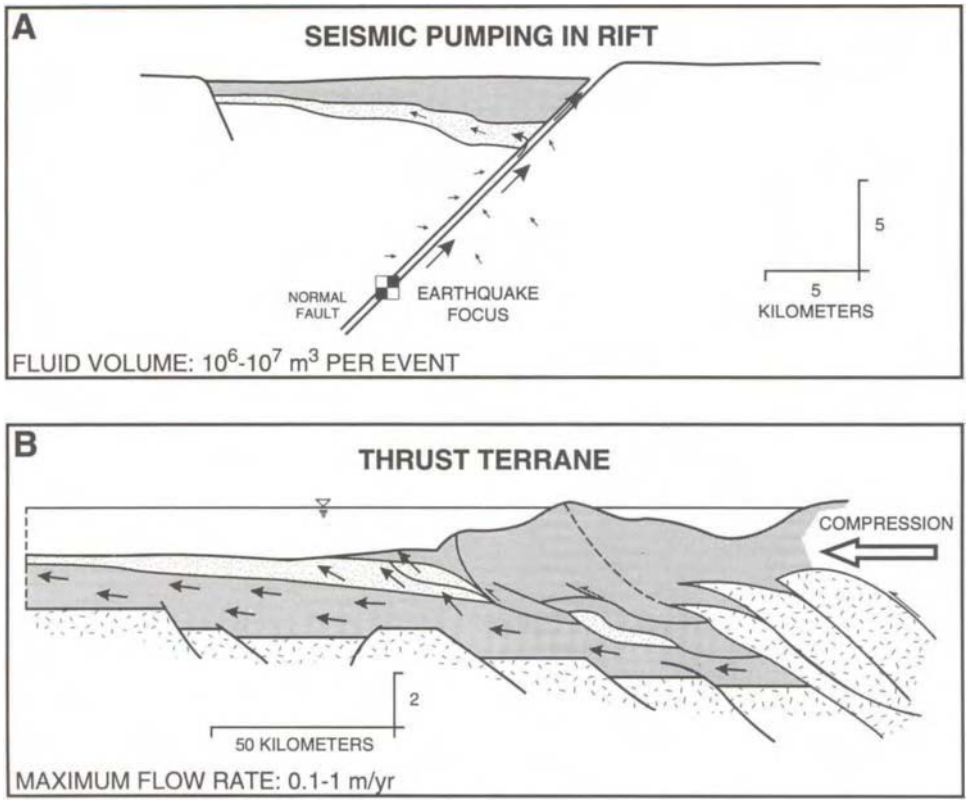


Fig. 6. Tectonically-driven groundwater flow (after Garven and Raffensperger, in press, used with permission of the authors).

from the orogen (Fig. 6B; Bethke and Marshak, 1990). Ge and Garven (1992) developed numerical models of coupled groundwater flow and tectonic rock deformation. Their results indicate that foreland compression is capable of producing transient flow rates of centimeters to meters per year, which dissipate in 10^3 to 10^4 years.

Each of these mechanisms may be anticipated to occur within any given basin at some point in its long history, although the basin setting (i.e., foreland versus intracratonic or marginal marine) and evolution may favor one mechanism over another. Each represents a different pattern, volume, and rate of groundwater flow, which may be discerned using geochemical observations. There are many complications in basin simulation: large time and length scales, physical and chemical heterogeneity at a variety of scales, difficulty in obtaining data (especially at depth), and our inability to directly observe some of the dynamic processes involved. Despite these difficulties, progress has been made in the past decade in our ability to analyze processes at this scale using numerical simulation.

2. Governing equations

In this section, the basic governing equations for fluid flow, heat transport, and reactive multicomponent solute transport in porous media will be developed. The conservation equations are based on a continuum (or REV) approach described by Bear (1972). The equations derived are valid for heterogeneous and anisotropic porous media containing inhomogeneous and slightly compressible fluids. Equations of state and specification of appropriate boundary conditions are also discussed.

2.1. Groundwater flow

2.1.1. *Fluid mass conservation in a nondeformable porous medium*

The excess of inflow over outflow during a time interval δt through the surfaces of a fixed control volume may be expressed as

$$-\left(\frac{\partial J_x}{\partial x}+\frac{\partial J_y}{\partial y}+\frac{\partial J_z}{\partial z}\right)\delta x\,\delta y\,\delta z\,\delta t \tag{2.1}$$

where vector $\mathbf{J}$, with components J_x, J_y, and J_z, denotes the mass flux (mass per unit time per unit area) of a fluid of density ρ. Applying the mass conservation principle, this must be equal to the change in mass within the control volume during the time interval δt, which is given by

$$\left[\frac{\partial(\phi\rho\delta x\delta y\delta z)}{\partial t}\right]\delta t \tag{2.2}$$

Combining equations (2.1) and (2.2) and assuming a constant control volume with no internal fluid sources or sinks

$$\nabla\cdot\mathbf{J}+\frac{\partial\phi\rho}{\partial t}=0 \tag{2.3}$$

The mass flux may be expressed as $\mathbf{J}=\rho\mathbf{q}$, such that the final conservation equation becomes (Bear, 1972; Marsily, 1986)

$$\nabla\cdot(\rho\mathbf{q})+\frac{\partial\phi\rho}{\partial t}=0 \tag{2.4}$$

or, for steady state flow

$$\nabla\cdot(\rho\mathbf{q})=0 \tag{2.5}$$

where ρ is the fluid density (dimensions of the parameters are provided in the Glossary), $\mathbf{q}$ is the specific discharge vector and ϕ is the porosity of the porous medium. If the medium is rigid, the ϕ term may be removed from the time derivative in equation (2.4), and if the fluid is incompressible and homogeneous

(ρ = constant), the density term may be removed from the expression altogether. Equation (2.4) excludes internal fluid sources or sinks.

At this point, we must make a distinction between continuity expressed for an "incompressible" fluid and that expressed for a variable-density fluid (2.4). If we define an incompressible fluid as one which satisfies the condition

$$\nabla \cdot \mathbf{q} \equiv 0 \tag{2.6}$$

then by expanding equation (2.4)

$$\rho \nabla \cdot \mathbf{q} + \mathbf{q} \cdot \nabla \rho = -\frac{\partial \phi \rho}{\partial t} \tag{2.7}$$

we see that incompressibility in the sense of equation (2.6) requires

$$\mathbf{q} \cdot \nabla \rho = -\frac{\partial \phi \rho}{\partial t} \tag{2.8}$$

For steady flow, this becomes

$$\mathbf{q} \cdot \nabla \rho = 0 \tag{2.9}$$

As pointed out by Bear (1972), equation (2.9) implies that in steady flow, streamlines will follow contours of constant ρ.

Another way of considering incompressibility in the flow of an inhomogeneous fluid is described by Yih (1961) and de Josselin de Jong (1969). Equation (2.6) describes continuity for an incompressible fluid if we consider that fluid elements preserve their density during displacement. This is only valid if density variations are due to variations in the concentration of dissolved species and no dispersion or diffusion occurs. In that case (Knudsen, 1962)

$$\frac{D\rho}{Dt} = \frac{\partial \rho}{\partial t} + \frac{1}{\phi} \mathbf{q} \cdot \nabla \rho = 0 \tag{2.10}$$

where $D(\rho)/Dt$ is the material derivative. For an incompressible medium (ϕ = constant), equation (2.10) is identical to equation (2.8). Only equations (2.4) or (2.5) are valid descriptions of mass conservation for a fluid in which $\rho = \rho(p, C, T)$.

2.1.2. Darcy's law

Darcy's empirical law governing flow through a porous medium is generally written (Freeze and Cherry, 1979)

$$q = -K \frac{dh}{dl} \tag{2.11}$$

where K is the hydraulic conductivity, h is the hydraulic head, and dh/dl is the hydraulic gradient. The hydraulic head may be defined as the mechanical energy per unit weight of the moving fluid and is the sum of two components (Hubbert, 1940)

$$h = \frac{p}{\rho g} + Z \tag{2.12}$$

where the first term is the pressure head and Z is the elevation head. The hydraulic conductivity is related to the medium intrinsic permeability (k) and fluid density and viscosity:

$$K = \frac{k\rho g}{\mu} \tag{2.13}$$

Incorporating equations (2.12) and (2.13), Darcy's law in three dimensions may be written

$$\mathbf{q} = -\frac{\mathbf{k}}{\mu}(\nabla p + \rho g \nabla Z) \tag{2.14}$$

where $\mathbf{q}$ is the specific discharge vector, $\mathbf{k}$ is the intrinsic permeability of the medium, a second order tensor, μ is the fluid dynamic viscosity, p is the fluid pressure and Z is the height above some datum. This equation is valid for an inhomogeneous fluid in laminar flow through an anisotropic porous medium.

For variable-density fluids, it is often desirable to define an equation of motion using equivalent freshwater head, rather than pressure. Defining the relative quantities

$$\mu_r = \frac{\mu_o}{\mu} \tag{2.15}$$

$$\rho_r = \frac{(\rho - \rho_o)}{\rho_o} \tag{2.16}$$

where μ_o and ρ_o are a chosen reference viscosity and density, respectively, the equivalent freshwater head may be defined as (Lusczynski, 1961)

$$h = \frac{p}{\rho_o g} + Z \tag{2.17}$$

We may also define the hydraulic conductivity tensor $\mathbf{K}$ as

$$\mathbf{K} = \frac{\mathbf{k}\rho_o g}{\mu_o} \tag{2.18}$$

We may then restate Darcy's law [equation (2.14)] as (Garven, 1989)

$$\mathbf{q} = -\mathbf{K}\mu_r(\nabla h + \rho_r \nabla Z) \tag{2.19}$$

Important parameters involved in groundwater flow calculations include the hydraulic conductivity (or intrinsic permeability) and porosity of the medium. The permeability or hydraulic conductivity of a porous medium may be determined using measurements on cores, or in situ measurements from pump tests. However, often direct measurements are not available, and values must be estimated. A

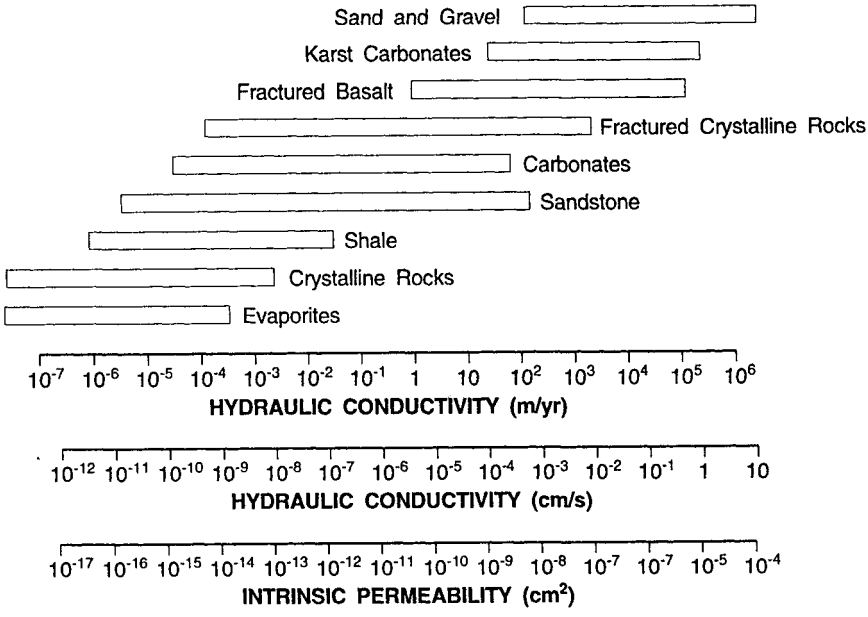


Fig. 7. Ranges of K and k for common rock types (after Garven and Freeze, 1984b, reprinted by permission of American Journal of Science).

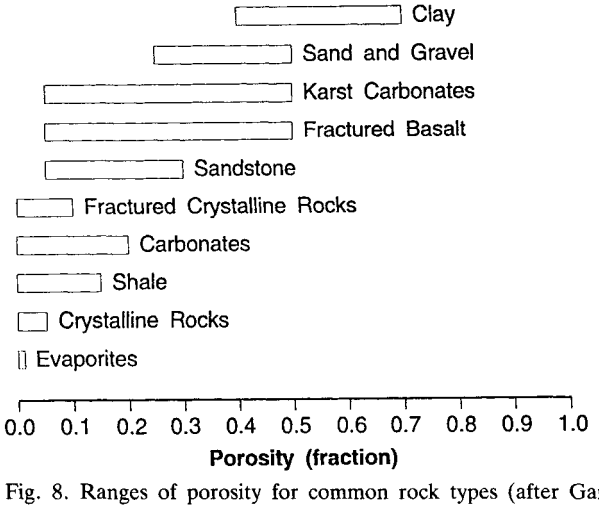


Fig. 8. Ranges of porosity for common rock types (after Garven and Freeze, 1984b, reprinted by permission of American Journal of Science).

variety of compilations of permeability data, based on lithology, are available (Davis and DeWiest, 1966; Davis, 1969; Freeze and Cherry, 1979; Brace, 1980; Mercer et al., 1982). These data are summarized for a variety of rock types in Fig. 7. Similarly, data for porosity are summarized in Fig. 8.

There is considerable evidence that hydraulic conductivity (and other hydrogeological parameter) measurements are dependent on the scale of observation (Fig.

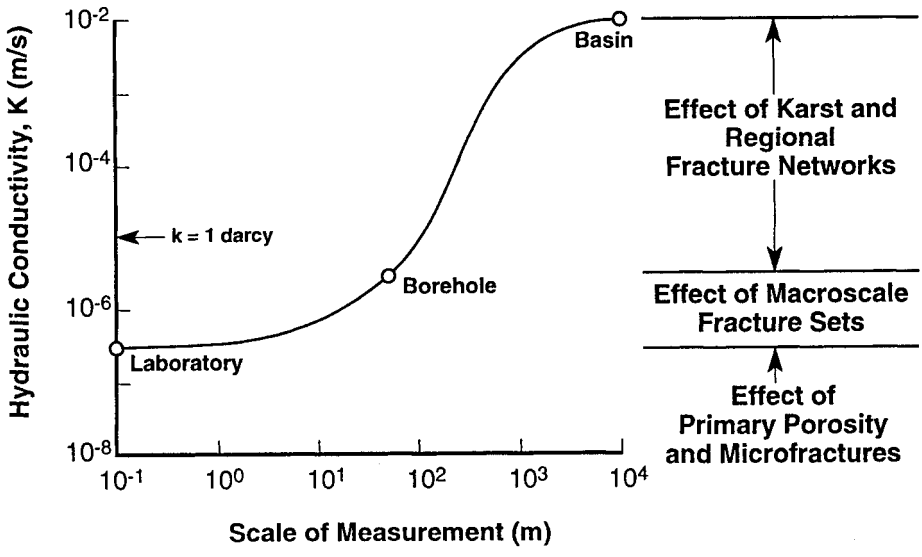


Fig. 9. Dependence of hydraulic conductivity on scale of measurement (after Garven, 1994, reprinted by permission of American Journal of Science).

9), which must also be considered when modeling groundwater flow at large scales (Garven, 1986; Bethke, 1989). For example, in a study of the Dakota aquifer in South Dakota, Bredehoeft et al. (1983) found that in situ and laboratory hydraulic conductivity measurements of the Cretaceous shale which confines the aquifer were one to three orders of magnitude lower than values indicated by numerical analyses. They suggested that leakage through the shale is largely through fractures. Dagan (1986) recognized that flow domains are characterized by their length scale and defined three such "fundamental" scales: the laboratory, the local, and the regional scale. Neuman (1990) presents a theoretical assessment of this scale effect.

2.1.3. Boundary conditions

In order to fully define a mathematical problem, the interaction of the system under consideration with its surroundings, i.e., the conditions on the boundaries of the domain in question, needs to be specified. The following discussion will refer to Fig. 10 which presents graphically the various boundary condition types which will be defined. As the primary dependent variables for which we seek a solution are equivalent freshwater head [h, defined by equation (2.17)] and specific discharge ($\mathbf{q}$, defined by Darcy's law), we will be concerned with two basic types of boundaries, one being a prescribed head boundary and the other a prescribed flux boundary. The condition for a prescribed head boundary may be expressed as

$$h = h(x, z, t) = \text{constant} \tag{2.20}$$

This type of boundary (Dirichlet or first-type) occurs wherever the flow domain is adjacent to a homogeneous fluid continuum.

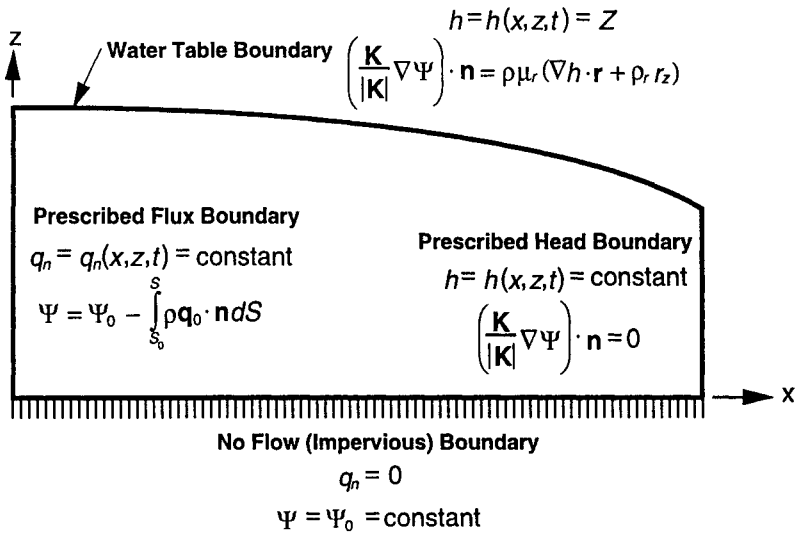


Fig. 10. Boundary conditions for flow and stream function equations.

The second boundary condition which needs to be defined is the prescribed flux (or second-type or Neumann) boundary. Along a boundary of the second-type, the flux normal to the bounding surface is fixed for all points on the boundary as a function of position and time

$$q_n = \mathbf{q} \cdot \mathbf{n} = q_n(x, z, t) = \text{constant} \tag{2.21}$$

For a no-flow (impervious) boundary, this becomes

$$q_n = \mathbf{q} \cdot \mathbf{n} = q_n(x, z, t) \equiv 0 \tag{2.22}$$

For the case of a prescribed water table (free or phreatic surface) of fixed position, we have

$$p = p(x, z, t) \equiv 0 \tag{2.23a}$$

or

$$h = h(x, z, t) = Z \tag{2.23b}$$

which represents a special case of the prescribed head (Dirichlet) boundary condition.

2.1.4. Equations of state

In order to be able to solve the equations of mass conservation (2.4) and motion (2.19) for an inhomogeneous fluid, equations of state are required which describe fluid density and viscosity as a function of pressure, solute concentration, and temperature. Phillips et al. (1981, 1983) present equations of state for calculation of fluid viscosity and density as functions of temperature, pressure, and concentration. For density

$$\rho(T, C, p) = 1000.0(A + Bx + Cx^2 + Dx^3) \tag{2.24}$$

where

$$x = c_1 e^{a_1 m} + c_2 e^{a_2 T} + c_3 e^{a_3 p} \tag{2.25}$$

and where m is concentration (molality), T is temperature (°C), and p is pressure (bars). Density (ρ) has units of kg/m^3. The coefficients A through D, a_i, and c_i are given in Phillips et al. (1981). These equations may be used to calculate densities for the following range of conditions

$$\begin{aligned} &0 < T < 350°\text{C} \\ &0 < m < 5 \text{ molal} \\ &0.1 < p < 100 \text{ MPa} \end{aligned} \tag{2.26}$$

The viscosity of water as a function of temperature and pressure is given by Watson et al. (1980)

$$\mu = \mu(T, p) = \mu_0(T) \exp\left[\frac{\rho}{317.763}\left(\sum_{i=0}^{5}\sum_{j=0}^{6} a_{ij} X^i Y^j\right)\right] \tag{2.27}$$

where

$$X = \left(\frac{T(°\text{K})}{647.27}\right)^{-1} - 1.0 \tag{2.28a}$$

$$Y = \frac{\rho}{317.763} - 1.0 \tag{2.28b}$$

$$\frac{\mu_0}{10^{-6}\text{Pa·s}} = \sqrt{\frac{T(°\text{K})}{647.27}}\left\{\sum_{k=0}^{3}\left[\frac{a_k}{(T(°\text{K})/647.27)^k}\right]\right\}^{-1} \tag{2.28c}$$

All coefficients are given in Watson et al. (1980). This result can then be corrected for salinity using the correlation (Phillips et al., 1981)

$$\mu(T, C, p) = \mu(T, p)\left[\sum_{i=0}^{3} f_i m^i + dT(1.0 - e^{km})\right] \tag{2.29}$$

Units of dynamic viscosity (μ) are Pa · seconds. The equations for viscosity [(2.27)–(2.29)] are valid for the following ranges

$$\begin{aligned} &10 < T < 350°\text{C} \\ &0 < m < 5 \text{ molal} \\ &0.1 < p < 50 \text{ MPa} \end{aligned} \tag{2.30}$$

2.1.5. Stream function

It is often useful to formulate the flow equation in terms of the stream function in modeling groundwater flow. Such formulations are essential when seeking analytical solutions for two-dimensional flow problems and when modeling free

convection. The importance of the stream function arises from its application to constant-density flow problems in which hydraulic head is a potential function that completely describes the flow system. In these circumstances (i.e., for potential flow) equipotentials are everywhere normal to flow lines, and the stream function and hydraulic head satisfy the Cauchy-Riemann conditions, thereby lending themselves to solutions using the mathematics of complex variables.

In cases of variable-density groundwater, flow is not described by a potential function. This, however, does not preclude the use of the stream function as a convenient tool for representing the flow field. Classic papers by Yih (1961) and de Josselin de Jong (1969) provide notable applications to the flow of inhomogeneous groundwater. In these cases, the stream function provides a useful mathematical tool as well as a practical way to visualize flow, and it relates flow directly to vorticity arising from lateral density variations (de Josselin de Jong, 1969).

There are several advantages in using the stream function to describe the flow of inhomogeneous groundwater. The stream function provides a scalar description of the groundwater velocity field such that contours of the stream function represent the paths that a fluid parcel follows during flow. The difference in the numerical value of the stream function between two points is a measure of the total flux of fluid across any surface through those points which is normal to the plane of view. The stream function representation provides an unambiguous picture of the flow field that can be difficult to infer from discrete velocity arrows. Moreover, fluid velocities are proportional to the contour spacing, so the relative magnitude of fluid velocities can also be inferred from a plot of the stream function.

In addition to its value in analytical solutions, the stream function presents significant advantages in numerical simulations involving very small hydraulic gradients (Frind and Matanga, 1985a, 1985b). The stream function also has significant numerical advantages when modeling the flow of variable-density groundwater. In particular, any solution of the flow field in terms of the stream function guarantees conservation of fluid mass. Numerically, this is perhaps the best reason for using the stream function.

Velocities are easy to calculate from the stream function and remain consistent from node to node. Velocity calculations are typically difficult and inaccurate with density-dependent flow even when pressure or head has been accurately calculated (Yeh, 1981). Errors in specific discharge estimates can arise because velocity depends on the pressure *gradient*, but the *magnitude* of density. Thus while pressure is discretized node-wise, density is averaged over an element (Voss, 1984). For free convection problems, estimating specific discharge can be particularly problematic because the magnitude of errors introduced by averaging density can be larger than the pressure gradients themselves. This problem is eliminated with the stream function formulation of the groundwater flow equation.

There are several disadvantages to using the stream function for calculating patterns and rates of groundwater flow. The greatest disadvantages are the inability to include internal fluid sources or sinks, and the difficulty in applying some boundary conditions (Frind and Matanga, 1985a). In addition, the stream function equation [to be developed subsequently, equation (2.44)] does not include a time derivative, and so is strictly valid only for steady flow. This is a clear disadvantage

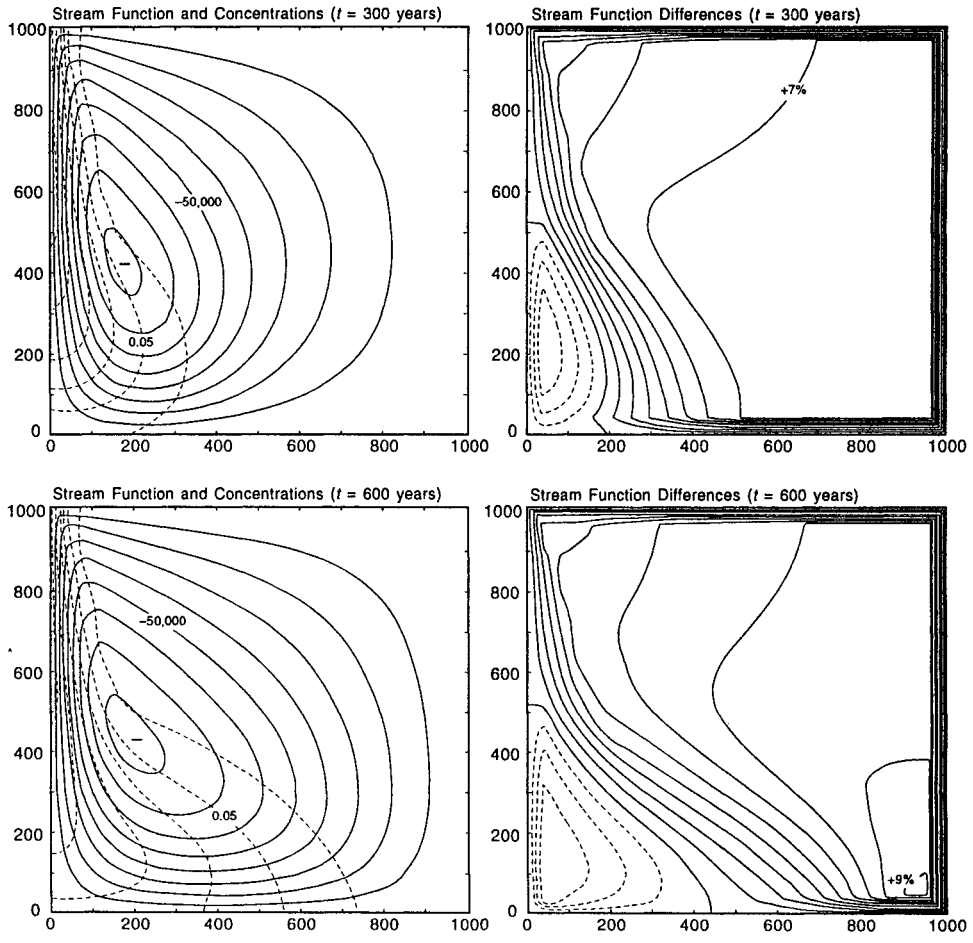


Fig. 11. Results of a numerical simulation indicating the magnitude of the relative errors produced by the use of the volume-based stream function for the case of a developing plume of high-density groundwater. Axes units are meters (from Evans and Raffensperger, 1992, *Water Resources Research*, 28(8), 2141–2145, copyright by the American Geophysical Union).

when investigating transient groundwater flow arising from changes in groundwater storage (see Section 3.1). However, problems of transient variable-density flow, arising from evolving temperature or salinity fields, are often treated by numerically solving coupled stream function and transient (heat or solute mass) transport equations. In this approach, the transient flow field is viewed as a succession of steady states (Norton and Knight, 1977).

In this section, the governing equation for groundwater flow will be developed in terms of a mass-based stream function. The importance of using this form of the stream function, over the more common volume-based stream function, are presented in Evans and Raffensperger (1992). For strongly buoyancy-driven flow, use of the volume-based stream function may lead to significant errors in the flow field (Fig. 11).

We begin with a statement of Darcy's law valid for inhomogeneous fluids

$$\mathbf{q} = -\mathbf{K}\mu_r(\nabla h + \rho_r \nabla Z) \tag{2.19}$$

The streamline **r** (Bear, 1972; Norton and Knight, 1977) is defined as the curve that is everywhere tangent to the fluid mass flux vector, $\rho\mathbf{q}$. It may be shown that the usual definition of the stream function as being tangential to the specific discharge, **q**, implies that $\nabla \cdot \mathbf{q} = 0$, which is the Boussinesq assumption, and is not strictly valid for compressible fluids (Evans and Raffensperger, 1992). The condition of tangency is

$$(\rho\mathbf{q}) \times d\mathbf{r} = 0 \tag{2.31}$$

The cross product may be expanded as

$$\frac{dx}{\rho q_x} = \frac{dz}{\rho q_z} \tag{2.32}$$

or

$$\rho q_z dx - \rho q_x dz = 0 \tag{2.33}$$

which is an exact differential by equation (2.5). By definition, the stream function $\Psi = \Psi(x, z)$ is constant along a streamline **r** (Bear, 1972). The exact differential then may be written

$$d\Psi = \frac{\partial \Psi}{\partial x} dx + \frac{\partial \Psi}{\partial z} dz = 0 \tag{2.34}$$

This must be an exact differential if the stream function is to be single-valued (de Josselin de Jong, 1969), i.e.

$$\frac{\partial^2 \Psi}{\partial x \partial z} = \frac{\partial^2 \Psi}{\partial z \partial x} \tag{2.35}$$

Comparing equations (2.33) and (2.34) results in

$$\rho q_x = -\frac{\partial \Psi}{\partial z} \tag{2.36a}$$

$$\rho q_z = \frac{\partial \Psi}{\partial x} \tag{2.36b}$$

using the convention that $\nabla\Psi$ is obtained from $\rho\nabla h$ (assuming a homogeneous, isotropic medium and a homogeneous fluid) by a counterclockwise rotation. Expanding equation (2.18) and combining with equation (2.36)

$$\begin{Bmatrix} q_x \\ q_z \end{Bmatrix} = -\mu_r \begin{bmatrix} K_{xx} & K_{xz} \\ K_{zx} & K_{zz} \end{bmatrix} \begin{Bmatrix} \partial h/\partial x \\ \partial h/\partial z + \rho_r \end{Bmatrix} = \frac{1}{\rho} \begin{Bmatrix} \partial \Psi/\partial z \\ \partial \Psi/\partial x \end{Bmatrix} \tag{2.37}$$

This may also be written

$$\frac{\mathbf{K}^{-1}}{\mu_r}\mathbf{q} = -(\nabla h + \rho_r \nabla Z) = \frac{\mathbf{K}^{-1}}{\rho\mu_r}\left(\frac{\partial \Psi}{\partial x} - \frac{\partial \Psi}{\partial z}\right) \tag{2.38}$$

where

$$\mathbf{K}^{-1} = \frac{1}{|\mathbf{K}|}\begin{bmatrix} K_{zz} & -K_{zx} \\ -K_{xz} & K_{xx} \end{bmatrix} \tag{2.39}$$

and where $|\mathbf{K}|$ is the determinant of the hydraulic conductivity tensor. Because (∇h) is a gradient field, we may make use of the identity

$$\nabla \times (\nabla h) \equiv 0 \tag{2.40}$$

Therefore (Norton and Knight, 1977; Frind and Matanga, 1985a)

$$\nabla \times \left(-\frac{\mathbf{K}^{-1}}{\mu_r}\mathbf{q} - \rho_r \nabla Z\right) \equiv 0 \tag{2.41}$$

Expanding equation (2.41)

$$\begin{vmatrix} \dfrac{\partial}{\partial x} & \dfrac{\partial}{\partial z} \\ -\dfrac{K_{zz}}{|\mathbf{K}|\mu_r}q_x + \dfrac{K_{zx}}{|\mathbf{K}|\mu_r}q_z & \dfrac{K_{xz}}{|\mathbf{K}|\mu_r}q_x - \dfrac{K_{xx}}{|\mathbf{K}|\mu_r}q_z - \rho_r \end{vmatrix} = 0 \tag{2.42}$$

Substituting equation (2.36) results in

$$\frac{\partial}{\partial x}\left[-\frac{K_{xz}}{|\mathbf{K}|\rho\mu_r}\frac{\partial \Psi}{\partial z} - \frac{K_{xx}}{|\mathbf{K}|\rho\mu_r}\frac{\partial \Psi}{\partial x} - \rho_r\right] - \frac{\partial}{\partial z}\left[\frac{K_{zz}}{|\mathbf{K}|\rho\mu_r}\frac{\partial \Psi}{\partial z} + \frac{K_{zx}}{|\mathbf{K}|\rho\mu_r}\frac{\partial \Psi}{\partial x}\right] = 0 \tag{2.43}$$

Rearranging and simplifying

$$\nabla \cdot \left(\frac{\mathbf{K}}{|\mathbf{K}|}\frac{1}{\rho\mu_r}\nabla \Psi\right) = -\frac{\partial \rho_r}{\partial x} \tag{2.44}$$

where the stream function (Ψ) has units of $[\mathrm{M\,L^{-1}\,T^{-1}}]$. This equation is valid for inhomogeneous compressible fluids in an inhomogeneous anisotropic medium.

The specification of boundary conditions for the stream function is analogous to that for the equation of mass conservation. Referring to Fig. 9, the first-type (Dirichlet) boundary condition, which may also be termed a prescribed stream function boundary, may be expressed as

$$\Psi = \Psi(x, z, t) = \text{constant} \tag{2.45}$$

This boundary type corresponds to a second-type (impervious boundary) for head. For the case of a specified (non-zero) fluid flux, this becomes

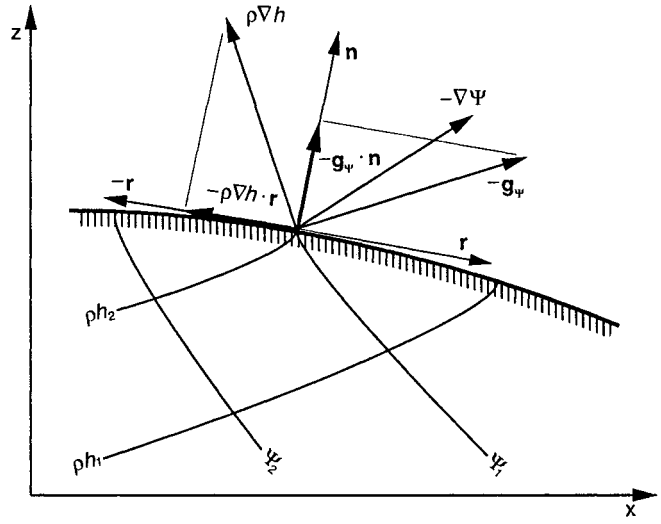


Fig. 12. Relationship between hydraulic and stream function gradients at a water table boundary. Terms are described in the text. To construct this figure, it was assumed that the medium was homogeneous, but anisotropic. If the medium is isotropic, the vectors $\nabla\Psi$ and $\mathbf{g}_\Psi$ are identical. The fluid is assumed to be homogeneous.

$$\Psi = \Psi_0 - \int_{S_0}^{S} \rho \mathbf{q}_0 \cdot \mathbf{n} dS \tag{2.46}$$

where $\mathbf{q}_0$ is the specified fluid flux and $\mathbf{n}$ is the unit normal vector.

In order to derive the second-type or Neumann boundary condition, we may consider the normal component of the gradient (see Fig. 12)

$$\mathbf{g}_\Psi \cdot \mathbf{n} = \left(\frac{\mathbf{K}}{|\mathbf{K}|}\nabla\Psi\right) \cdot \mathbf{n} \tag{2.47}$$

which may be expanded as

$$\begin{Bmatrix} g_\Psi^x \\ g_\Psi^z \end{Bmatrix} = \frac{1}{|\mathbf{K}|}\begin{bmatrix} K_{xx} & K_{xz} \\ K_{zx} & K_{zz} \end{bmatrix}\begin{Bmatrix} \partial\Psi/\partial x \\ \partial\Psi/\partial z \end{Bmatrix} \tag{2.48}$$

Expanding equation (2.48) and substituting equation (2.37) yields

$$\begin{Bmatrix} g_\Psi^x \\ g_\Psi^z \end{Bmatrix} = \frac{1}{|\mathbf{K}|}\begin{bmatrix} K_{xx} & K_{xz} \\ K_{zx} & K_{zz} \end{bmatrix}\begin{Bmatrix} \partial\Psi/\partial x \\ \partial\Psi/\partial z \end{Bmatrix} = \rho\mu_r\begin{Bmatrix} -(\partial h/\partial z) - \rho_r \\ \partial h/\partial x \end{Bmatrix} \tag{2.49}$$

which may be written

$$\mathbf{g}_\Psi \cdot \mathbf{n} = -\rho\mu_r\left(\frac{\partial h}{\partial z} + \rho_r\right)n_x + \rho\mu_r\frac{\partial h}{\partial x}n_z \tag{2.50}$$

where n_x and n_z are the x- and z-components of the unit normal vector. These are related to the components of the unit tangential vector by

$$n_x = -r_z \tag{2.51a}$$

$$n_z = r_x \tag{2.51b}$$

Substituting these relations in equation (2.50) yields

$$\mathbf{g}_\Psi \cdot \mathbf{n} = \rho \mu_r (\nabla h \cdot \mathbf{r} + \rho_r r_z) \tag{2.52}$$

where $\mathbf{r}$ is the unit tangential vector and r_z is the z-component of the unit tangential vector. This may be simplified by assuming variations in the relative density along the water table are insignificant

$$\mathbf{g}_\Psi \cdot \mathbf{n} = \rho \mu_r (\nabla h \cdot \mathbf{r}) \tag{2.53}$$

Finally, the second-type (Neumann) boundary condition may be expressed as (Fig. 9)

$$\left(\frac{\mathbf{K}}{|\mathbf{K}|} \nabla \Psi\right) \cdot \mathbf{n} = \rho \mu_r (\nabla h \cdot \mathbf{r} + \rho_r r_z) \tag{2.54}$$

where, as in equation (2.53), the relative density term may be ignored. This condition corresponds to a first-type (constant head) boundary condition for flow. The same condition may be applied to water table boundaries. When the specified head is identical at all points along the boundary, equation (2.54) simplifies to

$$\left(\frac{\mathbf{K}}{|\mathbf{K}|} \nabla \Psi\right) \cdot \mathbf{n} = 0 \tag{2.55}$$

2.2. Solute transport

2.2.1. Mass conservation of a conservative species in solution

Beginning with a general statement of mass conservation [equation (2.3)], and letting the solute mass flux be given by the sum of the advective and dispersive (i.e., mechanical dispersion and molecular diffusion) fluxes (Bear, 1972; Lichtner, 1985)

$$\mathbf{J} = (\phi \mathbf{v} \rho_i) - \phi(\mathbf{D}_m + D_i^d \mathbf{T}) \nabla \rho_i \tag{2.56}$$

where ρ_i is the mass density of solute species i, $\mathbf{v}$ is the average linear velocity, $\mathbf{D}_m$ is the coefficient of mechanical dispersion tensor, D_i^d is the molecular diffusivity, and $\mathbf{T}$ is the tortuosity of the medium, and canceling porosity terms which are assumed constant

$$\nabla \cdot [\mathbf{v} \rho_i - (\mathbf{D}_m + D_i^d \mathbf{T}) \nabla \rho_i] = -\frac{\partial \rho_i}{\partial t} \tag{2.57}$$

Simplifying this expression and assuming $\rho_i \nabla \cdot \mathbf{v} \approx 0$ (Bear, 1972), we can write

$$\nabla \cdot [(\mathbf{D}_m + D_i^d \mathbf{T})\nabla \rho_i] - \mathbf{v} \cdot \nabla \rho_i = \frac{\partial \rho_i}{\partial t} \tag{2.58}$$

We can make the following assumptions and simplifications

$$D^* = D_i^d \mathbf{T} \tag{2.59}$$

$$\rho_i = C \tag{2.60}$$

$$\mathbf{D}_m = \boldsymbol{\alpha} \mathbf{v} \tag{2.61}$$

$$\mathbf{D} = \mathbf{D}_m + D^* = \boldsymbol{\alpha} \mathbf{v} + D^* \tag{2.62}$$

Equation (2.59) defines an *effective* molecular diffusivity, D^*, for the porous medium. In equation (2.60), the mass density of species i is replaced with the solute concentration, C. In equation (2.61), the coefficient of mechanical dispersion is related to the dispersivity, $\boldsymbol{\alpha}$. Finally, equation (2.62) defines the dispersion coefficient tensor, $\mathbf{D}$. The average linear velocity is defined by

$$\mathbf{v} = \frac{\mathbf{q}}{\phi} \tag{2.63}$$

Incorporating equations (2.59) through (2.62) we may write equation (2.58) as

$$\nabla \cdot (\mathbf{D} \nabla C) - \mathbf{v} \cdot \nabla C = \frac{\partial C}{\partial t} \tag{2.64}$$

The dispersion coefficient is an assumed symmetric second order tensor (Marsily, 1986) which consists of a hydrodynamic or kinematic dispersive component and a diffusive component

$$D_{ij} = \alpha_{ij} v_i + D^* \tag{2.65}$$

where α_{ij} is the dispersivity (m), and D^* is the molecular diffusivity (effective for the porous media; units are m^2/yr). In most hydrogeological settings, molecular diffusion will be important only when fluid velocities are very small. In unconsolidated sediments, diffusion generally proceeds at one-half to one-twentieth the rate in free solution (Manheim, 1970). Lerman (1979) suggests that the value of the diffusivity in a porous medium is equal to the diffusivity in free or bulk solution multiplied by ϕ^2. Typical values for the effective molecular diffusivity range between 10^{-9} and 10^{-11} m^2/s (10^{-2} to 10^{-4} m^2/yr) (Freeze and Cherry, 1979; Lerman, 1979).

If the media is hydraulically isotropic and the dispersion tensor is expressed in its principal directions of anisotropy (i.e., the coordinate system is aligned with the streamlines or flow vector), it is limited to three components

$$\mathbf{D} = \begin{bmatrix} D_L & 0 & 0 \\ 0 & D_T & 0 \\ 0 & 0 & D_T \end{bmatrix} \tag{2.66}$$

where the subscripts L and T refer to longitudinal and transverse, respectively. In this case

$$D_L = \alpha_L |\mathbf{v}| + D^* \tag{2.67a}$$

$$D_T = \alpha_T |\mathbf{v}| + D^* \tag{2.67b}$$

In general, the flow direction will vary throughout a region, such that the dispersion tensor (assuming the medium is hydraulically isotropic) becomes (Pickens and Lennox, 1976)

$$D_{xx} = \alpha_L \frac{v_x^2}{|\mathbf{v}|} + \alpha_T \frac{v_z^2}{|\mathbf{v}|} + D^* \tag{2.68a}$$

$$D_{zz} = \alpha_L \frac{v_z^2}{|\mathbf{v}|} + \alpha_T \frac{v_x^2}{|\mathbf{v}|} + D^* \tag{2.68b}$$

$$D_{xz} = D_{zx} = (\alpha_L - \alpha_T) \frac{v_x v_z}{|\mathbf{v}|} \tag{2.68c}$$

Transverse dispersivities are generally much smaller than longitudinal dispersivities (Freeze and Cherry, 1979; Pickens and Grisak, 1981). Studies of contaminant plumes have shown that transverse dispersivities can be up to four orders of magnitude smaller than longitudinal dispersivities (Frind and Germain, 1986). Although not discussed in this section, the dispersion coefficient is a fourth order tensor (Bear, 1961). In materials that are anisotropic, the longitudinal and transverse dispersivities alone may not adequately describe dispersive transport. Gelhar et al. (1992) summarize data which indicate that transverse dispersivities measured in the vertical direction are typically an order of magnitude smaller than those measured in the horizontal direction. Jensen et al. (1993) reported the following dispersivity values from a large-scale (200 m in the direction of flow) tracer test conducted in a sandy aquifer: longitudinal, 0.45 m; transverse horizontal, 0.001 m; and transverse vertical, 0.0005 m.

The effect of scale on measured dispersivity, like hydraulic conductivity, is well recognized (Schwartz, 1977; Pickens and Grisak, 1981). Measurements at the laboratory scale (on the order of 10^{-2} to 1 cm; Domenico and Schwartz, 1990) are typically much smaller than those determined from field-scale experiments

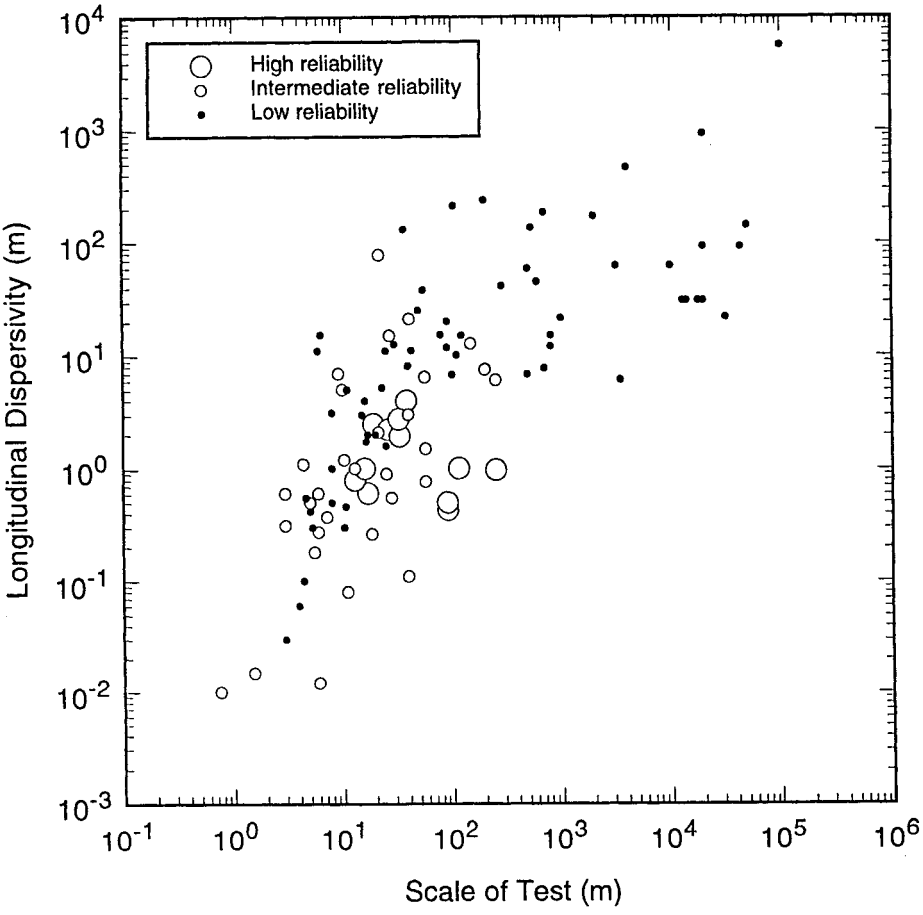


Fig. 13. Ranges of longitudinal dispersivity, α_L, for a variety of scales of measurement, ranked according to data reliability (after Gelhar et al., 1992, *Water Resources Research*, 28(7), 1955–1974, copyright by the American Geophysical Union).

(Fig. 13). This presents a problem when attempting to develop quantitative models of mass transport at the basin scale. This scale-dependence is generally attributed to heterogeneities at the field scale (lenses, layering) which manifest themselves as enhanced or macroscopic dispersion (Schwartz, 1977; Smith and Schwartz, 1980). Significant effort in recent years has been directed toward understanding the nature and scale-dependence of field-scale dispersion (Smith and Schwartz, 1980; Smith and Schwartz, 1981a; Smith and Schwartz, 1981b; Gelhar and Axness, 1983; Neuman, 1990; Gelhar et al., 1992).

2.2.2. Boundary conditions

The first-type or Dirichlet boundary condition (prescribed concentration) may be expressed as

$$C = C(x, z, t) = \text{constant} \tag{2.69}$$

This may also be used for a prescribed fluid flux boundary with incoming flow (Marsily, 1986). For a prescribed flux, we have either

$$(\mathbf{v}C - \mathbf{D}\nabla C) \cdot \mathbf{n} = \text{constant} \tag{2.70}$$

at an outflow boundary or a second-type (Neumann) boundary condition at an impervious boundary

$$(\mathbf{D}\nabla C) \cdot \mathbf{n} = \frac{\partial C}{\partial \mathbf{n}} = \text{constant}(0) \tag{2.71}$$

Although the boundary condition given by equation (2.71) ignores the advective solute flux across the boundary, it is generally used for an outflow boundary as well (Marsily, 1986).

2.2.3. Mass conservation of a reactive species in solution

We begin by defining the following values: $\hat{c}$ is the number of chemical components in the system of interest. Chemical components are defined as linearly independent chemical entities, such that every species can be uniquely represented as a combination of these components, yet no one component as a combination of other components (Yeh and Tripathi, 1989). In addition, these components are defined to correspond to species in the aqueous phase (mobile), referred to as "component species" (Reed, 1982). The use of these components, rather than neutral species, elements, or oxides, reduces the computer storage requirements significantly (Helgeson et al., 1970). The total or global mass of a component defined in this manner will be reaction-invariant (Rubin, 1983); $\hat{s}$ is the number of aqueous complexed species and other secondary species (mobile). These are aqueous species which are not used to define the system (as component species are), and which must be defined by some linear combination of the component species; and $\hat{m}$ is the number of precipitated mineral species (immobile).

Using these values and definitions, we may define the total dissolved concentration of an aqueous component ($M^T_{c,\text{aq}}$) as

$$M^T_{c,aq} = M_c + \sum_{s=1}^{\hat{s}} \tau_{cs} M_s \tag{2.72}$$

where c is a component species; s is a secondary species; M is the concentration (molarity); τ_{cs} is the composition coefficient (moles of component per formula weight).

The total non-aqueous or solid phase concentration of a component ($M^T_{c,\text{sol}}$) may be defined as

$$M^T_{c,\text{sol}} = \sum_{m=1}^{\hat{m}} \tau_{cm} M_m \tag{2.73}$$

Finally, we may define the total analytical concentration of a component (M^T_c), which will serve as the primary dependent variable

$$M_c^T = M_c + \sum_{s=1}^{\hat{s}} \tau_{cs} M_s + \sum_{m=1}^{\hat{m}} \tau_{cm} M_m \tag{2.74}$$

where all terms are as defined previously. No charge balance equation needs to be included, because charge balance is implicitly accommodated by the complete set of mass balance equations (Reed, 1982). The total analytical concentrations (M_c^T) are used as the primary variables, which simplifies the calculation procedure (Yeh and Tripathi, 1989; Mangold and Tsang, 1991).

The general advection-dispersion-reaction equation may be written for an aqueous component species as

$$\nabla \cdot (\phi \mathbf{D} \nabla M_c) - \phi \mathbf{v} \cdot \nabla M_c = \frac{\partial \phi M_c}{\partial t} - \phi R_c \tag{2.75}$$

where R_c is the rate of production of the aqueous component species per unit fluid volume (moles $L^{-3} T^{-1}$). This formulation assumes that the porous medium is saturated and no sorption reactions occur. We may write a similar expression for the secondary species

$$\nabla \cdot (\phi \mathbf{D} \nabla M_s) - \phi \mathbf{v} \cdot \nabla M_s = \frac{\partial \phi M_s}{\partial t} - \phi R_s \tag{2.76}$$

Since it is assumed that precipitated species (solid phases) are not subject to hydrological transport, one may write for a solid species

$$\frac{\partial \phi M_m}{\partial t} = \phi R_m \tag{2.77}$$

Multiplying equation (2.76) by τ_{cs} and summing over $\hat{s}$, multiplying equation (2.77) by τ_{cm} and summing over $\hat{m}$, adding the results to equation (2.75), and substituting equation (2.74) results in the general transport relation

$$\nabla \cdot (\phi \mathbf{D} \nabla M_{c,\mathrm{aq}}^T) - \phi \mathbf{v} \cdot \nabla M_{c,\mathrm{aq}}^T = \frac{\partial \phi M_c^T}{\partial t} \tag{2.78}$$

In writing equation (2.78), it has been assumed that total analytical concentrations are conservative or reaction-invariant, i.e.

$$R_c + \sum_{s=1}^{\hat{s}} \tau_{cs} R_s + \sum_{m=1}^{\hat{m}} \tau_{cm} R_m \equiv 0 \tag{2.79}$$

This will be true as long as there are no internal chemical sources or sinks.

The first-type or Dirichlet boundary condition (prescribed concentration) may be expressed as

$$M_{c,\mathrm{aq}}^T = M_{c,\mathrm{aq}}^T(x, z, t) = \text{constant} \tag{2.80}$$

This may also be used for a prescribed fluid flux boundary with incoming flow (Marsily, 1986). For a prescribed flux, we have either

$$(\mathbf{v} M_{c,\mathrm{aq}}^T - \mathbf{D} \nabla M_{c,\mathrm{aq}}^T) \cdot \mathbf{n} = \text{constant} \tag{2.81}$$

at an outflow boundary or a second-type (Neumann) boundary condition at an impervious boundary

$$(\mathbf{D}\nabla M^T_{c,\mathrm{aq}}) \cdot \mathbf{n} = \frac{\partial M^T_{c,\mathrm{aq}}}{\partial \mathbf{n}} = \text{constant(0)} \tag{2.82}$$

Although the boundary condition given by equation (2.82) ignores the advective solute flux across the boundary, it is generally used for an outflow boundary as well (Marsily, 1986).

2.2.4. Chemical equilibrium

In general, chemical reactions may be classified as occurring either entirely in a single macroscopic phase (homogeneous) or at the interface between two phases (heterogeneous). Both types of reactions are common in geological systems. Complexation, which is homogeneous, involves the combination of aqueous species, and is often considered very important in transporting metals and other ions of low solubility in geochemical systems (Skinner, 1979). The precipitation and dissolution of mineral phases, which are examples of heterogeneous reactions, are also very common.

Many geological systems may be considered to be in a state of partial equilibrium (Helgeson, 1968), such that at least one equilibrium reaction exists. As a consequence, at least one non-equilibrium reaction exists, i.e., one species is not in equilibrium with the remaining species. How the system progresses toward equilibrium is the subject of non-equilibrium thermodynamics, and consequently involves some form of kinetic rate expression or, alternatively, an evaluation of the reaction progress variable (Helgeson, 1968, 1979; Hewett, 1986).

Chemical equilibrium may be described by the law of mass action (Morel and Morgan, 1972; Truesdell and Jones, 1974). Incorporating the notation for aqueous component species, complexes, and precipitated species, we may write mass action expressions for each dissociation and dissolution reaction as follows (Reed, 1982)

$$K = \frac{\prod_{c=1}^{\hat{c}} \gamma_c^{\nu_{cs}} m_c^{\nu_{cs}}}{\gamma_s m_s} \tag{2.83a}$$

$$K^{sp} = \frac{\prod_{c=1}^{\hat{c}} \gamma_c^{\nu_{cm}} m_c^{\nu_{cm}}}{a_m} \tag{2.83b}$$

where K^{sp} is the solubility product for a mineral, m is the molality of the subscripted species, γ is the activity coefficient of the subscripted species, and ν is a stoichiometric reaction coefficient. Reactions are assumed to be written for one mole of the species under consideration (complex or solid). When the solid is not a solid solution, $a_m = 1$ in equation (2.83b).

We may write $\hat{c}$ mass balance equations, one for each component, $\hat{s}$ mass action expressions for the complexes [equation (2.83a)], and $\hat{m}$ mass action expressions for mineral phases [equation (2.83b)]. The result is $\hat{c} + \hat{s} + \hat{m}$ equations which

must be solved simultaneously for the $\hat{c} + \hat{s} + \hat{m}$ (concentrations of all species) unknowns. The matrix of equations is large and relatively sparse (hampering numerical stability). A significant advantage may be gained if the chemical system is predefined (i.e., all species including possible solid phases are known *a priori*) and the mass action expressions [equations (2.83)] are directly inserted into the mass balance expressions.

The thermodynamics of multicomponent systems requires that the number of components designated be the minimum required to fully describe the system, and therefore, that no component can be expressed by a combination of other components (Denbigh, 1981). For aqueous systems involving proton transfer or acid/base reactions (Stumm and Morgan, 1981), this constraint requires that among the species H_2O, H^+, and OH^-, only two may be included as components (Reed, 1982). In this discussion, H_2O and OH^- will be included as components. Some studies have neglected a formal mass balance on H_2O (Morel and Morgan, 1972; Truesdell and Jones, 1974), but as Reed (1982) points out, this omission precludes exact calculation of pH in systems involving redox reactions, variable temperatures, or heterogeneous equilibrium or non-equilibrium reactions.

Incorporation of acid/base reactions is straightforward and requires only the addition of two transport and mass balance equations (for OH^- and H_2O) and a mass action expression for H^+, given as the ion product of water (Stumm and Morgan, 1981)

$$K^w = \frac{(\gamma_{OH^-} m_{OH^-})(\gamma_{H^+} m_{H^+})}{a_{H_2O}} \tag{2.84}$$

In this case, H^+ is considered a secondary species, and mass balance expressions are only written for OH^- and H_2O. This treatment allows for the accurate calculation of pH under a range of conditions:

- alteration of the concentration of H^+, OH^-, and H_2O by hydrolysis, redox, and precipitation/dissolution reactions;
- variable temperature;
- and dilution of the aqueous phase by a pure H_2O source.

The chemistry of metals with varying valences, and in particular uranium, is dependent on the redox state of the system, which may play a large role in the element's solubility (Langmuir, 1978; Drever, 1982). Although many redox reactions are very slow (Stumm and Morgan, 1981), such that the concentrations of many oxidizable or reducible species may be far from those predicted by equilibrium thermodynamics, in this discussion we will assume that redox reactions are reversible and at equilibrium.

Redox reactions involve a transfer of electrons. Therefore, in one approach, these reactions may be incorporated by invoking the principle of conservation of electrons in place of the mass conservation relation (Morel and Morgan, 1972). In this case, the incorporation of redox reactions requires two additional modifications: (1) a transport equation for the "operational electrons" (Walsh et al., 1984; Yeh and Tripathi, 1989), and (2) a statement of electron or charge conservation.

Simply put, the concentration of operational electrons constitutes one additional component species.

Alternatively, two components may be specified which contain the same element in different oxidation states (Reed, 1982). This alternative makes somewhat more sense, as "free" electrons do not actually occur in aqueous solution. The designated redox pair is constrained by mass action expressions which are not written in terms of free electrons (e.g., "half-cell" reactions). Not all redox pairs need be expressed as separate components. For example, if Fe^{2+} is designated a component, Fe^{3+} may be treated as a secondary species, as long as a separate redox pair is designated as components (e.g., CO_3^{2-} and CH_4^0).

Redox reactions may be incorporated then through the addition of suitable redox-pair components, with accompanying transport and mass balance equations, and subsidiary mass action expressions for secondary species of variable oxidation state. The primary constraint is that balanced redox reactions must be established for all species (and may not include free electrons) in order to insure electrical neutrality.

2.2.5. Chemical kinetics

Several quantitative modeling efforts in recent years have sought to include kinetic rate expressions for mineral precipitation and dissolution, avoiding the limitations inherent in the assumption of local chemical equilibrium (see Section 2.2.6). In a kinetic approach, the mass action equations for solids (2.83b) are replaced by differential equations describing kinetic rate expressions. Often these expressions are founded in transition state theory (Aagaard and Helgeson, 1982); for reviews see Lasaga (1981), Stumm and Wollast (1990), and Lasaga et al. (1994). In a very general form, the rate of mineral precipitation or dissolution in aqueous solution may be written (Steefel and Lasaga, 1994)

$$\text{rate} = r = Sk_m f(a_i) f(\Delta G) \tag{2.85}$$

where r is the rate of mineral precipitation or dissolution per unit volume rock, S is the mineral specific reactive surface area, k_m is a rate constant, $f(a_i)$ is some function of the activities of the individual ions in solution, and $f(\Delta G)$ is some function of the free energy of the solution. Regardless of the specific form of kinetic rate expression used, most published models directly incorporate the rate expressions to produce conservation equations of the form [see equations (2.75) and (2.78)]

$$\nabla \cdot (\phi \mathbf{D} \nabla M_{c,\text{aq}}^T) - \phi \mathbf{v} \cdot \nabla M_{c,\text{aq}}^T = \frac{\partial \phi M_{c,\text{aq}}^T}{\partial t} + \sum_{m=1}^{\hat{m}} \tau_{cm} r_m \tag{2.86}$$

In this form, it is assumed that aqueous phase reactions (i.e., complexation) occur instantaneously (Lichtner, 1985; Steefel and Lasaga, 1994).

2.2.6. Local equilibrium versus kinetic descriptions

Several published studies assume local chemical equilibrium, i.e., at any point in the system, no mutually incompatible phases are in contact, even though the

system as a whole may not be in equilibrium (Helgeson, 1968). Knapp (1989) defines this assumption as requiring that any disequilibrium condition instantaneously relax to an equilibrium state. The assumption of local equilibrium is analogous to the case where the rates for all reactions approach infinity (Lichtner, 1993). In real geochemical systems, however, typically at least one reaction is not at equilibrium (Helgeson, 1968) but proceeds according to some kinetic rate law. Lichtner (1991) summarizes the advantages and disadvantages of the local equilibrium assumption or approximation. Its advantages (relative to a kinetic description) are that the mathematical representation of mineral reaction rates is simpler, there are fewer independent parameters involved, and that certain features of the coupled reactive transport system appear to be independent of kinetics, such as the propagation rate of mineral reaction fronts (Lichtner, 1988). Use of the local equilibrium approximation avoids the need to quantify mineral reacting surface areas and how they change through time, and also avoids potential difficulties related to the form of the kinetic rate laws involved, the values of the associated rate constants at temperatures and pressures found in sedimentary basins, and the probable lack of knowledge regarding reaction mechanisms. These advantages are largely responsible for the proliferation of reactive transport models which are based on the approximation.

The disadvantages of the local equilibrium assumption are also discussed by Lichtner (1991). Most significant is the inability of models based on the assumption to incorporate kinetically-inhibited reactions. Numerous examples can be found where thermodynamically-favored reactions simply do not occur, or do occur, but at very slow rates. In these cases, the local equilibrium assumption may not accurately describe the rates of geochemical change or even the correct sequence of reactions. With these advantages and disadvantages noted, this section will review theoretical and numerical modeling studies which compare and assess the effects of assuming local chemical equilibrium.

As a fluid, undersaturated with respect to a particular mineral phase, moves through a region, the distance to attainment of saturation tends to increase with increasing rates of dispersion and flow velocity, and decreases with increasing reaction rates (Palciauskas and Domenico, 1976). The equilibration length, l_e (Phillips, 1991), will be zero under local equilibrium. In general, $l_e \neq 0$, but if the equilibration length (and equilibration time, t_e) are less than the scales-of-interest for a particular system, then Knapp (1989) suggested that the assumption of local equilibrium is a valid approximation. It is worth briefly considering the ramifications of the assumption, in order to assess the applicability of the models invoking local equilibrium to basin-scale simulation of reactive solute transport.

Phillips (1991) has examined the approach to equilibrium conditions at reaction fronts. For the case of one-dimensional advection-dominant transport ($v \gg D/l_e$) the equilibration length is approximated by

$$l_e \approx \frac{v}{R} \tag{2.87}$$

where v is the average linear velocity, and R is the reaction rate. If $v \ll D/l_e$, then transport is dominated by dispersion (D), and

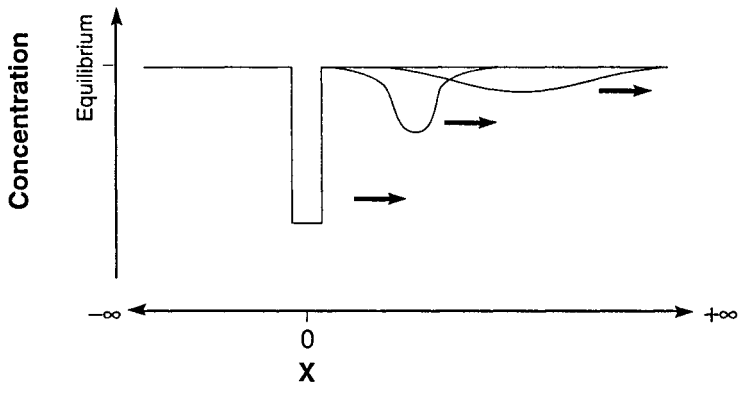


Fig. 14. Diagram of an initial slug of moving groundwater, not in local equilibrium, relaxing toward an equilibrium concentration. Spatial and temporal equilibration scales are defined by the distance and time required for relaxation to 99% of the equilibrium concentration (Re-drafted from Geochimica et Cosmochimica Acta, Volume 53, Knapp, R. B., Spatial and temporal scales of local equilibrium in dynamic fluid-rock systems, pages 1955–1964, Copyright (1989), with kind permission from Elsevier Science Ltd, The Boulevard, Langford Lane, Kidlington 0X5 1GB, UK).

$$l_e \approx \left(\frac{D}{R}\right)^{1/2} \tag{2.88}$$

This is in agreement with the findings of Palciauskas and Domenico (1976). According to Phillips (1991), the equilibration length, l_e, expresses the characteristic distance in the direction of flow over which the fluid remains in disequilibrium with respect to a given reaction. Moreover, he suggests that if the mineralogy, temperature, or pressure varies smoothly over length scales that are large compared to l_e, then the interstitial fluid is everywhere close to local equilibrium.

Knapp (1989) analyzes the spatial as well as temporal scales of local equilibrium for the case of a fluid initially in disequilibrium with quartz (Fig. 14). He shows that for relaxation to 99% of the equilibrium concentration, the advection-dispersion-reaction equation (2.86) for a single component (SiO_2) may be solved to give

$$2\mathrm{Da}\tau_e + \ln \mathrm{Pe} - 6.679316 = 0 \tag{2.89}$$

where τ_e is the dimensionless equilibration time, Pe is the Peclet number, and Da is the Damköhler number, given by

$$\mathrm{Pe} = \frac{\nu L}{D} \tag{2.90}$$

$$\mathrm{Da} = \frac{RL}{\nu} \tag{2.91}$$

where L is an arbitrary length scale (taken to be 1 m in his analysis), D is the dispersion coefficient, and R is the reaction rate. The length scale L is arbitrary, but is often chosen to represent some characteristic length of the system (Knapp, 1989).

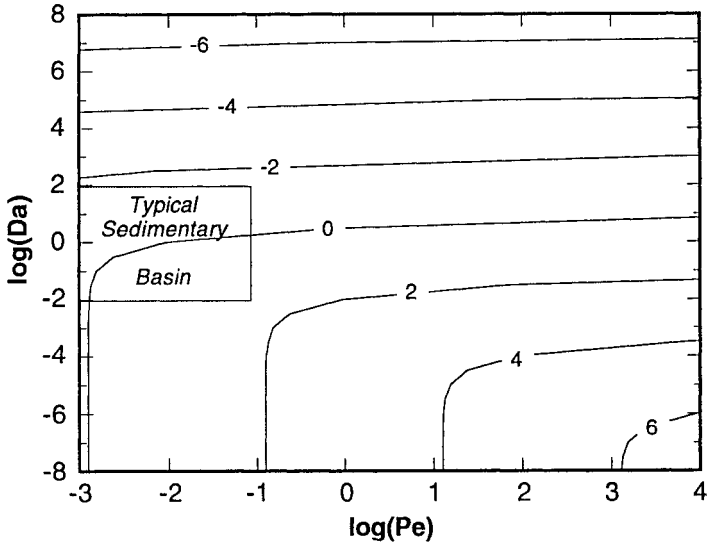


Fig. 15. Contours of $\log(\tau_e)$ for a range of Peclet and Damköhler numbers (Re-drafted from Geochimica et Cosmochimica Acta, Volume 53, Knapp, R. B., Spatial and temporal scales of local equilibrium in dynamic fluid-rock systems, pages 1955–1964, Copyright (1989), with kind permission from Elsevier Science Ltd, The Boulevard, Langford Lane, Kidlington 0X5 1GB, UK).

For the chosen length scale (1 m), the Peclet number becomes [for $D^* \ll D_m$, equation (2.62)]

$$\mathrm{Pe} = \frac{1}{\alpha} \tag{2.92}$$

where α is the dispersivity. The dimensionless time, τ_e, is related to the equilibration length, l_e, and time, t_e, by

$$l_e = \tau_e L \tag{2.93a}$$

$$t_e = \frac{\tau_e L}{v} \tag{2.93b}$$

Values of $\log(\tau_e)$ are plotted in Fig. 15. For a typical sedimentary basin, values of the Peclet number range between 10^{-3} and 10^{-1}, while values of the Damköhler number range between 10^{-2} and 10^{2} (Knapp, 1989). For these ranges, the value of τ_e ranges between 10^{-2} and 10 (Fig. 15). Therefore, the ranges of equilibration length (l_e) and time (t_e) will be 0.01–10.0 m and 10^{-3}–100 yr (for a velocity between 0.1 and 10.0 m/yr). Knapp (1989) notes that these values are less than the scales-of-interest for a sedimentary basin, which may be 10^3–10^5 m and 10^4–10^7 yr.

This analysis lends some confidence to the local equilibrium assumption as a valid approximation for processes occurring in sedimentary basins over geological time scales. However, geological media contain other minerals and competing

reactions. Therefore, this analysis may over- or under-estimate the true value of l_e or t_e. In addition, Knapp (1989) suggests that because some fluid-rock interactions are irreversible, and therefore that equilibrium fluid compositions and mineral assemblages are dependent on the chemical path (Helgeson, 1979), the compositions and assemblages predicted using local equilibrium may differ significantly from calculations involving irreversible reactions. Finally, the scales-of-interest for a numerical simulation are defined by the discretization of space and time. The grid and time step sizes should be greater than l_e and t_e, respectively, if the local equilibrium assumption is to produce valid results.

Lichtner (1991, 1993) has examined rigorously the implications of the local equilibrium assumption for the propagation of reaction fronts in one spatial dimension. He develops scaling relationships (Lichtner, 1993) for the advection-diffusion-reaction equation (2.86), which, for reaction zone boundaries (separating regions of presence and absence of a particular mineral), take the form

$$\sigma l(t; \sigma\{k_m\}, \sigma^{-1}D^*, q) = l(\sigma t; \{k_m\}, D^*, q) \tag{2.94}$$

In other words, the position of the reaction front (l) at time σt (where σ is a constant scaling parameter), corresponding to a set of rate constants $\{k_m\}$ and diffusion coefficient D^*, is equal to σ times the position of the front at time t corresponding to the scaled rate constants $\sigma\{k_m\}$ and diffusion coefficient $\sigma^{-1}D^*$. Alternatively, scaling the rate constants by a common factor and the diffusion coefficient by the reciprocal of the same factor is equivalent to scaling both the time and space coordinates by that factor. Lichtner (1993) develops similar scaling relationships for reaction front propagation rate and other functions.

This result [equation (2.94)] carries significant implications. For early times, the local equilibrium solution may be very different from the kinetic solution (Lichtner, 1993, p. 281). However, after sufficient time, the form of the two solutions begin to resemble one another. Specifically, reaction fronts propagate at a constant velocity, independent of the solution method (Fig. 16). The reaction front velocities in a kinetic description approach asymptotically the local equilibrium values; by scaling both the time and space coordinates of the kinetic solution, the limiting case of local chemical equilibrium can be determined. Since scaling the spatial coordinate does not change the amplitudes of the concentrations, the kinetic and local equilibrium solutions will have the same maxima and minima. However, reaction zone widths and solute and solid concentration profiles will be different (Fig. 17).

The analyses described above apply to one-dimensional isothermal systems and reaction front propagation. Unfortunately, relatively few direct comparisons of kinetic and local equilibrium solutions for more complicated problems are available. However, Steefel and Lasaga (1994) examine the applicability of the local equilibrium solution to two-dimensional flow (free convection) in a fractured-rock hydrothermal system. They determined that significant disequilibrium (they used a kinetic description) can occur in thermal boundary layers, with a length scale much smaller than the size of the whole system. They determine a Damköhler number [see equation (2.91)]

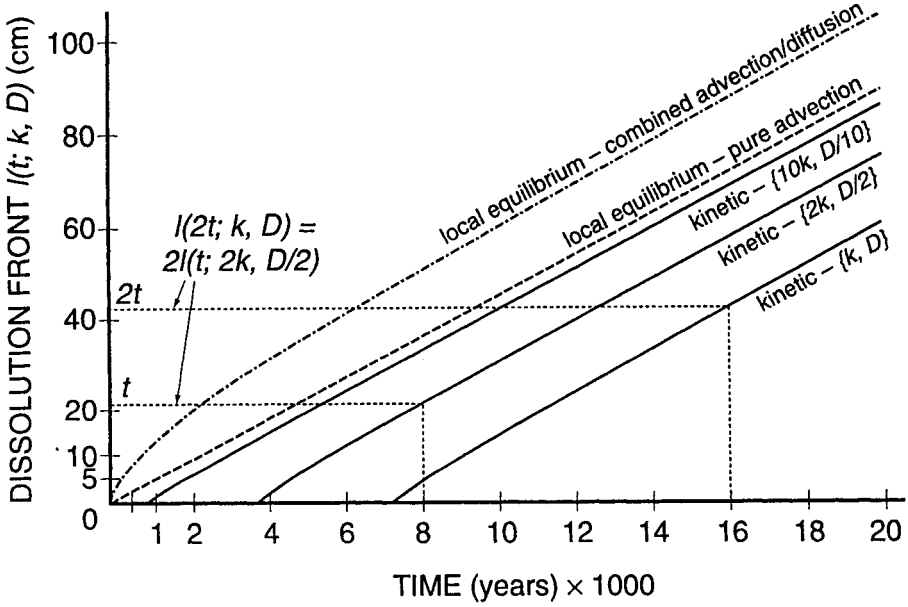


Fig. 16. Scaling relationships of a dissolution front for a single-component, one-dimensional isothermal system. Parameters correspond approximately to the dissolution rate of quartz at 100°C for a grain size of 1 mm. The scaled solution to the kinetic advection-diffusion-reaction equation (solid lines) approaches the local equilibrium solution (dashed line) for the case of pure advection. The local equilibrium solution with diffusion is displaced by the characteristic length $\lambda = \phi D^*/q$. At large times, the velocity of reaction front propagation is the same for all solutions (after Lichtner, 1993, reprinted by permission of American Journal of Science).

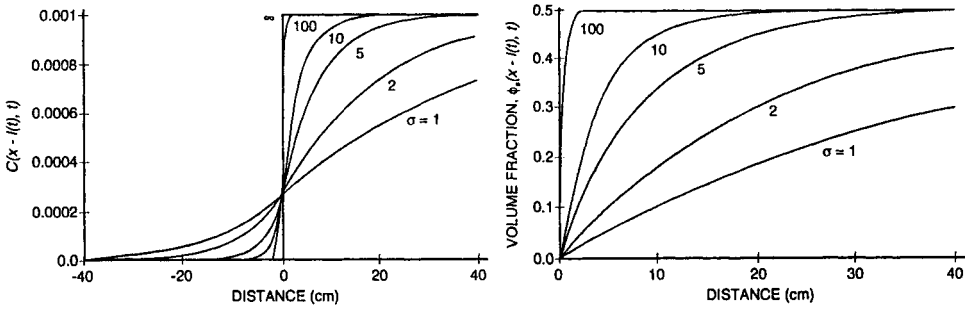


Fig. 17. Shape of the solute concentration front (left) and mineral dissolution front (right), both plotted relative to the position of the reaction front, for a single-component (SiO_2) one-dimensional system at $t = 250$ years (parameters as in Figure 16). Scaling the kinetic solution produces solute concentration profiles approaching the local equilibrium limit ($\sigma = \infty$). Note that with increasing time for a given rate constant, the kinetic solution will approach a steady-state limit (curves labeled $\sigma = 1$) which does not correspond to the local equilibrium solution. The local equilibrium and kinetic solutions will only begin to coincide when both space and time scales are scaled (after Lichtner, 1993, reprinted by permission of American Journal of Science).

$$\mathrm{Da} = \frac{R\kappa}{v_z^2} \tag{2.95}$$

where κ is the thermal diffusivity [equation (2.107)]. Values of the Damköhler number determined from this relationship will tend to be smaller than those determined using a different length scale, such as the height of the convection cell. Therefore, the equilibration length and time scales will be larger (Fig. 15), and local equilibrium less valid.

One other analysis of the importance of (dissolution) kinetics is provided by Sanford and Konikow (1989b), who coupled a two-dimensional variable-density flow model with a reaction path code (PHREEQE) using a unique scheme in which reaction path model results were tabulated for the range of conditions expected in their simulations. Within the coupling scheme, chemical reactions relationships are not solved directly, but reaction results are simply determined from the tabulated data. The problem they considered involved calcite dissolution in a coastal mixing zone. One conclusion reached by the study was that the results were relatively insensitive to the rate of calcite dissolution. The authors note, however, that other diagenetic reactions may be more strongly coupled to reaction kinetics.

2.2.7. Permeability and feedback coupling

Precipitation and dissolution of solids will affect the porosity and permeability of the medium. When the concentrations of all the mineral phases are known, the porosity may be calculated as (Hewett, 1986)

$$\phi = 1 - \sum_{m=1}^{\hat{m}} \frac{\omega_m \phi M_m}{\rho_m} \tag{2.96}$$

where ω_m is the molecular weight and ρ_m the density of mineral phase m. Changes in porosity at a point in the system as a consequence of chemical reactions involving mineral phases may then be calculated as

$$\frac{\partial \phi}{\partial t} = - \sum_{m=1}^{\hat{m}} \frac{\omega_m}{\rho_m} \frac{d\phi M_m}{dt} \tag{2.97}$$

To develop a "fully coupled" model of reactive solute transport we must consider temporal changes in porosity and permeability, and how they in turn can modify groundwater flow (Fig. 18). This is sometimes referred to as "feedback" coupling (Tsang, 1987). A relationship between porosity and permeability is needed to accomplish this. Porosities may be calculated directly once mineral volume fractions have been determined [equation (2.96)].

The relationship between porosity (as well as other geometrical properties of a porous medium) and permeability is a fundamental area of study in hydrogeology. Considerable work has been devoted to trying to understand the influence of microscale pore geometry on macroscale parameters of fluid flow in natural as well as man-made porous materials (Dullien, 1992). The incredible complexity of natural porous media means that a simple functional relationship between porosity

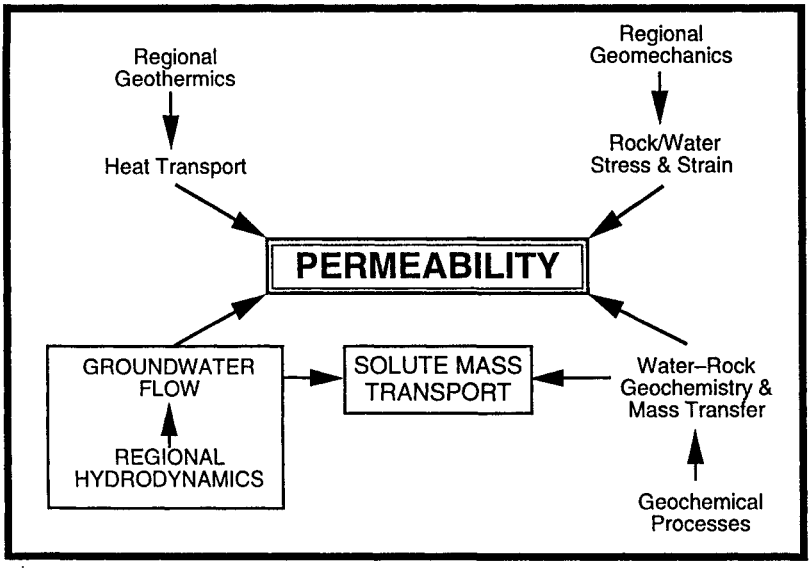


Fig. 18. Factors influencing the permeability of geological materials over large space and time scales.

and permeability is most likely not realistically attainable (e.g., Raffensperger and Ferrell, 1990).

Virtually hundreds of models have been proposed, both empirical and theoretical (Van Brakel, 1975). Steefel and Lasaga (1990) used a Kozeny-Carman model to calculate permeability. In general, however, this model is only applicable to simple granular materials (Bear, 1972), and can be very inaccurate for more complex media. Verma and Pruess (1988) used idealized models of porous media to relate changes in porosity to corresponding changes in permeability. Their geometric model considers the medium as a set of non-intersecting channels of varying cross-sectional shape. Dewers and Ortoleva (1994) used the Kozeny-Carman model to describe matrix permeability, combined with a cubic law for the fracture permeability. They determined that the exact form of the porosity-permeability relationship strongly influenced the theoretical possibility for and nature of fluid release from basin compartments. A cubic law was also used by Steefel and Lasaga (1994) to determine fracture permeability in a study of hydrothermal systems.

Several studies of sandstone core acidization have developed empirical relationships between porosity and permeability (Fogler et al., 1976; Lund and Fogler, 1976; Hekim and Fogler, 1980; Hekim et al., 1982), which generally take the form

$$\ln \frac{k}{k_i} = f(\phi, \phi_i) \tag{2.98}$$

where the subscript i refers to the initial values of intrinsic permeability (k) and porosity (ϕ). Examination of data from sandstones (Fig. 19) leads to the following

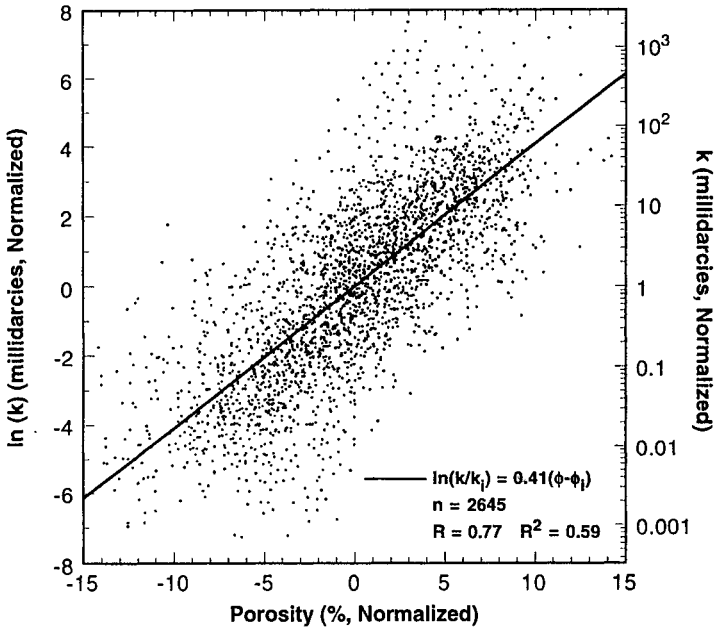


Fig. 19. Relationship between measured porosity and intrinsic permeability for several different sandstones. To construct the figure, over 2600 published measurements from several different sandstones were normalized to have a mean $\ln(k)$ of 0.0 md and ϕ of 0.0. Also shown (solid line) is the fitted empirical relationship. Data are from Füchtbauer (1967), Shenhav (1971), Bourbie and Zinszner (1985), Doyen (1988), Dixon et al. (1989), Bloch et al. (1990), Moraes (1991), Dutton and Diggs (1992), Forbes et al. (1992), Taylor and Soule (1993), Bowers et al. (1994), Fu et al. (1994), and Jian et al. (1994).

$$\ln \frac{k}{k_i} = 0.41(\phi - \phi_i) \tag{2.99}$$

where k has units of millidarcies and ϕ is expressed as a percentage. A similar relationship was used by Sanford and Konikow (1989b) to assess permeability changes produced by calcite dissolution in a coastal mixing zone.

2.3. Heat transport

In addition to transporting dissolved species, groundwater may also transport thermal energy in the form of heat (Bear, 1972). When vertical flow velocities are significant (Person, 1990), the normal or conductive temperature profile may be altered (Phillips, 1991). Since temperature directly affects fluid density, any lateral variation in temperature may lead to free convection, driven by the buoyancy of the fluid (Lapwood, 1948; Straus and Schubert, 1977; Bories, 1987). In other words, groundwater flow and heat transport are coupled processes, through the terms $\mathbf{v}$, ρ, and to a lesser extent, μ [equations (2.4), (2.5), (2.14), (2.44)].

The effects of basin-scale groundwater flow on thermal profiles have been studied extensively through the use of analytical and numerical models (Domenico

and Palciauskas, 1973; Garven and Freeze, 1984b; Person, 1990). Free convection may be a significant driving force in some hydrogeological regimes, and has also received considerable attention (Cathles, 1977; Norton and Knight, 1977; Fehn et al., 1978; Parmentier and Spooner, 1978; Cathles, 1981; Wood and Hewett, 1982; Davis et al., 1985; Sams and Thomas-Betts, 1988; Evans and Nunn, 1989). From these studies it is apparent that not only may groundwater flow affect the regional distribution of thermal energy, but that temperature may influence the patterns of mineralogical changes in a geological porous medium (Phillips, 1991).

In general, heat may be transported by conduction, convection, or radiation. For this discussion, radiation will be considered negligible. In a porous medium, the following modes of heat transport may be delineated (Bear, 1972): (a) heat transfer through the solid phase by conduction; (b) heat transfer through the fluid phase by conduction; (c) heat transfer through the fluid phase by advection; (d) heat transfer through the fluid phase by dispersion; and (e) heat transfer from the solid phase to the fluid phase, and vice versa.

2.3.1. Conservation of thermal energy in a porous medium

Conservation of thermal energy in the fluid phase may be expressed as (Bear, 1972)

$$\rho_f c_f \left(\frac{\partial T_f}{\partial t} + \mathbf{v} \cdot \nabla T_f \right) = \nabla \cdot (\lambda_f \nabla T_f) + \nabla \cdot (\epsilon_f \nabla T_f) \tag{2.100}$$

where ρ_f is the fluid density, c_f is the fluid heat capacity, T_f is the fluid temperature, λ_f is the fluid thermal conductivity, and ϵ_f is the fluid thermal dispersion coefficient. In the equation, heat transfer between the solid and fluid is assumed negligible and ignored.

For the solid phase, the thermal energy conservation equation becomes

$$\rho_s c_s \frac{\partial T_s}{\partial t} = \nabla \cdot (\lambda_s \nabla T_s) \tag{2.101}$$

Incorporating porosity relations, and noting that thermal equilibrium between the fluid and solid phases is assumed (i.e., $T_s = T_f = T$), we can combine equations (2.100) and (2.101) to obtain

$$[\phi \rho_f c_f + (1 - \phi) \rho_s c_s] \frac{\partial T}{\partial t} + \rho_f c_f \mathbf{v} \cdot \nabla T = \nabla \cdot \{[\phi \lambda_f + (1 - \phi) \lambda_s + \phi \epsilon_f] \nabla T\} \tag{2.102}$$

Defining an effective volumetric heat capacity and thermal conductivity (Fig. 20) for the porous medium (fluid plus solid)

$$(\rho c)_e = \phi \rho_f c_f + (1 - \phi) \rho_s c_s \tag{2.103}$$

$$\lambda_e = \lambda_f^{\phi} \lambda_s^{(1-\phi)} \tag{2.104}$$

equation (2.102) becomes

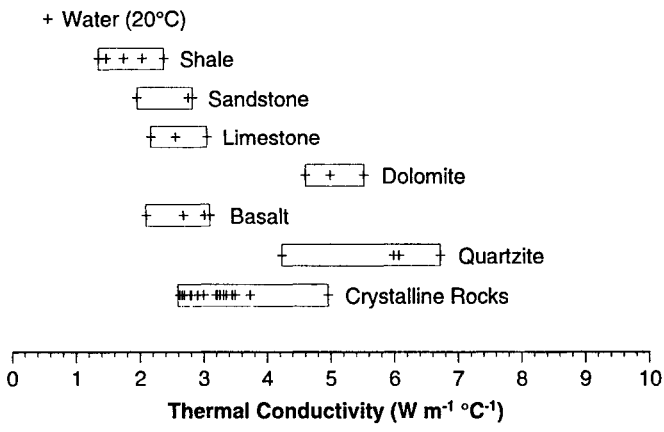


Fig. 20. Ranges of λ_e for some common rock types. Data are from Clark (1966). The symbols (+) indicate mean values for several measurements on a single rock type. Most of these values were measured at 20°C.

$$\nabla \cdot [(\lambda_e + \phi\epsilon_f)\nabla T] - \phi\rho_f c_f \mathbf{v} \cdot \nabla T = (\rho c)_e \frac{\partial T}{\partial t} \tag{2.105}$$

Marsily (1986) suggests that in order to employ units of [L] for the thermal dispersivity (analagous to the dispersivity for solute transport), the following simplification be made

$$\boldsymbol{\lambda}^* = \lambda_e + \phi\epsilon_f = \lambda_e + \epsilon\rho_f c_f |\mathbf{q}| \tag{2.106}$$

Here, we define an effective thermal dispersion coefficient, $\boldsymbol{\lambda}^*$, which is composed of an isotropic (assumed) effective thermal conductivity, λ_e, and a thermal dispersivity, ϵ, which is multiplied by the density and heat capacity of the fluid and the specific discharge. The analogy between the effective thermal dispersion coefficient and the solute dispersion coefficient, $\mathbf{D}$, becomes more apparent if we define the thermal diffusivity (Carslaw and Jaeger, 1959)

$$\kappa = \frac{\lambda_e}{\rho_f c_f} \tag{2.107}$$

which is assumed isotropic in this case. This is analogous to the effective molecular diffusivity for porous media [equation (2.59)]. Both have units of $L^2 T^{-1}$. Equation (2.105) then becomes

$$\nabla \cdot (\boldsymbol{\lambda}^* \nabla T) - \rho_f c_f \mathbf{q} \cdot \nabla T = (\rho c)_e \frac{\partial T}{\partial t} \tag{2.108}$$

For this result, we assume steady incompressible flow in an incompressible porous medium, and thermal equilibrium ($T_f = T_s$) in a saturated porous medium.

The heat capacity of water, c_f, is approximately equal to 4217.0 J/kg °C with λ_f approximately equal to 0.6 W/m °C. Typically, values of the heat capacity for common rock types vary between 500 and 2500 J/kg °C (Mercer et al., 1982). As

was the case for the solute dispersion tensor, the effective thermal dispersion tensor may be expressed in its principal directions as

$$\boldsymbol{\lambda}^* = \begin{bmatrix} \lambda_L & o & 0 \\ 0 & \lambda_T & 0 \\ 0 & 0 & \lambda_T \end{bmatrix} \tag{2.109}$$

The components of the effective thermal dispersion tensor in cartesian coordinates are determined using the relations

$$\lambda_{xx} = \lambda_e + \epsilon_L \rho_f c_f \frac{q_x^2}{|\mathbf{q}|} + \epsilon_T \rho_f c_f \frac{q_z^2}{|\mathbf{q}|} \tag{2.110a}$$

$$\lambda_{zz} = \lambda_e + \epsilon_L \rho_f c_f \frac{q_z^2}{|\mathbf{q}|} + \epsilon_T \rho_f c_f \frac{q_x^2}{|\mathbf{q}|} \tag{2.110b}$$

$$\lambda_{xz} = \lambda_{zx} = (\epsilon_L - \epsilon_T) \rho_f c_f \frac{q_x q_z}{|\mathbf{q}|} \tag{2.110c}$$

Two other quantities of relative interest are the thermal Peclet number (Pe_T) and the Rayleigh number (Ra). The Peclet number for solute transport (2.90) has been presented earlier. For heat transport, it takes the form

$$\mathrm{Pe}_T = \frac{qL}{\kappa} \tag{2.111}$$

where L is again a characteristic length and the other variables have been previously defined. Comparing this with equation (2.90), the thermal Peclet number involves the specific discharge, q, rather than the average linear velocity, v, a result of the fact that heat is transported through both fluid and solid phases, while solute is transported only through the fluid (Phillips, 1991).

In general, thermal Peclet numbers will be much smaller than solute Peclet numbers, due to the greater efficiency of thermal diffusion (or conduction) over chemical diffusion. For example, for $v = 0.09$ m/hr and $q = 0.03$ m/hr, with $L =$ 2 mm, the effective molecular diffusion, D^*, may be only 10^{-9} m^2/s, while the thermal diffusivity, κ, may be 2×10^{-7} m^2/s (Marsily, 1986). In this example, the solute Peclet number is approximately 50, while the thermal Peclet number is only 0.1.

Considering equation (2.44), it should be apparent that any horizontal gradient in fluid density will drive fluid flow, even in the absence of a pressure or head gradient. Horizontal density gradients may be due to lateral variations in salinity or temperature, and lead to the phenomenon of free convection (Combarnous and Bories, 1975; Blanchard and Sharp, 1985). In this regard, an important dimensionless quantity is the Rayleigh number, defined for a saturated isotropic homogeneous porous medium as

$$\mathrm{Ra} = \frac{g\rho\beta_T k\Delta TH}{\mu\kappa} \tag{2.112}$$

where β_T is the fluid thermal expansivity (typically 10^{-3} to $10^{-4}\,°C^{-1}$), ΔT is the temperature difference across a layer of thickness H, and the other variables have been defined previously. The Rayleigh number expresses the ratio of buoyant forces (promoting fluid flow) to viscous forces (hampering fluid flow).

Although horizontal isopycnals (lines of constant density) should produce no free convection, it is possible for organized cellular motion to develop as a result of an internal instability, if the Rayleigh number becomes too large (Phillips, 1991). As a result, a great deal of theoretical and experimental work has been done to determine the critical Rayleigh number for the onset of free convection, beginning with Lapwood (1948), through the classic studies of Elder (1967), Wooding (1957, 1958, 1960, 1963), and McKibbin (1980, 1982, 1983, 1986), some of which are reviewed by Combarnous and Bories (1975). Their results have been applied to geological settings by Donaldson (1962), Wood and Hewett (1982), Davis et al. (1985), Blanchard and Sharp (1985), and Bjorlykke et al. (1988). The critical Rayleigh number is often quoted as $4\pi^2$, but is dependent on the boundary conditions (Nield, 1968).

The critical Rayleigh number concept presumes horizontal isopycnals, which will rarely if ever be found in hydrogeological environments. However, the magnitude of the Rayleigh number may also provide some indication of how vigorous free convection will be, as well as what form the convective cells will take (Combarnous and Bories, 1975; Phillips, 1991). Taking mean values for density, viscosity, and thermal expansivity at 100°C, the Rayleigh number may be approximated by

$$\mathrm{Ra} \approx 2.6 \times 10^{-4} K\Delta TH \tag{2.113}$$

where the units are m/yr (K), °C (T), and m (H). It is important to bear in mind that parameters appearing in the expression for the Rayleigh number may be very sensitive to depth, temperature, and salinity (Straus and Schubert, 1977; Blanchard and Sharp, 1985). Finally, most geological porous media are anisotropic; Combarnous and Bories (1975) suggest the following form of the Rayleigh number for anisotropic porous media

$$\mathrm{Ra} = \frac{g\rho\beta_T\Delta TH}{\mu\kappa} \cdot \frac{4k_x k_z}{(k_x^{1/2} + k_z^{1/2})^2} \tag{2.114}$$

2.3.2. Boundary conditions

Two types of boundary conditions will be discussed, which are analagous to those described for the advection-dispersion equation. The first-type or Dirichlet boundary condition (prescribed temperature) may be expressed as

$$T = T(x, z, t) = \text{constant} \tag{2.115}$$

For a prescribed flux, we have either

$$(\mathbf{v}T - \boldsymbol{\lambda}^*\nabla T) \cdot \mathbf{n} = \text{constant} \tag{2.116}$$

or a second-type (Neumann) boundary condition (impervious boundary)

$$(\boldsymbol{\lambda}^*\nabla T) \cdot \mathbf{n} = \frac{\partial T}{\partial \mathbf{n}} = \text{constant}(0) \tag{2.117}$$

3. Numerical solution

This section will review numerical solution approaches to the governing sets of coupled partial differential equations describing groundwater, heat, and reactive solute mass fluxes in sedimentary basins. Special attention will be given to methods for solving the nonlinear equations describing reactive solute mass transport [Section (3.2.6)]. Although analytical solutions have been applied to hydrogeological problems encountered in sedimentary basins (for a recent review see Person et al., 1996), the problem complexity often necessitates numerical solution. Although numerical solutions have been developed using finite difference, integrated finite difference, and other numerical approaches, this section will concentrate on reviewing applications of the finite element method. Development of the finite element equations for groundwater flow (including the stream function), solute transport, and heat transport will be described for the two-dimensional case (vertical plane). Equations will be developed for heterogeneous, anisotropic, incompressible media and fluids of variable density, where density may be a function of pressure, solute concentration, and temperature. The governing equations have been derived in the previous section.

The finite element method has seen increasing application to problems of groundwater flow (Garven and Freeze, 1984a, 1984b; England and Freeze, 1988), solute transport (Pinder, 1973; Garven, 1989), and heat transport (Mercer et al., 1975; Smith and Chapman, 1983; Woodbury and Smith, 1985; Forster and Smith, 1988a, 1988b; Person and Garven, 1992). Although traditionally more difficult to program, the finite element method has the following advantages (Mercer and Faust, 1980): (1) flexibility in the geometry of boundaries and internal regions, (2) better evaluation of cross-product terms, and (3) simpler treatment of specified fluxes. Details of the method will not be presented here. These may be found in a variety of general texts (Zienkiewicz, 1977; Segerlind, 1984; Johnson, 1987), as well as numerous review papers and texts specific to groundwater hydrology (Remson et al., 1971; Pinder and Gray, 1977; Anderson, 1979; Wang and Anderson, 1982; Huyakorn and Pinder, 1983; Javandel et al., 1984; van der Heijde et al., 1985; Bear and Verruijt, 1987; Istok, 1989).

3.1. Groundwater flow

The equations which govern groundwater flow in porous media are the continuity equation (2.4), and Darcy's law (2.19). The transient terms in equation (2.4) can be expanded and simplified to account for transient changes in the fluid mass

balance within a given control volume due to changes in fluid density and medium porosity brought on by changes in head (or pressure), temperature, and solute concentration. Expanding the terms on the right side of equation (2.4) gives

$$\frac{\partial \phi \rho}{\partial t} = \phi\left[\left(\frac{\partial \rho}{\partial t}\right)_{T,C} + \left(\frac{\partial \rho}{\partial t}\right)_{h,C} + \left(\frac{\partial \rho}{\partial t}\right)_{T,h}\right] + \rho\left[\left(\frac{\partial \phi}{\partial t}\right)_{T,C} + \left(\frac{\partial \phi}{\partial t}\right)_{h,C} + \left(\frac{\partial \phi}{\partial t}\right)_{T,h}\right] \tag{3.1}$$

where the subscripts refer to variables assumed constant for the particular partial derivative. Equation (3.1) simply states that the changes in fluid density and medium porosity are a function of the individual contributions of these changes due to changes in head (h), temperature (T), and solute concentration (C). This equation may be rewritten (using the Chain Rule) as

$$\frac{\partial \phi \rho}{\partial t} = \phi\left[\left(\frac{\partial \rho}{\partial h}\frac{\partial h}{\partial t}\right)_{T,C} + \left(\frac{\partial \rho}{\partial T}\frac{\partial T}{\partial t}\right)_{h,C} + \left(\frac{\partial \rho}{\partial C}\frac{\partial C}{\partial t}\right)_{T,h}\right] + \rho\left[\left(\frac{\partial \phi}{\partial h}\frac{\partial h}{\partial t}\right)_{T,C} + \left(\frac{\partial \phi}{\partial T}\frac{\partial T}{\partial t}\right)_{h,C} + \left(\frac{\partial \phi}{\partial C}\frac{\partial C}{\partial t}\right)_{T,h}\right] \tag{3.2}$$

Equation (3.2) contains six terms; the fifth and sixth are often assumed to be zero, as the change in porosity as a result of changing temperature will be negligible, and that resulting from changes in solute concentration (neglecting precipitation and dissolution) will be zero. The first and fourth terms describe the changes in fluid volume as a result of changes in head, which may be written as (Freeze and Cherry, 1979)

$$\phi\left(\frac{\partial \rho}{\partial h}\frac{\partial h}{\partial t}\right)_{T,C} + \rho\left(\frac{\partial \phi}{\partial h}\frac{\partial h}{\partial t}\right)_{T,C} = \rho S_s \frac{\partial h}{\partial t} \tag{3.3}$$

where

$$S_s = \rho g(\eta + \phi\beta) \tag{3.4}$$

Here, S_s is the specific storage, η is the aquifer compressibility, and β is the compressibility of water. We are neglecting physical (non-elastic) compaction of the aquifer material. Employing the coefficient of isobaric thermal expansion for the fluid (Bear, 1972), and combining with equation (3.1), equation (3.3) becomes

$$\frac{\partial \phi \rho}{\partial t} = \rho S_s \frac{\partial h}{\partial t} - \phi \rho \beta_T \frac{\partial T}{\partial t} + \phi \frac{\partial \rho}{\partial C}\frac{\partial C}{\partial t} \tag{3.5}$$

where

$$\beta_T = -\frac{1}{\rho}\frac{\partial \rho}{\partial T} \tag{3.6}$$

Introducing an analogous expression for the isobaric and isothermal density variation of the fluid as a function of solute concentration

$$\beta_C = \frac{1}{\rho}\frac{\partial \rho}{\partial C} \tag{3.8}$$

The units for β_C are the inverse of those used to express concentration. (Note that the sign of the expression for β_C is positive since an increase in solute concentration results in an increase in fluid density, whereas an increase in temperature results in a decrease in fluid density.) Summarizing, the transient term may be written as

$$\frac{\partial \phi \rho}{\partial t} = \rho S_s \frac{\partial h}{\partial t} - \phi \rho \beta_T \frac{\partial T}{\partial t} + \phi \rho \beta_C \frac{\partial C}{\partial t} \tag{3.8}$$

We can now rewrite the general continuity equation for variable density groundwater flow as

$$\nabla \cdot (\rho \mathbf{q}) + \rho S_s \frac{\partial h}{\partial t} - \phi \rho \beta_T \frac{\partial T}{\partial t} + \phi \rho \beta_C \frac{\partial C}{\partial t} - Q = 0 \tag{3.9}$$

where Q is an internal fluid source/sink term.

3.1.1. Formulation of finite element equations

Combining equations (2.19) and (3.9), and neglecting the transient storage terms arising from temporal changes in temperature and solute concentration, we may apply the Galerkin formulation of the finite element method by initially defining the operator

$$L(h) = \nabla \cdot [\rho \mathbf{K} \mu_r (\nabla h + \rho_r \nabla Z)] - \rho S_s \frac{\partial h}{\partial t} \tag{3.10}$$

and using the interpolation formula (trial function)

$$h \approx \hat{h} = \sum_{m=1}^{N} h_m \xi_m \tag{3.11}$$

where N is the number of nodes. The weighted residual equation becomes

$$\iint_R \left\{ \nabla \cdot [\rho \mathbf{K} \mu_r (\nabla \hat{h} + \rho_r \nabla Z)] - \rho S_s \frac{\partial \hat{h}}{\partial t} + Q \right\} \xi_n dR = 0 \tag{3.12}$$

Simplifying

$$\iint_R \{\nabla \cdot [\rho \mathbf{K} \mu_r \nabla \hat{h}]\} \xi_n dR + \iint_R \{\nabla \cdot [\rho \rho_r \mathbf{K} \mu_r \nabla Z]\} \xi_n dR$$

$$-\iint_R \left(\rho S_s \frac{\partial \hat{h}}{\partial t}\right)\xi_n dR + \iint_R Q\xi_n dR = 0 \tag{3.13}$$

Applying Green's first integral identity, which may be expressed as

$$\iint_R (u\nabla^2 w + \nabla u \cdot \nabla w)dR = \int_S \left(u\frac{\partial w}{\partial n}\right)dS \tag{3.14}$$

using the variable substitutions

$$u = \xi_n \tag{3.15a}$$

$$\nabla w = \rho \mathbf{K}\mu_r \nabla \hat{h} \tag{3.15b}$$

for the first term and

$$u = \xi_n \tag{3.16a}$$

$$\nabla w = \rho\rho_r \mathbf{K}\mu_r \nabla Z \tag{3.16b}$$

for the second term, equation (3.13) becomes

$$\iint_R \rho\mathbf{K}\mu_r \nabla\hat{h}\cdot\nabla\xi_n dR - \int_S \rho\mathbf{K}\mu_r\nabla\hat{h}\cdot\mathbf{n}\xi_n dS + \iint_R \rho\rho_r\mathbf{K}\mu_r\nabla Z\cdot\nabla\xi_n dR$$
$$-\int_S \rho\rho_r\mathbf{K}\mu_r\nabla Z\cdot\mathbf{n}\xi_n dS + \iint_R \rho S_s\frac{\partial\hat{h}}{\partial t}\xi_n dR - \iint_R Q\xi_n dR = 0 \tag{3.17}$$

Rewriting equation (3.17) and neglecting the internal fluid source term

$$\iint_R \rho\mathbf{K}\mu_r\nabla\hat{h}\cdot\nabla\xi_n dR + \iint_R \rho\rho_r\mathbf{K}\mu_r\nabla Z\cdot\nabla\xi_n dR + \iint_R \rho S_s\frac{\partial\hat{h}}{\partial t}\xi_n dR$$
$$= -\int_S \rho\mathbf{q}\cdot\mathbf{n}\xi_n dS \tag{3.18}$$

Replacing equation (3.18) as a summation over each finite element (R^e), and incorporating the trial solution [equation (3.11)] and simplifying, we may write

$$\sum_m \left[\sum_e \iint_{R^e} \rho\mathbf{K}^e\mu_r\nabla\xi_n^e\cdot\nabla\xi_m^e dR^e\right]h_m + \sum_e \iint_R \rho\rho_r\mathbf{K}^e\mu_r\nabla Z\cdot\nabla\xi_n^e dR$$
$$+\sum_m \left[\sum_e \iint_R \rho S_s^e\xi_n^e\xi_m^e dR^e\right]\frac{dh_m}{dt} = -\sum_e \int_{S^e}\rho\mathbf{q}^e\cdot\mathbf{n}\xi_n^e dS^e \tag{3.19}$$

Here, the summation over m refers to the summation over all nodes and the summation over e refers to all elements. Several other comments are necessary.

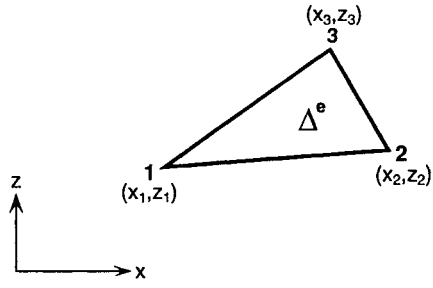


Fig. 21. Linear triangular finite element.

As the equation has been written as a summation over all the elements, with each element subregion being considered individually, values of certain parameters are considered element-wise, and are so indicated using the superscript e (e.g., ϕ^e). Density, viscosity, and their relative counterparts are considered as mean values for each element. The h_m values are spatially constant and so are removed from the interior of the first and third terms. In addition, the summation over m is exterior to the element-wise summation of the integral expressions in terms 1 and 3.

Simplifying the notation, equation (3.19) becomes

$$\sum_m A_{nm}h_m + \sum_m C_{nm}\frac{dh_m}{dt} = -Q_n \tag{3.20}$$

where

$$A_{nm} = \sum_e A^e_{nm} = \sum_e \iint_{R^e} \rho \mathbf{K}^e \mu_r \nabla \xi^e_n \cdot \nabla \xi^e_m dR^e \tag{3.21a}$$

$$C_{nm} = \sum_e C^e_{nm} = \sum_e \iint_{R^e} \rho S^e_s \xi^e_n \xi^e_m dR^e \tag{3.21b}$$

$$Q_n = \sum_e \iint_{R^e} \rho \rho_r \mathbf{K}^e \mu_r \nabla Z \cdot \nabla \xi^e_n dR^e + \sum_e \int_{S^e} \rho \mathbf{q}^e \cdot \mathbf{n} \xi^e_n dS^e \tag{3.21c}$$

3.1.2. Element basis functions

Using triangular elements (Fig. 21) and assuming linear variation

$$\xi_n(x, z) = a + bx + cz \tag{3.22}$$

Solving for a, b, and c

$$\xi_n = \frac{1}{2\Delta}(\alpha_n + \beta_n x + \gamma_n z) \tag{3.23}$$

where

$$\begin{aligned} \alpha_1 &= x_2 z_3 - x_3 z_2 & \beta_1 &= z_2 - z_3 & \gamma_1 &= x_3 - x_2 \\ \alpha_2 &= x_3 z_1 - x_1 z_3 & \beta_2 &= z_3 - z_1 & \gamma_2 &= x_1 - x_3 \\ \alpha_3 &= x_1 z_2 - x_2 z_1 & \beta_3 &= z_1 - z_2 & \gamma_3 &= x_2 - x_1 \end{aligned} \tag{3.24}$$

and Δ refers to the element area

$$2\Delta = \gamma_2 \beta_1 - \gamma_1 \beta_2 \tag{3.25}$$

The general integration formula given by Zienkiewicz (1977) for linear triangular elements may be written

$$\iint_R \xi_1^a \xi_2^b \xi_3^c dR = \frac{a!b!c!}{(a+b+c+2)!} 2\Delta \tag{3.26}$$

3.1.3. Evaluating the integrals

All that remains is to evaluate the integrals [equations (3.21)]. The stiffness matrix A_{nm} may be integrated, using equation (3.26), to give

$$A_{nm} = \sum_e \left[\frac{\bar{\rho}\bar{\mu}_r}{4\Delta^e} (K_{xx}^e \beta_n \beta_m + K_{xz}^e \beta_n \gamma_m + K_{zx}^e \gamma_n \beta_m + K_{zz}^e \gamma_n \gamma_m) \right] \tag{3.27}$$

where overbars indicate mean values for the element (e superscripts are implied). If the cartesian coordinate axes (x, z) are also the principal directions of the permeability tensor, the two off-diagonal terms (K_{xz}, K_{zx}) are zero (Bear, 1972).

The expression for the storage matrix, C_{nm}, may be integrated, assuming S_s is constant in R^e, to give

$$C_{nm} = \sum_e \bar{\rho} S_s^e \begin{cases} \dfrac{\Delta^e}{6} & \text{for } n = m \\ \dfrac{\Delta^e}{12} & \text{for } n \neq m \end{cases} \tag{3.28}$$

The flux array consists of a buoyancy term and a specified flux term, which may be integrated to give

$$Q_n = \sum_e \left[\bar{\rho}\bar{\rho}_r \bar{\mu}_r \left(K_{xz}^e \frac{\beta_n}{2} + K_{zz}^e \frac{\gamma_n}{2} \right) - \bar{\rho} \frac{q_n l^e}{2} \right] \tag{3.29}$$

where q_n is the specified fluid flux at node n and l^e is the length of the element boundary. Note that this term is negated so that by convention, q_n is positive for inflow and negative for outflow.

3.1.4. Transient and steady-state equations

For the time discretization, a weighted finite difference scheme may be constructed for the general expression

$$\sum_m A_{nm}h_m + \sum_m C_{nm}\frac{dh_m}{dt} = -Q_n \tag{3.20}$$

which takes the form

$$\sum_m \left[(1-\theta)A_{nm}h_m^k + \theta A_{nm}h_m^{k+1} + C_{nm}\frac{h_m^{k+1}-h_m^k}{\Delta t}\right] = -Q_n \tag{3.30}$$

where it is assumed that the $k+1$ time step is that being solved for. Specific cases are as follows

Fully explicit:	$\theta = 0$	(3.31a)
Crank-Nicolson:	$\theta = \frac{1}{2}$	(3.31b)
Galerkin:	$\theta = \frac{2}{3}$	(3.31c)
Fully implicit:	$\theta = 1$	(3.31d)

Rearranging equation (3.30) gives (using square brackets to indicate matrices and curly brackets to indicate arrays)

$$\left(\theta[A] + \frac{1}{\Delta t}[C]\right)\{h\}^{k+1} = \left[(\theta-1)[A] + \frac{1}{\Delta t}[C]\right]\{h\}^k - \{Q\} \tag{3.32}$$

where the global matrices [given in equations (3.27) through (3.29)] are derived by summing over the local matrices. On boundaries of prescribed head, h_m are known, and therefore the equations of these nodes can be removed from the matrices. On boundaries of prescribed fluid flow, values of q_n are inserted into the appropriate terms.

In the case of steady-state flow, equation (3.20) simplifies to

$$\sum_m A_{nm}h_m = -Q_n \tag{3.33}$$

where the stiffness matrix A_{nm} is given in equation (3.27) and the flux vector is given by equation (3.29). Boundary conditions are handled in the same manner as for transient equations.

3.1.5. Rotation of the hydraulic conductivity tensor

Given the maximum and minimum values (principal values) of the hydraulic conductivity tensor

$$\mathbf{K}' = \begin{bmatrix} K_{\max} & 0 \\ 0 & K_{\min} \end{bmatrix} \tag{3.34}$$

and an angle θ_K between the principal directions or axes and the orthogonal cartesian axes (x, z), the components of the hydraulic conductivity tensor used in equations (3.27) and (3.29)

$$\mathbf{K} = \begin{bmatrix} K_{xx} & K_{xz} \\ K_{zx} & K_{zz} \end{bmatrix} \tag{3.35}$$

may be determined using the relations (Bear, 1972)

$$K_{xx} = \frac{K_{\max} + K_{\min}}{2} + \frac{K_{\max} - K_{\min}}{2} \cos 2\theta_K \tag{3.36a}$$

$$K_{xz} = K_{zx} = \frac{K_{\max} - K_{\min}}{2} \sin 2\theta_K \tag{3.36b}$$

$$K_{zz} = \frac{K_{\max} + K_{\min}}{2} - \frac{K_{\max} - K_{\min}}{2} \cos 2\theta_K \tag{3.36c}$$

3.1.6. Solution of the matrix equations

In general, the matrix expression we wish to solve [equations (3.20) or (3.33)] takes the form

$$[A]\{x\} = \{b\} \tag{3.37}$$

where $[A]$ is the coefficient matrix, $\{b\}$ is an array of knowns, and $\{x\}$ is an array of unknowns. For the case of the groundwater flow problem, matrix $[A]$ will be a diagonally-dominant, symmetric, banded matrix, while for the case of the transport problem (heat or solute) the matrix will be non-symmetric.

There are a large variety of methods available to solve equation (3.37). In general, these methods may be classified as either direct or iterative. Iterative methods may be more computationally efficient, but convergence is not guaranteed. Direct methods, while not always as efficient, are reliable. Although they may involve a large number of repetitive mathematical operations, leading to round-off error, the accuracy of modern digital computers precludes this problem.

3.1.7. Stream function

The equation for the mass-based stream function is

$$\nabla \cdot \left(\frac{\mathbf{K}}{|\mathbf{K}|} \frac{1}{\rho \mu_r} \nabla \Psi \right) = - \frac{\partial \rho_r}{\partial x} \tag{2.44}$$

Typical units of the stream function are kg/m yr. Employing the operator

$$L(\Psi) = \nabla \cdot \left(\frac{\mathbf{K}}{|\mathbf{K}|} \frac{1}{\rho \mu_r} \nabla \Psi \right) \tag{3.38}$$

and using the trial function

$$\Psi \approx \hat{\Psi} = \sum_{m=1}^{N} \Psi_m \xi_m \tag{3.39}$$

the weighted residual equation may be written

$$\iint_R \left[\nabla \cdot \left(\frac{\mathbf{K}}{|\mathbf{K}|} \frac{1}{\rho \mu_r} \nabla \hat{\Psi} \right) + \frac{\partial \rho_r}{\partial x} \right] \xi_n dR = 0 \tag{3.40}$$

Simplifying

$$\iint_R \left[\nabla \cdot \left(\frac{\mathbf{K}}{|\mathbf{K}|}\frac{1}{\rho\mu_r}\nabla\hat{\Psi}\right)\right]\xi_n dR + \iint_R \left(\frac{\partial \rho_r}{\partial x}\right)\xi_n dR = 0 \tag{3.41}$$

Using Green's theorem [equation (3.14)] with the variable substitutions

$$u = \xi_n \tag{3.42a}$$

$$\nabla w = \frac{\mathbf{K}}{|\mathbf{K}|}\frac{1}{\rho\mu_r}\nabla\hat{\Psi} \tag{3.42b}$$

results in

$$\iint_R \left(\frac{\mathbf{K}}{|\mathbf{K}|}\frac{1}{\rho\mu_r}\nabla\hat{\Psi}\cdot\nabla\xi_n\right)dR - \int_S \left(\frac{\mathbf{K}}{|\mathbf{K}|}\frac{1}{\rho\mu_r}\nabla\hat{\Psi}\cdot\mathbf{n}\xi_n\right)dS - \iint_R \left(\frac{\partial\rho_r}{\partial x}\right)\xi_n dR = 0 \tag{3.43}$$

Writing equation (3.43) as a summation over all the element subregions, and incorporating the trial function [equation (3.39)]

$$\sum_m \left[\sum_e \iint_{R^e} \left(\frac{\mathbf{K}^e}{|\mathbf{K}^e|}\frac{1}{\rho\mu_r}\nabla\xi_m^e\cdot\nabla\xi_m^e\right)dR^e\right]\Psi_m$$

$$-\sum_e \int_{S^e}\left(\frac{\mathbf{K}^e}{|\mathbf{K}^e|}\frac{1}{\rho\mu_r}\nabla\Psi\cdot\mathbf{n}\xi_m^e\right)dS^e - \sum_e \iint_{R^e}\frac{\partial\rho_r}{\partial x}\xi_n^e dR^e = 0 \tag{3.44}$$

Simplifying the notation

$$\sum_m R_{nm}\Psi_m = T_n \tag{3.45}$$

where

$$R_{nm} = \sum_e R_{nm}^e = \sum_e \iint_{R^e}\left(\frac{\mathbf{K}^e}{|\mathbf{K}^e|}\frac{1}{\rho\mu_r}\nabla\xi_m^e\cdot\nabla\xi_n^e\right)dR^e \tag{3.46a}$$

$$T_n = \sum_e \int_{S^e}\left(\frac{\mathbf{K}^e}{|\mathbf{K}^e|}\frac{1}{\rho\mu_r}\nabla\Psi\cdot\mathbf{n}\xi_n^e\right)dS^e + \sum_e \iint_{R^e}\frac{\partial\rho_r}{\partial x}\xi_n^e dR^e \tag{3.46b}$$

Matrix R_{nm} is termed the resistance matrix by Frind and Matanga (1985a), and may be integrated to give

$$R_{nm} = \sum_e \left[\frac{1}{4\Delta^e\bar{\rho}\bar{\mu}_r|\mathbf{K}^e|}\left(K_{xx}^e\beta_n\beta_m + K_{xz}^e\beta_n\gamma_m + K_{zx}^e\gamma_n\beta_m + K_{zz}^e\gamma_n\gamma_m\right)\right] \tag{3.47}$$

The array T_n, following the analysis presented by Frind and Matanga (1985a) and Garven (1989) becomes

$$T_n = \sum_e \frac{T_n^s}{2} + \sum_e \frac{\rho_{rm}\beta_m}{6} \tag{3.48}$$

where the subscript m implies summation over the three element nodes, and T_n^s represents a term arising from a specified head boundary condition, which may be written (assuming fluid density does not vary along the water table boundary) as

$$T_n^s = -\Delta h^e \tag{3.49}$$

where

$$\Delta h^e = h_{n-1} - h_n \qquad \text{for } S^e \text{ with } n-1, n \tag{3.50a}$$

$$\Delta h^e = h_n - h_{n+1} \qquad \text{for } S^e \text{ with } n, n+1 \tag{3.50b}$$

Here, n, $n-1$, and $n+1$ refer to the node being considered, the previous water table node, and the next water table node, respectively. When the prescribed heads are constant and identical along a boundary, this term vanishes.

Boundary conditions for the stream function equation are known once fluid flow (head) boundaries are prescribed. Constant head and water table boundaries correspond to stream function "flux" or specified gradient boundaries and are accounted for in the T_n array. For a no-flow boundary, the stream function is a constant, and equations for these boundary nodes can be removed from the matrices. In general, one no-flow boundary will be the region base, which is conventionally assigned a zero constant stream function value. For a constant (non-zero) flux boundary, the values of the stream function are also constant, and may be calculated from (Frind and Matanga, 1985a)

$$\Psi(z) = \Psi_0 - \int_0^z \rho q_n dz \tag{3.51}$$

where $\Psi(z)$ is the constant value at some point (z) along the boundary (assumed vertical), Ψ_0 is the value at the base of the region (generally zero), and q_n is the normal component of the specified flux.

3.2. Solute transport

The equation for the advective-dispersive transport of a conservative solute in a porous medium is given by

$$\nabla \cdot (\mathbf{D}\nabla C) - \mathbf{v} \cdot \nabla C = \frac{\partial C}{\partial t} \tag{2.64}$$

where C is the solute concentration (used here as a mass concentration), and $\mathbf{v}$ is the average linear velocity.

3.2.1. Formulation of finite element equations

The procedure for formulating the appropriate finite element equations is similar to the development outlined previously (Sections 3.1.1 through 3.1.4). Using the operator

$$L(C) = \nabla \cdot (\mathbf{D}\nabla C) - \mathbf{v} \cdot \nabla C - \frac{\partial C}{\partial t} \tag{3.52}$$

and the trial function

$$C \approx \hat{C} = \sum_{m=1}^{N} C_m \xi_m \tag{3.53}$$

the weighted residual equation may be written

$$\iint_R \left[\nabla \cdot (\mathbf{D}\nabla \hat{C}) - \mathbf{v} \cdot \nabla \hat{C} - \frac{\partial \hat{C}}{\partial t}\right] \xi_n dR = 0 \tag{3.54}$$

Simplifying and applying the appropriate Green's theorem [equation (3.14)] with the variable substitutions

$$u = \xi_n \tag{3.55a}$$

$$\nabla w = \mathbf{D}\nabla \hat{C} \tag{3.55b}$$

this becomes

$$\iint_R \mathbf{D}\nabla \hat{C} \cdot \nabla \xi_n dR - \int_S \mathbf{D}\nabla \hat{C} \cdot \mathbf{n} \xi_n dS + \iint_R \mathbf{v} \cdot \nabla \hat{C} \xi_n dR + \iint_R \frac{\partial \hat{C}}{\partial t} \xi_n dR = 0 \tag{3.56}$$

Rearranging, and writing each integral as the summation over all the individual element subregions

$$\sum_e \left(\iint_{R^e} \mathbf{D}^e \nabla \hat{C} \cdot \nabla \xi_n^e dR^e + \iint_{R^e} \mathbf{v}^e \cdot \nabla \hat{C} \xi_n^e dR^e + \iint_{R^e} \frac{\partial \hat{C}}{\partial t} \xi_n^e dR^e \right)$$

$$= \sum_e \left(\int_{S^e} \mathbf{D}^e \nabla \hat{C} \cdot \mathbf{n} \xi_n^e dS^e \right) \tag{3.57}$$

Incorporating the trial function [equation (3.53)] and replacing the right hand side of equation (3.57) with a flux term (Fick's first law)

$$\mathbf{F} = -\mathbf{D}\nabla C \tag{3.58}$$

equation (3.57) becomes

$$\sum_m \left(\sum_e \iint_{R^e} \mathbf{D}^e \nabla \xi_m^e \cdot \nabla \xi_n^e dR^e + \sum_e \iint_{R^e} \mathbf{v}^e \cdot \nabla \xi_m^e \cdot \xi_n^e dR^e \right) C_m$$

$$+ \sum_m \left(\sum_e \iint_{R^e} \xi_m^e \xi_n^e dR^e \right) \frac{dC_m}{dt} = - \sum_e \left(\int_{S^e} \mathbf{F}^e \cdot \mathbf{n} \xi_n^e dS^e \right) \tag{3.59}$$

As before, the summation over m is over all the nodes and the summation over e is over all the elements. Simplifying the notation, equation (3.59) becomes

$$\sum_m E_{nm} C_m + \sum_m F_{nm} \frac{dC_m}{dt} = -G_n \tag{3.60}$$

where

$$E_{nm} = \sum_e E_{nm}^e = \sum_e \left(\iint_{R^e} \mathbf{D}^e \nabla \xi_m^e \cdot \nabla \xi_n^e dR^e + \iint_{R^e} \mathbf{v}^e \cdot \nabla \xi_m^e \cdot \xi_n^e dR^e \right) \tag{3.61a}$$

$$F_{nm} = \sum_e F_{nm}^e = \sum_e \left(\iint_{R^e} \xi_m^e \xi_n^e dR^e \right) \tag{3.61b}$$

$$G_n = \sum_e \left(\int_{S^e} \mathbf{F}^e \cdot \mathbf{n} \xi_n^e dS^e \right) \tag{3.61c}$$

3.2.2. Evaluating the integrals

In order to evaluate the integrals given in equations (3.61), the shape functions described previously are used. The expression for matrix E_{nm} (3.61a) may be integrated

$$E_{nm} = \sum_e E_{nm}^e = \sum_e \frac{1}{4\Delta^e} (D_{xx}^e \beta_n \beta_m + D_{xz}^e \beta_n \gamma_m + D_{zx}^e \gamma_n \beta_m + D_{zz}^e \gamma_n \gamma_m)$$

$$+ \sum_e \frac{1}{6} (v_x^e \beta_m + v_z^e \gamma_m) \tag{3.62}$$

In equation (3.62), the components of the dispersion tensor in cartesian coordinates are derived from the longitudinal and transverse dispersion coefficients using the relations given in equation (2.68). The next integral [equation (3.61b)] is easily evaluated

$$F_{nm} = \sum_e \begin{cases} \Delta^e/6 & \text{for } n = m \\ \Delta^e/12 & \text{for } n \neq m \end{cases} \tag{3.63}$$

The final integral [equation (3.61c)] is evaluated as follows

$$G_n = -\sum_e \left(\frac{c_n l^e}{2}\right) \tag{3.64}$$

In equation (3.64), the variable c_n is used to represent the specified solute flux at node n and l^e is the length of the element boundary. In general, the solute flux will be specified by assuming a constant concentration at an inflow boundary, so this term will not be used.

3.2.3. Determination of average linear velocities

Before the solute transport equations may be solved, average linear velocities for the flow region must be calculated. These may be determined from either the hydraulic gradient or the calculated stream function values. Substitution of the trial function for heads [equation (3.11)] into Darcy's law [equation (2.14)] leads to the following components of the specific discharge

$$q_x^e = -\sum_{i=1}^{3} \left(K_{xx}^e \bar{\mu}_r \frac{\beta_i}{2\Delta^e} + K_{xz}^e \bar{\mu}_r \frac{\gamma_i}{2\Delta^e}\right) h_i - K_{xz}^e \bar{\mu}_r \bar{\rho}_r \tag{3.65a}$$

$$q_z^e = -\sum_{i=1}^{3} \left(K_{zx}^e \bar{\mu}_r \frac{\beta_i}{2\Delta^e} + K_{zz}^e \bar{\mu}_r \frac{\gamma_i}{2\Delta^e}\right) h_i - K_{zz}^e \bar{\mu}_r \bar{\rho}_r \tag{3.65b}$$

As may be seen, the specific discharge is determined for each element by summing over the three nodes in the element. Average linear velocities are determined by dividing the specific discharge by the element porosity.

Note that we have not consistently discretized ∇h and ρ_r, which may result in spurious velocities for strongly density-dependent groundwater flow. It is possible to consistently discretize these two terms such that the approximations have consistent spatial dependencies (Voss, 1984). However, it is more convenient to use the stream function formulation of the governing groundwater flow equation in these cases (Evans and Raffensperger, 1992), in which case the consistency problem is avoided.

Stream function values may also be used to determine average linear velocities (Frind and Matanga, 1985a). Substitution of the trial stream function [equation (3.39)] into equation (2.36) yields

$$\bar{\rho} q_x^e = -\sum_{i=1}^{3} \left(\frac{\gamma_i}{2\Delta^e}\right) \Psi_i \tag{3.66a}$$

$$\bar{\rho} q_z^e = \sum_{i=1}^{3} \left(\frac{\beta_i}{2\Delta^e}\right) \Psi_i \tag{3.66b}$$

3.2.4. Transient equations

The general expression for solute transport, in matrix form, is given by equation (3.60). Discretization or time-stepping is performed using a weighted finite difference scheme which takes the form (again using matrix notation)

$$\left(\theta[E] + \frac{1}{\Delta t}[F]\right)\{C\}^{k+1} = \left[(\theta - 1)[E] + \frac{1}{\Delta t}[F]\right]\{C\}^{k} - \{G\} \tag{3.67}$$

where θ is the weight for which specific cases are given in equations (3.31). The fully explicit method ($\theta = 0$) is known to be conditionally stable (Segerlind, 1984). Solutions using $\theta = \frac{1}{2}$ or $\theta = \frac{2}{3}$ are unconditionally stable, but may contain numerical oscillations when the time step size is too large. The fully implicit method is unconditionally stable, and the calculated values do not oscillate about the correct values. The fully implicit method is therefore favored, although it does become less accurate for large values of time (Segerlind, 1984).

The matrices in equation (3.67) are given in equations (3.62) through (3.64). For boundary nodes with specified constant solute concentration, C_m are known and equations for these nodes may be removed from the matrices. In general, solute fluxes are not specified. Instead, concentrations are specified to be constant at an inflow boundary node. Impervious boundaries are handled by setting c_n to zero in equation (3.64).

3.2.5. On the numerical solution of the advection-dispersion equation

The numerical solution of the advection-dispersion equation may be hampered by numerical dispersion and/or spatial oscillations near the concentration front (Pinder and Gray, 1977, p. 159–160; Huyakorn and Pinder, 1983, p. 206–207). These problems are particularly severe when transport is advection-dominant.

Several means exist of minimizing these numerical inaccuracies. Numerical techniques, such as upstream weighting (Huyakorn and Pinder, 1983), may be used, but may introduce numerical dispersion while reducing oscillation. Careful gridding and choice of time step size (when computational costs are not a problem), as well as the choice of weights used in time stepping, may also help avoid numerical problems.

Theoretical investigation and actual testing have shown that numerical inaccuracies may be greatly reduced if the grid Peclet number (Pe*) does not exceed 2. The grid Peclet number [cf. equation (2.90)] is defined as

$$\text{Pe}^* = \frac{v\Delta L}{D} \tag{3.68}$$

where ΔL is a characteristic element length, which may be taken as $\max(\Delta x, \Delta z)$. Since hydrodynamic dispersion is in most cases much greater than diffusion, equation (3.68) becomes

$$\text{Pe}^* = \frac{\Delta L}{\alpha} \tag{3.69}$$

Therefore, the grid size is restricted by the following relationship

$$\Delta L \leqslant 2\alpha \tag{3.70}$$

Also, the time step size should be selected so that the local Courant number, defined as

$$Cr = \frac{v\Delta t}{\Delta l} \tag{3.71}$$

is less than or equal to 1 (Noorishad et al., 1992). In practice, this number should be smaller than $\frac{1}{3}$ (Marsily, 1986). To obtain a solution that is second-order accurate in time, Crank-Nicolson time stepping ($\theta = \frac{1}{2}$) may be used (Huyakorn and Pinder, 1983).

Segerlind (1984) notes several other practical considerations for the finite element solution of transient equations when using linear triangular elements. Triangular elements should not have any interior angles greater than 90°. Due to the fact that the length dimension is always in the numerator of the time step calculation [equation (3.63)], one way of increasing the time step size is to increase the size of the element [equation (3.71)]. Therefore, Segerlind (1984) suggests that one make the elements as large as is reasonably possible.

3.2.6. Finite element equations for reactive solute transport

A general mathematical statement for the transport of a reactive solute by advection and dispersion due to steady flow in porous media may be written [referring to equation (2.75)]

$$\nabla \cdot (\phi \mathbf{D} \nabla c_i) - \phi \mathbf{v} \cdot \nabla c_i = \frac{\partial \phi c_i}{\partial t} - \phi R_i \qquad i = 1, 2, \ldots, I \tag{3.72}$$

where **D** is the dispersion tensor (which includes the effects of both mechanical dispersion and diffusion), c_i is the concentration of species i, **v** is the average linear velocity, and R_i is the rate of addition of species i to the fluid by all reactions. R_i is negative if species i is removed from the fluid by adsorption or precipitation of solids. Solution of the set of partial differential equations (3.72) requires knowledge of the flow field and the rate of addition to the fluid phase of each chemical species. If local equilibrium is assumed (Rubin, 1983), these rates are constrained by appropriate mass action expressions. Otherwise, kinetic rate expressions must be used. In either case, the set of transport relations is nonlinear.

Several approaches to solving the reactive mass transport equations have been taken (Table 1), although traditional finite element and finite difference methods are the most common. Analytical solutions have been developed (Lund and Fogler, 1976; Cameron and Klute, 1977; Baumgartner and Ferry, 1991), but are greatly limited in terms of the physical processes represented and the complexity of the chemical system. For instance, one-dimensional flow is commonly assumed, and solute dispersion or diffusion are ignored. Typically, these solutions have been applied to simple binary ion exchange, although Palciauskas and Domenico (1976) derive simple analytical expressions which incorporate dissolution of calcium carbonate. Phillips (1990) also derives some simplified relations, based in part on scaling theory, which are useful in describing the general nature of different types of flow-controlled reactions. Despite the approximations and simplifications entailed by these studies, analytical solutions provide a benchmark for verifying numerical models and for analyzing some of the important effects of coupled flow and chemical reactions.

TABLE 1

Summary of features of selected hydrochemical models

Study (Year)	Methods	Dimensions	Application
Rubin & James (1973)	FD/dir/(C-T)	1	Ion exchange
Schwartz & Domenico (1973)	FD/dir/(C-T)	2	Watershed hydrochemistry
Palciauskas & Domenico (1976)	ANL/dir/(C-T)	1	Dissolution of carbonates
Schulz & Reardon (1983)	ANL/MC/seq/(C-T)	2	Ion exchange
Miller & Benson (1983)	FD/dir/(C-T)	1	Contaminant transport
Nguyen et al. (1983)	COL/dir/(C-T)	1	Uranium in situ mining
Walsh et al. (1984)	FD/seq/(C-T)	1	Uranium roll front ores
White et al. (1984)	IFD/seq/(C-F)	3	
Verma & Pruess (1985, 1987, 1988)	IFD/dir/(C-F)	2	Silica redistribution
Noorishad et al. (1985)	FD/dir/(C-T)	1	Carbonate dissolution
Lichtner (1985, 1986, 1988, 1992)	FD/dir/(C-T)	1	Weathering, supergene Cu ores
Hewett (1986)	ANL/dir/(C-T)	2	Diagenesis
Bryant et al. (1986, 1987)	FD/seq/(C-T)	1	Alkaline flooding
Carnahan (1987, 1990)	FD/dir/(C-T-H)	1	Uraninite dissolution
Ortoleva et al. (1987)	FD/dir/(C-F)	1	Various
Mundell & Kirkner (1988)	FE/dir/(C-F)	1	Quartz dissolution
Sanford & Konikow (1989a, 1989b)	FD/MOC/seq/(C-F)	2	Carbonate dissolution
Liu & Narasimhan (1989a, 1989b)	IFD/seq/(C-F)	2–3	Supergene Cu enrichment
Ague & Brimhall (1989)	IFD/seq/(C-T)	1–3	Supergene Cu enrichment
Jamet et al. (1989)	FE/seq/(C-T)	2	Uranium deposition
Phillips (1990, 1991)	ANL/dir/(C-T)	1	Flow-controlled reactions
Steefel & Lasaga (1990, 1992, 1994)	FD/dir/(C-F-H)	1–2	Hydrothermal systems
Yeh & Tripathi (1991)	FE/dir or seq/(C-T)	2	Various
Engesgaard & Kipp (1992)	FD/seq/(C-T)	1	Pyrite oxidation
Raffensperger (1993)	FE/seq/C-F-H	2	Sedimentary ore formation
Lee & Bethke (1994)	FD/seq/C-F-H	2	Diagenesis

KEY: FD – Finite difference; FE – Finite element; IFD – Integrated finite difference; ANL – Analytical; MC – Mixing cell; MOC – Method of characteristics; dir – Direct; seq – Sequential; C-T – chemistry-solute transport; C-F – chemistry-fluid flow; C-T-H – chemistry-solute transport-heat transport; C-F-H – chemistry-fluid flow-heat transport.

Methods for solving the coupled transport and chemical relations fall into two main categories: direct substitution and sequential iteration. Direct methods incorporate chemical equilibrium expressions or rate expressions directly in the transport equations, thereby solving both sets of equations simultaneously. The earliest modeling efforts generally used direct coupling methods, but again with limitations imposed by simple chemical and/or flow systems. Many of these studies have examined ion exchange, following pioneering work by Rubin and James (1973). The CHEMTRN code (Miller and Benson, 1983) solves both sets of

equations simultaneously (Lichtner, 1985), and has undergone several revisions (Noorishad et al., 1985; Carnahan, 1987).

Lichtner (1985) used the finite difference method to solve the set of general one-dimensional transport equations

$$\frac{\partial \phi c_i}{\partial t} + \frac{\partial(\phi v c_i - \phi D \nabla c_i)}{\partial x} = \sum_{r=1}^{M} \nu_{ir} \frac{\partial \Xi_r}{\partial t} \qquad i = 1, 2, \ldots, N \tag{3.73}$$

where N is the number of reacting aqueous species, M is the number of reacting minerals, v is the average linear velocity, ν_{ir} is the set of stoichiometric reaction coefficients, and Ξ_r is the reaction progress density for a mineral reaction, expressed in units of moles per unit volume of bulk porous medium (reaction progress, ξ_r, is defined as having units of moles). Both reversible and irreversible reactions were accounted for by a set of nonlinear algebraic equations which were solved simultaneously with the transport equations.

Lichtner (1988) described the application of the quasi-stationary state approximation to mass transport and fluid-rock interaction which allows coupled transport and reactive processes to be integrated over geologically significant time spans. The approximation essentially neglects the first derivative on the left side of equation (3.73), i.e., $\partial(\phi c_i)/\partial t = 0$. In this case, assuming the dispersion coefficient and porosity are constant, the one-dimensional transport equations take the form

$$\phi D \frac{d^2 c_i}{dx^2} - \phi v \frac{dc_i}{dx} = -\sum_{r=1}^{M} \nu_{ir} \frac{\partial \Xi_r}{\partial t} \qquad i = 1, 2, \ldots, N \tag{3.74}$$

These equations are solved for the case of pure advective transport ("multiple reaction path formulation") using the finite difference method and an adaptive grid (Lichtner, 1988, 1992).

Steefel and Lasaga (1994) describe a one-step or *global implicit* method for simultaneously solving the transport and chemical reaction equations, which uses a kinetic description of the reactions. The partial differential equations incorporating the reaction rate laws directly [see equation (2.86)] are discretized using an integrated finite difference formulation. The resulting system of equations is solved at each time step using Newton-Raphson iteration (see Section 3.3.5). Within a time step, successive over-relaxation is used to solve the matrix expressions. Steefel and Lasaga (1994) cite the following advantages of one-step methods over sequential methods: (a) the global convergence properties of the one-step method may be better than the two-step (sequential) methods, and (b) it may be possible to take larger time steps with the one-step method, especially when the governing equations are particularly *stiff* (i.e., characterized by orders of magnitude variation of parameters), which may be the case when both very slow and very fast reactions are considered. The successful application of this method to complicated multicomponent problems refutes previous arguments that sequential methods are necessary for any problems involving more than a few chemical components (Yeh and Tripathi, 1989).

Sequential solution methods have been the most commonly employed, for several reasons. Ease of programming is perhaps the most frequently noted advantage, since several chemical speciation codes are available which may be readily adapted for coupling with transport codes. Potentially large computer storage requirements for direct coupling methods involving more than a few chemical components was seen as a limitation that could be overcome using sequential methods (Yeh and Tripathi, 1989). In this approach, the mass transport and reaction equations are solved separately and sequentially; iteration may be required to treat the nonlinearities. Examples which make use of the sequential approach are provided by Walsh et al. (1984), Cederberg et al. (1985), and Yeh and Tripathi (1991). Often these codes will incorporate external chemical speciation codes, such as MINEQL (Kirkner et al., 1985), or reaction path codes, such as PHREEQE (Sanford and Konikow, 1989b) and EQ3/EQ6 (Ague and Brimhall, 1989). The difficulty in this approach is that these chemical submodels usually require large amounts of computer time, which may make them impractical for geologic-scale simulations.

Walsh et al. (1984) developed mass balance equations for individual chemical elements

$$\frac{\partial \phi C_i^T}{\partial t} + \phi \mathbf{v} \frac{\partial}{\partial x}\left(\sum^{J} \nu_{ij} C_j\right) - \frac{\partial^2}{\partial x^2}\left(\sum^{J} \phi \mathbf{D} C_j\right) = 0 \qquad i = 1, 2, \ldots, I \tag{3.75}$$

where I is the number of elements, J is the number of species, ν_{ij} is the stoichiometric number of elements i in species j, C_i^T is the total concentration of element i, and C_j is the concentration of aqueous species j. Since the total elemental concentrations are reaction-invariant, no source/sink term due to chemical reactions is required. Speciation was determined by a set of charge, electron, and element balances (local equilibrium was assumed), which were solved separately. The transport equations were solved using the finite difference method.

The governing equation for reactive solute transport was derived in Section (2.2.3), and may be written as

$$\nabla \cdot (\phi \mathbf{D} \nabla M_{c,\mathrm{aq}}^T) - \phi \mathbf{v} \cdot \nabla M_{c,\mathrm{aq}}^T = \frac{\partial \phi M_c^T}{\partial t} \tag{2.78}$$

The finite element approximation for this equation is similar to that for conservative solute transport (see Sections 3.2.1 through 3.2.4)

$$\sum_m E_{nm} (M_{c,\mathrm{aq}}^T)_m + \sum_m F_{nm} \frac{d(M_c^T)_m}{dt} = -G_n \tag{3.76}$$

where

$$E_{nm} = \sum_e E_{nm}^e = \sum_e \frac{\phi^e}{4\Delta^e} (D_{xx}^e \beta_n \beta_m + D_{xz}^e \beta_n \gamma_m + D_{zx}^e \gamma_n \beta_m + D_{zz}^e \gamma_n \gamma_m) \tag{3.77}$$

$$+ \sum_e \frac{\phi^e}{6} (v_x^e \beta_m + v_z^e \gamma_m)$$

$$F_{nm} = \sum_e \phi^e \begin{cases} \Delta^e/6 & \text{for } n = m \\ \Delta^e/12 & \text{for } n \neq m \end{cases} \tag{3.78}$$

$$G_n = -\sum_e \left[\frac{\phi^e (M^T_{c,\text{aq}})_n I^e}{2} \right] \tag{3.79}$$

Note that the porosity term is now found in the coefficient matrices and that the concentrations are now expressed in units of moles/liter or molarity. This assumes that porosity is a constant within an element. The next step is to determine a method for approximating the time derivative in equation (3.76). Four alternative methods will be reviewed.

The simplest scheme uses a backward or fully explicit finite difference approximation

$$[E]\{M^T_{c,\text{aq}}\}^k + [F]\frac{\{M^T_c\}^{k+1} - \{M^T_c\}^k}{\Delta t} = -\{G\} \tag{3.80}$$

This scheme has been used by Walsh (1983), but requires the use of very small time steps due to its conditional stability. However, this method is the simplest to program, and does not require iteration within a time step.

Due to the conditional stability of the fully explicit scheme [equation (3.80)], a more common approach uses a forward difference or implicit formulation of the time derivative, with iteration within a time step. Procedures of this type are referred to as the sequential iteration approach, or SIA (Yeh and Tripathi, 1989). The simplest example of an implicit scheme is

$$[E]\{M^T_{c,\text{aq}}\}^{k+1} + [F]\frac{\{M^T_c\}^{k+1} - \{M^T_c\}^k}{\Delta t} = -\{G\} \tag{3.81}$$

A scheme similar to this is used by Cederberg (1985). Obviously, iteration within a time step is required to update values of $\{M^T_{c,\text{aq}}\}^{k+1}$.

As pointed out by Yeh and Tripathi (1991), the implicit formulation above is prone to negative total analytical concentrations if $[E]\{M^T_{c,\text{aq}}\}^{k+1}$ is positive. They suggest therefore a rearrangement which takes the following form

$$\left([E] + \frac{[F]}{\Delta t}\right)\{M^T_c\}^{k+1} = [E]\{M^T_{c,\text{sol}}\}^{k+1} + \frac{[F]}{\Delta t}\{M^T_c\}^k - \{G\} \tag{3.82}$$

In this case, iteration within a time step is used to update values of $\{M^T_{c,\text{sol}}\}^{k+1}$. Yeh and Tripathi (1991) refer to this as the "implicit" scheme. This scheme is very accurate, and is not prone to negative total concentration values, but may require many iterations within a time step. Since time-consuming chemical speciation at each node must be recalculated at each iteration, this scheme may require excessive amounts of computer time for geologic-scale problems.

A predictor-corrector scheme was suggested by Raffensperger (1993) which allows large-scale calculations to be carried out with speed comparable to the non-iterative, but conditionally stable, explicit scheme, and which is unconditionally stable. Compared with explicit or implicit methods, the predictor-corrector scheme

offers several advantages for the numerical solution of nonlinear differential equations (Douglas and Jones, 1963). The predictor-corrector solution is second-order accurate, whereas explicit solutions are only first-order accurate. Therefore, a significant increase in accuracy can be obtained at the expense of doubling the computational effort at each time step. Since the explicit scheme is conditionally stable, relatively small time steps are required; the predictor-corrector scheme, on the other hand, can be shown to be unconditionally stable. Therefore, since this implies a significant reduction in the number of time steps required to maintain a prescribed accuracy, the use of the predictor-corrector scheme can dramatically reduce the computational effort. Implicit solutions are also second-order accurate, but require iteration within a time step (Yeh and Tripathi, 1989, 1991). Oran and Boris (1987) discuss the application of predictor-corrector methods to the solution of nonlinear transient ordinary differential equations encountered in reactive fluid flow problems.

Following the suggestion of Yeh and Tripathi (1991), equation (3.76) may be written as

$$\sum_m E_{nm}(M_c^T)_m + \sum_m F_{nm}\frac{d(M_c^T)_m}{dt} = \sum_m E_{nm}(M_{c,\mathrm{sol}}^T)_m - G_n \tag{3.83}$$

The predictor-corrector algorithm consists of two steps. In the first step, an implicit scheme is used to solve for $\{M_c^T\}$ at the $k+\frac{1}{2}$ time step, using values of $\{M_{c,\mathrm{sol}}^T\}$ from the previous pair of time steps. This is analogous to assuming $d(M_{c,\mathrm{sol}}^T)_m/dt = \text{constant}$. The matrix expression for the predictor step may be written

$$\left([E] + \frac{[F]}{\Delta t/2}\right)\{M_c^T\}^{k+1/2} - [E]\{M_{c,\mathrm{sol}}^T\}^{k+1/2} = \frac{[F]}{\Delta t/2}\{M_c^T\}^k - \{G\} \tag{3.84}$$

where

$$\{M_{c,\mathrm{sol}}^T\}^{k+1/2} = \{M_{c,\mathrm{sol}}^T\}^k + \frac{1}{2}(\{M_{c,\mathrm{sol}}^T\}^k - \{M_{c,\mathrm{sol}}^T\}^{k-1}) \tag{3.85}$$

This expression [equation (3.84)] is solved, after imposing constant concentration (M_c^T) boundary conditions. The chemical speciation is then recalculated to obtain *updated* values of $M_{c,\mathrm{sol}}^T$ at the $k+\frac{1}{2}$ time step. The corrector step consists of a time-centered (Crank-Nicolson) scheme which uses a linear extrapolation of the change in solid concentration from time step k to time step $k+\frac{1}{2}$ to obtain an estimate of $\{M_{c,\mathrm{sol}}^T\}$ at the $k+1$ time step

$$\left(\frac{[E]}{2} + \frac{[F]}{\Delta t}\right)\{M_c^T\}^{k+1} = \left(-\frac{[E]}{2} + \frac{[F]}{\Delta t}\right)\{M_c^T\}^k + \frac{[E]}{2}[2\{M_{c,\mathrm{sol}}^T\}^{k+1/2}] - \{G\} \tag{3.86}$$

After imposing the boundary conditions, this equation is solved for $\{M_c^T\}$ at the new time step $(k+1)$. The extrapolation scheme assumes the following

$$\{M_{c,\mathrm{sol}}^T\}^{k+1} - \{M_{c,\mathrm{sol}}^T\}^{k+1/2} = \{M_{c,\mathrm{sol}}^T\}^{k+1/2} - \{M_{c,\mathrm{sol}}^T\}^k \tag{3.87}$$

In other words, the rate of precipitation or dissolution is approximately constant over a time step. If no precipitation or dissolution occurs, the approximation is trivially satisfied.

3.2.7. Numerical algorithm

The algorithm for the solution of the coupled equations of groundwater flow, heat transport and reactive multicomponent solute transport (using the predictor-corrector solution scheme described in Section 3.2.6) consists of a time-stepping loop (Fig. 22) in which the groundwater flow equation and heat transport equation are first solved, followed by the reactive transport equations. The flow and heat transport equations may be solved for either a transient or a steady-state case. For variable-density flow, iteration between the flow and heat transport solutions may be used to resolve the nonlinear coupled equations. Once the flow equation has been solved, average linear velocities for each finite element may be determined using either hydraulic head or stream function values. These are required for transport (heat and solute) calculations.

Initially and within each time step, chemical speciation would calculated by calling a geochemical subroutine for each node in the finite element grid. In the case of a local equilibrium approach, the subroutine solves the nonlinear algebraic mass balance and mass action equations describing heterogeneous chemical equilibrium as a function of temperature. For a kinetically-described approach, the initial conditions would be input, although most of these approaches assume homogeneous equilibrium, which may require intial speciation. Within the time-stepping loop, solution of the groundwater flow and heat transport equations is followed by the predictor step in which the set of transport equations is solved for each component sequentially. After calculating the speciation at the midpoint of the time step, the corrector scheme is used to solve for the concentration of all components at the end of the time step, and the speciation is recalculated. For chemical-feedback simulations, the porosities and permeabilities are updated by quadrilateral (pair of triangular elements) at the end of the time step.

3.3. Chemical equilibrium

If local chemical equilibrium is assumed, then the distribution of all aqueous species as well as the volume fractions of all solids and the porosity must calculated by a chemical submodel (Fig. 23). The fundamental procedures for constructing and solving the set of nonlinear algebraic mass balance and mass action equations are reviewed in this section, much of which is described by Morel and Morgan (1972), Wolery (1978), Reed (1982), and Walsh (1983).

3.3.1. Equilibrium without solids

We may define our chemical system as consisting of $\hat{c}$ chemical components or component species, $\hat{s}$ secondary aqueous species, and $\hat{m}$ saturated minerals. Since the components are actually aqueous species, they may be considered a special subset of the total aqueous species, $\hat{c} + \hat{s}$. Initially, we will consider only homogeneous equilibrium between the aqueous species. We will also begin by assuming

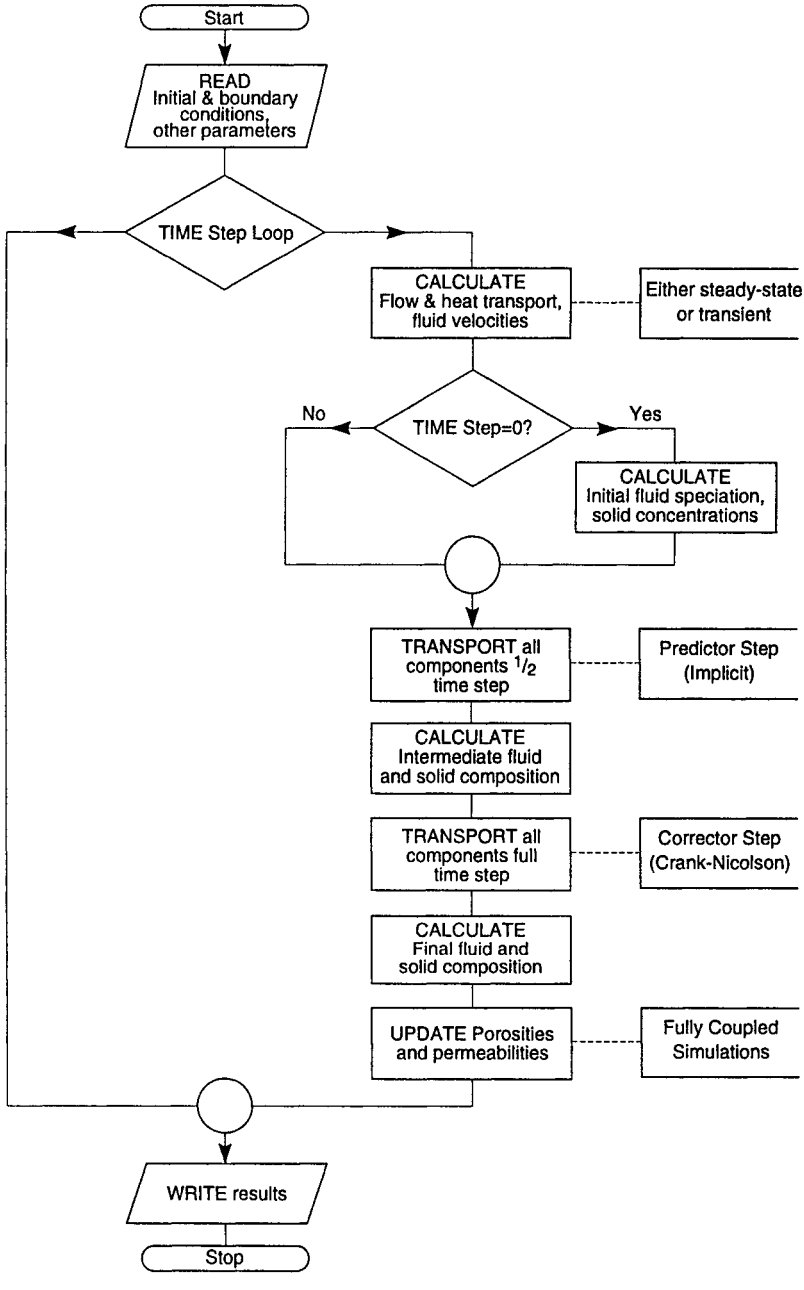


Fig. 22. Flowchart outlining the basic procedure for solving the coupled equations describing hydrochemical processes in sedimentary basins. Chemical speciation is determined within a time step using a separate subroutine. Alternatively, direct solution procedures would solve the transport and chemical equations simultaneously.

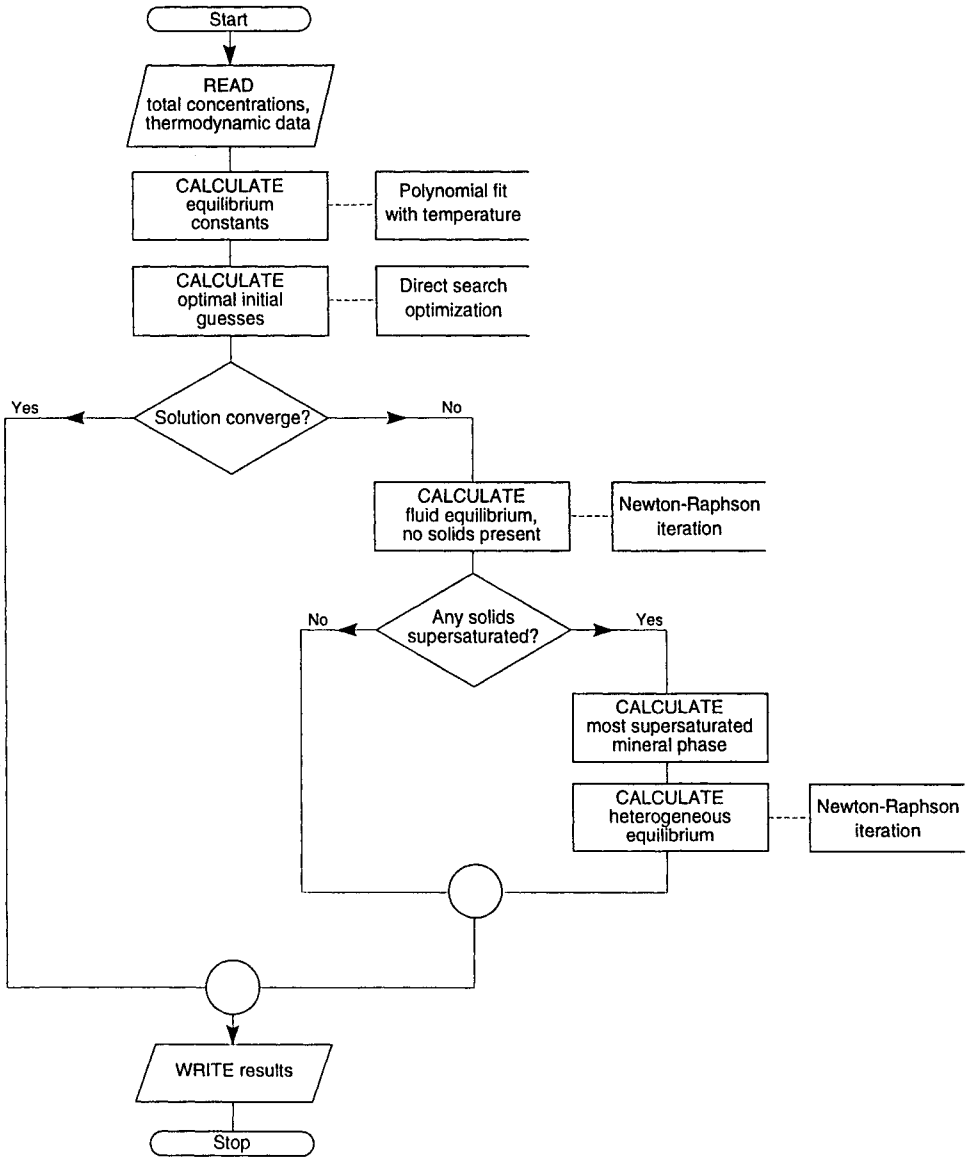


Fig. 23. Flowchart for a typical equilibrium geochemical submodel used to determine heterogeneous speciation at every point in the spatial grid.

an ideal solution, such that activity coefficients (γ) are all equal to 1. Concentrations will be expressed as molarity (M) or moles/liter. Molarity-molality conversions are ignored. With these assumptions, mass conservation and chemical equilibrium are described by the following set of equations

$$Y_j = M_j + \sum_{i=1+\hat{c}}^{\hat{c}+\hat{s}} \tau_{ji} M_i - M_j^T \qquad j = 1, \ldots, \hat{c} \tag{3.88}$$

$$M_i = \frac{\prod_{j=1}^{\hat{c}} M_j^{\nu_{ji}}}{K_i} \qquad i = 1, \ldots, \hat{c} + \hat{s} \tag{3.89}$$

for which the solution is the set of M_j ($j = 1, \ldots, \hat{c}$) such that $Y_j = 0$ given K_i, M_j^T, τ_{ji}, and ν_{ji}. In equations (3.88) and (3.89), Y_j represents the set of residuals or differences between the specified total concentration (M_j^T) and the calculated concentrations of aqueous species. The coefficient τ_{ji} is a composition coefficient representing the number of moles of component j in one mole of species i. The coefficient ν_{ji} is the stoichiometric reaction coefficient for aqueous species i. To simplify calculations, all reactions will be written for one mole of the dissociating or dissolving species, in which case, $\nu_{ji} = \tau_{ji}$.

The first step in solving the equations (3.88) and (3.87) will be to transform our variables (Walsh, 1983)

$$X_j = \log M_j \qquad j = 1, \ldots, \hat{c} \tag{3.90a}$$

$$10^{X_j} = M_j \qquad j = 1, \ldots, \hat{c} \tag{3.90b}$$

This transformation overcomes the problem of large corrections during Newton-Raphson iteration producing negative concentrations (van Zeggeren and Storey, 1970).

Implementation of the Newton-Raphson iteration scheme for solving nonlinear equations requires calculation of the elements of the Jacobian (derivative) matrix

$$\begin{bmatrix} \frac{\partial Y_1}{\partial X_1} & \cdots & \frac{\partial Y_1}{\partial X_{\hat{c}}} \\ \vdots & & \vdots \\ \frac{\partial Y_{\hat{c}}}{\partial X_1} & \cdots & \frac{\partial Y_{\hat{c}}}{\partial X_{\hat{c}}} \end{bmatrix}$$

The elements in the Jacobian matrix can be described by

$$J_{ij} = \frac{\partial Y_i}{\partial X_j} \qquad i, j = 1, \ldots, \hat{c} \tag{3.91}$$

because X_j is only a function of M_j [equation (3.90)], we can apply the Chain Rule and write

$$J_{ij} = \frac{\partial Y_i}{\partial M_j} \frac{\partial M_j}{\partial X_j} \qquad i, j = 1, \ldots, \hat{c} \tag{3.92}$$

where, from equation (3.90b)

$$\frac{\partial M_j}{\partial X_j} = M_j \ln 10 = 2.303 M_j \tag{3.93}$$

Because Y_i is a function of M_k ($k = 1, \ldots, \hat{c} + \hat{s}$), we can write

$$\frac{\partial Y_i}{\partial M_j} = \sum_{k=1}^{\hat{c}+\hat{s}} \frac{\partial Y_i}{\partial M_k} \frac{\partial M_k}{\partial M_j} \qquad i, j = 1, \ldots, \hat{c} \tag{3.94}$$

We may evaluate the first derivative in the summation by reference to equation (3.88)

$$\frac{\partial Y_i}{\partial M_k} = \tau_{ik} \qquad i = 1, \ldots, \hat{c} \qquad k = 1, \ldots, \hat{c} + \hat{s} \tag{3.95}$$

For $k = 1, \ldots, \hat{c}$, $\tau_{ik} = 1.0$ when $i = j = k$ and $\tau_{ij} = 0.0$ otherwise. Similarly, the second derivative can be determined from equation (3.89), which gives

$$\frac{\partial M_k}{\partial M_j} = \frac{\nu_{jk}}{K_j M_j} \prod_{i=1}^{\hat{c}} M_i^{\nu_{ik}} \qquad j = 1, \ldots, \hat{c} \qquad k = 1, \ldots, \hat{c} + \hat{s} \tag{3.96}$$

For the component species ($k = 1, \ldots, \hat{c}$) this reduces to

$$\frac{\partial M_k}{\partial M_j} = 1.0 \qquad j, k = 1, \ldots, \hat{c} \tag{3.97}$$

Equation (3.96) may be simplified for the secondary species as well ($k = \hat{c} + 1, \ldots, \hat{c} + \hat{s}$) by substituting equation (3.89)

$$\frac{\partial M_k}{\partial M_j} = \frac{\nu_{jk} M_k}{M_j} \qquad j = 1, \ldots, \hat{c} \qquad k = \hat{c} + 1, \ldots, \hat{c} + \hat{s} \tag{3.98}$$

Finally, substituting equations (3.97), (3.98), (3.95), (3.94), and (3.93) into equation (3.92) yields

$$J_{ij} = 2.303\left(\sum_{k=1}^{\hat{c}} \tau_{ik} M_k + \sum_{l=\hat{c}+1}^{\hat{c}+\hat{s}} \nu_{jl} \tau_{il} M_l\right) \qquad i, j = 1, \ldots, \hat{c} \tag{3.99}$$

For a given set of M_j ($j = 1, \ldots, \hat{c}$), equation (3.89) can be used to compute M_l ($l = \hat{c} + 1, \ldots, \hat{c} + \hat{s}$) and these values can be used in equation (3.99) to determine J_{ij} ($i, j = 1, \ldots, \hat{c}$).

3.3.2. Equilibrium with solids

The problem of determining the correct equilibrium mineral assemblage is a significant one, and great care must be taken when adding or removing phases to or from this assemblage. In the computational procedure (Fig. 23), minerals are added to the assemblage one by one, according to their degree of saturation. In

order to determine the degree of saturation, reaction (dissolution) affinities are calculated for each possible mineral by the relation (Wolery, 1978)

$$A = RT \ln \frac{Q}{K^{sp}} \tag{3.100}$$

where T is the temperature (°K), R is the gas constant (1.98719 cal/mol °K), K^{sp} is the equilibrium constant for the dissolution reaction, or solubility product, and Q is the activity quotient. If the mineral is in equilibrium with the fluid, its affinity will be zero. If the mineral is undersaturated, Q will be less than K^{sp}, and the affinity will be less than zero. Units of affinity are calories.

The most supersaturated mineral should be the one with the highest affinity. However, affinities are dependent on molecular formulas (and reaction coefficients), and therefore choosing a new phase on the basis of chemical affinity has a built-in bias in favor of minerals with large molecular formulas (Wolery, 1978). The affinities may be scaled by dividing by a factor τ_i', defined by

$$\tau_i' = \sum_{j=1}^{\hat{c}} \tau_{ij} \qquad i = 1, \ldots, \hat{m} \tag{3.101}$$

Then, the mineral with the highest scaled affinity is added to the assemblage. This scaling factor procedure is similar to that suggested by Wolery (1978) who used the sum of the absolute values of the stoichiometric coefficients. Trial and error testing of various procedures showed the scaling factor scheme above [equation (3.101)] to be efficient and reliable (Raffensperger, 1993).

A second difficulty which may arise when seeking the equilibrium mineral assemblage involves possible Gibbs phase rule violations. Phase rule violations may be real, i.e., the number of phases equals the number of components, excluding H_2O, which is both a phase and a component in the system, or apparent, i.e., involving the possible addition of a phase which is some linear combination of mineral phases already included in the assemblage (Wolery, 1979). Both of these cases may be checked for, and if found, corrected. This may be accomplished by removing a previously chosen solid on the basis of its similarity to the most recently added phase.

The problem of equilibrium in an ideal system containing $\hat{m}$ solids, $\hat{c}$ component species, and $\hat{s}$ secondary aqueous species can be described by appropriate mass balance and mass action equations

$$Y_j = M_j + \sum_{i=1+\hat{c}}^{\hat{c}+\hat{s}} \tau_{ji} M_i + \sum_{k=1}^{\hat{m}} \eta_{jk} M_k - M_j^T \qquad j = 1, \ldots, \hat{c} \tag{3.102}$$

$$F_k = \prod_{j=1}^{\hat{c}} M_j^{\upsilon_{jk}} - K_k^{sp} \qquad k = 1, \ldots, \hat{m} \tag{3.103}$$

subject to equation (3.101) for which the solution is the set of M_j ($j = 1, \ldots, \hat{c}$) and M_k ($k = 1, \ldots, \hat{m}$) such that Y_j ($j = 1, \ldots, \hat{c}$) = 0 and F_k ($k = 1, \ldots, \hat{m}$) = 0 given τ_{ji}, η_{jk}, M_j^T, K_k^{sp}, K_i, ν_{ji}, and ν_{kj} ($i = 1, \ldots, \hat{c}$; $j = 1, \ldots, \hat{c}$; $k = 1, \ldots, \hat{m}$). In equation (3.102), η_{jk} represents a composition coefficient equal to

the number of moles of component species j in one mole of mineral k. This problem may be viewed mathematically as one of solving $\hat{c} + \hat{m}$ nonlinear algebraic equations for the $\hat{c} + \hat{m}$ (M_j, M_k) unknowns. Walsh (1983) has shown that by simple algebraic rearrangement of the equations, this problem may be reduced to a series of two sequential problems, one of $\hat{c}$ independent unknowns which is solved by Newton-Raphson iteration, and a second of $\hat{m}$ independent unknowns which may be solved directly. This manipulation will always be possible since, by the phase rule, $\hat{m} \leqslant \hat{c}$.

As Walsh (1983) has shown, for a given number of solids, equation (3.102) can be transformed into

$$\tilde{Y}_j = \sum_{i=1}^{\hat{c}+\hat{s}} \tilde{\tau}_{ji} M_i - \tilde{M}_j^T \qquad j = 1, \ldots, \hat{c} - \hat{m} \tag{3.104}$$

where the values of the new coefficients are related to the original values. The rearrangement procedure for a system involving any number of solids can be summarized by recursion formulas which are repeated through $\hat{m}$ elimination steps, in which the values of τ_{ji} and M_j^T for the lth elimination step are given by

$$\tau_{ji}^{l} = \tau_{ji}^{l-1} - \tau_{\hat{c}+1-l,i}^{l-1} \frac{\eta_{jl}^{l-1}}{\eta_{\hat{c}+1-l,l}^{l-1}} \qquad j = 1, \ldots, \hat{c} - l \tag{3.105}$$

and for $i = 1, \ldots, \hat{s}$,

$$M_j^{T,l} = M_j^{T,l-1} - M_{\hat{c}+1-l}^{T,l-1} \frac{\eta_{jl}^{l-1}}{\eta_{\hat{c}+1-l,l}^{l-1}} \qquad j = 1, \ldots, \hat{c} - l \tag{3.106}$$

where

$$\eta_{jk}^{l} = \eta_{jk}^{l-1} - \eta_{\hat{c}+1-l}^{l-1} \frac{\eta_{jl}^{l-1}}{\eta_{\hat{c}+1-l,l}^{l-1}} \qquad j = 1, \ldots, \hat{c} - l \tag{3.107}$$

By definition, the zeroth elimination step ($l = 0$) corresponds to the original values of τ_{ji}, η_{jk}, and M_j^T. After $\hat{m}$ elimination steps ($l = \hat{m}$), these equations [(3.105), (3.106), and (3.107)] will determine the final values of the coefficients required in equation (3.104).

During the elimination procedure, if at any step l the value of $\eta_{\hat{c}+1-l,l}^{l-1}$ is zero, then it and its corresponding $\tau_{\hat{c}+1-l,i}^{l-1}$ and $M_{\hat{c}+1-l}^{T,l-1}$ must be replaced by a non-zero η_{jl}^{l-1} and its corresponding τ_{jl}^{l-1} and $M_j^{T,l-1}$ such that $j < \hat{c} + 1 - l$. This replacement is simply a row interchange between rows $\hat{c} + 1 - l$ and j where $j < \hat{c} + 1 - l$. If in the case there is no non-zero η_{jl}^{l-1} such that $j < \hat{c} + 1 - l$, then the lth elimination step is unnecessary and should be skipped.

Once the elimination process is complete, and the adjusted values for the coefficients determined, the independent aqueous concentrations M_j ($j = 1, \ldots, \hat{c}$) can be calculated from equations (3.103) and (3.104) using the Newton-Raphson method.

The matrix equation which must be solved to determine the concentrations of the aqueous component species may be written

$$\begin{bmatrix} -\tilde{Y}_1 \\ \vdots \\ -\tilde{Y}_{\hat{c}-\hat{m}} \\ -F_1 \\ \vdots \\ -F_{\hat{m}} \end{bmatrix}^l = \begin{bmatrix} J_{11} & \cdots & \cdots & \cdots & \cdots & J_{1\hat{c}} \\ \vdots & \ddots & & & & \vdots \\ \vdots & & \ddots & & & \vdots \\ \vdots & & & \ddots & & \vdots \\ \vdots & & & & \ddots & \vdots \\ J_{\hat{c}} & \cdots & \cdots & \cdots & \cdots & J_{\hat{c}\hat{c}} \end{bmatrix}^l \begin{bmatrix} \Delta X_1 \\ \vdots \\ \vdots \\ \vdots \\ \vdots \\ \Delta X_{\hat{c}} \end{bmatrix}^l \tag{3.108}$$

where l is the iteration step, with the derivatives defined as follows

$$J_{ij} = \frac{\partial \tilde{Y}_i}{\partial X_j} = 2.303\left(\sum_{k=1}^{\hat{c}} \tilde{\tau}_{ik} M_k + \sum_{l=\hat{c}+1}^{\hat{c}+\hat{s}} \tilde{\tau}_{il} \nu_{jl} M_l \right) \tag{3.109}$$

$$i = 1, \ldots, \hat{c} - \hat{m} \qquad j = 1, \ldots, \hat{c}$$

$$J_{ij} = \frac{\partial F_i}{\partial X_j} = \nu_{ji} \qquad i = 1, \ldots, \hat{m} \qquad j = 1, \ldots, \hat{c} \tag{3.110}$$

and where the residuals are given by

$$Y_j = M_j + \sum_{i=1+\hat{c}}^{\hat{c}+\hat{s}} \tau_{ji} M_k - M_j^T \qquad j = 1, \ldots, \hat{c} \tag{3.102}$$

$$F_k = \sum_{j=1}^{\hat{c}} \nu_{jk} X_j - \log K_k^{sp} \qquad k = 1, \ldots, \hat{m} \tag{3.111}$$

Given the aqueous concentrations, equation (3.102) can be used to determine the M_k $(k = 1, \ldots, \hat{m})$. Equation (3.102) represents $\hat{c}$ equations that are linear with respect to M_k $(k = 1, \ldots, \hat{m})$. However, because $\hat{c} \geqslant \hat{m}$, there are more equations than unknowns, and the proper subset of $\hat{m}$ equations in the form of equation (3.102) must be selected. The following criteria were used by Walsh (1983): (i) each selected equation must be a function of at least one solid concentration, and (ii) the collective subset of equations must include all solid concentrations. The subset of $\hat{m}$ equations are linear and can be solved directly.

For the case of a single solid species, equation (3.102) reduces to

$$M_1 = \frac{M_j^T - \sum_{i=1}^{\hat{c}+\hat{s}} \tau_{ji} M_i}{\eta_{j1}} \tag{3.112}$$

where j is chosen such that η_{j1} is non-zero. For the general case of multiple solids, equation (3.102) may be rearranged to form a subset of linear equations in M_k $(k = 1, \ldots, \hat{m})$

$$\sum_{k=1}^{\hat{m}} \eta_{jk} M_k = M_j^T - \sum_{i=1}^{\hat{c}+\hat{s}} \tau_{ji} M_i \qquad j = 1, \ldots, \hat{m} \tag{3.113}$$

where j represents the subset of mass balance equations meeting the criteria listed above.

3.3.3. Equilibrium with activity coefficients

Activity coefficients are required for non-ideal aqueous solutions. For individual ions, activity coefficients may be determined using several methods (Stumm and Morgan, 1981). The Davies equation is commonly used for solution ionic strengths up to 0.5 molal

$$\log \gamma_i = -Az^2\left(\frac{\sqrt{I}}{1+\sqrt{I}} - 0.3I\right) \qquad i = 1, \ldots, \hat{c} + \hat{s} \tag{3.114}$$

where the ionic strength (I) is given by

$$I = \frac{1}{2}\sum_{i=1}^{\hat{c}+\hat{s}} m_i z_i^2 \tag{3.115}$$

and where $A \approx 0.5$, $B \approx 0.3$, and z is the charge of the ion.

For more concentrated solutions, typically encountered in basinal brines, a modified extended Debye-Hückel equation was suggested by Helgeson et al. (1981) which provides an adequate geochemical approximation for NaCl brines up to 6 molal. As given by Oelkers and Helgeson (1990), this equation may be written

$$\log \gamma_j = -\frac{A_\gamma Z_j^2 \bar{I}^{1/2}}{1 + \mathring{a}B_\gamma \bar{I}^{1/2}} + \Gamma_\gamma + b_{\gamma,\mathrm{NaCl}}\bar{I} \qquad j = 1, \ldots, \hat{c} + \hat{s} \tag{3.116}$$

(here Z is used to represent the charge of the ion) where the mole fraction to molality conversion term is given by

$$\Gamma_\gamma = -\log(1 + 0.0180153m^*) \tag{3.117}$$

where m^* is the sum of molalities of all solute species, and the effective or "true" ionic strength is given by

$$\bar{I} = \frac{1}{2}\sum_{i=1}^{\hat{c}+\hat{s}} Z_i^2 m_i \tag{3.118}$$

The Debye-Hückel coefficients (A_γ and B_γ) are temperature-dependent functions. Walsh (1983) gives polynomial fits for their calculation

$$A_\gamma = 0.2891 + (1.587 \times 10^{-3})T - (5.96 \times 10^{-6})T^2 + (1.045 \times 10^{-8})T^3 \tag{3.119a}$$

$$B_\gamma = 0.4416(A_\gamma)^{1/2} \tag{3.119b}$$

The ion size parameter is given by

$$\mathring{a}_{\mathrm{NaCl}} = r_{e,\mathrm{Na}^+} + r_{e,\mathrm{Cl}^-} \tag{3.120}$$

The effective electrostatic radii may be calculated from (Shock and Helgeson, 1988)

$$r_{e,j} = r_{x,j} + |Z_j|\Gamma_{\pm} \tag{3.121a}$$

$$\Gamma_{\pm} = k_z + g \tag{3.121b}$$

where

$$k_z = 0.0 \quad \text{(for anions)} \tag{3.122a}$$

$$k_z = 0.94 \quad \text{(for cations)} \tag{3.122b}$$

Assuming g to be zero (which is valid for lower temperatures), and using data from Shock and Helgeson (1988), this gives a value of 3.72 Å for $\mathring{a}_{\mathrm{NaCl}}$.

Finally, the extended term coefficient may be calculated as a function of temperature by fitting a curve to data from Oelkers and Helgeson (1990)

$$b_{\gamma,\mathrm{NaCl}}(x10^2) = 4.144 + (0.111)T - (1.083 \times 10^{-3})T^2 + (3.8611 \times 10^{-6})T^3 - (5.8009 \times 10^{-9})T^4 \tag{3.123}$$

This equation is valid up to 350°C along the liquid-vapor saturation (P_{sat}) curve only. Finally, it is often assumed that $\gamma = 1$ for neutral species (Helgeson et al., 1981). The activity of H_2O, as well as the activities of all pure mineral phases, may be assumed to be unity without introducing significant error (Helgeson et al., 1970). Clearly, special circumstances may occur where these assumptions may not be valid.

Mass balance equations are unaffected by these corrections, but mass action expressions must be modified appropriately. The activity of an aqueous species (a) is defined as follows

$$a_i = \gamma_i m_i \qquad i = 1, \ldots, \hat{c} + \hat{s} \tag{3.124}$$

Equation (3.89) then becomes

$$a_i = \frac{\prod_{j=1}^{\hat{c}} a_j^{\nu_{ij}}}{K_i} \qquad i = 1, \ldots, \hat{c} + \hat{s} \tag{3.125}$$

Neglecting molality-molarity conversion, this may be written

$$M_i = \frac{\prod_{j=1}^{\hat{c}} \gamma_j^{\nu_{ji}} M_j^{\nu_{ji}}}{\gamma_i K_i} \qquad i = 1, \ldots, \hat{c} + \hat{s} \tag{3.126}$$

Similarly, the mass action constraint for saturated minerals [equation (3.103)] becomes

$$F_k = \prod_{j=1}^{\hat{c}} \gamma_j^{\nu_{jk}} M_j^{\nu_{jk}} - K_k^{sp} \qquad k = 1, \ldots, \hat{m} \tag{3.127}$$

Making the logarithmic transformation [equation (3.90)] this becomes

$$F_k = \sum_{j=1}^{\hat{c}} \nu_{jk} \log(\gamma_j M_j) - \log K_k^{sp} \qquad k = 1, \ldots, \hat{m} \tag{3.128}$$

Walsh (1983) has shown that the elements of the Jacobian matrix [equations (3.109) and (3.110)] are unaffected by the addition of activity coefficients.

3.3.4. Direct search optimization

The Newton-Raphson method, to be described in section (3.3.5), is *locally convergent* (Ortega and Rheinboldt, 1970) and so is likely to converge only if initial guesses are sufficiently accurate. In order to assure convergence, a direct search optimization procedure was used by Walsh (1983) to determine initial guesses. The basic function of this algorithm is to minimize an objective function, which is a function of the initial guesses, given by

$$f_{\text{obj}}(x_1, x_2, \ldots, x_N) = \sum_{i=1}^{N} (Y_i)^2 \tag{3.129}$$

where x_i is the set of initial estimates. The optimization proceeds as follows. Prior to the first iteration of the Newton-Raphson procedure, f_{obj} is evaluated using an initial set of x_i. Regardless of the value of f_{obj}, an attempt is made to improve the set of initial estimates. This is accomplished by changing one x_i at a time while keeping all others constant until a minimum in f_{obj} is reached. After each x_i is searched and possibly improved, the procedure is repeated using the improved set of x_i and tested for additional improvement.

3.3.5. Newton-Raphson iteration

The set of N functional relations to be zeroed takes the form (Press et al., 1986)

$$f_i(x_1, x_2, \ldots, x_N) = 0 \qquad i = 1, \ldots, N \tag{3.130}$$

Letting $\mathbf{X}$ denote the entire vector of values x_i then, in the neighborhood of $\mathbf{X}$, each of the functions may be expanded in Taylor series

$$f_i(\mathbf{X} + \delta\mathbf{X}) = f_i(\mathbf{X}) + \sum_{j=1}^{N} \frac{\partial f_i}{\partial x_j} \delta x_j + O(\delta\mathbf{X}^2) \tag{3.131}$$

By neglecting terms of order $\delta\mathbf{X}^2$ and higher, a set of linear equations is obtained for the corrections $\Delta\mathbf{X}$ that move each function closer to zero simultaneously, namely

$$\sum_{j=1}^{N} \alpha_{ij} \Delta x_j = \beta_i \tag{3.132}$$

where

$$\alpha_{ij} \equiv \frac{\partial f_i}{\partial x_j} \tag{3.133a}$$

$$\beta_i \equiv -f_i \tag{3.133b}$$

The linear matrix equation (3.132) is solved and the corrections are added to the solution vector

$$x_i^{\text{new}} = x_i^{\text{old}} + \Delta x_i \qquad i = 1, \ldots, N \tag{3.134}$$

This process is repeated until convergence is achieved.

In order to improve the stability of convergence, a dampening procedure may be used (Wolery, 1978; Walsh, 1983). If $|\Delta x_i|$ is greater than some value (e.g., 3 logarithmic units), it is set to that value. In practice, more complex dampening procedures may be necessary when treating heterogeneous equilibrium, which consider the rate of convergence and other factors.

As noted by Walsh (1983), coupled transport solutions require several thousands of different speciation calculations. Therefore, it is essential that speciation algorithms be sufficiently robust to avoid prematurely ending a simulation. Occasionally, solutions may begin to diverge when several solids are involved. This may be due to poor initial estimates, an ill-conditioned Jacobian matrix, insufficient dampening, especially during the first few iterations, or other reasons. For these reasons, coupled numerical models will often rely on tested available speciation codes.

3.4. Heat transport

In general, heat transfer in porous media is governed by three separate mechanisms (Marsily, 1986): (1) conduction in the solid matrix, (2) transport in the fluid phase (convection), and (3) heat exchange between the fluid phase and the solid matrix.

In practice, the third mechanism is assumed to be insignificant. Heat transport is characterized by (1) convection, and (2) a phenomenon similar to the dispersion of a solute: (a) conduction in the two phases (solid and fluid), which is analogous to molecular diffusion, and (b) the heterogeneity of the real velocity, which gives rise to a kinematic or hydrodynamic dispersion.

Conservation of hydrothermal energy gives rise to the following equation

$$\nabla \cdot (\boldsymbol{\lambda}^* \nabla T) - \rho_f c_f \mathbf{q} \cdot \nabla T = (\rho c)_e \frac{\partial T}{\partial t} \tag{2.108}$$

where T is the temperature, ρ_f is the fluid density, c_f is the specific heat capacity of the fluid, $\mathbf{q}$ is the specific discharge vector, $(\rho c)_e$ is the effective volumetric heat capacity [equation (2.103)], and $\boldsymbol{\lambda}^*$ is the tensor of effective or equivalent thermal conductivity, which combines the isotropic effective thermal conductivity (λ_e) of the porous medium (fluid plus solid) in the absence of flow with a term for the macrodispersivity.

3.4.1. Formulation of finite element equations

The governing equation for heat transport (2.108) is similar to the advection-dispersion equation for conservative solute transport (2.64), so formulation of the finite element equations is straightforward. Using the operator

$$L(T) = \nabla \cdot (\boldsymbol{\lambda}^* \nabla T) - \phi \rho_f c_f \mathbf{v} \cdot \nabla T - (\rho c)_e \frac{\partial T}{\partial t} \tag{3.135}$$

and the trial function

$$T \approx \hat{T} = \sum_{m=1}^{N} T_m \xi_m \tag{3.136}$$

the weighted residual equation becomes

$$\iint_R \left[\nabla \cdot (\boldsymbol{\lambda}^* \nabla \hat{T}) - \phi \rho_f c_f \mathbf{v} \cdot \nabla \hat{T} - (\rho c)_e \frac{\partial \hat{T}}{\partial t} \right] \xi_n dR = 0 \tag{3.137}$$

Simplifying and applying the appropriate Greens theorem [equation (3.14)] using

$$u = \xi_n \tag{3.138a}$$

$$\nabla w = \boldsymbol{\lambda}^* \nabla \hat{T} \tag{3.138b}$$

this becomes

$$\iint_R \boldsymbol{\lambda}^* \nabla \hat{T} \cdot \nabla \xi_n dR - \int_S \boldsymbol{\lambda}^* \nabla \hat{T} \cdot \mathbf{n} \xi_n dS + \iint_R \phi \rho_f c_f \mathbf{v} \cdot \nabla \hat{T} \xi_n dR + \iint_R (\rho c)_e \frac{\partial \hat{T}}{\partial t} \xi_n dR = 0 \tag{3.139}$$

Rearranging, and writing each integral as the summation over all the individual element subregions

$$\sum_e \left(\iint_{R^e} \boldsymbol{\lambda}^{*e} \nabla \hat{T} \cdot \nabla \xi_n^e dR^e + \iint_{R^e} \phi^e \rho_f^e c_f \mathbf{v}^e \cdot \nabla \hat{T} \xi_n^e dR^e + \iint_{R^e} (\rho c)_e^e \frac{\partial \hat{T}}{\partial t} \xi_n^e dR^e \right) = \sum_e \left(\int_{S^e} \boldsymbol{\lambda}^{*e} \nabla \hat{T} \cdot \mathbf{n} \xi_n^e dS^e \right) \tag{3.140}$$

Incorporating the trial function (3.136) and replacing the right hand side of equation (3.140) with a flux term (Fourier's law)

$$\mathbf{J} = -\boldsymbol{\lambda}^* \nabla T \tag{3.141}$$

equation (3.140) becomes

$$\sum_m \left(\sum_e \iint_{R^e} \boldsymbol{\lambda}^{*e} \nabla \xi_m^e \cdot \nabla \xi_n^e dR^e + \sum_e \iint_{R^e} \phi^e \rho_f^e c_f \mathbf{v}^e \cdot \nabla \xi_m^e \cdot \xi_n^e dR^e \right) T_m$$

$$+ \sum_m \left(\sum_e \iint_{R^e} (\rho c)_e^e \xi_m^e \xi_n^e dR^e \right) \frac{dT_m}{dt} = -\sum_e \left(\int_{S^e} \mathbf{J}^e \cdot \mathbf{n} \xi_n^e dS^e \right) \tag{3.142}$$

As before, the summation over m is over all the nodes and the summation over e is over all the elements. Simplifying the notation, equation (3.142) becomes

$$\sum_m O_{nm} T_m + \sum_m P_{nm} \frac{dT_m}{dt} = -U_n \tag{3.143}$$

where

$$O_{nm} = \sum_e O_{nm}^e = \sum_e \left(\iint_{R^e} \boldsymbol{\lambda}^{*e} \nabla \xi_m^e \cdot \nabla \xi_n^e dR^e + \iint_{R^e} \phi^e \rho_f^e c_j \mathbf{v}^e \cdot \nabla \xi_m^e \cdot \xi_n^e dR^e \right) \tag{3.144a}$$

$$P_{nm} = \sum_e P_{nm}^e = \sum_e \left(\iint_{R^e} (\rho c)_e^e \xi_m^e \xi_n^e dR^e \right) \tag{3.144b}$$

$$U_n = \sum_e \left(\int_{S^e} \mathbf{J}^e \cdot \mathbf{n} \xi_n^e dS^e \right) \tag{3.144c}$$

3.4.2. Evaluating the integrals

The next step is to evaluate the integrals presented in equations (3.144). Matrix O_{nm} may be found by integrating equation (3.144a)

$$O_{nm} = \sum_e O_{nm}^e = \sum_e \frac{1}{4\Delta^e} (\lambda_{xx}^{*e} \beta_n \beta_m + \lambda_{xz}^{*e} \beta_n \gamma_m + \lambda_{zx}^{*e} \gamma_n \beta_m + \lambda_{zz}^{*e} \gamma_n \gamma_m)$$

$$+ \sum_e \frac{1}{6} \phi^e \bar{\rho}_f c_f (v_x^e \beta_m + v_z^e \gamma_m) \tag{3.145}$$

In this equation, the components of the conductivity tensor in cartesian coordinates are derived from the longitudinal and transverse dispersivities using the relations given in equation (2.110). The next integral [equation (3.144b)] is easily evaluated

$$P_{nm} = \sum_e (\rho c)_e^e \begin{cases} \Delta^e/6 & \text{for } n = m \\ \Delta^e/12 & \text{for } n \neq m \end{cases} \tag{3.146}$$

The final integral [equation (3.144c)] is evaluated as follows

$$U_n = -\sum_e \left(\frac{u_n l^e}{2}\right) \tag{3.147}$$

Here, the variable u_n is used to represent the specified heat flux at node n and l^e is the length of the element boundary.

3.4.3. Transient and steady-state equations

The general expression for solute transport, in matrix form, is given in equation (3.143). Discretization or time-stepping is performed using a weighted finite difference scheme which takes the form

$$\left(\theta[O] + \frac{1}{\Delta t}[P]\right)\{T\}^{k+1} = \left[(\theta - 1)[O] + \frac{1}{\Delta t}[P]\right]\{T\}^k - \{U\} \tag{3.148}$$

where θ is the weight for which specific cases are given in equation (3.31). For boundaries of specified temperature, T_m are known, and equations for these nodes can be removed from the matrices. Specified heat fluxes are inserted as u_n values in the appropriate terms. For an impervious boundary, u_n values may be set to zero.

In Section 3.2.5, some of the difficulties and limitations of numerical solutions to the advection-dispersion equation were noted, especially with reference to the grid Peclet number and Courant number. Likewise, a thermal grid Peclet number (Pe_T^*) may be defined

$$\mathrm{Pe}_T^* = \frac{q\Delta L}{\lambda^*/\rho_f c_f} \tag{3.149}$$

If thermal dispersion is ignored, and we require $\mathrm{Pe}_T^* \leq 2$, then

$$\Delta L \leq \frac{2\kappa}{q} \tag{3.150}$$

Typically, $\kappa \approx 15\ \mathrm{m^2/yr}$, so for a specific discharge of 0.25 m/yr, the grid spacing should be less than 120 m. If thermal dispersion is greater than conduction ($\epsilon|\mathbf{q}| > \kappa$), then

$$\Delta L \leq 2\epsilon \tag{3.151}$$

The point to be made is that the restriction of equation (3.150) is not that significant, since thermal conduction is more efficient than molecular diffusion by a factor of 100 (Bear, 1972) to 400–1000 (Marsily, 1986). The Courant number restriction [equation (3.71)] is the same for heat transport.

The steady-state form of the heat transport equation is derived by simplifying equation (3.143)

$$\sum_m O_{nm} T_m = -U_n \tag{3.152}$$

where the stiffness matrix O_{nm} and the flux vector U_n are as given in equations (3.145) and (3.147). Boundary conditions are incorporated in the same manner as for the transient equations.

4. Applications

Models of hydrological, geochemical, and thermal processes at the basin scale generally involve either analytical or numerical solution to two or more sets of coupled partial differential equations (Fig. 24). These equations and their numerical solution have been reviewed in the previous sections. Ultimately, application of these models seeks to provide some additional explanation of our observations of large sedimentary basins. Numerical simulation has become an important tool for testing conceptual models (see Section 1.1) of basin hydrogeology (Garven, 1995). Currently, however, numerical models which include reactive multicomponent mass transport have not been applied to problems involving entire sedimentary basins. The exceptions to this statement have relied in most cases on dramatic simplification of geochemical processes. The two factors hampering our ability to conduct numerical experiments at the basin scale are: (i) computer processing time and memory limitations, and (ii) the lack of sufficiently detailed spatial data on physical parameters (K, ϕ) and the distribution of chemical mass. While the former limitation becomes less severe with time, it is likely that the latter will persist.

Models of coupled flow and reactive mass transport at very large scales have demonstrated the importance of mass transport over long times and distances as a mechanism for alteration of sediments and sedimentary rocks. Phillips (1990, 1991) broadly classified such transport-controlled reactions as follows: (1) isothermal reaction fronts, separating mineralogically distinct zones, which propagate in the direction of flow, (2) gradient reactions, the result of fluid movement through temperature and pressure gradients, producing more pervasive alteration, and (3) mixing reactions, which occur when two or more fluids of different composition mix, often producing highly localized alteration.

This classification will be used throughout this discussion of model applications. In addition to reviewing selected analytical and numerical model applications from the published literature, this section will provide some simple simulations to illustrate general features of transport-controlled geochemical processes.

4.1. One-dimensional reaction-front propagation

As a fluid within a porous medium crosses a compositional boundary, geochemical reactions will occur driving the composition of the fluid toward equilibrium with the rock. In the context of basin-scale hydrochemical processes, mineral precipitation and dissolution will be the primary geochemical reactions of interest.

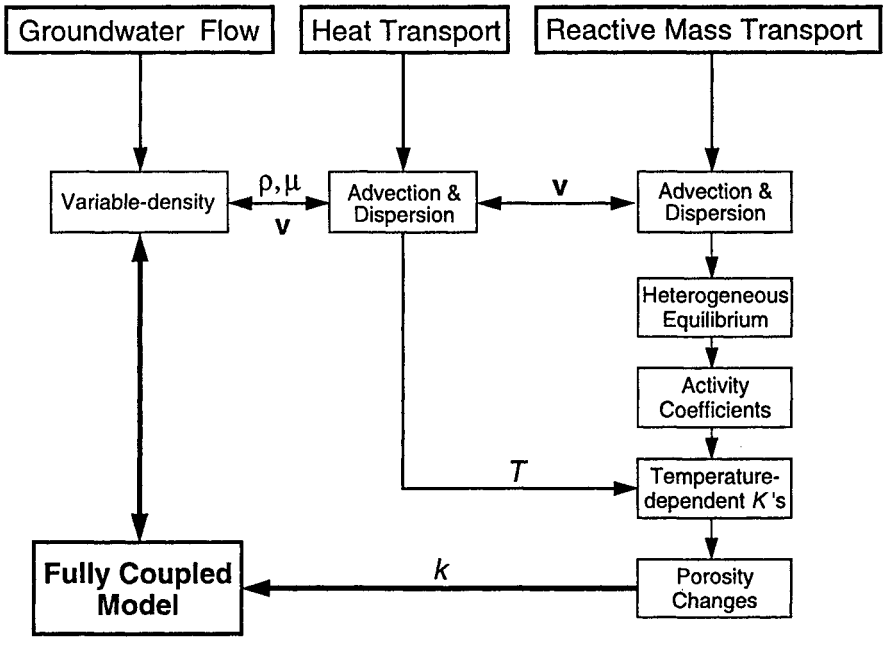


Fig. 24. Schematic diagram of the processes represented in a fully coupled model of basin-scale hydrological, geochemical, and thermal processes, showing terms involved in the coupling of the various processes.

A region of fluid-mineral disequilibrium will separate unaltered rock from regions in which one or more phases have been completely dissolved (and possibly new phases precipitated). The width of this region will depend on the fluid velocity, reaction kinetics, and solute dispersion (Phillips, 1990; Lichtner, 1993), but in the local equilibrium limit will occur as a sharp "reaction front" separating regions of distinctly different mineralogy (see also Section 2.2.6). These reaction fronts will propagate in the direction of fluid flow, but at some rate that is less than the average linear velocity. Laboratory studies which have examined the propagation of (mineralogical) reaction fronts include Lund and Fogler (1976), Hekim and Fogler (1980), and Hekim et al. (1982). Other studies that have developed mathematical and numerical models of reaction-front propagation include Walsh et al. (1984), Bryant et al. (1986, 1987), Willis and Rubin (1987), Dria et al. (1987), Mundell and Kirkner (1988), Novak et al. (1988), and Sevougian et al. (1993). Several studies have examined reaction-front propagation due to sorption reactions (Cameron and Klute, 1977; Charbeneau, 1981; Kirkner et al., 1984; Brusseau et al., 1992; Bajracharya and Barry, 1993; Bosma and van der Zee, 1993; Yeh et al., 1993; Schweich et al., 1993a, 1993b); Brusseau (1994) provides a recent review of the progress in modeling chemical transport with sorption reactions. Bahr and Rubin (1987) compare local equilibrium and kinetic formulations of the reactive transport equation for sorption reactions.

Reaction-front-related geological phenomena which have been the subject of numerical modeling studies include weathering (Liu and Narasimhan, 1989b;

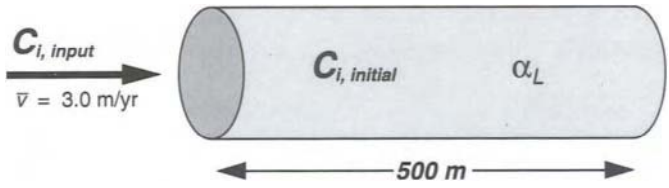


Fig. 25. Conceptual one-dimensional domain and parameters used for simulations of reaction-front propagation shown in Figs. 4.3 through 4.6.

Lichtner and Waber, 1992; Merino et al., 1993), supergene enrichment of porphyry copper deposits (Ague and Brimhall, 1989; Liu and Narasimhan, 1989b; Lichtner and Biino, 1992), sediment diagenesis and reactive-infiltration instabilities (Ortoleva et al., 1987; Ortoleva et al., 1987; Hinch and Bhatt, 1990; Steefel and Lasaga, 1990; Wei and Ortoleva, 1990; Ortoleva, 1994), and redox behavior (Auchmuty et al., 1986; Ortoleva et al., 1986; Liu and Narasimhan, 1989a, 1989b; Engesgaard and Kipp, 1992; Lichtner and Waber, 1992). Walsh (1983), Phillips (1990, 1991), and Lichtner (1991, 1993) provide excellent overviews of the general behavior of propagating reaction fronts.

Consider an initially homogeneous one-dimensional domain (Figure 25) and allow a fluid not in equilibrium with the starting mineral assemblage to move through the domain. In the limiting case of local chemical equilibrium, minerals will precipitate or dissolve at the upstream end of the domain *instantaneously* to achieve equilibrium. Bearing in mind that local equilibrium is really only valid at large length and time scales, we shall consider a 500-m long domain. Initially, we will consider only calcite and anhydrite as possible mineral phases. If the domain contains anhydrite initially, and the reacting fluid is in equilibrium with calcite but undersaturated with respect to anhydrite, the anhydrite will dissolve, eventually forming a reaction front that moves through the rock at some rate that is less than the average linear velocity of the fluid (Fig. 26A). The greater the amount of anhydrite initially present, the slower the rate of front propagation. Downstream of the front, concentrations of calcium and sulfate must be in equilibrium with anhydrite; upstream, the fluid is undersaturated with respect to anhydrite. Calcite begins to precipitate at the entrance to the domain, but the precipitation front does not propagate with the anhydrite dissolution front. Downstream of the precipitation front, the fluid remains in equilibrium with calcite, despite its absence. This is referred to as the "downstream equilibrium condition", and is a result of the imposed local equilibrium assumption (Walsh et al., 1984).

Alternatively, when we begin with a calcite-bearing domain (all of these examples are essentially sandstone with minor cements), and allow a fluid to infiltrate which is in equilibrium with anhydrite and not calcite, the results are different (Figure 26B). In this case, calcite dissolution, which must precede anhydrite precipitation, occurs so slowly that *neither* front propagates quickly. Under the assumption of local chemical equilibrium, a precipitation front can not advance faster than a dissolution front. This is due to the fact that downstream of a precipitation front, the fluid must be *in equilibrium* with the precipitating mineral such that no supersaturation can occur. In order to continue to precipitate the

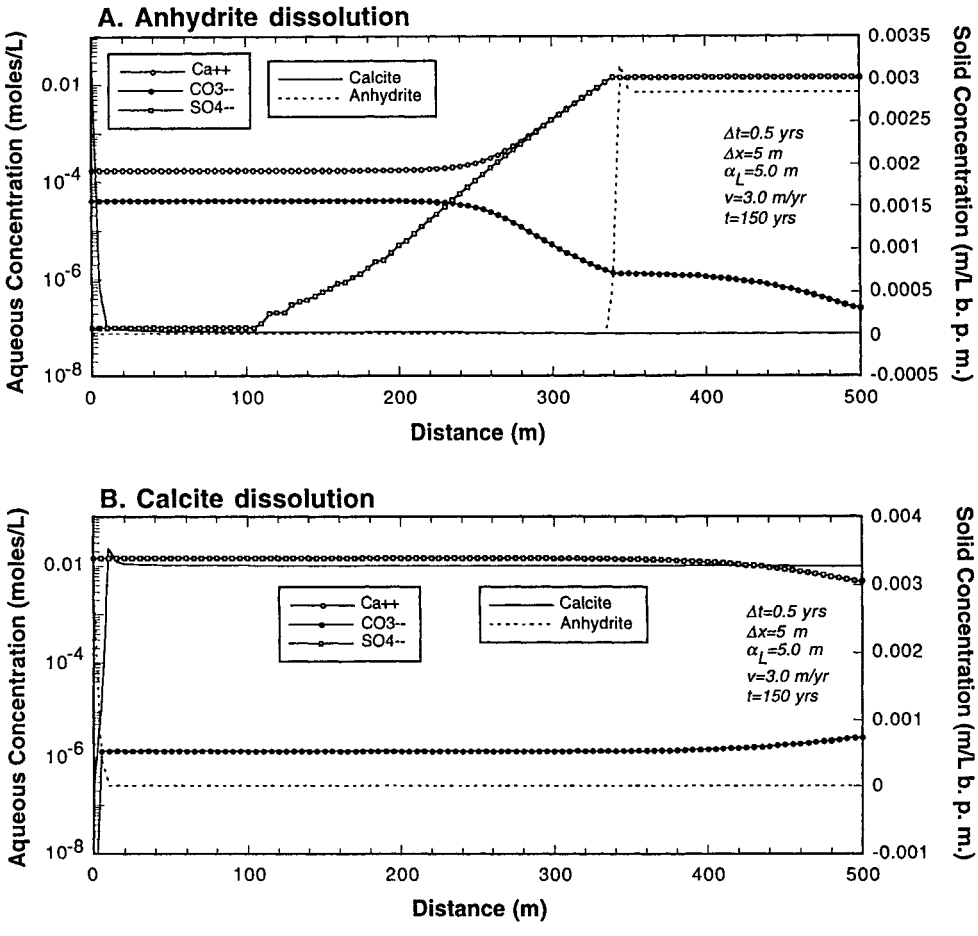


Fig. 26. Simulations of anhydrite (A) and calcite (B) dissolution-front propagation. In Figures 4.3 through 4.6, the abbreviation "m/L b.p.m." refers to molar concentration per liter of saturated porous material.

mineral in the downstream direction, the fluid must gain calcium (in this example) through *dissolution of the downstream phase*. In addition, the saturation index and relative concentrations of product species determine the amount of dissolution that can occur before equilibrium is reached. In these examples, the calcite-bearing lithology is much more undersaturated with respect to anhydrite than the anhydrite-bearing lithology is with respect to calcite. Furthermore, the initial carbonate concentrations are much lower than the initial sulfate concentrations. Therefore, in Figure 26A, the anhydrite dissolution front propagates quickly, while in Figure 26B, the calcite dissolution front propagates slowly. It is also apparent from Figure 26A that the calcium produced by dissolution of anhydrite is not sufficient to precipitate significant quantities of calcite. Figure 27 shows the results of a calcite- and anhydrite-bearing domain infiltrated by a fluid which is capable of dissolving both. In this case both minerals dissolve, but the reaction fronts

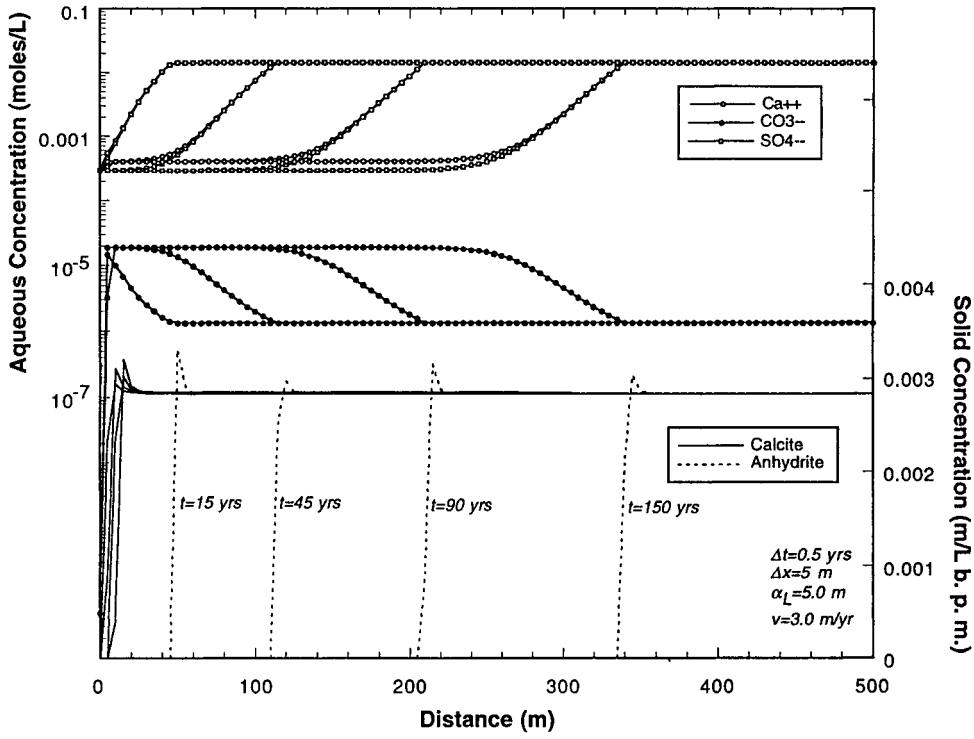


Fig. 27. Simulation of simultaneous anhydrite and calcite dissolution-front propagation.

propagate at different rates, depending on the degree of undersaturation in the incoming fluid and the relative concentrations of the product species.

Several studies have addressed the relative importance of dispersive mixing in determining the behavior of reaction fronts (Phillips, 1990; Steefel and Lasaga, 1992; Lichtner, 1993). This has been somewhat of an issue in numerically modeling reactive solute transport, since both older and recent approaches (Lichtner, 1992) have neglected dispersion. Considering the results shown in Figure 28, it appears that dispersion has an effect on the *initial* rate of reaction-front propagation, but at longer times the reaction fronts propagate at a rate that is independent of the longitudinal dispersivity. This result was also demonstrated by Lichtner (1993), and was discussed in Section 2.2.6. A much more complicated example is shown in Figure 29, involving four mineral phases: calcite, dolomite, magnesite, and anhydrite. Initially, the domain comprises quartz, calcite, and anhydrite. The infiltrating fluid is in equilibrium with magnesite only. In this case, rather than simple calcite/magnesite dissolution/precipitation fronts, we see the formation of an intermediate product, dolomite, which occupies a distinct zone. An additional complication is that anhydrite is observed to precipitate just upstream of the calcite dissolution front, but dissolves completely a few meters farther upstream. The dolomite zone increases with dispersivity (compare Figs. 29A and 29B), and also appears to increase with time (or distance of propagation), since the fronts defining the zone will initially advance at different rates. At longer times, we would

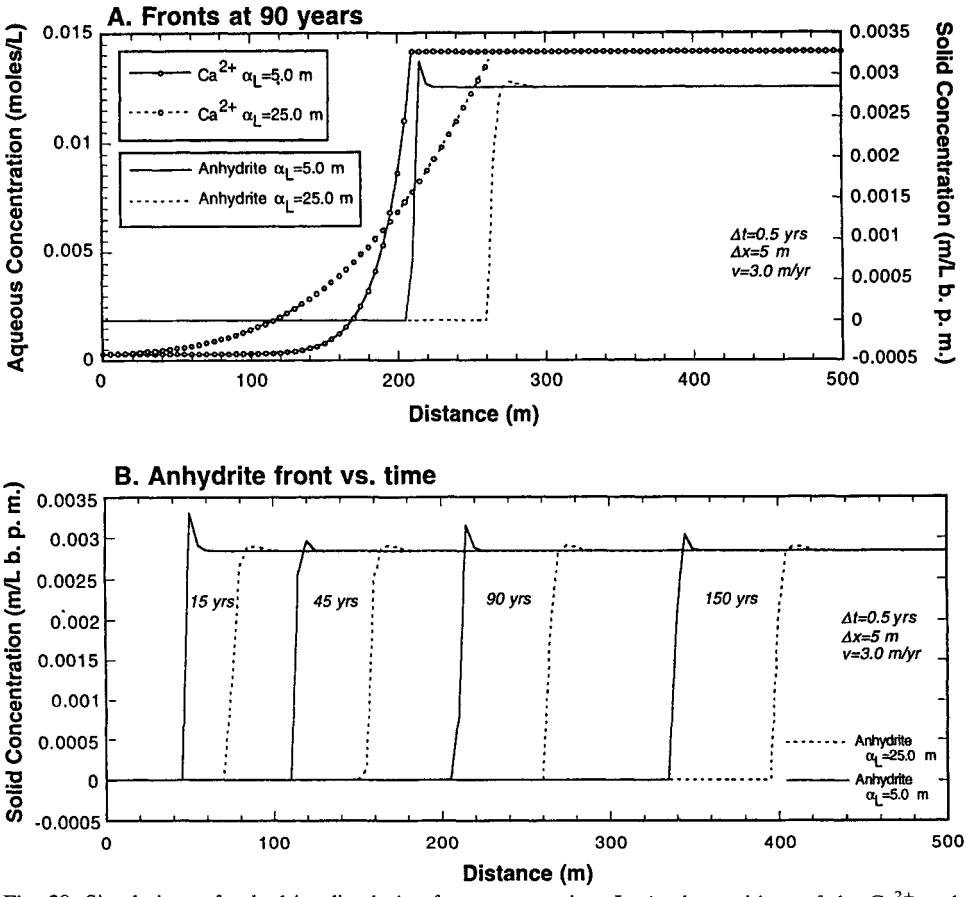


Fig. 28. Simulations of anhydrite dissolution-front propagation. In A, the positions of the Ca^{2+} and anhydrite fronts are shown after 90 years for different values of the longitudinal dispersivity. In B, the anhydrite fronts for the two dispersivities are shown as a function of time. At long times, the front propagates at a constant rate, independent of the value of the longitudinal dispersivity (see also Fig. 16).

anticipate that the rates would become independent of the dispersivity. However, unless the alteration rates are identical at each front, the intermediate zone should continue to widen through time.

These examples considered mineral reaction-front propagation under the assumption of local chemical equilibrium. Steefel and Lasaga (1992) compare the rates of mineral reaction as a function of time and space, using a kinetic approach. Their results (Figure 30) indicate that dispersive mixing may influence the distribution of mineral reaction rates, which led the authors to conclude that ignoring the coupling between hydrodynamic dispersion and geochemical reactions can produce inaccurate predictions of the rates of reaction, and possibly what reactions will occur, along a flow path.

Obviously, even when dealing with simple chemical systems, the nature of the spatial and temporal distribution of geochemical reactions can be quite complex,

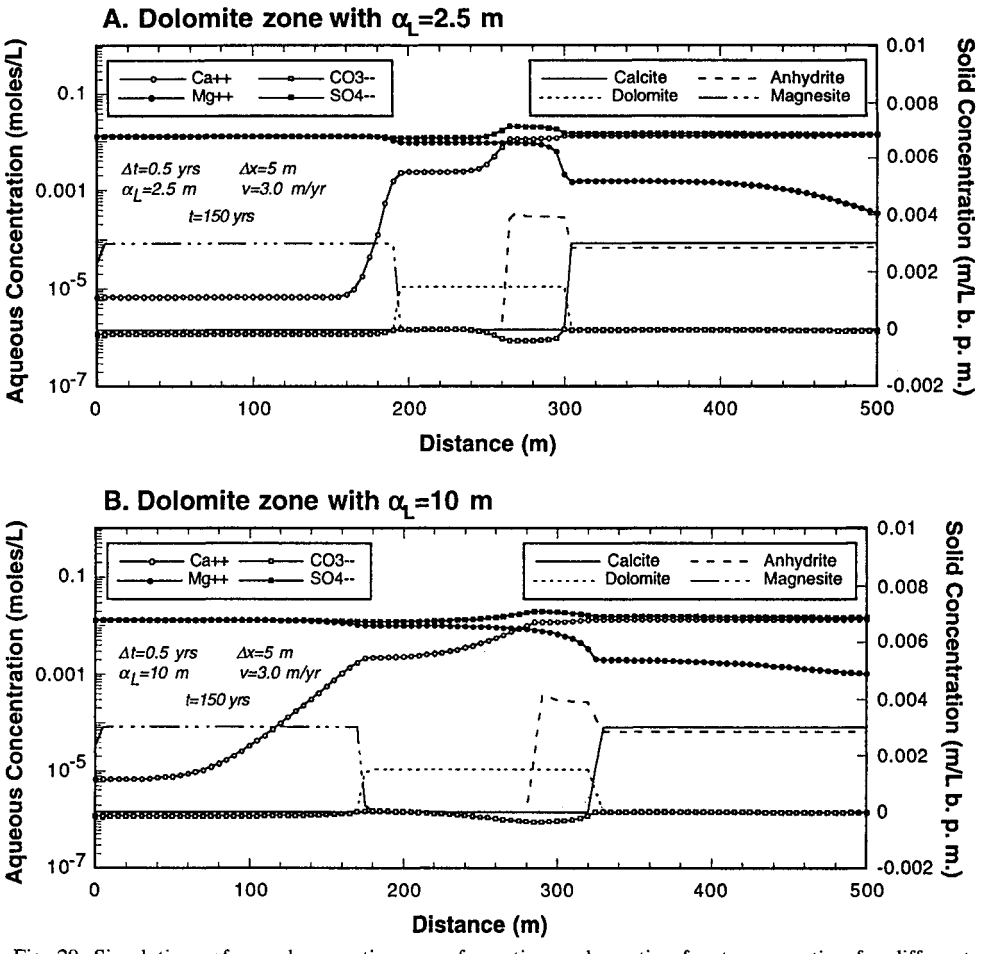


Fig. 29. Simulations of complex reaction-zone formation and reaction-front propagation for different values of the longitudinal dispersivity.

and difficult to predict based on static geochemical calculation approaches. The concentrations of aqueous species are controlled by these competing reaction fronts, and ultimately the fluid compositions exiting the domain are a complicated function of the time-space continuum of geochemical reactions.

4.1.1. Supergene copper enrichment

Many copper ore deposits, especially hydrothermal porphyry copper deposits, experience supergene enrichment near the water table, in which hydrochemical differentiation due to weathering transports copper from a source region above the water table to be re-precipitated below the water table as secondary ore minerals (Maynard, 1983; Ague and Brimhall, 1989). In general, this process involves oxidation and leaching of copper in the unsaturated zone, which is then transported below the water table and reduced to form a zone of enrichment. Although supergene enrichment has been recognized as an important mechanism

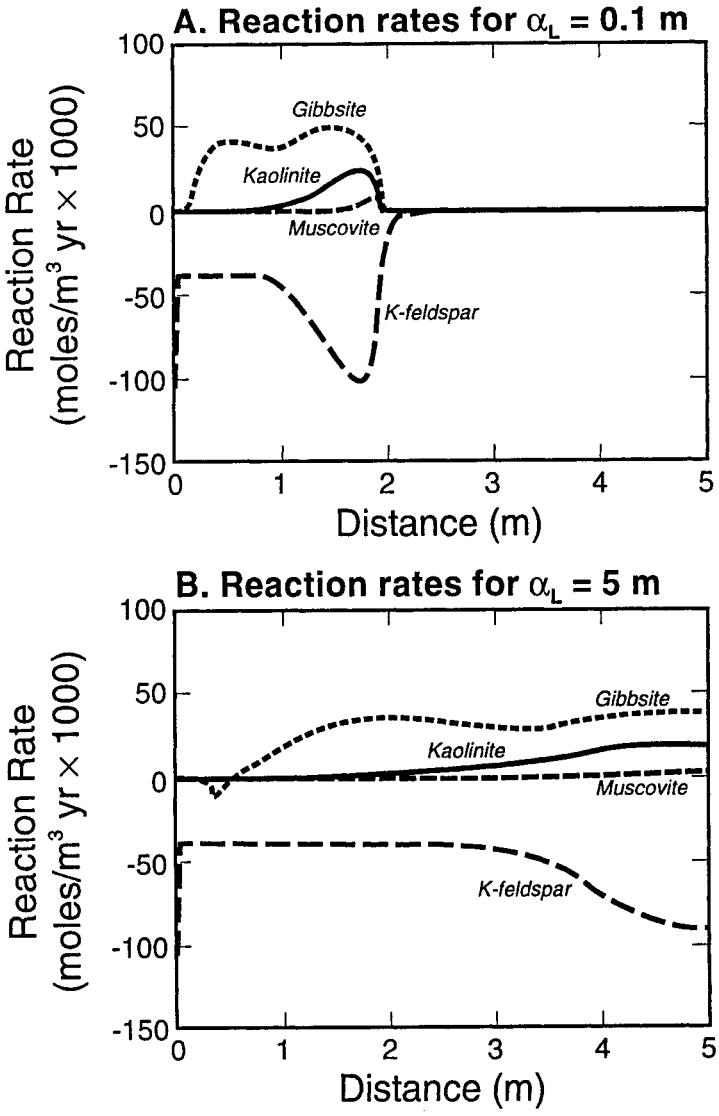


Fig. 30. Comparison of instantaneous reaction rates for different values of the longitudinal dispersivity, using a kinetic description of mineral precipitation and dissolution (after Steefel and Lasaga, 1992, used with permission of the authors).

for the formation of economic ore deposits for decades, only in the past ten years have numerical models of coupled flow and reactive mass transport been developed and applied to increase our understanding of the interaction between hydrological and geochemical processes (Brimhall et al., 1985; Ague and Brimhall, 1989; Alpers and Brimhall, 1989; Liu and Narasimhan, 1989b; Lichtner and Biino, 1992).

The formation of sediment-hosted ore deposits represents possibly the most often studied hydrochemical processes occurring in sedimentary basins, and several

numerical modeling studies have addressed questions regarding the nature of the transport and concentration of ore metals. Garven and Freeze (1984a, 1984b) examined regional gravity-driven flow systems and the transport of metal-bearing brines in foreland basins and demonstrated that this mechanism of flow (and transport) could have been responsible for the formation of Mississippi-valley type lead-zinc deposits. However, their approach to coupling mass transport with geochemical reactions considered only a single spatial point, where the metal-bearing brines reach the site of ore deposition. Since that study, several coupled numerical models have been developed and applied to the formation of sediment-hosted ore deposits (for a recent review, see Garven and Raffensperger, in press).

Since supergene copper enrichment generally involves vertical fluxes of mass (Brimhall et al., 1985), one-dimensional models are often applied. The process may be viewed as one of reaction-front propagation. Liu and Narasimhan (1989b) applied a kinetically-based model of multicomponent reactive mass transport (Liu and Narasimhan, 1989a) to the formation of the Butte ore district, in Montana. Their results indicate that complete leaching of the source zone occurs on a time scale of 10^4 to 10^5 yr. Precipitation of copper as chalcocite (Cu_2S), covellite (CuS), and bornite (Cu_5FeS_2) below the water table produces a blanket or enrichment zone in which copper is enriched, relative to the source zone. In their simulations, the vertical spatial dimension was discretized into 10 nodes, with a nodal spacing of 10 m.

Ague and Brimhall (1989) also studied supergene enrichment of porphyry copper deposits, using a numerical model which coupled a model of one-dimensional advective transport in a variably-saturated domain with the reaction path code EQ6 (Wolery, 1978, 1979). Due to computer limitations, their simulations used only five "volume elements," each 30 m long in the vertical direction and 1 m^2 in cross-section. They concluded from their simulations that in natural oxidative weathering, the supergene enrichment process conserves copper, i.e., no copper was found to be transported out of the supergene system. Furthermore, these simulations demonstrated that the dominant source of sulfur for secondary copper sulfide mineral formation is the preexisting protore sulfides, rather than reduced sulfate transported from the leached zone.

Lichtner and Biino (1992) noted the coarse spatial resolution of the simulations reported previously, and applied the reactive mass transport model developed by Lichtner (1992) to the problem of supergene copper enrichment. This model, based on the quasi-stationary state approximation (Lichtner, 1988) enables the governing transport equations to be integrated over long time spans, which allowed Lichtner and Biino (1992) to perform their calculations with significantly greater spatial resolution. As a result, they could accurately simulate the complex zones of alteration and copper mineral deposition associated with supergene enrichment. In their simulations, enrichment was found to occur at the top of the blanket (Figure 31), due to precipitation of chalcocite; below the narrow zone of enrichment, the copper concentration remained constant and equal to its value in the protore. This zone of enrichment at the top of the blanket grows continuously with increasing time. One important result of their work was that increased copper enrichment occurred in zone of higher flow velocities or permeabilities.

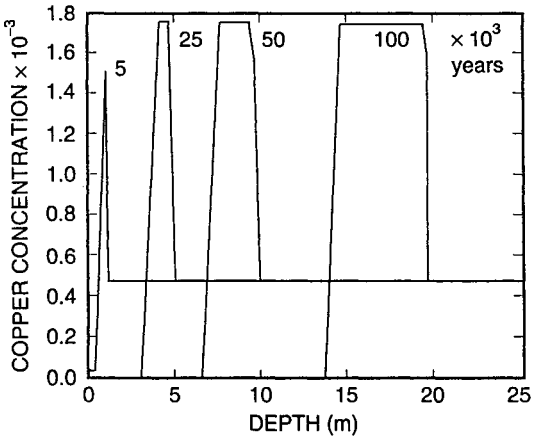


Fig. 31. Results of a numerical simulation of supergene copper enrichment showing copper concentrations in the solid phase as a function of depth at various times. Units of concentration are mol/cm^3 (Re-drafted from Geochimica et Cosmochimica Acta, Volume 56, Lichtner, P. C., and G. G. Biino, A first principles approach to supergene enrichment of a porphyry copper protore: I. Cu-Fe-S subsystem, pages 3987–4013, Copyright (1992), with kind permission from Elsevier Science Ltd, The Boulevard, Langford Lane, Kidlington 0X5 1GB, UK).

4.2. Two-dimensional simulations

As may be inferred from the previous discussion of geological applications of one-dimensional models of coupled flow and reactive mass transport, relatively few geological problems of interest may be studied by neglecting two- or three-dimensional flow and transport. Applications of one-dimensional models have concentrated on studies of reaction-front propagation. To examine more complicated reactions involving flow through gradients and fluid mixing, two- or three-dimensional models are required. However, with few exceptions (Schwartz and Domenico, 1973), two-dimensional models have only recently been developed (see Table 1). Before presenting applications of two-dimensional models to these phenomena in sedimentary basins, we will examine the nature of reaction-front propagation in two spatial dimensions.

4.2.1. Dispersion and two-dimensional reaction fronts

Two-dimensional models are capable of including hydrostratigraphy and its effects on both the geometry of the flow system and the nature of reactive mass transport. In this section, two-dimensional simulations will be presented that examine the effect of simple stratigraphic layering. The domain for the problem consists of a shale unit overlying a sandstone aquifer in a large hillslope basin (Figure 32). The longitudinal dispersivity (α_L) initially is 100 m, and the transverse dispersivity (α_L) is 10 m. Minor amounts of K-feldspar and calcite are present initially in the sandstone, and minor amounts of kaolinite are present initially in the shale. Steady-state hydraulic heads and streamlines (contours of the stream function) are shown in Fig. 32.

The spatial distributions of calcite, K-feldspar, and kaolinite at 3000 years are

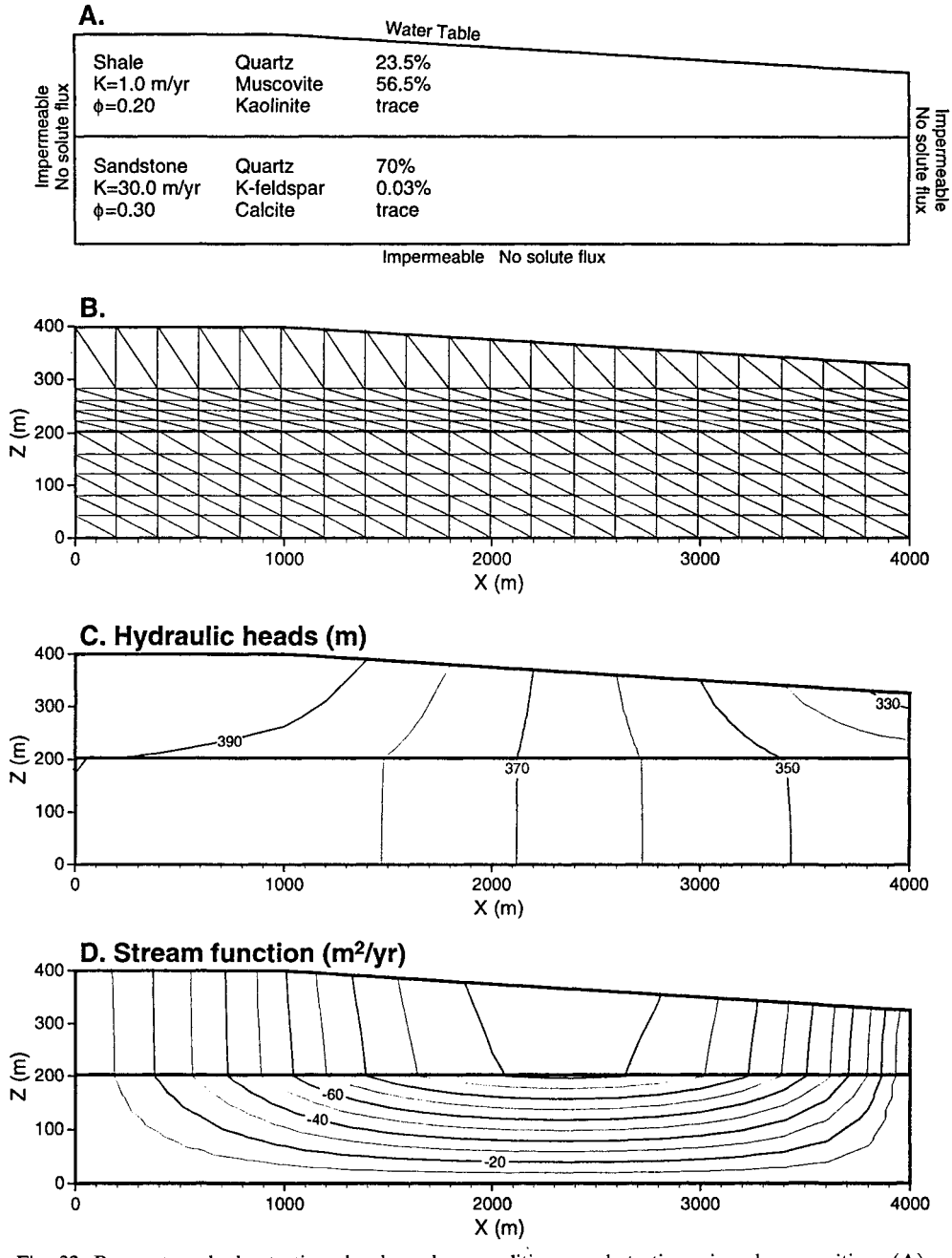


Fig. 32. Parameters, hydrostratigraphy, boundary conditions, and starting mineral compositions (A), finite element grid (B), steady-state hydraulic heads (C), and streamlines (D) for the example two-dimensional simulation. Note that vertical exaggeration is present in Figs. 32 through 34.

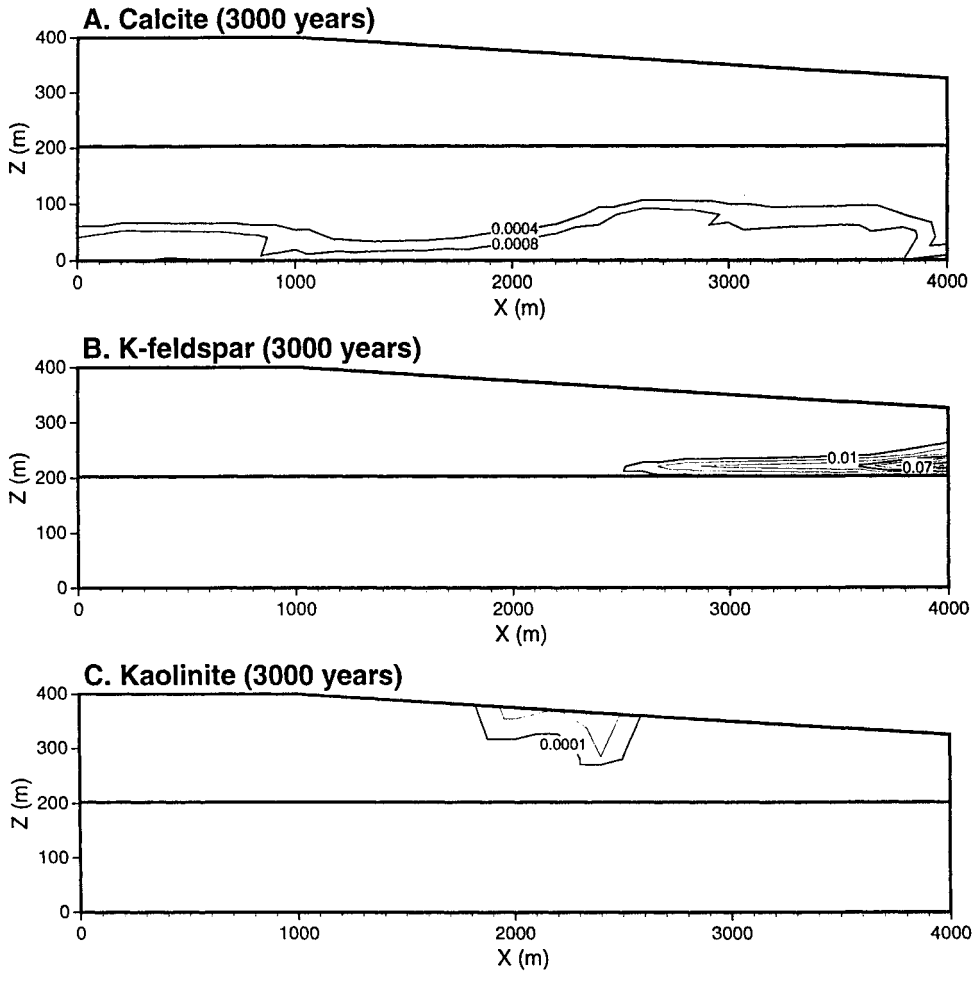


Fig. 33. Two-dimensional simulation results at 3000 years for a longitudinal dispersivity of 100 m. Concentration units are m/L b.p.m.

shown in Fig. 33. Calcite is dissolving from the sandstone, both where recharging water enters the sandstone from the shale, and where groundwater, now in equilibrium with calcite, crosses back into the shale near the discharge zone. Dispersion is again an important process; this result would not be anticipated if dispersion were not present. At the discharge end of the region, groundwater in equilibrium with the minor K-feldspar is entering the overlying shale, precipitating K-feldspar and dissolving muscovite (not shown) and kaolinite. Kaolinite is dissolving at both recharge and discharge ends of the basin, but at different rates. By 3000 years, all of the K-feldspar and most of the calcite has been dissolved from the sandstone, significant quantities of K-feldspar have precipitated in the discharge zone, and kaolinite remains only near the hinge line separating recharge and discharge areas. Figure 34 shows the results at 3000 yr for the same simulation, but with 200 m and

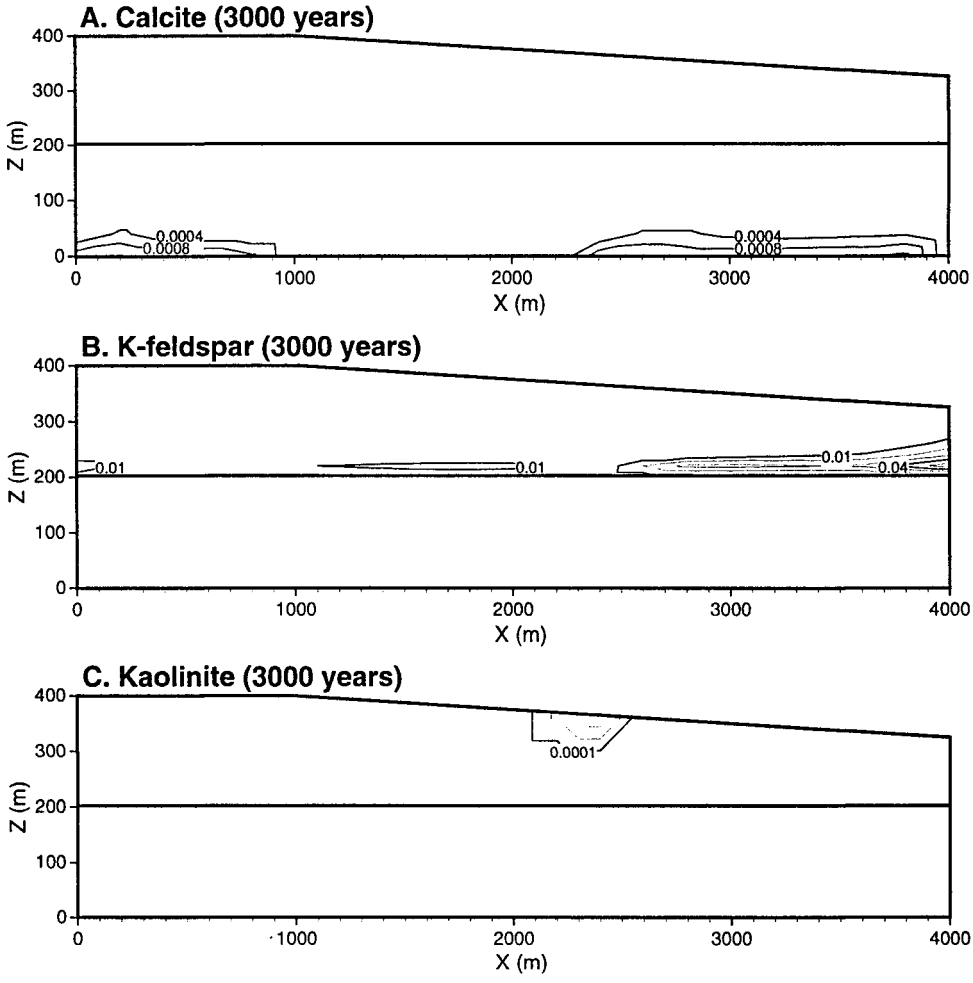


Fig. 34. Two-dimensional simulation results at 3000 years for a longitudinal dispersivity of 200 m. Concentration units are m/L b.p.m.

20 m longitudinal and transverse dispersivities, respectively. Increased dispersion increases the rate of calcite removal from the sandstone, and leads to the precipitation of K-feldspar along a greater length of the compositional boundary.

4.2.2. Sediment diagenesis

The study of sandstone diagenesis has significant impact on petroleum reservoir analysis and understanding the history of fluid flow and geochemical reactions in sedimentary basins (Bjorlykke et al., 1989; Bjorlykke and Egeberg, 1993). The source of cementing material and timing of cementation are important questions which remain unresolved (Blatt, 1979; McBride, 1989). Sediment diagenesis may involve relatively complicated geochemical reactions (Surdam et al., 1989; Ehrenberg, 1993), as well as a combination of mass transfer due to fluid flow and physical

compaction (Angevine and Turcotte, 1983; Houseknecht, 1987; Wood, 1989; Dewers and Ortoleva, 1990, 1991). In general, however, there is considerable evidence that significant fluxes of both energy and solute mass are involved in sediment diagenesis (Hardie, 1987; Sharp et al., 1988; Land, 1991; Gluyas and Coleman, 1992; Land and Macpherson, 1992; McManus and Hanor, 1993). Recently, the role of diagenetically-produced permeability variations has been suggested as a means of segregating sedimentary basin into individual fluid "compartments" (Hunt, 1990; Powley, 1990; Weedman et al., 1992; Deming, 1994; Dewers and Ortoleva, 1994).

Petroleum migration and accumulation in sedimentary basins are significant areas of study that have benefited from recent advances in coupling groundwater flow and reactive mass transport. Lee and Bethke (1994) developed paleohydrological models of compaction- and topographically-driven groundwater flow within the Denver basin in order to examine petroleum accumulation and diagenetic reactions in the Permian Lyons Sandstone. Their models included mineral precipitation and dissolution driven by fluid movement through temperature and pressure gradients, as well as mixing of fluids within the Lyons Sandstone, assuming local chemical equilibrium. Their analysis demonstrated important relationships between diagenetic facies observed in the sandstone and petroleum accumulation within the basin.

Another possible mechanism for diagenetic alteration of sandstones involves free or thermally-driven convection. Wood and Hewett (1982, 1984) developed a quantitative analytical model for diagenetic cementation which established possible patterns of cementation, and suggested time scales for quartz cementation and accompanying porosity changes. As fluids circulate through temperature gradients, minerals are preferentially dissolved or precipitated. Since quartz solubility increases with temperature, quartz will dissolve where fluid flow is up the temperature gradient and will precipitate (ignoring kinetic inhibition) where flow is down the temperature gradient (Fig. 35). Minerals exhibiting retrograde solubility (such as calcite) should simultaneously precipitate in regions where quartz dissolves. Over geological time the flow pattern itself may be modified as porosity, and hence permeability, are altered as a result of diagenetic cementation (Wood and Hewett, 1982). Other studies have refined this general picture (Palm, 1990; Ludvigsen et al., 1992).

Diagenesis produced by gradient reactions, such as suggested by Wood and Hewett (1982, 1984) do not necessarily require the presence of free convection. Wood (1986), Wood and Hewett (1986), and Hewett (1986) examined the role of forced convection through temperature fields, generally in the context of folded sandstone layers. These studies developed analytical solutions to the governing transport equations, using a single chemical component and assuming local chemical equilibrium. These studies noted that the rate of diagenetic alteration is proportional to the quantity $|\mathbf{v} \cdot \nabla T|$ (Phillips, 1991). Complete depletion of individual minerals can produce propagating reaction fronts, which may affect dissolution and precipitation rates both downstream and upstream of the fronts (Figs. 36 and 37).

Davis et al. (1985) developed analytical solutions for single component mass

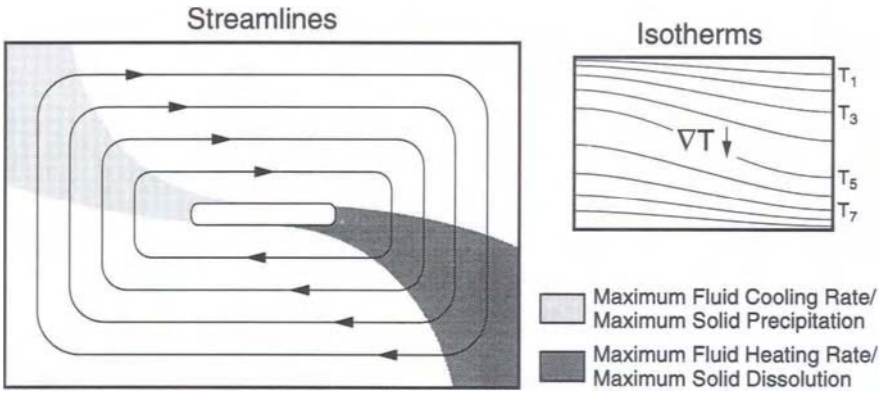


Fig. 35. Source/sink regions for diagenetic quartz cementation due to free convection in a sandstone layer (Re-drafted from Geochimica et Cosmochimica Acta, Volume 46, Wood, J. R., and T. A. Hewett, Fluid convection and mass transfer in porous sandstonesfla theoretical model, pages 1707–1713, Copyright (1982), with kind permission from Elsevier Science Ltd, The Boulevard, Langford Lane, Kidlington 0X5 1GB, UK).

transfer and transport due to free convection in domed sheets. In this case, variations in thermal conductivity between the layers and the surrounding material created lateral temperature gradients, driving free convection within the (permeable) sheets. The patterns of diagenesis produced (Figure 38) show maximum precipitation and dissolution rates occurring where maximum slopes are found, but with strong variations vertically across the layer, depending on whether fluid flow was up or down the temperature gradient. The dynamics of this system were found to depend strongly on the geometry of the layer, and the ratio of thermal conductivities of the layer and surrounding rocks.

A significant question in all of the work discussed above has involved the time scales for significant porosity (and permeability) modification. Wood and Hewett estimated that a 50% reduction in porosity could occur within 3.5 Ma (million years). However, the analytical solutions involve several simplifications, and most notably, ignore the feedback between the porosity/permeability changes and the flow field. Raffensperger (1993) reported the results of a fully coupled simulation involving variable-density fluid flow, heat transport, and reactive mass transport for a system involving quartz and calcite, two common minerals that together form the bulk of the diagenetically-produced pore filling in sandstones (Blatt, 1979). The results of a similar calculation, involving only quartz, are shown in Fig. 39. The domain for the problem is a 100 m square box consisting initially of 80 volume percent quartz (176.4 mol/L) and 20% porosity. The domain is discretized using 441 nodes (21 by 21) for a total of 800 elements. No-flow boundaries are assumed for all sides. The bottom boundary is assigned a constant temperature of 155°C and the top boundary is assigned a constant temperature of 150°C. The hydraulic conductivity is assumed to be isotropic and is initially 330 m/yr ($\approx$1 darcy). The longitudinal and transverse dispersivities are 2.5 and 0.5 m, respectively. Initially, the maximum average linear velocity is approximately 9 m/yr.

This simplified geometry ignores certain aspects of real geological systems which

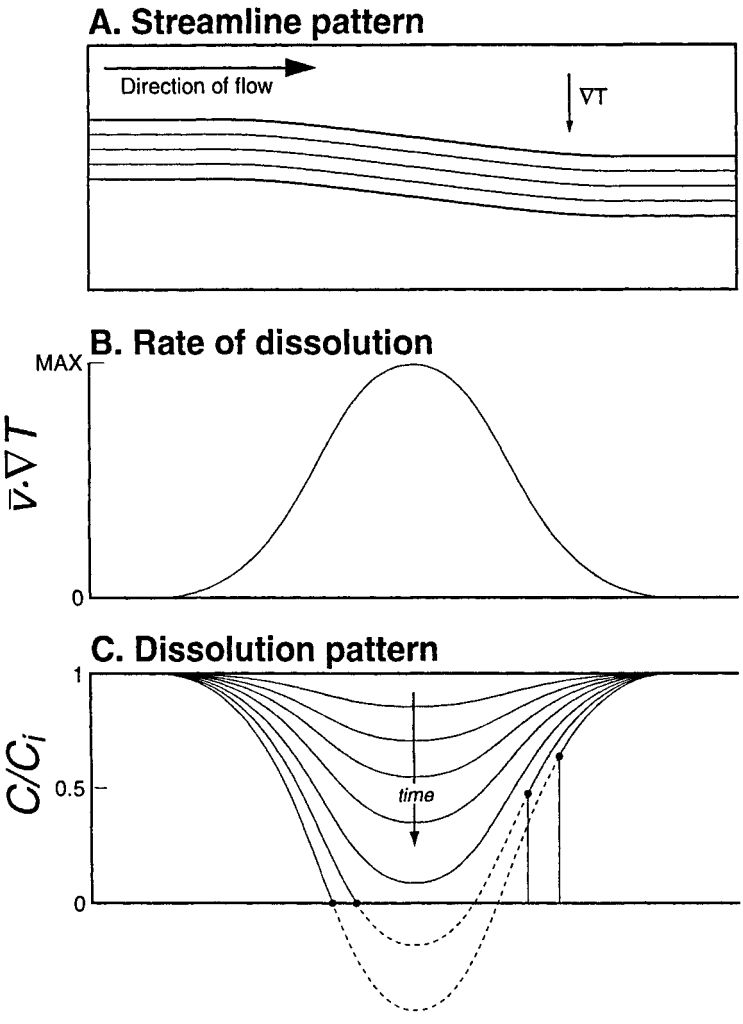


Fig. 36. Theoretical prediction of diagenetic behavior resulting from fluid flow through a gently folded layer (monocline), showing streamlines (A), relative dissolution rate produced by fluid warming (B), and the pattern of dissolution within the layer at various times (C). The dashed lines in (C) indicate the values that would be obtained if mass transfer to negative values were physically possible. Once complete removal has occurred in the middle of the monocline, reaction fronts propagate both forward and backward of the point of maximum dissolution, but at different rates. Based on an analytical solution to the advection-reaction equation for a single mineral phase, assuming local chemical equilibrium (Hewett, 1986).

must be mentioned. First, permeable layer thicknesses may be less than 100 m, although sandstone thicknesses greater than 2 km are found in Proterozoic basins in Canada and Australia (Raffensperger, 1993). Thin permeable beds may produce calculated convection velocities of only cm/yr (Rabinowicz et al., 1985), or, if interbedded with low permeability units, may be too thin to allow free thermal convection (Bjorlykke et al., 1988). However, beds as thin as 2 m in the North Sea

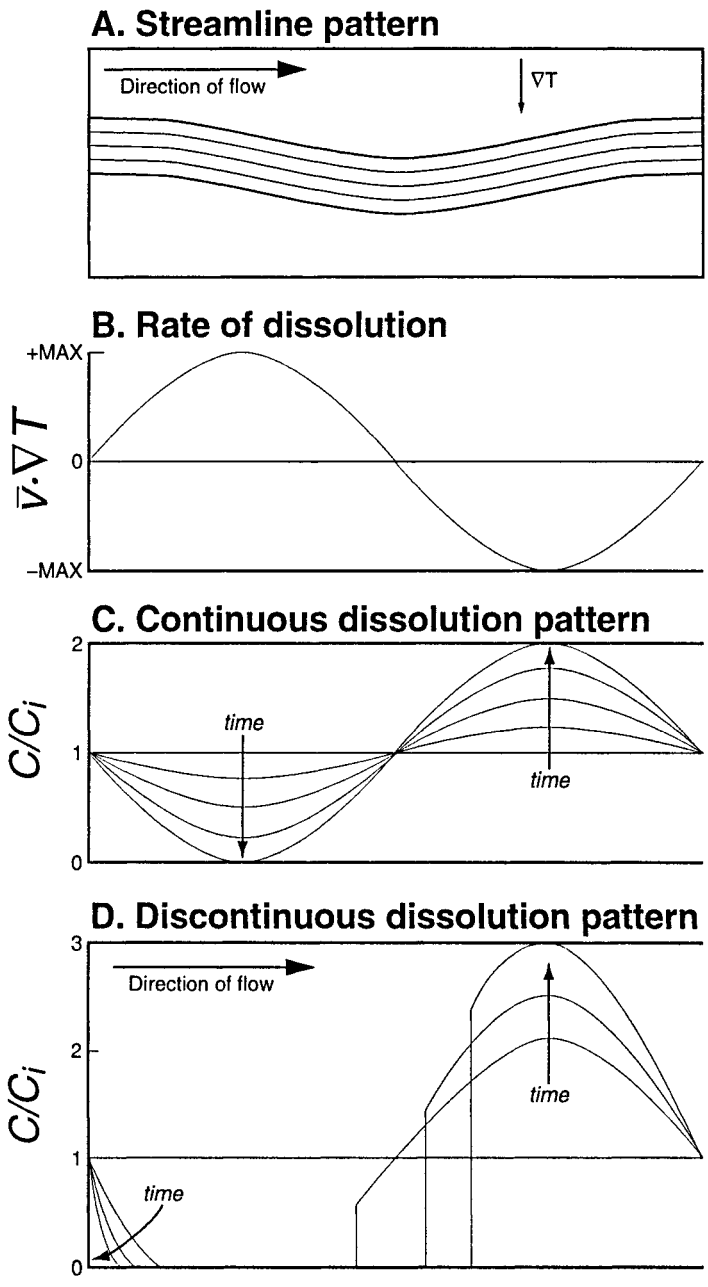


Fig. 37. Theoretical prediction of diagenetic behavior resulting from fluid flow through a gently folded layer (syncline), showing streamlines (A), relative dissolution rate produced by fluid warming (B), and the pattern of dissolution within the layer at various times for continuous (C) and discontinuous (D) dissolution. In the case of continuous dissolution (C), maximum precipitation (dissolution) rates occur at the points of maximum layer slope, corresponding to the positions of maximum cooling (warming). For the discontinuous case (D), once complete removal has occurred at the center of the left portion of the syncline, reaction fronts propagate both forward and backward of the point of maximum dissolution, but at different rates. Based on an analytical solution to the advection-reaction equation for a single mineral phase, assuming local chemical equilibrium (Hewett, 1986).

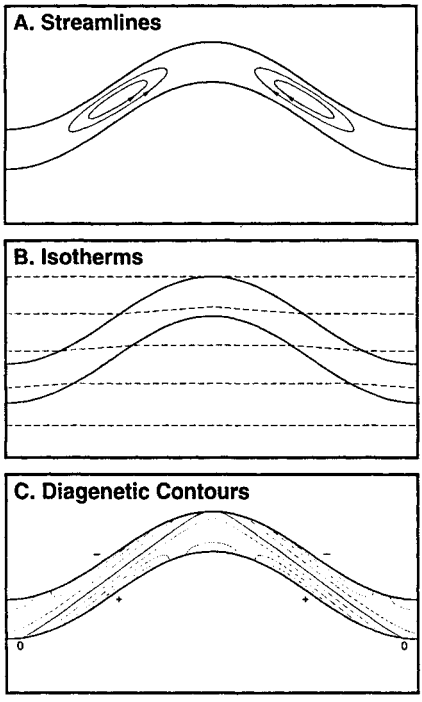


Fig. 38. Theoretical prediction of diagenetic behavior resulting from free convection in a gently folded layer (anticline), showing streamlines (A), isotherms (B), and the pattern of dissolution and precipitation within the layer (C). The geometry of the free convection in (A) is based on the assumption that the layer has a lower thermal conductivity than the surrounding material. Maximum rates of precipitation and dissolution occur where the slope of the layer is greatest, with precipitation occurring where fluid circulation is upward (cooling) and dissolution occurring where fluid circulation is downward (warming). Based on an analytical solution to the advection-reaction equation for a single mineral phase, assuming local chemical equilibrium (after Davis et al., 1985, reprinted by permission of American Journal of Science).

have been observed (Haszeldine et al., 1984) with authigenic quartz distributions mimicking the pattern described by Wood and Hewett (1982). Secondly, the assumption of impermeable boundaries at 100 m intervals is generally not valid for most geological systems; the results to be discussed in this section would most likely be altered in form if infinite or semi-infinite boundary conditions were used. Impermeable boundaries simply serve to confine the calculations to a single initial free convection cell.

For times less than 3 Ma, the distribution of quartz as a function of time (Fig. 39) resembles the pattern predicted by Wood and Hewett (1982) and Rabinowicz et al. (1985), which might be predicted on the basis of the simple argument that zones of maximum precipitation or dissolution should coincide with regions of maximum $|\mathbf{v} \cdot \nabla T|$. However, this argument is complicated by the fact that the flow pattern evolves as porosity and permeability change. This demonstrates the nature of the geochemical coupling between reactions and fluid flow. As a result of this feedback, the region of quartz dissolution in the lower right is more

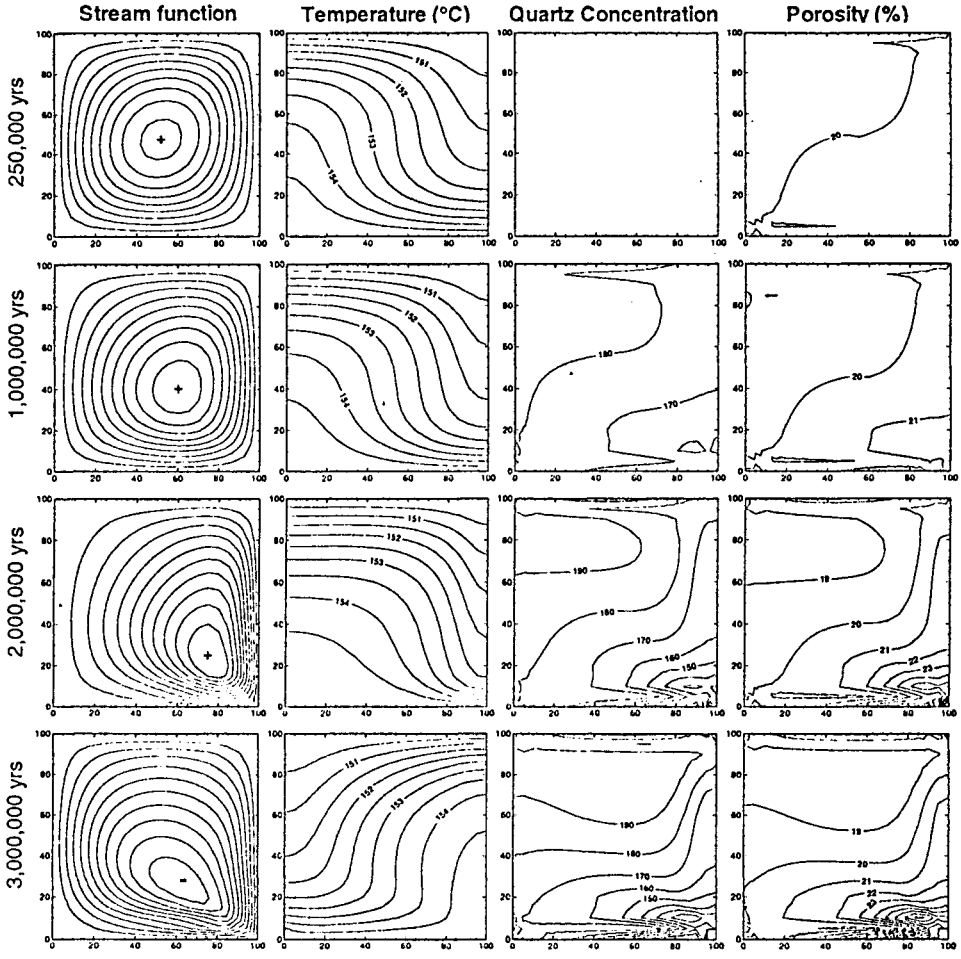


Fig. 39A,B. Fully coupled numerical simulation of diagenesis in a sandstone layer produced by free convection, showing streamlines, temperatures, quartz concentrations (mol/L), and porosity for times 0–3 Ma (million years; A) and 4–6 Ma (B). Convection is initially clockwise, but reverses between 2 and 3 Ma, when significant dissolution at the lower right has occurred. Between 5 and 6 Ma, the single convection cell is no longer stable, and two cells develop. The resulting patterns of diagenesis are extremely complicated, although in general precipitation occurs throughout a greater volume than dissolution as a result of feedback coupling.

concentrated due to the positive feedback between flow and dissolution producing focusing of flow (Steefel and Lasaga, 1990). Negative feedback in the region of quartz precipitation (upper left) produces a more diffuse pattern.

Changes in permeability are reflected in the evolution of the pattern of groundwater flow, which in turn alters the temperature profile. At 2 Ma, the streamline pattern indicates enhanced groundwater flow rates in the lower right (Fig. 39A). Overall, the fluid mass flux in the region has increased. Between 2 and 3 Ma, the flow pattern changes radically, such that the sense of convection is reversed. At 3 Ma, the maximum average linear velocity approaches 30 m/yr.

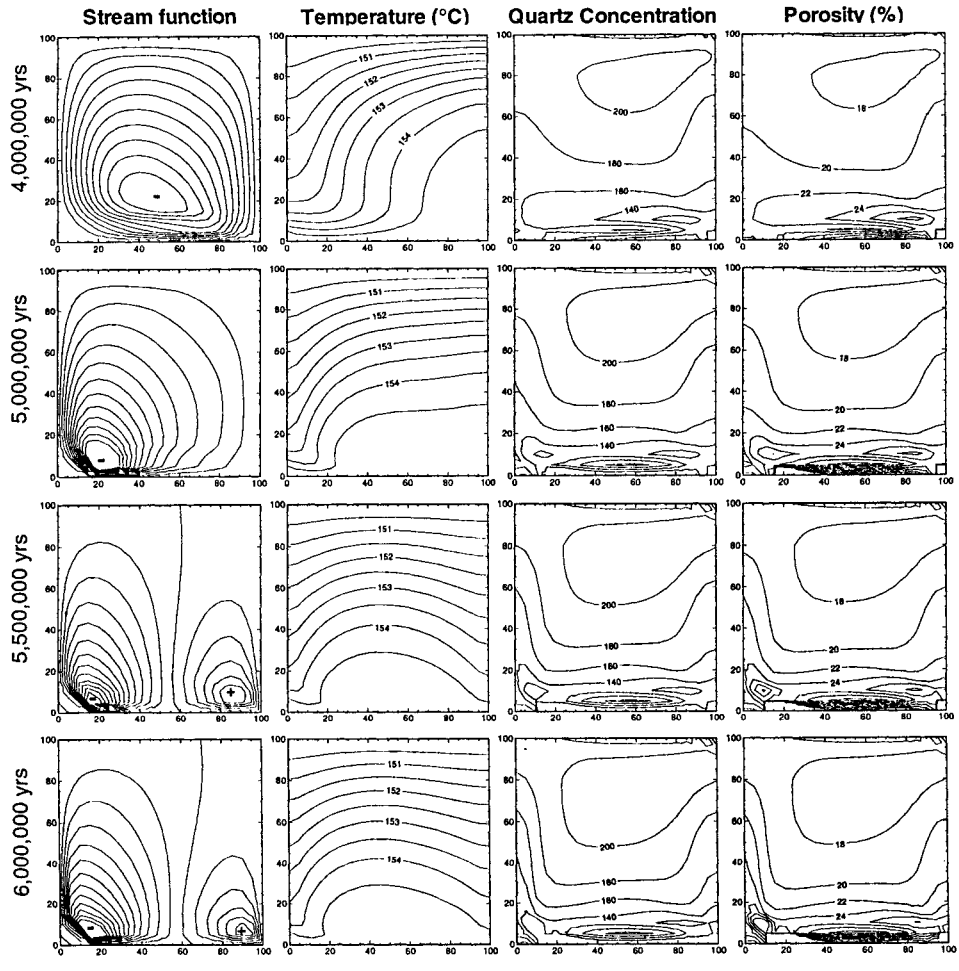


Fig. 39A,B. Continued.

Between 5 and 5.5 Ma, the pattern of flow again changes, as a single convection cell becomes unstable and two counter-rotating cells develop. The particular flow geometry observed after 5 Ma is partly a result of the domain geometry and imposed side boundary conditions, and will differ in more realistic domains. However, the fact that the flow pattern will evolve in some manner similar to this may be expected, due to the feedback. As a result, the potential exists for significantly more complicated and pervasive patterns of diagenetic cementation over geological time. These calculated patterns of diagenetic cementation indicate the importance of feedback coupling over geological time. In this regard, minerals with highly temperature-dependent solubilities will be especially important. Finally, the fact that the cementation patterns and flow system will co-evolve suggests that prolonged free convection might be capable of extensively cementing the sandstone.

Relatively little work has addressed this issue of the feedback between mineral-

ogical alteration and fluid flow, although the results shown in Fig. 39 indicate the potential importance of the coupling. Several studies have examined the reactive-infiltration instability, in which flow is focused into high-permeability zones, producing enhanced dissolution (Ortoleva et al., 1987; Hinch and Bhatt, 1990; Steefel and Lasaga, 1990; Wei and Ortoleva, 1990). Other studies have examined the formation of chemically- and physically-produced seals promoting zones of abnormally high pressure in sedimentary basins (Dewers and Ortoleva, 1994; Ortoleva et al., 1995). In their study of the Denver Basin, Lee and Bethke (1994) noted an association in time and space of oil migration and fluid mixing producing diagenetic alteration within the Lyons Sandstone. They suggested that since migration and diagenetic cementation were so closely linked, subsequent migration of petroleum was probably inhibited by cementation-reduced porosity and permeability of the reservoir. The diagenetic alteration halos surrounding unconformity-type uranium mineralization (Section 4.2.4) display significantly reduced porosity and permeability, which may have acted both to halt uranium mineralization and to preserve the ores for more than 1300 Ma (Raffensperger and Garven, 1995b; Raffensperger, in press).

4.2.3. Mixing-zone reactions in carbonate aquifers

Mixing of fluids with different chemical compositions has been suggested as a mechanism responsible for a variety of geochemical processes altering sediments and sedimentary rocks in basins. Examples include sediment-hosted ore deposits (Goldhaber et al., 1983; Anderson, 1991; Hofstra et al., 1991) and geochemical processes occurring in coastal mixing zones (Hanshaw et al., 1971; Badiozamani, 1973; Ward and Halley, 1985; Back et al., 1986; Stoessell et al., 1989; Wicks and Herman, 1994; Sacks et al., 1995; Wicks et al., 1995). Most geochemical models of mixing processes ignore the spatial distribution of mixing reactions. However, Sanford and Konikow (1989b) approached the problem of carbonate dissolution in coastal mixing zones using a fully coupled numerical model of variable-density groundwater flow and geochemical reactions (described in Section 2.2.6). Their results indicated that significant porosity enhancement should occur at distinct positions within the mixing zone, as long as the aquifer is homogeneous (Fig. 40A). When heterogeneity is included, however, this pattern is no longer observed. Although the mixing zone is still the region experiencing carbonate dissolution, significant porosity enhancement is focused at initially permeable zones (Fig. 40B). As a result of the feedback between the flow system and geochemically-produced porosity enhancement and destruction, the position of the mixing zone tends to migrate landward with time (Fig. 40D).

4.2.4. Unconformity-type uranium ores

More than 25% of known uranium resources are of Early to Middle Proterozoic age (1300–1600 Ma), associated with unconformable contacts between Archean-Early Proterozoic metasedimentary rocks and overlying Middle Proterozoic sandstones. The majority of these deposits are found within the Athabasca Basin, northern Saskatchewan, Canada, and the McArthur Basin, Northern Territory, Australia. These unconformity-type deposits are unique in their age, lithological

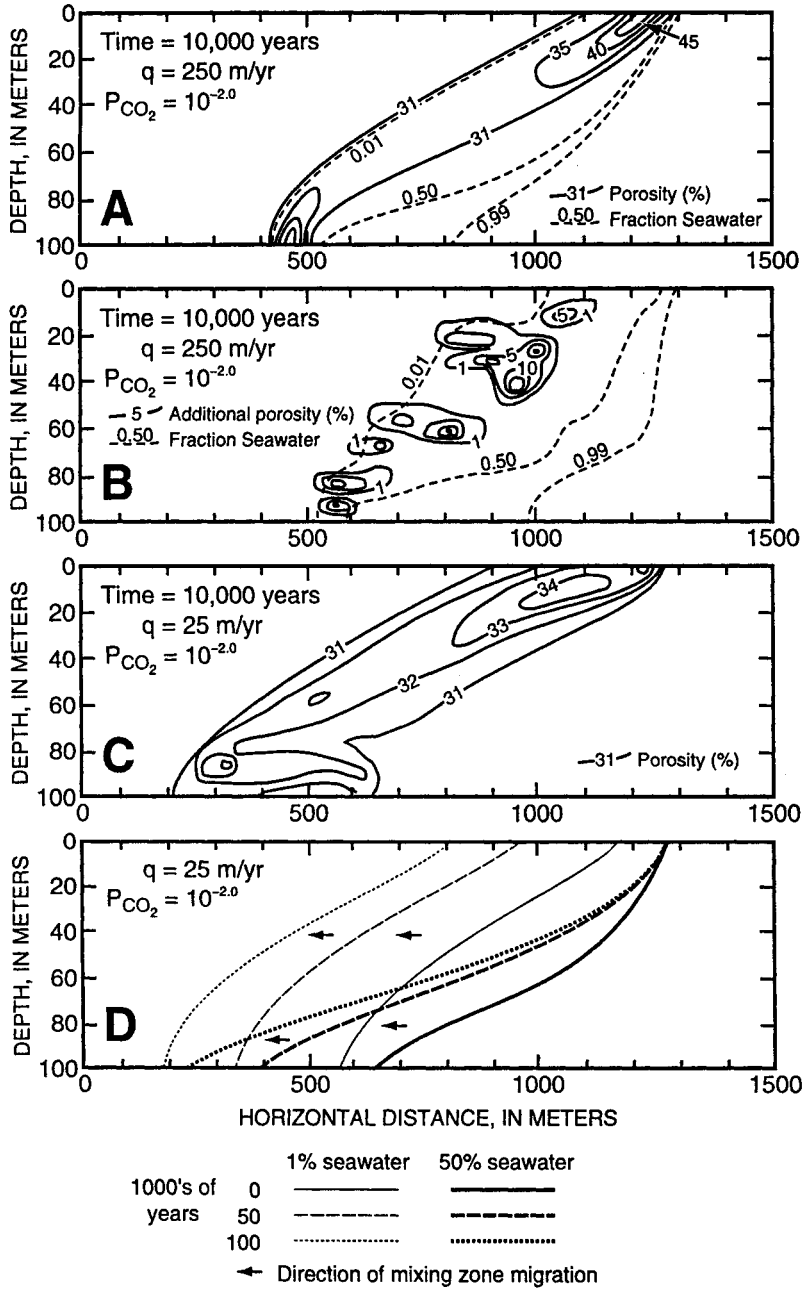


Fig. 40. Numerical simulations of variable-density groundwater flow and reactive mass transport, showing porosity evolution within the seawater mixing zone of a homogeneous (A) and heterogeneous (B) coastal carbonate aquifer. The freshwater inflow rate (q) is 250 m/yr in both simulations. In the homogeneous case (A), dissolution is most pronounced at the base and top of the mixing zone. This pattern, however, is strongly modified when heterogeneity is considered (B). Fully coupled simulations, allowing feedback between the flow system and evolving porosity-permeability structure, demonstrate the dynamic nature of the flow pattern (D) resulting from porosity modification (C; after Sanford and Konikow, 1989b).

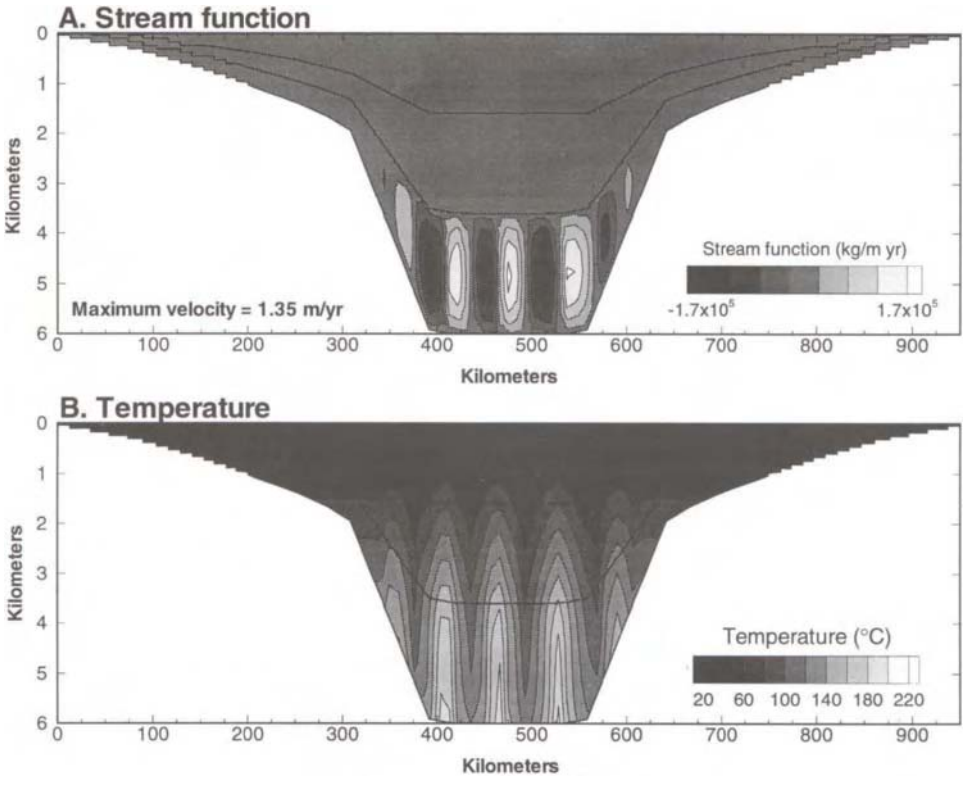


Fig. 41. Simulation of basin-scale free convection in a conceptual Proterozoic sandstone basin: contours of the stream function (A), and contours of temperature (B). The maximum average linear velocity is 1.3 m/yr, and lighter shades (warmer colors) indicate clockwise convection (in A). The contour interval for temperature (C) is 20°C (after Raffensperger and Garven, 1995a, reprinted by permission of American Journal of Science).

associations, and alteration history. Some workers favor a hydrothermal-diagenetic model for the formation of these deposits in which warm basinal brines encounter reducing conditions at or near the unconformity as they circulate within the basin (Hoeve and Sibbald, 1978; Hoeve and Quirt, 1984).

Raffensperger and Garven (1995a, 1995b) examined the diagenetic-hydrothermal hypothesis for the formation of unconformity-type uranium deposits using a series of numerical calculations of coupled variable-density groundwater flow and heat transport in a generic intracratonic sedimentary basin. They examined the relative contribution of alternative driving mechanisms (gravity/forced convection, free convection) to the possible evolution of the hydrological system, and found that free convection is a viable mechanism for driving regional scale groundwater flow within a sandstone-rich sedimentary basin (Fig. 41). Horizontal hydraulic conductivities as low as 50 m/yr ($K_x/K_z = 100$) were shown to be sufficient to drive m/yr fluid convection at depths of 3 to 6 km. The most important factors influencing flow pattern geometry were found to be basin geometry and hydrostratigraphy.

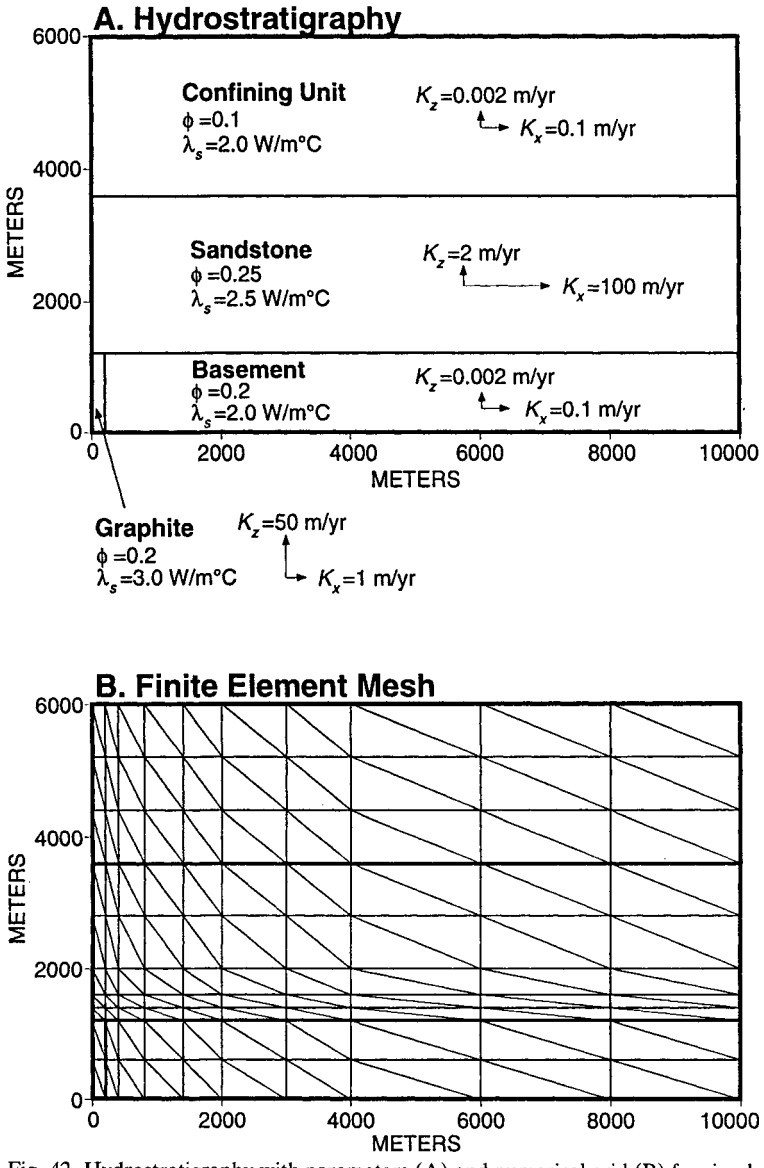


Fig. 42. Hydrostratigraphy with parameters (A) and numerical grid (B) for simulation of unconformity-type uranium mineralization (after Raffensperger and Garven, 1995b, reprinted by permission of American Journal of Science).

The permeability and anisotropy of the sandstone were found to control flow rate and convective cell geometry, respectively.

Simulations of reactive mass transport within a single free convection cell (Fig. 42) were performed using the predictor-corrector scheme described in Section 3.2.6. These results indicate that free convection within a sedimentary basin of a uranium-bearing chloride brine, under moderately oxidizing conditions, may

precipitate ore-grade quantities of uraninite in the vicinity of the unconformity between basin sandstones and basement graphite schists (Fig. 43). Temperatures at the unconformity are elevated by vertical flow of groundwater, reaching nearly 190°C (Fig. 43B). Moderate concentrations of aqueous uranium in the form of uranyl-chloride complexes and flow rates on the order of 1 m/yr are sufficient to produce significant quantities of ore within 10^5 to 10^6 yr.

Changes in mass composition associated with the alteration halos around the ore deposits were found to result from mass transport through temperature gradients and across compositional boundaries (Fig. 44). Once chemical reaction fronts develop due to dispersion across the unconformity, they propagate in the direction of flow until they stabilize at the point of focused groundwater flow above the unconformity. The form of this alteration can not be predicted by simpler equilibrium speciation or reaction-path models, and indicates the importance of modeling reactive mass transport in order to understand large-scale geochemical change over geological time. An additional result of this work was the conclusion that the three classes of transport-controlled reactions presented by Phillips (1990), isothermal reaction fronts, gradient reactions, and mixing reactions, were all involved in the formation of unconformity-type uranium deposits.

5. Summary

Sedimentary basins represent large-scale porous media, and are important hosts to a significant portion of the world's economic energy and mineral resources. Many sedimentary basins have been extensively explored in search of these resources. At present, much of what we know about the geochemistry and hydrogeology of sedimentary basins is the direct result of explorations efforts. Coupled with this is our interest in how these resources accumulated, both as a scientific question and in order to improve exploration strategies. Over the past ten years, renewed interest in crustal-scale fluid flow and transport processes (National Research Council, 1990; Torgersen, 1990, 1991), continental-scale fluid migration and ore-forming processes (Sverjensky and Garven, 1992), coupled processes associated with nuclear waste disposal (Tsang, 1987), and basin hydrodynamics (Belitz and Bredehoeft, 1988; Harrison and Summa, 1991; Ge and Garven, 1992; Person and Garven, 1992; Dewers and Ortoleva, 1994), and concurrent concern with contaminant transport in the near subsurface (Brusseau, 1994), has led to the development of sophisticated models that couple hydrogeological, geochemical, mechanical, and thermal processes. This paper has reviewed these developments, focusing on coupled numerical models of reactive solute transport that have been developed and applied to processes occurring over long distances and times in sedimentary basins.

Processes occurring in sedimentary basins include groundwater flow, heat transport, and reactive mass transport. Quantitative models of flow and transport in these settings can provide insight into the processes that control the evolution of sedimentary basins by enabling the examination of processes that may occur too

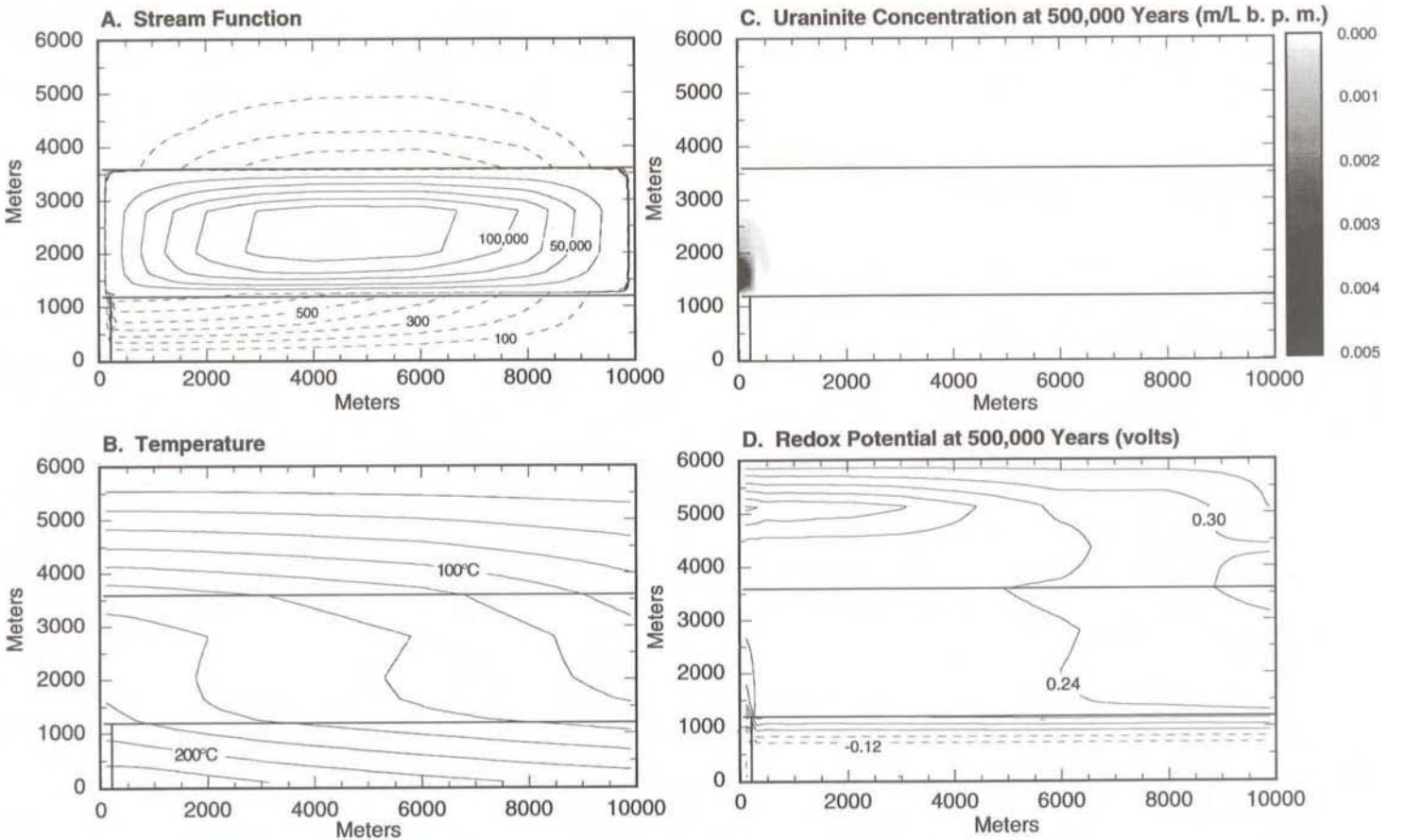


Fig. 43. Calculated steady state streamlines (A), temperature (B), uraninite precipitated (C), and *Eh* (D) for the reactive solute transport simulation. Flow is clockwise in (A). The contour interval is 25,000 kg/m yr (100 kg/m yr for dashed lines) for the stream function, 20°C for temperature, and 0.06 volts for *Eh*. Units are moles/L bulk porous medium for concentration (C), and solid lines indicate unit boundaries (after Raffensperger and Garven, 1995b, reprinted by permission of American Journal of Science).

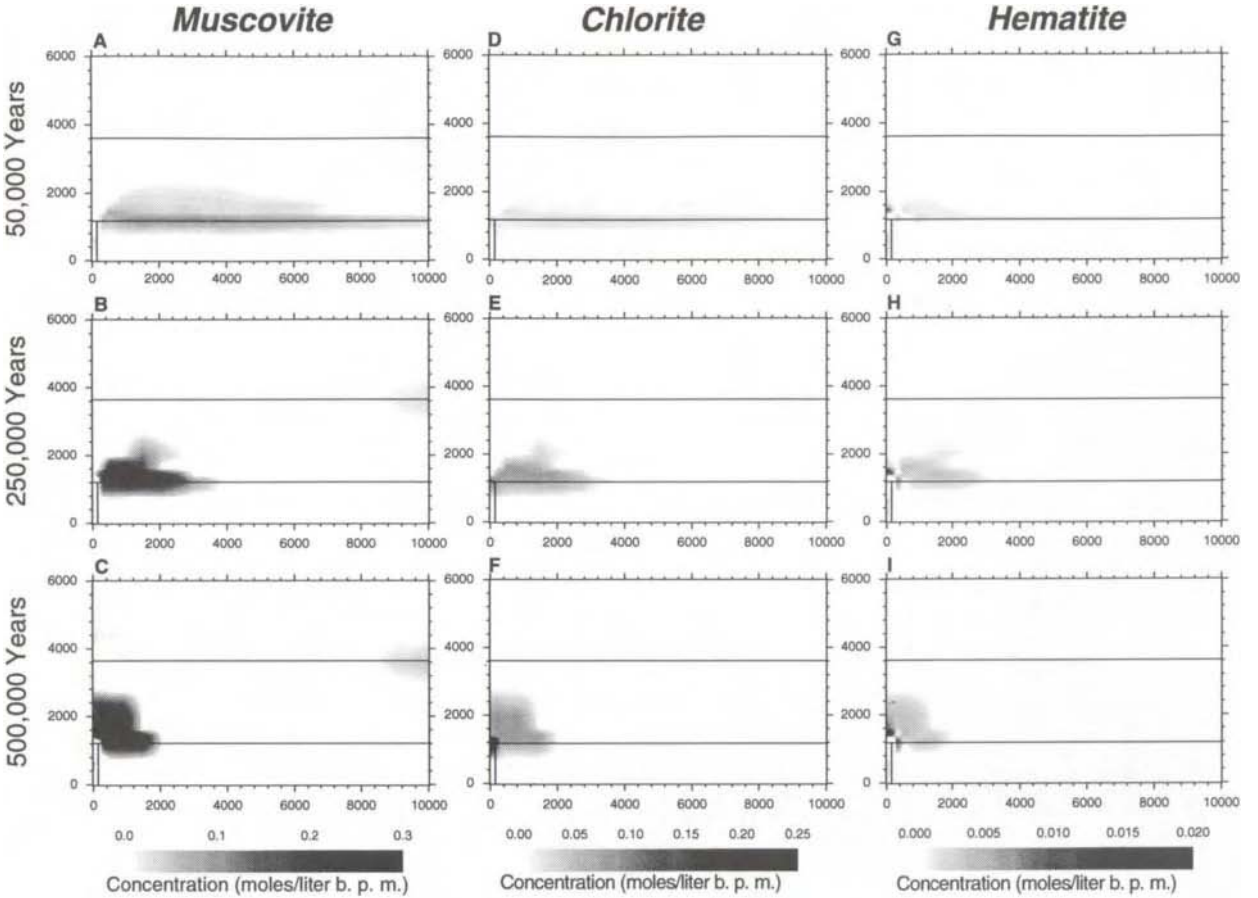


Fig. 44. Calculated patterns of alteration accompanying unconformity-type uranium mineralization showing amounts of muscovite (A-C), chlorite (D-F), and hematite (G-I) precipitated at various times, indicated to the left. Axes units are meters, and solid lines indicate hydrostratigraphic boundaries (after Raffensperger and Garven, 1995b, reprinted by permission of American Journal of Science).

slowly to be observed in the field or laboratory. In many cases, such models may be the only available tool for studying processes occurring over geological time and space scales (Bethke, 1989; Person et al., 1996). Geochemical equilibrium speciation codes and reaction path codes have been developed in order to understand the nature of geochemical reactions, but generally neglect important mass transport processes. Only by considering coupled mass transport and geochemical reactions can we hope to fully understand the temporal and spatial evolution of these complex systems. In addition, it may be suggested that coupled hydrochemical models, which are potentially capable of testing hypotheses regarding fluid flowpaths in the subsurface, may be used to address the central question of fluid flow mechanisms in the deep subsurface.

It is important to consider the behavior of the processes occurring in sedimentary basins simultaneously, since they are generally coupled. Groundwater flow is controlled by the boundary conditions and the distribution of hydraulic conductivity; as a result, flow velocities vary spatially and temporally. This circulation is capable of transporting thermal energy and dissolved mass. In general, flow rates will be sufficiently small that the water will reach approximate equilibrium with each lithology along the flow path at the ambient temperature and pressure. These successive equilibria produce changes in the chemical composition of the fluid, resulting in reactions with the medium (i.e., precipitation, dissolution), which in turn modify the porosity and permeability. This modification may be insignificant at a human time scale, but very significant at the geological time scale.

The hydrogeological flow field then is a coupled hydrological-thermal-geochemical system, requiring solution to three sets of coupled partial differential equations. More correctly, mechanical processes (e.g., compaction, fracturing, faulting) must also be considered as an additional set of coupled equations (Bethke, 1985; Ge and Garven, 1992). These processes have been incorporated into numerical models of fluid flow and heat transport in sedimentary basin settings (Bethke, 1985; Dewers and Ortoleva, 1990; Ge and Garven, 1992; Person and Garven, 1992); their exclusion from this discussion results from the fact that very few models have been developed to address the complete interaction between these processes. Exceptions to this observation are summarized in Ortoleva (1994). Various numerical solution procedures have been described in the literature, which often use the finite difference or finite element method. The central concerns of research in this area over the past decade have involved the development of accurate and computationally efficient algorithms for solving large sets of nonlinear coupled equations. It is recognized that significant advances in this area have been made in a number of fields. The most common approach to solving the reactive mass transport equations has been based on the approximation or assumption of local chemical equilibrium, which represents simply an end-member case in the broader spectrum of kinetically-controlled geochemical reactions. This approach has been favored for a number of reasons, and arguments regarding its validity for problems involving large time- or length-scales have been made in the literature. However, ultimately an assumption this dramatic will provide only an approximate description of the real processes. Recent work by Steefel and Lasaga (1992, 1994), and the development of the quasi-stationary state approximation by Lichtner (1988,

1991, 1992), have demonstrated the feasibility of incorporating kinetically-controlled reactions into models of mass transport, even for large-scale problems.

Applications of coupled models to a variety of geological problems, such as the propagation of mineral reaction fronts, have noted the importance of hydrodynamic dispersion and its control on the spatial distribution of reaction rates and products. As a result, neglecting hydrodynamic dispersion may, in some cases, lead to inaccurate predictions of mineral reaction zones. At the scale of a large sedimentary basin (10's to 100's of kilometers), macroscopic dispersivities may be large since in general numerical transport models involve discretizing the basin into blocks or elements that are large (100's of meters to kilometers), thus homogenizing and removing smaller-scale heterogeneity. How dispersion at the scale of a sedimentary basin is to be measured and incorporated into hydrogeological transport models remains a significant question.

Relatively few two-dimensional simulations are available in the literature, and virtually no studies have involved simulations of coupled flow and heat and reactive mass transport at the scale of an entire sedimentary basin. Rather, portions of the system tend to be isolated for study. These studies have noted the importance of transport-controlled reaction-front propagation, fluid mixing and gradient reactions, which all occur to varying degrees in a heterogeneous sedimentary basin. Future developments and extension of these models to entire basins will require greater computer capability, but the work reviewed to date demonstrates that quantitative study of coupled hydrological, geochemical, and thermal processes in evolving sedimentary basins is currently possible. Eventually, three-dimensional models, which have been developed for contaminant transport problems (Burr et al., 1994) as well as for flow and heat transport (Woodbury and Smith, 1985; Garven and Toptygina, 1993) may be expanded to include geochemical reactions of importance in sedimentary basins and which may be applied to large-scale problems. Use of supercomputers and parallel or vector-based algorithms has received some interest in the recent literature (Bethke et al., 1988; Tompson et al., 1989; Barry, 1990; Tripathi and Yeh, 1993; Williams, 1994; Zhang et al., 1994), which may eventually allow complicated three-dimensional problems to be addressed.

Finally, the role of hydrogeological heterogeneity remains a fundamental problem when considering flow and transport processes in the subsurface. Heterogeneity not only directly impacts calculated patterns of mineral alteration (Sanford and Konikow, 1989b; Gerdes et al., 1995), but has other implications as well. When addressing our capability to model heterogeneous systems at large space and time scales, the question of grid resolution becomes important. At this point in time, it seems unlikely that natural geological heterogeneity at the meter scale or smaller can be incorporated in modeling efforts at the 10's to 100's of kilometers scale. As long as this remains an obstacle, the question of adequate scaling relationships for parameters such as dispersivity and permeability remains crucial. Future improvements in our understanding of basin-scale hydrochemical processes will require careful consideration of natural heterogeneity, and will likely focus increasing attention on application to field settings where sufficient data exist to eliminate, or at least reduce, large-scale parameter estimation uncertainty.

Glossary

The following list includes dimensions (M, mass; L, length; T, time; θ, temperature), but not units, which may be specific to the particular models discussed in the review. Variables occurring only once are defined within the text. Other variables which are infrequently used, especially those presented in Section 3.3, are also not included.

a_{H_2O}	activity of liquid water.
a_m	activity of solid species.
$[A]$, A_{nm}	global stiffness matrix for groundwater flow.
A^e_{nm}	local stiffness matrix for groundwater flow.
c	designation for an aqueous component species.
$\hat{c}$	number of aqueous component species.
c_i	mass concentration of species i.
c_f	heat capacity for the fluid, $L^2\ T^{-2}\ \theta^{-1}$.
c_s	heat capacity for the solid, $L^2\ T^{-2}\ \theta^{-1}$.
C	solute concentration, $M\ L^{-3}$.
$\hat{C}$	trial function for solute concentration.
$[C]$, C_{nm}	global storage matrix for groundwater flow.
C^e_{nm}	local storage matrix for groundwater flow.
$\mathbf{D}$, D_{ij}	dispersion tensor, $L^2\ T^{-1}$.
D_L	longitudinal dispersion coefficient, $L^2\ T^{-1}$.
D_T	transverse dispersion coefficient, $L^2\ T^{-1}$.
$D_{xx} \ldots D_{zz}$	components of dispersion tensor, $L^2\ T^{-1}$.
$\mathbf{D}_m$	mechanical dispersion tensor, $L^2\ T^{-1}$.
D^d_i	molecular diffusivity, $L^2\ T^{-1}$.
D^*	effective molecular diffusivity, $L^2\ T^{-1}$.
Da	dimensionless Damköhler number.
$[E]$, E_{nm}	global stiffness matrix for solute transport.
E^e_{nm}	local stiffness matrix for solute transport.
$[F]$, F_{nm}	global storage matrix for solute transport.
F^e_{nm}	local storage matrix for solute transport.
$\mathbf{g}$, g	gravitational acceleration constant, $L\ T^{-2}$.
$\{G\}$, G_n	global solute flux array.
h	hydraulic head, L.
$\hat{h}$	trial function for hydraulic head.
$\mathbf{J}$	flux term, $M\ L^{-2}\ T^{-1}$.
$\mathbf{k}$, k	intrinsic permeability, L^2.
k_i	initial intrinsic permeability, L^2.
k_m	rate constant for a mineral reaction, moles $L^{-2}\ T^{-1}$.
K	equilibrium constants for secondary aqueous species.
$\mathbf{K}$	hydraulic conductivity tensor, $L\ T^{-1}$.
$K_{xx} \ldots K_{zz}$	components of hydraulic conductivity tensor, $L\ T^{-1}$.
K^{sp}	solubility product.
K^w	equilibrium constant for the dissociation of water.
l^e	length of element boundary, L.
l_e	equilibration length, L.
m	designation for a solid species.
$\hat{m}$	number of solid species.
M_{OH^-}	concentration of OH^-, molarity.
M_{H^+}	concentration of H^+, molarity.
M_c	concentration of aqueous component species, molarity.
M^T_c	total analytical concentration, molarity.
$\{M^T_c\}$	array of nodal total analytical concentrations, molarity.

$M^T_{c,\mathrm{aq}}$	total aqueous concentrations, molarity.
$\{M^T_{c,\mathrm{aq}}\}$	array of nodal total aqueous concentrations, molarity.
$M^T_{c,\mathrm{sol}}$	total solid concentration, molarity.
$\{M^T_{c,\mathrm{sol}}\}$	array of nodal total solid concentrations, molarity.
M_m	concentration of solid species, molarity.
M_s	concentration of secondary aqueous species, molarity.
$\mathbf{n}$	unit normal vector.
p	fluid pressure, M L^{-1} T^{-2}.
pH	pH value.
Pe	dimensionless Peclet number.
$\mathrm{Pe_T}$	dimensionless thermal Peclet number.
$\mathbf{q}$	specific discharge vector, L T^{-1}.
$\{Q\}$, Q_n	global fluid mass flux array.
r	rate of mineral precipitation/dissolution per unit volume rock, moles L^{-3} T^{-1}.
Ra	dimensionless Rayleigh number.
R_c	rate of addition of component species to solution.
R_i	net rate of addition of species i to solution.
R_m	rate of addition of solid species to solution.
R_s	rate of addition of secondary species to solution.
R_{nm}	global resistance matrix for the stream function.
R^e_{nm}	local resistance matrix for the stream function.
s	designation for a secondary aqueous species.
$\hat{s}$	number of secondary species.
S	mineral specific reactive surface area, L^2 L^{-3}.
S_s	specific storage, L^{-1}.
t	time, T.
t_e	equilibration time, T.
Δt	time step size, T.
T	temperature, θ.
$\mathbf{T}$	dimensionless porous medium tortuosity.
T_n	global "flux" array for the stream function.
$\mathbf{v}$, v_i	average linear velocity vector, L T^{-1}.
v_x, v_z	velocity components, L T^{-1}.
x	x coordinate, L.
z	z coordinate, L.
Z	elevation, L.
$\boldsymbol{\alpha}$, α_{ij}	solute dispersivity tensor, L.
α_L	longitudinal solute dispersivity, L.
α_T	transverse solute dispersivity, L.
α_n	alpha values for element shape function, L^2.
β	compressibility of water, M L^{-1} T^{-2}.
β_n, β_m	beta values for element shape function, L.
β_T	fluid thermal expansivity, θ^{-1}.
γ_{OH^-}	activity coefficient for OH^-.
γ_{H^+}	activity coefficient for H^+.
γ_c	activity coefficients for aqueous component species.
γ_s	activity coefficients for secondary aqueous species.
γ_n, γ_m	gamma values for element shape function, L.
Δ^e	element area, L^2.
ϵ_f	fluid thermal dispersion coefficient, L M T^{-3} θ^{-1}.
ϵ	thermal dispersivity, L.
η	aquifer compressibility, M L^{-1} T^{-2}.
θ	weights used in finite difference approximations of temporal derivatives.

θ_K	angle of rotation between principal directions of hydraulic conductivity tensor and coordinate directions.
κ	thermal diffusivity, $L^2\ T^{-1}$.
$\boldsymbol{\lambda}^*$	effective thermal dispersion tensor, $L\ M\ T^{-3}\ \theta^{-1}$.
λ_L	longitudinal effective thermal dispersion coefficient, $L\ M\ T^{-3}\ \theta^{-1}$.
λ_T	transverse effective thermal dispersion coefficient, $L\ M\ T^{-3}\ \theta^{-1}$.
λ_e	effective isotropic thermal conductivity, $L\ M\ T^{-3}\ \theta^{-1}$.
λ_f	thermal conductivity of the fluid, $L\ M\ T^{-3}\ \theta^{-1}$.
λ_s	solid thermal conductivity, $L\ M\ T^{-3}\ \theta^{-1}$.
μ	fluid viscosity, $M\ L^{-1}\ T^{-1}$.
μ_o	reference fluid viscosity, $M\ L^{-1}\ T^{-1}$.
μ_r	relative fluid viscosity, dimensionless.
ν_{cm}	stoichiometric coefficient for solids.
ν_{cs}	stoichiometric coefficient for secondary aqueous species.
ξ_r	reaction progress, mol.
ξ_n, ξ_m	basis function.
Ξ_r	reaction progress density, $mol\ L^{-3}$.
ρ, ρ_f	fluid density, $M\ L^{-3}$.
ρ_o	reference fluid density, $M\ L^{-3}$.
ρ_r	relative fluid density, dimensionless.
ρ_s	density of solid matrix, $M\ L^{-3}$.
ρ_m	density of solid species, $M\ L^{-3}$.
$(\rho c)_e$	effective volumetric heat capacity for the saturated porous medium, $M\ L^{-1}\ T^{-3}\ \theta^{-1}$.
σ	dimensionless scaling parameter.
τ_{cm}	stoichiometric coefficient matrix for solids.
τ_{cs}	stoichiometric coefficient matrix for secondary aqueous species.
τ_e	dimensionless equilibration time.
ϕ	porosity, fraction.
ϕ_i	initial porosity, fraction.
Ψ	mass-based stream function, $M\ L^{-1}\ T^{-1}$.
ω_m	molecular weight of solid species, $M\ mol^{-1}$.

Acknowledgments

Acknowledgment is made to the donors of The Petroleum Research Fund, administered by the ACS, for partial support of this research. The author would also like to acknowledge the assistance of Jeffrey Lawton and James Monohan in preparing Fig. 19.

References

Aagaard, P., and Helgeson, H.C., 1982. Thermodynamic and kinetic constraints on reaction rates among minerals and aqueous solutions, I. Theoretical considerations. Amer. J. Sci., 282: 237–285.

Abriola, L.M., 1987. Modeling contaminant transport in the subsurface: an interdisciplinary challenge. Rev. Geophys., 25(2): 125–134.

Ague, J.J. and Brimhall, G.H., 1988. Geochemical modeling of steady state fluid flow and chemical reaction during supergene enrichment of porphyry copper deposits. Econ. Geol., 84: 506–528.

Alpers, C.N. and Brimhall, G.H., 1989. Paleohydrologic evolution and geochemical dynamics of cumulative supergene metal enrichment at La Escondida, Atacama Desert, northern Chile. Econ. Geol., 84(2): 229–255.

Anderson, G.M., 1991. Organic maturation and ore precipitation in southeast Missouri. Econ. Geol., 86(5): 909–926.

Anderson, M.P., 1979. Using models to simulate the movement of contaminants through groundwater flow systems. CRC Crit. Rev. Env. Control, 9(2): 97–156.

Anderson, R.N., Hobart, M.A., and Langseth, M.G., 1979. Geothermal convection through oceanic crust and sediments in the Indian Ocean. Science, 204: 828–832.

Angevine, C.L. and Turcotte, D.L., 1983. Porosity reduction by pressure solution: a theoretical model for quartz arenites. G.S.A. Bull., 94: 1129–1134.

Auchmuty, G., Chadam, J., Merino, E., Ortoleva, P., and Ripley, E., 1986. The structure and stability of propagating redox fronts. S.I.A.M. J. Appl. Math., 46(4): 588–604.

Back, W., Hanshaw, B.B., Herman, J.S., and van Driel, J.N., 1986. Differential dissolution of a Pleistocene reef in the ground-water mixing zone of coastal Yucatan, Mexico. Geol., 14(2): 137–140.

Badiozamani, K., 1973. The Dorag dolomitization model—application to the Middle Ordovician of Wisconsin. J. Sed. Pet., 43(4): 965–984.

Bahr, J.M. and Rubin, J., 1987. Direct comparison of kinetic and local equilibrium formulations for solute transport affected by surface reactions. Water Resources Res., 23(3): 438–452.

Bajracharya, K. and Barry, D.A., 1993. Mixing cell models for nonlinear nonequilibrium single species adsorption and transport. Water Resources Res., 29(5): 1405–1413.

Barry, D.A., 1990. Supercomputers and their use in modeling subsurface solute transport. Rev. Geophys., 28(3): 277–295.

Baumgartner, L.P. and Ferry, J.M., 1991. A model for coupled fluid-flow and mixed-volatile mineral reactions with applications to regional metamorphism. Contrib. Mineral. Petrol., 106: 273–285.

Bear, J., 1961. On the tensor form of dispersion in porous media. J. Geophys. Res., 66(4): 1185–1197.

Bear, J., 1972. Dynamics of Fluids in Porous Media. Dover Publications, New York, N.Y., 764 pp.

Bear, J. and Verruijt, A., 1987. Modeling Groundwater Flow and Pollution. D. Reidel, Boston, M.A., 414 pp.

Belitz, K. and Bredehoeft, J., 1988. Hydrodynamics of Denver Basin: explanation of subnormal fluid pressures. A.A.P.G. Bull., 72(11): 1334–1359.

Bethke, C.M., 1985. A numerical model of compaction-driven groundwater flow and heat transfer and its application to the paleohydrology of intracratonic sedimentary basins. J. Geophys. Res., 90(B8): 6817–6828.

Bethke, C.M., 1986. Hydrologic constraints on the genesis of the Upper Mississippi Valley mineral district from Illinois Basin brines. Econ. Geol., 81(2): 233–249.

Bethke, C.M., 1989. Modeling subsurface flow in sedimentary basins. Geologische Rundschau, 78(1): 129–154.

Bethke, C.M., Harrison, W.J., Upson, C., and Altaner, S.P., 1988. Supercomputer analysis of sedimentary basins. Science, 239: 261–267.

Bethke, C.M. and Marshak, S., 1990. Brine migrations across North America—the plate tectonics of groundwater. Ann. Rev. Earth Planet. Sci., 18: 287–315.

Bjorlykke, K. and Egeberg, P.K., 1993. Quartz cementation in sedimentary basins. A.A.P.G. Bull., 77(9): 1538–1548.

Bjorlykke, K., Mo, A., and Palm, E., 1988. Modelling of thermal convection in sedimentary basins and its relevance to diagenetic reactions. Mar. Pet. Geol., 5: 338–351.

Bjorlykke, K., Ramm, M., and Saigal, G.C., 1989. Sandstone diagenesis and porosity modification during basin evolution. Geologische Rundschau, 78(1): 243–268.

Blanchard, P.E. and Sharp, Jr., J.M., 1985. Possible free convection in thick Gulf Coast sandstone sequences, in Southwest Section AAPG 1985 Transactions. American Association of Petroleum Geologists, pp. 6–12.

Blatt, H., 1979. Diagenetic processes in sandstones. In: P.A. Scholle and P.R. Schluger (Editors), Aspects of Diagenesis. Special Publication No. 26, Society of Economic Paleontologists and Mineralogists, Tulsa, O.K., pp. 141–157.

Bloch, S., McGowen, J.H., Duncan, J.R., and Brizzolara, D.W., 1990. Porosity prediction, prior to

drilling, in sandstones of the Kekiktuk Formation (Mississippian): North Slope of Alaska. A.A.P.G. Bull., 74(9): 1371–1385.

Bories, S., 1987. Natural convection in porous media. In: J. Bear and M.Y. Corapcioglu (Editors), Advances in Transport Phenomena in Porous Media. Martinus Nijhoff, Boston, M.A., pp. 77–141.

Bosma, W.J.P. and van der Zee, S.E.A.T.M., 1993. Transport of reacting solute in a one-dimensional, chemically heterogeneous porous medium. Water Resources Res., 29(1): 117–131.

Bourbie, T. and Zinszner, B., 1985. Hydraulic and acoustic properties as a function of porosity in Fountainebleau sandstone. J. Geophys. Res., 90(B13): 11524–11532.

Bowers, M.C., Ehrlich, R., and Clark, R.A., 1994. Determination of petrographic factors controlling permeability using petrographic image analysis and core data, Satun field, Pattani Basin, Gulf of Thailand. Mar. Pet. Geol., 11(2): 148–156.

Brace, W.F., 1980. Permeability of crystalline and argillaceous rocks. International Journal of Rock Mechanics and Mining Sciences, 17: 241–251.

Bredehoeft, J.D., Neuzil, C.E., and Milly, P.C.D., 1983. Regional flow in the Dakota aquifer: a study of the role of confining layers. Water-Supply Paper 2237, U.S. Geological Survey, 45 pp.

Brimhall, G.H., Alpers, C. N., and Cunningham, A.B., 1985. Analysis of supergene ore-forming processes and ground-water solute transport using mass balance principles. Econ. Geol., 80(5): 1227–1256.

Brusseau, M.L., 1994. Transport of reactive contaminants in heterogeneous porous media. Rev. Geophys., 32(3): 285–313.

Brusseau, M.L., Jessup, R.E., and Rao, P.S.C., 1992. Modeling solute transport influenced by multi-process nonequilibrium and transformation reactions. Water Resources Res., 28(1): 175–182.

Bryant, S.L., Schechter, R.S., and Lake, L.W., 1986. Interactions of precipitation/dissolution waves and ion exchange in flow through permeable media. Amer. Inst. Chem. Eng. J., 32(5): 751–764.

Bryant, S.L., Schechter, R.S., and Lake, L.W., 1987. Mineral sequences in precipitation/dissolution waves. Amer. Inst. Chem. Eng. J., 33(8): 1271–1287.

Burr, D.T., Sudicky, E.A., and Naff, R.L., 1994. Nonreactive and reactive solute transport in three-dimensional heterogeneous porous media: Mean displacement, plume spreading, and uncertainty. Water Resources Res., 30(3): 791–815.

Cameron, D.R. and Klute, A., 1977. Convective-dispersive solute transport with a combined equilibrium and kinetic adsorption model. Water Resources Res., 13(1): 183–188.

Carnahan, C.L., 1987. Simulation of chemically reactive solute transport under conditions of changing temperature. In: C.-F. Tsang (Editor), Coupled Processes Associated with Nuclear Waste Repositories. Academic Press, New York, N.Y., pp. 249–257.

Carnahan, C.L., 1990. Coupling of precipitation-dissolution reactions to mass diffusion via porosity changes. In: D.C. Melchior and R.L. Bassett (Editors), Chemical Modeling in Aqueous Systems II. ACS Symposium Series 416, American Chemical Society, Washington, D.C., pp. 234–242.

Carslaw, H.S. and Jaeger, J.C., 1959. Conduction of Heat in Solids. 2nd ed., Oxford University Press, New York, N.Y., 510 pp.

Cathles, L.M., 1977. An analysis of the cooling of intrusives by ground-water convection which includes boiling. Econ. Geol., 72: 72–804.

Cathles, L.M., 1981. Fluid flow and genesis of hydrothermal ore deposits. Econ. Geol., 75th Anniversary Volume, 424–457.

Cathles, L.M. and Smith, A.T., 1983. Thermal constraints on the formation of Mississippi valley-type lead-zinc deposits and their implications for episodic basin dewatering and deposit genesis. Econ. Geol., 78: 983–1002.

Cederberg, G.A., 1985. TRANQL: a ground-water mass-transport and equilibrium chemistry model for multicomponent systems. Ph.D. thesis, Stanford University, Stanford, C.A., 117 pp.

Cederberg, G.A., Street, R.L., and Leckie, J.O., 1985. A groundwater mass transport and equilibrium chemistry model for multicomponent systems. Water Resources Res., 21(8): 1095–1104.

Charbeneau, R.J., 1981. Groundwater contaminant transport with adsorption and ion exchange chemistry: method of characteristics for the case without dispersion. Water Resources Res., 17(3): 705–713.

Clark, S.P., Jr., 1966. Thermal conductivity. In: S.P. Clark Jr. (Editor), Revised ed., Handbook of Physical Constants. Memoir 97, The Geological Society of America, pp. 459–482.

Combarnous, M.A. and Bories, S.A., 1975. Hydrothermal convection in saturated porous media. Adv. Hydrosci., 10: 231–307.

Dagan, G., 1986. Statistical theory of groundwater flow and transport: pore to laboratory, laboratory to formation, and formation to regional scale. Water Resources Res., 22(9): 120S–134S.

Davis, S.H., Rosenblat, S., Wood, J.R., and Hewett, T.A., 1985. Convective fluid flow and diagenetic patterns in domed sheets. Amer. J. Sci., 285: 207–223.

Davis, S.N., 1969. Porosity and permeability of natural materials. In: R.J.M. De Wiest (Editor), Flow Through Porous Media. Academic Press, New York, N.Y., pp. 53–89.

Davis, S.N. and DeWiest, R.J.M., 1966. Hydrogeology. Wiley, New York, N.Y., 463 pp.

de Josselin de Jong, G., 1969. Generating functions in the theory of flow through porous media. In: R.J.M. De Wiest (Editor), Flow Through Porous Media. Academic Press, New York, N.Y., pp. 377–400.

Deming, D., 1994. Factors necessary to define a pressure seal. A.A.P.G. Bull., 78(6): 1005–1009.

Deming, D. and Nunn, J.A., 1991. Numerical simulations of brine migration by topographically driven recharge. J. Geophys. Res., 96(B2): 2485–2499.

Deming, D., Nunn, J.A., and Evans, D.G., 1990. Thermal effects of compaction-driven groundwater flow from overthrust belts. J. Geophys. Res., 95(B5): 6669–6683.

Denbigh, K., 1981. The Principles of Chemical Equilibrium. 4th ed., Cambridge University Press, Cambridge, 494 pp.

Dewers, T. and Ortoleva, P., 1990. A coupled reaction/transport/mechanical model for intergranular pressure solution, stylolites, and differential compaction and cementation in clean sandstones. Geochim. Cosmochim. Acta, 54: 1609–1625.

Dewers, T. and Ortoleva, P., 1991. Influences of clay minerals on sandstone cementation and pressure solution. Geol., 19: 1045–1048.

Dewers, T. and Ortoleva, P., 1994. Nonlinear dynamical aspects of deep basin hydrology: fluid compartment formation and episodic fluid release. Amer. J. Sci., 294: 713–755.

Dixon, S.A., Summers, D.M., and Surdam, R.C., 1989. Diagenesis and preservation of porosity in Norphlet Formation (Upper Jurassic): southern Alabama. A.A.P.G. Bull., 73(6): 707–728.

Domenico, P.A. and Palciauskas, V.V., 1973. Theoretical analysis of forced convective heat transfer in regional ground-water flow. G.S.A. Bull., 84: 3803–3814.

Domenico, P.A. and Schwartz, F.W., 1990. Physical and Chemical Hydrogeology, Wiley, New York, N.Y., 824 pp.

Donaldson, I.G., 1962. Temperature gradients in the upper layers of the Earth's crust due to convective water flows. J. Geophys. Res., 67(9): 3449–3459.

Douglas, J. and Jones, B.F., 1963. On predictor-corrector methods for nonlinear parabolic differential equations. Journal of the Society for Industrial and Applied Mathematics, 11(1): 195–204.

Doyen, P.M., 1988. Permeability, conductivity, and pore geometry of sandstone. J. Geophys. Res., 93(B7): 7729–7740.

Drever, J.I., 1982. The Geochemistry of Natural Waters, Prentice-Hall, Englewood Cliffs, N.J., 388 pp.

Dria, M.A., Bryant, S.L., Schechter, R.S., and Lake, L.W., 1987. Interacting precipitation/dissolution waves: the movement of inorganic contaminants in groundwater. Water Resources Res., 23(11): 2076–2090.

Dullien, F.A.L., 1992. Porous Media: Fluid Transport and Pore Structure. 2nd ed., Academic Press, San Diego, C.A., 574 pp.

Dutton, S.P. and Diggs, T.N., 1992. Evolution of porosity and permeability in the Lower Cretaceous Travis Peak Formation, east Texas. A.A.P.G. Bull., 76(2): 252–269.

Ehrenberg, S.N., 1993. Preservation of anomalously high porosity in deeply buried sandstones by grain-coating chlorite: examples from the Norwegian continental shelf. A.A.P.G. Bull., 77(7): 1260–1286.

Elder, J.W., 1967. Steady free convection in a porous medium heated from below. J. Fluid Mech., 27(1): 29–48.

Engesgaard, P. and Kipp, K.L., 1992. A geochemical transport model for redox-controlled movement of mineral fronts in groundwater flow systems: a case of nitrate removal by oxidation of pyrite. Water Resources Res., 28(10): 2829–2843.

England, L.A. and Freeze, R.A., 1988. Finite-element simulation of long-term transient regional ground-water flow. Ground Water, 26(3): 298–308.

Evans, D.G. and Nunn, J.A., 1989. Free thermohaline convection in sediments surrounding a salt column. J. Geophys. Res., 94(B9): 413–422.

Evans, D.G., Nunn, J.A., and Hanor, J.S., 1991. Mechanisms driving groundwater flow near salt domes. Geophys. Res. Lett., 18(5): 927–930.

Evans, D.G. and Raffensperger, J.P., 1992. On the stream function for variable-density groundwater flow. Water Resources Res., 28(8): 2141–2145.

Fehn, U., Cathles, L.M., and Holland, H.D., 1978. Hydrothermal convection and uranium deposits in abnormally radioactive plutons. Econ. Geol., 73: 1556–1566.

Ferry, J.M., 1987. Metamorphic hydrology at 13-km depth and 400–550°C. Amer. Mineral., 72: 39–58.

Fogler, H.S., Lund, K., and McCune, C.C., 1976. Predicting the flow and reaction of HCl/HF acid mixtures in porous sandstone cores. Soc. Pet. Eng. J., October, 1976: 248–260.

Forbes, P.L., Ungerer, P., and Mudford, B.S., 1992. A two-dimensional model of overpressure development and gas accumulation in Venture Field, eastern Canada. A.A.P.G. Bull., 76(3): 318–338.

Forster, C. and Smith, L., 1988a. Groundwater flow systems in mountainous terrain 1. Numerical modeling technique. Water Resources Res., 24(7): 999–1010.

Forster, C. and Smith, L., 1988b. Groundwater flow systems in mountainous terrain 2. Controlling factors. Water Resources Res., 24(7): 1011–1023.

Freeze, R.A. and Cherry, J., 1979. Groundwater. Prentice-Hall, New York, N.Y., 604 pp.

Freeze, R.A. and Witherspoon, P.A., 1967. Theoretical analysis of regional groundwater flow: 2. Effect of water-table configuration and subsurface permeability variation. Water Resources Res., 3(2): 623–634.

Frind, E.O. and Germain, D., 1986. Simulation of contaminant plumes with large dispersive contrast: evaluation of alternating direction Galerkin models. Water Resources Res., 22(13): 857–1873.

Frind, E.O. and Matanga, G.B., 1985a. The dual formulation of flow for contaminant transport modeling 1. Review of theory and accuracy aspects. Water Resources Res., 21(2): 159–169.

Frind, E.O. and Matanga, G.B., 1985b. The dual formulation of flow for contaminant transport modeling 2. The Borden aquifer. Water Resources Res., 21(2): 170–182.

Fu, L., Milliken, K.L., and Sharp Jr., J.M., 1994. Porosity and permeability variations in fractured and liesegang-banded Breathitt sandstones (Middle Pennsylvanian): eastern Kentucky: diagenetic controls and implications for modeling dual-porosity systems. J. Hydrol., 154: 351–381.

Füchtbauer, H., 1967. Influence of different types of diagenesis on sandstone porosity. In: Seventh World Petroleum Congress Proceedings. Volume 2: Origin of Oil, Geology, and Geophysics, Elsevier Science, New York, N.Y., pp. 353–369.

Garven, G., 1986. The role of regional fluid flow in the genesis of the Pine Point deposit, western Canada sedimentary basin—a reply. Econ. Geol., 81(4): 1015–1020.

Garven, G., 1989. A hydrogeologic model for the formation of the giant oil sands deposits of the Western Canada Sedimentary Basin. Amer. J. Sci., 289(2): 105–166.

Garven, G., 1994. Reply to a comment by C. W. Clendenin on "Genesis of stratabound ore deposits in the Midcontinent basins of North America. 1. The role of regional groundwater flow" by Garven, G., Ge, S., Person, M.A., and Sverjensky, D.A., Amer. J. Sci., 294: 760–775.

Garven, G., 1995. Continental-scale groundwater flow and geologic processes. Ann. Rev. Earth Planet. Sci., 24: 89–117.

Garven, G. and Freeze, R.A., 1984a. Theoretical analysis of the role of groundwater flow in the genesis of stratabound ore deposits 1. Mathematical and numerical model. Amer. J. Sci., 284: 1085–1124.

Garven, G. and Freeze, R.A., 1984b. Theoretical analysis of the role of groundwater flow in the genesis of stratabound ore deposits 2. Quantitative results. Amer. J. Sci., 284: 1125–1174.

Garven, G. and Raffensperger, J.P., in press. Hydrogeology and geochemistry of ore genesis in sedimentary basins. In: H.L. Barnes (Editor), Geochemistry of Hydrothermal Ore Deposits. 3rd ed. Wiley, New York, N.Y.

Garven, G. and Toptygina, V.I., 1993. Numerical modeling of three-dimensional, variable density

groundwater flow systems and heat transport in large sedimentary basins [abst.]. G.S.A., Abstracts with Programs, 25(6): A182.

Ge, S. and Garven, G., 1989. Tectonically induced transient groundwater flow in foreland basin. In: R.A. Price (Editor), Origin and Evolution of Sedimentary Basins and Their Energy and Mineral Resources. Geophysical Monograph 48, American Geophysical Union, Washington, D.C., pp. 145–157.

Ge, S. and Garven, G., 1992. Hydromechanical modeling of tectonically driven groundwater flow with application to the Arkoma foreland basin. J. Geophys. Res., 97(B6): 9119–9144.

Gelhar, L.W. and Axness, C.L., 1983. Three-dimensional stochastic analysis of macrodispersion in aquifers. Water Resources Res., 19(1): 61–180.

Gelhar, L.W., Welty, C., and Rehfeldt, K.R., 1992. A critical review of data on field-scale dispersion in aquifers. Water Resources Res., 28(7): 1955–1974.

Gerdes, M.L., Baumgartner, L.P., and Person, M., 1995. Stochastic permeability models of fluid flow during contact metamorphism. Geol., 23(10): 945–948.

Gluyas, J. and Coleman, M., 1992. Material flux and porosity changes during sediment diagenesis, Nature, 356: 52–54.

Goldhaber, M.B., Reynolds, R.L., and Rye, R.O., 1983. Role of fluid mixing and fault-related sulfide in the origin of the Ray Point Uranium District, south Texas. Econ. Geol., 78: 1043–1063.

Hanor, J.S., 1987. Kilometre-scale thermohaline overturn of pore waters in the Louisiana Gulf Coast. Nature, 327: 501–503.

Hanshaw, B.B., Back, W., and Deike, R.G., 1971. A geochemical model for dolomitization by ground water. Econ. Geol., 66: 710–724.

Hardie, L.A., 1987. Dolomitization: a critical review of some current views. J. Sed. Pet., 57(1): 166–183.

Harrison, W.J. and Summa, L.L., 1991. Paleohydrology of the Gulf of Mexico Basin. Amer. J. Sci., 291: 109–176.

Haszeldine, R.S., Samson, I.M., and Cornford, C., 1984. Quartz diagenesis and convective fluid movement: Beatrice oilfield, UK North Sea. Clay Min., 19: 391–402.

Hekim, Y. and Fogler, H.S., 1980. On the movement of multiple reaction zones in porous media. Amer. Inst. Chem. Eng. J., 26(3): 403–411.

Hekim, Y., Fogler, H.S., and McCune, C.C., 1982. The radial movement of permeability fronts and multiple reaction zones in porous media. Soc. Pet. Eng. J., February, 1982: 99–107.

Helgeson, H.C., 1968. Evaluation of irreversible reactions in geochemical processes involving minerals and aqueous solutions—I. Thermodynamic relations. Geochim. Cosmochim. Acta, 32: 853–877.

Helgeson, H.C., 1969. Thermodynamics of hydrothermal systems at elevated temperatures and pressures. Amer. J. Sci., 267: 729–804.

Helgeson, H.C., 1979. Mass transfer among minerals and hydrothermal solutions. In: H.L. Barnes (Editor), Geochemistry of Hydrothermal Ore Deposits. 2nd ed. Wiley, New York, N.Y., pp. 568–610.

Helgeson, H.C., Brown, T.H., Nigrini, A., and Jones, T.A., 1970. Calculation of mass transfer in geochemical processes involving aqueous solutions. Geochim. Cosmochim. Acta, 34: 569–592.

Helgeson, H.C., Kirkham, D.H., and Flowers, G.C., 1981. Theoretical prediction of the thermodynamic behavior of aqueous electrolytes at high pressures and temperatures. IV. Calculation of activity coefficients, osmotic coefficients, apparent molal and standard and relative partial molal properties to 5 kb and 600°C. Amer. J. Sci., 281: 1241–1516.

Hewett, T.A., 1986. Porosity and mineral alteration by fluid flow through a temperature field. In: L.W. Lake and H.B. Carroll (Editors), Reservoir Characterization. Academic Press, New York, N.Y., pp. 83–140.

Hinch, E.J. and Bhatt, B.S., 1990. Stability of an acid front moving through porous rock. J. Fluid Mech., 212: 279–288.

Hitchon, B., 1969a. Fluid flow in the western Canada sedimentary basin: 1. Effect of topography. Water Resources Res., 5(1): 186–195.

Hitchon, B., 1969b. Fluid flow in the western Canada sedimentary basin: 2. Effect of geology. Water Resources Res., 5(2): 460–469.

Hoeve, J. and Quirt, D., 1984. Mineralization and host rock alteration in relation to clay mineral

diagenesis and evolution of the Middle-Proterozoic, Athabasca Basin, northern Saskatchewan, Canada. SRC Technical Report 187, Saskatchewan Research Council, 187 pp.

Hoeve, J. and Sibbald, T.I.I., 1978. On the genesis of Rabbit Lake and other unconformity-type uranium deposits in northern Saskatchewan, Canada. Econ. Geol., 73: 1450–1473.

Hofstra, A.H., Leventhal, J.S., Northrop, H.R., Landis, G.P., Rye, R.O., Birak, D.J., and Dahl, A.R., 1991. Genesis of sediment-hosted disseminated-gold deposits by fluid mixing and sulfidization: chemical-reaction-path modeling of ore-depositional processes documented in the Jerritt Canyon district, Nevada. Geol., 19: 36–40.

Houseknecht, D.W., 1987. Assessing the relative importance of compaction processes and cementation to reduction of porosity in sandstones. A.A.P.G. Bull., 71(6): 633–642.

Hubbert, M.K., 1940. The theory of ground-water motion. J. Geol., 48(8): 785–944.

Hunt, J.M., 1990. Generation and migration of petroleum from abnormally pressured fluid compartments. A.A.P.G. Bull., 74(1): 1–12.

Huyakorn, P.S. and Pinder, G.F., 1983. Computational Methods in Subsurface Flow. Academic Press, New York, N.Y., 473 pp.

I, T.-P. and Nancollas, G.H., 1972. EQUIL—a general computational method for the calculation of solution equilibria. Anal. Chem., 44(12): 1940–1950.

Istok, J., 1989. Groundwater Modeling by the Finite Element Method. Water Resources Monograph 13, American Geophysical Union, Washington, D.C., 495 pp.

Jamet, P., Lachassagne, P., Doublet, R., and Ledoux, E., 1989. Modelling of the Needle's Eye natural analogue. Technical Report WE/89/64, British Geological Survey, 43 pp.

Javandel, I., Doughty, C., and Tsang, C.-F., 1984. Groundwater Transport: Handbook of Mathematical Models. Water Resources Monograph 10, American Geophysical Union, Washington, D.C., 228 pp.

Jensen, K.H., Bitsch, K., and Bjerg, P.L., 1993. Large-scale dispersion experiments in a sandy aquifer in Denmark: observed tracer movements and numerical analyses. Water Resources Res., 29(3): 673–696.

Jian, F.X., Chork, C.Y., Taggart, I.J., McKay, D.M., and Bartlett, R.M., 1994. A genetic approach to the prediction of petrophysical properties. J. Pet. Geol., 17(1): 71–88.

Johnson, C., 1987. Numerical Solution of Partial Differential Equations by the Finite Element Method. Cambridge University Press, New York, N.Y., 279 pp.

Kirkner, D.J., Jennings, A.A., and Theis, T.L., 1985. Multisolute mass transport with chemical interaction kinetics. J. Hydrol., 76: 107–117.

Kirkner, D.J., Theis, T.L., and Jennings, A.A., 1984. Multicomponent solute transport with sorption and soluble complexation. Adv. Water Resources, 7: 120–125.

Knapp, R.B., 1989. Spatial and temporal scales of local equilibrium in dynamic fluid-rock systems. Geochim. Cosmochim. Acta, 53: 1955–1964.

Knudsen, W.C., 1962. Equations on fluid flow through porous media—incompressible fluid of varying density. J. Geophys. Res., 67(2): 733–737.

Land, L.S., 1991. Evidence for vertical movement of fluids, Gulf Coast sedimentary basin. Geophys. Res. Lett., 18(5): 919–922.

Land, L.S. and Macpherson, G.L., 1992. Origin of saline formation waters, Cenozoic section, Gulf of Mexico sedimentary basin. A.A.P.G. Bull., 76(9): 1344–1362.

Langmuir, D., 1978. Uranium solution-mineral equilibria at low temperatures with applications to sedimentary ore deposits. Geochim. Cosmochim. Acta, 42: 547–569.

Lapwood, E.R., 1948. Convection of a fluid in a porous medium. Proc. Cambridge Phil. Soc., 44: 508–521.

Lasaga, A.C., 1981. Rate laws of chemical reactions. In: A.C. Lasaga and R.J. Kirkpatrick (Editors), Kinetics of Geochemical Processes. Reviews in Mineralogy, Volume 8, Mineralogical Society of America, pp. 1–68.

Lasaga, A.C., Soler, J.M., Ganor, J., Burch, T.E., and Nagy, K.L., 1994. Chemical weathering rate laws and global geochemical cycles. Geochim. Cosmochim. Acta, 58(10): 2361–2386.

Lee, M.-K. and Bethke, C.M., 1994. Groundwater flow, late cementation, and petroleum accumulation in the Permian Lyons Sandstone, Denver Basin. A.A.P.G. Bull., 78(2): 217–237.

Lerman, A., 1979. Geochemical Processes: Water and Sediment Environments. Robert E. Krieger Pub. Co., Malabar, F.L., 481 pp.

Lichtner, P.C., 1985. Continuum model for simultaneous chemical reactions and mass transport in hydrothermal systems. Geochim. Cosmochim. Acta, 49: 779–800.

Lichtner, P.C., 1988. The quasi-stationary state approximation to coupled mass transport and fluid-rock interaction in a porous medium. Geochim. Cosmochim. Acta, 52: 143–165.

Lichtner, P.C., 1991. The quasi-stationary state approximation to fluid/rock reaction: local equilibrium revisited. In: J. Ganguly (Editor), Diffusion, Atomic Ordering and Mass Transport. Advances in Physical Geochemistry 8, pp. 454–562.

Lichtner, P.C., 1992. Time-space continuum description of fluid/rock interaction in permeable media. Water Resources Res., 28(12): 3135–3155.

Lichtner, P.C., 1993. Scaling properties of time-space kinetic mass transport equations and the local equilibrium limit. Amer. J. Sci., 293: 257–296.

Lichtner, P.C. and Biino, G.G., 1992. A first principles approach to supergene enrichment of a porphyry copper protore: I. Cu-Fe-S subsystem. Geochim. Cosmochim. Acta, 56: 3987–4013.

Lichtner, P.C., Oelkers, E.H., and Helgeson, H.C., 1986. Interdiffusion with multiple precipitation/dissolution reactions: transient model and the steady-state limit. Geochim. Cosmochim. Acta, 50: 1951–1966.

Lichtner, P.C. and Waber, N., 1992. Redox front geochemistry and weathering: theory with application to the Osamu Utsumi uranium mine, Poços de Caldas, Brazil. Journal of Geochemical Exploration, 45: 521–564.

Liu, C.W. and Narasimhan, T.N., 1989a. Redox-controlled multiple-species reactive chemical transport 1. Model development. Water Resources Res., 25(5): 869–882.

Liu, C.W. and Narasimhan, T.N., 1989b. Redox-controlled multiple-species reactive chemical transport 2. Verification and application. Water Resources Res., 25(5): 883–910.

Ludvigsen, A., Palm, E., and McKibben, R., 1992. Convective momentum and mass transport in porous sloping layers. J. Geophys. Res., 97(B9): 12315–12325.

Lund, K. and Fogler, H.S., 1976. Acidization—V: the prediction of the movement of acid and permeability fronts in sandstone. Chem. Eng. Sci., 31: 381–392.

Lusczynski, N.J., 1961. Head and flow of ground water of variable density. J. Geophys. Res., 66(12): 4247–4256.

Mangold, D.C. and Tsang, C.-F., 1991. A summary of subsurface hydrological and hydrochemical models. Rev. Geophys., 29(1): 51–79.

Manheim, F.T., 1970. The diffusion of ions in unconsolidated sediments. Earth Planet. Sci. Lett., 9: 307–309.

Marsily, G. de, 1986. Quantitative Hydrogeology. Marsily, G. de, Translator, Academic Press, New York, N.Y., 440 pp.

Maynard, J.B., 1983. Geochemistry of Sedimentary Ore Deposits. Springer-Verlag, New York, N.Y., 305 pp.

McBride, E.F., 1989. Quartz cement in sandstones: a review. Earth-Science Rev., 26: 69–112.

McKibbin, R., 1986. Thermal convection in a porous layer: effects of anisotropy and surface boundary conditions. Trans. Porous Media, 1: 271–292.

McKibbin, R. and O'Sullivan, M.J., 1980. Onset of convection in a layered porous medium heated from below. J. Fluid Mech., 96(2): 375–393.

McKibbin, R. and Tyvand, P.A., 1982. Anisotropic modelling of thermal convection in multilayered porous media. J. Fluid Mech., 118: 315–339.

McKibbin, R. and Tyvand, P.A., 1983. Thermal convection in a porous medium composed of alternating thick and thin layers. Int. J. Heat Mass Transfer, 26(5): 761–780.

McManus, K.M. and Hanor, J.S., 1993. Diagenetic evidence for massive evaporite dissolution, fluid flow, and mass transfer in the Louisiana Gulf Coast. Geol., 21: 727–730.

Mercer, J.W. and Faust, C.R., 1980. Ground-water modeling: numerical models. Ground Water, 18(4): 395–409.

Mercer, J.W., Pinder, G.F., and Donaldson, I.G., 1975. A Galerkin-finite element analysis of the hydrothermal system at Wairakei, New Zealand. J. Geophys. Res., 80(17): 2608–2621.

Mercer, J.W., Thomas, S.D., and Ross, B., 1982. Parameters and variables appearing in repository siting models. NUREG/CR-3086, U.S. Nuclear Regulatory Commission, 244 pp.

Merino, E., Nahon, D., and Wang, Y., 1993. Kinetics and mass transfer of pseudomorphic replacement: application to replacement of parent minerals and kaolinite by Al, Fe, and Mn oxides during weathering. Amer. J. Sci., 293: 135–155.

Miller, C.W. and Benson, L.V., 1983. Simulation of solute transport in a chemically reactive heterogeneous system: model development and application. Water Resources Res., 19(2): 381–391.

Moraes, M.A.S., 1991. Diagenesis and microscopic heterogeneity of lacustrine deltaic and turbiditic sandstone reservoirs (Lower Cretaceous): Potiguar Basin, Brazil. A.A.P.G. Bull., 75(11): 1758–1771.

Morel, F. and Morgan, J., 1972. A numerical method for computing equilibria in aqueous chemical systems. Env. Sci. Tech., 6(1): 58–67.

Mundell, J.A. and Kirkner, D.J., 1988. Numerical studies of dissolution-induced moving boundary problems from aqueous diffusion in porous media. J. Geophys. Res., 93(B9): 10397–10407.

Musgrove, M. and Banner, J.L., 1993. Regional ground-water mixing and the origin of saline fluids: Midcontinent, United States. Science, 259: 1877–1882.

National Research Council, 1990. Overview and recommendations. In: The Role of Fluids in Crustal Processes, Studies in Geophysics, National Academy Press, Washington, D.C., pp. 3–23.

Neuman, S.P., 1990. Universal scaling of hydraulic conductivities and dispersivities in geologic media. Water Resources Res., 26(8): 1749–1758.

Nguyen, V.V., Pinder, G.F., Gray, W.G., and Botha, J.F., 1983. Numerical simulation of uranium in-situ mining. Chem. Eng. Sci., 38(11): 1855–1862.

Nield, D.A., 1968. Onset of thermohaline convection in a porous medium. Water Resources Res., 4(3): 553–560.

Noorishad, J., Carnahan, C.L., and Benson, L.V., 1985. Development of a kinetic-equilibrium chemical transport code [abst.]. EOS, Trans., Amer. Geophys. Union, 66(18): 274.

Noorishad, J., Tsang, C.-F., Perrochet, P., and Musy, A., 1992. A perspective on the numerical solution of convection-dominated transport problems: a price to pay for the easy way out. Water Resources Res., 28(2): 551–561.

Nordstrom, D.K., Plummer, L.N. et al., 1979. Comparison of computerized chemical models for equilibrium calculations in aqueous systems. In: E.A. Jenne (Editor), Chemical Modeling in Aqueous Systems. ACS Symposium Series 93, American Chemical Society, Washington, D.C., pp. 857–892.

Norton, D. and Knight, J., 1977. Transport phenomena in hydrothermal systems: cooling plutons. Amer. J. Sci., 277: 937–981.

Novak, C.F., Schechter, R.S., and Lake, L.W., 1988. Rule-based mineral sequences in geochemical flow processes. Amer. Inst. Chem. Eng. J., 34(10): 1607–1614.

Nunn, J.A., 1994. Free thermal convection beneath intracratonic basins: thermal and subsidence effects. Basin Res., 6: 115–130.

Oelkers, E.H. and Helgeson, H.C., 1990. Triple-ion anions and polynuclear complexing in supercritical electrolyte solutions. Geochim. Cosmochim. Acta, 54: 727–738.

Oliver, J., 1986. Fluids expelled tectonically from orogenic belts: their role in hydrocarbon migration and other geologic phenomena. Geol., 14: 99–102.

Oran, E.S. and Boris, J.P., 1987. Numerical Simulation of Reactive Flow. Elsevier, New York, N.Y., 601 pp.

Ortega, J.M. and Rheinboldt, W.C., 1970. Iterative Solution of Nonlinear Equations in Several Variables. Academic Press, New York, N.Y., 572 pp.

Ortoleva, P., Al-Shaieb, Z., and Puckette, J., 1995. Genesis and dynamics of basin compartments and seals. Amer. J. Sci., 295: 345–427.

Ortoleva, P., Auchmuty, G., Chadam, J., Hettmer, J., Merino, E., Moore, C.H., and Ripley, E., 1986. Redox front propagation and banding modalities. Physica, 19D, 334–354.

Ortoleva, P., Chadam, J., Merino, E., and Sen, A., 1987. Geochemical self-organization II: the reactive-infiltration instability. Amer. J. Sci., 287: 1008–1040.

Ortoleva, P., Merino, E., Moore, C., and Chadam, J., 1987. Geochemical self-organization I: reaction-transport feedbacks and modeling approach. Amer. J. Sci., 287: 979–1007.

Ortoleva, P.J., 1994. Geochemical Self-Organization. Oxford Monographs on Geology and Geophysics No. 23, Oxford University Press, New York, N.Y., 411 pp.

Palciauskas, V.V. and Domenico, P.A., 1976. Solution chemistry, mass transfer, the approach to chemical equilibrium in porous carbonate rocks and sediments. G.S.A. Bull., 87: 207–214.

Palm, E., 1990. Rayleigh convection, mass transport, and change in porosity in layers of sandstone. J. Geophys. Res., 95(B6): 8675–8679.

Parkhurst, D.L., Thorstenson, D.C., and Plummer, L.N., 1980. PHREEQE—A Computer Program for Geochemical Calculations. Water-Resources Investigations 80–96, U.S. Geological Survey, Reston, V.A., 210 pp.

Parmentier, E.M. and Spooner, E.T.C., 1978. A theoretical study of hydrothermal convection and the origin of the ophiolitic sulphide ore deposits of Cyprus. Earth Planet. Sci. Lett., 40: 33–44.

Person, M. and Garven, G., 1992. Hydrologic constraints on petroleum generation within continental rift basins: theory and application to the Rhine graben. A.A.P.G. Bull., 76(4): 468–488.

Person, M. and Garven, G., 1994. A sensitivity study of the driving forces on fluid flow during continental-rift basin evolution. G.S.A. Bull., 106: 461–475.

Person, M., Raffensperger, J.P., Ge, S., and Garven, G., 1996. Basin-scale hydrogeologic modeling. Rev. Geophys., 34(1): 61–87.

Person, M.A., 1990. Hydrologic constraints on the thermal evolution of continental rift basins: implications for petroleum maturation. Ph.D. thesis, The Johns Hopkins University, Baltimore, M.D., 271 pp.

Phillips, O.M., 1990. Flow-controlled reactions in rock fabrics. J. Fluid Mech., 212: 263–278.

Phillips, O.M., 1991. Flow and Reactions in Permeable Rocks, Cambridge University Press, New York, N.Y., 285 pp.

Phillips, S.L., Igbene, A., Fair, J.A., Ozbek, H., and Tavana, M., 1981. A technical data book for geothermal energy utilization. DE81–029868, NTIS, 46 pp.

Phillips, S.L., Ozbek, H., and Silvester, L.F., 1983. Density of sodium chloride solutions at high temperatures and pressures. DE84–004883, NTIS, 51 pp.

Pickens, J.F. and Grisak, G.E., 1981. Scale-dependent dispersion in a stratified granular aquifer. Water Resources Res., 17(4): 1191–1211.

Pickens, J.F. and Lennox, W.C., 1976. Numerical simulation of waste movement in steady groundwater flow systems. Water Resources Res., 12(2): 171–180.

Pinder, G.F., 1973. A Galerkin-finite element simulation of groundwater contamination on Long Island, New York. Water Resources Res., 9(6): 1657–1669.

Pinder, G.F. and Gray, W.G., 1977. Finite Element Simulation in Surface and Subsurface Hydrology. Academic Press, San Diego, C.A., 295 pp.

Powley, D.E., 1990. Pressures and hydrogeology in petroleum basins. Earth-Science Rev., 29: 215–226.

Press, W.H., Flannery, B.P., Teukolsky, S.A., and Vetterling, W.T., 1986. Numerical Recipes: The Art of Scientific Computing. Cambridge University Press, Cambridge, 818 pp.

Rabinowicz, M., Dandurand, J.-L., Jakubowski, M., Schott, J., and Cassan, J.-P., 1985. Convection in a North Sea oil reservoir: inferences on diagenesis and hydrocarbon migration. Earth Planet. Sci. Lett., 74: 387–404.

Raffensperger, J.P., 1993. Quantitative evaluation of the hydrologic and geochemical processes involved in the formation of unconformity-type uranium deposits. Ph.D. thesis, The Johns Hopkins University, Baltimore, M.D., 679 pp.

Raffensperger, J.P., in press. Evidence and modeling of large-scale groundwater convection in Precambrian sedimentary basins. In: I.P. Montañez, J.M. Gregg, and K.L. Shelton (Editors), Basin-wide Fluid Flow and Associated Diagenetic Patterns: Integrated Petrologic, Geochemical and Hydrologic Considerations. Special Publication SEPM, Tulsa, O.K.

Raffensperger, J.P. and Ferrell Jr., R.E., 1990. Permeant-induced changes in the permeability, microtexture, and pore structure of unconsolidated water-sensitive sediments. Proceedings of the 9th International Clay Conference, Strasbourg, 1989: Sci. Géol., Mém., 87: 75–83.

Raffensperger, J.P. and Garven, G., 1995a. The formation of unconformity-type uranium ore deposits 1. Coupled groundwater flow and heat transport modeling. Amer. J. Sci., 295(5): 581–636.

Raffensperger, J.P. and Garven, G., 1995b. The formation of unconformity-type uranium ore deposits 2. Coupled hydrochemical modeling. Amer. J. Sci., 295(6): 639–696.

Reed, M.H., 1982. Calculation of multicomponent chemical equilibria and reaction processes in systems involving minerals, gases and an aqueous phase. Geochim. Cosmochim. Acta, 46: 513–528.

Remson, I., Hornberger, G.M., and Molz, F.J., 1971. Numerical Methods in Subsurface Hydrology. Wiley, New York, N.Y., 389 pp.

Rubin, J., 1983. Transport of reacting solutes in porous media: relation between mathematical nature of problem formulation and chemical nature of reactions. Water Resources Res., 19(5): 1231–1252.

Rubin, J. and James, R.V., 1973. Dispersion-affected transport of reacting solutes in saturated porous media: Galerkin method applied to equilibrium-controlled exchange in unidirectional steady water flow. Water Resources Res., 9(5): 1332–1356.

Sacks, L.A., Herman, J.S., and Kauffman, S.J., 1995. Controls on high sulfate concentrations in the Upper Floridan aquifer in southwest Florida. Water Resources Res., 31(10): 2541–2551.

Sams, M.S. and Thomas-Betts, A., 1988. Models of convective fluid flow and mineralization in southwest England. J. Geol. Soc., London, 145: 809–817.

Sanford, W.E. and Konikow, L.F., 1989a. Porosity development in coastal carbonate aquifers. Geol., 17: 249–252.

Sanford, W.E. and Konikow, L.F., 1989b. Simulation of calcite dissolution and porosity changes in saltwater mixing zones in coastal aquifers. Water Resources Res., 25(4): 655–667.

Schulz, H.D. and Reardon, E.J., 1983. A combined mixing cell/analytical model to describe two-dimensional reactive solute transport for unidirectional groundwater flow. Water Resources Res., 19(2): 493–502.

Schwartz, F.W., 1977. Macroscopic dispersion in porous media: the controlling factors. Water Resources Res., 13(4): 743–752.

Schwartz, F.W. and Domenico, P.A., 1973. Simulation of hydrochemical patterns in regional groundwater flow. Water Resources Res., 9(3): 707–720.

Schweich, D., Sardin, M., and Jauzein, M., 1993a. Properties of concentration waves in presence of nonlinear sorption, precipitation/dissolution, and homogeneous reactions 1. Fundamentals. Water Resources Res., 29(3): 723–733.

Schweich, D., Sardin, M., and Jauzein, M., 1993b. Properties of concentration waves in presence of nonlinear sorption, precipitation/dissolution, and homogeneous reactions 2. Illustrative examples. Water Resources Res., 29(3): 735–741.

Segerlind, L.J., 1984. Applied Finite Element Analysis. 2nd ed., Wiley, New York, N.Y., 427 pp.

Senger, R.K. and Fogg, G.E., 1987. Regional underpressuring in deep brine aquifers, Palo Duro Basin, Texas 1. Effects of hydrostratigraphy and topography. Water Resources Res., 23(8): 1481–1493.

Senger, R.K., Kreitler, C.W., and Fogg, G.E., 1987. Regional underpressuring in deep brine aquifers, Palo Duro Basin, Texas 2. The effect of Cenozoic basin development. Water Resources Res., 23(8): 1494–1504.

Sevougian, S.D., Schechter, R.S., and Lake, L.W., 1993. Effect of partial local equilibrium on the propagation of precipitation/dissolution waves. Industrial and Engineering Chemistry Research, 32: 2281–2304.

Sharp, J.M., Jr., Galloway, W.E. et al., 1988. Diagenetic processes in northwestern Gulf of Mexico sediments. In: G.V. Chilingarian and K.H. Wolf (Editors), Diagenesis, II. Developments in Sedimentology 43, Elsevier, New York, N.Y., pp. 43–113.

Shenhav, H., 1971. Lower Cretaceous sandstone reservoirs, Israel: petrography, porosity, permeability. A.A.P.G. Bull., 55(12): 2194–2224.

Shock, E.L. and Helgeson, H.C., 1988. Calculation of the thermodynamic and transport properties of aqueous species at high pressures and temperatures: correlation algorithms for ionic species and equation of state predictions to 5 kb and 1000°C. Geochim. Cosmochim. Acta, 52: 2009–2036.

Sibson, R.H., Moore, J.M., and Rankin, A.H., 1975. Seismic pumping—a hydrothermal fluid transport mechanism. J. Geol. Soc. London, 131: 653–659.

Skinner, B.J., 1979. The many origins of hydrothermal mineral deposits. In: H.L. Barnes (Editor), Geochemistry of Hydrothermal Ore Deposits. 2nd ed. Wiley, New York, N.Y., pp. 1–21.

Skinner, B.J. and Barton, P.B., 1973. Genesis of mineral deposits. Ann. Rev. Earth Planet. Sci., 1: 183–211.

Smith, L. and Chapman, D.S., 1983. On the thermal effects of groundwater flow 1. Regional scale systems. J. Geophys. Res., 88(B1): 593–608.

Smith, L. and Schwartz, F.W., 1980. Mass transport 1. A stochastic analysis of macroscopic dispersion. Water Resources Res., 16(2): 303–313.

Smith, L. and Schwartz, F.W., 1981a. Mass transport 2. Analysis of uncertainty in prediction. Water Resources Res., 17(2): 351–369.

Smith, L. and Schwartz, F.W., 1981b. Mass transport 3. Role of hydraulic conductivity data in prediction. Water Resources Res., 17(5): 1463–1479.

Steefel, C.I. and Lasaga, A.C., 1990. Evolution of dissolution patterns: permeability change due to coupled flow and reaction. In: D.C. Melchior and R.L. Bassett (Editors), Chemical Modeling in Aqueous Systems II. ACS Symposium Series 416, American Chemical Society, Washington, D.C., pp. 212–225.

Steefel, C.I. and Lasaga, A.C., 1992. Putting transport into water-rock interaction models. Geol., 20(8): 680–684.

Steefel, C.I. and Lasaga, A.C., 1994. A coupled model for transport of multiple chemical species and kinetic precipitation/dissolution reactions with application to reactive flow in single phase hydrothermal systems. Amer. J. Sci., 294: 529–592.

Steefel, C.I. and Van Cappellen, P., 1990. A new kinetic approach to modeling water-rock interaction: the role of nucleation, precursors, and Ostwald ripening. Geochim. Cosmochim. Acta, 54: 2657–2677.

Stoessell, R.K., Ward, W.C., Ford, B.H., and Schuffert, J.D., 1989. Water chemistry and $CaCO_3$ dissolution in the saline part of an open-flow mixing zone, coastal Yucatan Peninsula, Mexico. G.S.A. Bull., 101: 159–169.

Straus, J.M. and Schubert, G., 1977. Thermal convection of water in a porous medium: effects of temperature- and pressure-dependent thermodynamic and transport properties. J. Geophys. Res., 82(2): 325–333.

Stumm, W. and Morgan, J.J., 1981. Aquatic Chemistry: An Introduction Emphasizing Chemical Equilibria in Natural Waters. 2nd ed., Wiley, New York, N.Y., 780 pp.

Stumm, W. and Wollast, R., 1990. Coordination chemistry of weathering: kinetics of the surface-controlled dissolution of oxide minerals. Rev. Geophys., 28(1): 53–69.

Surdam, R.C., Crossey, L.J., Hagen, E.S., and Heasler, H.P., 1989. Organic-inorganic interactions and sandstone diagenesis. A.A.P.G. Bull., 73(1): 1–23.

Sverjensky, D. and Garven, G., 1992. Tracing great fluid migrations. Nature, 356: 481–482.

Taylor, T.R. and Soule, C.H., 1993. Reservoir characterization and diagenesis of the Oligocene 64–Zone sandstone, North Belridge Field, Kern County, California. A.A.P.G. Bull., 77(9): 1549–1566.

Tompson, A.F.B., Dougherty, D.E., and Bagtzoglou, A., 1989. Particle methods for reactive transport: 2. vector and parallel implementation and examples [abst.]. EOS, Trans., Amer. Geophys. Union, 70(43): 1078.

Torgersen, T., 1990. Crustal-scale fluid transport. EOS, Trans., Amer. Geophys. Union, 71(1): 1–4.

Torgersen, T., 1991. Crustal-scale fluid transport: magnitude and mechanisms. Geophys. Res. Lett., 18(5): 917–918.

Tóth, J., 1962. A theory of groundwater motion in small drainage basins in central Alberta, Canada. J. Geophys. Res., 67(11): 4375–4387.

Tóth, J., 1963. A theoretical analysis of groundwater flow in small drainage basins. J. Geophys. Res., 68(16): 4795–4812.

Tripathi, V.S. and Yeh, G.T., 1993. A performance comparison of scalar, vector, and concurrent vector computers including supercomputers for modeling transport of reactive contaminants in groundwater. Water Resources Res., 29(6): 1819–1823.

Truesdell, A.H. and Jones, B.F., 1973. WATEQ, a computer program for calculating chemical equilibria of natural waters. PB-220 464, NTIS, 73 pp.

Truesdell, A.H. and Jones, B.F., 1974. WATEQ, a computer program for calculating chemical equilibria of natural waters. J. Research U.S. Geol. Survey, 2(2): 233–248.

Tsang, C.-F. (Editor), 1987. Coupled Processes Associated with Nuclear Waste Repositories. Academic Press, New York, N.Y., 801 pp.

Tsang, C.-F., 1987. Introduction to coupled processes. In: C.-F. Tsang (Editor), Coupled Processes Associated with Nuclear Waste Repositories. Academic Press, New York, N.Y., pp. 1–6.

Van Brakel, J., 1975. Pore space models for transport phenomena in porous media: review and evaluation with special emphasis on capillary liquid transport. Powder Tech., 11: 205–236.

van der Heijde, P., Bachmat, Y., Bredehoeft, J., Andrews, B., Holtz, D., and Sebastian, S., 1985. Groundwater Management: The Use of Numerical Models. 2nd ed., Water Resources Monograph 5, American Geophysical Union, Washington, D.C., 180 pp.

van Zeggeren, F. and Storey, S.H., 1970. The Computation of Chemical Equilibria. Cambridge University Press, Cambridge, 176 pp.

Verma, A. and Pruess, K., 1985. Porosity and permeability changes from silica redistribution in non-isothermal flow [abst.]. EOS, Trans., Amer. Geophys. Union, 66(18): 273.

Verma, A. and Pruess, K., 1987. Effects of silica redistribution on performance of high-level nuclear waste repositories in saturated geologic formations. In: C.-F. Tsang (Editor), Coupled Processes Associated with Nuclear Waste Repositories. Academic Press, New York, N.Y., pp. 541–563.

Verma, A. and Pruess, K., 1988. Thermohydrological conditions and silica redistribution near high-level nuclear wastes emplaced in saturated geological formations. J. Geophys. Res., 93(B2): 1159–1173.

Voss, C.I., 1984. A finite-element simulation model for saturated-unsaturated, fluid-density-dependent ground-water flow with energy transport or chemically-reactive single-species solute transport. Water-Resources Investigations Report 84–4369, U.S. Geological Survey, 409 pp.

Walsh, M.P., 1983. Geochemical flow modeling. Ph.D. thesis, University of Texas, Austin, T.X., 502 pp.

Walsh, M.P., Bryant, S.L., Schechter, R.S., and Lake, L.W., 1984. Precipitation and dissolution of solids attending flow through porous media. Amer. Inst. Chem. Eng. J., 30(2): 317–328.

Wang, H.F. and Anderson, M.P., 1982. Introduction to Groundwater Modeling: Finite Difference and Finite Element Methods. W. H. Freeman and Company, New York, N.Y., 237 pp.

Ward, W.C. and Halley, R.B., 1985. Dolomitization in a mixing zone of near-seawater composition, Late Pleistocene, northeastern Yucatn Peninsula. J. Sed. Pet., 55(3): 407–420.

Watson, J.T.R., Basu, R.S., and Sengers, J.V., 1980. An improved representative equation for the dynamic viscosity of water substance. J. Phys. Chem. Ref. Data, 9(4): 1255–1290.

Weedman, S.D., Brantley, S.L., and Albrecht, W., 1992. Secondary compaction after secondary porosity: can it form a pressure seal? Geol., 20: 303–306.

Wei, C. and Ortoleva, P., 1990. Reaction front fingering in carbonate-cemented sandstones, Earth-Science Rev., 29: 183–198.

White, A.F., Delany, J.M., Narasimhan, T.N., and Smith, A., 1984. Groundwater contamination from an inactive uranium mill tailings pile 1. Application of a chemical mixing model. Water Resources Res., 20(11): 1743–1752.

Wicks, C.M. and Herman, J.S., 1994. The effect of a confining unit on the geochemical evolution of ground water in the Upper Floridan aquifer system. J. Hydrol., 153: 139–155.

Wicks, C.M. Herman, J.S., Randazzo, A.F., and Jee, J.L., 1995. Water-rock interactions in a modern coastal mixing zone. G.S.A. Bull., 107(9): 1023–1032.

Williams, G.P., 1994. Comment on "A performance comparison of scaler, vector, and concurrent vector computers including supercomputers for modeling transport of reactive contaminants in groundwater" by Vijay S. Tripathi and G. T. Yeh. Water Resources Res., 30(5): 1635–1637.

Willis, C. and Rubin, J., 1987. Transport of reacting solutes subject to a moving dissolution boundary: numerical methods and solutions. Water Resources Res., 23(8): 1561–1574.

Wolery, T.J., 1978. Some chemical aspects of hydrothermal processes at mid-oceanic ridges. I. Basalt-sea water reaction and chemical cycling between the oceanic crust and the oceans. II. Calculation of chemical equilibrium between aqueous solutions and minerals. Ph.D. thesis, Northwestern University, Evanston, I.L., 263 pp.

Wolery, T.J., 1979. Calculation of chemical equilibrium between aqueous solution and minerals: the EQ3/EQ6 software package. UCRL-52658, NTIS, 41 pp.

Wood, J.R., 1986. Thermal mass transfer in systems containing quartz and calcite. In: D.L. Gautiern

(Editor), Roles of Organic Matter in Sediment Diagenesis. Special Publication No. 38, Society of Economic Paleontologists and Mineralogists, Tulsa, O.K., pp. 169–180.

Wood, J.R., 1989. Modeling the effect of compaction and precipitation/dissolution on porosity. In: I.E. Hutcheon (Editor), Burial Diagenesis. Mineralogical Association of Canada Short Course Handbook 15, Mineralogical Association of Canada, pp. 311–362.

Wood, J.R. and Hewett, T.A., 1982. Fluid convection and mass transfer in porous sandstones—a theoretical model. Geochim. Cosmochim. Acta, 46: 1707–1713.

Wood, J.R. and Hewett, T.A., 1984. Reservoir diagenesis and convective fluid flow. In: D.A. McDonald and W.C. Surdam (Editor), Clastic Diagenesis. AAPG Memoir 27, American Association of Petroleum Geologists, Tulsa, O.K., pp. 99–111.

Wood, J.R. and Hewett, T.A., 1986. Forced fluid flow and diagenesis in porous reservoirs—controls on the spatial distribution. In: D.L. Gautier (Editor), Roles of Organic Matter in Sediment Diagenesis. Special Publication No. 38, Society of Economic Paleontologists and Mineralogists, Tulsa, O.K., pp. 181–187.

Woodbury, A.D. and Smith, L., 1985. On the thermal effects of three-dimensional groundwater flow. J. Geophys. Res., 90(B1): 759–767.

Wooding, R.A., 1957. Steady state free thermal convection of liquid in a saturated permeable medium. J. Fluid Mech., 2: 273–285.

Wooding, R.A., 1958. An experiment on free thermal convection of water in saturated permeable material. J. Fluid Mech., 3: 582–600.

Wooding, R.A., 1960. Instability of a viscous liquid of variable density in a vertical Hele-Shaw cell. J. Fluid Mech., 7: 501–515.

Wooding, R.A., 1963. Convection in a saturated porous medium at large Rayleigh number or Peclet number. J. Fluid Mech., 15: 527–544.

Yeh, G.T., 1981. On the computation of Darcian velocity and mass balance in the finite element modeling of groundwater flow. Water Resources Res., 17(5): 1529–1534.

Yeh, G.T. and Tripathi, V.S., 1989. A critical evaluation of recent developments in hydrogeochemical transport models of reactive multichemical components. Water Resources Res., 25(1): 93–108.

Yeh, G.T. and Tripathi, V.S., 1991. A model for simulating transport of reactive multispecies components: model development and demonstration. Water Resources Res., 27(12): 3075–3094.

Yeh, T.C.J., Srivastava, R., Guzman, A., and Harter, T., 1993. A numerical model for water flow and chemical transport in variably saturated porous media. Ground Water, 31(4): 634–644.

Yih, C.-S., 1961. Flow of a non-homogeneous fluid in a porous medium. J. Fluid Mech., 10: 133–140.

Zhang, H., Schwartz, F.W., and Sudicky, E.A., 1994. On the vectorization of finite element codes for high-performance computers. Water Resources Res., 30(12): 3553–3559.

Zienkiewicz, O.C., 1977. The Finite Element Method. 3rd ed., McGraw-Hill, London, 787 pp.

This Page Intentionally Left Blank

Chapter 4

Stabilization/solidification of hazardous wastes in soil matrices

EVAN R. COOK and BILL BATCHELOR

Abstract

Cementitious solidification/stabilization (s/s) treatment processes combine Portland cement or lime/-pozzolan mixtures with waste materials or contaminated soils to immobilize contaminants by physical and chemical mechanisms. It is a low cost remedial alternative and is commonly used at Superfund sites for treatment of soils, sludges and debris. Although widely utilized, s/s processes do not preclude migration of contaminants, but they can substantially reduce the rates of release to the environment. Evaluation of the impact of these releases requires appropriate applicaton of risk assessment techniques.

Problems associated with accurate prediction of leach rates are exacerbated in stabilized soil/waste matrices by (1) reactions between soil components and cement hydration or pozzolanic reaction products and (2) interactions between stabilized soil/waste matrices and adjacent media. This paper assesses effects of soil/cement reactions and environmental interactions on solid and solution phase characteristics of stabilized soil/waste matrices. First, available information on soil S/S applications will be evaluated to ascertain plausible disposal scenarios for stabilized soil/waste matrices. Second, cement hydration reactions, soil/cement reactions and environmental interactions that affect solid and solution phase characteristics of stabilized soil/waste matrices and, consequently, long-term leach rates will be delineated. Finally, techniques for predicting long-term leach rates will be evaluated.

1. Introduction

To control releases of hazardous constituents, large quantities of soils contaminated with hazardous wastes must be treated and/or disposed in the course of remedial activities mandated by provisions of the Comprehensive Environmental Response, Compensation, and Liability Act (CERCLA) and corrective action provisions of the Resource Conservation and Recovery Act (RCRA). Low-cost alternatives are necessary for treatment of soils at sites where extensive excavation and/or intensive treatment or recovery operations are technically infeasible, economically unwarranted, or environmentally unnecessary. Cementitious stabilization/solidification (S/S) processes are often appropriate under such circumstances.

Such processes have been employed as at least one component of remedial activities at 26 percent of all CERCLA sites (USEPA, 1993); the most prevalent waste matrices at such sites are soil and debris.

Cementitious S/S processes combine Portland cement or lime/pozzolan mixtures and various additives with waste materials to chemically or physically immobilize hazardous constituents. Such processes decrease the mobility of hazardous constituents through precipitation, sorption, oxidation/reduction, or diadochy reactions. They also decrease the potential for diffusive or advective transport by encapsulating mobile constituents in solid matrices of relatively low permeability and surface area.

Cementitious S/S processes are particularly appropriate for treatment of inorganic elemental contaminants because, unlike organic contaminants, elemental contaminants can not be destroyed or transformed to nontoxic compounds. Thus, the only remedial alternatives applicable to inorganic elemental contaminants are (1) immobilization (i.e. S/S processes), (2) sequestration in landfills or containment areas, (3) extraction from waste matrices and concentration in other forms (e.g. soil washing, metal recovery, acid/base leaching), or (4) some combination of these processes.

Cementitious S/S processes are demonstrated techniques for treatment of nonwastewater matrices contaminated with metallic constituents, particularly metals that form insoluble precipitates at high pH levels intrinsic to cement or lime-pozzolan matrices. Such processes have been identified as the "best demonstrated available technology" (BDAT) or one component of a treatment train that constitutes BDAT for nonwastewater treatability subcategories of 57 RCRA hazardous wastes (USEPA, 1993).

Because cementitious S/S processes are relatively inexpensive, they are generally appropriate for treatment of high-volume wastes, such as contaminated soils. Efficacy of such processes for treatment of metallic constituents in soil/waste matrices was demonstrated in several Superfund Innovative Technology Evaluation (SITE) projects (Barth, 1992; Bates, 1992; de Percin, 1989; Grube, 1990a; Sawyer, 1989a; Sawyer, 1989b; USEPA, 1991).

Nonetheless, appropriate applications of cementitious S/S processes for soil remediation are limited. Such processes do not preclude migration of metallic constituents, albeit they do substantially reduce leach rates of many metallic constituents, ideally to levels that can be assimilated by the environment. Thus, appropriate use of such processes requires accurate risk assessment to ensure long-term compliance with CERCLA remediation goals or RCRA corrective action cleanup goals.

Migration of metallic constituents into groundwater is generally the exposure pathway of concern in S/S applications. Risks associated with groundwater migration of metallic constituents depend upon (1) location and sensitivity of potential human or environmental receptors, (2) site-specific hydrogeological conditions, (3) secondary containment characteristics, and (4) leach rates of specific constituents.

The crux of methodologies for risk assessment in S/S applications is prediction of leach rates over long time intervals based upon short-term leach tests or intrinsic

waste properties. Given accurate predictions for leach rates, groundwater concentrations at points of compliance can be calculated using available landfill, vadose zone and/or groundwater fate and transport models, then risks can be assessed using intake and dose-response formulas.

Leach rates for metallic constituents in cementitious waste matrices generally depend upon (1) characteristics of the waste constituents, such as molecular diffusivity and aqueous solubility of various species; (2) physical characteristics of the stabilized waste matrix, such as permeability, durability, and surface area; (3) chemical characteristics of the stabilized waste matrix such as porewater pH, concentrations of major cations and anions, and cation exchange capacity; and (4) characteristics of the leachant, such as velocity and acidity.

Problems associated with accurate prediction of leach rates are exacerbated in stabilized soil/waste matrices by (1) reactions between soil components and cement hydration or pozzolanic reaction products and (2) interactions between stabilized soil/waste matrices and adjacent media. This paper assesses effects of soil/cement reactions and environmental interactions on solid and solution phase characteristics of stabilized soil/waste matrices. First, available information on soil S/S applications will be evaluated to ascertain plausible disposal scenarios for stabilized soil/waste matrices. Second, cement hydration reactions, soil/cement reactions and environmental interactions that affect solid and solution phase characteristics of stabilized soil/waste matrices and, consequently, long-term leach rates will be delineated. Finally, techniques for predicting long-term leach rates will be evaluated.

2. Soil stabilization/solidification applications

Portland cement is generally the principal ingredient in admixtures employed by commercial soil S/S processes (de Percin, 1989; Stinson, 1990; USEPA, 1991; Bates, 1992; Grube, 1990a). Cement content ranges from 15 percent (Stinson, 1990) to 300 percent (Grube, 1990a) by dry weight of soil/waste mixtures. High cement content is generally correlated with high organic content of soil/waste matrices (de Percin, 1989; Grube, 1990a). Cement content in soils with low organic content typically ranges from 15 to 70 percent (Grube, 1990a) by dry weight of soil/waste mixtures.

Reagents can be mixed with contaminated soils either ex situ or in situ. Effectiveness of mixers used for different soil S/S processes varies substantially (de Percin, 1989; Stinson, 1990; USEPA, 1991). Soil/cement/waste mixtures from ex situ processes are generally molded into one cubic yard monoliths for landfill disposal or disposed in pits on-site to cure (dePercin, 1989; Bates, 1992; Grube, 1990a).

Soil S/S applications can be broadly classified into three categories based upon disposal conditions: (1) S/S treatment followed by monofill disposal, (2) S/S treatment followed by municipal landfill disposal and (3) S/S treatment followed by open disposal or in situ treatment. Open disposal refers to placement of soil/ce-

TABLE 1

Leachant characteristics

Ion	Soil (mM)	MSW leachate (mM)	Carbonate GW (mM)	Crystalline GW (mM)
OH^-	10^{-6}–10^{-3}	1.6×10^{-5}	3×10^{-4}	3×10^{-5}
Ca^{2+}	0.8–8	35	1.2–1.5	0.01–0.3
Mg^{2+}	0.2–2	13	0.5–2.5	0.004–0.2
Si^{4+}	0.4–2	NA	NA	0.1–1.4
K^+	0.02–0.2	27	0.03–0.2	0.02–0.09
Na^+	0.02–0.2	NA	0.1–1.6	0.01–0.7
Al^{3+}	<0.001	1.5	NA	NA
Cl^-	2–20	37	0.2–0.8	0.01–0.6
SO_4^{2-}	0.5–5	NA	0.2–1	0.004–0.1
HCO_3^-	0.0046–4.6	NA	2.6–6.8	0.03–1

NA = no data available.

Sources: Bohn et al., 1979; Plaster, 1992; Maris et al., 1984; Freeze and Cherry, 1979; Uloth and Mavinic, 1977.

ment/waste mixtures or monoliths in pits without synthetic liners. Under this latter scenario, soil/cement/waste matrices directly contact adjacent soils or geologic formations. These different disposal scenarios have important implications with regard to long-term leach rates because extrinsic factors that affect leach rates, such as leachant velocity and composition, differ significantly under different disposal scenarios.

Under landfill disposal scenarios, leachant is generally static. Acidity in leachant generated by percolation of rainwater through soil cover materials probably consists primarily of carbonic acid and bicarbonate ion; organic acids contribute minimal acidity (Freeze and Cherry, 1979). Concentrations of other components in leachant generated by rainwater percolation are probably comparable to soil solutions. Unlike soil solutions, however, soluble component concentrations in landfills isolated from adjacent media can not be replenished by desorption or dissolution processes. Moreover, concentrations of most components decrease with time due to washout from soil cover materials. Carbonic acid, on the other hand, can be continuously generated by microbial and root respiration in soil cover materials.

Acidity in municipal landfill leachant substantially exceeds acidity in leachant generated by rainwater percolation through soil cover material due to formation of organic acids by anaerobic decomposition of organic wastes. Bishop (1986) suggested that acidity in municipal landfill leachant is approximately 100 meq/l compared to 1 meq/l in groundwater. Concentrations of other components (e.g., calcium, magnesium, potassium, chloride, and dissolved organic matter) are generally high relative to cement porewater and soil solutions or groundwater as indicated in Table 1. In addition, oxidation/reduction potential is generally low. Solids in municipal landfills may provide some buffer capacity for soluble components.

Under open disposal or *in situ* treatment scenarios, leachant flows around or

TABLE 2

28-Day hydraulic conductivity values for stabilized soil/waste matrices

Process	Hydraulic conductivity (cm/s)	Source
IWT/Geo-Con	0.24×10^{-7}–8.3×10^{-7}	Stinson, 1990
Silicate technology	$0.33 \times 10^{-7} - 2.5 \times 10^{-7}$	Bates, 1992
Solidtech	8.3×10^{-7}–2.1×10^{-9}	Grube, 1990b
Hazcon	8.4×10^{-9}–$5.0 + 10^{-10}$	Barth, 1992
Chemfix	1×10^{-6}–3.6×10^{-7}	USEPA, 1991

through soil/cement/waste monoliths. Leachant acidity, which consists primarily of carbonic acid and bicarbonate ions, is low relative to municipal landfill leachant, but it can be regenerated by microbial and root respiration in soils. Concentrations of other components are generally low relative to municipal landfill leachant. However, dissolution, desorption, or diffusive transport processes can replenish soluble component concentrations.

Leachant composition at depths below the soil zone generally differs somewhat from soil solutions. Furthermore, component concentrations differ in carbonate and crystalline rock formations. Variations of leachant composition with depth may affect leach rates under some *in situ* treatment scenarios because certain *in situ* processes, in particular, the Geo-Con process, can be employed at substantial depths. At the IWT/Geo-Con SITE demonstration, for example, sandy soil underlain by limestone was treated to depths of 14 to 18 feet, approximately 10 feet below the local water table.

Leachant flows through soil/cement/waste monoliths if hydraulic conductivity values are comparable to adjacent media. Leach rates are generally higher when leachant flows through waste monoliths because advective transport rates generally exceed diffusive transport rates, which govern leach rates when leachant flows around monoliths (Côté and Bridle, 1987). Hydraulic conductivity values for soil/cement/waste matrices are generally low relative to soils or geologic materials, at least initially. Hydraulic conductivity values for soil/cement/waste matrices at 28 days range from about 10^{-6} cm/s to about 10^{-9} cm/s as indicated in Table 2. Except for Soliditech samples, which were cured in a warehouse, values in Table 2 are representative within one order of magnitude of hydraulic conductivity values for soil/waste matrices treated by these processes and cured in the field. Some seasonal and geographical bias may exist since soil/waste matrices treated by different processes were cured in different climatic settings at different times of year (de Percin and Sawyer, 1991; Stinson, 1990; Bates, 1992; Grube, 1990a; USEPA, 1991).

Nonetheless, these values compare well to hydraulic conductivity values for unconsolidated soils, which range from about 10^{-2} cm/s for sandy soils to about 10^{-7} cm/s for clayey soils (Freeze and Cherry, 1979). They also compare well to hydraulic conductivity values for most rocks. Hydraulic conductivity of karst limestone, for example, ranges from approximately 10^{0} to 10^{-3} cm/s. Hydraulic conductivity values for fractured igneous and metamorphic rocks range from 10^{-2} to 10^{-5} cm/s. For limestone and dolomite, hydraulic conductivity values range

TABLE 3

Long-term hydraulic conductivity values for Hazcon and IWT products

IWT/Geo-Con (cm/s × 10^7)			Hazcon (cm/s × 10^9)			
Sample	1 mo.	12 mo.	Sample	1 mo.	9 mo.	18 mo.
B-6	4.2	2.4	LAN	3.6	57.0	3.7
B-6	–	5.6	DSA	1.5	115.0	2.3
B-7	5.9	0.07	FSA	84.0	95.0	3.4
B-21	8.3	0.05	LFA	4.5	37.0	2.4
B-22	4.1	0.13	PFA	6.3	3.4	2.6
C-1	0.24	0.16	LAS	3.1	19.9	3.6
C-7	4.1	2.8				
C-16	4.6	0.13				
C-17	2.5	2.5				

from 10^{-4} to 10^{-8} cm/s; and for unfractured igneous and metamorphic rocks and shale, they range from $10^{-}7$ to 10^{-11} cm/s (Freeze and Cherry, 1979). In addition, hydraulic conductivity values for soil/cement/waste matrices compare well to design values for compacted clay liners (i.e. 10^{-7} cm/s).

Changes in hydraulic conductivity of soil/cement/waste matrices with time are uncertain. Long-term hydraulic conductivity values have only been reported for Hazcon (de Percin and Sawyer, 1991) and IWT/Geo-Con products (Stinson, 1990); those values are summarized in Table 3. Long-term values for Hazcon products were probably not significantly different from one month values because they only differed by about one order to magnitude. Stegemann and Côté (1990) found that intralaboratory hydraulic conductivity measurements of replicate samples varied by about one order of magnitude.

Hydraulic conductivity values measured at one year for two samples from the IWT/Geo-Con demonstration (B-7 and B-21) probably were significantly lower than values measured at one month. Changes in hydraulic conductivity values of those samples may have been caused by further cement hydration reactions or, possibly, formation of calcium carbonate occlusions. IWT/Geo-Con's deep soil mixing process drilled through a limestone layer and mixed it into the soil/cement/waste column (Stinson, 1990). Other long-term hydraulic conductivity values for IWT/Geo-Con products probably were not significantly different from values at one month.

Environmental exposure may degrade soil/cement/waste matrices and engender higher hydraulic conductivity values. Durability of soil/cement/waste matrices has typically been measured by exposing stabilized soil/waste samples to repetitive wet/dry and freeze/thaw cycles. Soil/cement/waste matrices generally exhibit good durability as measured by those tests. Every soil S/S process evaluated by EPA as part of the SITE program, except the IWT/Geo-Con process, exhibited weight losses of one percent or less after 12 wet/dry or freeze/thaw cycles (Bates, 1992; de Percin, 1989; Grube, 1990c; Sawyer, 1989a; Sawyer, 1989b; USEPA, 1991; Stinson, 1990; Sawyer, 1990). IWT/Geo-Con products exhibited less than 0.1

TABLE 4

Composition of Portland cements

Cement	Component (percent by weight anhydrous cement)				
	$(CaO)_3SiO_2$	$(CaO)_2SiO_2$	$(CaO)_3Al_2O_3$	$(CaO)_4Al_2O_3Fe_2O_3$	$CaSO_4 \cdot 2H_2O$
I	50	25	12	8	5
II	45	30	7	12	5
IV	25	50	5	12	4
V	40	40	4	10	4

Source: Mindess and Young, 1981.

percent weight loss after 12 wet-dry cycles, but they exhibited from 0.5 to 30 percent weight loss (average 6 percent) after 12 freeze/thaw cycles.

Pertinence of wet/dry and freeze/thaw durability to specific soil S/S applications depends upon site conditions. Freeze/thaw durability was not pertinent at the IWT/Geo-Con demonstration site, for example, because it was located in Hialeah, Florida. Furthermore, exposure to wet/dry and freeze/thaw conditions can be controlled by capping. Every soil S/S process evaluated by EPA exhibited sufficient unconfined compressive strength (i.e. greater than 50 psi) to support construction of a RCRA landfill cover.

Thus, soil S/S processes can be designed to withstand wet/dry and freeze/thaw cycles, or if necessary, covers can be constructed to protect stabilized soil/waste monoliths from their effects. Wet/dry and freeze/thaw cycles are not the only factors, however, that affect long-term stability (i.e. capability to adequately attenuate migration of hazardous constituents) of soil/cement/waste matrices. Stability can also be adversely affected by carbonation, alkali-silica reactions, and sulfate reactions.

Under most open disposal or *in situ* treatment scenarios, it is reasonable to assume, at least initially, that water flows around soil/cement/waste matrices. Consequently, hazardous constituents leach via diffusion. Under some landfill disposal scenarios (e.g. landfill cover failure), water may flow through soil/cement/waste matrices. However, advective transport under such scenarios is probably negligible due to low hydraulic gradients (Côté, Bridle, and Benedek, 1986). Advective transport under landfill, open disposal, or *in situ* treatment scenarios may become non-negligible with time due to soil/cement reactions or environmental interactions.

3. Cement hydration reactions

Table 4 lists compositions of Portland cements. Type I is ordinary Portland cement, the type typically employed in soil S/S applications. Types II and V are moderate and high sulfate resistant cements, respectively. Type II exhibits slightly lower heat of hydration than type I. Type IV exhibits minimal heat of hydration and moderate sulfate resistance, but it develops strength slowly. Type III Portland

cement, which hardens quickly but exhibits high heat of hydration, is not listed in Table 4. Rapid strength development is relatively unimportant for soil S/S applications, and high heat of hydration can cause thermal cracks to develop in cement structures greater than 0.5 m thick (Mindess and Young, 1981) such as soil/cement/waste monoliths. Thus, type III is unlikely to be used for soil S/S applications.

The ferrite phase in Portland cement may differ substantially from $(CaO)_4Al_2O_3Fe_2O_3$. Lea (1971) noted that it is actually a solid solution with composition ranging from $(CaO)_6Al_2O_3(Fe_2O_3)_2$ to $(CaO)_6(Al_2O_3)_2Fe_2O_3$. Nonetheless, Lea (1971) suggested that hydration of $(CaO)_4Al_2O_3Fe_2O_3$ typifies hydration of the ferrite phase. Mindess and Young (1981) further noted that variations in the Al/Fe ratio only affect the rate of hydration. Taylor (1990) concluded, however, that pure $(CaO)_4Al_2O_3Fe_2O_3$ may not behave like the ferrite phase in Portland cement due to variation of the Al/Fe ratio and effects of impurity oxides. According to Taylor (1990), the ferrite phase typically contains about 21.4 percent by weight Fe_2O_3 in comparison to $(CaO)_4Al_2O_3Fe_2O_3$ which contains 32.9 percent by weight Fe_2O_3, and it contains about 10 percent impurity oxides due to isomorphic substitutions of Mg^{2+}, Si^{4+}, and Ti^{4+} for Fe^{3+}.

Portland cements also contain small amounts (<6 percent) of periclase (MgO). In addition, Portland cements typically contain about 0.5 percent by weight potassium and 0.2 percent by weight sodium (Mindess and Young, 1981), which strongly affect porewater pH of Portland cement pastes. About 70 percent of potassium and 35 percent of sodium occur as readily soluble sulfates; the remainder occur as impurities in calcium silicates and calcium aluminate (Taylor, 1990).

Tricalcium silicate and dicalcium silicate react with water to form calcium silicate hydrates and calcium hydroxide (portlandite) in accordance with equations 1 and 2, respectively.

$$(CaO)_3SiO_2 + 5H_2O \rightarrow (CaO)_xSiO_2\cdot(2+x)H_2O + (3-x)Ca(OH)_2 \quad (1)$$

$$(CaO)_2SiO_2 + 4H_2O \rightarrow (CaO)_xSiO_2\cdot(2+x)H_2O + (2-x)Ca(OH)_2 \quad (2)$$

Calcium:silicon ratios of calcium silicate hydrates may vary from 0.8 to 2.0 (Soroka, 1979), but average calcium:silicon ratios are generally about 1.5–1.7 under metastable equilibrium conditions (Taylor, 1990).

Tricalcium aluminate reacts initially with gypsum and water to form ettringite ($(CaO)_3Al_2O_3(CaSO_4)_3\cdot32H_2O$) in accordance with equation (3).

$$(CaO)_3Al_2O_3 + 3CaSO_4\cdot2H_2O + 26H_2O \rightarrow (CaO)_3Al_2O_3(CaSO_4)_3\cdot32H_2O \quad (3)$$

Ettringite reacts further with tricalcium aluminate to form calcium monosulfoaluminate ($(CaO)_3Al_2O_3CaSO_4\cdot12H_2O$) in accordance with equation (4).

$$2(CaO)_3Al_2O_3 + (CaO)_3Al_2O_3(CaSO_4)_3\cdot32H_2O + 4H_2O \rightarrow 3(CaO)_3Al_2O_3CaSO_4\cdot12H_2O \quad (4)$$

Relative proportions of monosulfoaluminate and ettringite in cement pastes at

equilibrium depend upon molar ratios of gypsum to tricalcium aluminate. At molar ratios greater than three, ettringite exists at equilibrium. At molar ratios between one and three, ettringite and monosulfoaluminate co-exist at equilibrium (Mindess and Young, 1981). At molar ratios less than one, tetracalcium aluminate hydrate ($(CaO)_4Al_2O_3 \cdot 13H_2O$) co-exists with monosulfoaluminate either in solid solution with it or separate crystals (equation (5)) (Mindess and Young, 1981; Taylor, 1990).

$$(CaO)_3Al_2O_3 + Ca(OH)_2 + 12H_2O \rightarrow (CaO)_4Al_2O_3 \cdot 13H_2O \quad (5)$$

Cement compositions cited above indicate that gypsum:tricalcium aluminate molar ratios in type I Portland cement are approximately 0.6, whereas molar ratios in types II, IV, and V are approximately 1.1, 1.3, and 1.6, respectively (Mindess and Young, 1981). Thus, monosulfoaluminate predominates at equilibrium (Reardon, 1992), but types II, IV, and V contain some ettringite, which co-exists with monosulfoaluminate, whereas type I contains some calcium aluminate hydrate.

Hydration of the ferrite phase forms solid solutions of calcium sulfoaluminates and calcium sulfoferrites analogous to products of tricalcium aluminate hydration (Mindess and Young, 1981; Taylor, 1990; Lea, 1971; Soroka, 1979) and iron-rich hydrogarnet (Taylor, 1990; Lea, 1971). The ferrite phase reacts initially with gypsum to form a solid solution of calcium sulfoaluminate and calcium sulfoferrite similar to ettringite with an Al/Fe ratio greater than tetracalcium aluminoferrite (equation (6)). Excess iron (III) forms an iron-rich hydrogarnet ($(CaO)_3(Al_2O_3, Fe_2O_3) \cdot 6H_2O$), in contrast to reaction of pure tetracalcium aluminoferrite with gypsum and calcium hydroxide in which excess iron (III) precipitates as iron hydroxides or oxides (Taylor, 1990). Products of hydration of the ferrite phase exhibit variable stoichiometry, but Fukuhara et al., cited by Taylor (1990), concluded that solid solutions of calcium sulfoaluminate and sulfoferrite in Portland cements exhibit Al/Fe ratios of about 3:1. Thus, equation (6) is probably a reasonable approximation of this reaction.

$$\begin{aligned}(CaO)_4Al_2O_3Fe_2O_3 + 3CaSO_4 \cdot 2H_2O + 2Ca(OH)_2 + 30H_2O \rightarrow \\ (CaO)_3(Al_2O_3)_{0.75}(Fe_2O_3)_{0.25}(CaSO_4)_3 \cdot 32H_2O + \\ (CaO)_3(Al_2O_3)_{0.25}(Fe_2O_3)_{0.75} \cdot 6H_2O\end{aligned} \quad (6)$$

Lea (1971) concluded that trisulfate solid solutions convert to monosulfate solid solutions ($(CaO)_3(Al_2O_3, Fe_2O_3)CaSO_4 \cdot 12H_2O$) in a manner analogous to conversion of ettringite to monosulfoaluminate except for cements with low tricalcium aluminate content. Lea (1971) also concluded that $(CaO)_4(Al_2O_3, Fe_2O_3) \cdot 13H_2O$ may form during hydration of the ferrite phase in Portland cement. However, stoichiometry for those reactions and gypsum:tetracalcium aluinoferrite molar ratios or tricaclium aluminate levels at which conversion occurs have not been delineated. Taylor (1990) noted that only about two-thirds of iron(III) in Portland cement occurs in calcium aluminoferrite; the remainder exists as impurities in tricalcium silicate or tricalcium aluminate. Iron (III) in those phases substitutes for aluminum in monosulfoaluminate or tetracalcium aluminate hydrate.

TABLE 5

Solids in Portland cement pastes

Solid (mmoles/g anhydrous cement)	I	II	IV	V
$(CaO)_{1.5}SiO_2 \cdot 3H_2O$	3.6	3.7	4.0	4.1
$Ca(OH)_2$	4.0	3.8	3.1	3.8
$(CaO)_3Al_2O_3CaSO_4 \cdot 12H_2O$	0.44	0.26	0.19	0.15
$(CaO)_3(Al_2O_3, Fe_2O_3)(CaSO_4)_3 \cdot 32H_2O$	0.16	0.25	0.25	0.21
$(CaO)_3(Al_2O_3, Fe_2O_3) \cdot 6H_2O$	0.16	0.25	0.25	0.21

Portland cement pastes also contain small amounts of periclase, which hydrates slowly to brucite ($Mg(OH)_2$), and hydrotalcite ($Mg_4Al_2(OH)_{14} \cdot 2H_2O$), which precipitates from magnesium impurities, particularly within calcium aluminoferrite phases (Taylor, 1990).

Table 5 lists approximate molar quantities for primary solids present in Portland cement pastes at equilibrium. Quantities in Table 5 were calculated under the following assumptions: (1) cement hydrates completely, (2) composition of calcium silicate hydrate can be approximated as $(CaO)_{1.5}SiO_2 \cdot 3H_2O$, (3) tricalcium aluminate forms only monosulfoaluminate, and (4) tetracalcium aluminoferrite forms $(CaO)_3(Al_2O_3, Fe_2O_3)(CaSO_4)_3 \cdot 32H_2O$ and $(CaO)_3(Al_2O_3, Fe_2O_3) \cdot 6H_2O$. This latter assumption may be incorrect, particularly for Type I Portland cements. Nevertheless, proportions of calcium sulfoaluminate and sulfoferrite hydrates relative to other solids in Portland cement are probably reasonably accurate.

Approximately 0.24 grams of water are required per gram anhydrous cement to form these products (Mindess and Young, 1981). Usually, the amount of water added to cement exceeds this amount; approximately 0.30 grams of water per gram anhydrous cement are required to achieve normal plasticity without plasticizers (Glasser, 1993). Nevertheless, complete cement hydration usually does not occur because dense layers of reaction products form around anhydrous cement particles, and slow diffusion of water through these layers limits the extent of reaction. Thus, the solid phase assemblage in cement pastes also includes occluded cement particles that do not affect solution phase characteristics.

Table 5 suggests that solid phase characteristics of cement matrices depend largely upon characteristics of calcium hydroxide and calcium silicate hydrate. Those solids do constitute primary pH buffer phases in cement matrices. In addition, calcium silicate hydrates govern surface characteristics of cement matrices due to their relatively large surface area (Glasser, 1993). Other solids may affect mobility of specific toxic constituents, however. For example, diadochy reactions or isomorphic substitution of CrO_4^{2-}, AsO_4^{2-}, and SeO_4^{2-} for SO_4^{2-} in monosulfoaluminate or ettringite may limit mobility of chromium, arsenic, and selenium in cementitious matrices (Glasser, 1993).

Potassium, sodium, and hydroxide ions dominate solution phases in cement matrices not open to environmental interactions. Potassium and sodium levels are relatively high in cement porewater even though potassium and sodium are minor components of Portland cements because no precipitates control potassium and sodium concentrations under metastable equilibrium conditions. Hydroxide ions counterbalance potassium and sodium ions to maintain electroneutrality of the

TABLE 6

Cement porewater characteristics

Ion	Concentration (mM)							Average	Std. Dev.
OH^-	743	590	440	477	546	689	651	591	111
Ca^{2+}	2	0.6	–	1	<1	<1	<1	1	0.7
Si^{4+}	–	–	–	–	0.9	–	1	1	0.07
K^+	639	420	490	376	442	547	519	490	88
Na^+	323	250	560	136	110	156	173	244	157
Al^{3+}	–	–	–	–	–	–	0.1	0.1	–
SO_4^{2-}	27	–	–	–	4	3	19	13	12

Source: Reardon, 1992.

solution phase (Reardon, 1992). Because a constant fraction of potassium and sodium in cement are soluble regardless of available water content, potassium and sodium concentrations in cement porewater solutions vary inversely with water:cement ratio. Consequently, hydroxide ion concentrations also vary inversely with water:cement ratio (Lawrence, 1966).

Calcium in cement porewater exists in quasi-equilibrium with portlandite. However, calcium levels are substantially lower in cement porewater than $CaO—H_2O$ systems due to high hydroxide ion concentrations (i.e., common ion effect). Silicon in cement porewater exists in quasi-equilibrium with calcium silicate hydrates or calcium silicate hydrates with alkali substituents. Aluminum exists in quasi-equilibrium with calcium monosulfoaluminate and ettringite or calcium aluminate hydrates. Magnesium exists in quasi-equilibrium with brucite or, possibly, hydrotalcite, and sulfate exists in quasi-equilibrium with monosulfoaluminate or ettringite (Atkins and Glasser, 1992).

Concentrations of major components in porewater expressed from ordinary Portland cement pastes with water:cement ratios of approximately 0.5, cured for time periods from 28 to 180 days, are presented in Table 6.

Oxidation/reduction potential of cement porewater ranges from 0 to +100 mV, but cement porewater is not well poised; its redox potential can be readily altered by electroactive species in additives or leachant, such as municipal landfill leachant (Atkins and Glasser, 1992).

Portland cement pastes are usually about 40 percent hydrated within one day at 15 to 25 °C, 70 percent hydrated within one month (Reardon, 1992), and 95 percent hydrated within one year (Atkins and Glasser, 1992). Typically, metastable equilibrium conditions are presumed to exist after one month.

4. Soil/cement reactions

Solid and solution phase characteristics of soil/cement matrices may differ substantially from cement matrices due to soil/cement reactions. Reactions between soil components and cement hydration products that affect solid and solution phase

characteristics of soil/cement/waste matrices include (1) pozzolanic reactions, (2) alkali metal reactions, and (3) alkali-silica reactions. In addition, soil components can interfere with cement hydration reactions.

Pozzolanic reactions in soil/cement matrices increase proportions of calcium silicate and aluminate hydrates and decrease proportions of calcium hydroxide in comparison to cement matrices. In addition, pozzolanic reactions may reduce calcium:silicon ratios of calcium silicate hydrates. Pozzolanic reactions do not reduce acid neutralization capacities of soil/cement matrices relative to cement matrices, but they may reduce pH levels of solutions in equilibrium with solid phase assemblages in soil/cement matrices. In addition, they affect cation exchange capacities of soil/cement/waste matrices. Alkali metal reactions reduce potassium and sodium concentrations in solution phases of soil/cement/waste matrices relative to cement matrices. Alkali-silica reactions may cause cracks to develop and, consequently, increase secondary permeability of soil/cement/waste matrices.

Soil/cement reactions generally attain equilibrium more slowly than cement hydration reactions. Pozzolanic reactions in clay/cement matrices may require up to 120 days to attain metastable equilibrium conditions. However, time requirements to attain equilibrium depend upon specific surface area of soil components. Therefore, soils with large proportions of coarse components may require longer time periods to attain equilibrium. Pozzolanic reactions may affect alkali metal concentrations; thus, alkali metal reactions also require long time periods to attain equilibrium. Alkali-silica reaction rates depend upon silica reactivity, and time requirements to attain equilibrium vary from 1 to 20 years (Mindess and Young, 1981).

4.1. Pozzolanic reactions

Pozzolanic reactions can occur between calcium and hydroxide ions generated by cement hydration reactions and silicate and aluminosilicate minerals in soils. These reactions can transform calcium hydroxide and calcium silicate hydrates with high calcium:silicon ratios into calcium silicate hydrates with low calcium:silicon ratios and calcium aluminate hydrates. Calcium silicate hydrates with low calcium:silicon ratios tend to buffer pH at lower levels than calcium silicate hydrates with high calcium:silicon ratios. In addition, calcium silicate hydrates with low calcium:silicon ratios exhibit net negative surface charge whereas calcium silicate hydrates with high calcium:silicon ratios exhibit net positive charge (Glasser, 1993). Thus, positively charged metals may adsorb more readily onto calcium silicate hydrates with low calcium:silicon ratios than calcium silicate hydrates with high calcium:silicon ratios.

Reactions between calcium and hydroxide ions and aluminosilicate minerals can probably be described in general by equation (7) for 2:1 layer aluminosilicate minerals, such as smectite, vermiculite, illite, and chlorite, and by equation (8) for 1:1 layer aluminosilicate minerals, such as kaolinite. Calcium:silicon ratios of calcium silicate hydrates (x) formed by pozzolanic reactions range from 0.8 to 2.

$$Al_2Si_4O_{10}(OH)_2 + (4x + 4)Ca^{2+} + (8x + 8)OH^- + 16H_2O \rightarrow$$
$$4[(CaO)_xSiO_2 \cdot (2 + x)H_2O] + (CaO)_4Al_2O_3 \cdot 13H_2O \quad (7)$$

$$Al_2Si_2O_5(OH)_4 + (2x + 4)Ca^{2+} + (4x + 8)OH^- + 11H_2O \rightarrow$$
$$2[(CaO)_xSiO_2 \cdot (2 + x)H_2O] + (CaO)_4Al_2O_3 \cdot 13H_2O \quad (8)$$

Equation (7) depicts pyrophillite, a 2:1 layer aluminosilicate mineral without substituents, as representative of 2:1 aluminosilicate minerals in general. However, isomorphic substitutions of Fe^{3+}, Fe^{2+}, or Mg^{2+} for Al^{3+} and Al^{3+} for Si^{4+} occur in most 2:1 layer aluminosilicate minerals. Also, chlorite contains an interlayer of aluminum or magnesium hydroxide (Bohn et al., 1979). Nonetheless, these equations indicate an approximate stoichiometry for pozzolanic reactions applicable to most common clay minerals.

Pozzolanic reactions usually generate calcium silicate hydrates and tetracalcium aluminate hydrate. Other pozzolanic reaction products such as tricalcium aluminate hexahydrate (Ford, Moore, and Hajek, 1982; Diamond, White, and Dolch, 1963) have been identified in soil/lime matrices, but such products are usually formed under abnormal conditions (i.e. high temperature). Most researchers agree that quaternary compounds (e.g. gehlenite hydrate) are usually not found in soil/lime matrices. Moh (1965), however, identified Stratling's compound (C_2ASH_x) in soil/cement matrices. Diamond, White, and Dolch (1963) and Glenn and Handy (1963) have suggested that isomorphic substitution of aluminum in calcium silicate hydrates occurs if no calcium aluminate hydrate phase develops, particularly in soils that contain relatively small amounts of aluminum (e.g., montmorillonitic soils).

Dissolution of portlandite and calcium silicate hydrates supply calcium and hydroxide ions required for pozzolanic reactions. Calcium silicate hydrates dissolve incongruently in accordance with equation (9) (Glasser, MacPhee, and Lachowski, 1987).

$$(CaO)_xSiO_2 \cdot (2+x)H_2O \rightarrow yCa^{2+} + 2yOH^- +$$
$$(CaO)_{x-y}SiO_2 \cdot (2 + x - y)H_2O \quad (9)$$

Because portlandite and calcium silicate hydrates function as primary pH buffer phases in cementitious matrices open to environmental interactions, the extent of pozzolanic reactions strongly affects pH levels in soil/cement/waste matrices under typical disposal conditions. Equilibrium hydroxide concentrations drop at clay:cement ratios of approximately 1.0 for soil/cement matrices dominated by 2:1 layer aluminosilicate minerals. At clay:cement ratios greater than 1.0, hydroxide ion concentrations are approximately one order of magnitude lower than hydroxide concentrations in cement matrices that do not contain clay or similar pozzolanic materials.

Pozzolanic reactions increase cation exchange capacities of cementitious matrices. Data from Komarneni, Roy, and Kumar (1983) show that cation exchange capacities of cementitious matrices increase by one order of magnitude from approximately 0.04 meq/g to approximately 0.4 meq/g with addition of 30 percent

silica fume by weight anhydrous cement. Higher cation exchange capacities result partially from generation of additional calcium silicate hydrates and partially from reduction of surface charges on calcium silicate hydrates.

Komarneni, Roy, and Kumar (1983) used x-ray diffraction and scanning electron microscopy/energy dispersive x-ray analysis to confirm that proportions of calcium hydroxide decrease and proportions of calcium silicate hydrates increase relative to cement matrices as cation exchange capacities increase due to pozzolanic reactions. Generation of additional calcium silicate hydrates can not, however, wholly account for incremental changes in cation exchange capacities measured by Komarneni, Roy, and Kumar (1983). Complete reaction of 30 percent by weight SiO_2 with portlandite in accordance with equation 10 generates only 5.0 mmoles calcium silicate hydrate/g anhydrous cement. With this additional calcium silicate hydrate, total quantities of calcium silicate hydrates in cementitious matrices with 30 percent SiO_2 are only 2.4 times greater than quantities in cement matrices, assuming that calcium:silicon ratios of calcium silicate hydrates are approximately 1.5 (see Table 5).

$$3Ca^{2+} + 6OH^- + 2SiO_2 + 3H_2O \rightarrow 2(CaO)_{1.5}SiO_2 \cdot 3H_2O \quad (10)$$

Reduction of surface charges on calcium silicate hydrates may explain incremental increases in cation exchange capacities in excess of levels attributable to generation of additional calcium silicate hydrates. Glasser (1993) stated that surface charges on calcium silicate hydrates decrease from net positive values at calcium:silicon ratios greater than 1.2 to net negative values at calcium:silicon ratios less than 1.2.

Pozzolanic reactions may decrease rather than increase cation exchange capacities of soil/cement/waste matrices relative to untreated soils because pozzolanic reactions dissolve clay minerals. Some clay minerals, such as vermiculite and montmorillonite, exhibit high cation exchange capacities, approximately 1 to 1.5 meq/g (Plaster, 1992). Formation of calcium silicate hydrates from those minerals may decrease overall cation exchange capacities of soil/cement/waste matrices. Other clay minerals, such as kaolinite, exhibit relatively low cation exchange capacities, approximately 0.03 to 0.15 meq/g (Plaster, 1992). Formation of calcium silicate hydrates from those minerals probably increases overall cation exchange capacities.

4.1.1. Soil reactivity

The magnitude of pH and cation exchange capacity shifts in soil/cement/waste matrices depend upon the extent of pozzolanic reactions. Amounts of reactive aluminosilicate and silicate minerals and amounts of available calcium and hydroxide ions limit the extent of pozzolanic reactions. Amounts of silicon and aluminum available for pozzolanic reactions can generally be ascertained from stoichiometry of aluminosilicate and silicate minerals in clay and silt fractions of soils. However,

organic and iron (oxy)hydroxide surface layers may limit silicon and aluminum availability.

4.1.1.1. Particle size distribution. Pozzolanic reaction rates depend upon specific surface area. However, there is no specific size range that dictates limits for pozzolanic reactivity. For example, Eades, Nichols, and Grim (1962) found that cementitious material surrounded and penetrated fractures in large particles of quartz, mica, and feldspar. They also noted that quartz grains appeared to be serrated; they interpreted these serrations as indicative of calcium hydroxide attack. Plaster and Noble (1970) also observed that large quartz and feldspar grains were often coated with cementitous material. Minerals in those size fractions react more slowly than clay particles, however, and they may not contribute significant amounts of silicon and aluminum if large amounts of clay are present and availability of calcium or hydroxide ions limits the extent of pozzolanic reactions.

Particle size affects reaction rates because pozzolanic reactions occur initially at particle surfaces, in particular, at edge surfaces. Substantial evidence exists from x-ray diffraction and electron microscopic analyses to support this conclusion. Eades and Grim (1960) used x-ray diffraction data to conclude that calcium hydroxide attacks edges of kaolinite particles. Diamond, White, and Dolch (1963) confirmed their conclusion. They observed kaolinite particles with frayed edges indicative of calcium hydroxide attack using electron microscopy. Sloane (1964) further confirmed that calcium hydroxide reacts at kaolinite edges. He observed reaction products along edges of kaolinite particles 48 hours after lime treatment. Seventy-two hours after treatment, these reaction products detached from kaolinite particles and aggregated into foliate clusters that continued to grow throughout 15 days of observation. Sloane (1964) also observed dissolution of kaolinite edges not directly associated with reaction products. Ormsby and Bolz (1966) concluded that nucleation of reaction products is not limited to particle edges. They further concluded that calcium hydroxide attacks both basal and edge surfaces of kaolinite particles.

Evidence for 2:1 layer aluminosilicate minerals is somewhat contradictory. Eades and Grim (1960) concluded that calcium hydroxide causes general structural deterioration of illite and montmorillonite micelles. In contrast, Diamond, White, and Dolch (1963) concluded that calcium hydroxide reacts at edges of illite and montmorillonite, and their structural integrity remains intact even in later stages of decomposition.

Mitchell and El Jack (1965) investigated cement/kaolinite, cement/silica flour/-montmorillonite, and cement/soil mixtures by electron microscopy and observed the same general pattern: formation of calcium silicate hydrate gels along the edges of groups of clay particles, followed by further deterioration of soil particles and diffusion of cement throughout the mixture until soil and cement were no longer distinguishable as separate phases.

Some controversy still exists about specific pozzolanic reaction mechanisms. Two mechanisms have been postulated: 1) topochemical and 2) dissolution-precipi-

tation. Stocker (1972) suggested with regard to soil/lime matrices that "... lime in solution reacts directly with clay crystal edges, generating ... calcium silicates and aluminates at or near these edges ...".

Greenburg (1956) and Diamond (1964) and Diamond and Kinter (1965) suggested possible topotactic reaction mechanisms. Greenburg (1956) concluded that calcium hydroxide reacts with silanol groups in accordance with equation (11).

$$2 \equiv SiOH + 2OH^- + Ca^{2+} \leftrightarrow (\equiv SiO)_2Ca + 2H_2O \quad (11)$$

Diamond (1964) and Diamond and Kinter (1965) implied that calcium hydroxide reacts with aluminol groups in accordance with equation (12).

$$2 \equiv AlOH + 2OH^- + Ca^{2+} \leftrightarrow (\equiv AlO)_2Ca + 2H_2O \quad (12)$$

Data of Ho and Handy (1963) and Davidson et al. (1965) suggest, however, that hydroxide attack is necessary to initiate pozzolanic reactions. Ho and Handy's (1963) data indicate that pozzolanic reactions do not occur below pH 11, and data presented by Davidson et al. (1965) indicate that pozzolanic reactions do not occur below pH 10.5.

Volk and Jackson (1963) stated that extensive dissolution of clay minerals occurs above pH 10. Furthermore, Handy et al. (1965) and Plaster and Noble (1970) noted large increases in dissolved silica and alumina associated with pozzolanic reactions. Thus, apparently, sorption of calcium ions onto aluminol groups with a pKa of about 7.5 (Volk and Jackson, 1963), or silanol groups with a pKa of about 9.5 (Bohn, et al., 1979), is insufficient to engender formation of calcium aluminate or silicate hydrates; pH levels high enough to induce dissolution of clay minerals are also necessary.

According to Srinivasan (1967), dissolution of silica occurs due to rupture of Si—O bonds of silanol groups by hydroxide ions. This process begins at particle surfaces and proceeds inward via diffusion of hydroxide ions. Presumably, dissolution of alumina proceeds via similar mechanisms. Silanol groups and aluminol groups are generally exposed at edge surfaces; however, Bohn et al. (1979) noted that some hydroxyl ions are exposed on basal surfaces. Moreover, Srinivasan (1967) suggested that rehydration effects on siloxane surfaces can induce formation of silanol groups. He further suggested that structural disorder affects pozzolanic reactions more than surface area because it affects the degree of structural strain on Si—O bonds and, consequently, their tendency to rupture in response to hydroxide attack.

Whether pozzolanic reactions proceed via dissolution of silica and alumina followed by reaction with calcium ions in solution or topochemically via complexation of calcium and hydroxide ions followed by rupture of Si—O or Al—O bonds, surface area strongly affects the rate of pozzolanic reactions. Thus, clay particles probably supply the bulk of silicon and aluminum for pozzolanic reactions in soil/cement matrices.

4.1.1.2. Clay mineralogy. The most prevalent minerals in clay fractions of soils are aluminosilicate minerals such as montmorillonite, vermiculite, chlorite, illite, and kaolinite, although primary silicates and aluminosilicates such as quartz, mus-

covite, biotite, and feldspars and metal (oxy)hydroxides such as goethite and gibbsite also may be present. Various researchers have shown that montmorillonite, vermiculite, chlorite, illite, kaolinite, quartz, and mica, which includes muscovite and biotite, can react with calcium and hydroxide ions to various degrees to form calcium silicate or aluminate hydrates.

Eades and Grim (1960) found that kaolinite and, to a lesser extent, illite react with calcium hydroxide to form calcium silicate hydrates. They also found that montmorillonite reacts with calcium hydroxide albeit at a slower rate. Although they could not identify any reaction products in montmorillonite/calcium hydroxide mixtures, they noted that unconfined compressive strength did increase after addition of about 4 to 6 percent calcium hydroxide, and they concluded that amorphous calcium silicate hydrates were probably present. Deterioration of clay mineral structures was noted in mixtures of lime and mixed layer illite, chlorite, and montmorillonite, but no reaction products were identified. Hilt and Davidson (1960) identified tetracalcium aluminate hydrate in montmorillonite/calcium hydroxide mixtures. Diamond and Kinter (1965) suggested that Hilt and Davidson's(1960) data also indicate presence of calcium silicate hydrates.

Glenn and Handy (1963) found that montmorillonite and kaolinite react with calcium hydroxide to form tetracalcium aluminate hydrate ($(CaO)_4Al_2O_3 \cdot 13H_2O$), calcium silicate hydrate (gel), calcium silicate hydrate (I), and, possibly, calcium silicate hydrate (II). They also found that vermiculite and, possibly, muscovite react with calcium hydroxide, to a lesser extent, to form tetracalcium aluminate hydrate. They suggested that montmorillonite exhibits the greatest pozzolanic reactivity, followed in decreasing order by kaolinite, vermiculite, and muscovite. They concluded that quartz does not react with calcium hydroxide. However, they did not specify the size range of quartz particles used in their investigations. Eades, Nichols, and Grim (1962) identified calcium silicate hydrates in three soils, dominated by kaolinite, vermiculite, and illite, three to four years after treatment with calcium hydroxide in the field.

Diamond, White, and Dolch (1963) found that kaolinite, montmorillonite, illite, pyrophillite, and mica react with calcium hydroxide to form calcium silicate hydrate (gel) or calcium silicate hydrate (I) and tetracalcium aluminate hydrate. They concluded that talc does not react with calcium hydroxide, but quartz, ground to pass a No 270 sieve (i.e., clay or silt size particles), does react with calcium hydroxide to form calcium silicate hydrate (gel). Ormsby and Bolz (1966) noted formation of calcium silicate hydrate (I) and calcium silicate hydrate (II) in kaolinite/lime mixtures.

Plaster and Noble (1970) did not attempt to identify any reaction products, but they did note that kaolinite was substantially diminished or completely dissolved by pozzolanic reactions in soil/cement matrices. Montmorillonite and vermiculite were also substantially diminished, but illite, chlorite, and feldspar were apparently only slightly diminished. They suggested that pozzolanic reactivity decreases in the following order: montmorillonite, kaolinite, illite. Ford, Moore, and Hajek (1982) identified tetracalcium aluminate hydrate, calcium silicate hydrate (gel), and calcium silicate hydrate (II) in soil/lime matrices dominated by kaolinite. Calcium silicate hydrate (II) was identified in soils dominated by montmorillonite.

Ford, Moore, and Hajek (1982) also noted reduction of gibbsite in soil/lime matrices.

In summary, all clay minerals can react with calcium and hydroxide ions generated by cement hydration reactions. Products of those reactions are usually calcium silicate and aluminate hydrates. Primary silicates and aluminosilicates in clay and silt fractions of soils also may react with calcium hydroxide to form calcium silicate and aluminate hydrates. However, reactivity generally decreases as specific surface area decreases.

4.1.1.3. Organic matter content. Thompson (1966) found that lime reactivity decreases significantly in soils with greater than one percent soil organic matter. He concluded that organic surface layers on soil particles inhibit pozzolanic reactions by decreasing availability of silicon and aluminum. His results show that treatment with hydrogen peroxide to remove soil organic matter significantly increases soil reactivity as indicated by unconfined compressive strength whereas additional lime, up to 15 percent by weight of soil, without hydrogen peroxide treatment does not significantly increase reactivity.

Cation exchange capacity of humus measured at pH 7 ranges from 1 to 3 meq/g (Plaster, 1992). In soil/cement matrices, the cation exchange capacity of humus is probably higher, possibly, as much as two times higher than its cation exchange capacity at pH 7 because the pK_a for phenolic hydroxyl groups, a major acidic functional group on humic substances, is about 10. Nonetheless, soils with one percent humus can not sorb more than approximately 0.01 to 0.03 meq Ca^{2+}/g soil. In comparison, 15 percent lime by weight of soil is equivalent to 4 meq Ca^{2+}/g soil. Thus, inhibition occurs even if relatively large amounts of calcium are available. Thompson (1966) suggested that silicon and aluminum availability limits pozzolanic reactions in soil/lime matrices with greater than 1 percent organic matter because soil organic matter "masks" surfaces of clay or silt particles. Effects of soil organic matter on pozzolanic reactivity of clay or silt particles in soil/cement matrices are unknown. Humic substances dissolve at pH levels of approximately 13.7 (Sposito, 1989). Thus, a substantial portion of soil organic matter may dissolve at pH levels intrinsic to soil/cement matrices.

4.1.1.4. Iron (III) content. Thompson (1966) also suggested that inhibition of pozzolanic reactions by iron (III) (oxy)hydroxide layers on soil particles may partially explain differences in lime reactivity of poorly-drained versus well-drained soils. Poorly-drained soils generally contain more iron (II) than well-drained soils because oxidation/reduction potential is generally lower in poorly-drained than well-drained soils. Since iron (II) is generally more soluble than iron (III) (Lindsay, 1979), iron (oxy)hydroxides occur less frequently on soil particles in poorly-drained soils than well-drained soils.

Other factors also affect pozzolanic reactivity of poorly-drained versus well-drained soils. Poorly-drained soils, for example, generally contain more silicon because they weather more slowly than well-drained soils. To ascertain whether iron (III) content significantly affects pozzolanic reactivity, Thompson (1966) extracted iron from two well-drained soils using a dithionate-citrate extraction

method. Lime reactivity of those soils after iron extraction was substantially greater than lime reactivity before iron extraction.

Iron (III) (oxy)hydroxide layers probably affect pozzolanic reactivity of soil/cement matrices, too. Solubilities of iron (III) (oxy)hydroxides increase by approximately one order of magnitude from pH 12.5 to 13.5, but the amount of soluble iron is still negligible relative to total iron. Total soluble iron in equilibrium with $Fe(OH)_3$ at pH = 13.5 and pe = 8 is approximately 4×10^{-2} mg/kg soil; whereas, the average iron content of soils is 26,000 mg/kg according to Sposito (1989). Availability of silicon and aluminum as a function of iron (III) content in soil/cement matrices has not yet been assessed.

4.1.2. Calcium hydroxide availability

Amounts of cement relative to soil largely govern availability of calcium and hydroxide ions in soil/cement matrices. However, only a portion of calcium and hydroxide ions in cement hydration products participate in pozzolanic reactions. Portlandite and calcium silicate hydrates supply calcium and hydroxide ions required for pozzolanic reactions. Amounts of those two solids in soil/cement/waste matrices depend upon the degree of cement hydration. Furthermore, calcium silicate hydrates generated by cement hydration only supply calcium and hydroxide ions until they attain equilibrium with calcium, silicon, and hydroxide in the solution phase and aluminosilicate minerals in the solid phase (i.e., complete decalcification does not occur). X-ray diffraction data from Komarneni, Roy and Kumar (1983) suggest that calcium monosulfoaluminate, ettringite, and calcium aluminate hydrates do not dissolve to supply calcium ions for pozzolanic reactions.

Moreover, one to seven percent calcium hydroxide by weight of clay may be unavailable for pozzolanic reactions due to various "lime retention" mechanisms (Hilt and Davidson, 1960; Eades and Grim, 1960; Ho and Handy, 1963). Hilt and Davidson (1960) and Ho and Handy (1963) concluded that pozzolanic reactions can not occur unless the "affinity of soil for lime is satisfied" (Hilt and Davidson, 1960). Lime retention mechanisms postulated by various researchers include (1) cation exchange reactions, (2) pH dependent cation exchange reactions, (3) sorption of calcium hydroxide ion pairs, (4) double layer compression, and (5) sorption of calcium hydroxide ion triplets. Those researchers focused primarily on reactions between lime and clay minerals. Reactions between cement and clay minerals differ somewhat from reactions between lime and clay minerals as discussed further below. Also, soil components other than clay minerals, in particular, soil organic matter, may affect availability of calcium or hydroxide ions.

Significance of lime retention, with regard to solid and solution phase characteristics of soil/cement matrices, depends upon the quantities of calcium or hydroxide ions effectively sequestered from subsequent pozzolanic reactions. Available evidence suggests that most calcium ions initially removed from solution by lime retention mechanisms participate directly in pozzolanic reactions (i.e. topotactic reactions), or they can re-enter the solution phase to maintain equilibrium as dissolved calcium concentrations decline due to cement hydration or pozzolanic reactions. Likewise, some portion of hydroxide ions removed from solution participate in pozzolanic reactions.

Cation exchange capacities of temperate, inorganic soils typically range from about 0.10 to 0.30 meq/g soil at pH 7 (Plaster, 1992), and percentage calcium saturation is usually about 75 percent at that pH level (Bohn et al., 1979). In comparison, amounts of calcium available in calcium hydroxide and calcium silicate hydrates generated by cement hydration in 20 percent Portland cement/soil mixtures, for example, are approximately 3 meq/g soil, even if decalcification of calcium silicate hydrates supplies only one mole calcium per mole calcium silicate hydrate. Thus, cation exchange reactions can remove 2.5 to 7.5 percent of available calcium in 20 percent cement/soil mixtures at pH 7, at least temporarily.

Cation exchange capacities of inorganic soil components increase as pH increases due to deprotonation of hydroxyl groups on clay minerals and metal (oxy)hydroxides. Helling et al. (1964) found, for example, that average cation exchange capacity of clay minerals in 60 Wisconsin soils increased approximately 20 percent from 0.54 meq/g at pH 5 to 0.64 meq/g at pH 8. Incremental increases in cation exchange capacity measured by Helling et al. (1964) were caused by deprotonation of aluminol groups. Cation exchange capacities of soil/cement matrices probably increase even more than Helling et al.'s (1964) data suggest because the pKa for silanol groups on clay minerals is approximately 9.5. Moreover, formation of $CaOH^+$ ion pairs at high pH levels may increase sorption of calcium onto permanent charge sites on clay minerals (Stocker, 1972). Sposito (1989) noted that metal hydroxide ion pairs may sorb more strongly than uncomplexed metals because they desolvate more easily. Ho and Handy (1963) further postulated that clay particles retain calcium ions in excess of typical cation exchange capacities due to double layer compression. In effect, high bulk calcium concentrations reduce concentration gradients between bulk and interfacial solutions and, thereby, decrease diffusion of calcium ions from diffuse double layers of clay particles.

These mechanisms may remove substantial amounts of calcium from solution during initial stages of soil/cement reactions. They may even temporarily delay cement hydration reactions. However, these mechanisms probably do not sequester calcium from subsequent pozzolanic reactions in soil/cement matrices. In contrast to soil/lime matrices, potassium and sodium ions in soil/cement matrices can displace calcium from metal (oxy)hydroxide and permanent charge cation exchange sites on clay minerals. Although calcium concentrations initially exceed potassium and sodium concentrations in cement porewater, they decline substantially about one day after initiation of cement hydration reactions due to precipitation of portlandite (Soroka, 1979). Thereafter, sorption of potassium or sodium is preferential from the standpoint of mass action. Calcium-hydroxide ion pairs may compete effectively for permanent charge exchange sites against sodium ions if they form inner sphere surface complexes, but they probably can not compete effectively against potassium ions which also form inner sphere complexes (Bohn et al., 1979). Thus, calcium sorption onto metal (oxy)hydroxides and permanent charge cation exchange sites on clay minerals probably does not sequester calcium from pozzolanic reactions.

Calcium ions that sorb onto pH-dependent cation exchange sites on clay minerals probably form surface complexes with aluminol or silanol groups in accord-

ance with equations (11) and (12) as a preliminary step in formation of calcium silicate and aluminate hydrates. Thus, sorption onto pH-dependent exchange sites on clay minerals probably does not sequester calcium from pozzolanic reactions. Moreover, calcium ions removed from solution due to double layer compression are probably not sequestered from pozzolanic reactions; outward diffusion probably occurs as calcium concentrations in solution decline.

Diamond and Kinter (1965) suggested that calcium hydroxide ion triplets physically sorb onto clay particles. They did not postulate a mechanism for this process, but they did note that portlandite possesses hexagonal structure which suggests that calcium hydroxide ion triplets may exhibit some polarity. Diamond and Kinter (1965) further suggested that calcium hydroxide sorbed onto clay particles subsequently reacts with silanol and aluminol groups to form calcium silicate and aluminate hydrates, so this mechanism apparently does not sequester calcium hydroxide from pozzolanic reactions.

Soil organic matter may remove small amounts of calcium from solution. Cation exchange capacity of humic substances is high relative to clay minerals, approximately 4 to 9 meq/g at pH 7 (Sposito, 1989), but surface horizons of soils other than peat or muck soils only contain about 0.5 to 5 percent organic matter by weight, and percent calcium saturation is about 75 percent at pH 7 (Bohn et al., 1979). Cation exchange capacity of soil organic matter in soil/cement matrices is probably somewhat higher than cation exchange capacity in soils because the pK_a for phenolic hydroxyl groups on humic substances is about 10. Nonetheless, the amount of calcium removed from solution by soil organic matter is negligible relative to available calcium in typical soil/cement mixtures. Moreover, potassium and sodium can displace calcium from soil organic matter as calcium concentrations in solution decline.

Complexation of calcium by organic ligands may limit calcium availability. Generally, concentrations of organic ligands in soil solutions are relatively low. However, dissolution of soil organic matter within soil/cement matrices may substantially increase organic ligand concentrations. Additional data on dissolution of soil organic matter at high pH is necessary to assess effects of organic complexation on calcium availability.

Substantial quantities of hydroxide ions generated by cement hydration reactions may be consumed by non-pozzolanic reactions. Major base neutralization reactions in noncalcerous soils include (1) neutralization of exchangeable H^+ or H_3O^+ ions, (2) neutralization of exchangeable Al^{3+} and polymeric aluminum species, (3) carbonic acid reactions, (4) deprotonation of carboxyl groups on soil organic matter, (5) deprotonation of aluminol groups on clay minerals, (6) bicarbonate reactions, (7) deprotonation of hydroxyl groups on metal (oxy)hydroxides, (8) deprotonation of silanol groups on clay minerals, (9) deprotonation of phenolic hydroxyl groups on soil organic matter, (10) dissolution of aluminosilicate minerals, and (11) dissolution of soil organic matter. Three of these reactions, deprotonation of aluminol groups, deprotonation of silanol groups, and dissolution of clay minerals, can probably be categorized as pozzolanic reactions.

Volk and Jackson (1963) measured base neutralization capacities to pH 10 for twelve soils. Base neutralization capacities for those soils ranged from 0.05 meq/g

to 0.20 meq/g. Clay content, mineralogy, organic matter content, and degree of weathering affect base neutralization capacity in soils. Mineralogy and degree of weathering largely determine initial soil pH, and initial pH largely determines which reactions cited above occur during base titration of any particular soil. Titration of soils to pH 10 may involve all of those reactions cited above except dissolution of clay minerals and soil organic matter, which generally occur above pH 10. Base titration of soils with initial pH values lower than about 7.5 includes base required for deprotonation of aluminol groups, and base titration of soils with initial pH values less than about 9.5 includes base required for deprotonation of silanol groups. Thus, some portion of base neutralized during Volk and Jackson's (1963) experiments was consumed by reactions that can be categorized as pozzolanic reactions. Nonetheless, base neutralization capacities measured by Volk and Jackson (1963) are small relative to quantities of available hydroxide in soil/cement matrices.

For example, a soil/cement mixture with 20 percent type I Portland cement by weight of soil contains about 0.80 mmoles calcium hydroxide and 0.72 mmoles calcium silicate hydrate per gram of soil. Dissolution of portlandite in this mixture generates about 1.6 milliequivalents hydroxide per gram of soil, and decalcification of calcium silicate hydrate generates an additional 2.2 milliequivalents hydroxide per gram of soil. Based upon Volk and Jackson's (1963) data, non-pozzolanic base neutralization reactions may consume approximately 1 to 5 percent of hydroxide generated by dissolution of portlandite and decalcification of calcium silicate hydrate in this soil/cement mixture. This estimate does not, however, include hydroxide ions required for dissolution of soil organic matter.

4.2. Alkali metal reactions

Potassium and sodium concentrations also affect calcium and hydroxide ion concentrations in cement matrices. To maintain electroneutrality, hydroxide ions counterbalance potassium and sodium ions in solution phases of cementitious matrices (Reardon, 1992). Elevated hydroxide concentrations suppress calcium concentrations due to the common ion effect on precipitation of portlandite and calcium silicate hydrate.

Hydroxide ions are also the principal counterions in soil/cement matrices. Major anions in soil solutions do not significantly affect the cation-anion balance. Chloride concentrations in soil solutions, about 2 to 20 mM (Bohn et al., 1979), are relatively low in comparison to potassium and sodium concentrations in cement porewater, about 500 mM and 250 mM, respectively. Silica concentrations in soil solutions, about 0.4 to 2 mM (Bohn et al., 1979), are also low relative to potassium and sodium concentrations. Moreover, silica ions are likely to precipitate as calcium silicate hydrates. Sulfate concentrations in soil solutions, about 0.5 to 5 mM (Bohn et al., 1979), are low relative to potassium and sodium concentrations, and furthermore, sulfate ions precipitate as monosulfoaluminate or ettringite.

Glasser (1993) concluded that pH elevation, above levels buffered by calcium hydroxide, due to potassium and sodium ions in solution, occurs regardless of availability of other anions, at least at low levels, because other anions are seques-

tered within solid phases, and hydroxide ions replace them in solution. Due to alkali hydroxides, initial pH levels up to approximately 13.5 may exist in soil/cement matrices.

In addition to water:cement ratio, soil:cement ratio affects potassium and sodium concentrations and, consequently, hydroxide ion concentrations in soil/cement matrices. Potassium content of soils is approximately 0.8 percent by weight; sodium content is approximately 0.6 percent by weight (Lindsay, 1979). Potassium and sodium weight percentages in Type I Portland cement in comparison are approximately 0.5 and 0.2, respectively (Mindess and Young, 1981). Both potassium and sodium exist primarily as exchangeable cations in soils. However, potassium is strongly adsorbed by certain 2:1 layer aluminosilicate minerals (Bohn et al., 1979). Potassium and sodium concentrations in porewater of temperate soils typically range from 0.2 mM in humid regions to 2 mM in arid regions (Bohn et al., 1979). Thus, potassium and sodium concentrations in soil solutions are low relative to sodium and potassium concentrations in cement porewater. However, soils may contribute substantial amounts of potassium and sodium in soil/cement matrices as ion exchange reactions and dissolution of clay minerals release potassium and sodium into solution.

Under typical disposal conditions, potassium, sodium, and hydroxide ions leach rapidly due to high concentration gradients between soil/cement matrices and adjacent media. However, potassium, sodium, and hydroxide ion concentrations also decline due to alkali metal reactions and pozzolanic reactions in soil/cement matrices not open to environmental interactions. Three possible mechanisms exist for removal of alkali metals from porewater of soil/cement matrices not open to environmental interactions.

First, potassium and, possibly, sodium may be sorbed onto calcium silicate hydrates. Glasser and Marr (1984) suggested that sorption removes potassium and, possibly, sodium from solution, concurrently with removal of hydroxide by pozzolanic reactions, as calcium:silicon ratios of calcium silicate hydrates decrease in response to pozzolanic reactions. Glasser, Luke, and Angus (1988) found that sorptive potential of calcium silicate hydrates increases in direct proportion to amounts of silica additive. Glasser and Marr (1984) found that potassium sorbs in preference to sodium on calcium silicate hydrates. Glasser, Luke, and Angus (1988) found that pozzolanic reactions do not significantly increase sodium sorptive capacity of calcium silicate hydrates.

Second, Glasser and Marr (1984), Reardon (1990), and Moh (1965) have suggested that alkali silicates may precipitate from solution. Moh (1965) concluded that sodium precipitates as sodium-calcium silicate hydrates at high soluble sodium:calcium ratios; however, he did not report any solubility data for this compound. Alkali silicates may precipitate as calcium:silicon ratios of calcium silicate hydrates decrease because silica concentrations in equilibrium with calcium silicate hydrates increase as calcium:silicon ratios decrease (Atkins and Glasser, 1992).

Third, potassium and sodium may sorb onto soil components. Although calcium sorption is preferential from the standpoint of both ionic potential and mass action during the initial phase of hydration in soil/cement matrices, potassium may be preferentially adsorbed by illite, vermiculite, and, to a lesser extent, montmorillon-

ite (Bohn et al., 1979; Grim, 1968). Potassium readily dehydrates (Bohn et al., 1979), so it can form inner-sphere complexes with clay minerals (Sposito, 1989). Due to its size and coordination number, anhydrous potassium fits into hexagonal holes on siloxane surfaces of illite, vermiculite, and other 2:1 layer clay minerals (Grim, 1968). Because it forms inner sphere complexes, potassium does not readily desorb (Bohn et al., 1979). Moreover, potassium collapses interlayer spaces of expansive clay minerals, such as vermiculite and smectite, and consequently, it can be retained between adjacent 2:1 layers, particularly under alkaline or dry conditions (Grim, 1968; Bohn et al., 1979). Fixation of potassium may require several months under normal soil conditions, probably due to slow diffusion of potassium into interlayer spaces (Grim, 1968). Potassium diffusion probably occurs more rapidly in soil/cement matrices, however, due to high concentration gradients. Moreover, sorption of potassium and sodium is preferential from the standpoint of mass action after calcium concentrations decline due to precipitation of portlandite.

4.3. Alkali-silica reactions

Alkali-silica reactions may cause expansive cracks to develop throughout soil/cement/waste matrices due to formation of alkali silica gels that absorb water (Mindess and Young, 1981; Taylor, 1990). Presumably, this reaction proceeds in accordance with equation (13) for potassium and, likewise, for sodium.

$$SiO_2 + 2KOH + xH_2O \rightarrow K_2SiO_2(OH)_2 \cdot xH_2O \quad (13)$$

Severity of alkali-silica reactions generally depends upon (1) type of reactive silica, (2) amount of reactive silica, (3) particle size of reactive material, (4) amount of available water, and (5) amount of available alkali (Mindess and Young, 1981).

Alkali-silica reactions usually occur due to dissolution of siliceous aggregates, especially aggregates that contain amorphous silica or poorly crystallized quartz, such as siliceous limestone and sandstone, chert, shale, or flint. Sand, sandstone, quartzite, and many igneous and metamorphic rocks may also react with alkali hydroxides if they contain microcrystalline or strained quartz. Crystalline quartz may react slowly. Synthetic glass is highly reactive (Mindess and Young, 1981). Soil/cement/waste matrices may contain any of these materials.

Alkali-silica deterioration involves reaction of isolated siliceous particles with alkali metal ions from surrounding cement to form potassium and sodium silicate hydrates that absorb water and, consequently, engender high, localized expansive forces. At high levels of reactive material, expansive forces become too diffuse to cause cracks. Thus, severity of alkali-silica reactions in cementitious matrices increases up to some percentage of reactive silica, called the pessimum percentage, then decreases at higher levels (Mindess and Young, 1981). For amorphous silica, the pessimum percentage is about 10 percent; for less reactive material, the pessimum percentage may be higher (Taylor, 1990). Similarly, severity of alkali-silica reactions depends upon particle size. Reactive particles in the 0.1–1.0 mm range engender high localized expansive forces; expansive forces due to particles less than 10 μm are negligible.

Taylor (1990) indicated that alkali-silica reactions are unlikely to occur in cementitious matrices that contain less than 4 kg/m^3 of equivalent $Na_2O(Na_2O + 0.66K_2O)$. A typical sandy or silty clay soil with dry bulk density of 60 lb/ft^3 may contain 14 kg/m^3 equivalent Na_2O. Most potassium and sodium exists in soils as exchangeable ions. However, potassium and sodium may be released by ion exchange reactions or dissolution of clay minerals in soil/cement matrices. Thus, alkali-silica reactions are plausible.

Pozzolans, such as clays, tend to reduce the severity of alkali-silica reactions in cementitious matrices if they contain low levels of potassium and sodium. Pozzolanic reactions reduce hydroxide ion concentrations and, consequently, the extent of silica dissolution. However, pozzolanic reactions also reduce calcium ion concentrations; calcium can stabilize alkali silica gels via formation of calcium silicate hydrates.

4.4. Soil interference

Clay particles and soil organic matter can interfere with cement hydration reactions in soil/cement/waste matrices. Both clay particles and soil organic matter can adsorb water and, thereby, reduce the amount of water available for cement hydration and pozzolanic reactions. Soil organic matter can also interfere with cement hydration reactions by inhibiting growth of calcium hydroxide and calcium silicate hydrate.

4.4.1. Clay particles

Davidson et al. (1962) found that water requirements increase as clay content increases in soil/cement matrices. They investigated effects of clay content on unconfined compressive strength. For a specific clay content, unconfined compressive strength increases due to increased cement hydration as available water content increases, then decreases due to increased porosity as available water content, in excess of the amount required for hydration, increases. Davidson et al. (1962) concluded that water requirements increase because water adsorbed onto clay particles is unavailable for cement hydration. Data extracted from graphs presented by Davidson et al. (1962) are summarized in Table 7. The last column contains the linear correlation coefficient for optimum moisture content as a function of clay content.

Degree of cement hydration governs the relative proportions of anhydrous cement, calcium hydroxide, and calcium silicate and aluminate hydrates in solid phases of soil/cement/waste matrices. Amounts of calcium silicate hydrates and calcium hydroxide in soil/cement/waste matrices largely govern long term performance characteristics, in particular acid neutralization capacity. However, data required to estimate the degree of cement hydration in soil/cement/waste matrices are not yet available. The amount of water adsorbed by clay particles in soil/cement mixtures depends upon clay content, clay mineralogy, exchangeable cations, and cement content.

TABLE 7

Optimum moisture content for 28-day unconfined compressive strength of sand-clay mixtures

Clay mineral	Cement (percent)	Optimum moisture content (percent) for sand:clay ratios					R
		100:0	75:25	50:50	25:75	0:100	
K	8	8.8	10.3	16.2	23.0	26.5	0.98
I	8	8.8	9.7	17.2	23.0	24.3	0.97
M	8	8.8	11.8	15.7	20.0	30.0	0.97
K	12	10.1	10.7	16.1	22.3	28.9	0.97
I	12	10.1	10.8	15.7	22.0	25.3	0.98
M	12	10.1	12.3	18.0	19.4	29.4	0.96
K	16	8.3	11.1	15.5	22.0	28.5	0.99
I	16	8.3	9.8	15.4	21.5	25.9	0.99
M	16	8.3	13.5	16.2	22.0	29.3	0.99

K = Kaolinite.
I = Illite.
M = Montmorillonite.

4.4.2. Soil organic matter

Soil organic matter can adsorb water in quantities comparable to some clay minerals, approximately 80 to 90 percent by weight (Bohn et al., 1979). In addition, soil organic matter can interfere with cement hydration reactions. Clare and Sherwood (1954) measured unconfined compressive strength in samples of an organic sandy soil (<10 percent clay and silt) treated with 10 percent Portland cement by weight of soil; greater than 70 percent of those samples exhibited unconfined compressive strength less than 50 psi after seven days. However, Clare and Sherwood (1954) found no correlation between unconfined compressive strength and total organic content, measured by loss on ignition. They concluded that retardation of cement hydration reactions was probably correlated with some "active" fraction of soil organic matter, rather than total organic content.

They found that glucose at 0.10 percent by weight of soil retards set for at least 28 days, and nucleic acid at less than 0.25 percent retards set for 7 days. They also found that 7-day unconfined compressive strength of 10 percent Portland cement/sand mixtures decreases from approximately 500 psi to 25 psi after addition of 0.50 percent pectin by weight of soil, and unconfined compressive strength of 10 percent Portland cement/sand mixtures decreases to about 10 psi after addition of 1 percent carboxymethylcellulose.

Taylor (1990) concluded that organic retarders delay cement hydration because they coat surfaces of calcium hydroxide and calcium silicate hydrate particles and, thereby, inhibit further growth. With regard to sucrose inhibition, the species that causes inhibition, according to Taylor (1990), is R—O—Ca—OH where R represents the sucrose anion. Carboxyl and phenolic hydroxyl groups, the two predominant surface functional groups on soil organic matter, can form similar structures via complexation of calcium and hydroxide ions. Indeed, Weitzman and Hamel (1989) found that adverse effects of organics on cement hydration correlate with abundance of carboxyl and hydroxyl groups. They also suggested that adverse

effects of soil organic matter are correlated with abundance of carbonyl groups, although the mechanism for formation of R—O—Ca—OH species from carbonyl groups is unclear.

Validity of this mechanism is further substantiated by results from Clare and Sherwood (1954) who found that addition of calcium chloride at 3 percent by dry weight of soil overcomes inhibitory effects of soil organic matter. According to Taylor (1990), calcium chloride accelerates hydration of tricalcium silicate. Thus, calcium chloride promotes growth of calcium silicate hydrates and calcium hydroxide, whereas soil organic matter hinders growth of those compounds.

Results from Clare and Sherwood (1954) suggest that high pH levels in soil/cement matrices may exacerbate adverse effects of soil organic matter. Dissolution of soil organic matter may substantially increase concentrations of organic retarders in soil/cement matrices. Cellulose, for example, is composed of glucose monomers; if cellulose dissolves at high pH, glucose concentrations may increase substantially. Whereas cellulose at one percent by weight of soil only decreases 7-day unconfined compressive strength of soil/cement matrices by approximately 100 psi, glucose completely inhibits cement hydration at 0.1 percent (Clare and Sherwood, 1954). Presumably, dissolution of cellulose did not adversely affect cement hydration reactions in Clare and Sherwood's (1954) experiments because they employed a water:cement ratio of one; thus, alkali hydroxide concentrations and, consequently, pH were relatively low (<13.5)., below levels required to dissolve humic substances Dissolution of soil organic matter may also inhibit cement hydration reactions due to complexation of cement matrix components by dissolved organic matter or consumption of hydroxide ions. Additional data on dissolution of soil organic matter at high pH is necessary to assess effects of organic complexation on cement hydration reactions.

In summary, pozzolanic reactions between calcium and hydroxide ions generated by cement hydration and, primarily, clay minerals in soils can lower porewater pH levels and raise cation exchange capacities of soil/cement matrices relative to cement matrices. The extent of pozzolanic reactions in soil/cement matrices depends upon amounts of reactive silicon and aluminum in soils and calcium and hydroxide ions in cement hydration products. Amounts of silicon and aluminum available for pozzolanic reactions can generally be ascertained from stoichiometry of aluminosilicate minerals in clay fractions of soils. However, organic and iron (oxy)hydroxide surface layers on clay particles can reduce availability of silicon and aluminum. Amounts of calcium and hydroxide ions depend upon amounts of portlandite and calcium silicate hydrate in soil/cement matrices, and amounts of portlandite and calcium silicate hydrates depend upon soil:cement ratio and extent of cement hydration. Clay and soil organic matter in soils affect the extent of cement hydration. Calcium sorption and complexation on soil components probably does not significantly reduce amounts of calcium available for pozzolanic reactions. Non-pozzolanic reactions may substantially reduce amounts of hydroxide ions available for pozzolanic reactions. Potassium and sodium concentrations also affect hydroxide and calcium levels in soil/cement matrices. In addition, alkali-silica reactions in soil/cement matrices may increase secondary permeability of soil/cement matrices.

5. Environmental interactions

Because soil/cement/waste matrices are not closed systems, environmental interactions also affect solid and solution phase characteristics. Such interactions include diffusive transport of matrix components from soil/cement/waste matrices into adjacent media and reactions with external components that diffuse into soil/cement/waste matrices including acids, carbonate ions, sulfate ions, and magnesium ions. Diffusive transport rates frequently dictate time requirements to attain equilibrium for these reactions.

5.1. Intermedia transport

Diffusive transport occurs due to concentration gradients between soil/cement/waste matrices and adjacent media. Comparison of average cement porewater concentrations in Table 6 with leachant concentrations in Table 1 suggests that hydroxide, potassium, sodium, aluminum and sulfate tend to diffuse outward from soil/cement/waste matrices. In contrast, magnesium and carbonate probably diffuse from soil solutions, groundwater, or municipal landfill leachant into soil/cement/waste matrices. Calcium may diffuse from soil solutions and municipal landfill leachant into soil/cement/waste matrices. However, it probably diffuses from soil/cement/waste matrices into groundwater of carbonate and crystalline rock formations. Porewater concentrations in soil/cement matrices are comparable to concentrations in cement matrices (Table 6) at low clay:cement ratios (i.e., <1). At high clay:cement ratios, however, hydroxide ion concentrations decline due to pozzolanic reactions. In addition, potassium, sodium, and calcium concentrations decline as clay:cement ratios increase (Atkins and Glasser, 1992; Reardon, 1992; Larbi, Fraay, and Bijen, 1990).

Diffusive transport rates depend upon (1) mobile component concentrations in soil/cement/waste matrices and adjacent media, (2) leachant velocity, (3) matrix geometry (i.e., surface area:volume ratio), and (4) porosity, tortuosity, and water content of soil/cement/waste matrices and adjacent media. If leachant velocity is low relative to diffusive transport rates (e.g., monofill or municipal landfill disposal scenarios), leachant concentrations approach equilibrium with soil/cement porewater concentrations and, consequently, leach rates depend upon leachant flow rate and soil/cement porewater concentrations (Batchelor, 1993a)

$$F_l = Q_l C(MW) \tag{14}$$

where F_l = leach rate (mass/time), Q_l = leachant flow rate (volume/time), C = mobile component concentration (moles/volume), and MW = molecular weight of component (mass/mole).

If leachant velocity is high relative to diffusive transport rates (e.g., open disposal or *in situ* treatment scenarios), fresh leachant with low component concentrations continually contacts waste monoliths. Under this condition, diffusive transport rates within soil/cement/waste matrices govern leach rates. A one-dimensional

material balance that describes diffusive transport without reactions for soil/cement/waste matrices with rectangular geometry can be expressed as equation (15)

$$\frac{\partial C}{\partial t} = D_e \frac{\partial^2 C}{\partial X^2} \tag{15}$$

where D_e = effective diffusivity (length^2/time). Effective diffusivity is smaller than molecular diffusivity because flux is measured in one direction in porous solids, but components follow tortuous pathways through pores. A one-dimensional model is appropriate for symmetric waste forms, and it is reasonable to presume that waste forms are symmetrical for many soil S/S scenarios. It is also reasonable to assume that waste forms are rectangular for most soil S/S scenarios. However, equation (15) is valid for nonrectangular waste forms at early leach times.

Crank (1975) solved equation (15) analytically using the following boundary conditions: (1) zero concentration at interface between waste monolith and leachant at all times and (2) concentration at midpoint of waste monolith approximately equal to initial concentration at all times. This second boundary condition is reasonable if less than 20 percent of the initial component mass has leached from the waste matrix (Cheng and Bishop, 1992). Crank's (1975) initial condition requires that component concentrations be uniform for all points X within the solid at time $t = 0$; this condition does not always exist in soil/cement/waste matrices, but it is not unreasonable as an approximation. Equation (16) is Crank's solution

$$C(X, t) = C_0 \operatorname{erf}\left(\frac{X}{(4D_e t)^{0.5}}\right) \tag{16}$$

where C_0 = initial mobile component concentration, erf = error function, and X = distance into the waste monolith from the interface.

Calculation of component mass leached at any time requires integration of the concentration profile over the entire slab (Crank, 1975)

$$M_t = \frac{2M_0}{LC_0} \int_0^L (C_0 - C)\, dX \tag{17}$$

where L = distance from the interface to the centerline of the waste monolith, M_0 = initial mass of component within waste monolith, and M_t = mass of component leached from waste monolith at any time, t. For waste forms with nonrectangular geometry, L = volume/surface area. Equation (17) can be solved using the concentration distribution in equation (16) to yield equation (18)

$$M_t = \frac{2M_0}{L}\left(\frac{D_e t}{\pi}\right)^{0.5} \tag{18}$$

dM_t/dt equals the leach rate, F_l, in disposal environments with high leachant velocity

$$F_l = \frac{M_0}{L}\left(\frac{D_e}{\pi t}\right)^{0.5} \tag{19}$$

Equations (16) and (19) presume the leachant does not contain the component of interest at significant concentrations. This presumption is probably valid for most contaminants. However, leachant concentrations may not be negligible for matrix components (e.g., calcium, silicon, sodium, potassium, aluminum, and magnesium), even if leachant velocity is high relative to diffusive transport rates, as indicated in Table 1. Thus, the first boundary condition for Crank's solution (equation (16)) may be invalid for many disposal scenarios.

Equations (16) and (19) are also invalid when effective diffusivity values within adjacent soils or geologic media approach values within soil/cement/waste matrices. Equation (20) is appropriate under those conditions (Crank, 1975)

$$C(X,t) = \frac{C_0}{1 + (D_2/D_1)^{1/2}} \left[1 + (D_2/D_1)^{1/2} \operatorname{erf}\left(\frac{X}{(4D_1t)^{1/2}}\right)\right] \tag{20}$$

where D_1 = effective diffusivity within the waste matrix and D_2 = effective diffusivity in adjacent soils or geologic media.

Under most soil S/S disposal scenarios, $(D_2/D_1)^{1/2} \gg 1$ (i.e., effective diffusivity within adjacent soils or geologic media exceeds effective diffusivity within the waste matrix), and equation (20) is approximately equal to equation (16). Oblath (1989), for example, found comparable leach rates from waste monoliths in water, sand at 80 percent saturation, and soil at 32 percent saturation. However, Oblath (1989) also found that effective diffusivity values for dry soils (i.e., 4 percent saturation) approach values for stabilized waste matrices, and consequently, leach rates decline in accordance with equation (20). Moisture content also affects effective diffusivity values within soil/cement/waste matrices. Impacts of variable moisture content on leach rates are generally disregarded, however, because leach rates under saturated conditions constitute worst-case conditions.

Desorption and dissolution reactions, on the other hand, can not be disregarded. Equation (19) is premised upon the assumption that mobile components are neither generated nor removed by processes other than diffusive transport. In effect, the amount of component initially present in mobile form constitutes the total amount of that component in the waste matrix. Dissolution or desorption of components from the solid phase as solution phase concentrations decrease due to diffusive transport precludes utilization of equation 19 without modification. These types of processes generally do occur for components of interest in soil/cement/waste matrices. A one-dimensional material balance for soil/cement/waste matrices with rectangular geometry that includes such reactions can be expressed as equation (21) (Myers and Hill, 1986)

$$\frac{\partial C}{\partial t} = D_e \frac{\partial^2 C}{\partial X^2} - \frac{\partial C_{im}}{\partial t} \tag{21}$$

where C_{im} = immobile component concentration (moles component/volume porewater).

If local equilibrium exists, linear partitioning between mobile and immobile phases (i.e., $K_p = C_{im}/C$) can be incorporated into equation (21) in accordance with equation (22).

$$\frac{\partial C}{\partial t} = D_e \frac{\partial^2 C}{\partial X^2} - \frac{\partial (K_p C)}{\partial t} \tag{22}$$

Many sorption reactions can be adequately described by linear partitioning at least at low concentrations, and the local equilibrium assumption is generally appropriate for sorption reactions that do not involve inner sphere surface complexation. If K_p does not vary as a function of time, equation (22) can be rearranged to yield equation (23).

$$\frac{\partial C}{\partial t} = \frac{D_e}{(1 + K_p)} \frac{\partial^2 C}{\partial X^2} \tag{23}$$

An observed diffusivity for components that undergo linear partitioning can be defined as equation (24)

$$D_{obs} = \frac{D_e}{(1 + K_p)} \tag{24}$$

Equation (23) is identical to equation (15) after substitution of D_{obs}. Thus, the leach rate with linear partitioning can be expressed in a form identical to equation (19) with substitution of D_{obs} for D_e.

$$F_l = \frac{M_0}{L} \left(\frac{D_{obs}}{\pi t} \right)^{0.5} \tag{25}$$

For solubility-limited dissolution processes, the rate of change of immobile component concentration with time can be expressed as equation (26)

$$\frac{\partial C_{im}}{\partial t} = -k(C_e - C) \tag{26}$$

where C_e = mobile component concentration in equilibrium with the solid phase (moles component/volume porewater). Thus, equation (21) can be expressed as equation (27) (Côté, Constable, and Moreira, 1987)

$$\frac{\partial C}{\partial t} = D_e \frac{\partial^2 C}{\partial X^2} + k(C_e - C) \tag{27}$$

where k = dissolution rate constant (1/time). Equation (28) is Godbee and Joy's solution of equation (27) (Côté, Constable, and Moreira, 1987) for a semi-infinite medium with zero surface concentration and uniform initial concentration (i.e., the same boundary and initial conditions as equation (16))

$$F_l = C_e A (D_e k)^{1/2} \left[\text{erf}(kt)^{1/2} + \frac{e^{-kt}}{(\pi kt)^{1/2}} \right] \tag{28}$$

where A = surface area of the waste monolith. The mobile component concentration in equilibrium with the solid phase can be calculated using the solubility product.

Alternatively, an observed diffusivity value analogous to equation (24) can

be defined for components that undergo solubility-limited dissolution reactions (Batchelor, 1990)

$$D_{obs} = \frac{\pi[F_m(1 - F_m) + 0.5F_m^2]D_e}{2} \tag{29}$$

where F_m = mobile fraction of component at time $t = 0$. Given this definition of D_{obs}, leach rates for components that undergo dissolution reactions can be expressed as equation (25). Thus, a simple leach model based upon diffusion with no reactions (equation (19)) can be modified to include diffusion with linear sorption reactions or diffusion with dissolution reactions by substitution of appropriate values for D_{obs}.

This latter approach is advantageous because diffusivity values ascertained from semidynamic leach tests based upon this simple leach model (i.e., ANS 16.1) can be decomposed using equations (29) and (24) into components associated with physical and chemical immobilization mechanisms. In accordance with equation (18), a plot of component mass leached at time t (M_t) versus $t^{0.5}$ is a straight line with slope (S) described by equation (30).

$$S = \frac{2M_0}{L}\left(\frac{D_{obs}}{\pi}\right)^{0.5} \tag{30}$$

Observed diffusivity values can be calculated given this slope. Except for nonreactive components, however, diffusivity values obtained from semidynamic leach tests are not equal to effective diffusivity values, which describe only mobility of soluble forms of components and, consequently reflect only physical immobilization mechanisms. Diffusivity values observed during semidynamic leach tests depend upon both physical and chemical immobilization mechanisms.

Differentiation of physical and chemical immobilization mechanisms facilitates a systematic approach to minimization of observed diffusivity values. Physical components of observed diffusivity (D_{obs}) as represented by effective diffusivity (D_e) in equations (24) and (29) can be quantified using the electrical conductivity/resistivity method developed by Taffinder and Batchelor (1993). Chemical components of observed diffusivity as represented by mobile fraction (F_m) in equation (29) and partition coefficient (K_p) in equation (24) can be quantified by porewater expression (Barneyback and Diamond, 1981) and batch sorption experiments, respectively. Thus, independent effects of chemical and physical immobilization mechanisms on observed diffusivity can be investigated using equations (24) and (29).

Although these equations facilitate development of S/S processes that minimize observed diffusivity values under laboratory conditions, they can only describe leach rates under conditions that emulate the assumptions underlying their solutions (e.g. zero concentration at interface between waste form and leachant). They can not predict leach rates under field conditions. Interactions with external components invalidate assumptions underlying solutions of these equations under field conditions. For example, acids that diffuse into soil/cement/waste matrices from adjacent media can react with hydroxide ions in solution and, consequently,

increase soluble concentrations of components that exist in equilibrium with hydroxide solids. Moreover, components of interest may exhibit multiple behaviors including precipitation/dissolution, sorption/desorption and complexation. An approach that accounts for multicomponent interactions will be discussed in the section on long-term performance assessment. Changes in solid and solution phase characteristics of soil/cement matrices due to reactions with external components are discussed in the following sections.

5.2. Acid reactions

Acid reactions reduce equilibrium pH levels and acid neutralization capacities of soil/cement/waste matrices. Portlandite buffers porewater pH levels at about 12.4 after alkali hydroxide concentrations decline in cementitious matrices. Hydrogen ions react with portlandite in accordance with equation (31).

$$Ca(OH)_2 + 2H^+ \rightarrow Ca^{2+} + 2H_2O \tag{31}$$

Calcium silicate hydrates buffer pH after dissolution of portlandite. Hydrogen ions react with calcium silicate hydrates in accordance with equation (32).

$$(CaO)_x SiO_2 \cdot (2 + x)H_2O + 2yH^+ \rightarrow$$
$$yCa^{2+} + (CaO)_{x-y} SiO_2 \cdot (2 + x - y)H_2O + 2yH_2O \tag{32}$$

Calcium silicate hydrates with calcium:silicon ratios greater than or equal to 1.5 buffer pH levels near 12.4. As calcium:silicon ratios decrease from 1.5 to 1.1, pH decreases from 12.4 to 11.8. As calcium:silicon ratios decrease from 1.1 to 0.85, pH decreases from 11.8 to 11.1 (Atkins and Glasser, 1992).

Tricalcium aluminate hexahydrate (i.e., hydrogarnet) also buffers pH between 11.8 and 11.0 (Atkins and Glasser, 1992). Tetracalcium aluminate hydrate buffers pH at slightly higher levels. Hydrogen ions react with tetracalcium aluminate hydrate in accordance with equation (33).

$$(CaO)_4Al_2O_3 \cdot 13H_2O + 8H^+ \rightarrow 4Ca^{2+} + 2Al(OH)_{3(s)} + 14H_2O \tag{33}$$

Ettringite buffers pH at approximately 11 (Atkins and Glasser, 1992). Monosulfoaluminate buffers pH at slightly higher levels. Hydrogen ions react with monosulfoaluminate and ettringite in accordance with equations (34) and (35), respectively.

$$(CaO)_3Al_2O_3CaSO_4 \cdot 12H_2O + 6H^+ \rightarrow 4Ca^{2+} + 2Al(OH)_{3(s)} + SO_4^{2-} + 12H_2O \tag{34}$$

$$(CaO)_3Al_2O_3(CaSO_4)_3 \cdot 32H_2O + 6H^+ \rightarrow$$
$$6Ca^{2+} + 2Al(OH)_{3(s)} + 3SO_4^{2-} + 32H_2O \tag{35}$$

Lea (1971) stated that calcium aluminate and calcium sulfoaluminate hydrates with iron substituents generally exhibit low solubilities. Acid neutralization capacities of calcium aluminate, calcium sulfoaluminate, calcium ferrite, and calcium sulfoferrite hydrates are relatively insignificant in cement matrices because amounts of those solids are small relative to calcium hydroxide and calcium silicate hydrates.

In soil/cement matrices with low clay/cement ratios, pH evolution proceeds in accordance with this sequence of mineralogical tranformations. However, in soil/cement matrices with high clay:cement ratios, calcium silicate hydrate with low calcium:silicon ratios and tetracalcium aluminate hydrate replace portlandite. Although acid neutralization capacities in soil/cement matrices with high clay:cement ratios are equivalent to cementitious matrices with equal amounts of anhydrous cement, the solid phase assemblage buffers pH at lower levels.

Poon et al. (1985) confirmed decalcification of calcium silicate hydrates and dissolution of calcium sulfoaluminate hydrates due to acidic reactions in cement/silicate matrices using scanning electron microscopy and energy dispersive x-ray analysis. Primary hydration products identified by Poon et al. (1985) in these cement/silicate samples prior to acidic reactions were calcium silicate hydrates, monosulfoaluminate and ettringite. Overall calcium:silicon ratios were approximately 3 : 1. After 2 days in contact with 0.5 M acetic acid, calcium silicate hydrates were not identifiable; instead, a calcium silicate gel with high silicon content was present. After 3 days, relatively small amounts of ettringite were present, and overall calcium : silicon ratios were approximately 1 : 1. After 4 days, ettringite was not identifiable, and overall calcium:silicon ratios were approximately 0.4. After 5 days, cement paste structure had been completely destroyed, leaving a residue of amorphous gel, and overall calcium : silicon ratios were approximately 0.2.

Poon's data on calcium : silicon ratios were corroborated by Bishop (1988) and Cheng and Bishop (1992a). Bishop (1988) found that 8 percent of calcium initially present in cementitious matrices is extant after 15 sequential extractions with 0.04 M acetic acid whereas 80 percent of silicon, 90 percent of aluminum, and 98 percent of iron are extant (Bishop, 1988). Cheng, Bishop, and Isenburg (1992) visually observed distinct boundaries between leached portions and unleached portions of cementitious waste forms using pH indicators. Overall calcium:silicon ratios decreased from approximately 5 in unleached portions to approximately 0.4 in portions leached with acetic acid as indicated by energy dispersive x-ray analysis and atomic absorption spectrophotometry (Cheng and Bishop, 1992a). pH decreased from levels greater than 12 within unleached portions to levels less than 6 within leached portions (Cheng, Bishop, and Isenburg, 1992).

Cheng and Bishop (1992b) found that inward movement of the leach boundary was linearly proportional to the square root of time which indicates that diffusive transport limits dissolution rates (see equation (25)). Diffusive transport rates depend upon total soluble hydrogen (e.g., $[H^+] - [OH^-] + \Sigma [HA_i]$) concentration gradients between soil/cement/waste matrices and adjacent media as well as effective diffusivity values for soil/cement/waste matrices and adjacent media. Batchelor (1990) approximated observed diffusivity values for components in solids that dissolve due to acid reactions as equation (36)

$$D_{obs} = \frac{\pi C_{b,HA} D_{e,HA}}{2nC_i^0} \theta_c^0 \tag{36}$$

where $C_{b,HA}$ = concentration of acid in bath (moles/bath volume), $D_{e,HA}$ = effective diffusivity of acid in solid (length^2/time), θ_c^0 = initial capillary porosity, n =

moles of acid required to react with one mole of component in solid, and C_i^0 = initial concentration of component in solid (moles/porewater volume). Equation (36) assumes that acids diffuse into solid matrices from semi-infinite baths.

Data presented by Cheng and Bishop (1992b) show that acid penetration depth as a function of time does increase as leachant acid concentrations increase as indicated by equation (36). They found, for example, that fraction leached at 30 days was approximately 0.46 for cementitious matrices leached with 0.2 N acetic acid, 0.52 for 0.3 N acetic acid, 0.68 for 0.4 N acetic acid, and 0.72 for 0.5 N acetic acid. Data presented by Poon et al. (1985) further demonstrate that dissolution rates of cementitious matrices depend upon total soluble hydrogen concentration gradients, not hydrogen ion concentration gradients. Poon et al. (1985) measured leachant pH during semi-dynamic leach tests of cement/silicate matrices with three different types of leachants; leachants used during these tests had equal initial pH values but different buffer intensities. Leachant pH decreased from approximately 12 to approximately 5 in 15 elutions for leachant with a buffer intensity of 0.160, 11 elutions for leachant with a buffer intensity of 0.315, and 8 elutions for leachant with a buffer intensity of 0.528. Data presented by Cheng and Bishop (1992b) also show that acid penetration depth as a function of time decreases as leachant velocity decreases. After 28 days, for example, acid penetration depths in semi-dynamic leach tests were approximately 0.6 cm; whereas, acid penetration depths in static leach tests were approximately 0.3 cm.

Dissolution of portlandite and decalcification of calcium silicate hydrates can increase effective diffusivity values in leached portions of soil/cement/waste matrices. Research by Buil et al. (1992) suggest that changes in effective diffusivity may be approximated by equation (37)

$$D_e(C_p) = D_e^0\left(\frac{\theta_c(C_p)}{\theta_c^0}\right) \tag{37}$$

where D_e^0 = effective diffusivity of a soil/cement/waste matrix before leaching begins, $\theta_c(C_p)$ = capillary porosity as a function of solid phase calcium concentration (C_p), and θ_c^0 = initial capillary porosity. Changes in effective diffusivity values for leached portions of soil/cement/waste matrices affect both outward diffusion of cement matrix components such as calcium and inward diffusion of hydrogen and other external components such as inorganic carbon compounds, magnesium, and sulfate.

Model results from Buil et al. (1992) indicate that capillary porosity generated by dissolution of portlandite and decalcification of calcium silicate hydrates is approximately equal to one molar volume of portlandite per mole of calcium dissolved from solid phases. Thus, porosity changes due to dissolution processes can be approximated by equation (38) (Buil et al., 1992)

$$\theta_c(C_p) = \theta_c^0\left(1 + \frac{MW_{CH}}{\gamma_{CH}}(C_p^0 - C_p)\right) \tag{38}$$

where MW_{CH} = molecular weight of calcium hydroxide ($Ca(OH)_2$), γ_{CH} = density of portlandite, C_p^0 = initial solid phase calcium concentration (moles/porewater

volume), and C_p = solid phase calcium concentration. The initial capillary porosity can be approximated by equation (39) (Soroka, 1979)

$$\theta_c^0 = \frac{\omega - 0.384\alpha}{0.32 + \omega} \tag{39}$$

where w = water:cement weight ratio and α = degree of hydration. Equation (39) assumes that (1) the specific volume of anhydrous cement is 0.32 cm^3/g, and (2) the volume of cement gel is 2.2 times the volume of anhydrous cement.

5.3. Carbonation

Carbonation can reduce porewater pH levels of soil/cement/waste matrices and transform calcium hydroxide, calcium silicate hydrates, calcium aluminate hydrates, and calcium sulfoaluminate hydrates to calcium carbonate, silica gel, and aluminum and iron (oxy)hydroxides. Carbonation can also reduce permeability of soil/cement/waste matrices, but cracks induced by carbonation may short-circuit low permeability surface layers caused by external carbonation.

Atmospheric $CO_{2(g)}$ and $CO_{2(g)}$ generated by microbial and root respiration diffuse into soil/cement/waste matrices or adjacent media or mix with soil/cement/waste mixtures during treatment. Carbon dioxide reacts with water to form carbonic acid, which, under most pH conditions in soil/cement matrices, dissociates to yield carbonate ions. In cement matrices, carbonate ions react first with portlandite ($Ca(OH)_{2(s)}$) to form calcium carbonate. Overall, the reaction between carbon dioxide and portlandite can be characterized by equation 40 (Dayal and Reardon, 1992).

$$Ca(OH)_{2(s)} + CO_{2(g)} \rightarrow CaCO_{3(s)} + H_2O \tag{40}$$

Lea (1970) suggested that aragonite ($CaCO_3$) and vaterite ($CaCO_3$) may precipitate initially, then transform later to calcite ($CaCO_3$). Lindsay (1979) suggested that solubilities of aragonite and calcite are sufficiently similar that they can coexist.

Subsequent carbonation converts tetracalcium aluminate hydrate to calcium carboaluminate (Taylor, 1990) in accordance with equation (41).

$$(CaO)_4Al_2O_3{\cdot}13H_2O_{(s)} + CO_{2(g)} \rightarrow (CaO)_3Al_2O_3CaCO_3{\cdot}11H_2O_{(s)} + 2H_2O \tag{41}$$

Further exposure to inorganic carbon induces transformation of ettringite and monosulfoaluminate to calcium carbonate, gypsum, and aluminum (oxy)hydroxide (Taylor, 1990) in accordance with equations (42) and (43), respectively.

$$(CaO)_3Al_2O_3(CaSO_4)_3{\cdot}32H_2O_{(s)} + 3CO_{2(g)} \rightarrow$$
$$3CaCO_{3(s)} + 2Al(OH)_{3(s)} + 3CaSO_4{\cdot}2H_2O_{(s)} + 27H_2O \tag{42}$$

$$(CaO)_3Al_2O_3CaSO_4{\cdot}12H_2O_{(s)} + 3CO_{2(g)} \rightarrow$$
$$3CaCO_{3(s)} + 2Al(OH)_{3(s)} + CaSO_4{\cdot}2H_2O_{(s)} + 7H_2O \tag{43}$$

Additional exposure to inorganic carbon induces transformation of calcium carboaluminate to calcium carbonate and aluminum (oxy)hydroxide (Taylor, 1990) in accordance with equation (44).

$$(CaO)_3Al_2O_3CaCO_3 \cdot 11H_2O_{(s)} + 3CO_{2(g)} \rightarrow 4CaCO_{3(s)} + 2Al(OH)_{3(s)} + 8H_2O \quad (44)$$

Subsequent carbonation reduces the calcium:silicon ratio of calcium silicate hydrate in accordance with equation (45) and, ultimately, transforms it into calcium carbonate and silica gel (Dayal and Reardon, 1992; Suzuki et al., 1985; Lea, 1970; Taylor, 1990).

$$(CaO)_xSiO_2 \cdot (2 + x)H_2O + yCO_2 \rightarrow yCaCO_3 + (CaO)_{x-y}SiO_2 \cdot (2 + x - y)H_2O + yH_2O \quad (45)$$

Dayal and Reardon (1992) suggested the sequence of mineralogical transformations implied by the order of equations (40) through (45) based upon chemical equilibrium modeling.

Changes in solid phase characteristics caused by carbonation also affect solutions in equilibrium with carbonated regions of soil/cement/waste matrices. Most significant, pH of solutions in equilibrium with cementitious matrices altered by carbonation decrease linearly from about 11.5 at 10 percent $CaCO_3$ to 10.5 at 90 percent $CaCO_3$, then drop rapidly to about 9 at $CaCO_3$ levels greater than 90 percent (Parrott and Killoh, 1989). Taylor (1990) indicated that porewater pH levels in equilibrium with fully carbonated cement matrices are 8.5 or lower based upon phenolphthalein tests. Equilibrium modeling indicates that pH of solutions in equilibrium with calcium carbonate at a fixed CO_2 partial pressure of 0.0003 atm, the normal atmospheric CO_2 partial pressure, is 8.3; pH of solutions in equilibrium with calcium carbonate at a fixed CO_2 partial pressure of 0.003 atm, a typical CO_2 partial pressure in soil atmospheres, is about 7.6.

Impacts of carbonation are probably limited under most scenarios. Carbonation via diffusive transport of atmospheric carbon dioxide or aqueous inorganic carbon species probably only affects regions near interfaces between waste matrices and adjacent media. Carbonation caused by inorganic carbon species present in soil/waste matrices prior to treatment may affect bulk solid and solution phase characteristics, but impacts are probably negligible under most circumstances. Carbonation caused by mixing of atmospheric $CO_{2(g)}$ into alkaline soil solutions during treatment, on the other hand, may substantially impact solid and solution phase characteristics of soil/cement/waste matrices.

Atmospheric $CO_{2(g)}$ will probably not penetrate more than 100 mm into cementitious matrices even after long periods of exposure. Parrot and Killoh (1989) found, for example, that atmospheric carbon dioxide had only penetrated about 65 mm into one concrete column after 36 years of exposure. Calcium hydroxide had been completely converted to $CaCO_3$ only at depths less than about 25 mm. Carbon dioxide that diffuses into soil/cement/waste matrices from adjacent soils may penetrate further than atmospheric $CO_{2(g)}$ because the partial pressure of carbon dioxide in soil air is higher than its partial pressure in the atmosphere.

Due to microbial and root respiration, carbon dioxide levels within soil matrices are generally 10 to 100 times higher than atmospheric carbon dioxide levels, typically ranging from 0.003 to 0.03 atmospheres (Bohn et al., 1979; Lindsay, 1979). High carbon dioxide partial pressures may substantially increase carbonation. For example, Ho and Lewis (1987) demonstrated that carbonation of cement specimens at 4 percent carbon dioxide for one week is equivalent to carbonation under normal atmospheric conditions for one year.

Because diffusion limits the rate of carbonation due to atmospheric $CO_{2(g)}$ or $CO_{2(g)}$ from adjacent soils (Dayal and Reardon, 1992; Ho and Lewis, 1987), the extent of carbonation via these pathways depends upon moisture content, porosity, and pozzolan content, as well as exposure time and carbon dioxide partial pressure. Approximately 50 percent relative humidity is optimal for carbonation via these two pathways (Dayal and Reardon, 1992; Soroka, 1979; Lea, 1970). Unsaturated conditions favor carbonation because $CO_{2(g)}$ can diffuse more rapidly through air-filled pores than water-filled pores. The diffusion coefficient for carbon dioxide in saturated cementitious matrices is approximately three orders of magnitude lower (10^{-9} m^2/s) than the diffusion coefficient for carbon dioxide in gas-filled cementitious matrices (10^{-6} m^2/s). Some water is necessary, however, to facilitate mineral transformations (Dayal and Reardon, 1992).

Carbonation can reduce effective diffusivity in soil/cement/waste matrices due to blockage of pores by calcium carbonate. Calcite has a molar volume 11 percent greater than portlandite, and aragonite has a molar volume 3 percent greater than portlandite (Lea, 1970). Diffusion coefficients measured by Dayal and Reardon (1992) for tritiated water under saturated conditions decreased from 1.8×10^{-12} m^2/s in uncarbonated cement grout to 0.6×10^{-12} m^2/s in fully carbonated cement grout. Thus, carbonation may cause low permeability regions to develop near surfaces of soil/cement/waste monoliths and, consequently, hinder further diffusion of $CO_{2(g)}$ and aqueous inorganic carbon species.

Cracks caused by carbonation shrinkage may, however, penetrate through this surface layer in soil/cement/waste matrices exposed to the atmosphere or unsaturated soils. According to Lea (1971), carbonation shrinkage probably occurs due to reduction of the nonevaporable water content of cement hydration products. However, shrinkage may also occur due to polymerization and dehydration of hydrous silica carbonation products (Lea, 1971; Soroka, 1979) Lea (1971) noted that depth of crazing – networks of fine, surface cracks – coincides with depth of carbonation in concrete specimens, and he concluded that carbonation shrinkage causes crazing. Depth of carbonation may coincide with depth of crazing because crazing fosters diffusion of $CO_{2(g)}$. Nonetheless, carbonation does cause shrinkage, and shrinkage can induce cracking.

Because pozzolanic reactions consume calcium hydroxide, less calcium carbonate accumulates in cement/pozzolan matrices. Thus, $CO_{2(g)}$ and aqueous inorganic carbon species can diffuse more readily into cement/pozzolan matrices than cement matrices given comparable effective diffusivities; consequently, carbonation generally affects cement/pozzolan matrices more than cement matrices. For example, one survey found that, after 20 years, the maximum depth of carbonation in concrete samples with fly ash was 16 mm; whereas, the maximum depth of

carbonation in concrete samples without fly ash was only about 4 mm. Another survey found that, after 25 years, maximum depths of carbonation in concrete samples with and without fly ash were 23 and 5 mm respectively (Ho and Lewis, 1987). Nonetheless, carbonation via diffusive transport mechanisms in soil/cement/waste matrices only affects regions near interfaces between waste matrices and adjacent media.

Carbonation caused by inorganic carbon species present in soil/waste matrices prior to treatment may occur throughout soil/cement/waste matrices, but impacts will probably be negligible. Even under a reasonable worst case scenario (i.e., $pH \approx 8$, $P(CO_2) = 0.03$ atm.), the total amount of inorganic carbon in soil solutions is two orders of magnitude less than the amount of calcium ions in, for example, a 5 percent cement/soil mixture.

In contrast, the amount of inorganic carbon that can potentially be adsorbed from the atmosphere ($P(CO_2) = 0.0003$ atm.) into alkaline soil solutions ($pH \approx 12.5$) during treatment is several orders of magnitude greater than the amount of calcium in soil/cement mixtures typically used for S/S processes. Extensive carbonation of soil/lime matrices in the field was reported by Eades, Nichols, and Grim (1962). They found 2.5 percent calcium carbonate in soils treated with 5 percent lime after 3 to 4 years. No calcium carbonate was initially present in the soils. Impacts of carbonation via this pathway depend upon the type of mixing process. Extensive carbonation may occur with backhoe mixing processes, backhoe-mounted injector-type *in situ* processes, tractor-mounted hollow tine injectors, and rotary tillers.

Carbonation can affect leaching behavior even if it only affects a small region near the surface of soil/cement/waste monoliths. Carbonated surface layers may slow diffusion, and, consequently, reduce the concentration gradients that drive diffusive transport. Changes in pH or carbonate content may cause toxic metals to precipitate or dissolve, increasing or decreasing concentration gradients, respectively.

Impacts of carbonation are not necessarily adverse. Carbonation may be beneficial for immobilization of some metals. Copper, nickel, and lead, for example, exhibit minimum solubility at about pH 9 (Conner, 1990). Also, carbonate ions in solution may react with certain metals, particularly cadmium and lead, to form highly insoluble carbonate precipitates. Lindsay (1979) noted that Cd(II) concentrations decrease 100-fold for each unit increase in pH above 7.84 at carbon dioxide partial pressures typical of soil atmospheres (0.003 atm.). Carbonate compounds also govern lead solubility in soils at carbon dioxide partial pressures greater than 0.0003 atmospheres. In addition, carbonated soil/cement matrices exhibit lower solubility than noncarbonated matrices.

5.4. Sulfate reactions

Sulfate reactions that occur after cement has hardened may adversely affect durability and solid and solution phase characteristics of soil/cement/waste matrices. Guidelines from the U.S. Bureau of Reclamation cited by Soroka (1979) indicate that sulfate concentrations as low as 2 mM in soil solutions or groundwater

can cause cracks to develop in concrete that contains type I Portland cement, and sulfate concentrations as low as 20 mM can cause "severe" deterioration. Soroka (1979) suggested that "considerable" deterioration occurs at sulfate concentrations greater than approximately 6 mM.

Sulfate concentrations in pore solutions of temperate soils typically range from 0.5 mM in humid regions to 5 mM in arid regions (Bohn et al., 1979). Sulfate concentrations in groundwater from carbonate rock formations typically range from about 0.2 to 1.0 mM. Sulfate concentrations in groundwater of crystalline rock formations typically range from about 0.004 to 0.1 mM (Freeze and Cherry, 1979). Thus, sulfate attack from external sources is problematic only for soil/cement/waste matrices in direct contact with soils in arid regions. Sulfate attack from internal sources may also occur, but that type of attack also occurs predominantly in arid soils.

Sulfate ions in excess of levels stabilized by equilibrium with monosulfoaluminate can induce ettringite precipitation. Taylor (1990) concluded on the basis of microstructural observations that ettringite precipitates from solution in accordance with equation (46)

$$6Ca^{2+} + 2Al(OH)_4^- + 4OH^- + 3SO_4^{2-} + 26H_2O \rightarrow$$
$$(CaO)_2Al_2O_3(CaSO_4)_3{\cdot}32H_2O \qquad (46)$$

Sulfate concentrations required for ettringite precipitation depend upon calcium, aluminum, and hydroxide ion concentrations, and concentrations of other soluble species that can complex those species. Potassium and sodium, for example, can complex significant amounts of sulfate and, consequently, increase total sulfate concentrations necessary for ettringite precipitation.

Ettringite precipitation induces dissolution of monosulfoaluminate which supplies aluminum ions plus some calcium and sulfate ions required for further ettringite precipitation. Overall, this reaction can be characterized by equation (47).

$$(CaO)_3Al_2O_3CaSO_4{\cdot}12H_2O_{(s)} + 2Ca^{2+} + 2SO_4^{2-} + 20H_2O \rightarrow$$
$$(CaO)_3Al_2O_3(CaSO_4)_3{\cdot}32H_2O_{(s)} \qquad (47)$$

Dissolution of tetracalcium aluminate hydrate can also supply aluminum and calcium ions for ettringite formation (Lea, 1971; Soroka, 1979). Overall, this reaction can be characterized by equation (48).

$$(CaO)_4Al_2O_3{\cdot}13H_2O + 2Ca^{2+} + 3SO_4^{2-} + 2H^+ + 18H_2O \rightarrow$$
$$(CaO)_3Al_2O_3(CaSO_4)_3{\cdot}32H_2O_{(s)} \qquad (48)$$

More calcium and sulfate ions are required, however, to precipitate additional ettringite. Dissolution of portlandite, decalcification of calcium silicate hydrates, or diffusive transport from adjacent media replenish calcium ions.

Dissolution of gypsum present in soil/waste matrices prior to treatment or inward diffusive transport from adjacent media replenish sulfate ions (Taylor, 1990). Diffusive transport of sulfate ions from adjacent media probably occurs slowly under most disposal scenarios due to low concentration gradients as indi-

cated by comparison of Tables 1 and 6. Outward diffusion of sulfate ions rather than inward diffusion probably occurs under many disposal scenarios due to high porewater concentrations in soil/cement matrices. Soluble sulfate present in soil/waste matrices prior to treatment probably does not cause cracks; instead, soluble sulfate reacts with tricalcium aluminate to form ettringite before hardening occurs. However, if gypsum is present in soil/waste matrices prior to treatment, an atypical situation except in arid soils (Lindsay, 1979), it may dissolve and react with monosulfoaluminate or tetracalcium aluminate hydrate to form ettringite after hardening occurs (Taylor, 1990).

Ettringite formation can engender expansive forces that cause cracks to develop in cementitious matrices because its molar volume is substantially greater than molar volumes of monosulfoaluminate and tetracalcium aluminate hydrate (Soroka, 1979; Taylor, 1990; Mindess and Young, 1981; Lea, 1970). Molar volume of ettringite is 715 cm^3; whereas, molar volumes of monosulfoaluminate and calcium aluminate hydrate are 313 cm^3 and 277 cm^3, respectively (Soroka, 1979; Lea, 1971). If available space is inadequate to accommodate ettringite expansion, cracks can develop.

Sulfate ions can also induce precipitation of gypsum in accordance with equation (49).

$$Ca^{2+} + SO_4^{2-} + H_2O \rightarrow CaSO_4 \cdot 2H_2O_{(s)} \tag{49}$$

Formation of gypsum from calcium hydroxide is expansive. Molar volume of gypsum is 74.2 cm^3, and molar volume of calcium hydroxide is 33.3 cm^3. However, Mindess and Young (1981) concluded that gypsum formation does not directly contribute to expansive forces in cementitous matrices at sulfate concentrations below about 10 mM, and it is secondary to ettringite formation at concentrations below about 40 mM, probably because the solubility of gypsum is greater than ettringite.

Monosulfate solid solutions of calcium sulfoaluminate and calcium sulfoferrite from hydration of tetracalcium aluminoferrite resist sulfate attack. Mechanisms of sulfate resistance have not been ascertained. However, replacement of tricalcium aluminate with tetracalcium aluminoferrite in sulfate resistant Portland cements (types V, IV, and II) and, consequently, replacement of monosulfoaluminate with calcium sulfoaluminate/sulfoferrite solid solutions in solid phase assemblages of cement pastes reduces severity of sulfate attack.

Because sulfate can react with tetracalcium aluminate hydrates generated by pozzolanic reactions to form ettringite, sulfate resistant cements can not preclude adverse sulfate reactions in soil/cement/waste matrices. Hunter (1988) and others cited therein have confirmed the presence of ettringite in lime-stabilized soils. Their observations indicate that calcium aluminate hydrates generated by pozzolanic reactions between lime and clay minerals can react with sulfate ions to form ettringite in the absence of monosulfoaluminate. Formation of calcium aluminate hydrates by pozzolanic reactions is particularly germane because clayey soils are generally associated with high sulfate levels (Mindess and Young, 1981; Lea, 1971). However, sulfate resistant Portland cements probably can reduce the severity of sulfate attack in soil/cement/waste matrices because the only sulfate

sources for ettringite formation in the absence of monosulfoaluminate are diffusive transport from adjacent media and dissolution of gypsum present in soil/waste matrices prior to treatment.

Expansive cracking due to ettringite or gypsum formation is not the only deleterious effect of sulfate attack. Dissolution of calcium hydroxide and decalcification of calcium silicate hydrates to supply calcium ions for ettringite formation also affect metal attenuation mechanisms in soil/cement/waste matrices. Lea (1971) concluded that sulfate reactions can not induce decalcification of calcium silicate hydrates, but Taylor (1990) cited scanning electron microscopic data to buttress his contention that decalcification can occur in solutions that contain low calcium concentrations. Calcium silicate hydrates with low calcium:silicon ratios tend to buffer pH at lower levels than calcium silicate hydrates with high calcium:silicon ratios.

Severity of sulfate reactions depends upon other anions in solution. Carbonate ions can react with silica and ettringite to form thaumasite ($Ca_3Si(OH)_6(SO_4)(CO_3)12H_2O$) at temperatures below 15 °C (Taylor, 1990; Hunter 1988). Transformation of ettringite to thaumasite involves substitution of silica for aluminum and carbonate for sulfate in accordance with equation 50 (Hunter 1988).

$$(CaO)_3Al_2O_3(CaSO_4)_3\cdot 32H_2O_{(s)} + 2H_2SiO_4^{2-} + 2CO_3^{2-} + 6O_2 \rightarrow$$
$$2Ca_3Si(OH)_6SO_4CO_3\cdot 12H_2O_{(s)} + 2Al(OH)_4^- + SO_4^{2-} + 4OH^- + 10H_2O \quad (50)$$

Thaumasite "severely" softens cementitious matrices (Taylor, 1990; Hunter, 1988). Hunter (1988) has identified it in lime-stabilized soils. Calcium carbonate, on the other hand, may ameliorate sulfate reactions due, possibly, to blockage of pores, or formation of calcium carboaluminate ($(CaO)_3Al_2O_3CaCO_3\cdot 11H_2O$) (Taylor, 1990). This latter compound may hinder ettringite formation by sequestering Al_2O_3 (Lea 1970).

Severity of sulfate reactions also depend upon environmental conditions, primarily availability of water. External sulfate attack can not proceed without sufficient moisture for diffusive transport. Soroka (1979) noted, however, that deterioration due to sulfate attack increases when concrete is exposed to alternate wet/dry cycles. Deterioration may increase under such circumstances because saturated conditions allow sulfate ions to diffuse into the matrix, then evaporation concentrates them until levels required for reaction 46 to proceed are attained.

Although sulfate penetration can not be precluded under most circumstances, diffusive transport rates and, consequently, deterioration rates due to external sulfate attack decline as permeability decreases. High cement content, low water content, and pozzolanic additives reduce permeability of soil/cement/waste matrices and, consequently, reduce the severity of external sulfate attack. Pozzolanic additives, however, are only effective if they have a relatively high $SiO_2/Al_2O_3 + Fe_2O_3$ ratios. Silica in pozzolanic materials reacts with lime generated by cement hydration reactions to form calcium silicate hydrates, which reduce permeability by obstructing pores. Also, Lea (1970) suggested that calcium silicate hydrates may coat calcium aluminates, protecting them from sulfate attack. In contrast,

alumina in pozzolanic materials reacts with lime to form calcium aluminate hydrates that react with sulfate to form ettringite as discussed earlier.

5.5. Magnesium reactions

Magnesium ions react with hydroxide ions to form brucite ($Mg(OH)_2$) in accordance with equation (51) (Soroka, 1979; Taylor 1990; Lea, 1970)

$$Mg^{2+} + 2OH^- \rightarrow Mg(OH)_{2(s)} \quad (51)$$

Brucite exhibits low solubility. Continuous exposure to fresh leachant that contains magnesium ions may deplete hydroxide ions and induce dissolution of portlandite and monosulfoaluminate and decalcification of calcium silicate hydrates (Taylor, 1990; Mindess and Young, 1981). According to Lea (1970), silica gel that remains after decalcification of calcium silicate hydrates can react slowly with brucite to form hydrated magnesium silicate of approximate composition $(MgO)_4$-$SiO_2 \cdot 8.5H_2O$. In contrast to silica gel, this compound has no cementitous characteristics (Lea, 1970). Lea (1970) also suggested that ettringite is unstable in the presence of brucite and eventually decomposes into gypsum and hydrated alumina.

Deterioration of cementitious matrices due to external magnesium attack may be limited by precipitation of brucite in pores. Lea (1970) and Taylor (1990) noted that hard, dense surface layers form on cementitous structures exposed to magnesium sulfate solutions, and consequently, further penetration of magnesium ions is limited. Cementitious matrices exposed to magnesium sulfate ultimately decompose into hard, granular particles in contrast to cementitious matrices exposed to sodium or calcium sulfate solutions, which decompose into soft pastes.

6. Long term performance assessment

To summarize, problems associated with accurate prediction of leach rates are exacerbated in soil/cement/waste matrices by reactions between soil components and cement hydration products and interactions between soil/cement/waste matrices and adjacent media. Pozzolanic, acidic, carbonate, magnesium, and sulfate reactions alter equilibrium solid phase assemblages in soil/cement/waste matrices. Generally, those reactions transform calcium hydroxide and calcium silicate hydrates, the primary pH buffer phases in cementitious matrices, into solids that buffer solution phases of soil/cement matrices at lower pH levels than cement matrices. Acidic reactions also reduce acid neutralization capacities of soil/cement/waste matrices. Moreover, carbonate, magnesium, sulfate, and alkali-silica reactions may affect structural integrity and/or permeability of soil/cement/waste matrices.

Soil characteristics, such as particle size distribution, mineralogy, reactive silica content, organic matter content, degree of weathering, and concentrations of major cations and anions, affect the extent of soil/cement reactions and environmental interactions. Clay content and organic matter content also affect the extent of cement hydration reactions in soil/cement matrices. Because soils vary substan-

tially both horizontally and vertically within relatively short distances, bench-scale leach tests can not fully reproduce in situ soil characteristics. Thus, thorough knowledge of potential impacts of soil properties on solid and solution phase characteristics and, consequently, attenuative properties of soil/cement/waste matrices, is necessary to accurately translate bench-scale test results to full-scale applications or extrapolate results to different soil matrices.

Moreover, soil/cement/waste matrices and adjacent media are dynamic systems whose characteristics change over time scales much longer than times usually employed for leach tests but, nonetheless, within time scales of interest in soil S/S applications. Thus, long-term performance of soil/cement/waste matrices can not be wholly assessed by leach tests. Even hybrid leach tests that combine bench-scale tests with mass transport models (e.g. bulk diffusive transport models in combination with ANS 16.1) are inadequate for prediction of long-term performance because such tests presume that soil/cement/waste matrix characteristics do not change except through dissolution reactions after the initial curing period.

A mechanistic model that can approximate long-term effects of soil/cement reactions and environmental interactions is necessary to supplement such tests. This type of model could ideally be employed as a screening tool to evaluate the sensitivity of metallic constituents to various soil properties and pinpoint conditions likely to cause failure (i.e., excessive leach rates) of soil/cement/waste matrices. A numerical model is requisite because the numerous variables that affect long-term performance of soil/cement/waste matrices preclude analytical solutions.

Because diffusive transport rates depend upon solution phase concentrations within soil/cement/waste matrices and adjacent media, a numerical model used for soil S/S applications must account for soluble component concentrations in both soil/cement/waste matrices and adjacent media. Complexation, precipitation/dissolution, and sorption/desorption reactions affect soluble component concentrations; thus, a numerical model for soil S/S applications must further account for total amounts of each component in different phases (i.e., soluble, sorbed, and solid). Algorithms to solve equilibrium precipitation/dissolution equations must account for incongruent dissolution of calcium silicate hydrates. Additionally, a numerical model for soil S/S applications must account for variable surface charges in soil/cement/waste matrices as a function of calcium:silicon ratios of calcium silicate hydrates, and it should contain algorithms to calculate activity coefficients under high ionic strength conditions.

Because dissolution of calcium hydroxide and decalcification of calcium silicate hydrates can increase capillary porosity within soil/cement/waste matrices, a numerical model used for soil S/S applications should accommodate variable effective diffusivity coefficients. Furthermore, a numerical model for soil S/S applications should incorporate advective transport. Advection is particularly important with regard to component concentrations in soil solutions or groundwater, but advection may also become non-negligible with time within soil/cement/waste matrices due to soil/cement reactions and environmental interactions.

6.1. SOLTEQ

A model with all of these capabilities does not yet exist, but Batchelor and co-workers have developed models with many of these capabilities. A mechanistic

model to predict chemical speciation under metastable equilibrium conditions in cement/waste matrices, SOLTEQ, has been developed by Batchelor and Wu (1993b) and refined by Sabharwal (1993). SOLTEQ was constructed from MINTEQA2 (Allison et al., 1991). MINTEQA2 serves as a good foundation because it can model equilibrium precipitation/dissolution, complexation, and sorption/desorption reactions. It includes a large thermodynamic database for solids and soluble complexes of common elements. It also includes surface complexation models that can predict sorption under different conditions of pH, ionic strength, and concentrations of competing cations and anions, although it does not include parameters required for those models. SOLTEQ was constructed from MINTEQA2 by (1) addition of equations to calculate activity coefficients at high ionic strength, (2) expansion of MINTEQA2's thermodynamic database to include cement hydration products, and (3) addition of equations to calculate equilibrium constants and calcium : silicon ratios of calcium silicate hydrates.

Pitzer's ion interaction model was employed in SOLTEQ to calculate activity coefficients because it is accurate at high ionic strengths typical of cement porewater. For those ions without virial coefficients required for Pitzer's model, a modification of the operational $B\cdot$ method was used to calculate activity coefficients (Batchelor and Wu, 1993b). Incongruent dissolution of calcium silicate hydrates was modeled using equations (52) and (53). Equations (52) and (53) are regression equations based upon numerous data for calcium silicate hydrates in $CaO—SiO_2—H_2O$ systems. Equation (52) was developed by Reardon (1990); it correlates calcium : silicon ratios of calcium silicate hydrates with calcium and silicon activities in solution. Equation (53) was derived by Wu (1992) from equations developed by Reardon (1990); it correlates formation constants for calcium silicate hydrates with calcium and silicon activities in solution.

$$(Ca/Si)_{CSH} = 0.48548 + 0.11563R + 0.0104536R^2 \tag{52}$$

$$\log K_{CSH} = -5.01650 - 1.90658R - 0.273487R^2 \tag{53}$$

where $R = \log[\{Ca^{2+}\}/\{H_4SiO_4^0\}]$.

SOLTEQ is premised upon the assumption that equations (52) and (53), derived for $CaO—SiO_2—H_2O$ systems, are valid in complex cement/waste systems. Batchelor and Wu (1993b) validated this assumption by comparison of SOLTEQ predictions with major cation and anion concentrations in porewater expressed from Portland cement paste. Concentrations of hydroxide and other major matrix components (Ca, Si, Al, and Mg) predicted by SOLTEQ generally compared well with porewater concentrations. However, concentrations of iron predicted by SOLTEQ were high possibly due to a lack of thermodynamic data for tetracalcium aluminoferrite. Iron is a relatively minor component of cementitous matrices, and its effects on mobility of toxic metals are probably minimal. Nonetheless, this discrepancy highlights one obvious limitation of SOLTEQ – its predictions are only as good as thermodynamic data input to it. Thermodynamic data for species formed at high pH levels intrinsic to cement porewater, particularly trace metals, are generally limited.

6.2. SOLDIF

Sabharwal (1993) combined SOLTEQ with a bulk diffusive transport model developed by Batchelor (1992) to create SOLDIF. The core of SOLDIF is equation 21 which describes bulk diffusive transport of soluble components with concurrent precipitation/dissolution or sorption/desorption from solid phases. Equation (21) can be rearranged to yield equation (54).

$$\frac{\partial T}{\partial t} = D_e \frac{\partial^2 C}{\partial x^2} \tag{54}$$

where $T = C + C_{im}$ is the total component concentration (moles/porewater volume) including soluble, sorbed, and solid phases. Equation (54) states that, at any point within a cementitious matrix, the total concentration of any component varies with time due to diffusive transport of the mobile (i.e. soluble) portion of that component. Precipitation/dissolution, sorption/desorption, and complexation reactions do not change total component concentrations; they change only their speciation. Only redox reactions can change one component into another component. SOLDIF presumes that redox reactions do not occur, and other reactions occur quickly enough that local equilibrium exists at all nodes. Other assumptions inherent in SOLDIF include the following: (1) contaminants are uniformly distributed throughout the waste matrix before leaching begins, (2) the waste matrix is symmetrical (i.e. leaching can be approximated with a one-dimensional transport model), (3) effective diffusivity of the waste matrix does not change with time, and (4) all mobile species of each component diffuse at equivalent rates.

Equation (54) contains two dependent variables. To reduce the number of dependent variables, mobile concentration is expressed as a product of total concentration and mobile fraction, G, where the mobile fraction of any component is a function of the total concentration of all components.

$$\frac{\partial T}{\partial t} = D_e \frac{\partial^2 (GT)}{\partial x^2} \tag{55}$$

To facilitate solution, SOLDIF uses dimensionless parameters.

$$\bar{T} = \frac{T}{T^0} \tag{56}$$

$$\bar{X} - \frac{X}{L} \tag{57}$$

$$\bar{t} - \frac{tD_e}{L^2} \tag{58}$$

$$\beta = \frac{D_e}{D_e^0} \tag{59}$$

where $\bar{T}$ = dimensionless total component concentration, $\bar{T}^0$ = initial total component concentration, $\bar{X}$ = dimensionless distance, L = distance from center of solid

to boundary with bath, $\bar{t}$ = dimensionless time, and D_e^0 = standard effective diffusivity. Thus, equation (55) becomes equation (60)

$$\frac{\partial \bar{T}}{\partial \bar{t}} = \beta \frac{\partial^2 (G\bar{T})}{\partial \bar{X}^2} \tag{60}$$

SOLDIF solves a Crank--Nicolson finite difference approximation of equation (60)

$$\frac{\bar{T}_i^{j+1} - \bar{T}_i^j}{\Delta \bar{t}} = \frac{\beta}{2}\left[\frac{(G_{i+1}\bar{T}_{i+1} - 2G_i\bar{T}_i + G_{i-1}\bar{T}_{i-1})^{j+1} + (G_{i+1}\bar{T}_{i+1} - 2G_i\bar{T}_i + G_{i-1}\bar{T}_{i-1})^j}{\Delta \bar{X}^2}\right] \tag{61}$$

where i = space step index and j = time step index.

Crank–Nicolson was chosen because it is unconditionally stable, unlike explicit finite difference methods, and it is more accurate than fully implicit finite difference methods near initial conditions. The Crank–Nicolson method does tend, however, to overshoot or undershoot solutions for unsmooth solution surfaces. Unsmooth solution surfaces can be defined for this model by equation (62)

$$\left(\frac{\partial \bar{T}}{\partial \bar{X}}\right)^i \neq \left(\frac{\partial \bar{T}}{\partial \bar{X}}\right)^{i+\Delta \bar{t}} \tag{62}$$

To mitigate these effects, SOLDIF uses an adaptive time step control algorithm to compute the time step size. Solutions are calculated for full time steps and half time steps for each component, and the maximum difference in these solutions is considered the truncation error (Δ_1). If the truncation error exceeds the acceptable error (i.e., $\Delta_1 > \Delta_0$), SOLDIF computes a smaller step size for the current time step using equation (62). If the truncation error is less than the acceptable error (i.e., $\Delta_1 < \Delta_0$), SOLDIF computes a larger step size for the next time step.

$$h_{\text{new}} = h_{\text{present}} \left|\frac{\Delta_0}{\Delta_1}\right|^{0.5} \tag{63}$$

where h = one-half of the time step size, Δ_0 = desired error, and Δ_1 = truncation error.

For each time step, SOLDIF calls SOLTEQ to calculate G at all nodes; however, G^{j+1}, the mobile fraction at the next time step, is unknown. To estimate G^{j+1}, SOLDIF linearly extrapolates from G values obtained at previous time steps. Calculation of G using SOLTEQ presupposes that local equilibrium exists at all nodes. This local equilibrium assumption is valid for most sorption/desorption and complexation reactions. It is also valid for many dissolution reactions because diffusive transport generally limits rates of dissolution reactions. Diffusive transport from solid surfaces into the pore network occurs over distances of approximately one-half of an average pore radius, whereas diffusive transport through the pore network to the waste/leachant interface occurs over distances of approximately one-half of an average pore length (Batchelor, 1992). Diffusive transport

into the pore network probably occurs more rapidly than diffusive transport through the pore network for distances greater than several pore diameters. Thus, an assumption of local chemical equilibrium is probably reasonable for dissolution of solids at most nodes within the waste matrix.

7. Conclusions and recommendations

Soil/cement reactions and environmental interactions may significantly affect solid and solution phase characteristics and, consequently, metal attenuation capacities of soil/cement/waste matrices over time. Bench-scale leach tests do not account for such reactions; thus, they are not wholly adequate for long-term performance assessment. A mechanistic model capable of predicting changes in solid and solution phase characteristics of soil/cement/waste reactions due to soil/cement reactions and environmental interactions is necessary to supplement such tests.

Modeling fate and transport of toxic metals in soil/cement/waste matrices and adjacent media will likely be limited by the paucity of data available on metal speciation at high pH. However, a model built upon the framework of SOLDIF, capable of predicting solid and solution phase characteristics of soil/cement/waste matrices over long time periods, might be combined with laboratory data correlating contaminant mobility with waste matrix characteristics to predict leach rates over time in a manner analogous to Côté, Bridle, and Benedek's (1986) model.

Additional data requirements for this type of model include the following: (1) effects of soil organic matter on cement hydration and pozzolanic reactions in soil/cement matrices, (2) effects of iron (III) content on pozzolanic reactivity of clay minerals in soil/cement matrices, (3) effects of clay on cement hydration in soil/cement matrices, (4) partition coefficients for potassium and sodium as a function of calcium:silicon ratios of calcium silicate hydrates, (5) solubility product constants for sodium-calcium silicate hydrates, (6) effects of alkali-silica reactions on hydraulic conductivity and effective diffusivity in soil/cement matrices, (7) calcium carbonate and brucite precipitation kinetics and consequent effects on effective diffusivity in soil/cement matrices, (8) extent of carbonation due to absorption of atmospheric $CO_{2(g)}$ into alkaline soil solutions during various treatment processes, (9) effects of crazing on hydraulic conductivity and effective diffusivity in soil/cement matrices, and (10) effects of sulfate reactions on hydraulic conductivity and effective diffusivity in soil/cement matrices.

Determination of the extent of carbonation during treatment is probably most important from both application and modeling perspectives. Theoretical calculations and experience (Eades, Nichols, and Grim, 1962) suggest that carbonation during treatment may significantly affect solid and solution phase characteristics of soil/cement/waste matrices, particularly porewater pH. From a modeling perspective, effects of soil organic matter and iron (oxy)hydroxide on availability of silicon and aluminum ions in soil/cement matrices and changes in effective diffusivity due to environmental interactions are also important.

Glossary

A	surface area of soil/cement/waste matrix (length^2)
C	mobile component concentration (moles/porewater volume)
$C_{b,HA}$	concentration of acid (HA) in bath (moles/bath volume)
C_e	mobile component concentration in equilibrium with solid phase (moles/porewater volume)
C_i^0	initial component concentration in solid phase (moles/porewater volume)
C_{im}	immobile component concentration (moles/porewater volume)
C_0	initial mobile component concentration (moles/porewater volume)
C_p	calcium concentration in solid phase (moles/porewater volume)
C_p^0	initial calcium concentration in solid phase (moles/porewater volume)
D_e	effective diffusivity (length^2/time)
$D_{e,HA}$	effective diffusivity of acid (HA) in soil/cement/waste matrix (length^2/time)
D_e^0	standard effective diffusivity (length^2/time)
D_0	initial effective diffusivity (length^2/time)
D_{obs}	observed diffusivity (length^2/time)
D_1	effective diffusivity within soil/cement/waste matrix (length^2/time)
D_2	effective diffusivity within adjacent geologic media (length^2/time)
erf	error function
F_l	leach rate (mass/time)
F_m	mobile fraction at time $t = 0$
G	mobile fraction
h	one-half timestep size
k	dissolution rate constant (time^4)
K_p	linear partition coefficient
L	distance from interface to centerline of soil/cement/waste matrix
M_0	initial component mass within soil/cement/waste matrix
M_t	component mass leached from soil/cement/waste matrix at any time, t
MW	component molecular weight (mass/mole)
MW_{CH}	calcium hydroxide ($Ca(OH)_2$) molecular weight (mass/mole)
n	moles acid required to react with one mole of component in solid phase
Q_l	leachant flow rate (volume/time)
R	$=\log[\{Ca^{2+}\}/\{H_2SiO_4^0\}]$
T	total component concentration (moles/porewater volume)
T^0	initial total component concentration
$\bar{T}$	dimensionless total component concentration
$\bar{t}$	dimensionless time
X	distance into soil/cememt/waste matrix from interface
$\bar{X}$	dimensionless distance
α	degree of cement hydration
β	dimensionless effective diffusivity
Δ_0	acceptable error
Δ_1	truncation error
γ_{CH}	portlandite density (mass/volume)
$\theta_e(C_p)$	capillary porosity as a function of solid phase calcium concentration
θ_e^0	initial capillary porosity
ω	water:cement weight ratio

References

Allison, J.D., Brown, D.S., and Novo-Gradac, Kevin J., 1990. MINTEQA2/PRODEFA2, A Geochemical Assessment Model for Environmental Systems. Version 3.0 User's Manual. Environmental

Research Laboratory, Office of Research and Development, U.S. Environmental Protection Agency, Athens, G.A.

Atkins, M. and Glasser, F. P., 1992. Application of Portland cement-based materials to radioactive waste immobilization. Waste Management, 12: 105–131.

Barneyback, R.S., Jr. and Diamond, S., 1981. Expression and analysis of pore fluids from hardened cement pastes and mortars. Cement and Concrete Research, 11: 279–285.

Barth, E.F., 1992. Summary of solidification/stabilization SITE demonstrations at uncontrolled hazardous waste sites. In: T.M. Gilliam and C.C. Wiles (Editors), Stabilization and Solidification of Hazardous, Radioactive, and Mixed Wastes, Second Volume, ASTM STP 1123, American Society for Testing and Materials, Philadelphia, P.A., pp. 409–414.

Batchelor, B., 1990. Leach models: theory and application. J. Hazardous Materials, 24: 255–266.

Batchelor, B., 1992. A numerical leaching model for solidified/stabilized wastes. Water Science and Technology, 26: 107–115.

Batchelor, B., 1993a. A Framework for Risk Assessment of Disposal of Solidified/Stabilized Wastes and Contaminated Soils, Symposium on Treatment and Modeling of Hazardous Waste Processes, 24th Annual Meeting of the Fine Particle Society, Chicago, I.L., August 24–28.

Batchelor, B. and Wu, K., 1993b. Effects of equilibrium chemistry on leaching of contaminants from stabilized/solidified wastes. In: Roger D. Spence (Editor), Chemistry and Microstructure of Solidified Waste Forms, pp. 243–259.

Bates, E., 1992. Applications Analysis Report: Silicate Technology Corporation's Solidification/Stabilization Technology for Organic and Inorganic Contaminants in Soils. EPA/540/AR-92/010 (1992).

Bishop, P.L., 1986. Prediction of heavy metal leaching rates from stabilized/solidified hazardous wastes. In: Toxic and Hazardous Waste: Proceedings of the 18th Mid-Atlantic Industrial Waste Conference, pp. 236–252.

Bishop, P.L., 1988. Leaching of inorganic hazardous constituents from stabilized/solidified hazardous wastes. Hazardous Waste & Hazardous Materials, 5: 129–143 (1988).

Bohn, L.H., McNeal, B.L., and O'Connor, G. A., 1979. Soil Chemistry, Wiley Interscience, New York, N.Y.

Buil, M., Revertegat, E., and Oliver, J., 1992. A model of the attack of pure water or undersaturated lime solutions on cement. In: T. Gilliam and C. Wiles (Editors), Solidification and Stabilization of Hazardous, Radioactive, and Mixed Wastes, ASTM STP 1123, pp. 227–241.

Cheng, K.Y. and Bishop, P.L., 1992a. Metals distribution in solidified/stabilized waste forms after leaching. Hazardous Waste & Hazardous Materials, 9(2): 163–171.

Cheng, K.Y. and Bishop, P.L., 1992b. Leaching boundary movement in solidified/stabilized waste forms. J. Air Waste Management Assoc., 42: 164–168.

Cheng, K.Y., Bishop, P.L., and Isenburg, J., 1992. Leaching boundary in cement-based waste forms. J. Hazardous Materials, 30: 285–295.

Clare, K.E. and Sherwood, P.T., 1954. The effect of organic matter on the setting of soil-cement mixtures. J. Appl. Chem., 4: 625–630.

Conner, J., 1990. Chemical Fixation and Solidification of Hazardous Wastes, Van Nostrand Reinhold, New York, N.Y.

Côté, P.L. and Bridle, T.R., 1987. Long-term leaching scenarios for cement-based waste forms. Waste Management and Research, 5: 55–66.

Côté, P.L., Bridle, T.R., and Benedek, A., 1986. An approach for evaluating long-term leachability from measurement of intrinsic waste properties. In: D. Lorenzen et al. (Editors), Hazardous and Industrial Solid Waste Testing and Disposal: Sixth Volume, ASTM STP 933, American Society for Testing and Materials, Philadelphia, P.A., pp. 63–78.

Côté, P.L. and Constable, T., 1987. An evaluation of cement-based waste forms using the results of approximately two years of dynamic leaching. Nuclear and Chemical Waste Management, 7: 129–139.

Crank, J., 1975. The Mathematics of Diffusion, Clarendon Press, Oxford.

Davidson, D.T., Pitre, G.L., Mateos, M., and George, K.P., 1962. Moisture-density, moisture-strength and compaction characteristics of cement-treated soil mixtures. HRB Bulletin 353: 42–63 (1962).

Davidson, L.K., Demirel, T., and Handy, R.L., 1985. Soil pulverization and lime migration in soil-lime stabilization. Highway Research Record, 92: 103–118.

Dayal, R. and Reardon, E.J., 1992. Cement-based engineered barriers for carbon-14 isolation. Waste Management, 12: 189–200.

de Percin, P.R., 1989. Description of EPA SITE Demonstration of the HAZCON Stabilization Process at the Douglassville, Pennsylvania Superfund Site. EPA 600/J-89/325.

de Percin, P.R. and Sawyer, S., 1991. Long-term monitoring of the hazcon stabilization process at the Douglassville, Pennsylvania superfund site. J. Air Waste Management Assoc., 41(1): 88–91.

Diamond, S., 1964. Rapid reaction of lime with hydrous alumina. Nature, 204: 183–185.

Diamond. S. and Kinter, E.B., 1965. Mechanisms of soil-lime stabilization: an interpretive review. Highway Research Record, 92: 83–102.

Diamond, S., White, J.L., and Dolch, W.L., 1963. Transformation of clay minerals by calcium hydroxide attack. Proceedings of the Twelfth National Conference on Clays and Clay Minerals, pp. 359–378.

Eades, J.L. and Grim, R.E., 1960. Reaction of hydrated lime with pure clay minerals in soil stabilization. Highway Research Board Bulletin, 262: 51–63.

Eades, J.L., Nichols, F.P. Jr., and Grim, R.E., 1962. Formation of new minerals with lime stabilization as proven by field experiments in Virginia. Highway Research Board Bulletin, 335: 31–39.

Ford, C.M., Moore, R.K., and Hajek, B.F., 1982. Reaction products of lime-treated southeastern soils. Transportation Research Record, 839: 38–40.

Freeze, R.A. and Cherry, J.A., 1979. Groundwater, Prentice-Hall, Englewood Cliffs, N.J.

Glasser, F.P., 1993. Chemistry of cement-solidified waste forms. In: R.D. Spense (Editor), Chemistry and Microstructure of Solidified Waste Forms Lewis Publishers, Boca Raton, F.L., pp. 1–39.

Glasser, F.P., Luke, K., and Angus, M.J., 1988. Modification of cement pore fluid compositions by pozzolanic additives. Cement and Concrete Research 18: 165–178.

Glasser, F.P., MacPhee, D.E., and Lachowski, E.E., 1987. Solubility modeling of cements: implications for radioactive waste immobilization. In: J.K. Bates and W.B. Seefeldt (Editors), Scientific Basis for Nuclear Waste Management X. Materials Research Society Symposium Proceedings, Vol. 84, pp. 331–341.

Glasser, F.P. and Marr, J., 1984. The effect of mineral additives on the composition of cement pore fluids. Proceedings of the British Ceramic Society, 35: 419–428.

Glenn, G.R. and Handy, R.L., 1963. Lime-clay mineral reaction products. Highway Research Record, 29: 70–82.

Greenburg, S.A., 1956. The chemisorption of calcium hydroxide by silica.

Grim, R.E., 1968. Clay Mineralogy, McGraw-Hill, New York, N.Y.

Grube, W.E., 1990a. Evaluation of waste stabilized by the soliditech SITE technology. J. Air & Waste Management, 40(3): 310–316.

Grube, W.E., 1990b. Physical and Morphological Measures of Waste Solidification Effectiveness. EPA/600/D-t91/164.

Grube, W.E., 1990c. Soliditech, Inc. Solidification/Stabilization Process: Applications Analysis Report. EPA/540/A5–89/005.

Handy, R.L., Demirel, T., Ho, C., Nady, R.M., and Ruff, C.C., 1965. Discussion of Diamond, S. and Kinter, E.B. Mechanisms of soil-lime stabilization: an interpretive review. Highway Research Record, 92: 83–102.

Hilt, G.H. and Davidson, D.T., 1960. Lime fixation in clayey soils. Highway Research Board Bulletin, 262: 20–32 (1960).

Helling, C.S., Chesters, G., and Corey, R.B., 1964. Contribution of organic matter and clay to soil cation exchange capacity as affected by pH of the saturating solution. Proc. Soil Sci. Soc. Amer., 28: 517–520.

Ho, C. and Handy, R.L., 1963. Characteristics of lime retention by montmorillonitic clays. Highway Research Board, 29: 35–69.

Ho, D.W.S. and Lewis. R.K., 1987. Carbonation of concrete and its prediction. Cement and Concrete Research, 17: 489–504.

Hunter, D., 1988. Lime-induced heave in sulfate-bearing clay soils. J. Geotech. Eng., 114: 151–167.

Komarneni, S., Roy, D.M., and Kumar, A., 1984. Cation-exchange properties of hydrated cements. Nuclear Waste Management, American Ceramic Society, Columbus, O.H., pp. 441–447.

Larbi, J.A., Fraay, A.L.A., and Bijen, M.J.M., 1990. The chemistry of the pore fluid of silica fume-blended cement systems. Cement and Concrete Research, 20: 506–516.

Lawrence, C.D., 1966. Changes in composition of the aqueous phase during hydration of cement pastes and suspensions. In: Highway Research Board Special Report 90: Symposium on Structure of Portland Cement Paste and Concrete, pp. 378–391.

Lea, F.M., 1971. The Chemistry of Cement and Concrete. Chemical Publishing Company, New York, N.Y.

Lindsay, W.L., 1979. Chemical Equilibria in Soils. Wiley, New York, N.Y.

Maris, P.J. et al., 1984. Leachate treatment with particular reference to aerated lagoons. Water Pollution Control, 83(4): 521.

Mindess, S. and Young, J.F., 1981. Concrete. Prentice-Hall, Englewood Cliffs, N.J.

Mitchell, J.K. and El Jack, A., 1965. The fabric of soil-cement and its formation. Fourteenth National Conference on Clays and Clay Minerals, pp. 297–305.

Moh, Z-C., 1965. Reactions of soil minerals with cement and chemicals. Highway Research Record, 86: 39–61.

Myers, T.E. and Hill, D.O., 1986. Extrapolation of leach test data to the field situation. J. Mississippi Academy of Sciences, 31: 27–46.

Oblath, S.B., 1989. Leaching from solidified waste forms under saturated and unsaturated conditions. Environ. Sci. Technol., 23: 1098–1102.

Ormsby, W.C. and Bolz, L.H., 1966. Microtexture and composition of reaction products in the system kaolin-lime-water. J. Amer. Ceramic Soc., 49: 364–366.

Parrott, L.J. and Killoh, D.C., 1989. Carbonation in a 36 year old, in-situ concrete. Cement and Concrete Research, 19: 649–656.

Plaster, E.J., 1992. Soil Science and Management, Second Edition. Delmar Publishers, Albany, New York, N.Y.

Plaster, R.W. and Noble, D.F., 1970. Reactions and strength development in Portland cement-soil mixtures. Highway Research Record, 315: 46–63.

Poon, C.S., Clark, A.I., and Perry, R., 1985. Mechanisms of metal fixation and leaching by cement based fixation processes. Waste Management and Research, 3: 127–142.

Reardon, E.J., 1990. An ion interaction model for the determination of chemical equilibria in cement/water systems. Cement and Concrete Research, 20: 175–192.

Reardon, E.J., 1992. Problems and approaches to the prediction of the chemical composition in cement/water systems. Waste Management, 12: 221–239.

Sawyer, S., 1989a. Technology Evaluation Report: SITE Program Demonstration Test, HAZCON Solidification, Douglassville, Pennsylvania, P.A., Vol. 1. EPA/540/5—89/001a.

Sawyer, S., 1989b. Technology Evaluation Report: SITE Program Demonstration Test, International Waste Technologies In Situ Stabilization/Solidification, Hialeah, F.L., Vol. 1. EPA/540/5–89/004a.

Sawyer, S., 1990. International Waste Technologies/Geo-Con In Situ Stabilization/Solidification: Applications Analysis Report. EPA/540/A5–89/004.

Sloane, R.L., 1964. Early reaction determination in two hydroxide-kaolinite systems by electron microscopy and diffraction. Proceedings of the Thirteenth National Conference on Clays and Clay Minerals, pp. 331–339.

Soroka, I., 1979. Portland Cement Paste and Concrete. MacMillan Press, London.

Sposito, G., 1989. The Chemistry of Soils, Oxford University Press, Oxford.

Stegemann, J. and Côté, P.L., 1991. Investigation of Test Methods for Solidified Waste Evaluation – A Cooperative Program. Wastewater Technology Center, Conservation and Protection, Environment Canada.

Stocker, P.T., 1972. Diffusion and diffuse cementation in lime and cement stabilized clayey soils. Australian Road Research Board Special Report, No. 8 (1972).

Srinivasan, N.R., 1967. Influence of the structural state of silica on lime-silica reactions. Highway Research Record, 192: 1–13.

Stinson, M.K., 1990. EPA Site Demonstration of the International Waste Technologies/GEO-CON In Situ Stabilization/Solidification Process. EPA/600/J-90/413.

Suzuki, K., Nishikawa, T., and Ito, S., 1985. Formation and carbonation of C—S—H in water. Cement and Concrete Research, 15: 213–224.

Taffinder, G.G. and Batchelor, B., 1993. Measurement of effective diffusivities in solidified wastes. J. Environ. Eng., 119: 17–33.

Taylor, H.F.W., 1990. Cement Chemistry. Academic Press, New York, N.Y.

Thompson, M.R., 1966. Lime reactivity of Illinois soils. J. Soil Mechanics and Foundations Division, 92: 67–93.

Uloth, V.C. and Mavinic, D.S., 1977. Aerobic biotreatment of a high stength leachate. J. Environ. Eng. Div., 103(4): 652.

U.S. Environmental Protection Agency, 1993. Technical Resource Document: Solidification/Stabilization and Its Applications to Waste Materials. EPA/530/R-93/012.

U.S. Environmental Protection Agency, 1991. Applications Analysis Report: Chemfix Technologies, Inc. Solidification/Stabilization Process. EPA/540/A5–89/011.

Volk, V.V. and Jackson, M.L., 1963. Inorganic pH dependent cation exchange charge of soils. Proceedings of the Twelfth National Conference on Clay and Clay Minerals, pp. 281–294.

Weitzman, L. and Hamel, L.E., 1989. Evaluation of Solidification/Stabilization Technology as a Best Demonstrated Available Technology for Contaminated Soils. EPA/600/2–89/049.

Wu, K., 1993. A Chemical Equilibrium Model for Contaminants in Stabilized/Solidified Waste. Civil Engineering Dept., Texas A&M University, T.X.

This Page Intentionally Left Blank

Chapter 5

Propagation of waves in porous media

M. YAVUZ CORAPCIOGLU and KAGAN TUNCAY

Abstract

Wave propagation in porous media is of interest in various diversified areas of science and engineering. The theory of the phenomenon has been studied extensively in soil mechanics, seismology, acoustics, earthquake engineering, ocean engineering, geophysics, and many other disciplines. This review presents a general survey of the literature within the context of porous media mechanics. Following a review of the Biot's theory of wave propagation in linear, elastic, fluid saturated porous media which has been the basis of many analyses, we present various analytical and numerical solutions obtained by several researchers. Biot found that there are two dilatational waves and one rotational wave in a saturated porous medium. It has been noted that the second kind of dilatational wave is highly attenuated and is associated with a diffusion type process. The influence of coupling between two phases has a decreasing effect on the first kind wave and an increasing effect on the second wave. Procedures to predict the liquefaction of soils due to earthquakes have been reviewed in detail. Extension of Biot's theory to unsaturated soils has been discussed, and it was noted that, in general, equations developed for saturated media were employed for unsaturated media by replacing the density and compressibility terms with modified values for a water-air mixture. Various approaches to determine the permeability of porous media from attenuation of dilatational waves have been described in detail. Since the prediction of acoustic wave speeds and attenuations in marine sediments has been extensively studied in geophysics, these studies have been reviewed along with the studies on dissipation of water waves at ocean bottoms. The mixture theory which has been employed by various researchers in continuum mechanics is also discussed within the context of this review. Then, we present an alternative approach to obtain governing equations of wave propagation in porous media from macroscopic balance equations. Finally, we present an analysis of wave propagation in fractured porous media saturated by two immiscible fluids.

1. Introduction

The dynamic response of porous media is of interest in various areas of engineering and physics. Underground nuclear explosions generate shock waves propagating through the porous medium surrounding the blast. Liquefaction of saturated sands due to dynamic loads has been studied extensively in earthquake engineer-

ing. Attenuation of waves in geologic formations is of importance in seismic studies at very low frequencies (1–100 Hz). On the other hand, full-wave acoustic logging requires a much higher frequency range, almost up to 100 KHz. Elastic wave propagation in wet paper layers or the articulating cartilage is modeled as dynamic loads moving with a velocity across a poroelastic layer. Propagation of tidal fluctuations through groundwater aquifers or wave induced pressure fluctuations at ocean bottoms are other examples of wave propagation in porous media. Although liquid saturated materials attenuate waves gradually, dry porous materials exhibit pore crushing and pore collapse. Shock-wave compaction of porous metals has received considerable attention in mechanical engineering. Furthermore, due to their energy absorption characteristics, dry porous substances such as elastomeric foam are used as shock attenuators for commercial packaging purposes. Finally, one can note the soil-structure interaction due to pile driving, rotary machines, and moving heavy traffic in geotechnical engineering as examples of wave propagation in porous materials.

As seen in this brief listing of areas where the response of porous materials to dynamic loads plays a role, the study of wave propagation in porous media would cover a large number of disciplines. However, the conservation of mass and momentum principles form the basis of an analysis of problems arising in many diversified fields. In this theory, the deformable porous medium is viewed as a continuum consisting of a solid phase (either compressible or incompressible) and one or more fluids (gases and liquids). The solid phase constitutes the solid matrix with interconnected void space filled by fluids. These relations are introduced into the conservation of linear momentum and solid and fluid mass balance equations. Elastic constants of the constitutive relations are either obtained experimentally (e.g., Biot and Willis, 1957) or determined theoretically employing a theory such as that used by Duffy and Mindlin (1957). In this study, the governing equations of the phenomenon will be presented at a macroscopic level. That is, they are obtained by averaging the microscopic equations which are valid at a point within an individual phase present in the system over a representative elementary volume (REV) of the porous medium.

An alternative to continuum approach is the "distinct element" approach which treats the granular medium as an assemblage of individual particles with a particular geometry (circular disks, spheres, etc.). This approach employs Newtonian rigid body mechanics to simulate the translational and rotational motion of each element under dynamic loading. Dynamic photoelastic experiments provide experimental information (Sadd et al., 1989; Shukla and Zhu, 1988). This type of modeling effort started with Iida (1939) and included researchers like Gassman (1951), Brandt (1955), Duffy and Mindlin (1957), Goodman and Cowin (1972), Nunziato et al. (1978), Schwartz (1984), Sadd and Hossain (1989), and Chang et al. (1992) among many others. Since it is beyond the scope of this research, distinct element approach will not be covered in this review. The reader is referred to any one of these references for a more detailed treatment of the subject.

Therefore, it is the purpose of this review to present various continuum approach methodologies to formulate the wave propagation in porous media in different fields of interest. We will try to achieve this in such a way that the reader

unfamiliar with the subject can follow the material within the context of porous media mechanics.

2. Biot's theory

Although the wave propagation in porous media has been studied quite some time, Biot's (1956a, b) work on wave propagation appears to be the first one employing the fundamentals of porous media mechanics. In addition to his dynamic theory, Biot (1941) also presented a quasi-static theory for elastic porous solids saturated with a fluid. Biot's work dominated the field over three decades, and influenced the direction of future research more than any other person who ever worked in this area. Not only the work published in the Western literature, but also research conducted by Russian researchers was affected by Biot's theory. For a review of Russian literature, we refer the reader to Nikolaevskij (1990). To do justice to this most significant work, we will start our review by presenting the Biot's formulation.

2.1. Stress-strain relationships for a fluid saturated elastic porous medium

The deformation of a porous medium can be related to the average displacement fields by using the theory of infinitesimal strain, i.e., the second and higher order displacement derivatives are neglected. Introducing the fundamental notation, the components of strain tensor of the solid matrix are

$$\epsilon_{xx} = \frac{\partial u_x}{\partial x}, \quad \epsilon_{yy} = \frac{\partial u_y}{\partial y}, \quad \epsilon_{zz} = \frac{\partial u_z}{\partial z} \tag{2.1}$$

$$\gamma_{xy} = \frac{\partial u_x}{\partial y} + \frac{\partial u_y}{\partial x}, \quad \gamma_{xz} = \frac{\partial u_z}{\partial x} + \frac{\partial u_x}{\partial z}, \quad \gamma_{yz} = \frac{\partial u_y}{\partial z} + \frac{\partial u_z}{\partial y} \tag{2.2}$$

The dilatation, ϵ, is expressed in terms of displacement vector, $\boldsymbol{u}$, as

$$\epsilon = \nabla . \boldsymbol{u} \tag{2.3}$$

The components of the rotation vector, $\boldsymbol{\omega}$, are expressed as

$$\omega_x = \frac{1}{2}\left(\frac{\partial u_z}{\partial y} - \frac{\partial u_y}{\partial z}\right), \quad \omega_y = \frac{1}{2}\left(\frac{\partial u_x}{\partial z} - \frac{\partial u_z}{\partial x}\right), \quad \omega_z = \frac{1}{2}\left(\frac{\partial u_y}{\partial x} - \frac{\partial u_x}{\partial y}\right) \tag{2.4}$$

and the rotation $\boldsymbol{\omega}$ of the solid is given by

$$\boldsymbol{\omega} = \frac{1}{2}\nabla x \boldsymbol{u} \tag{2.5}$$

if $\boldsymbol{\omega} = 0$, the strain is irrotational. Similarly, the components U_x, U_y, and U_z of the fluid displacement vector $\boldsymbol{U}$ are related to the dilatation of the fluid

$$e = \nabla . U \tag{2.6}$$

Similarly, the rotation in the fluid is given by

$$\Omega = \frac{1}{2} \nabla x U \tag{2.7}$$

It should be pointed out that this expression is not the actual strain in the fluid but simply the divergence of the fluid displacement which itself is derived from the average volume flow through the pores.

Following Biot (1956a), we assume that the solid skeleton of the porous medium is isotropic and for the relatively small deviations it is perfectly elastic. For such a solid matrix, the stress-strain relationships are expressed by

$$\sigma_{xx} = 2N\epsilon_{xx} + A\epsilon + Qe \tag{2.8}$$

$$\sigma_{yy} = 2N\epsilon_{yy} + A\epsilon + Qe \tag{2.9}$$

$$\sigma_{zz} = 2N\epsilon_{zz} + A\epsilon + Qe \tag{2.10}$$

$$\tau_{xy} = N\gamma_{xy} \tag{2.11}$$

$$\tau_{xz} = N\gamma_{xz} \tag{2.12}$$

$$\tau_{yz} = N\gamma_{yz} \tag{2.13}$$

where

$$\epsilon = \epsilon_{xx} + \epsilon_{yy} + \epsilon_{zz} \tag{2.14}$$

where σ_{xx}, σ_{yy}, and σ_{zz} are the normal stresses in x, y, and x, directions, respectively. τ_{xy}, τ_{xz}, and τ_{yz} are the shear stresses. ϵ and e denote the dilatation in the solid matrix and the fluid, respectively. The coefficient N represents the shear modulus of the solid. The coefficients A and N correspond to Lame constants. In the theory of elasticity, they are denoted by λ and G, respectively. The coefficient Q is the cross coupling term between the volume changes of the solid matrix and the fluid. The stress in the fluid, σ, is proportional to the fluid pressure p by

$$-\sigma = np \tag{2.15}$$

where n is the effective porosity which represents the interconnected pore space. Biot considers the sealed pore space as part of the solid. Note that solid stresses are positive in tension, and the fluid pressure is positive in compression. Although Biot neglects shear stresses in the fluid due to viscosity. Then the stress-strain relationship for the fluid is given by

$$\sigma = Q\epsilon + Re \tag{2.16}$$

where R is defined by Biot as a measure of the fluid pressure to force a certain volume of the fluid into the porous medium while the total volume of the porous medium stays constant. If a stress is applied to the solid matrix while the fluid pressure is zero, the dilatation of the solid (and an associated decrease in porosity) would produce a reverse dilatation (volume expansion) of the fluid. As seen in

equation (2.16), the ratio of dilatation would be equal to the ratio of Q/R. Fatt (1959) determined the values of four constants, A, N, Q, and R, by experiments of kerosene flow through Boise sandstone. Biot and Willis (1957) express A, N, Q, and R as

$$Q = \frac{n(\alpha - n)}{\gamma + \alpha\alpha^*}$$

$$R = \frac{n^2}{\gamma + \alpha\alpha^*}$$

$$A = \frac{\gamma/K + n^2 + \alpha(1 - 2n)}{\gamma + \alpha\alpha^2} - \frac{2G}{3}$$

$$N = G$$

where $\alpha = 1 - \alpha^*/K$, $\gamma = n(1/\beta - \alpha^*)$, G is the shear modulus of the solid matrix, α^* is the unjacketed compressibility (grain compressibility) which is the inverse of bulk modulus of solid grains, K is the jacketed compressibility. Geertsma (1957) and Stoll (1979) also evaluated Biot's coefficients. The frequency dependence of the elastic moduli was investigated by Schmidt (1988)

2.2. Equations of motion

Biot (1956a) derived his theory of wave propagation in porous media by introducing the Lagrangian viewpoint and the concept of generalized coordinates. In Lagrangian description, one follows the movement of the REV rather than interpreting in terms of what happens at a fixed REV (Eulerian description). In this case, kinetic energy function, T, and dissipation function, D, are expressed in terms of six displacement components of solid and fluid phases. The kinetic energy, T, of the saturated isotropic porous medium per unit volume is expressed as

$$2T = \rho_{11}\left[\left(\frac{\partial u_x}{\partial t}\right)^2 + \left(\frac{\partial u_y}{\partial t}\right)^2 + \left(\frac{\partial u_z}{\partial t}\right)^2\right] + 2\rho_{12}\left[\frac{\partial u_x}{\partial t}\frac{\partial U_x}{\partial t} + \frac{\partial u_y}{\partial t}\frac{\partial U_y}{\partial t} + \frac{\partial u_z}{\partial t}\frac{\partial U_z}{\partial t}\right]$$
$$+ \rho_{22}\left[\left(\frac{\partial U_x}{\partial t}\right)^2 + \left(\frac{\partial U_y}{\partial t}\right)^2 + \left(\frac{\partial U_z}{\partial t}\right)^2\right] \tag{2.17}$$

T depends only on six displacement components. The dissipation depends on the relative movement between the solid and the fluid. When there is no relative motion, the dissipation function, D, vanishes. Then

$$2D = b\left[\left(\frac{\partial u_x}{\partial t} - \frac{\partial U_x}{\partial t}\right)^2 + \left(\frac{\partial u_y}{\partial t} - \frac{\partial U_y}{\partial t}\right)^2 + \left(\frac{\partial u_z}{\partial t} - \frac{\partial U_z}{\partial t}\right)^2\right] \tag{2.18}$$

where b is a constant (drag coefficient) for an isotropic medium and it is related to the fluid viscosity μ_f and permeability k by

$$b = \frac{\mu_f n^2}{k} \tag{2.19}$$

Biot calls ρ_{11}, ρ_{12}, and ρ_{22} "mass coefficients", and they are related to densities of solid (ρ_s) and fluid (ρ_f) phases by

$$\rho_{11} + \rho_{12} = (1 - n)\rho_s \tag{2.20a}$$

$$\rho_{12} + \rho_{22} = n\rho_f \tag{2.20b}$$

The coefficient ρ_{12} represents the mass coupling parameter (virtual mass effect) between the fluid and the solid phases and is always negative.

Then, if we denote the total force acting on the solid and fluid phases per unit volume in the x-direction by F_x^s and F_x^f, respectively, we can derive the following from Lagrange's equations

$$F_x^s = \frac{\partial}{\partial t}\left[\frac{\partial T}{\partial(\partial u_x/\partial t)}\right] + \frac{\partial D}{\partial(\partial u_x/\partial t)} = \frac{\partial^2}{\partial t^2}(\rho_{11}u_x + \rho_{12}U_x) + b\frac{\partial}{\partial t}(u_x - U_x) \tag{2.21}$$

$$F_x^f = \frac{\partial}{\partial t}\left[\frac{\partial T}{\partial(\partial U_x/\partial t)}\right] + \frac{\partial D}{\partial(\partial U_x/\partial t)} = \frac{\partial^2}{\partial t^2}(\rho_{12}u_x + \rho_{22}U_x) - b\frac{\partial}{\partial t}(u_x - U_x) \tag{2.22}$$

Similar equations may be written in the y- and z-directions. If we express the force components, F_x^s and F_x^f as stress gradients, equations (2.21) and (2.22) can be rewritten in the following form

$$\frac{\partial \sigma_{xz}}{\partial x} + \frac{\partial \tau_{xy}}{\partial y} + \frac{\partial \tau_{xz}}{\partial z} = \frac{\partial^2}{\partial t^2}(\rho_{11}u_x + \rho_{12}U_x) + b\frac{\partial}{\partial t}(u_x - U_x) \tag{2.23}$$

$$\frac{\partial \sigma}{\partial x} = \frac{\partial^2}{\partial t^2}(\rho_{12}u_x + \rho_{22}U_x) - b\frac{\partial}{\partial t}(u_x - U_x) \tag{2.24}$$

Since stresses are related to displacements by employing equations (2.8)–(2.16), the equations of motion can be stated as

$$N\nabla^2 u_x + (A + N)\frac{\partial \epsilon}{\partial x} + Q\frac{\partial e}{\partial x} = \frac{\partial^2}{\partial t^2}(\rho_{11}u_x + \rho_{12}U_x) + b\frac{\partial}{\partial t}(u_x - U_x) \tag{2.25}$$

$$N\nabla^2 u_y + (A + N)\frac{\partial \epsilon}{\partial y} + Q\frac{\partial e}{\partial y} = \frac{\partial^2}{\partial t^2}(\rho_{11}u_y + \rho_{12}U_y) + b\frac{\partial}{\partial t}(u_y - U_y) \tag{2.26}$$

$$N\nabla^2 u_z + (A + N)\frac{\partial \epsilon}{\partial z} + Q\frac{\partial e}{\partial z} = \frac{\partial^2}{\partial t^2}(\rho_{11}u_z + \rho_{12}U_z) + b\frac{\partial}{\partial t}(u_z - U_z) \tag{2.27}$$

$$Q\frac{\partial \epsilon}{\partial x} + R\frac{\partial e}{\partial x} = \frac{\partial^2}{\partial t^2}(\rho_{12}u_x + \rho_{22}U_x) - b\frac{\partial}{\partial t}(u_x - U_x) \tag{2.28}$$

TABLE 1

Frequency range of wave propagation in porous media

Frequency range of Poiseuille flow	Critical < frequency, f_t	Characteristic < frequency, f_c	High < frequency range
	Viscous forces dominate <------> inertial forces dominate		
	μ_f	$\mu_f = \mu_f(f/f_c)$	

$$Q\frac{\partial \epsilon}{\partial y} + R\frac{\partial e}{\partial y} = \frac{\partial^2}{\partial t^2}(\rho_{12}u_x + \rho_{22}U_y) - b\frac{\partial}{\partial t}(u_y - U_y) \tag{2.29}$$

$$Q\frac{\partial \epsilon}{\partial z} + R\frac{\partial e}{\partial z} = \frac{\partial^2}{\partial t^2}(\rho_{12}u_z + \rho_{22}U_z) - b\frac{\partial}{\partial t}(u_z - U_z) \tag{2.30}$$

Equations (2.25)–(2.30) with six dependent variables, u_x, U_x, u_y, U_y, u_z, and U_z, formulate the wave propagation in a fluid saturated isotropic porous medium. As noted by Biot (1956a), an acceleration of the solid matrix without any motion of fluid causes a pressure gradient in the fluid due to the coupling coefficient, ρ_{12}.

Biot assumed that the fluid flow $(\boldsymbol{U} - \boldsymbol{u})$ relative to the solid is of the Poiseuille type. The coefficient b, as given by equation (2.19), is for Poiseuille flow. This assumption restricts the solution domain to low frequency range. For wave motions in high frequency range, Poiseuille flow assumption does not hold. At higher frequency range, a boundary layer develops on solid phase surfaces. The friction forces developing in this layer increases with frequency. The flow field in this layer is different than the flow beyond the boundary layer. Thus "the friction force of the fluid on the solid becomes out of phase with relative rate of flow and exhibits a frequency dependence" (Biot, 1962a). Biot (1956a) limits the lower frequency range with a "critical frequency" value, f_t, defined by

$$f_t = \frac{\mu_f \pi}{4\rho_f d^2} \tag{2.31}$$

where d is the diameter of the pores and μ_f is the dynamic viscosity. By equation (2.31), the relative size of wave length of elastic waves is limited to an order of the pore diameter. This assumption can be avoided if we assume that the fluid is an ideal one. Furthermore, above the characteristic frequency, f_c, which depends on the kinematic viscosity of the fluid and the size of the pores, the viscosity must be considered frequency dependent (Table 1).

Since the use of Poiseuille flow concept is a major assumption in Biot formulation, we will briefly look at the Poiseuille equation. In fluid mechanics, steady state laminar flow due to pressure drop along a tube is called Poiseuille flow. The velocity distribution for such a flow in a tube with radius r_0 can be written in cylindrical coordinates. Let us take x-axis as the axis of the tube. The only velocity component, u, will be in the x-direction and will be independent of x. Then by neglecting gravity effects

$$-\frac{\partial p}{\partial x}+\mu_f \frac{1}{r}\frac{\partial}{\partial r}\left(r\frac{\partial u}{\partial r_2}\right)=0 \tag{2.32}$$

By integrating equation (2.32) twice, employing boundary conditions at $r = 0$, $u = u_{max}$ and at $r = r_0$, $u = 0$, and noting that $u_{ave} = u_{max}/2$ where u_{ave} is the average velocity, we obtain

$$\frac{dp}{dx}=\frac{32\mu_f}{d^2}u_{ave}=\frac{C\mu_f u_{max}}{R_H^2} \tag{2.33}$$

where d is the diameter of the tube. Note that in equation (2.32) there is no inertia term. In equation (2.33), R_H is the hydraulic radius ($=d/4$ for circular pipes), and C is a constant (Kozeny's constant, or a shape factor). In porous media flow, R_H will be a measure of the size of pores. A comparison of equation (2.33) with equation (2.19) shows that for a porous medium $k = nR_H^2/C$. Tiller (1975) illustrates the variation of Kozeny's constant with porosity. For $0 < C < 10$, C can be calculated by

$$C=\frac{3.5n^3}{\sqrt{(1-n)}}[1+57(1-n)^3] \tag{2.33a}$$

2.3. Derivation of dilatational wave propagation equations

If we differentiate both sides of equation (2.25) with respect to x, both sides of equation (2.26) with respect to y, and both sides of equation (2.27) with respect to z and add using equation (2.14) and assuming constant ρ_{11}, ρ_{22}, and ρ_{12}, we obtain

$$\nabla^2(P\epsilon+Qe)=\frac{\partial^2}{\partial t^2}(\rho_{11}\epsilon+\rho_{12}e)+b\frac{\partial}{\partial t}(\epsilon-e) \tag{2.34}$$

where $P = A + 2N$. If we perform same operations and make the same assumptions for equations (2.28)–(2.30), then

$$\nabla^2(Q\epsilon+Re)=\frac{\partial^2}{\partial t^2}(\rho_{12}\epsilon+\rho_{22}e)-b\frac{\partial}{\partial t}(\epsilon-e) \tag{2.35}$$

Equations (2.34) and (2.35) govern the propagation of dilatational waves in a porous medium. These two equations clearly show the coupling between them.

If we neglect the dissipative forces, and consider purely elastic waves, i.e., $b = 0$ in equations (2.34) and (2.35), the velocities of two dilatational waves, V_1 and V_2 are obtained from the solution of a quadratic equation by assuming solutions to equations (2.34) and (2.35) to be represented by

$$\epsilon = C_1 e^{i(\beta x+\theta t)}$$

$$e = C_2 e^{i(\beta x+\theta t)}$$

The velocity, V, of these waves is $V = \beta/\theta$ which is determined by substituting ϵ and e expressions into equations (2.34) and (2.35) as

$$\frac{PR - Q^2}{H^2} Z^2 - \left[\frac{PR}{H^2} + \frac{R\rho_{11} - 2Q\rho_{12}}{H(\rho_{11} + \rho_{22} + 2\rho_{12})}\right] Z + \left[\frac{\rho_{11}\rho_{22} - \rho_{12}^2}{(\rho_{11} + \rho_{22} + 2\rho_{12})^2}\right] = 0$$

$$V_1^2 = \frac{H}{(\rho_{11} + \rho_{22} + 2\rho_{12})Z_1}, \quad V_2^2 = \frac{H}{(\rho_{11} + \rho_{22} + 2\rho_{12})Z_2} \tag{2.36}$$

where $H = P + R + 2Q$. β and θ denote to wave number and circular frequency, respectively. Biot designates the high-velocity compression wave as the wave of the "first kind", and the low-velocity wave as the wave of the "second kind". However, we must note that in general, neither of these waves propagate as a wave in the fluid or in the solid matrix alone, both travel jointly in the matrix and the fluid. If coupling is weak (see the solution of Garg et al. (1974) in section 3.1) waves propagate in a form which closely resemble a wave in the solid matrix alone, and a wave in the fluid alone.

Biot (1956a) demonstrated the possible existence of an elastic wave, in which no relative motion between the fluid and solid phases occurs ($\epsilon = e$) and the dissipation due to fluid friction disappears. This is obtained when a "dynamic compatibility" condition is satisfied between the elastic and dynamic constants, i.e.

$$\frac{(A + 2N + Q)(\rho_{11} + 2\rho_{12} + \rho_2)}{(\rho_{11} + \rho_{12})(A + 2N + R + 2Q)} = \frac{(R + Q)(\rho_{11} + 2\rho_{12} + \rho_{22})}{(\rho_{22} + \rho_{12})(a + 2N + R + 2Q)} = 1$$

The propagation velocity of this wave is given by

$$V^2 = \frac{A + 2N + R + 2Q}{\rho_{11} + 2\rho_{12} + \rho_{22}}$$

As b increases (i.e., higher frequencies), $(\boldsymbol{u} - \boldsymbol{U})$ would decrease. This implies that both phases would eventually have the same velocity field. Then one might use a single velocity field and a single stress-strain relation. This would correspond to Biot's single elastic wave with no attenuation, satisfying the "compatibility condition".

If the dissipation is included, then the quadratic equation becomes

$$(Z - Z_1)(Z - Z_2) + iM(Z - 1) = 0 \tag{2.37}$$

where $i = (-1)^{1/2}$, and M is a frequency variable in terms of b, P, R, Q, ρ_{11}, ρ_{22}, ρ_{12}, and a characteristic frequency, f_c

$$f_c = \frac{b}{2\pi\rho_f n} \tag{2.38}$$

The characteristic frequency, f_c is proportional to the critical frequency, f_t [e.g., (2.31)] which defines the limit of Poiseuille flow. The proportionality depends on the detailed pore geometry. For pores represented by circular tubes,

$$\frac{f_t}{f_c} = 0.154$$

TABLE 2

Coefficient combinations for Figures 1–6

Case #	P/H	R/H	Q/H	ρ_{11}/ρ	ρ_{22}/ρ	ρ_{12}/ρ	Z_1	Z_2
1	0.610	0.305	0.043	0.500	0.500	0	0.812	1.674
2	0.610	0.305	0.043	0.666	0.333	0	0.984	1.203
3	0.610	0.305	0.043	0.800	0.200	0	0.650	1.339
4	0.610	0.305	0.043	0.650	0.650	−0.150	0.909	2.394
5	0.500	0.500	0	0.500	0.500	0	1.000	1.000
6	0.740	0.185	0.037	0.500	0.500	0	0.672	2.736

Where $H = P + R + 2Q$, $P = A + 2N$, $\rho = \rho_{11} + \rho_{22} + 2\rho_{12}$.

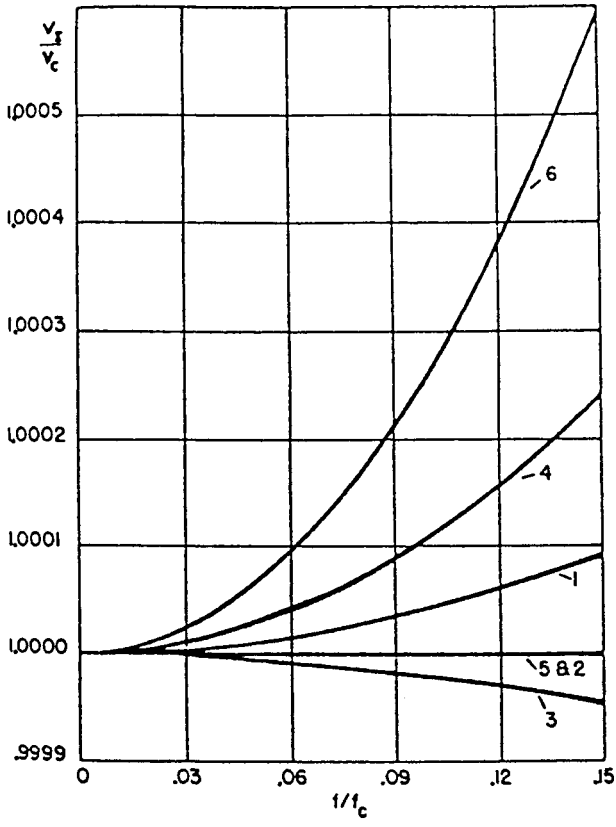


Fig. 1. Phase velocity v_1 of dilatational waves of the first kind (after Biot, 1956a).

At frequencies below characteristic frequency viscous forces, and above it inertial forces are significant with no coupling between the fluid and the solid (see Table 2).

The first root of equation (2.37) which reaches to unity at zero frequency corresponds to waves of the first kind while the second root corresponds to waves of the second kind. Biot (1956a) presents velocity expressions and their graphical representations in the range $0 < f/fc < 0.15$ (see Table 2 and Figs. 1–4).

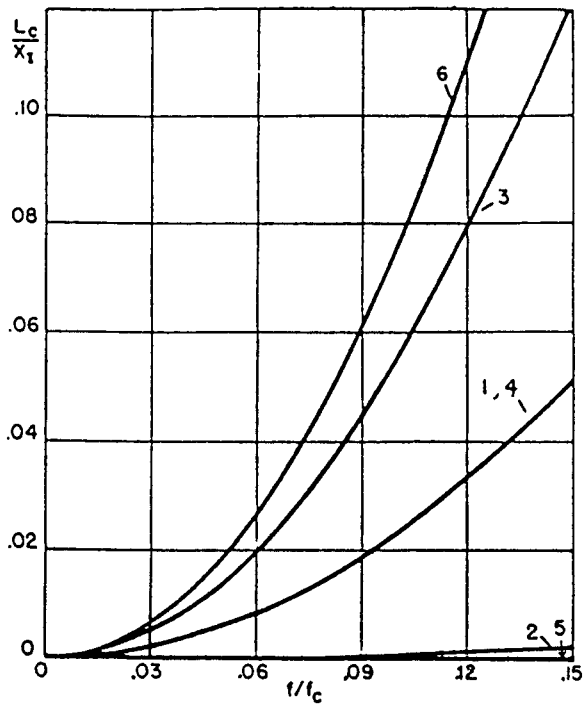


Fig. 2. Attenuation coefficient of dilatational waves of the first kind (after Biot, 1956a).

2.4. Derivation of rotational wave propagation equations

If we eliminate $[(A + N)\epsilon + Qe]$ between equations (2.25) and (2.26) by differentiating both sides of equation (2.25) with respect to y and of equation (2.26) with respect to x and subtract, we obtain an equation in terms of ω_z and Ω_z. Similar equations are obtained for ω_x, Ω_x, ω_y and Ω_y from equations (2.26) and (2.27) and equations (2.25) and (2.27), respectively. By adding these three equations, we obtain the equation for rotational waves for the solid phase

$$N\nabla^2\boldsymbol{\omega} = \frac{\partial^2}{\partial t^2}(\rho_{11}\boldsymbol{\omega} + \rho_{12}\boldsymbol{\Omega}) + b\frac{\partial}{\partial t}(\boldsymbol{\omega} - \boldsymbol{\Omega}) \tag{2.39}$$

If we perform same operations for equations (2.28)–(2.30) we obtain the equation for rotational waves for the fluid phase

$$\frac{\partial^2}{\partial t^2}(\rho_{12}\boldsymbol{\omega} + \rho_{22}\boldsymbol{\Omega}) - b\frac{\partial}{\partial t}(\boldsymbol{\omega} - \boldsymbol{\Omega}) = 0 \tag{2.40}$$

If we neglect the dissipation term in these equations, and eliminate $\boldsymbol{\Omega}$ from both, we obtain

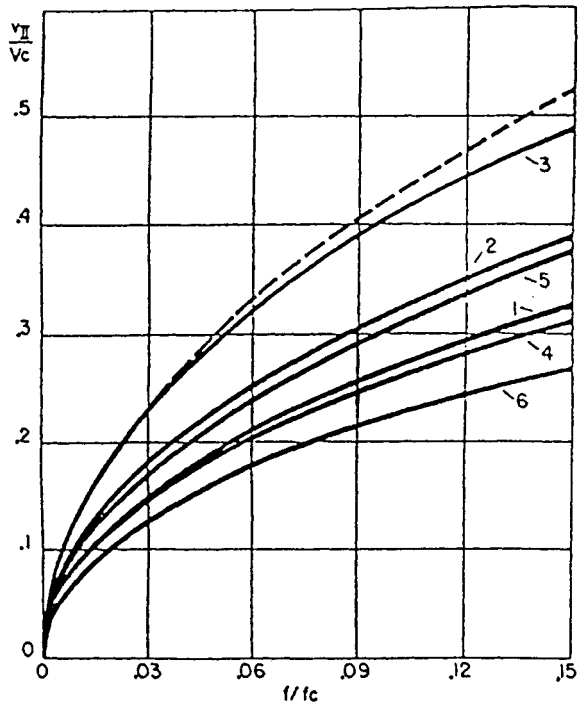


Fig. 3. Phase velocity v_{II} of dilatational waves of the second kind (after Biot, 1956a).

$$N\nabla^2\boldsymbol{\omega} = \rho_{11}\left[1 - \frac{\rho_{12}^2}{\rho_{11}\rho_{12}}\right]\frac{\partial^2\boldsymbol{\omega}}{\partial t^2} \tag{2.41}$$

Equation (2.41) shows that there is only one type of rotational wave with velocity

$$V_c^2 = \frac{N}{\rho_{11}\left[1 - \dfrac{\rho_{12}^2}{\rho_{11}\rho_{22}}\right]} \tag{2.42}$$

The rotation of the fluid, $\boldsymbol{\Omega}$ is calculated by

$$\boldsymbol{\Omega} = -\frac{\rho_{12}\boldsymbol{\omega}}{\rho_{22}} \tag{2.43}$$

Since $\rho_{12} < 0$, $\boldsymbol{\Omega}$ and $\boldsymbol{\omega}$ are both in the same direction. Biot noted that although there is no circulation in a frictionless fluid at microscopic level, the line integral of the volume flow (volume of fluid per unit time per unit cross sectional area of the medium) can be nonzero. Since there is no coupling of rotational (shear) wave of the fluid and the solid phase, the shear waves in a saturated porous medium signifies the shear waves in the solid matrix. However, there is a strong effect of coupling involved in both compression waves (see Section 2.3), i.e., the presence of water exerts an influence on the dilatational wave velocities, but produces a very minor effect on the rotational wave velocity.

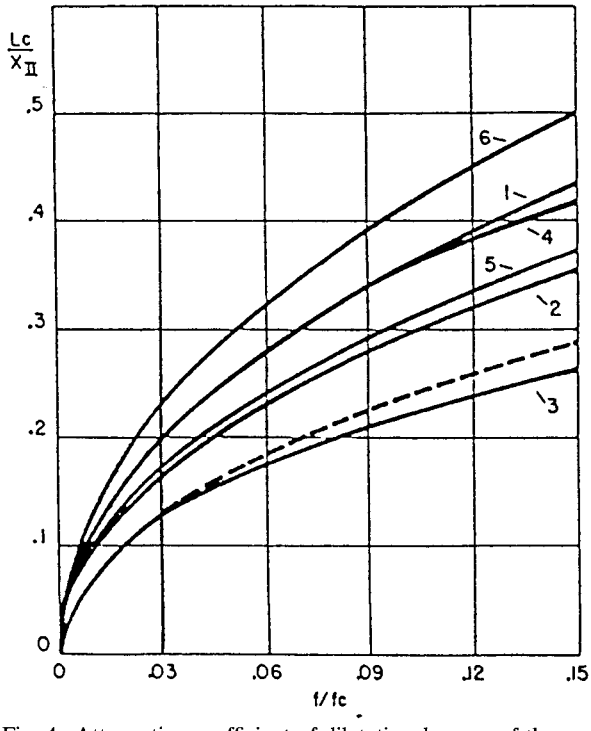


Fig. 4. Attenuation coefficient of dilatational waves of the second kind (after Biot, 1956a).

In seismology, compression waves known as primary or *P* waves arrive first at some distance away from an earthquake. These waves are predominantly longitudinal, and followed by secondary (rotational) waves or *S* waves corresponding to a transverse wave in which the direction of motion is normal to the direction of propagation. In an infinite isotropic saturated porous medium, there are only two types of waves (*P* and *S*) that can be propagated. However, in regions close to surface, a third type of wave arrives after the body waves. These are known as Rayleigh waves and have both vertical and horizontal components. The former dominates, and the amplitude diminishes exponentially with depth. Love waves which appear due to stratification of the earth arrive last. Rayleigh waves have been studied by Jones (1961), Levy and Sanchez-Palencia (1977), Deresiewicz (1962), and Foda and Mei (1983) in homogeneous porous media, and by Beskos et al. (1989b) in fissured porous media. Love waves were investigated by Deresiewicz (1961, 1964a, 1965) and Chattopadhyay and De (1983). Variable frequency interface waves known as Stoneley waves have been analyzed by Stoll (1980) and Pascal (1986).

2.5. Modifications of Biot's theory

In a companion paper, Biot (1956b) extended his theory to high-frequency range. In this case the coefficient b which is the ratio of the total friction force to the average relative fluid velocity for oscillatory motion is multiplied by frequency

correction factor, $F(\kappa)$ which represents the deviation from Poiseuille friction as the frequency increases. He proposed various expressions for $F(\kappa)$ by assuming certain pore structures (e.g., parallel tubes in the direction of flow). In general

$$F(\kappa) = F\left[\delta\left(\frac{f}{f_c}\right)^{1/2}\right] \tag{2.44}$$

where δ is the "structural factor" and f is the frequency of the wave and f_c is a characteristic frequency defined by equation (2.38). As noted by Biot (1962a) such a correction is also needed for mass coefficients, ρ_{11}, ρ_{12}, and ρ_{22} to take into account the deviation from the Poiseuille flow. A functional form of $F(\kappa)$ is given by Stoll (1977) (see equation [7.10]).

Later, Biot (1962a) modified his original theory slightly by employing the general principles of nonequilibrium thermodynamics and extended to an anisotropic medium with an elastic matrix. Modifications include a new definition of b as μ_f/k. The elastic coefficients N, A, Q, and R were replaced by new elastic constants, $[\lambda + M(\alpha - n)^2]$, $n(\alpha - n)M$, and n^2M where $M = Q$. For an incompressible fluid $\alpha = 1$. Equations (2.21) and (2.22) were replaced by

$$\nabla \cdot \tau = \frac{d}{dt}\left[\frac{\partial T}{\partial(\partial u/\partial t)}\right] \tag{2.45}$$

$$-\nabla p = \frac{d}{dt}\left[\frac{\partial T}{\partial(\partial w/\partial t)}\right] + \frac{\partial D}{\partial(\partial w/\partial t)} \tag{2.46}$$

where

$$w = n(U - u) \tag{2.47}$$

For a uniform porosity, Biot called $\zeta = -\nabla.w$ "fluid content". Equation (2.46) takes into account the relative motion of the fluid with respect to the solid matrix. This approach is more in line with relative Darcy's law concept used in a deforming porous medium. It is the specific discharge relative to the moving solid that is expressed by Darcy's law. Biot started with a thermodynamic system initially under equilibrium to apply the thermodynamics of irreversible processes. The initial state was defined as the one with no pressure gradients or gravity forces acting on the fluid phase. A disequilibrium force was applied to perturb the system. Biot expressed this disequilibrium force in a form conjugate to the flow coordinate. Then, he used Onsager's principle to express Darcy's law in a three-dimensional space.

Biot's modified equations can be stated as follows with constant parameters.

$$\mu\nabla^2 u + (N + \lambda)\nabla\epsilon - \alpha M\nabla\zeta = \frac{\partial^2}{\partial t^2}(\rho u + \rho_f w) \tag{2.48}$$

$$\nabla(\alpha M\epsilon - M\zeta) = \frac{\partial^2}{\partial t^2}(\rho_f u + mw) + \frac{\mu_f}{k}\frac{\partial w}{\partial t} \tag{2.49}$$

where $\rho = \rho_{11} + \rho_{22} + 2\rho_{12} = (1-n)\rho_s + \rho_f$. m is mass coefficient for an isotropic

medium and it is related to ρ_f. If we multiply equation (2.49) by n and subtract from equation (2.48), we obtain equations (2.25–2.30).

Note that the term within the parentheses on the left had side of equation (2.49) is p. Also, $\rho_{11} = \rho - 2\rho_f n + mn^2$, $\rho_{22} = mn^2$, and $\rho_{12} = \rho_f n - mn^2$.

Equations of dilatational wave propagation can be given in terms of solid dilatation, ϵ, and fluid content, ζ as

$$\nabla^2(H\epsilon - \alpha M\zeta) = \frac{\partial^2}{\partial t^2}(\rho\epsilon - \rho_f\zeta) \tag{2.50}$$

$$\nabla^2(-\alpha M\epsilon + M\zeta) = \frac{\partial^2}{\partial t^2}(-\rho_f\epsilon + m\zeta) + \frac{\mu_f}{k}\frac{\partial \zeta}{\partial t} \tag{2.51}$$

where $H = \lambda + 2N$. The coefficient m is given by

$$m = \delta\frac{\rho_f}{n} \tag{2.52}$$

where δ is the structural factor indicating the apparent increase in fluid inertia caused by the tortuosity of the pore space (Stoll and Bryan, 1970). For a random system of uniform pores, $\delta = 3$. Berryman (1980a,b) theoretically determined δ as

$$\delta = 1 - r_0\left[1 - \frac{1}{n}\right] \tag{2.53}$$

where r_0 is a coefficient $(1 > r_0 > 0)$. $(r_0\rho_f)$ is the induced mass caused by the oscillation of solid particles in the fluid. Berryman noted that r_0 should be determined from microscopic models. Berryman's (1981a) switch from macroscopic displacement parameters used by Biot to microscopic fluid displacement (and strain) parameters caused him to arrive at erroneous results in his analysis (Korringa, 1981). Later Berryman (1981b) has shown that his error arose due to misinterpretation of fluid content, ζ.

Hovem and Ingram (1979) used the real part of $F(\kappa)$ (see equation (7.10)) to multiply with μ_f in equation (2.51). Also, they defined m by

$$m = \frac{\rho_f}{n}\left[1 + \frac{n\mu_f F(\kappa)}{\rho_f k f}\right] \tag{2.54}$$

The term within the parentheses is the structural factor, δ. Hovem and Ingram showed that for low frequencies

$$\delta = 1 + \frac{R^*}{6} \tag{2.55}$$

where R^* is a coefficient taking into account the pore shape and the tortuosity of the pores (e.g., $R^* = 2$ for circular tubes, $R^* = 5$ for spherical grains). At high frequencies, coefficients N, λ, α, M, H, m, and μ_f are replaced by equivalent terms to introduce frequency dependance of these coefficients.

Biot (1962b) presented new features of the theory in more detail and generalized

it by introducing a viscodynamic operator. In addition, a more detailed analysis of viscoelastic and solid dissipation is given.

2.6. Elaboration on Biot's work by other researchers

A large number of researchers modified, revised, and solved Biot's formulation. In this section we will review some of these works.

Hardin (1965) described column test studies for evaluating the damping in sands and gave an example of the application of Biot's theory to a water-saturated body of quartz sand. He also presented the application of Kelvin–Voight model (viscous damping) and found that this model satisfactorily represented the behavior of sands in small-amplitude vibration tests. Hardin and Richart (1963) showed that the shear modulus of soils is essentially dependent on various variables such as average effective confining pressure, void ratio, and frequency among others. They showed that the grain size and grading had almost no effect on shear modulus, and the degree of saturation had a minor effect only at low pressures. Allen et al. (1980) conducted laboratory experiments to determine Biot relationships between pore pressure, time, degree of saturation, and compression wave velocity. The effect of saturation has been investigated in detail by Santos et al. (1990a) (Section 5).

Ishihara (1967) revised Biot's theory and obtained dilatational wave propagation equations with dissipation in terms of e and ζ [see equations (2.48) and (2.49)]. After eliminating ζ between two equations, they were reduced to a fourth-order differential equation in terms of wave velocity V. The material parameters of the resulting equation were expressed as functions of measurable quantities. By doing this, Ishihara redefined Biot coefficients in terms of basic compressibilities. This is similar to Geertsma and Smit's (1961) approach which redefined Biot's elastic constants in terms of compressibilities of the phases and porosity. Ishiara has shown that the wave of the first kind at low frequencies would travel without drainage of water, and its velocity can be calculated by using undrained tests. This also implies that there is no movement of water relative to the solid matrix and the first kind wave travel without causing pore volume change through the solid-water-system. At high frequencies (e.g., ultrasonic vibrations in soils) $f > f_c$, the first kind waves cause rapid fluctuations in pore pressure due to strain, so that there is not enough time for water to drain due to pressure gradients and the attenuation disappears. The stress condition is a drained condition. Furthermore, at higher frequencies the wavelength is short, and therefore the travel distance for water is also short. However, at low frequencies, although there is enough time to travel, the distance is much larger due to larger wave length, thus, the drainage does not progress. The lack of drainage is not because of the movement of the wave as erroneously assumed by some engineers (Ishihara, 1967). Waves due to earthquakes and explosions are usually waves of the first kind at low-frequencies.

The waves of the second kind usually correspond to consolidation deformation at low frequencies. In this kind of waves, wave energy is quickly lost due to large attenuations. Thus, the disturbance cannot travel as a wave but rather it propagates

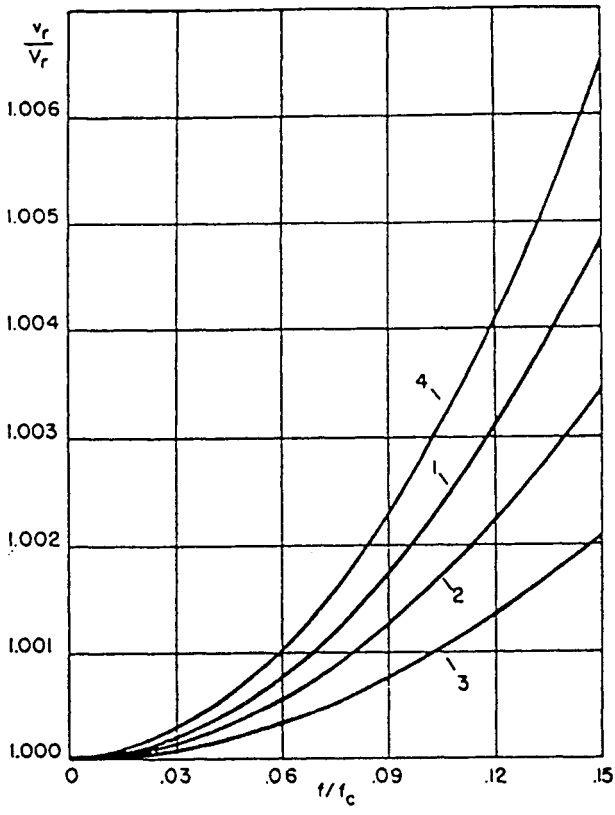


Fig. 5. Phase velocity v_r of rotational waves (after Biot, 1956a).

in a form similar to diffusion (i.e., consolidation) and the phase velocity is reduced to zero. The pore compressibility has predominant effect on the wave behavior. These waves can only progress where there is a change in pore volume. At higher frequencies, the disturbance travels as a wave under drained conditions similar to the first kind waves. Ishihara (1967) calculated the velocities of all four types of waves. The velocity of the wave of the first kind is the same as the one derived by Geerstma and Smit (1961).

A comparison of the first and second kind of waves and rotational waves can be illustrated in Figs. 1–6. The numbers in all figures refer to different combinations of Biot coefficients (see Table 2). In all cases $\rho_{12} = 0$ except at case 4 which gives the highest rotational (shear) wave velocity due to cross coupling of fluid and solid phase rotations, $\boldsymbol{\omega}$ and $\boldsymbol{\Omega}$. Number 5 refers to $Q = 0$, i.e., no cross coupling between the volume changes of the solid, e, and the fluid, e. Number 6 refers to a case with a large $(A + 2N)$ in comparison to other parameters, i.e., purely elastic dilatational waves, and no rotational waves. Case 6 also assumes equal fluid and solid masses $\rho_{11} = \rho_{22}$. Number 3 refers to a case with a large ρ_{11}, and $(A + 2N)$, i.e., low porosity medium. Since ρ_{11} represents the total effective mass of solid moving in the fluid, case 3 waves mostly travel in the fluid.

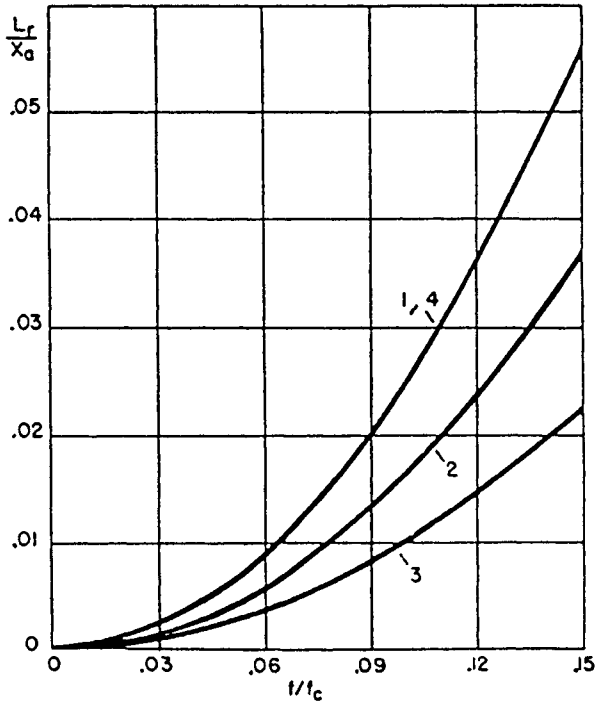


Fig. 6. Attenuation coefficient of rotational waves (after Biot, 1956a).

In summary, Biot found that the phase velocity of rotational waves increases slightly with frequency. The attenuation is proportional to the square of the frequency. The first kind dilatational waves are "true waves". The phase velocity changes with frequency depending on the elastic Biot coefficients. The attenuation is also proportional to the square of the frequency. When the dissipation due to fluid friction disappears, so does the attenuation of those waves. Dilatational waves of second kind attenuate highly. As noted earlier their propagation is diffusive and slower than that of the wave of the first kind.

In a series of ten papers, Deresiewicz and his coworkers (1960)–(1967) obtained solutions of various problems of wave reflection and refraction at the interfaces, and studied the effects of boundaries in a liquid saturated porous medium by using Biot's theory. Dunn (1986) investigated the effect of boundary conditions of a porous rock cylinder at low frequencies, and discovered the existence of an "artificial attenuation" caused by the open-pore boundary conditions. Lovera (1987) studied the boundary conditions for a fluid saturated porous solid. Wu et. al. (1990) and Santos et al. (1992) computed reflection and refraction coefficients for various interface conditions.

Sun et. al. (1993) studied harmonic wave propagation through an anisotropic, periodically layered porous medium by using Biot's theory to describe the constitutive relations. They presented results for a layered, fluid saturated, fabric material. Sharma and Gogna (1991b) employed Biot's theory to investigate the propagation of plane harmonic seismic waves in a transversely isotropic porous medium. They

concluded that anisotropy has significant effect on the velocities of body waves. They also presented frequency equation for surface waves.

Albert (1993) compared propagation characteristic of water filled and air filled materials in 10 Hz–100 kHz band. Analogous to an elastic medium, Deresiewicz (1962) and Jones (1961) independently showed the existence of surface waves in saturated porous media. They examined surface waves by considering the coupled transverse wave and one of the compressional waves. Later Tajuddin (1984) presented a study of Rayleigh waves considering all three types of body waves. Tajuddin (1984) extended the study to convex cylindrical pervious and impervious surfaces and found that phase velocity is higher for the impervious surface than for the pervious surface. Foda and Mei (1983) proposed a boundary layer theory for Rayleigh waves. Weng and Yew (1990) examined the behavior of leaky Rayleigh waves generated by a line source. Philippacopoulos (1987) investigated Rayleigh waves in partially saturated layered half spaces. However, we should note that his model consist of a saturated porous half space and a dry elastic layer. Hence, his results are not applicable to unsaturated porous media. Feng and Johnson (1983) numerically searched for the velocities of various surface modes at an interface between a fluid half space and a half space of a fluid saturated porous medium. Attenborough and Chen (1990) modified Biot's theory and obtained dispersion equations for a rigid porous half space, for a poroelastic half space, and for a layered poroelastic half space. They predicted the possibility of two additional types of surface waves at an air/air-filled poroelastic interface.

Love waves which appear due to stratification of the earth were studied by Deresiewicz (1961, 1964a, 1965) and Chattopadhyay and De (1983). Sharma and Gogna (1991a) obtained the dispersion equation for Love waves in a slow elastic layer overlying a saturated porous half space. Tajuddin (1991) investigated dynamic interaction of a saturated porous medium and an elastic half space.

2.7. Applicability of Biot's theory

Existence, uniqueness, and regularity of the solution of Biot's equations were presented by Santos (1986). The applicability of the Biot theory has been investigated by Hovem and Ingram (1979), Hovem (1980), and Ogushwitz (1985) for various types of porous media with a wide range of porosity. Ogushwitz (1985) determined that the Biot's theory predicts compressional and shear wave speeds within 3% for a porous sintered glass saturated with water (Plona, 1980), 1% for Berea Sandstone, 5% for Bedford limestone saturated with brine, 8% for water saturated Bedford limestone, 25 to 30% for water saturated Massilon sandstone. The last one could be an indication of water sensitivity of sandstone which might reduce the shear modules of the solid matrix due to release of colloidal particles. All these materials represent low-porosity porous media. For suspensions which represent the other end of porosity spectrum, the Biot model agrees well with the experimental data. For porous medium with mid-range porosity values, the Biot's theory matched within 3% for Ottawa sandpack, 10% for glass bead pack. Ogushwitz's (1985) work is similar to that of Hovem (1980) except that a theoretically derived structure factor was employed instead of an experimental value. Stoll and

Bryan (1970) and Stoll (1974, 1977) demonstrated the applicability of the Biot theory to marine sediments. Berryman (1980a) gave supporting theoretical evidence to Plona's (1980) experimental data for the dilational waves of the second kind with the identification of coefficients given by Geertsma (1957), Biot and Willis (1957), and Stoll (1979). Plona and Johnson (1984) also provided experimental data verifying Biot's theory. Salin and Schon (1981) provided data for ultrasonic pulse propagation in packed glass beads. Holland and Brunson (1988) examined the Biot's theory as implemented by Stoll for accuracy for a variety of marine sediments. Out of 13 inputs needed, 10 of them were derived empirically and the other 3 were measured. Comparison of predicted and measured values of compressional velocity, attenuation and shear velocity showed excellent agreement. Beebe et al. (1982) compared the predictions of compressional attenuation to estimate velocities and showed good agreement between the predictions and measurements. Berryman (1986a,b) notes that Biot's theory was not successful at predicting the magnitude of the attenuation coefficient in the low-frequency (1–100 Hz) range (Murphy, 1982, 1984; Mochizuki, 1982). Berryman (1986b, 1988) attributed this to inhomogeneities in fluid permeability of porous geologic materials and showed that local flow effects dominate the wave attenuation. Johnson (1982) applied Biot's theory to acoustic wave propagation in snow, and obtained data for the 200–800 Hz frequency range.

As a criticism of Biot's formulation, Rice and Cleary (1976) noted that dead-end pores in a porous medium may be sealed off from fully interconnected pores. These dead end pores would not contribute to momentum transfer between the solid and the fluid. Instead, the "closed-off" pores would induce an apparent viscoelastic effect. Levy (1979) observed the effect of unconnected fluid in a similar way. We must point out that this can be avoided by using the "effective porosity" concept and modifying the stress-strain relations for any possible viscoelastic behavior due to dead-end pores. At this point we should note that pore crushing was not taken into account in Biot's theory. In dry porous materials, such a phenomenon can occur and must be included in the formulation (e.g., Carroll and Holt, 1972; Butcher et al., 1974).

Burridge and Keller (1981) provided theoretical justification for Biot's equations by considering the microstructure of porous media. They assumed the scale of the pores to be small in comparison to the macroscopic scale, so that the "two-space method of homogenization" can be used to obtain macroscopic equations. When a dimensionless fluid viscosity term is small, the resulting equations reduce to that of Biot. When the dimensionless viscosity is equal to unity, the equation of a viscoelastic solid is obtained. Pride et. al. (1992) rederived Biot's constitutive relations and obtained the same expressions for the coefficients by using the local volume averaging technique.

3. Solutions of Biot's formulation

A number of researchers in various fields solved Biot's formulation either numerically or analytically. In this section, we will review some of these solutions and point out some interesting results.

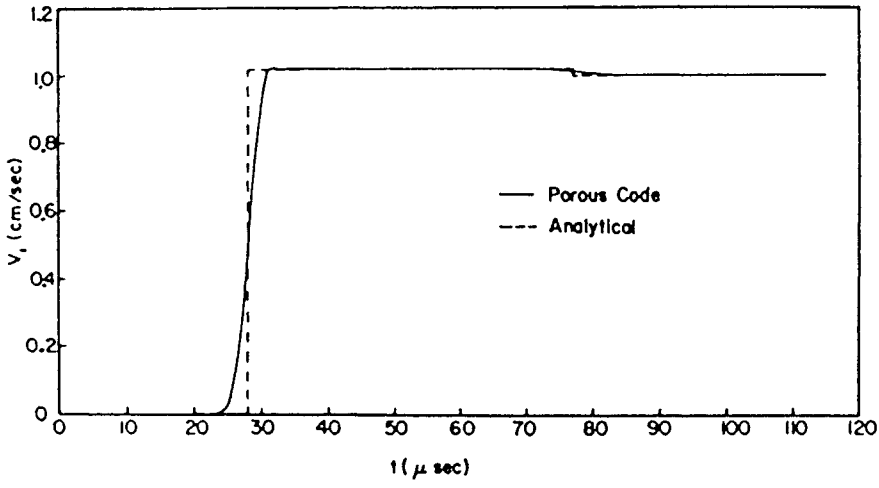


Fig. 7. Solid particle velocity history at 10 cm with $b = 0.219 \times 10^2$ g/cm^3 sec (after Garg et al., 1974).

3.1. Analytical solutions of Biot's formulation

Among various solutions obtained within last two decades, (e.g., Wijesinghe and Kingsbury's (1979, 1980) solution with no coupling, i.e., $b = 0$, for a harmonic loading of saturated porous layer or Cleary's (1977) solution without inertia, or Verruijt's (1982) solution for cyclic sea wave generated pore pressures), Garg and his coworkers' analytical solution (Garg et al., 1974) is an important one. Garg et al. solved Biot's equations for dilatational waves in terms of displacements u_x and U_x [equations (2.25) and (2.28)] for a one-dimensional column. They assumed $\rho_{12} = 0$. The column is initially at rest and is subjected to a time-dependent disturbance at time zero at the free boundary, $x = 0$. They assumed solutions of the form

$$V_j = A_j e^{i(\beta x - \theta t)}, \qquad j = 1, 2 \tag{3.1}$$

V_j is the velocity. Subscripts 1 and 2 refer to solid and fluid, respectively. β, θ, and A_j denote the complex wave number, the circular frequency and wave amplitude, respectively. The phase velocity is obtained by dividing θ by the real part of β. The imaginary part of β is an attenuation coefficient. Garg et al. took the Laplace transform of equations (2.25), (2.28), and (3.1) and obtained characteristic equation for two extreme cases of weak and viscous coupling, i.e., for small values of b (weak coupling), and for $b \to \infty$ (strong viscous coupling). They obtained the exact inverse Laplace transformation after making some simplifying assumptions. Hong et al. (1988) has compared Garg et al.'s solutions with solutions obtained by numerical inverses of the Laplace transformed solutions with no approximations. They found that the difference is insignificant. Garg et al. stated that strong viscous coupling causes the two wave fronts to merge to a single front and the porous medium behaves like a single medium with bulk properties. They presented finite difference solutions for the general case with no assumptions on viscous coupling.

Figures 7 and 8 show propagation of two fronts when the viscous coupling is

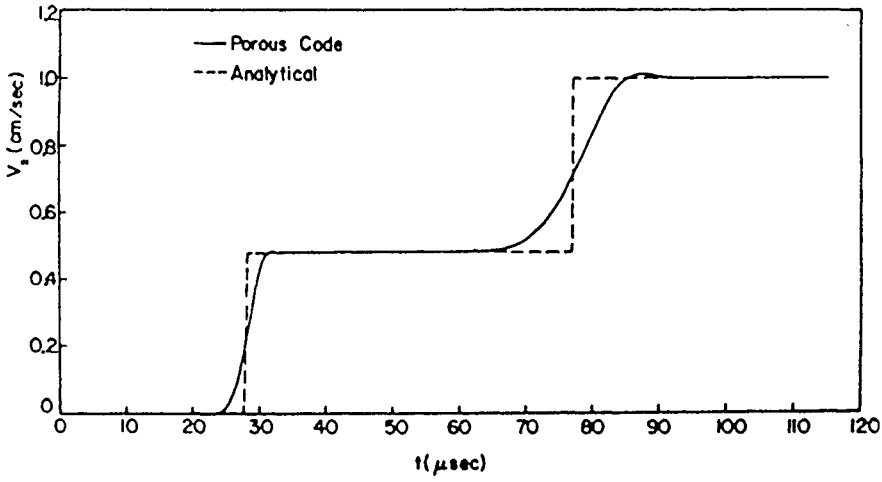


Fig. 8. Fluid velocity history at 10 cm with $b = 0.219 \times 10^2$ g/gm^3 sec (after Garg et al., 1974).

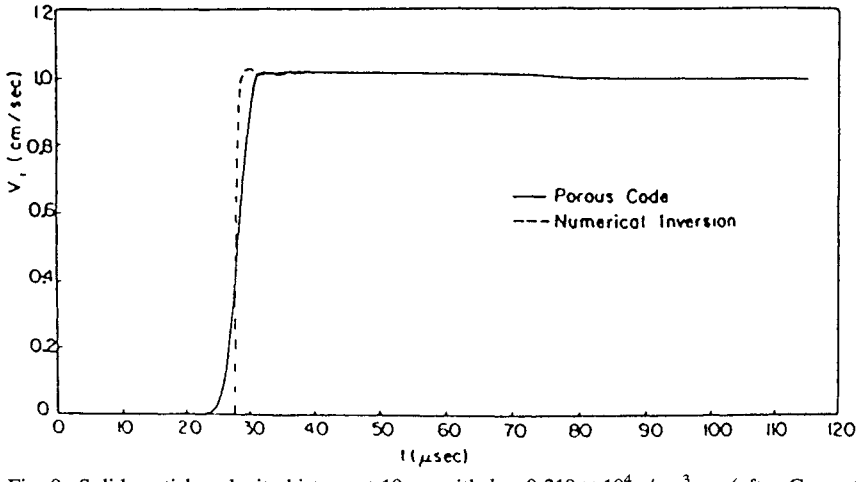


Fig. 9. Solid particle velocity history at 10 cm with $b = 0.219 \times 10^4$ g/cm^3 sec (after Garg et al., 1974).

weak ($b = 21.9$ g/cm^3 sec.). For moderate viscous coupling ($b = 2190$ g/cm^3 sec.), we also observe two waves. However as seen in Fig. 10 wave velocity in the fluid phase gradually increases between the two fronts. This gradual increase is due to viscous momentum transfer between the solid and fluid phases. Figure 11 shows that in the far field (distant to the boundary at $x = 0$), the wave of second kind disappears and becomes a standing wave with time. Garg et al. noted that oscillations in Fig. 11 at the head of the pulse are due to numerical approximations. For strong viscous coupling ($b = 2190 \times 10^4$ g/cm^3 sec.), two wave fronts merge into one (Fig. 12). We should note that for in all figures the numerical solutions cause the wave front(s) to smear. Yew and Jogi (1976) also obtained a solution by Laplace transformation similar to Garg et al's. (1974). Jones (1969) studied the propagation of a pulse wave in porous media.

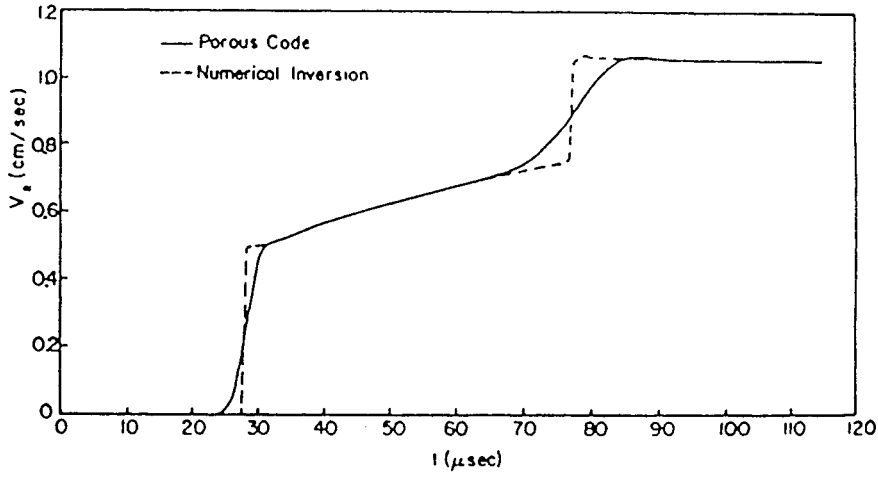


Fig. 10. Fluid velocity history at 10 cm with $b = 0.219 \times 10^4$ g/cm^3 sec (after Garg et al., 1974).

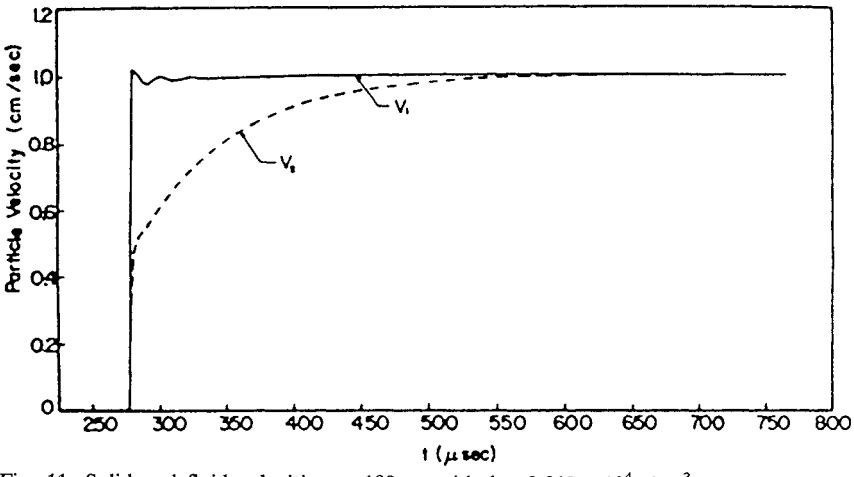


Fig. 11. Solid and fluid velocities at 100 cm with $b = 0.219 \times 10^4$ g/cm^3 sec, obtained by numerical inversion (after Garg et al., 1974).

Burridge and Vargas (1979) obtained analytical solutions for P and S waves due to an instantaneous point body force acting in a uniform whole space. Biot's equations [equations (2.48) and (2.49)] have been solved by introducing four scalar potentials to decouple the system of equations, and transforming them to symmetric hyperbolic systems to be solved by Laplace transformation. It has been found that P and S waves have the shape of a Gaussian instead of a sharp pulse shape. Norris (1985) derived the time harmonic Green function of Biot's equations for a point load in an infinite saturated porous medium. He obtained the solutions for rotational waves as well as compressional waves. As Burridge and Vargas (1979) did, Norris observed that Gaussian shaped pulses broaden with time and distance. The integral representation of displacement fields and pore pressure was

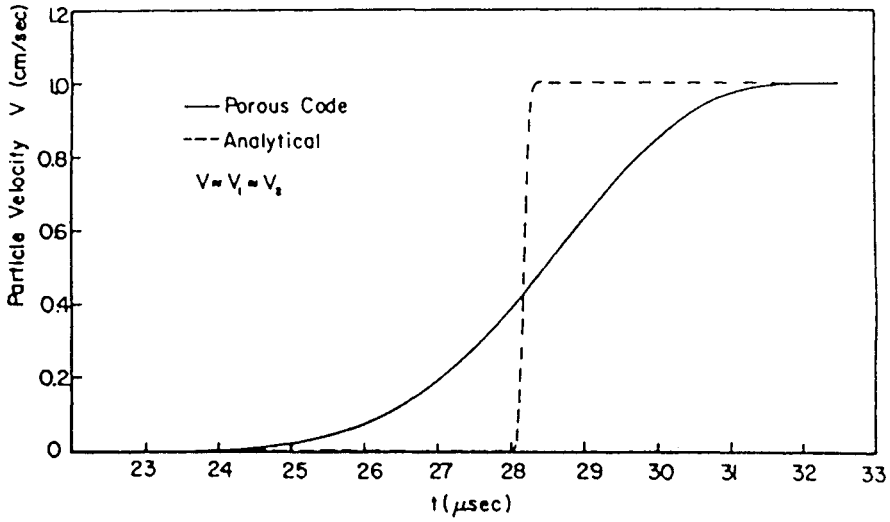


Fig. 12. Velocity histories at 10 cm with $b = 0.219 \times 10^8$ g/cm^3 sec (after Garg et al., 1974).

also suggested by Predeleanu (1984). Boutin et al. (1987) presented a new analytical formulation of Green's function. Their solution is valid at any frequency range. Parra (1991) developed an analytical solution for seismic wave propagation associated with a point source in a stratified saturated porous medium.

Based on the construction of synthetic seismograms, Boutin et al. concluded that the signal wave form is strongly dependent on the permeability value, thus raising the possibility of determining the permeability values from seismic explorations (see Section 6 for details). Bonnet (1987) provided an harmonic solution by an analogy with a thermoelasticity problem.

3.2. Numerical solutions

During the last fifteen years, the numerical solution of Biot's wave propagation equations on large scale computers have gained popularity due to ability to solve a large number of equations in a multi-dimensional space. Among many other studies, a finite element solution by Ghaboussi and Wilson (1972) appears to be one of the early studies. Ghaboussi and Wilson's formulation which is a generalization of Sandhu and Pister's (1970) technique, used the displacement of the solid, $\boldsymbol{u}$, and relative fluid displacement $(\boldsymbol{U} - \boldsymbol{u})$ as two field variables [equations (2.23) and (2.24)]. Ghaboussi and Wilson calculated the fluid pressure, p, from the volumetric changes of the solid and fluid through stress-strain relations. Differential equations were transformed by using the "Galerkin process of weighted residuals" to functional forms which are discretized by the finite element method. Step loading applied to half-space of saturated elastic porous solid was given as an example. Galerkin solution was also employed by Santos et al. (1986).

Later, Sandhu et al. (1989) presented a mixed variational formulation taking the soil displacement, relative fluid displacement, and fluid pressure as three field variables, as a special case of general variational principle of Sandhu and Hong

(1987). By taking pore pressure as a variable, a continuous solution for pressure has been obtained. Numerical solutions were compared with Garg et al.'s (1974) analytical solution for a special case.

Hiremath et al. (1988), Morland et al. (1987, 1988) solved Biot's equations for a one-dimensional case by employing the Laplace transformation and numerical inversion. These results were compared with a finite element solution. It has been concluded that numerical solutions compare favorably with the Laplace solutions for weak as well as strong viscous coupling.

Zienkiewicz and his co-workers obtained various finite element solutions for simplified Biot theory under transient conditions. Among various assumptions made, drained or undrained behavior depending on the permeability of the porous medium and rapidity of loading are the dominating factors to characterize a particular problem. For example, an earthquake which can be modeled as an impulse loading can be investigated as a completely undrained behavior if the permeability of the soil is not high. Similar assumptions have been also made by other researchers to study the effect of water waves on sea beds (Mei and Foda, 1981 in Section 7.2). Nur and Booker (1972) suggested that due to the agreement between computed rates of attenuation and observed rates of aftershock activity, aftershocks can be caused by the flow of groundwater due to changes in pore water pressures induced by large shallow earthquakes.

In a series of papers, Zienkiewicz et al. (1980, 1982a,c) solved the following simplified equations after making further assumptions for a numerical solution

$$\nabla\cdot\sigma + \rho g \nabla z = \rho \frac{\partial^2 \boldsymbol{u}}{\partial t^2} + \rho_f \frac{\partial^2 \boldsymbol{w}}{\partial t^2} \tag{3.2}$$

$$-\nabla p + \rho_f g \nabla z = \rho_f \frac{\partial^2 \boldsymbol{u}}{\partial t^2} + \frac{\rho_f}{n}\frac{\partial^2 \boldsymbol{w}}{\partial t^2} + \frac{\rho_f g}{k'}\frac{\partial \boldsymbol{w}}{\partial t} \tag{3.3}$$

$$\nabla \cdot \frac{\partial w}{\partial t} = -\frac{\partial \epsilon}{\partial t} - \frac{1-n}{K_s}\frac{\partial p}{\partial t} + \frac{1}{3K_s}\frac{\partial \sigma'}{\partial t} - \frac{n}{K_f}\frac{\partial p}{\partial t} \tag{3.4}$$

Equations (3.2)–(3.4) are the momentum balance equations for the porous medium, and fluid phase and mass balance equation for the fluid, respectively. σ is the total stress tensor. σ' is the effective stress tensor. K_s and K_f are the bulk modules of the solid grains and the fluid, respectively. The first term on the right hand side of equation (3.4) incorporates the solid matrix compressibility. The second and the third terms represent the rate of pore volume increase due to the increase in pore fluid pressure and effective stress change, respectively. The last term represents the compressibility of pore fluid. In equation (3.3), the term k' is the hydraulic conductivity. ρ is the "total density". For a correct interpretation, equations (3.2) and (3.3) should be compared with equations (2.48) and (2.49).

Zienkiewicz and Bettess (1982c) consider a case in which the acceleration in the fluid is neglected. The formulation for this "medium speed phenomena" is referred to as the $u-p$ formulation. If all acceleration terms are neglected, it corresponds to "very slow phenomena" which is the classical consolidation problem in soil mechanics. "Very rapid phenomena" occurs when the permeability

becomes very small or w, $\partial w/\partial t$, $\partial^2 w/\partial t^2$ never reach to significant values. This is the "undrained behavior" which is also known as the "penalty type" formulation. The total system can be expressed by omitting the momentum balance equation for fluid (equation (3.3)), thus u becomes the primary variable. "Drained behavior" is another extreme case which occurs when the permeability (or hydraulic conductivity) reaches to infinity. p can be calculated independently, and then u is calculated using the known values of p. This extreme case does not occur ever with dynamic effects and it is only possible when all transient behavior ceases.

For one dimensional case (a soil layer with thickness, L) i.e., $\sigma = \sigma' - p$, $e = \partial u/\partial z$, and $\sigma' = D\epsilon$ and neglecting the grain compressibility, two dilatational wave equations in terms of u and U are obtained (similar to equations (2.25) and (2.28) with different mass coefficients). For the periodic case (i.e., $\exp(-i\omega t)$ where ω is the angular frequency), these equations become

$$\left[D + \frac{K_f}{n}\right]\frac{d^2\bar{u}}{dz^2} + \frac{K_f}{\rho n}\frac{d^2\bar{w}}{dz^2} = -\omega^2\bar{u} - \omega^2\frac{\rho_f}{\rho}\bar{w} \tag{3.5}$$

$$\left[\frac{d^2\bar{u}}{dz^2} + \frac{d^2\bar{w}}{dz^2}\right]\frac{K_f}{\rho_f} = -\omega^2 n\bar{u} - \omega^2\bar{w} + \frac{i\omega n g}{k'}\bar{w} \tag{3.6}$$

where overbar denotes transformed variables in the Fourier space.

The coefficient of the first term of equation (3.5) is the square of compression wave velocity $V_c = K_f/\rho_f$ is the speed of sound in water. Results of Zienkiewicz et al. (1980) have shown that in the space of two dimensionless parameters π_1 and π_2 which are defined by

$$\pi_1 = \frac{k'V_c^2}{g(\rho_f/\rho)\omega L^2}, \qquad \pi_2 = \frac{\omega^2 L^2}{V_c^2} \tag{3.7}$$

There are three zones. In zone one, the propagation is slow so that the consolidation problem (C) would solve the problem. In zone II, the $u - p$ approximation (Z) would be satisfactory. Zone III includes extremely rapid motions which can be described by full Biot theory (B) as given by equations (3.2) through (3.4). Figure 13 shows the summary of basic conclusions. They noted the existence of small zones which are drained even when most of the medium is undrained. This "boundary layer" concept was studied by Mei and Foda (1981, 1982) (see Section 7.2). Zienkiewicz et al. (1982b) applied $u - p$ model to analyze the earthquake problem by neglecting the coupling acceleration term. They employed various plastic constitutive equations to represent the soil deformation.

Later Zienkiewicz and Shiomi (1984) added the convective fluid acceleration term $[\rho_f(\partial w/\partial t \nabla.\partial w/\partial t)/n]$ to the right hand side of equation (3.3). Similar adjustment was also introduced into equation (3.2).

Prevost (1982, 1984) solved the coupled equations of mass and momentum balance by using a finite element technique. Time integration is handled by an implicit/explicit predictor/multicorrector scheme. The method has been applied to one- and two-dimensional initial value problems. Later, Prevost (1985) allowed

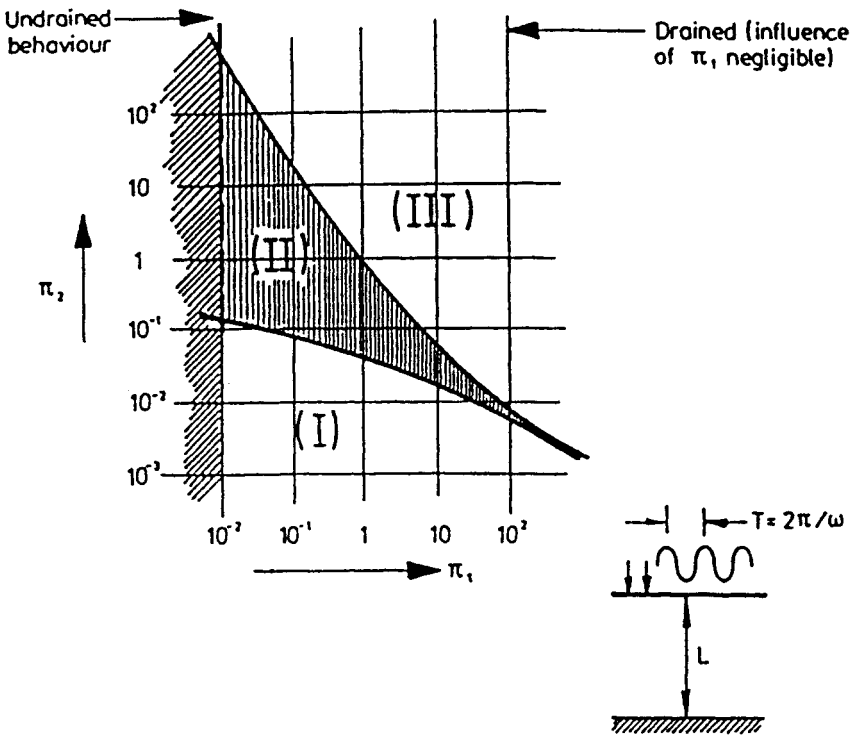


Fig. 13. Zones of applicability of various assumptions (after Zienkiewicz et al. (1980)). Zone 1: $B = Z = C$. Slow phenomena ($\partial^2 U/\partial t^2$ and $\partial^2 u/\partial t^2$ can be neglected). Zone 2: $B = Z \neq C$. Moderate speed ($\partial^2 U/\partial t^2$ can be neglected. Zone 3: $B \neq Z \neq C$. Fast phenomena ($\partial^2 U/\partial t^2$ can not be neglected), only full Biot equation [Equations (3.2) through (3.4)] valid.

the compressibility of fluid by treating the fluid contributions to the equations of momentum balance implicitly. This approach removed the restriction on the time step size. Halpern and Christiano (1986a,b) applied Biot's formulation to analyze various foundation problems.

Hassanzadeh (1991) presented an acoustic modelling method that involves numerical simulation of two-dimensional low frequency transient wave propagation. The method is based on explicit finite difference formulation of Biot's system of equations. Zhu and Mcmechan (1991) developed a two-dimensional finite difference method allowing investigation of spatial variations in porosity, permeability and fluid viscosity.

Bougacha and Tassoulas (1991) used the finite element method to analyze dam-reservoir-sediment-foundation interaction. They modelled the sediment by using Biot's formulation for saturated porous medium. Bougacha et al. (1993a) developed a spatially semi-discrete finite element technique for layered, saturated porous medium. Bougacha et al. (1993b) applied the formulation to calculate dynamic stiffness of strip and circular foundations. Chang et al. (1991) presented a singular integral solution technique for solving dynamic problems. They also

showed an analogy between thermoelasticity and dynamic poroelasticity in the frequency domain.

3.3. Solutions by the method of characteristics

The method of characteristics have been used widely to solve hyperbolic partial differential equations. By using the method characteristics, partial differential equations are transformed into time-dependent ordinary differential equations. These canonical equations are solved along the characteristic lines.

Streeter et al. (1974) applied the characteristics method to study the wave propagation in a layered soil due to earthquakes. Streeter et al. presented equation (2.23) in a form

$$\frac{\partial \tau_{xz}}{\partial z} - \rho \frac{\partial^2 u_x}{\partial t^2} = \frac{\partial \tau_{xz}}{\partial z} - \rho \frac{\partial v_x}{\partial t} = 0 \tag{3.8}$$

for a one-dimensional (vertical) soil column. ρ is the density of the soil. The displacement in the vertical direction is zero. Shearing stresses are set up by horizontal motions imposed at the base of the column (i.e., earthquake) and they travel in the vertical direction.

The soil is modeled as a viscoelastic solid with a constitutive equation

$$\tau_{xz} = G \frac{\partial u_x}{\partial z} + \mu_s \frac{\partial^2 u_x}{\partial z \partial t} \tag{3.9}$$

where G is the shear modulus and μ_s is the viscosity of soil. Differentiation of equation (3.9) gives

$$\frac{\partial \tau_{xz}}{\partial t} = G \frac{\partial v_x}{\partial z} + \mu_s \frac{\partial^2 v_x}{\partial z \partial t} \tag{3.10}$$

If the time derivative in equation (3.10) is approximated by finite difference equation, and then combined with equation (3.8) after multiplying with an unknown multiplier θ, to give

$$\left[\theta \frac{\partial \tau_{xz}}{\partial z} + \frac{\partial \tau_{xz}}{\partial t}\right] - \theta\rho\left[\frac{\partial v_x}{\partial z}\left(g + \frac{\mu_s}{\Delta t}\right)\frac{1}{\theta\rho} + \frac{\partial v_x}{\partial t}\right] + \frac{\mu_s}{\Delta t}\left(\frac{\partial v_x}{\partial z}\right)_c = 0 \tag{3.11}$$

where the subscript c represents the value determined at point c on the $z - t$ space. Partial derivatives in equation (3.11) are expressed in terms of total derivatives as

$$\frac{d\tau_{xz}}{dt} - \rho V_s \frac{dv_x}{dt} + \frac{\mu_s}{\Delta t}\left(\frac{\partial v_x}{\partial z}\right) = 0 \tag{3.12}$$

when

$$\frac{dz}{dt} = \theta = \frac{1}{\theta\rho}\left(G + \frac{\mu_s}{\Delta t}\right) \tag{3.13}$$

Equation (3.13) is solved for

$$\frac{dz}{dt} = \theta = \pm\left(\frac{G}{\rho} + \frac{\mu_s}{\rho\Delta t}\right)^{1/2} = \pm V_s \tag{3.14}$$

where V_s is the shear velocity. Equations (3.12) and (3.14) give four ordinary equations to be solved, replacing two partial differential equations [equations (3.8) and (3.10)]. One-dimensional pressure wave propagation is similar to shear wave propagation except that the velocity of the compression wave is given by

$$V_p = \pm\left(\frac{K_s}{\rho} + \frac{\mu_s}{\rho\Delta t}\right)^{1/2} \tag{3.15}$$

where K_s is the bulk modulus of the soil.

Propagation of pore pressure and water flux are analyzed by simultaneous solution of momentum and mass balance equations

$$K\frac{\partial h}{\partial z} + \frac{Kr^2}{g}\frac{\partial V_z}{\partial t} + V_z = 0 \tag{3.16}$$

$$\frac{\partial h}{\partial t} + \frac{V_p^2}{g}\frac{\partial V_z}{\partial z} - \frac{V_p^2}{g}\frac{1}{1+e}\frac{\Delta e}{\Delta t} = 0 \tag{3.17}$$

where e is the void ratio ($n/(1-n)$). Streeter et al. (1974) present various examples including the liquefaction of an earth dam. r is an inertia multiplier.

Van der Grinten et al. (1985) solved the conservation of mass and momentum equations for a saturated porous medium

$$\frac{\partial V_x}{\partial x} + \frac{1-n}{n}\frac{\partial v_x}{\partial x} = -\frac{1}{K_f}\frac{\partial p}{\partial x} \tag{3.18}$$

$$\frac{\partial v_x}{\partial x} = \frac{1}{K_s}\frac{\partial \sigma'}{\partial t} \tag{3.19}$$

$$[n\rho_f + (\alpha^{**} - 1)n\rho_f]\frac{\partial V_x}{\partial t} - (\alpha^{**} - 1)n\rho_f\frac{\partial v_x}{\partial t} = -n\frac{\partial p}{\partial x} + n\rho_f g + n^2\mu_f a'(v_x - V_x) \tag{3.20}$$

$$[(1-n)\rho_s + (\alpha^{**} - 1)n\rho_f]\frac{\partial v_x}{\partial t} - (\alpha^{**} - 1)n\rho_f\frac{\partial V_x}{\partial t} = -\frac{\partial \sigma'}{\partial x} - (1-n)\frac{\partial p}{\partial x} + (1-n)\rho_s g - n^2\mu_f a'(v_x - V_x) \tag{3.21}$$

where ρ_s is the density of solid. The term $(\alpha^{**} - 1)n\rho_f$ represents the mass coupling between the fluid and the solid matrix. The added mass parameter α^{**}

depends on the structure of the porous matrix (Johnson et al., 1982). Equations (3.18)–(3.21) were first presented by de Josselin de Jong (1956). Equations (3.20) and (3.21) can directly be obtained from Biot's equations [equations (2.23) and (2.24)]. Equation (3.18) is the mass balance equation for the fluid after some mathematical manipulations (Bear and Corapcioglu, 1981) and equation (3.19) is the elastic stress-strain relation for the solid matrix. By applying the method of characteristics, equations (3.18)–(3.21) are obtained in characteristic form

$$\left(\frac{\partial}{\partial t} + V_{\mathrm{p}} \frac{\partial}{\partial x}\right)(A\sigma' + Bp + Cv_x + DV_x) = E(v_x - V_x) \tag{3.22}$$

V_{p} is obtained from

$$FV_{\mathrm{p}}^4 + HV_{\mathrm{p}}^2 + 1 = 0 \tag{3.23}$$

where A, B, C, D, E, F and H are parameters in terms of equation coefficients. When the pore fluid is air, the compressibility of the matrix is much smaller than that of air. Therefore, the porous medium can be considered rigid. Since interactive forces are much larger than inertial forces, equations are decoupled. The momentum equation will reduce to Forcheimer equation by adding a term proportional to the velocity squared (see equation (6.11)). Then the governing equations reduce to

$$\frac{\partial \rho_{\mathrm{a}}}{\partial t} + \frac{\partial(\rho_{\mathrm{a}} V_{\mathrm{a}})}{\partial x} = 0 \tag{3.24}$$

$$\frac{\partial p_{\mathrm{a}}}{\partial x} = -na'\mu_{\mathrm{f}} V_{\mathrm{a}} - n^2 b' \rho_{\mathrm{a}} V_{\mathrm{a}} |V_{\mathrm{a}}| \tag{3.25}$$

where V_{a} is the air velocity, p_{a} is the air pressure, ρ_{a} is the density of the air, and a' and b' are Forcheimer coefficients. For an isothermal compression

$$\frac{d\rho_{\mathrm{a}}}{\rho_{\mathrm{a}}} = \frac{dp_{\mathrm{a}}}{p_{\mathrm{a}}} \tag{3.26}$$

when the solid matrix is filled by air instead of water, the wave is strongly damped, and the permeability is not frequency dependent. As concluded by other studies, when the pore fluid is water, the permeability is strongly dependent on frequency due to viscosity. In a dry porous medium, the dilatational wave of the second kind which is strongly attenuated is the only wave observed in the pores. Furthermore, it is determined that transient permeability is approximately one-third of the stationary value. The contribution of added mass which is neglected by most researchers (e.g., Garg et al., 1974; Mei and Foda, 1981) was found to be significant. Later, van der Grinten et al., (1987a) provided new experimental evidence by measuring pore pressures and strain simultaneously. They concluded that the behavior of the wave of the second kind is affected by the boundary conditions at the top of the solid matrix. The influence of boundary conditions is also discussed by Geertsma and Smit (1961) and Zolotarjew and Nikolaevskij (1965). Van der

Grinten et al. (1987a) used approximations of frequency correction factor [see equations (2.44) and (7.10)] for low and high frequencies, respectively.

$$F(\kappa) = 1 + i\left(\frac{\kappa^2}{24}\right) \quad \text{as} \quad \kappa \to 0 \tag{3.27}$$

$$F(\kappa) = [(1+i)/4\sqrt{2}]\kappa \quad \text{as} \quad \kappa \to \infty \tag{3.28}$$

where κ is the transient Reynolds number defined as

$$\kappa = \mathrm{Re} = R_p \sqrt{\frac{\omega}{\upsilon_f}} \tag{3.29}$$

where R_p is the radius of cylinders of the cylindrical duct model representing the porous medium. The reader should compare the definition of Reynold's number given here with equation (6.10) given by Geertsma (1974). Later, van der Grinten et al. (1987b), extended their analysis to partially saturated medium by varying the bulk modulus of fluid. The reader is referred to Section 5 for a review of this type of treatment to model unsaturated porous medium.

4. Liquefaction of soils

When loose saturated sands are subjected to vibrations, their porosity decreases. If the pore water pressure increases due to lack of drainage, the effective stress vanishes when the pore pressure reaches the overburden pressure (total stress) with continuous vibration. This can be stated by the effective stress principle

$$\sigma = \sigma' - pI \tag{4.1a}$$

where σ is the overburden pressure, σ' is the effective stress, I is the unit tensor, and p is the pore pressure. At this point, the sand looses its shear strength and behaves like a liquid. When this happens, the soil cannot support the weight of the structure resting on it. Structures sink into the soil as observed in Niigata (Japan) earthquake of 1964. This phenomenon is known as liquefaction in soil mechanics (Scott, 1986). Liquefaction can be observed even several hours after the initial shock. Since this is a problem of great practical importance, quite a number of studies tried to predict the liquefaction potential of soils.

In liquefaction studies, the soil is represented by one or more layers with homogeneous properties resting on a solid rock base. The earthquake excitation is at the base and resulting shear waves propagate vertically upward through the soil column. Shear stresses induced by the earthquake are approximated by cyclic horizontal shear stresses applied at the base. Since, liquefaction is caused by pore pressure increase, the pore pressure dissipation during and after a period of cyclic loading, needs to be calculated. A similar phenomenon can occur in sea-bed deposits of sand subjected to storm-wave loadings. The concept of pore pressure generation under cyclic loading condition was first introduced by Seed and his coworkers in various publications (e.g., DeAlba et al., 1976; Martin et al., 1975;

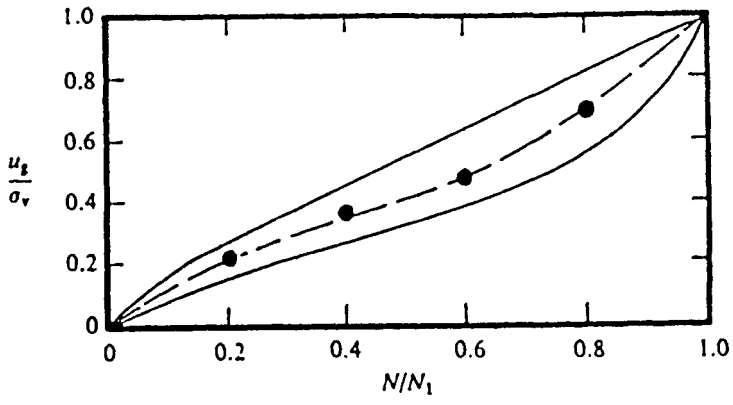


Fig. 14. Rate of pore water pressure buildup in cyclic simple shear test (after Seed and Brooker, 1977).

Rahman et al., 1977; Seed et al., 1976; Seed and Rahman, 1978) and outlined in Seed and Idriss (1982). Such an approach is known as "effective stress method." Seed and his coworkers have found that pore pressure generation in a cyclic undrained simple shear test falls within a narrow range as shown in Fig. 14. The average curve can be approximated by

$$r_p=\frac{p_g}{\sigma'_o}=\frac{2}{\pi}\sin^{-1}\left(\frac{N}{N_l}\right)^{1/2\theta} \tag{4.1}$$

where N is the number of stress cycles applied, N_M is the number of stress cycles needed for initial liquefaction, and $j=0.7$. σ'_o is the initial vertical effective stress. p_g is the generated pore pressure. Then, the rate of pore pressure generation is obtained from equation (4.1) as

$$\frac{\partial p_g}{\partial t}=\frac{\partial p_g}{\partial N}\frac{\partial N}{\partial t}=\frac{\sigma'_o}{\theta\pi T_D}\left(\frac{N_{eq}}{N_L}\right)\frac{1}{\sin^{2\theta-1}(\pi r_p/2)\cos(\pi r_p/2)} \tag{4.2}$$

Note that in equation (4.2), irregular cyclic loading is converted to an equivalent number of uniform stress cycles, N_{eq} occurring in a time span T_D by $\partial N/\partial t=N_{eq}/T_D$. Then, combined pore pressure generation and dissipation is obtained from the solution of

$$\frac{\partial p}{\partial t}=\frac{C_v}{r}\frac{\partial}{\partial r}\left(r\frac{\partial p}{\partial r}\right)+C_v\frac{\partial^2 p}{\partial z^2}+\frac{\partial p_g}{\partial t} \tag{4.3}$$

where C_v is the consolidation coefficient and r and z are the radial and vertical coordinates. An example given by Seed et al., 1976 (Fig. 15a) shows that the sand layer at a depth of 15 ft liquefies after about 21 seconds of shaking during the earthquake. Liquefied condition propagates to 40 ft at 40 seconds (Fig. 15a). After earthquake stops at 50 seconds, pore pressures below 15 ft dissipate. However, pore pressures above 15 ft continue to build up and after about 12 min., the water in the top foot would flow from the ground (Fig. 15b). Seed et al., noted that

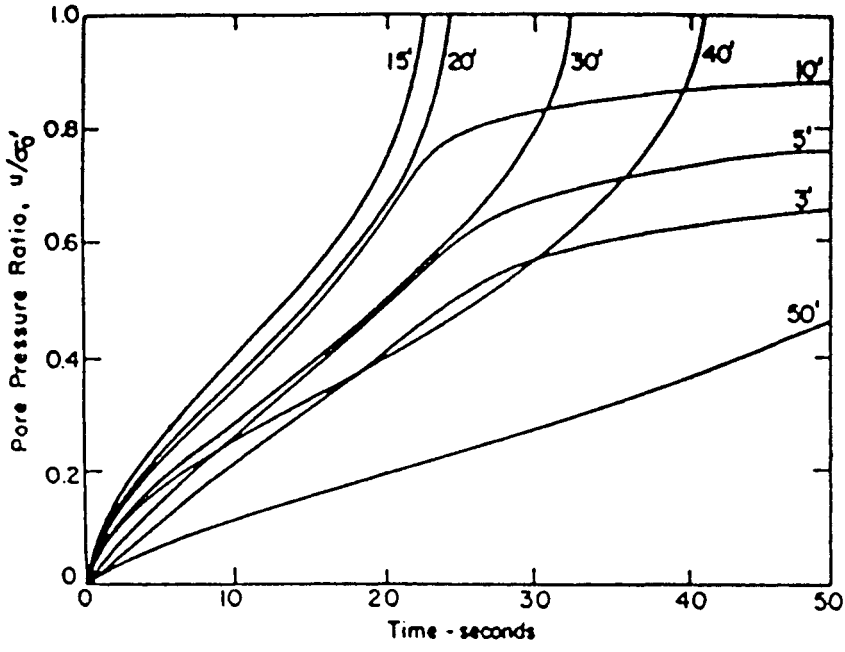


Fig. 15A. Computed development of pore water pressures during earthquake shaking (after Seed et al., 1976).

lower water table would decrease the liquefaction potential. Seed and Idriss (1982) noted that a more fundamental approach by Finn et al. (1977) shows only small differences in results.

Finn et al. (1976, 1977) developed a non-linear method of analysis of liquefaction in which the momentum balance equations was coupled by the pore water pressure generation model given by equation (4.3). Later, a more general approach by solving Biot equations were presented by Ishihara and Towhata (1982). Finn et al.'s (1976) stress-strain relations were used by Mansouri et al. (1983) to study the liquefaction potential of an earth dam.

Streeter et al. (1974) presented a characteristics method which treated responses of the pore water and the solid matrix separately as uncoupled problems. Pore pressures were introduced by defining volume changes. The details of Streeter et al.'s technique are given in Section 3.4 (equations (3.8)–(3.17)). Later Liou et al. (1977) developed a liquefaction analysis of saturated sands. They studied the propagation of shear and pressure induced by the earthquake motion at the base of the sand deposit. Liou et al.'s shear wave submodel is similar to that of Streeter et al.'s except the coefficient of viscosity in equation (3.9). Pressure wave submodel consists of momentum balance equation for the solid

$$\frac{\partial \sigma}{\partial t} + \rho g \nabla z = \rho \frac{\partial v}{\partial t} + n\rho_f \frac{\partial V_r}{\partial t} \tag{4.4}$$

momentum balance equation for the pore water,

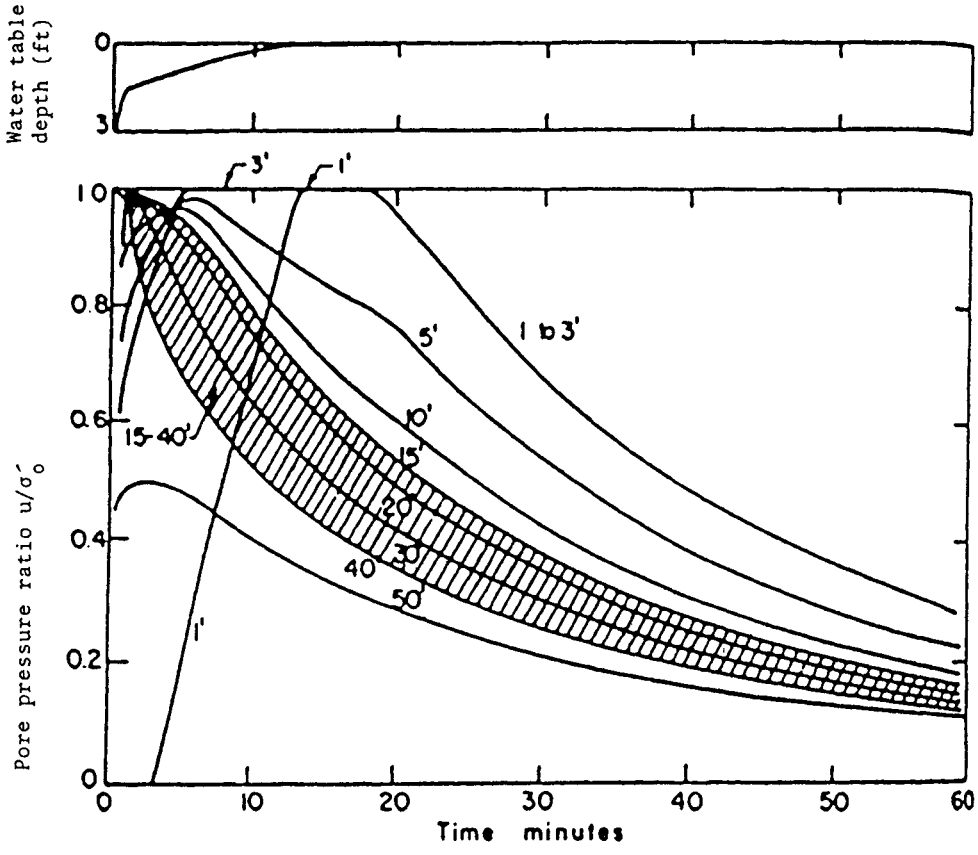


Fig. 15B. Computed variation of pore water pressures in 60-minute period following earthquake (after Seed et al., 1976).

$$\frac{\partial S}{\partial t} + n\rho_f g \nabla z - n\rho_f \frac{\partial v}{\partial t} - n^2 \rho_f \frac{g}{K} V_r = n\rho_f \frac{\partial V_r}{\partial t} \tag{4.5}$$

mass balance equation of pore water

$$\frac{\partial S}{\partial t} = \frac{1}{C_w}\frac{\partial v}{\partial z} + \frac{1}{C_w}\frac{\partial V_r}{\partial z} \tag{4.6}$$

and time derivative of the stress-strain relation

$$\frac{\partial S}{\partial t} = \left(\frac{1}{C_c} + \frac{1}{nC_w}\right)\frac{\partial V_r}{\partial z} + \frac{1}{C_w}\frac{\partial V_r}{\partial z} - \frac{1}{C_c}\left(\sigma - \frac{S}{n}\right)\frac{\partial C_c}{\partial t} \tag{4.7}$$

where

$$S = -np, \qquad \sigma = -\sigma' + \frac{S}{n}, \qquad V_r = \frac{\partial(U-u)}{\partial t}$$

C_w is the compressibility of water, and $(1/C_c)$ is the secant modulus of the soil skeleton. These four equations form a hyperbolic system to be solved by the method of characteristics. The first two equations (equations (4.4) and (4.5)) are similar to equations (2.48) and (2.49). The coupled solutions of shear wave and pressure wave propagation have been presented by Liou et al. to simulate Niigate earthquake.

Endochronic modeling of two phase porous medium was developed by Bazant and Krizek (1975, 1976) after the work of Valanis (1971). Bazant and Krizek combined the endochronic constitutive equations with governing equations to analyze the liquefaction phenomenon. Bazant et al. (1982) and Valanis and Read (1982) reviewed endochronic models for soils. This theory which is different from the conventional stress-strain relations are separated into a relation for the volumetric components, and another one for the deviatoric components. Inelastic behavior which is produced by the deviatoric strain increments is described by the endochronic law. A similar approach was also employed by Sawicki and Morland (1985) for dry and saturated sand by adding elastic and non-linear irreversible deformations.

Hiremath and Sandhu (1984) and Morland et al. (1987) applied their numerical solution techniques to study liquefaction problems. They noted that, in general, for long wave-length problems with strong coupling like liquefaction, the relative motion of fluid and solid which maximized the pore pressure has been neglected. Sandhu and his coworkers' numerical solution are discussed in Section 3.2

Ghaboussi and Dikmen (1978) treated horizontal layers of saturated sand as fluid saturated porous media in their analysis of seismic response and evaluation of liquefaction potential. Coupled conservation of momentum equations were solved with nonlinear soil properties such as yield, failure, and cyclic effects. Later, Ghaboussi and Dikmen (1981) extended their analysis to three dimensional earthquake base acceleration. Zienkiewicz et al. (1978, 1982) presented a numerical solution with non-associative plasticity models. A review of these works are given by Zienkiewicz (1982). A similar approach with an elastoplastic solid matrix was also taken by Vardoulakis (1987).

5. Wave propagation in unsaturated porous media

In contrast to saturated porous media, wave propagation in unsaturated porous media received little attention from researchers. The general trend is to extend the Biot formulation developed for saturated medium to unsaturated medium by replacing model parameters with the ones modified for air-water mixture. Modification is generally done by volume averaging the density and the compressibility coefficients. For example, Spooner's (1971) equation of motion [equation (6.1)] contained a correction term to incorporate the degree of saturation in the inertia term. As an alternative, as noted in Section 7.1, others increased the volume compressibility of water due to trapped air in the porous medium (e.g., van der Grinten et al. 1987b). In addition to Verruijt's (1969) formula, we might

also note Bishop and Eldin's (1950) expression for the compressibility of pore air-water mixture, C_w, as given by Ghaboussi and Kim (1984)

$$C_w = (1 - S_{wo} - H_c S_{wo}) \frac{p_{ao}}{p^2} \tag{5.1a}$$

where S_{wo} is the initial degree of saturation. H_c is the solubility coefficient, p_{ao} is the initial pore air pressure, and p is the pore water pressure. Schurman (1966) considered the surface tension between the air and the water ($= 0.5\ (p_a - p)R_a$) which is neglected in equation (5.1a). R_a is the radius of the air bubble, and p_a is the air pressure. Domenico (1974) defined the effective compressibility of the fluid, β, as

$$\beta = S_w \beta_g + S_w \beta_w \tag{5.1b}$$

where β_g and β_w are the compressibility coefficient of the gas and the water, respectively. Composite density ρ is obtained by adding equations (5.3) through (5.5). A similar approach was taken by Mochizuki (1982) by mass averaged parameters. Bedford and Stern (1983) developed a mixture theory for porous media saturated with a bubbly liquid which is equivalent to the Biot theory except that the inertial effect of bubble oscillations is included.

Brandt (1960) reported that in a water saturated quartz sand column, compressional wave velocity decreases linearly with the decreasing degree of water saturation, and levels off at 50% saturation. Gassman (1951) employed the "distinct element" technique by representing the medium by packed elastic spheres (see Section 1). Brutsaert (1964) employed Lagrangian formulation similar to Biot's (1956a) approach to obtain a mathematical model. By taking $\rho_{12} = 0$, the kinetic energy, T of an unsaturated porous medium was expressed by

$$2T = \rho'_{11}\left[\left(\frac{\partial u_x}{\partial t}\right)^2 + \left(\frac{\partial u_y}{\partial t}\right)^2 + \left(\frac{\partial u_z}{\partial t}\right)^2\right] + \rho'_{22}\left[\left(\frac{\partial u_x^g}{\partial t}\right)^2 + \left(\frac{\partial u_y^g}{\partial t}\right)^2 + \left(\frac{\partial u_z^g}{\partial t}\right)^2\right]$$
$$+ \rho'_{33}\left[\left(\frac{\partial U_x}{\partial t}\right)^2 + \left(\frac{\partial U_y}{\partial t}\right)^2 + \left(\frac{\partial U_z}{\partial t}\right)^2\right] \tag{5.2}$$

where u^g is the gas displacement. Mass coefficients ρ'_{11}, ρ'_{22}, ρ'_{33} are given by

$$\rho'_{11} = \rho_{11} = (1 - n)\rho_s \tag{5.3}$$

$$\rho'_{22} = \rho_g(1 - S_w)n \tag{5.4}$$

$$\rho'_{33} = \rho_f S_w n \tag{5.5}$$

where ρ_g is the density of gas. Equations (2.8) through (2.13) and (2.16) were generalized to include the dilatation of the gas, and an equation similar to equation (2.16) was proposed for the stress in the gas. The dissipation function given in equation (2.18) was modified to include the relative velocities between the gas and the solid, and the gas and the liquid phases. After this extension of Biot's theory, Brutsaert and Luthin (1964) provided experimental data which agrees with Brandt's (1960) conclusions. Also, Allen et al. (1980) provided laboratory data to

evaluate the relationships between degree of saturation, pore pressure, time, and compression wave velocity.

Garg and Nayfeh (1986) developed a mixture theory by neglecting inertial coupling ($\rho_{12} = 0$). Momentum exchange between phases was incorporated by including the relative velocities between the gas and the solid, and the gas and the liquid phases in the momentum balance equations of respective phases. The coefficient b was replaced by

$$b_{sf} = n^2(1 - S_w)^2\mu_f/(k_o k_{rw}) \tag{5.6}$$

$$b_{sg} = n^2 s_w^2 \mu_g/(k_o k_{rg}) \tag{5.7}$$

$$b_{fg} = 0 \tag{5.8}$$

where k_o is the intrinsic permeability of the medium, k_{rw} and k_{ro} are relative permeabilities for the water and the gas phase, respectively. μ_f and μ_g are respective viscosities. Equation (5.8) implies that there is no momentum transfer between two fluid phases due to negligible contact area between the water and the gas phase. Solubility of gas in water is incorporated in the model. Garg and Nayfeh's work is limited to low frequencies. At high frequencies b_{sf}, b_{sg}, and b_{fg} may not be constant, and furthermore, these constants and the capillary pressure $(p_a - p_w)$ should be taken as functions of frequency. Garg and Nayfeh assume linear elastic constitutive relations for all phases. Their solution for dilatational waves show three modes of propagation for weak viscous coupling. Three fronts merge into one with strong viscous coupling.

Kansa (1987, 1988, 1989) and Kansa et al. (1987) solved governing equations similar to that of Garg and Nayfeh (1986) by using an explicit Lagrangian code. They concluded that due to its small inertia, the gas phase response is basically uncoupled from solid and liquid phases. Gas phase also moves out of pores ("drained behavior") very readily in comparison to water which has a much larger inertia.

Based on their previous works (e.g., Berryman and Thigpen, 1985a,b,c,d), Berryman et al. (1988) presented a mixture theory for dilatational wave propagation. Their kinetic energy expression included terms for microstructural kinetic energy due to the dynamics of local expansion and contraction of individual phases and virtual mass due to relative flow of each phase in addition to usual kinetic energy terms given by equation (5.2). Drag coefficients were identical to that of Garg and Nayfeh (1986) (see equations (5.6) through (5.8)). However, Berryman et al. included the virtual mass effect in their formulation. They have shown that by neglecting effects due to changes in capillary pressure, governing equations reduce to equations similar to that of Biot for full saturation. Equation parameters incorporated the presence of the gas phase. This conclusion is analogous to the concept of replacing the coefficients of Biot equations with the ones modified for air-water mixture. Such an approach was reviewed earlier. Berryman et al.'s (1988) model can be expressed by

$$\mu^*\nabla^2\boldsymbol{u} + (H - \mu^*)\nabla\epsilon - c\nabla\xi + \omega^2(\rho_{uu}\boldsymbol{u} + \rho_{uw}\boldsymbol{w}) = 0 \tag{5.9}$$

$$C\nabla e - M\nabla\xi + \omega^2(\rho_{wu}\boldsymbol{u} + \rho_{ww}\boldsymbol{w}) = 0 \tag{5.10}$$

where μ^*, H, C, and M are parameters similar to that of Biot's. However, the inertial coefficients ρ_{uu}, ρ_{uw}, and ρ_{ww}, are much more complicated due to presence of gas phase. ξ is the divergence of total fluid (water plus gas) displacements. In derivation of equations (5.9) and (5.10), Berryman et al. introduced a Fourier time dependence of the form $\exp(-i\omega t)$ (ω = angular frequency) into the formulation. A comparison of equations (5.9) and (5.10) with equations (2.48) and (2.49) would demonstrate the analogy. Equation variables are identical in both sets of equations. Auriault et al. (1989) followed a similar approach by treating porous medium as a periodic media. Auriault et al. did not neglect the capillary pressures in their theoretical formulation. Lebaigue et al. (1987) applied this theory to analyze ultrasonic waves in a sheet of unsaturated wet paper. Ross et al. (1989) measured stress wave attenuation using the split Hopkinson pressure bar.

Santos et al. (1990b) presented a theory describing the wave propagation in a porous medium saturated by a mixture of two immiscible, viscous, compressible fluids by employing the principle of virtual complementary work. It was assumed that the two-phase flow in porous media obeys Darcy's law. Santos et al. (1990b) found that there are five possible body waves. Three of them correspond to compressional waves, and the other two, of identical speed, are associated with shear modes. This is a generalization of the single-phase Biot theory. The third kind dilatational wave is associated with the relative motion between two fluid phases. However, we must note that Darcy's law was not generalized to account for the relative motion of different phase fluids. The relative motion between the fluids might create a momentum exchange which in turn introduces additional head loss. Yuster (1951) tried to explain this by the remark that there is a shear transmitted at the two-phase interface which would actually entail such a phenomenon. A further discussion of the "Yuster effect" has been given by Scott and Rose (1953).

Santos et al. (1990b) stated the conservation of mass equation for oil and water phases as

$$\frac{\partial(n\rho_o S_o)}{\partial t} + \nabla \cdot \left(\rho_o K \frac{k_{ro}}{\mu_o} \nabla p_o \right) \tag{5.11}$$

$$\frac{\partial(n\rho_w S_w)}{\partial t} + \nabla \cdot \left(\rho_w K \frac{k_{rw}}{\mu_w} \nabla p_w \right) \tag{5.12}$$

where S_o and S_w denote the oil and water saturations, respectively. Note that

$$S_o + S_w = 1 \tag{5.13}$$

Oil and water densities are denoted by ρ_o and ρ_w, respectively. K is the intrinsic permeability. k_{ro} and k_{rw} are the relative permeability functions for the oil and water, respectively. They are expressed in terms of S_w. μ_o and μ_w denote the dynamic viscosities of the oil and water phases, respectively. p_o and p_w are the incremental oil and water pressures, respectively. Similar to Biot's work (see Section 2.2), the Lagrangian formulation of the equations of motion was stated by employing the kinetic energy density and dissipation energy density function

definitions. Then, using the assumption of time independence for the saturation, a linearization technique, and the assumption of constant coefficients, Santos et al. (1990b) obtained the wave propagation equations

$$\rho\frac{\partial^2 u_s}{\partial t^2}+\rho_o\bar{S}_o\frac{\partial^2 u^o}{\partial t^2}+\rho_w\bar{S}_w\frac{\partial^2 u^w}{\partial t^2}=N\nabla^2 u^s+\nabla[(\lambda+N)\epsilon+B_1e^o+B_2e^w] \tag{5.14}$$

$$\rho_o\bar{S}_o\frac{\partial^2 u^s}{\partial t^2}+\bar{g}_1\frac{\partial^2 u^o}{\partial t^2}+\bar{g}_3\frac{\partial^2 u^w}{\partial t^2}+(\bar{S}_o)^2\frac{\mu_o}{Kk_{ro}}\frac{\partial u^o}{\partial t}=\nabla[B_1\epsilon+M_1e^o+M_3e^w] \tag{5.15}$$

$$\rho_w\bar{S}_w\frac{\partial^2 u^s}{\partial t^2}+\bar{g}_3\frac{\partial^2 u^o}{\partial t^2}+\bar{g}_2\frac{\partial^2 u^w}{\partial t^2}+(\bar{S}_w)^2\frac{\mu_w}{Kk_{rw}}\frac{\partial u^w}{\partial t}=\nabla[B_2\epsilon+M_3e^o+M_2e^w] \tag{5.16}$$

where u^s, u^o, and u^w denote solid, oil, and water phase displacements, respectively. An overbar refers to a reference value. ϵ, e^o, and e^w denote volumetric dilatations of the solid, oil, and water phases respectively. ρ is defined by

$$\rho=(1-n)\rho_s+n(\rho_oS_o+\rho_wS_w) \tag{5.17}$$

where ρ_s is the solid density. λ, N, g_c, B_1, B_2, g_1, g_2, M_1, M_2, and M_3 are all material parameters. In formulating equations (5.14)–(5.16), Santos et al. ignored the friction effects between the oil and water phases in the dissipation energy function. We must note that instead of using the Lagrangian formulation to obtain the wave propagation equation, we can state the momentum conservation equations as shown by Baer and Corapcioglu (1989) (see Section 9). Santos et al. (1990b) obtained the equations governing the propagation of dilatational and rotational waves by applying the divergence and curl operators to equations (5.14)–(5.16), respectively.

In a companion paper, following the presentation of a method to determine the elastic constants for an isotropic porous medium saturated by a two-phase fluid, Santos et al. (1990a) calculated the phase velocities and attenuations for Berea sandstone saturated by mixtures of oil and water, and gas and water as functions of both frequency and saturation of the non-wetting phase. As shown in Figures 16, 17, and 19, Santos et al. observed that for low saturations, the phase velocities of first and second kind compressional waves, and shear waves approach to the corresponding water-saturated (i.e., $S_w = 1$) porous medium. As seen in Figure 17, the wave in gas-water mixture saturated medium is slower due to smaller relative motion of lower density fluids. The third kind dilatational wave which is directly associated with the presence of capillary pressures, increases with the saturation of non-wetting phase (oil or gas) (see Fig. 18. The phase velocity of the third kind wave is much slower than others and reaches to zero velocity at low saturations. Similar to the second kind waves, the third kind dilatational waves are diffusion-type waves. As seen in Fig. 19, the shear wave phase velocity increases almost linearly with the non-wetting phase saturation for both mixtures. Since, the bulk density of the gas-water mixture saturated porous medium is

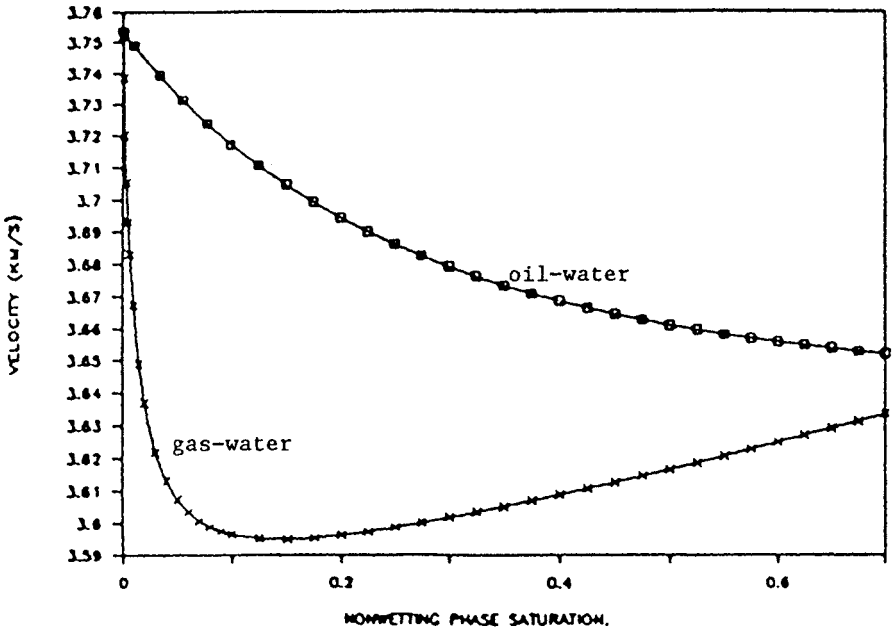


Fig. 16. Phase velocity of dilatational waves of the first kind (after Santos et al., 1990a).

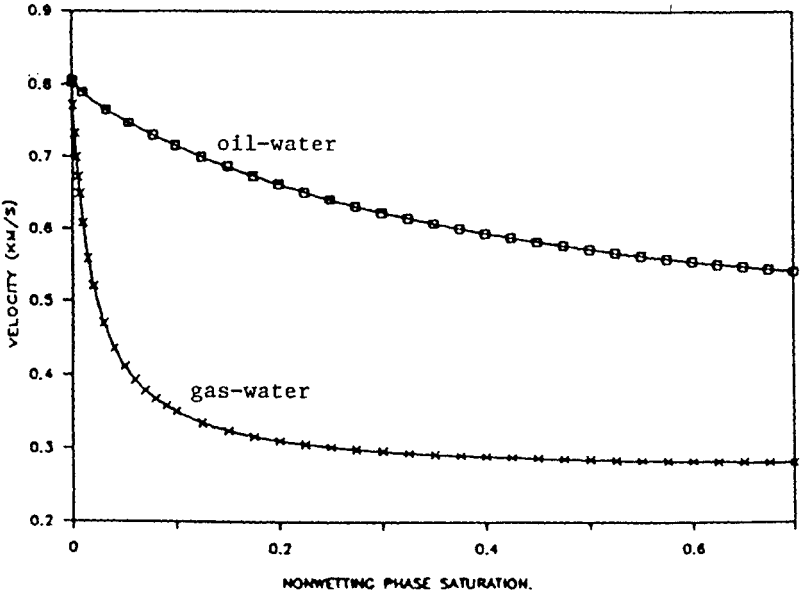


Fig. 17. Phase velocity of dilatational waves of the second kind (after Santos et al., 1990a).

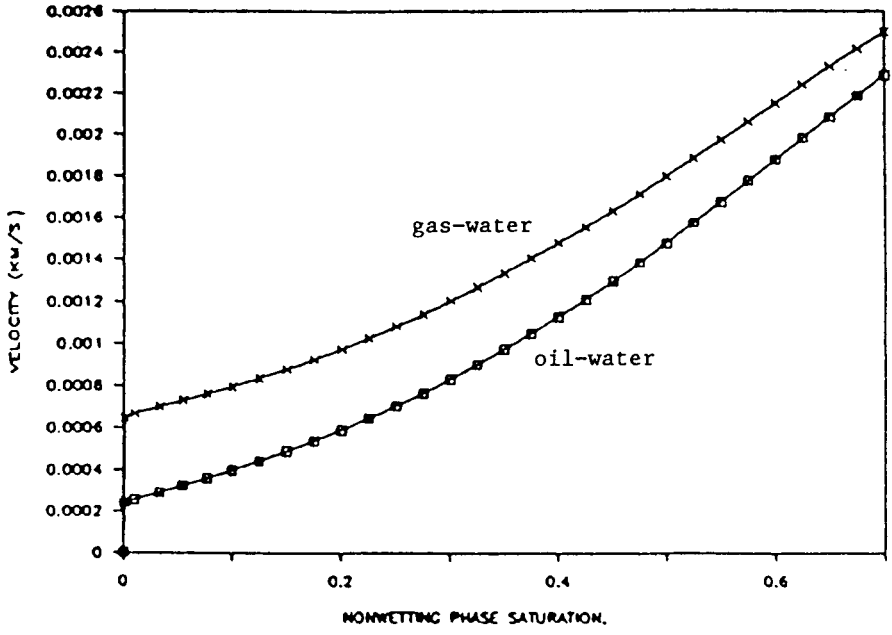


Fig. 18. Phase velocity of dilatational waves of the third kind (after Santos et al., 1990a).

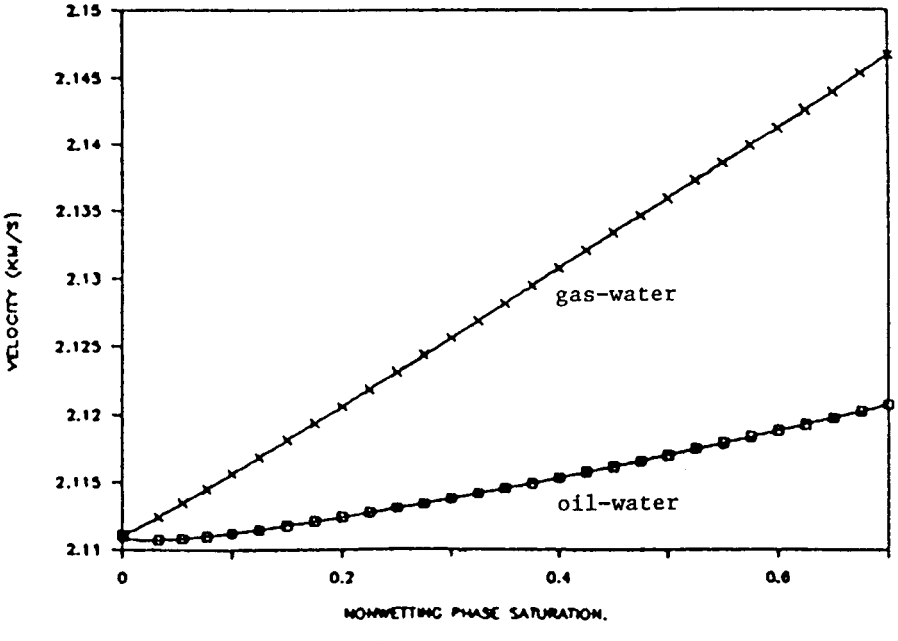


Fig. 19. Phase velocity of shear wave (after Santos et al., 1990a).

smaller than the oil-water saturated medium, it has higher shear wave phase velocity. Santos et al.'s model shows increasing phase velocities with frequency at low frequencies (< 5 Hz) and almost constant velocities at higher frequencies. They questioned the validity of their model at high frequencies, since the frequency dependence of dissipation for high frequencies has not been taken into account in their formulation (see Section 2.5). The attenuation coefficients of the first kind dilatational and shear waves were found to be almost zero at low frequencies and very small at high frequencies with peaks at a particular frequency.

White (1975) derived expressions by extending Gassmann's viewpoint to include coupling between the fluids. White considered a spherical region of gas or liquid surrounded by a concentric shell of liquid or gas. Norris (1992) developed a macroscopic theory that takes into account the type of microstructure in White's model.

Domenico (1974, 1976) experimentally investigated the effects of water saturation on reflection, refraction, and phase velocity of body waves and showed that the drainage process used in many laboratory studies (Gregory, 1976; Elliot and Wiley, 1975; Domenico, 1976) results in extremely heterogeneous gas distribution in the samples.

Murphy (1982) provided further data on the effects of partial water saturation on attenuation in high-porosity sandstone ($n = 0.23$) and porous glass ($n = 0.28$). Murphy concluded that attenuation is much more sensitive to degree of saturation than the wave velocity. In partially saturated sandstones, attenuation is strongly frequency dependent. Murphy also concluded that viscous dissipation is dominant over surface film mechanism at saturation levels over one percent. At very low saturations, monolayer of water react with the silicate surface, increasing the compressibility of the matrix significantly. Biot's theory does not take this effect into consideration. Murphy (1984) observed different results in tight sandstones ($n = 0.033 - 0.085$) which can be explained by contact relaxation mechanism. Although grain-to-grain response is elastic, water trapped in the contact gap adds a component stiffness to the matrix and creates a viscoelastic response.

Yin. et. al. (1992) used force-deformation method to examine the attenuation characteristics of unsaturated porous media and concluded that pore fluids within the rock affect attenuation not only by their degree of saturation but also by the history of the saturation.

6. Use of wave propagation equation to estimate permeability

An inspection of equation (2.19) reveals that the coefficient b of the dissipation term is related to the intrinsic permeability of the medium. Klimentos and McCann (1990) found relationships between the clay content, phase velocity and attenuation. Their results showed that the relationship between clay content and attenuation is very strong. Since permeability strongly depends on the clay content, dissipation is the key factor in determining the permeability of a porous medium. We should note that permeability is measured by quasi-static experiments where there is net flow. However, in wave propagation there is no net flow but oscil-

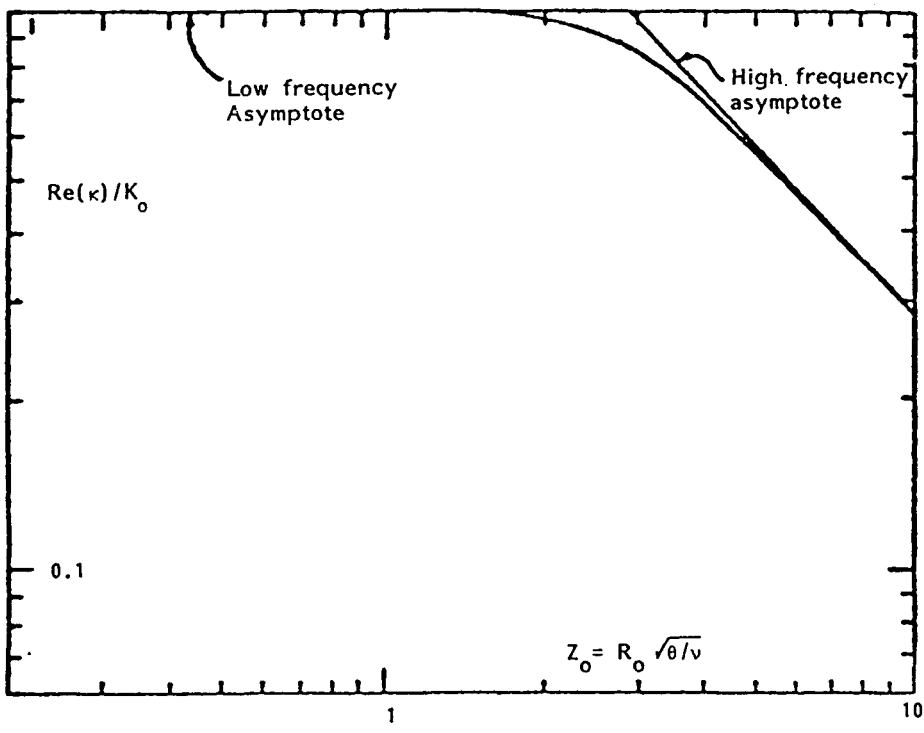


Fig. 20. Frequency dependence of hydraulic conductivity (after Misra and Monkmeyer, 1966).

lations about an equilibrium position. Hence, permeability that is back calculated by using wave propagation theory may differ from the quasi-static permeability of a porous medium. Similar statements were made by Berryman (1986b, 1988). Berryman warned against the use of Biot's theory to determine the permeability of rocks in the low-frequency range (1–100 Hz). He showed that since the intrinsic permeability of the rock is inhomogeneous and varies widely in magnitude, the spatial scale of Biot's theory is quite small. Therefore, Biot's theory predicts an order of magnitude of different permeability values than measured permeabilities. Nagy (1993) concluded that the observed discrepancy in attenuation coefficients is due to the irregular geometry that significantly reduces the high frequency dynamic permeability. Mochizuki (1982) argued that attenuation measurements of Murphy (1982) can not be explained by Biot's theory. Prasad and Meissner (1992) observed that other attenuation mechanisms exist in saturated sands. The discrepancy between Biot's theory and experimental results are believed to be because of the squirt flow in the microscale (Mavko and Nur, 1979; Murphy et al., 1986; Akbar et al., 1986). Some researchers used wave propagation equations to estimate the permeability of the medium. In this section, we will review some of these studies.

Wylie et al. (1962) suggested the use of Biot's theory to calculate the hydraulic conductivity by measuring the attenuation at two or more frequencies. However, they did not introduce a formalism to their proposal.

Spooner (1971) obtained the wave propagation equation for a partially saturated porous medium in terms of pore pressure by taking the divergence of the conservation of momentum equation

$$\frac{(S_w\rho_f + (1 - S_w\rho_g))m}{n}\frac{\partial q_r}{\partial t} = -\nabla p - \frac{\mu_f}{k}q_r \tag{6.1}$$

and differentiating the conservation of mass equation for the water phase

$$-\nabla \cdot \boldsymbol{q}_r = \left(S_w n\beta'' + \frac{\rho_g}{\rho_f}\frac{(1 - S_w)n}{p_0} + \left[S_w + \frac{\rho_g}{\rho_f}(1 - S_w)\right]a_v\right)\frac{\partial p}{\partial t} \tag{6.2}$$

and combining equations (6.1) and (6.2), and eliminating $\boldsymbol{q}_r$

$$\nabla^2 p = m[S_f\rho_f + (1 - S_w)\rho_g]\beta'\frac{\partial^2 p}{\partial t^2} + \frac{\mu_f n}{k}\beta'\frac{\partial p}{\partial t} \tag{6.3}$$

where m is the "structure factor" (see equation (2.52)) which is called mass coefficient by Biot. S_w is the degree of water saturation, ρ_g is the density of gas, p_o is the reference pressure. a_v is the coefficient of volume compressibility of the solid matrix ($= (1 - n)^{-1}\, dn/dp$). β'' is the compressibility of water. β' is considered as an "effective compressibility" and is equal to the coefficient on the right side of equation (6.2) divided by n. $\boldsymbol{q}_r$ is the relative specific discharge of water

$$\boldsymbol{q}_r = n\frac{\partial}{\partial t}(\boldsymbol{U} - \boldsymbol{u}) \tag{6.4}$$

Note that $\boldsymbol{q}_r = \boldsymbol{w}$ [see equation (2.47)]. A comparison of equation (6.1) for $S_w = 1$ (i.e., saturated porous medium) with equation (2.49) reveals that

$$-n\nabla p = -\rho_f m\frac{\partial^2}{\partial t^2}(u - U) - \frac{n^2\mu_f}{k}\frac{\partial}{\partial t}(u - U) \tag{6.5}$$

$$\nabla p = \frac{\partial^2}{\partial t^2}[\rho_f u + mn(U - u)] + \frac{\mu_f}{k}\frac{\partial}{\partial t}(U - u) \tag{2.49}$$

The parameter m has been introduced by Zwikker and Kosten (1949). It incorporates the increasing effect of "apparent density" $[S\rho_f + (1 - S)\rho_g]$ in the inertial term of the fluid. Zwikker and Kosten comment that as seen in equation (6.5) the fluid flow may not be in the direction of pressure gradient due to increase in the apparent inertia of the fluid which results from the vibration of the solid matrix. Furthermore, Zwikker and Kosten showed that the "resistance constant" ($= 1/k$) depends on the frequency of oscillation of the fluid. Zwikker and Kosten considered only two dilatational waves by using the concept of impedance. Same concept was also emphasized by Beranek (1947). The problem was also studied by Morse (1952) under the simplifying assumption of "rigid-frame theory." Rigid-frame theory assumes that the pore fluid is air, and the solid matrix is considered rigid. With a rigid matrix, there is only one dilatational wave, and it travels through the air. Morse considers high frequency range when inertial effects dominate over

viscous ones. He finds that $2.0 < m < 3.4$. $m = 2$ corresponds to uniform grain size materials while $m = 3.4$ is for non-uniform granular porous media.

If we rewrite equation (6.3) in one-dimension

$$\frac{\partial^2 p}{\partial x^2} = \frac{m}{C_o^2}\frac{\partial^2 p}{\partial t^2} + \frac{n\mu_f}{[\rho_f S_w + (1 - S_w)\rho_g]kC_o^2}\frac{\partial p}{\partial t} \tag{6.6}$$

The wave velocity, V_c, is given by

$$V_c = \frac{C_o}{\sqrt{m}} = \left[\frac{1}{[\rho_f S_w + (1 - S_w)\rho_g]m\beta''}\right]^{1/2} \tag{6.7}$$

Misra (1965) and Misra and Monkmeyer (1966) assumed a plane, progressive harmonic wave solution for the fluid pressure as

$$p(x, t) = p_o e^{i(\theta t - \beta x)} \tag{6.8}$$

where r is the frequency, and β is the complex wave number. The imaginary part of β is the attenuation constant and the real part is the phase constant. Misra and Monkmeyer (1966) have shown that by using capillary tube modeling of the porous medium, the steady state hydraulic conductivity, K_o ($= k\rho_f g/\mu_f$) is given by

$$K_o = \frac{\rho_f g n R_o^2}{8\mu_f m} \tag{6.9}$$

where R_o is the radius of the capillary tube. During wave propagation, K_o is a function of $z_o = R_o\,(r^*/\upsilon_f)^{1/2}$ where υ_f is the kinematic viscosity. Misra and Monkmeyer have shown that for low frequencies, i.e., small z_o (or low permeabilities) the hydraulic conductivity approaches its static value (i.e., $K = K_o$). For high frequencies (or high permeabilities), the permeability is proportional to the structure factor, w.

Geertsma (1974) defined the Reynolds number in terms of the "coefficient of inertial flow resistance"

$$\mathrm{Re} = \frac{\chi\rho_f q k}{\mu_f} \tag{6.10}$$

from the Forcheimer equation

$$-\nabla p = \frac{\mu_f}{k} q + \chi\rho_g |q| \cdot q \tag{6.11}$$

where $\boldsymbol{q}$ is the specific discharge of fluid (i.e., $\boldsymbol{q} = n\,\partial \boldsymbol{u}/\partial t$) and χ is the coefficient of inertial flow resistance. A comparison with Biot equations show that χ is similar to ρ_{12} (or m). The Reynolds number as given by equation (6.10) describes the upper limit of Darcy's law.

Smith and Greenkorn (1972) independently derived equation (6.3) and equation (6.9) for a saturated rigid porous medium, i.e., $a_v = 0$, $S = 1$. Smith et al. (1974a) presented experimental data obtained in nitrogen filled Ottawa sand to check the validity of their theory. The results of Spooner (1971) and Smith and Greenhorn

(1972a) are quite similar. Smith et al. (1972b) extended the theory to transient pressure response. Their results show that inertial effects exist for short distances and high permeabilities.

Turgut and Yamamoto (1990) studied attenuation of acoustic waves in fluid saturated sediments and obtained good agreement between the experimental and theoretical results. This enabled the remote estimation of porosity and permeability of marine sediments by using measured compressional and shear wave characteristics. They were able to estimate the porosity distribution of a 3×3 m vertical plane by a cross-hole tomography experiment. Porosities are calculated from the compressional wave velocities which are inverted from measured travel times by using singular decomposition technique.

7. Wave propagation in marine environments

7.1 Response of porous beds to water waves

When sea waves propagate over a porous bottom, they induce fluid flow in the medium and cause the bed to deform. In shallow waters, fluctuating wave pressures can generate high levels of energy resulting in soil failure and damage to structures such as pipelines and offshore terminals. Therefore, numerous investigations were carried out with various degrees of simplifications. Assumptions of a rigid bed and incompressible water leads to the Laplace equation in terms of pore pressure [$\nabla^2 p = 0$] (pressure waves), (e.g., Putnam, 1949; Reid and Kajiura, 1957; Oroveanu and Pascal, 1959; Sleath, 1970; Demars, 1983). Later, Moshagen and Torum (1975) introduced the compressibility of water, thus obtaining a diffusion type (parabolic) equation for the pore pressure. In contrast to Laplace equation, pore pressure response is highly affected by the permeability of the sea bed. Verruijt (1982) considered only standing waves in his analytical solution. Madsen (1978), Yamamoto et al. (1978), and Nataraja and Gill (1983) took into consideration the flow in the bed, compressibility of water and elastic bed in their formulation. Yamamoto et al. noted that even a very small amount of air trapped in the bed would increase the volume compressibility of water very drastically (Verruijt, 1969).

$$\beta = \beta_o + \frac{(1 - S_w)}{p_o}$$

where β and β_o are the compressibility coefficient of water and pure water, respectively. S_w is the degree of water saturation, p_o is the absolute pore pressure (taken as 1 atm by Yamamoto et al., 1978).

Yamamoto and Takahashi (1983) established a Froude-Mach similitude law for sea-seabed interaction. This law requires that three Mach numbers which are the ratios of water wave phase velocity to the velocities of the fast and slow compressional waves and the shear waves in the seabed should be equal in the prototype and physical scale model in addition to the geometric similarity and the

Froude number squared which is the ratio of inertial to gravity force. In general, the Mach number is a ratio of inertial to elastic force and it is an indicator of the importance of compressibility effects in a fluid flow. When the Mach number is small, the associated inertial force does not cause significant compressibility. Yamamoto and Takahashi found that the response of sand beds to water waves is linear and quasi-static. However, clay beds showed highly nonlinear and dynamically amplified response. This conclusion enforces the concept of internal loss due to the Coulomb friction between clay particles which is independent of loading frequency (Yamamoto and Schuckman, 1984). Therefore, the representation of seabed as a "fluid-like" material (e.g., Dalrymple and Liu, 1978) is inadequate.

In all these studies, the inertia term in the momentum balance equations were neglected. Although Massel (1976) included the inertia term in his equation, he concluded that the effect of permeability on the pressure variation is negligible, thus the governing equation gives results similar to that of the Laplace equation. Dalrymple and Lui (1982) extended Yamamoto's work to include the inertia term in the governing equations. They concluded that the inertial terms are important when a dimensionless parameter which is the ratio of the square of the wave speed for an elastic solid to the water wave speed, is close to one. When this parameter is less than one (i.e., soft sediments), the solid displacements and the shear stress, τ_{xy}, oscillate as they decay with depth. They further noted that ρ_{12} has negligible effects on solutions. Later, Liu and Dalrymple (1984) employed the generalized Darcy's law with an acceleration term obtained by Dagan (1979), to describe the oscillatory flow in soil bed. Basak and Madhav (1978), Wylie (1976), Wiggert and Wylie (1976), and Auriault et al. (1985) also included the acceleration term in Darcy's law. The inclusion of inertial effects can also be achieved by using the Forchheimer equation (Finjord, 1990).

Finn et al. (1982) reviewed the methods for estimating the response of seafloor to ocean waves and the determination of wave-induced pore pressures. Finn et al. have shown that transient pore pressures and the associated effective stress field may be investigated by Biot's (1941) theory of consolidation. We must note that by using this approach Finn et al. (1982) assume quasi-static (equilibrium) distribution of stresses.

As noted in Section 4, Seed and his coworkers (e.g., Seed and Rahman, 1978) introduced the concept of pore pressure generation under cyclic loading condition to investigate the response of seafloor sands subjected to storm wave loadings (see equation 4.1). Siddharthan (1987) combined this approach with that of Yamamoto and Madsen, to analyze the seafloor response to a storm wave group. Siddhartham found that for North Sea seafloor, the inclusion of inertia, damping and anisotropic permeabilities is not important. However, the thickness and the stiffness properties of the sediment govern the response of the deposit. Thus, the seafloor displacements are affected by residual pore pressures generated by waves.

7.2. Mei and Foda's boundary layer theory

Mei and Foda (1981) obtained a solution for Biot's equations for rapid water waves with high frequencies (i.e., ocean waves or seismic waves). Mei and Foda

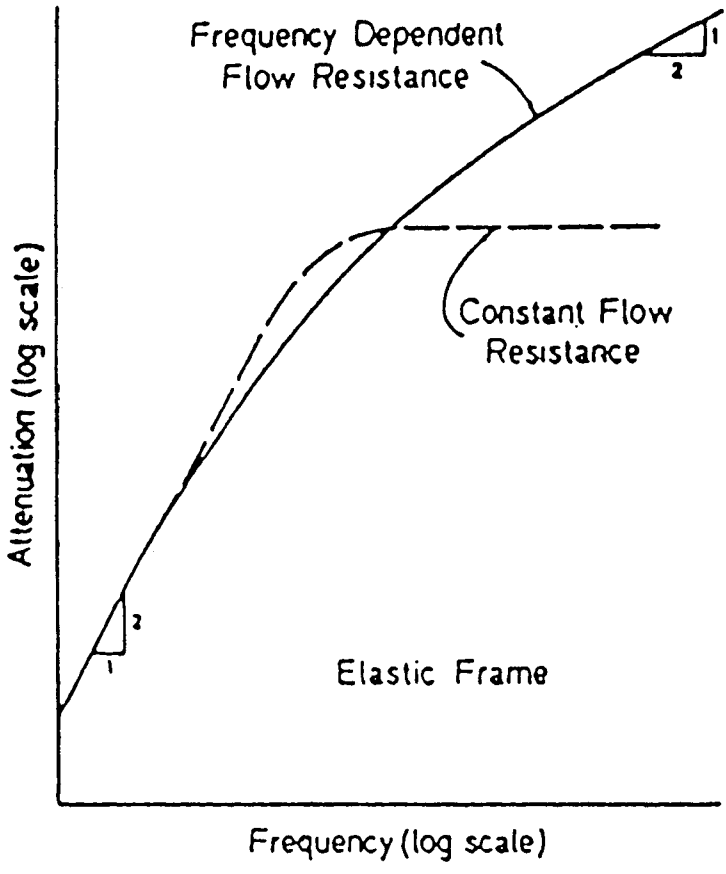


Fig. 21. Attentuation versus frequency for a linear elastic frame (after Stoll, 1974).

has concluded that the region close to the porous medium surface is drained and pore pressures in that region are independent of the wave length. The depth of this zone of consolidation is smaller than the wave length. This region is treated as a boundary layer of Stokes' type with one-dimensional flow. The boundary layer concept agrees well with the Biot's conclusion for the waves of the second kind which have very short attenuation distances and the disturbance propagates in a form similar to diffusion. Outside the boundary layer, the porous medium reacts undrained and the fluid and the solid matrix move together. Mei and Foda (1981, 1982) have shown that by neglecting the grain compressibility (unjacketed compressibility) and the apparent mass (ρ_{12}) from equation (2.28) and using elastic strain relation [equation (2.16)], they obtain

$$n\rho_f \frac{\partial V_x}{\partial t} = -n\frac{\partial p}{\partial x} - \frac{n^2}{k^*}(V_x - v_x) \tag{7.1}$$

V_x and v_x are the fluid and the solid velocities, respectively. Note that $v_x = \partial u_x/\partial t$ and $V_x = \partial U_x/\partial t$. By neglecting some parameters and eliminating $\nabla.\boldsymbol{u}$ from

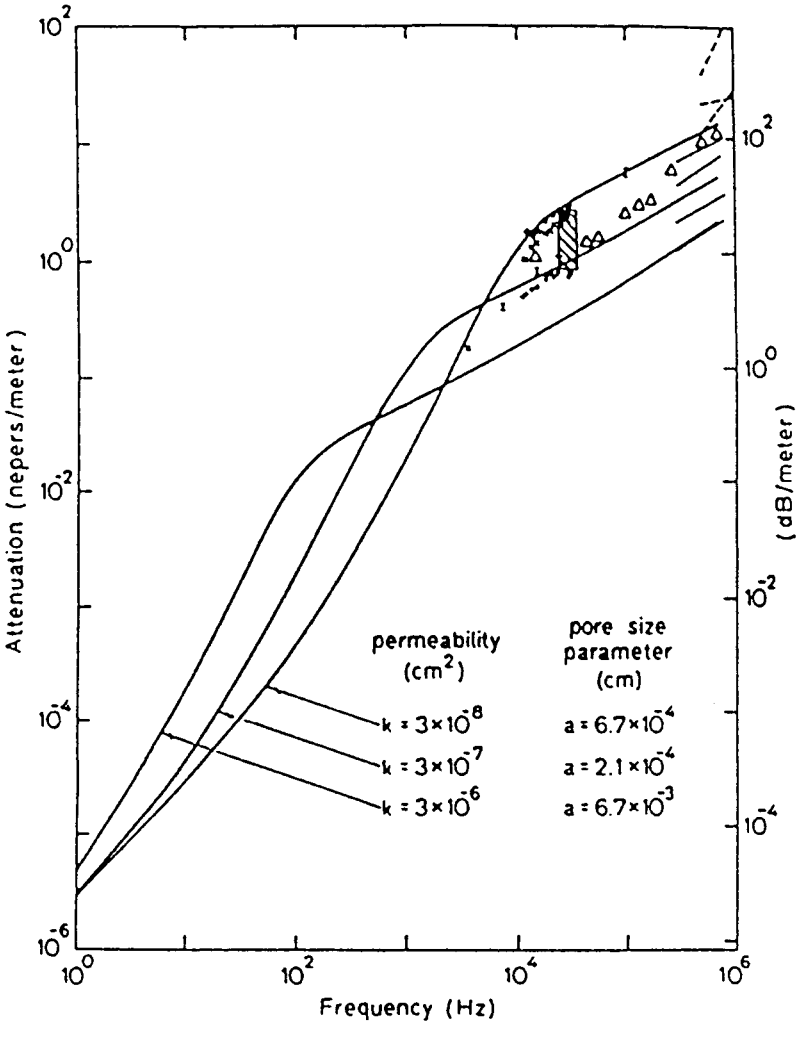


Fig. 22. Attenuation versus frequency for sands (after Stoll, 1974).

equation (2.25) by using equations (2.15) and (2.16) and inserting elastic stress-strain relations, Mei and Foda obtained,

$$(1-n)\rho_s \frac{\partial v_x}{\partial t} = \frac{\partial \sigma_{xx}}{\partial x} + \frac{\partial \tau_{xy}}{\partial y} + \frac{\partial \tau_{xz}}{\partial z} - (1-n)\frac{\partial p}{\partial x} + \frac{n^2}{k^*}(V_x - v_x) \tag{7.2}$$

Note that Mei and Foda's k^* is equal to Biot's k/μ_f. Similar equations can be obtained in the y- and z-directions. The conservation of mass equations for the solid and the fluid phases

$$\nabla\cdot[(1-n)\rho_s v] + \frac{\partial[(1-n)\rho_s]}{\partial t} = 0 \tag{7.3}$$

$$\nabla\cdot(n\rho_f V) + \frac{\partial(n\rho_f)}{\partial t} = 0 \tag{7.4}$$

are combined to obtain (in x-direction)

$$n\nabla\cdot(V - v) + \nabla\cdot v + \frac{n}{\beta}\frac{\partial p}{\partial t} = 0 \tag{7.5}$$

where β is the compressibility of water. Equation (7.5) has been obtained by various other researchers for the compressible groundwater aquifer problem (e.g., Bear and Corapcioglu, 1981).

By adding equations (7.1) and (7.2), and using the Hooke's law, Mei and Foda obtained

$$G(\nabla^2 v + \frac{1}{1-2v}\nabla\nabla\cdot v) - \nabla\frac{\partial p}{\partial t} = n\rho_f\frac{\partial^2 V}{\partial t^2} + (1-n)\rho_s\frac{\partial^2 v}{\partial t^2} \tag{7.6}$$

They eliminated ($\mathbf{V} - \mathbf{v}$) from equations (7.2) and (7.5)

$$k^*\nabla^2 p = \nabla\cdot v + \frac{n}{\beta}\frac{\partial p}{\partial t} - k^*\rho_f\frac{\partial}{\partial t}(\nabla\cdot V) \tag{7.7}$$

where G and ν are the shear modulus and Poisson ratio, respectively. Mei and Foda split the stress field into the outer solution and the boundary layer correction. For outer solution $V = v$ and the first and the last term of equation (7.7) is neglected since, the dimensionless parameter of $\rho_f\omega^2 L^2/G$ is very small for the seismic wave length $L = 100$–500 m, seismic frequency $\omega = 10\,\text{rad}\,\text{s}^{-1}$ and $\omega L^2/Gk^*$ is very large. These parameters appear in equation (7.7) after a non-dimensionalization is performed. The first one is the ratio of inertia to pressure (or stress) forces. The second is the ratio of Darcy's drag force to the pressure (or stress) gradient waves. Therefore the solid dilatation $\nabla.\mathbf{v}$ is directly related to the pore pressure change. Then, the velocity of compressional waves is

$$V_c^2 = \frac{\lambda_e + 2G}{n\rho_f + (1-n)\rho_s}$$

λ_e is the effective Lame constant $= \lambda + \beta/n$ where β^{-1} is the compressibility of water. Shear waves propagate with a velocity of $V_{s2} = G/[\rho_f n + (1-n)\rho_s]$. For gravity waves at the sea with $\omega = 0.5 - 1\,\text{rad}\,\text{s}^{-1}$, $L = 50$–200 m same approximations can be made. In general, one can conclude that since the permeability of soils is small, at high frequencies, the fluid is resisted by viscosity and cannot have a significant velocity relative to solid (Mei and Foda, 1982). But, near the mud line (free surface), fluid can drain, and relative velocity can not be neglected. Near the ground surface, vertical component of $G\nabla^2\mathbf{v}$ in equation (7.6) is dominant, and inertial terms in comparison are negligible. The boundary layer correction of the solid velocity is irrotational which implies that vertical velocities are much larger than the horizontal ones (Mei and Foda, 1981). In equation (7.7), the last term is neglected near the free surface, and it finally reduces to a diffusion equation in terms of p to be solved for the boundary layer correction.

$$k^* \frac{\partial^2 p^b}{\partial y^2} = \left[\frac{n}{\beta} + \frac{1-2\upsilon}{2G(1-\upsilon)}\right] \frac{\partial p^b}{\partial t} \tag{7.8}$$

The boundary layer thickness is determined from

$$\delta = \left(\frac{k^*}{\omega}\right)^{1/2} \left(\frac{n}{\beta} + \frac{1-2\upsilon}{2G(1-\upsilon)}\right)^{-1/2} \tag{7.8a}$$

As seen in equation (7.8a), the thickness of the boundary layer, δ, is very small for small permeability, or high frequency, or large compressibility of water, or large compressibility of the solid matrix. Mei and Foda (1981) have calculated δ of various earth materials changing from 0.002 m for granite to 10 m for coarse sand for $\omega = 1$ rad s^{-1}.

Solutions obtained for the boundary layer from the solution of equation (7.8) are added to the solutions obtained for the outer region. Using this approximation, Mei and Foda (1981) obtained solutions for progressive waves over a semi-infinite sea bed and a sea bed with finite thickness. In summary, Mei and Foda concluded that for many wave problems, the wave period is much smaller than the consolidation time of soils which in general have low permeability. Thus the relative movement between the fluid and solid is significant only near the free surface of the porous medium ("mudline"). Chen (1986) applied Mei and Foda's (1981) boundary layer theory to study the effect of sediment on earthquake-induced reservoir hydrodynamic response.

Rigid frame analysis of Morse (1952) was extended by Nolle et al. (1963) to allow the bulk modulus of the sand. Nolle et al. stated the equations of motion for solid matrix and fluid by

$$-(1-n)\frac{\partial p}{\partial x} = \rho_s(1-n)\frac{\partial v_x}{\partial t} + b(v_x - V_x)$$

$$-n\frac{\partial p}{\partial x} = \rho_f n \frac{\partial V_x}{\partial t} + b(V_x - v_x) \tag{7.9}$$

where v_x and V_x are the velocities of the solid and the fluid, respectively [compare with equations (7.1) and (7.2) with $\sigma_{xx} = \tau_{xy} = \tau_{xz} = 0$ due to rigidity of the matrix]. Nolle et al. expressed b by

$$b = -i\omega n\rho_f(Y-1) + h^2\sigma^*$$

where ω is the angular (circular) frequency, Y is a constant (>1) used to calculate the effective porosity ($=n/Y$), and σ^* is the specific flow resistance approximated by

$$\sigma^* = \frac{2\sqrt{2\rho_f \mu_f \omega}}{0.12nd}$$

where d is the average particle diameter.

Equations (7.9) are solved simultaneously with an equation of continuity

$$-\frac{\partial \rho}{\partial t} = \left[\frac{1}{n/\beta_l + (1-n)/\beta_s}\right]\left[n\frac{\partial V_x}{\partial x} + (1-n)\frac{\partial v_x}{\partial x}\right] \tag{7.9a}$$

where β_l and β_s are the bulk modules of the liquid and the sand grains, respectively. o is the true density of the porous medium. By introducing β_s, Nolle et al. allowed a finite compressibility for the solid while taking the elastic modulus of the skeleton to be zero. Equation (7.9a) can be compared with equations (6.2) and (7.5).

7.3. Modifications of the boundary layer theory

Later, Mynett and Mei (1983) applied the boundary layer theory to study the propagation of earthquake induced Rayleigh waves. The outer region is divided into two regions. The far field is the region at a distance from the structure and the wave length is the characteristic length. The region around the structure is the near field and has the structural dimension as the characteristic length. In the near field, inertial terms are small. Further applications were also given by Mynett and Mei (1982) and Mei and Mynett (1983).

In a later paper, Mei et al. (1985) included the convective component of the acceleration i.e., $n\rho_f U\,\partial V_x/\partial x$ in equation (7.1) and $(1-n)\rho_s U\,\partial v_x/\partial x$ in equation (7.2), on the left hand side of respective equations (similar approach was also taken by Derski, 1978) and assumed $\partial V_x/\partial t \ll U\,\partial V_x/\partial x$ and $\partial v_x/\partial t \ll U\,\partial v_x/\partial x$ to study the dynamic response of the ground to an air pressure distribution moving along the surface at a constant speed U. These approximations were carried out for a steady-state linearization of governing equations. Similarly, in equation (7.5) the convective component $U\,\partial p/\partial x$ was added to $\partial p/\partial t$, and assumed $\partial p/\partial t \ll U\,\partial p/\partial x$. The results were given for supersonic ($U/V_c > U/V_s > 1$), subsonic ($1 > U/V_c > U/V_s$) and transonic ($U/V_c > 1 > U/V_s$) loads. U/V_c and U/V_s are Mach numbers for compressional and shear waves, respectively.

7.4. Wave attenuation in marine sediments

Attenuation of waves in saturated marine sediments is important in seismic studies of these sediments at low frequency range (1–100 Hz). Acoustic soundings are conducted at a much higher range (up to 100 KHz). The evaluation of the attenuation of acoustic waves of low amplitude over relatively long distances has been a major interest in geophysics. To develop a unified theory over a wide range of frequencies, Stoll and Bryan (1970) started with Biot's theory [equations (2.49) and (2.50)] to study the attenuation of dilational wave of the first kind. Stoll and Bryan, by casting the parameters H, αM, and M of these equations in terms of bulk modulus of the discrete grains, the water, and the solid matrix, and the shear modules of the matrix, demonstrated that attenuation is controlled by the inelasticity of the matrix at low frequencies, and by viscosity of the fluid at higher frequencies. Thus at low frequencies, there is a linear dependence of attenuation on frequency, f. At high frequency, attenuation is controlled by f^n where n first increases from one to two, and then gradually decreases. At very high frequencies, matrix losses are dominant again, thus causing n to increase. The definition of

"low" and "high" is a relative term depending on the material. As noted by Stoll and Bryan, fluid losses dominate for granular materials like sand over most of the frequency range due to friction at contact points of grains. For materials like clays, losses are dominated by the solid matrix. Stoll and Bryan (1970) and Stoll (1974) used a functional form of frequency correction factor for high frequencies (Biot, 1956b).

$$F(\kappa) = \frac{\kappa T(\kappa)}{4(1 - 2T(\kappa)/i\kappa)} \tag{7.10}$$

where $T(\kappa)$ is given in terms of real and imaginary parts of the Kelvin function

$$T(\kappa) = \frac{\mathrm{ber}'(\kappa) + i\,\mathrm{ber}'(\kappa)}{\mathrm{ber}(\kappa) + i\,\mathrm{ber}(\kappa)} \tag{7.11}$$

and κ is defined by

$$\kappa = a\left(\frac{\omega\rho_f}{\mu_f}\right)^{1/2} \tag{7.12}$$

where a is the pore size parameter (for circular pores, it is the radius) and ω is the angular frequency. For low frequencies $F(\kappa)$ approaches to unity.

Stoll (1977) mentioned the significance of the dilatational waves of the second kind in multilayer systems where energy exchanges can occur at interfaces. Plona (1980) has demonstrated the existence of these waves in saturated porous sintered glass. Stoll (1980) noted the non-linear dependence of acoustic properties on cyclic strain amplitude and static stress level. In this study, Stoll developed a mathematical model based on the work of Biot (1956a). Stoll and Kan (1981) have shown the significance differences in the reflection of waves at a fluid-sediment interface depending on the type of modeling used to represent the sediment i.e., viscoelastic solid vs. water saturated porous viscoelastic matrix. A porous medium representation should be preferred for high permeability sediments or high frequency sources. Factors affecting the dilatational wave velocity in marine sediment was also investigated by Brandt (1960) by employing his model. Brandt's (1955) model represented the marine and sediments as liquid-saturated aggregate of spherical particles (distinct element model noted in Section 1). A correction factor incorporated the elasticity of pore fluid in an expression to calculate the wave velocity.

McCann and McCann (1969) and Smith (1974) have observed disappearance of solid friction for sediment grains finer than sand. For this type of sediment, the loss mechanism is entirely viscous. As the percentage of clay size particles increases, the effect of relative motion decreases. Then, the frequency dependence becomes quite complex. For very fine grained high porosity sediments of deep oceans, the medium behaves like seawater in its response to frequency variations.

8. Application of mixture theory

Treatment of particulate volume fraction as a constitutive variable in the mixture theory formulation for a multiphase medium like porous materials was introduced by Goodman and Cowin (1972) among others. Application of mixture theory to analyze the wave propagation in a fluid-solid mixture has received limited attention due to complexity of the theoretical exposition and difficulty in relating to practical problems. However, in the last few years, there are a number of papers providing a useful tool and an alternative to deal with wave propagation in porous media. A general treatment of the mixture theory is provided by Bowen (1976).

Raats' publications starting with Raats and Klute (1968) appear to be one of the first studies in this area. Raats has provided a framework for the construction of a mixture theory to study the balance of mass and momentum in porous media. Raats regarded the soil as a mixture of phases with an exchange of momentum taking place in the interfaces between them. Later, Raats (1969) presented an analysis of the propagation of sinusoidal pressure oscillations at a plane boundary into a structured porous medium. Pores of the medium have been classified into two: large and small pores. Raats has found that when the frequency of the oscillation is small, the heterogeneity of the medium is unnoticeable. Raats extended his analysis to include the effect of inertial forces into the jump conditions at the boundaries in addition to introducing an inertial force in the differential balance of forces.

A mixture theory for shock loading of wet tuff was presented by Drumheller (1987). Drumheller's work was a generalization of Herrmann's (1968, 1972) model. Drumheller considered an effective stress expression which corresponds to Biot and Willis' (1957) work [equation (2.16)] rather than the original expression of Terzaghi [(equation (4.1a)]. According to the Drumheller's theory, dilatancy occurs when the shear modulus is specified as a function of the porosity, and the n-p function is universal for all saturation values. Later, Grady et al. (1986) did similar work for dry and water-saturated porous calcite. In earlier works, others, e.g., Garg (1971, 1987), Garg and Kirsch (1973), Morland (1972), and Sawicki and Morland (1985) presented models for a water-saturated porous medium. Their theories similar to that of Bedford and Drumheller's (1979) work, were based on the adaptation of general mixture theory. However, they did not consider intrinsic behavior of immiscible constituents. Garg and Nayfeh (1986) extended the mixture theory approach to unsaturated soils [see equations (5.6)–(5.8)].

Garg (1971) developed a formulation based on the theory of interacting continua for a mixture of a solid and a fluid by defining effective stress and densities in terms of volume fractions of each phase, partial stresses and partial densities. Garg (1971) notes that the attenuation force (diffusive force as he called it) should be a function of partial pressures of each phase for large pressure gradients. Referring to Swift and Kiel (1962), he also suggested to have higher order terms of $(\mathbf{u} - \mathbf{U})$ for larger velocities. Later, Garg et al. (1975) generalized the constitutive relations of Garg (1971) and Morland (1972) to include thermodynamic effects. They solved the proposed model to study the shock wave propagation in tuff-

water mixture. Their numerical results indicate an increase in pulse rise time with increasing permeability.

Density variations in an inhomogeneous granular solid were considered in a mixture theory formulation developed by Nunziato and Walsh (1977) based upon concepts developed by Goodman and Cowin (1972). Later, Nunziato et al. (1978) applied their model to study one-dimensional wave propagation in an explosive material.

Bowen (1976) considered the saturated porous medium as a binary mixture of a linear elastic fluid and a linear elastic solid. Bowen and Reinicke (1978) stated four governing differential equations for displacements and temperatures of each phase, and they have shown that when there is momentum transfer between phases, there is only one mode of non-dispersive propagation in the low frequency range independent of the energy transfer. However, phase velocities and the attenuation coefficients depend on the presence of energy transfer between the phases. Thermal effects on wave propagation were also studied by Pecker and Deresiewicz (1973). Pecker and Deresiewicz have determined four distinct dilatational motions. The first two represent modifications of fast and slow waves (first and second P waves) at constant temperatures, and the other two are diffusion type modes similar to the thermal waves in a single-phase thermoplastic solid. Jones and Nur (1983) have observed that shear velocity and attenuation decrease with increasing temperature at all pressures in a saturated rock. In frozen soils, wave attenuation from low-level impact was found to be exponential (Dutta et al., 1990). Later, Bowen (1982) extended his mixture theory analysis (Bowen, 1980) to compressible porous media. Bowen compared his model to the one proposed by Biot (1962a). Bowen and Lockett (1982) have shown that long-term inertial effects cannot be neglected under certain circumstances such as the occurrence of resonance displacements for a harmonically varying compression at some loading frequencies. Neglecting inertia does not predict this type of behavior. We should note that in long-term diffusion type slow processes, the inertia terms have been generally neglected. Inertia terms were considered important at small times. We refer to Zienkiewicz and Bettess (1982c) as an example of this type of work, (see Section 3.3).

Katsube (1985) investigated Biot's constitutive relations by modifying Carroll's (1980) developments. Katsube and Carroll (1987) modified the mixture theory of Green and Naghdi (1965) and applied to porous media. They compared the resulting theory with Biot's theory and concluded that they are equivalent when fluid velocity gradients are ignored. Liu and Katsube (1990) predicted the existence of a second kind of a shear wave using the mixture theory of Crochet and Naghdi (1966). This wave is caused by the skew-symmetric portions of the partial stress tensors in the mixture theory of Crochet and Naghdi. Pride et. al. (1992) used local volume averaging technique in the derivation and argued that interaction torques caused by the skew-symmetrix portions should not be expected.

Loret (1990) and, Loret and Pervost (1991) studied dynamic strain localization in saturated porous media. Boer et al. (1993) formulated the field equations assuming both fluid and solid constituents are incompressible and obtained an analytical solution for transient wave propagation.

By employing the theory of mixtures and assuming that the mixture consists of two non-polar, incompressible constituents, Prevost (1980) obtained the conservation of mass and momentum equations for the solid and the fluid phases as

$$\frac{\partial n}{\partial t} + (1-n)\nabla\cdot v = 0 \tag{8.1}$$

$$\nabla\cdot[n(V-v)] + \nabla\cdot v = 0 \tag{8.2}$$

$$\nabla\cdot\sigma' - (1-n)\nabla p + n^2\rho_f k^{-1}(v-V) + (1-n)\rho_s b = (1-n)\rho_s \frac{d_s v}{dt} \tag{8.3}$$

$$n\rho_f(v-V)\colon \nabla V - n\nabla p - n^2\rho_f k^{-1}(v-V) + \rho_f n b = n\rho_f \frac{d_s V}{dt} \tag{8.4}$$

where d_s/dt is the material derivative with respect to moving solid phase. In deriving these equations Prevost assumed that since there is no moment of momentum supply between the two phases, the partial stress tensors for both phases are symmetric. It was also assumed that the fluid has no average shear viscosity. Later Prevost (1983, 1984, 1985) solved these equations by using a finite element technique.

Hsieh and Yew (1973) accounted for the change in porosity in their mixture theory formulation by expressing the porosity, n as

$$n = n_o + \Delta n \tag{8.5}$$

where n_o and vn are the initial porosity and small incremental change in porosity, respectively. Furthermore, the relationship among the pore fluid pressure, p, dilatation, ϵ, and Δn is expressed by

$$-p = Q^*\epsilon - N^*\Delta n \tag{8.6}$$

where coefficients Q^* and N^* which should be determined experimentally, do not correspond to Biot coefficients [see equation (2.16)]. Hsieh and Yew (1973) presented a numerical solution for the dilatational and rotational waves.

As noted in Section 5, Berryman (1988) presented a mixture theory for unsaturated porous media. Berryman published his theory in a series of papers which deal with different aspects of the problem such as inhomogeneity and normalization constraint (e.g., Berryman and Milton, 1985; Berryman, 1985).

In Section 2.7, we noted that Biot's theory does not take into account the time-dependent pore collapse of a porous matrix. However, dry porous materials, such as granular high energy solid propellants, granular explosives, dry metal powders exhibit pore crushing and pore collapse. Carroll and Holt (1972) and Butcher et al. (1974) described a time-dependent pore collapse mechanism for porous aluminum. Baer and Nunziato (1986), Baer (1988), Gokhale and Krier (1982) and Powers et al. (1989) provided two-phase continuum mixture equations to describe the motion of a mixture of solid particles and gas. These equations simulate the deflagration-to-detonation transition in a column of granular explosives. Powers

et al. (1989) stated these equations by neglecting the effects of diffusive momentum and energy transport, and the compaction work

$$\frac{\partial \rho_i \phi_i}{\partial t} + \frac{\partial (\rho_i \phi_i v_i)}{\partial x} = A_i \tag{8.7}$$

$$\frac{\partial \rho_i \phi_i v_i}{\partial t} + \frac{\partial (p_i \phi_i + \rho_i \phi_i v_i^2)}{\partial x} = B_i \tag{8.8}$$

$$\frac{\partial}{\partial t}\left[\rho_i \phi_i \left(e_i + \frac{v_i^2}{2}\right)\right] + \frac{\partial}{\partial t}\left[\rho_i \phi_i u_i \left(e_i + \frac{v_i^2}{2} + \frac{p_i}{\rho_i}\right)\right] = C_i \tag{8.9}$$

$$\frac{\partial \phi_2}{\partial t} + v_2 \frac{\partial \phi_2}{\partial x} = \phi_1 \frac{\phi_2}{\mu_c} [p_2 - p_1 - \sigma'(\phi_2)] \tag{8.10}$$

where ρ_i is the density, p_i is the pressure, e_i is the energy, v_i is the velocity, d_i is the volume fraction for each phase ($i = 1$ for the gas, $i = 2$ for the solid). Equations (8.7)–(8.9) are the balance equations for mass, momentum and energy of each phase. Interphase transport is represented by A_i, B_i, and C_i which are functions of other parameters such as densities, velocities, and pressures of each phase. By definition, the sum of each term is equal to zero, i.e., $A_1 + A_2 = 0$. Equation (8.10) similar to Butcher et al.'s (1974) pore collapse equation, is the "compaction equation" where m_c is the "compaction viscosity" and s' is the intergranular stress expressed as a function of volume fraction. Different phases of compaction, i.e., elastic, plastic, would generate different s' expressions (Carroll and Holt, 1972). Substitution of equation (8.10) into equations (8.7)–(8.9) would yield hyperbolic equations (Baer and Nunziato, 1986). State expressions will express p_i and e_i in terms of (ρ_i, T_i) and (p_i, ρ_i) respectively. T_i is the phase temperature. By definition $d_1 + d_2 = 1$. Powers et al.'s (1987) model admits both subsonic and supersonic compaction waves. They have shown that when compaction waves travel faster than the ambient sound speed of the solid, a shock preceding the compaction wave structure is expected. There was no leading shock for subsonic compaction waves.

Beskos (1989) studied the dynamic behavior of fluid saturated fissured rocks. Beskos developed his model along the lines of the theory of mixture formulation of Aifantis (1979) and, Wilson and Aifantis (1984) in a notational framework similar to the one employed by Vardoulakis and Beskos (1986). In companion papers, Beskos et al. (1989a, 1989b) studied the propagation of harmonic body and Rayleigh waves. Their analysis reveals the existence of three dilatational (compressional) waves and one rotational (shear) wave. The presence of fissures results in the appearance of an additional dilatational wave in a fissured porous medium.

Another approach of formulating multiphase equations is local volume averaging. This approach started after the development of the theorem for the local volume average of a gradient (Slattery, 1967; Anderson and Jackson, 1967; Whitaker, 1967). It has been recently applied to wave propagation problems. de la Cruz and Spanos (1985) made the first attempt to rederive Biot's theory. In a later

paper, de la Cruz and Spanos (1989) extended their theory to include thermodynamical coupling. Garg (1987) developed the complete set of balance laws for multiphase media. However, in all these works the main problem was the determination of the constitutive relations in terms of averaged variables. Recently, Pride et al. (1992) rederived Biot's equations and obtained the same expressions for the coefficients in Biot's theory. An alternative approach of homogenization is the two-space method. It was first developed and studied by Sanchez-Palancia (1980) and Keller (1977). It was applied to wave propagation by Burridge and Keller (1981), Levy (1979), and Auriault (1980, 1985). In principle both local volume averaging and two-space method yield the same results. However, application of local volume averaging is simpler and enables physical interpretations of the averaged expressions.

9. The use of macroscopic balance equations to obtain wave propagation equations in saturated porous media

In this section we will develop the governing equations for wave propagation in a saturated compressible porous medium from the macroscopic momentum and mass balance equations for both the solid matrix and fluid phase. The equations are written for an elastic solid matrix and a Newtonian compressible fluid that completely fills the void space. The constitutive equations for the elastic solid matrix are written in terms of the effective stresses. The resulting governing equations are in terms of fluid and solid velocities, effective stresses, displacements, fluid pressure, fluid density, and porosity. This approach has been presented by Bear and Corapcioglu (1989).

We assume that the compressible porous medium is fully saturated by a single-phase, single-component fluid. As a result of dynamic loading, stresses in the fluid change. This is accompanied by a corresponding change in the effective stresses in the solid matrix. A change in effective stress produces the deformation of the porous medium.

The approach we present in this chapter offers an alternative methodology to obtain the wave propagation equations. As opposed to Biot's approach which employs the kinetic energy density functions and dissipation energy functions, we state the conservation of momentum and mass equations to formulate the problem.

9.1. Mass balance equations for the fluid and the solid matrix

We start from the three-dimensional mass balance equation for a fluid that saturates a porous medium (e.g., Bear and Corapcioglu, 1981)

$$\nabla\cdot(\rho_f n V_f) + \frac{\partial(\rho_f n)}{\partial t} = 0 \tag{9.1}$$

where V_f is the mass-weighted velocity of the fluid, ρ_f is the density of the fluid, and n is the porosity of the medium. In deriving (9.1), we have neglected the

dispersive mass flux due to spatial variations in the fluid's density. Similarly, the balance equation for the solid mass can be written as

$$\nabla\cdot(\rho_s(1-n)V_s) + \frac{\partial(\rho_s(1-n))}{\partial t} = 0 \tag{9.2}$$

where V_s is the mass-weighted velocity of the solid due to deformation, ρ_s is the density of the solid. By introducing the definition of material derivative with respect to the moving solid particles $D_s(\ )/Dt$, and assuming that the solid's density is constant, equation (9.2) can be expressed by (Bear and Corapcioglu, 1981)

$$\nabla\cdot V_s = \frac{1}{1-n}\frac{D_s(1-n)}{Dt} \tag{9.3}$$

The mass balance equation for the fluid phase can be rewritten in a different form by making use of equation (9.3) (Bear and Corapcioglu, 1981).

$$\rho_f\nabla\cdot n(V_f - V_s) + n\frac{D_f\rho_f}{Dt} + \rho_f\frac{D_s n}{Dt} + \rho_f n\nabla\cdot V_s = 0 \tag{9.3a}$$

where $D_f(\ )/Dt$ is the material derivative with respect to an observer moving with the fluid.

9.2. Momentum balance equations for the fluid and solid phases

Macroscopic momentum balance equations for the fluid can be obtained by neglecting certain dispersive terms in the averaging process, in the form (Bear and Bachmat, 1984)

$$n\rho_f\frac{D_f V_f}{D_t} = \nabla\cdot n\sigma_f + n\rho_f F + \frac{1}{U_0}\int_{S_{fs}} \sigma_f.v_f\, dS \tag{9.4}$$

Similarly, for the solid matrix

$$(1-n)\rho_s\frac{D_s V_s}{D_t} = \nabla\cdot(1-n)\sigma_s + (1-n)\rho_s F + \frac{1}{U_0}\int_{S_{fs}} \sigma_s.v_s\, dS \tag{9.5}$$

where σ_f and σ_s are the stress tensors in the fluid and solid phases, respectively, F is the body force per unit mass, equal to the gravitational acceleration $g(= -g\nabla z)$ where z is the vertical coordinate, U_0 is the volume of a representative elementary volume, S_{fs} is the contact area between the solid and fluid phases within the representative elementary volume and n_f and n_s are the unit outward vectors on the interphase boundaries between them. The terms on the left hand side of equations (9.4) and (9.5) represent the inertial force per unit volume. The first two terms on the right hand side represent the stress and the body forces, respectively. The last terms in equations (9.4) and (9.5), represent the interfacial momentum transfer from the fluid phase to the solid phase and vice-versa. Their sum should vanish.

By adding equations (9.4) and (9.5), we obtain the momentum balance equation for the porous medium as a whole

$$n\rho_f \frac{D_f V_f}{Dt} + (1-n)\rho_s \frac{D_s V_s}{Dt} = \nabla\cdot\sigma + [n\rho_f + (1-n)\rho_s]g\nabla z \tag{9.6}$$

where σ is the total stress tensor, expressed as

$$\sigma = (1-n)\sigma_s + n\sigma_f \tag{9.7}$$

As we noted earlier each solid grain is assumed incompressible. The total stress is related to the effective stress, σ_s', and to the stress in the fluid, σ_f, by

$$\sigma = (1-n)(\sigma_s - \sigma_f) + \sigma_f = \sigma_s' + \sigma_f \tag{9.8}$$

In writing equation (9.8), we assume that solid matrix deformation is caused only by the stress in the solid matrix minus the isotropic effect of the fluid pressure surrounding each grain (e.g., Bear, Corapcioglu and Balakrishna, 1984). In soil mechanics, σ_s' corresponds to Terzaghi's definition of effective stress. When grain compressibility is taken into account, Verruijt (1984) has shown that

$$\sigma = \sigma_s' + (1-\gamma)\sigma_f \tag{9.9}$$

where γ is the ratio between the solid's compressibility and that of the soil. We shall assume that $\gamma \ll 1$.

Since Darcy's law expresses the mass weighted velocity of the fluid relative to the solid

$$n(V_f - V_s) = nV_r = \frac{K}{\mu_f}(\nabla p + \rho_f g\nabla z) \tag{9.9a}$$

It is convenient to rewrite equation (9.6) as

$$n\rho_f \frac{D_r V_r}{Dt} + [(1-n)\rho_s + n\rho_f]\frac{D_s V_s}{Dt} + [V_s{:}\nabla V_s + V_r{:}\nabla V_s]n\rho_f = \nabla\cdot\sigma + [(1-n)\rho_s + n\rho_f]g\nabla' z \tag{9.10}$$

The stress in the fluid phase can be divided into two components, i.e., the viscous shear, τ_f, and the average fluid pressure, p

$$\sigma_f = \tau_f - pI \tag{9.11}$$

where I is the unit tensor. For a Newtonian compressible fluid, the constitutive equation takes the form

$$\tau_f = \mu_f(\nabla V_f + (\nabla V_f)^T) + \lambda_f \nabla\cdot V_f I \tag{9.12}$$

where μ_f and λ_f are the fluid's dynamic and bulk viscosities. For an incompressible Newtonian fluid, the second term on the right hand side can be neglected. Similarly, for an isotropic, perfectly elastic solid matrix, the stress-strain relationship for the solid matrix assumed to take the form

$$\sigma_s' = G(\nabla W + (\nabla W)^T) + \lambda\nabla\cdot W I \tag{9.13}$$

where W is the displacement vector and G (shear modulus) and λ are the Lame constants. Note that by definition

$$V_s = \frac{D_s W}{Dt} \tag{9.13a}$$

Equation (9.12) can be written for an incompressible Newtonian fluid in terms of the relative velocity as

$$\tau_f = \mu_f(\nabla V_r + (\nabla V_r)^T + \nabla V_s + (\nabla V_s)^T) \tag{9.14}$$

The integral that expresses the momentum transfer from the solid to the fluid through their common surface, S_{fs}, per unit volume of porous medium can be expressed as

$$\frac{1}{U_0}\int_{S_{fs}} \tau_f . v_f \, dS = -\mu_f b_f . n V_r \tag{9.15}$$

where b_f is a macroscopic coefficient representing the effect of the microscopic configuration of the S_{fs} surface. It is related to a shape factor and the hydraulic radius of the void space (Bear and Bachmat, 1984). The substitution of equations (11), (14) and (15) into equation (4) yields ?????? where the tortuosity, T_f is a second rank symmetric tensor which is related to the geometric features of the microscopic distribution of the fluid phase in the vicinity of a point (Bear and Bachmat, 1984). If we neglect the effect of internal viscous resistance to the flow in the fluid

$$n\rho_f \frac{D_f V_f}{Dt} - \mu_f \nabla\cdot\{n(\nabla V_r + (\nabla V_r)^T + \nabla V_s + (\nabla V_s)^T)\}$$
$$+ T_f(\nabla p + \rho_f g \nabla z) + \mu_f b_f . n V_r \tag{9.16}$$

(i.e., $\nabla . n t_f = 0$), we obtain

$$\rho_f T_f^{-1} \frac{D_f V_f}{Dt} + \nabla p + \rho_f g \nabla z + n\mu_f K^{-1} V_r = 0 \tag{9.17}$$

where K is the permeability of the porous medium

$$K = n T_f b_f^{-1} \tag{9.18}$$

The momentum balance equation for the saturated porous medium as a whole can be obtained from equation (6) by substituting equations (8) and (11) and by neglecting the effect of internal friction as

$$n\rho_s \frac{D_f V_f}{Dt} + (1-n)\rho_s \frac{D_s V_s}{Dt} = \nabla\cdot\sigma_s' - \nabla p - (n\rho_f + (1-n)\rho_s) g \nabla z \tag{9.19}$$

9.3. Complete set of equations

If we summarize the complete set of three-dimensional governing equations in terms of V_f and V_s (note that $V_r = V_f - V_s$), we can list the following seventeen equations in a three dimensional system

- one mass balance equation for the fluid, equation (9.1) or (9.3a)
- one mass balance equation for the solid, equation (9.2) or (9.3)
- three momentum balance equations for the fluid, equation (9.17)
- three momentum balance equations for the saturated porous medium, equation (9.19)
- three equations defining the solid's velocity, equation (9.13a)
- six constitutive equations for an elastic solid matrix, equation (9.13)

for seventeen unknowns, i.e., three fluid velocities, V_f; three solid velocities, V_s; six effective stress components, σ_s; three displacements, W; porosity, n; and pore fluid pressure, p. Note that so far, we assumed a constant fluid and solid particle densities. If we assume a compressible fluid, then we need an additional constitutive equation to relate ρ_f to p.

As noted by Bear and Corapcioglu (1989), some simplifications can be introduced to the general formulation to show the derivation of various well-known equations. For example, if we neglect the inertial terms in equation (9.16), we obtain Darcy's law. Equilibrium equations satisfying the total stress field can be obtained from equation (9.19) by dropping the inertial terms. The resulting set of equations obtained by deleting the inertial terms in equations (9.17) and (9.19), constitutes the three-dimensional consolidation model of Biot (1941). This corresponds to "very slow phenomena" where all acceleration forces can be neglected (Zienkiewicz and Bettess, 1982c). "Very rapid phenomena" occur when the permeability becomes very small. Zienkiewicz and Bettess consider a case in which the acceleration in the fluid is neglected ("medium speed phenomena) (see Section 3.3). In this case, we define the fluid velocity V_f in terms of a fluid displacement W_f, $V_f = \partial W_f / \partial t$ by neglecting the convective term in the material derivative $D_f W_f / Dt$.

10. Wave propagation in fractured porous media saturated by two immiscible fluids

The single-porosity models are shown to be fairly successful to describe the behavior of porous materials. However, they are not suitable for fractured (or fissured) porous materials. In such systems, although most of the fluid mass is stored in the pores, the fracture permeability is much higher than the permeability of the pores. This leads to two distinct pressure fields: one in the fractures and the other in the pores. Barenblatt et al. (1960) appear to be the first researchers proposing a double-porosity model to represent naturally fractured porous media. A double-porosity model can be considered as a three phase system, i.e., solid

phase, fluid phase in the pores and fluid phase in the fractures, with fluid mass exchange between the pores and fractures.

Although flow in fractured porous media has been studied extensively (e.g., Barenblatt et al., 1960; Barenblatt, 1963; Bear and Berkowitz, 1987), there is limited work in deformable fractured porous media. Duguid and Lee (1977) considered incompressible solid grains and used double-porosity concept in the formulation. They simplified the governing equations by neglecting solid displacement from the flow equations and used the finite element method for numerical analysis. Aifantis and his co-workers published a series of papers on consolidation of saturated fractured porous media (Wilson and Aifantis, 1982; Beskos and Aifantis, 1986; Khaled et al. 1984). The final set of equations is a direct generalization of Biot's consolidation theory. The phenomenological coefficients of the theory were expressed in terms of measurable quantities by Wilson and Aifantis (1982). Uniqueness and some general solutions were presented by Beskos and Aifantis (1986). Khaled et al. (1984) employed the finite element method to solve the governing equations for some practical problems. They reduced the number of coefficients from fifteen to nine by simply "physically motivated arguments". Wilson and Aifantis (1984) extended Aifantis' work and studied wave propagation in saturated fractured porous media without detailed derivations. Their analysis showed three compressional waves. Similar results were obtained by Beskos who published a series of papers on the dynamics of fissured rocks (Beskos, 1989; Beskos et al. 1989a; Beskos et al., 1989b). Beskos (1989) assumed that the medium is linearly elastic. However, the effect of fluid pressure on the deformation of matrix was not considered. Beskos connected this to the definition of partial stresses. But when we assume that there is no relative movement between solid and fluid phases, Beskos' equation for the deformation of solid phase uncouples from fluid pressures. Bear and Berkowitz (1987) suggested a set of constitutive relations to model quasi-static behavior of fractured porous media. They assumed that the changes in the volume fraction of pores and fractures are linear functions of incremental pressures.

Tuncay and Corapcioglu (1996a) presented a theory of wave propagation in fractured porous media based on the double-porosity concept. The macroscopic constitutive relations, and mass and momentum balance equations were obtained by volume averaging the micro-scale balance and constitutive equations and assuming small deformations. In micro-scale the grains were assumed to be linearly elastic and the fluids are Newtonian. Momentum transfer terms were expressed in terms of intrinsic and relative permeabilities assuming the validity of Darcy's law in fractured porous media. The macroscopic constitutive relations of elastic porous media saturated by one or two fluids and saturated fractured porous media were obtained from the constitutive relations they developed. The macroscopic constitutive relations contain the bulk modulus of the fractured porous medium, bulk modulus of the nonfractured medium, bulk modulus of the solid grains and shear modulus of the solid matrix. The capillary pressure effects were taken into account by assuming the validity of the relationship between capillary pressure and saturation. The momentum transfer terms are expressed in terms of intrinsic

and relative permeabilities as a first order approximation. The final set of equations has an hyperbolic behavior with dissipation due to interaction terms. In the simplest case, the final set of governing equations reduce to Biot's equations containing the same parameters as of Biot and Willis (1957).

In their derivation, Tuncay and Corapcioglu (1996a) assumed immiscible fluid phases at rest. Furthermore, the solid phase is assumed to be isotropic, experiencing small deformations and providing all shear resistance of the porous medium. Momentum transfer terms are expressed in terms of intrinsic and relative permeabilities assuming the validity of Darcy's law in fractured porous media. The theory is limited to low frequency wave propagation. The medium is assumed to have fractures which are referred as secondary pores. The pores of the nonfractured part of the porous medium are referred as primary pores. The secondary pores are saturated by wetting fluid whereas the primary pores are saturated by wetting and non-wetting fluids. The mass transfer between the primary pores and secondary pores per unit volume is approximated by (Tuncay and Corapcioglu, 1996b)

$$\frac{1}{V}\int_{S_{2f}} \rho_2(u - v_2)\cdot n_2 dA = -\frac{1}{V}\int_{S_{f2}} \rho_2(u - v_f)\cdot n_f dA = R\rho_2(\bar{P}_f - \bar{P}_2) \tag{10.1}$$

where R is a material property of the porous medium and the wetting fluid, $\bar{P}_2$ and $\bar{P}_f$ are the pressures in fluid phase 2 and phase f, respectively. From now on, subscripts s, 1, 2 and f will refer to the solid phase, non-wetting phase, wetting phase in the primary pores, and the fluid phase in the fractures, respectively. Barenblatt et al. (1960) proposed R as

$$R = \frac{cK_f A^2}{\mu_2} \tag{10.2}$$

where A is the area of fracture-block contact per unit volume, c denotes a dimensionless shape factor of the fractured medium and K_f is the permeability of the fractures. The macroscopic constitutive relations were obtained as

$$\alpha_s \bar{\tau}_s = \left(a_{11}\nabla\cdot\bar{u}_s + a_{12}\nabla\cdot\bar{u}_1 + a_{13}\nabla\cdot\bar{u}_2 + a_{14}\nabla\cdot\bar{u}_f + \left(\frac{a_{14}}{\alpha_f} - \frac{a_{13}}{\alpha_2}\right)M\right)I + G_{fr}\left(\nabla\bar{u}_s + (\nabla\bar{u}_s)^T - \frac{2}{3}\nabla\cdot\bar{u}_s\right) \tag{10.3}$$

$$\alpha_1\bar{P}_1 = a_{21} + a_{22}\nabla\cdot\bar{u}_s\nabla\cdot\bar{u}_1 + a_{23}\nabla\cdot\bar{u}_2 + a_{24}\nabla\cdot\bar{u}_f + \left(\frac{a_{24}}{\alpha_f} - \frac{a_{23}}{\alpha_2}\right)M \tag{10.4}$$

$$\alpha_2\bar{P}_2 = a_{31}\nabla\cdot\bar{u}_s + a_{32}\nabla\cdot\bar{u}_1 + a_{33}\nabla\cdot\bar{u}_2 + a_{34}\nabla\cdot\bar{u}_f + \left(\frac{a_{34}}{\alpha_f} - \frac{a_{33}}{\alpha_2}\right)M \tag{10.5}$$

$$\alpha_f\bar{P}_f = a_{41}\nabla\cdot\bar{u}_s + a_{42}\nabla\cdot\bar{u}_1 + a_{43}\nabla\cdot\bar{u}_2 + a_{44}\nabla\cdot\bar{u}_f + \left(\frac{a_{44}}{\alpha_f} - \frac{a_{43}}{\alpha_2}\right)M \tag{10.6}$$

The reader is referred to Tuncay and Corapcioglu (1995a) for expressions of a_{ij}

in terms of material parameters: K_s, *bulk modulus of the solid grains*; K_{fr}, *bulk modulus of the fractured porous medium*; K_{fr}^{m}, bulk modulus of the nonfractured porous medium; α_i, volume fraction of phase i; S_1, saturation of the non-wetting fluid phase; K_1, bulk modulus of the non-wetting fluid phase; K_2, bulk modulus of the wetting fluid phase; P'_{cap}, derivative of the capillary pressure-saturation relation with respect to S_1; G_{fr}, shear modulus of the solid matrix and F, a material propertiy associated with the changes in volume fraction of fractures. M is given by

$$\frac{\partial M}{\partial t} = R(\bar{P}_f - \bar{P}_2) \tag{10.7}$$

We note that $\rho_2 \, \partial M/\partial t$ is equal to the mass transfer rate of wetting fluid phase between the primary pores and fractures. The volume averaged momentum balance equations are obtained as

$$\begin{aligned}\langle \rho_s \rangle \frac{\partial^2 \bar{u}_s}{\partial t^2} = \nabla\Bigg(&\left(a_{11} + \frac{G_{fr}}{3}\right)\nabla \cdot \bar{u}_s + a_{12}\nabla \cdot \bar{u}_1 + a_{13}\nabla \cdot \bar{u}_2 + a_{14}\nabla \cdot \bar{u}_f \\ &+ \left(\frac{a_{14}}{\alpha_f} - \frac{a_{13}}{\alpha_2}\right)M\Bigg) + \nabla \cdot (G_{fr}\nabla \bar{u}_s) + C_1(\bar{v}_1 - \bar{v}_s) \\ &+ C_2(\bar{v}_2 - \bar{v}_s) + C_3(\bar{v}_f - \bar{v}_s)\end{aligned} \tag{10.8}$$

$$\begin{aligned}\langle \rho_1 \rangle \frac{\partial^2 \bar{u}_1}{\partial t^2} = \nabla\Bigg(&a_{21}\nabla \cdot \bar{u}_s + a_{22}\nabla \cdot \bar{u}_1 + a_{23}\nabla \cdot \bar{u}_2 + a_{24}\nabla \cdot \bar{u}_f \\ &+ \left(\frac{a_{24}}{\alpha_f} - \frac{a_{23}}{\alpha_2}\right)M\Bigg) - C_1(\bar{v}_1 - \bar{v}_s)\end{aligned} \tag{10.9}$$

$$\begin{aligned}\langle \rho_2 \rangle \frac{\partial^2 \bar{u}_2}{\partial t^2} = \nabla\Bigg(&a_{31}\nabla \cdot \bar{u}_s + a_{32}\nabla \cdot \bar{u}_1 + a_{33}\nabla \cdot \bar{u}_2 + a_{34}\nabla \cdot \bar{u}_f + \left(\frac{a_{34}}{\alpha_f} - \frac{a_{33}}{\alpha_2}\right)M\Bigg) \\ &- C_1(\bar{v}_2 - \bar{v}_s)\end{aligned} \tag{10.10}$$

$$\begin{aligned}\langle \rho_f \rangle \frac{\partial^2 \bar{u}_f}{\partial t^2} = \nabla\Bigg(&a_{41}\nabla \cdot \bar{u}_s + a_{42}\nabla \cdot \bar{u}_1 + a_{43}\nabla \cdot \bar{u}_2 + a_{44}\nabla \cdot \bar{u}_f + \left(\frac{a_{44}}{\alpha_f} - \frac{a_{43}}{\alpha_2}\right)M\Bigg) \\ &- C_3(\bar{v}_f - \bar{v}_s)\end{aligned} \tag{10.11}$$

where

$$C_1 = \frac{(1 - \alpha_s - \alpha_f)^2 S_1^2 \mu_1}{K_p k_{r1}} \tag{10.12}$$

$$C_2 = \frac{(1 - \alpha_s - \alpha_f)^2 (1 - S_1)^2 \mu_2}{K_p k_{r2}} \tag{10.13}$$

$$C_3 = \frac{\alpha_f^2 \mu_2}{K_f} \tag{10.14}$$

In equations (10.13)–(10.14), K_p is the intrinsic permeability of the nonfractured porous medium and k_{ri} is the relative permeability of phase i, K_f is the intrinsic permeability of the fractures and μ_i is the viscosity of phase i. Equations (10.5)–(10.11) form the final set of fifteen equations with fifteen unknowns $\bar{u}_s$, $\bar{u}_1$, $\bar{u}_2$, $\bar{u}_f$, $\bar{P}_f$, $\bar{P}_2$ and M (twelve displacements, two pressures and M).

10.1. Compressional waves

To investigate compressional waves, we apply divergence to equations (10.8)–(10.11) to obtain

$$\langle \rho_s \rangle \frac{\partial^2 \epsilon_s}{\partial t^2} = a_{11}^* \nabla^2 \epsilon_s + a_{12} \nabla^2 \epsilon_1 + a_{13} \nabla^2 \epsilon_2 + a_{14} \nabla^2 \epsilon_f + \left(\frac{a_{14}}{\alpha_f} - \frac{a_{13}}{\alpha_2} \right) \nabla^2 M + C_1 \left(\frac{\partial \epsilon_1}{\partial t} - \frac{\partial \epsilon_s}{\partial t} \right) + C_2 \left(\frac{\partial \epsilon_2}{\partial t} - \frac{\partial \epsilon_s}{\partial t} \right) + C_3 \left(\frac{\partial \epsilon_f}{\partial t} - \frac{\partial \epsilon_s}{\partial t} \right) \tag{10.15}$$

$$\langle \rho_1 \rangle \frac{\partial^2 \epsilon_1}{\partial t^2} = a_{21} \nabla^2 \epsilon_s + a_{22} \nabla^2 \epsilon_1 + a_{23} \nabla^2 \epsilon_2 + a_{24} \nabla^2 \epsilon_f + \left(\frac{a_{24}}{\alpha_f} - \frac{a_{23}}{\alpha_2} \right) \nabla^2 M - C_1 \left(\frac{\partial \epsilon_1}{\partial t} - \frac{\partial \epsilon_s}{\partial t} \right) \tag{10.16}$$

$$\langle \rho_2 \rangle \frac{\partial^2 \epsilon_2}{\partial t^2} = a_{31} \nabla^2 \epsilon_s + a_{32} \nabla^2 \epsilon_1 + a_{33} \nabla^2 \epsilon_2 + a_{34} \nabla^2 \epsilon_f + \left(\frac{a_{34}}{\alpha_f} - \frac{a_{33}}{\alpha_2} \right) \nabla^2 M - C_2 \left(\frac{\partial \epsilon_2}{\partial t} - \frac{\partial \epsilon_s}{\partial t} \right) \tag{10.17}$$

$$\langle \rho_f \rangle \frac{\partial^2 \epsilon_f}{\partial t^2} = a_{41} \nabla^2 \epsilon_s + a_{42} \nabla^2 \epsilon_1 + a_{43} \nabla^2 \epsilon_2 + a_{44} \nabla^2 \epsilon_f + \left(\frac{a_{44}}{\alpha_f} - \frac{a_{43}}{\alpha_2} \right) \nabla^2 M - C_3 \left(\frac{\partial \epsilon_f}{\partial t} - \frac{\partial \epsilon_s}{\partial t} \right) \tag{10.18}$$

where $\epsilon_j = \nabla \cdot \bar{u}_j$ and $a_{11}^* = a_{11} + 4G_{fr}/3$. We state the dilatational plane harmonic waves propagating along the z direction by

$$\begin{aligned} \epsilon_j &= B_j e^{i(\xi z - \omega t)} \\ M &= B_m e^{i(\xi z - \omega t)} \\ P_f &= A_j e^{i(\xi z - \omega t)} \\ P_p &= A_p e^{i(\xi z - \omega t)} \end{aligned} \tag{10.19}$$

where B_j, B_m, A_f and A_p are the wave amplitudes, ξ is the wave number, ω is

the frequency and i is the imaginary number. The phase velocity is defined as $c = \omega/\xi_r$ where ξ_r is the real part of the wave number. The imaginary part of ξ is called the attenuation coefficient. Substitution of equation (10.19) in equations (10.5)–(10.11) yields a set of homogeneous algebraic equations and for non-trivial solution the determinant of the coefficient matrix must be equal to zero. The reader is referred to Corapcioglu and Tuncay (1996b) for an expression of the coefficient matrix. For a given ω, the determinant of the coefficient matrix equates to zero, and is known as the "dispersion equation" in wave mechanics literature. It is an eighth order polynomial in terms of wave number. The polynomial contains only the even powers of the wave number. Because the amplitude of the waves should decrease as they propagate, imaginary part of the wave number must be greater than zero. This implies the existence of four compressional waves. When $M = 0$, i.e., no mass exchange between the porous blocks and fractures, the number of unknowns reduce to twelve ($\bar{u}_s$, $\bar{u}_1$, $\bar{u}_2$ and $\bar{u}_f$) and the coefficient matrix reduces to a four by four matrix.

10.2. Rotational waves

To investigate the rotational waves, we apply curl operator to equations (10.8)–(10.11)

$$\langle \rho_s \rangle \frac{\partial^2 \Omega_s}{\partial t^2} = G_{fr} \nabla^2 \Omega_s + C_1 \left(\frac{\partial \Omega_1}{\partial t} - \frac{\partial \Omega_s}{\partial t} \right) + C_2 \left(\frac{\partial \Omega_2}{\partial t} - \frac{\partial \Omega_s}{\partial t} \right) + C_3 \left(\frac{\partial \Omega_f}{\partial t} - \frac{\partial \Omega_s}{\partial t} \right) \tag{10.20}$$

$$\langle \rho_1 \rangle \frac{\partial^2 \Omega_1}{\partial t^2} = -C_1 \left(\frac{\partial \Omega_1}{\partial t} - \frac{\partial \Omega_s}{\partial t} \right) \tag{10.21}$$

$$\langle \rho_2 \rangle \frac{\partial^2 \Omega_2}{\partial t^2} = -C_2 \left(\frac{\partial \Omega_2}{\partial t} - \frac{\partial \Omega_s}{\partial t} \right) \tag{10.22}$$

$$\langle \rho_f \rangle \frac{\partial^2 \Omega_f}{\partial t^2} = -C_3 \left(\frac{\partial \Omega_f}{\partial t} - \frac{\partial \Omega_s}{\partial t} \right) \tag{10.23}$$

where $\Omega_j = \nabla \times \bar{u}_j$.

10.3. Results

Tuncay and Corapcioglu (1996b) solved the governing equations in terms of wave number for a given frequency. The phase velocity is defined as $c = \omega/\xi_r$ where ξ_r is the real part of the wave number. The imaginary part of ξ is called the attenuation coefficient. Van Genuchten's (1980) closed form expressions for the capillary pressure-saturation relations are employed to obtain P'_{cap} which appear in a_{ij} expressions. Van Genuchten proposed that

$$\frac{S_2 - S_{r2}}{S_{m2} - S_{r2}} = \left(1 + \left(\frac{\alpha P_{cap}}{100}\right)^{n}\right)^{-m} \tag{10.24}$$

where P_{cap} is the capillary pressure (N/m^2), S_2 is the water saturation, S_{r2} is the irreducible water saturation, S_{m2} is the upper limit of water saturation, $m = 1 - 1/n$, and α and n are parameters.

From now on, we represent the compressional waves by "*P*" and rotational wave by "*S*". Since there are four compressional waves, we will number them according to the magnitude of their phase velocity, P1 being the fastest. Tuncay and Corapcioglu showed the existence of four compressional and one rotational waves. The fastest wave (P1) is analogous to Biot's fast wave. The second wave (P2) arises because of the fluid phase in the fractures and it vanishes when the medium is not fractured. The third compressional wave (P3) corresponds to the slow wave of Biot's theory. The fourth compressional wave (P4) is due to the second fluid phase (non-wetting fluid) in the primary pores. The second, third and fourth compressional waves disappear when the frequency approaches zero and are associated with diffusive-type processes i.e., highly attenuated. The rotational wave (*S*) is analogous to the rotational wave in elastic solids. All waves are dispersed and attenuated. Especially, the second, third and fourth compressional waves are highly attenuated. Because of the high attenuation, an experimental confirmation of these waves can be very difficult. Tuncay and Corapcioglu (1996b) numerically examined the frequency, saturation, volume fraction of fractures dependence of phase velocity and attenuation coefficient of body waves. The third and fourth compressional waves do not depend on the volume fraction of fractures. The phase velocities of the first compressional and rotational waves slightly change due to the volume fraction of fractures. However, Tuncay and Corapcioglu (1996b) observed a change in the order of magnitude of the attenuation coefficients of the first compressional and rotational waves due to the presence of the fractures. This can be explained by the high intrinsic permeability of the fractures.

References

Aifantis, E.C., 1979. On the response of fissured rocks. Proc. 16th Mid-western Mechanics Conf., Vol. 10, Kansas State Univ., Manhattan, Kansas, pp. 249–253.

Akbar, N., Dvorkin, J., and Nur, A., 1993. Relating P-wave attenuation to permeability. Geophysics, 58: 20–29.

Albert, D.G., 1993. A comparison between wave propagation in water-saturated and air-saturated porous materials. J. Appl. Phys., 73: 28–36.

Allen, N.F., Richart, F.E., and Woods, R.D., 1980. Fluid wave propagation in saturated and nearly saturated sands. J. Geotech. Eng., ASCE, 106: 235–254.

Anderson, T.B. and Jackson, R., 1967. A fluid mechnical description of fluidized beds. I&EC Fundamentals, 6: 527–539.

Attenborough, K. and Chen, Y., 1990. Surface waves at an interface between air and air-filled poroelastic ground. J. Acoust. Soc. Am., 87: 1010–1016.

Auriault, J.L., 1980. Dynamic behaviour of a porous medium saturated by a Newtonian fluid. Int. J. Engng. Sci., 18: 775–785.

Auriault, J.L., Borne, L., and Chambon, R., 1985. Dynamics of porous saturated media, checking of the generalized law of Darcy. J. Acoust. Soc. Am., 77: 1641–1650.

Auriault, J.L., Lebaique, O., and Bonnet, G., 1989. Dynamics of two immiscible fluids flowing through deformable porous media. Transport in Porous Media, 4: 105–128.

Baer, M.R., 1988. Numerical studies of dynamic compaction of inert and energetic granular material. J. Appl. Mech., 55: 36–43.

Baer, M.R. and Nunziato, J.W., 1986. A two-phase mixture theory for the deflagration to detonation transition (DDT) in reactive granular materials. Int. J. Multiphase Flow, 12: 861–889.

Barenblatt, G.I., Zheltow, I.P., and Kochina, T.N., 1960. Basic concepts in the theory of seepage of homogeneous liquids in fissured rocks. J. Appl. Math. Mech., 24: 1286–1303.

Barenblatt, G.I., 1963. On certain boundary value problems for the equations of seepage of a liquid in fissured rocks. J. Appl. Math. Mech., 27: 513–518.

Basak, P., and Madhav, M.R., 1978. Effect of the inertia term in one-dimensional fluid flow in deformable porous media. J. Hydrology, 38: 139–146.

Bazant, Z.P., and Krizek, R.J., 1975. Saturated sand as an inelastic two-phase medium. J. Eng. Mech., ASCE, 101: 317–332.

Bazant, Z.P., and Krizek, R.J., 1976. Endochronic constitutive law for liquefaction of sand. J. Eng. Mech. ASCE, 102: 225–238.

Bazant, Z.P., Ansal, A.M., and Krizek, R.J., 1982. Endochronic models for soils. In: G.N. Pande and O.C. Zienkiewicz (Editors), Soil Mechanics and Cyclic Loads. Wiley, Somerset, N.J., pp. 419–428.

Bear, J. and Bachmat, Y., 1984. Transport phenomena in porous media–basic equation. In: J. Bear and M.Y. Corapcioglu (Editors), Fundamentals of Transport Phenomena in Porous Media. Martinus Nijhoff, Dordrecht, The Netherlands, pp. 3–61.

Bear, J. and Berkowitz, B., 1987. Groundwater flow and pollution in fractured rock aquifers. In: P. Novak (Editor), Developments in Hydraulic Engineering. Elsevier Applied Science, New York, N.Y., pp. 175–238.

Bear, J. and Corapcioglu, M.Y., 1981. Mathematical model for regional land subsidence due to pumping, I. Integrated aquifer subsidence equations based on vertical displacement only. Water Resour. Research, 17: 937–946.

Bear, J., Corapcioglu, M. Y., and Balakrishna, J., 1984. Modeling of centrifugal filtration in unsaturated deformable porous media. Adv. Water Resources, 7: 150–167.

Bear, J. and Corapcioglu, M.Y., 1989. Wave propagation in saturated porous media—Governing equations. In: D. Karamanlidis and R.B. Stout (Editors), Wave Propagation in Granular Media. ASME, New York, N.Y., 91–94.

Bedford, A. and Drumheller, D.S., 1979. A variational theory of porous media. Int. J. Solids Structures, 15: 967–980.

Bedford, A. and Stern, M., 1983. A model for wave propagation in gassy sediments. J. Acoust. Soc. Am., 73: 409–417.

Beebe, J.H., McDaniel, S.T., and Rubano, L.A., 1982. Shallow water transmission loss prediction using the Biot sediment model. J. Acous. Soc. Am., 71: 1417–1426.

Beranek, L.L., 1947. Acoustical properties of homogeneous, isotropic rigid tiles and flexible blankets. J. Acoust. Soc. Am., 19: 556–568.

Berryman, J.G., 1980a. Confirmation of Biot's theory. Appl. Phys. Lett., 37: 382–384.

Berryman, J.G., 1980b. Long wave length propagation of composite elastic media. J. Acoust. Soc. Am., 68: 1809–1831.

Berryman, J.G., 1981a. Elastic wave propagation in fluid-saturated porous media. J. Acoust. Soc. Am., 69: 416–424.

Berryman, J.G., 1981b. Elastic wave propagation in fluid-saturated porous media II. J. Acoust. Soc. Am., 69: 1754–1756.

Berryman, J.G., 1985. Scattering by a spherical inhomogeneity in fluid saturated porous medium. J. Math. Phys., 26: 1408–1419.

Berryman, J.G., 1986. Elastic wave attenuation in rocks containing fluids. Appl. Phys. Lett., 49: 552–554.

Berryman, J.G., 1986a. Effective medium approximation for elastic constants of porous solids with microscopic heterogeneity. J. Appl. Phys., 59: 1136–1140.

Berryman, J.G., 1986b. Elastic wave attenuation in rocks containing fluids. Appl. Phys. Lett., 49: 552–554.

Berryman, J.G., 1988. Seismic wave attenuation in fluid saturated porous media. Pageoph, 128: 423–432.

Berryman, J.G. and Milton, G.W., 1985. Normalization constraint for variational bounds on fluid permeability. J. Chem. Phys., 83: 754–760.

Berryman, J.G. and Thigpen, L., 1985a. Effective constants for wave propagation through partially saturated porous media. Appl. Phys. Lett., 46: 722–724.

Berryman, J.G. and Thigpen, L., 1985b. Effective medium theory for partially saturated porous solids. In: Multiple Scattering of Waves in Random Media and Random Rough Surfaces. Penn. St. Univ., College Park, P.A., pp. 257–266.

Berryman, J.G. and Thigpen, L., 1985c. Linear dynamic poroelasticity with microstructure for partially saturated porous solids. J. Appl. Mech., 52: 345–350.

Berryman, J.G. and Thigpen, L., 1985d. Nonlinear and semilinear dynamic poroelasticity with microstructure. J. Mech. Phys. Solids, 33: 97–116.

Berryman, J.G., Thigpen, L., and Chin, R.C.Y., 1988. Bulk elastic wave propagation in partially saturated porous solids. J. Acoust. Soc. Am., 84: 360–373.

Beskos, D.E., 1989. Dynamics of saturated rocks, I: Equations of motion. J. Eng. Mech., ASCE, 115: 983–995.

Beskos, D.E. and Aifantis, E.C., (1986), 'On the theory of consolidation with double porosity. Int. J. Engng. Sci., 24: 1697–1716.

Beskos, D.E., Vgenopoulou, I., and Providakis, C.P., 1989a. Dynamics of Saturated rocks II: Body forces. J. Eng. Mech., ASCE, 115: 996–1016.

Beskos, D.E., Papadakis, C.N., and Woo, H.S., 1989b. Dynamics of saturated rocks, III: Rayleigh waves. J. Eng. Mech., ASCE, 115: 1017–1034.

Biot, M.A., 1941. General theory of three-dimensional consolidation. J. Appl. Physics, 12: 155–164.

Biot, M.A., 1956a. Theory of propagation of elastic wave in a fluid saturated porous solid, I. Low frequency range. J. Acoust. Soc. Am., 28: 168–178.

Biot, M.A., 1956b. Theory of propagation elastic waves in a fluid saturated porous solid, II. Higher frequency range. J. Acoust. Soc. Am., 28: 169–191.

Biot, M.A., 1962a. Mechanics of deformation and acoustic propagation in porous media. J. Appl. Phys., 33: 1482–1498.

Biot, M.A., 1962b. Generalized theory of acoustic propagation in porous dissipative media. J. Acoust. Soc. Am., 34: 1254–1264.

Biot, M.A. and Willis, D.G., 1957. The elastic coefficients of the theory of consolidation. J. Appl. Mech., 24: 594–601.

Bonnet, G., 1987. Basic singular solutions and boundary integral equations for a poroelastic medium in the dynamic range. J. Acoust. Soc., Am., 82: 1758–1762.

Bougacha, S., Tassoulas, J.L., and Roesset, J.M., 1993b. Analysis of foundations on fluid-filled poroelastic stratum. J. Eng. Mech., ASCE, 119: 1632–1648.

Bougacha, S., Roesset, J.M., and Tassoulas, J.L., 1993a. Dynamic stiffness of foundations on fluid-filled poroelastic stratum. J. Eng. Mech., ASCE, 119: 1649–1662.

Bougacha, S. and Tassoulas, J.L., 1991. Seismic analysis of gravity dams I: modelling of sediments. J. Eng. Mech., ASCE, 117: 1826–1837.

Boutin, C., Bonnet, G., and Bard, P.Y., 1987. Green functions and associated sources in infinite and stratified poroelastic media. Geophys. J. R. Astr. Soc., 90: 521–550.

Bowen, R.M., 1976. The theory of mixtures. In: A.C. Eringin (Editor), Continuum Physics, Vol. 3. Academic Press, New York, N.Y.

Bowen, R.M., 1980. Incompressible porous media models by use of the theory of mixtures. Int. J. Engng. Sci., 18: 1129–1148.

Bowen, R.M., 1982. Compressible porous media models by use of the theory of mixtures. Int. J. Engng. Sci., 20: 697–735.

Bowen, R.M., and Lockett, R.R., 1983. Inertial effects in poroelasticity. J. Appl. Mech., 50: 334–342.

Bowen, R.M. and Reinicke, K.M., 1978. Plane progressive waves in a binary mixture of linear elastic materials. J. Appl. Mech., 45: 493–499.

Brandt, H., 1955. A study of the speed of sound in porous granular media. J. Appl. Mech. 22: 479–486.

Brandt, H., 1960. Factors affecting compressional wave velocity in unconsolidated marine sand sediments. J. Acoust. Soc. Am., 32: 171–179.

Briones, A.A. and Vehara, G., 1977. Soil elastic constants: I. Calculations from sound velocities. Soil Sci. Soc. Am. J., 41: 22–25.

Brutsaert, W., 1964. The propagation of elastic waves in unconsolidated unsaturated granular mediums. J. Geophys. Res., 69: 243–257.

Brutsaert, W. and Luthin, J.N., 1964. The velocity of sound in soils near the surface as a function of the moisture content. J. Geophys. Res., 69: 643–652.

Burridge, R. and Vargas, C.A., 1979. The fundamental solution in dynamic poroelasticity. Geophys. J.R. Am. Soc., 58: 61–90.

Burridge, R. and Keller, J.B., 1981. Poroelasticity equations derived from microstructure. J. Acoust. Soc. Am., 70: 1140–1146.

Butcher, B.M., Carroll, M.M., and Holt, A.C., 1974. Shock wave compaction of porous aluminum. J. Appl. Phys., 45: 3864–3875.

Carroll, M.M. and Holt, A.C., 1972. Static and dynamic pore collapse relations for ductile porous materials. J. Appl. Phys., 43: 1626–1635.

Chang, Y., Kabir, M.G., and Chang, Y., 1993. Micromechanics modeling for stress-strain behavior of granular soils I: Evaluation. J. Geotech. Eng., ASCE, 118: 1975–1992.

Chattopadhyay, A. and De, R.K., 1983. Love type waves in a porous layer with irregular interface. Int. J. Engng. Sci., 21: 1295–1303.

Chen, A.H.D., 1986. Effect of sediment on earthquake induced reservoir hydrodynamic response. J. Engng. Mech., ASCE, 112: 654–663.

Cheng, A.H.D., Badmus, T., and Beskos, D.E., 1991. Integral equation for dynamic poroelasticity in frequency domain with BEM solution. J. Eng. Mech., ASCE, 1136–1157.

Ching, C.S., Chang, Y., and Kabir, M.G., 1993. Micromechanics modeling for stress-strain behavior of granular soils I. Theory. J. Geotech. Eng., ASCE, 118: 1959–1974.

Cleary, M.P., 1977. Fundamental solutions for a fluid-saturated porous solid. Int. J. Solids Structures, 13: 785–806.

Crochet, N.J. and Naghdi, P.M., 1966. On constitutive equations for flow of fluid through elastic porous media. Int. J. Engng. Sci., 4: 383–401.

Dagan. G., 1979. The generalization of Darcy's law for non-uniform flows. Water Resour. Res., 15: 1–17.

Dalrymple, R.A. and Liu, P.L.F., 1978. Wave over soft muds: A two-layer fluid model. J Phys. Oceanog., 8: 1121–1131.

Dalrymple, R.A. and Liu, P.L.F., 1982. Gravity waves over a poroelastic seabed. ASCE Ocean Structural Dynamics Symposium, Proc., Oregon State University, Corvallis, O.R., pp. 181–195.

de Alba, P., Seed, H.B., and Chan, C.K., 1976. Sand liquefaction in large-scale simple shear tests. J. Geotech. Engng., ASCE, 102: 909–927.

de Boer, R., Ehlers, W., and Liu, Zhangfang, 1993. One-dimensional transient wave propagation in fluid-saturated incompressible porous media. Arc. Appl. Mech., 65: 59–72.

de Josselin de Jong, G., 1956. What happens in soil during pile driving? De Ingenieur, 68: B77–B88.

de la Cruz, V. and Spanos, T.J.T., 1985. Seismic wave propagation in a porous medium. Geophysics, 50: 1556–1565.

de la Cruz, V. and Spanos, T.J.T., 1989. Thermomechanical coupling during seismic wave propagation in a porous medium. J. Geophys. Res., 94: 637–642.

Demars, K.R., 1983. Transient stresses induced in sandbed by wave loading. J. Geotech. Engng., ASCE, 109: 591–602.

Deresiewicz, H., 1960. The effect of boundaries on wave propagation in a liquid-filled porous solid:

I. Reflection of plane waves at a free plane boundary (non-dissipative case). Bull. Seism. Soc. Am., 50: 599–607.

Deresiewicz, H., 1961. The effect of boundaries on wave propagation in a liquid-filled porous solid: II. Love waves in a porous layer. Bull. Seism. Soc. Am., 51: 51–59.

Deresiewicz, H. and Rice J.T., 1962. The effect of boundaries on wave propagation in a liquid-filled porous solid: III. Reflection of plane waves at free plane boundary (general case). Bull. Seism. Soc. Am., 52: 595–625

Deresiewicz, H., 1962. The effect of boundaries on wave propagation in a liquid-filled porous solid: IV. Surface waves in a half-space. Bull. Seism. Soc. Am., 52: 627–638.

Deresiewicz, H. and Rice J.T., 1964. The effect of boundaries on wave propagation in a liquid-filled porous solid: V. Transmission across a plane interface. Bull. Seism. Soc. Am., 54: 409–416.

Deresiewicz, H., 1964a. The effect of boundaries on wave propagation in a liquid-filled porous solid: VI. Love waves in a double surface layer. Bull. Seism. Soc. Am., 54: 417–423.

Deresiewicz, H., 1964b. The effect of boundaries on wave propagation in a liquid-filled porous solid: VII. Surface waves in a half-space in the presence of a liquid layer. Bull. Seism. Soc. Am., 54: 425–430.

Deresiewicz, H. and Wolf, B., 1964. The effect of boundaries on wave propagation in a liquid-filled porous solid: VIII. Reflection of plane waves in an irregular boundary. Bull. Seism. Soc. Am., 54: 1537–1561.

Deresiewicz, H., 1965. The effect of boundaries on wave propagation in a liquid-filled porous solid: IX. Love waves in a porous internal stratum. Bull. Seism. Soc. Am., 55: 919–923.

Deresiewicz, H., and Levy, A., 1967. The effect of boundaries on wave propagation in a liquid-filled porous solid: X. Transmission through a stratified medium. Bull. Seism. Soc. Am., 57: 381–391.

Derski, W., 1978. Equations of motion for a fluid saturated porous solid. Bull. Academia Pol. Sci., 26: 11–16.

Digby, P.J. and Walton, K., 1989. Wave propagation through elastically-anisotropic fluid-saturated porous rocks. J. Appl. Mech., 56: 744–750.

Domenico, S.N., 1974. Effects of water saturation of sand reservoirs encased in shales. Geophysics, 29: 759–769.

Domenico, S.N., 1976. Effect of brine-gas mixture on velocity in an unconsolidated sand reservoir. Geophysics, 41: 882–894.

Drumheller, D.S., 1986. A theory for dynamic compaction of wet porous solids. Int. J. Solids Struct.

Duffy, J. and Mindlin, R.D., 1957. Stress-strain relations and vibration of a granular medium. J. Appl. Mech., 24: 585–593.

Duguid, J.O. and Lee, P.C.Y., 1977. Flow in fractured porous media. Water Resour. Res., 13: 558–566.

Dunn, K.J., 1986. Acoustic attenuation in fluid-saturated porous cylinders at low frequencies. J. Acoust. Soc. Am., 79: 1709–1721.

Dutta, P.K., Farrell, D., Kalafut, J., 1990. A laboratory study of shock waves in frozen soil. In: D.S. Sodhi (Editor), Cold Regions Engineering. Proc. 6th Int. Specs. Conf., ASCE, New York, N.Y., pp. 54–70.

Elliott, S.E. and Wiley, B.F., 1975. Compressional velocities of partially saturated, unconsolidated sands. Geophysics, 40: 949–954.

Fatt, I., 1959. The Biot-Willis elastic coefficients for a sandstone. J. Appl. Mech., 26: 296–297.

Feng, S. and Johnson, D.L., 1983. High-frequency acoustic properties of a fluid/porous solid interface I New surface mode. J. Acoust. Soc. Am., 74: 906–914.

Finjord, J., 1990. A solitary wave in a porous medium. Transport in Porous Media, 5: 591–607.

Finn, W.D.L., Byrne, P.M., and Martin, G.R., 1976. Seismic response and liquefaction of sands. J. Geotech. Engng., ASCE, 102: 841–856.

Finn, W.D.L., Lee, K.W., and Martin, G.R., 1977. An effective stress model for liquefaction. J. Geotech. Engng., ASCE, 103: 517–533.

Finn, W.D.L., Siddharthan, R., and Martin, G.R., 1983. Response of seafloor to ocean waves. J. Geotech. Eng., ASCE, 109: 556–572.

Foda, M.A. and Mei, C.C., 1983. A boundary layer theory for Rayleigh waves in a porous fluid-filled half space. Soil Dyn. Earth. Engng., 2: 62–65.

Garg, S.K., 1971. Wave propagation effects in a fluid saturated porous solid. J. Geophys. Res., 76: 7947–7962.

Garg, S.K., 1987. On balance laws for fluid saturated porous media. Mech. Materials, 6: 219–232.

Garg, S.K. and Kirsch, J.W., 1973. Steady shock waves in composite materials. J. Composite Materials, 7. 277–285.

Garg, S.K., Nayfeh, A.H., and Good, A.J., 1974. Compressional waves in fluid-saturated elastic porous media. J. Appl. Phys., 45: 1968–1974.

Garg, S.K., Brownell, C.H., Pritchett, and Herrman, R.G., 1975. Shock wave propagation in fluid saturated porous media. J. Appl. Phys., 46: 702–713.

Garg, S.K. and Nayfeh, A.H., 1986. Compressional wave propagation in liquid and/or gas saturated elastic porous media. J. Appl. Phys., 60: 3045–3055.

Gassman, F., 1951. Elastic waves through a packing of spheres. Geophysics, 16: 673–685.

Geertsma, J., 1957. The effect of fluid pressure decline on volume changes of porous rocks. Trans. Am. Inst. Mining Metallurgical Eng., 210: 331–340.

Geertsma, J., 1974. Estimating the coefficient of inertial resistance in fluid flow through porous media. Soc. Petroleum Eng. J., 257: 445–450.

Geertsma, J. and Smit, D.C., 1961. Some aspects of elastic wave propagation in fluid saturated porous solids. Geophysics, 26: 160–180.

Ghaboussi, J. and Wilson, E.L., 1972. Variational formulation of dynamics of fluid saturated porous elastic solids. J. Engng. Mech., ASCE, 98: 947–963.

Ghaboussi, A.M. and Dikmen, S.U., 1978. Liquefaction analysis of horizontally layered sands. J. Geotech. Eng., ASCE, 104: 341–356.

Ghaboussi, J. and Dikmen, S.U., 1981. Liquefaction analysis for multidirectional shaking. J. Geotech. Engng., ASCE, 107: 605–627.

Ghaboussi, J. and Kim, K.J., 1984. Quasistatic and dynamic analysis of saturated and partially saturated soils. In: C.S. Desai and R.H. Gallagher (Editors), Mechanics of Engineering Materials. Wiley, Somerset, N.J., pp. 277–296.

Gokhale, S.S. and Krier, H., 1982. Modeling of unsteady two-phase reactive flow in porous beds of propellant. Prog. Energy Combust. Sci., 8: 1–39.

Goodman, M.A. and Cowin, S.C., 1972. A continuum theory for granular materials. Arch. Rat. Mech. Anal., 44: 249–266.

Grady, D.E., Moody, R.L., and Drumheller, D.S., 1986. Release equation of state of dry and water saturated porous calcite. Sandia Report SAND 86–2110. Sandia Nat. Lab., Albuquerque, N.M.

Green, A.E., and Naghdi, P.M., 1965. A dynamical theory of interacting continua. Int. J. Engng. Sci., 3: 231–241.

Gregory, A.R., 1976. Fluid saturation effects on dynamic elastic properties of sedimentary rocks. Geophysics, 41: 895–921.

Halpern, M. and Christiano P., 1986a. Response of poroelastic halfspace to steady-state harmonic surface tractions. Int. J. Num. Anal. Meth. Geomech., 10: 609–632.

Halpern, M. and Christiano P., 1986b. Steady-state harmonic response of a rigid plate bearing on a liquid-saturated poroelastic halfspace. Earth. Engrg. Struct. Dyn., 14: 439–454.

Hardin, B.O., 1965. The nature of damping in sands. J. Soil Mech. Found., ASCE, 91: 63–97.

Hardin, B.O. and Richart, F.E., 1963. Elastic wave velocities in granular soils. J. Soil Mech. Found., ASCE, 89: 33–65.

Hermann, W., 1968. Constitutive equation for the dynamic compaction of ductile porous materials. J. Appl. Phys., 40: 2490–2499.

Hassanzadeh, S., 1991. Acoustic modeling in fluid-saturated porous media. Geophysics, 56: 424–435.

Hermann, W., 1972. Constitutive equations for compaction of porous materials. In: Applied Mechanics Aspects of Nuclear Effects in Materials. Sandia Lab., Albuquerque, N.M.

Hiremath, M.S. and Sandhu, R.S., 1984. A computer program for dynamic response of layered saturated sand. Ohio St. Univ., Geotech. Eng. Rep. Columbus, O.H.

Hiremath, M.S., Sandhu, R.S., Morland, L.W., and Wolfe, W.E., 1988. Analysis of one-dimensional wave propagation in a fluid saturated finite soil column. Int. J. Num. and Analy. Meth. Geomech., 12: 121–139.

Holland, C.W. and Brunson, B.A., 1988. The Biot–Stoll sediment model: An experimental assessment. J. Acous. Soc. Am., 84: 1427–1443.

Hong, S.J., Sandhu, R.S., and Wolfe, W.E., 1988. On Garg's solution of Biot's equations for wave propagation in a one-dimensional fluid saturated elastic porous solid. Int. J. Num. Analy. Meth. Geomech., 12: 627–637.

Hovem, J.M., 1980. Viscous attenuation of sound in suspensions and high porosity marine sediment. J. Acoust. Soc. Am., 67: 1559–1573.

Hovem, J.M. and Ingram, G.D., 1979. Viscous attenuation of sound in saturated sand. J. Acoust. Soc. Am., 66: 1807–1812.

Hsieh, L. and Yew, C.H., 1973. Wave motions in a fluid-saturated porous medium. J. Appl. Mech., 40: 873–878.

Iida, K., 1939. The velocity of elastic waves in sand. Bull. Earthquake Research Inst., Japan, 17: 738–808.

Ishihara, K., 1967. Propagation of compressional waves in a saturated soil. In: Proc. Int. Symp. Wave Propagation and Dynamic Properties of Earth Materials. Univ. of New Mexico Press, Albuquerque, N.M., pp. 451–467.

Ishihara, K., 1970. Approximate forms of wave equations for water saturated porous materials and related dynamic modulus. J. Soc. Soil Mech. and Found. Eng., 10: 10–38.

Ishihara, K., Shimizu, K., and Yamada, Y., 1981. Pore water pressures measured in sand deposits during an earthquake. Soils and Foundations (Japan), 21: 85–100.

Ishiara, K. and Towhata, I., 1982. Dynamic response analysis of level ground based on the effective stress method. In: G.N. Pande and O.C. Zienkiewica (Editors), Soil Mechanics—Transient and Cyclic Loads. Wiley, Somerset, N.J., pp. 133–172.

Johnson, D.L., Plona, T., Plona, J., Scala, C., Pasierb, F., and Kojima, H., 1982. Tortuosity and acoustic slow waves. Phys. Rev. Lett., 49: 1840–1844.

Johnson, J.B., 1982. On the application of Biot's theory to acoustic wave propagation in snow. Cold Regions Sci. Tech., 6: 49–60.

Jones, J., 1969. Pulse propagation in a poroelastic solid. J. Appl. Mech., ASME, 36: 878–880.

Jones, J.P., 1961. Rayleigh waves in a porous, elastic, saturated solid. J. Acoust. Soc. Am., 33: 959–962.

Jones, T. and Nur, A., 1983. Velocity and attenuation in sandstone at elevated temperatures and pressures. Geophys. Res. Lett., 10: 140–143.

Kansa, E.J., 1987. A guide to the transient three phase porous flow model implemented in the two-dimensional Cray-tensor code: Physics, numerics, and code description. Lawrence Livermore Nat. Lab. Rep. UCID-21260.

Kansa, E.J., 1989. The response of shocks in unsaturated geological media under a wide range of permeabilities. In: D. Karamanlidis and R.B. Stout (Editors), Wave Propagation in Granular Materials. ASME, New York, N.Y., pp. 95–101.

Kansa, E.J., 1988. Numerical solution of three phase porous flow under shock conditions. Mathl. Comput. Modelling, 11: 180–185.

Kansa, E.J., Kirk, T.M., and Swift, R.P., 1987. Multiphase flow in geological materials: Dynamic loading theory and numerical modeling. In: AIChE Symposium Series 257, Vol. 83, pp. 206–210.

Katsube, N., 1985. The constitutive theory for fluid-filled porous materials. J. Appl. Mech., 52: 185–189.

Katsube, N., and Carroll, M.M., 1987. The modified mixture theory for fluid-filled porous materials., J. Appl. Mech., 54: 35–40.

Khaled, M.Y., Beskos, D.E., and Aifantis, E.C., 1984) On the porosity of consolidation with double porosity – III: A finite element formulation. Int. J. Num. Meth. Eng., 8: 101–123.

Kim, Y.K. and Kingsbury, H.G., 1979. Dynamic characterization of poroelastic materials. Exp. Mech., 252–258.

Klimentos, T. and McCann, C., 1990. Relationships among compressional wave attenuation, porosity, clay content, and permeability in sandstones. Geophysics, 55: 998–1014.

Korringa, J., 1981. On the Biot–Gassman equations for the elastic moduli of porous rocks. (Critical comment on a paper by J.G. Berryman.) J. Acoust. Soc. Am., 70: 1752–1753.

Lebaigue, O.D., Bonnet, G.I., and Auriault, J.D., 1987. Transparency ultrasonic tests on a thin plate

of unsaturated porous medium application to wet paper. Ultrasonics Int. 87 Conf. Proc. London, pp. 635–640.

Levy, T., 1979. Propagation of waves in a fluid-saturated porous elastic solid. Int. J. Engng. Sci., 17: 1005–1014.

Levy, T. and Sanchez-Palencia, E., 1977. Equations and interface conditions for acoustic phenomena in porous media. J. Math. Analy. Applications, 61: 813–834.

Liou, C.P., Streeter, V.L., and Richart, F.E., 1977. Numerical model for liquefaction. J. Geotech. Engng., ASCE, 103: 589–606.

Liu, P.L.F. and Darlrymple, R.A., 1984. The damping of gravity water-waves due to percolation. Coastal Eng., 8: 33–49.

Liu, Q.R. and Katsube, N., 1990. The discovery of a second kind of rotational wave in a fluid-filled porous material. J. Acoust. Soc. Am., 88: 1045–1053.

Loret, B., 1990. Acceleration waves in elastic-plastic porous media: Interlacing and seperation properties. Int. J. Engng. Sci., 28: 1315–1320.

Loret, B. and Pervost, J.H., 1991. Dynamic strain localization in fluid-saturated porous media. J. Eng. Mech., ASCE, 117: 907–922.

Lovera, O.M., 1987. Boundary conditions for a fluid-saturated porous solid. Geophysics, 174–178.

Madsen, O.S., 1978. Wave-induced pore-pressures and effective stresses in a porous bed. Geotechnique, 28: 377–393.

Mann, R.W., 1979. Elastic Wave Propagation in Paper. Ph.D. Dissertation. Lawrence Univ., Appleton, W.I.

Martin, G.R., Finn, W.D.L., and Seed, H.B., 1975. Fundamentals of liquefaction under cyclic loading. J. Geotech. Engng., ASCE, 101: 423–438.

Mansouri, T.A., Nelson, J.D., and Thompson, E.G., 1983. Dynamic response and liquefaction of earth dam. J. Geotech. Eng., ASCE, 109: 89–100.

Massel, S.R., 1976. Gravity waves propagated over permeable beds. J. Waterways, Harbours, and Coastal Eng., ASCE, 102: 11–21.

Mavko, G.M. and Nur, A., 1979. Wave attenuation in partially saturated rocks. Geophysics, 44, 161–178.

McCann, C. and McCann, D.M., 1969. The attenuation of compressional waves in marine sediments. Geophysics, 34: 882–892.

Mei, C.C. and Foda, M.A., 1981. Wave-induced responses in a fluid-filled poro-elastic solid with a free surface–A boundary layer theory. Geophys. J.R. Astr., Soc., 66: 597–631.

Mei, C.C. and Foda, M.A., 1982. Boundary layer theory of waves in a poro-elastic sea bed. In: G.N. Pande and O.C. Zienkiewicz (Editors), Soil Mechanics—Transient and Cyclic Loads. Wiley, Somserset, N.J., pp. 17–35.

Mei, C.C. and Mynett, A.E., 1983. Two-dimensional stresses in a saturated poro-elastic foundation beneath a rigid structure, I. A dam in river. Int. J. Numer. Analy. Meth. Geomech., 7: 57–74.

Mei, C.C., Boon I.S., and Chen, Y.S., 1985. Dynamic response in a poro-elastic ground induced by a moving air pressure. Wave Motion, 7: 129–141.

Misra, H.C., 1965. Permeability of Porous Media to Transient Flow'. Ph.D. thesis, Univ. of Wisconsin, Madison, W.I.

Misra, H.C. and Monkmeyer, P.L., 1966. On the response of sound waves to the permeability of a porous medium. Presented at the 15th An. ASCE Hyd. Div. Conf., Madison, W.I.

Mochizuki, S., 1982. Attenuation in partially saturated rocks. J. Geophysical Res., 87: 8598–8604.

Morland, L.W., 1972. A simple constitutive theory for a fluid-saturated porous solid. J. Geophys. Res., 77: 890–900.

Morland, L.W., Sandhu, R.S., Wolfe, W.C., and Hiremath, M.S., 1987. Wave propagation in a fluid-saturated elastic layer. Geotechnical Eng., Rep. No. 25, Ohio State Univ., Columbus, O.H.

Morland, L.W., Sandhu, R.S., and Wolfe, W.E., 1988. Uni-axial wave propagation through fluid-saturated elastic soil layer. In: G. Swoboda (Editor), Numerical Methods in Geomechanics. Innsbruck, 1988, Balkema, Rotterdam, pp. 213–220.

Morse, R.W., 1952. Acoustic propagation in granular media. J. Acoust. Soc. Am., 24: 696–700.

Moshagen, H. and Torum, A., 1975. Wave induced pressures in permeable seabeds. J. Waterways, Harbours and Coastal Eng., ASCE, 101: 49–57.

Murphy, W.F., 1982. Effects of partial water saturation on attenuation in Massilon sandstone and Vycor porous glass. J. Acoust. Soc., Am., 71: 1458–1468.

Murphy, W.F., 1984. Acoustic measures of partial gas saturation in tight sandstones. J. Geophysical Res., 89: 11549–11559.

Murphy, W.F., Winkler, K.W., and Kleinberg, R.L., 1986. Acoustic relaxation in sedimentary rocks: Dependence on grain contacts and fluid saturation. Geophysics, 51: 757–766.

Mynett, A.E. and Mei, C.C., 1982. Wave-induced stresses in a saturated poro-elastic sea bed beneath a rectangular caisson. Geotechnique, 32: 235–247.

Mynett, A.E. and Mei, C.C., 1983. Earthquake induced stresses in a poro-elastic foundation supporting a rigid structure. Geotechnique, 33: 293–303.

Nagy, P.B., 1993. Slow wave propagation in air-filled permeable solids. J. Acoust. Soc. Am., 93: 3224–3234.

Nataraja, M.S. and Gill, H.S., 1983. Ocean wave-induced liquefaction analysis. J. Geotech. Eng., ASCE, 109: 573–590.

Nikolaevskij, V.N., 1990. Mechanics of Porous and Fractured Media, World Scientific, Singapore.

Nolle, A.W., Hoyer, W.A., Mifsud, J.F., Runyan, W.R., and Ward, M.B., 1963. Acoustical properties of water-filled sands. J. Acoust. Soc. Am., 35: 1394–1408.

Norris, A.N., 1985. Radiation from a point source and scattering theory in a fluid-saturated porous solid. J. Acoust. Soc. Am., 77: 2012–2023.

Norris, A.N., 1993. Low-frequency dispersion and attenuation in partially saturated rocks. J. Acoust. Soc. Am., 94: 359–370.

Nunziato, J.W. and Walsh, E.K., 1977. On the influence of void compaction and material non-uniformity on the propagation of one-dimensional acceleration waves in granular materials. Arch. Rational Mech. Anal., 64: 299–316.

Nunziato, J.W., Kennedy, J.E., and Walsh, E., 1978. The behaviour of one-dimensional acceleration waves in an inhomogeneous granular solid. Int. J. Engng. Sci., 16: 637–648.

Nur, A. and Booker, J.R., 1972. Aftershocks caused by pore fluid flow? Science, 885–887.

Ogushwitz, P.R., 1985. Applicability of the Biot theory: I. Low porosity materials II. Suspensions, III. Wave speeds versus depth in marine sediments. J. Acoust. Soc. Am., 77: 429–464.

Paria, G., 1963. Flow of fluids through porous deformable solids. Appl. Mech. Rev., 16.

Parra, J.O., 1991. Analysis of elastic wave propagation in stratified fluid-filled porous media for interwell seismic applications. J. Acoust. Soc. Am., 90: 2557–2575.

Pascal, H., 1986. Pressure wave propagation in a fluid flowing through a porous medium and problems related to interpretation of Stoneley's wave attenuation in acoustical well logging. Int. J. Engng. Sci., 24: 1553–1570.

Pecker, C. and Deresiewicz, H., 1973. Thermal effects on wave propagation in liquid filled porous media. Acta Mechanica, 16: 45–64.

Philippacopoulos, A.J., 1987. Waves in a partially saturated layered half-space analytic formulation. Bull. Seismological Soc. Amer., 77: 1838–1853.

Plona, T.J., 1980. Observation of a second bulk compressional wave in a porous medium at ultrasonic frequencies. App. Phys. Lett., 36: 259–261.

Plona, T.J. and Johnson, D.L., 1984. Acoustic properties of porous systems: I. Phenomenological description. In: D.L. Johnson and P.N. Sen (Editors), Physics and Chemistry of Porous Media, Vol. 107. American Institute of Physics, New York, N.Y., pp. 89–104.

Powers, J.M., Stewert, D.S., and Krier, H., 1989. Analysis of steady compaction waves in porous materials. J. Appl. Mech., 56: 15–24.

Prassad, M. and Meissner, R., 1992. Attenuations mechanisms in sands: Laboratory versus theoretical Biot data. Geophysics, 57: 710–719.

Predeleanu, M., 1984. Development of boundary element method to dynamic problems for porous media. Appl. Math. Modelling, 8: 378–382.

Prevost, J.H., 1980. Mechanics of continuous porous media. Int. J. Engng. Sci., 18: 787–800.

Prevost, J.H., 1982. Nonlinear transient phenomena in saturated porous media. Computer Meth. in Appl. Mech. Engng., 20: 3–18.

Prevost, J.H., 1984. Non-linear transient phenomena in soil media. In: C.S. Desai and R.H. Gallagher (Editors). Mechanics of Engineering Materials. Wiley, Somerset, N.J., pp. 515–533.

Prevost, J.H., 1985. Wave propagation in fluid-saturated porous media: An efficient finite element procedure. Soil Dynamics Earthquake Eng., 4: 183–202.

Pride, S.R., Gangi, A.F., and Morgan, F.D., 1992. Deriving equations of motion for porous isotropic media. J. Acoust. Soc. Am., 92: 3278–3290.

Putnam, J.A., 1949. Loss of wave energy due to percolation in a permeable sea bottom. Trans. Am. Geophys. Union, 30: 349–366.

Raats, P.A.C., 1969. The effect of a finite response time upon the propagation of sinusoidal oscillations of fluids in porous media. ZAMP, 20: 936–946.

Raats, P.A.C., 1972. The role of inertia in the hydrodynamics of porous media. Arch. Rat. Mech. Analysis, 44: 267–280.

Raats, P.A.C. and Klute, A., 1969. Transport in soils: The balance of momentum. Soil Sci. Soc. Amer. Proc., 32: 452–456.

Rahman, M.S., Seed, H.B., and Booker, J.R., 1977. Pore pressure development under offshore gravity structures. J. Geotech. Engng., ASCE, 103: 1419–1436.

Reid, R.O. and Kajivra, K., 1957. On the damping of gravity waves over a permeable seabed. Trans. Am. Geophys. Union, 38: 662–666.

Rice, J.R. and Cleary, M.P., 1976. Some basic stress-diffusion solutions for fluid saturated elastic porous media with compressible constituents. Rev. Geophys. Space Phys., 14: 227–241.

Richart, F.E., Jr., Hall, J.R., Jr., and Woods, R.D., 1970. Vibrations of Soils and Foundations. Prentice Hall, Englewood Cliffs, N.J.

Ross, C.A., Thompson, P.Y., Charlie, W.A., and Dohering, D.O., 1989. Transmission of pressure waves in partially saturated soils. Experimental Mech., March, 80–83.

Sadd, M.H., Shukla, A., Mei, H., and Zhu, C.Y., 1989. The effect of voids and inclusion on wave propagation in granular materials. In: G.J. Weng, M. Taya, and H. Abe (Editors), Micromechanics and Homogeneity. Springer-Verlag, New York, N.Y.

Sadd, M.H. and Hossain, M., 1989. Wave propagation in distributed bodies with applications to dynamic soil behaviour. J. Wave-Material Interaction, 4.

Salin, D. and Schon, W., 1981. Acoustics of water saturated packed glass spheres. J. Phys. Lett., 42: 477–480.

Sanchez-Palencia, E., 1980. Non-Homogeneous Media and Vibration Theory. Springer-Verlag, New York, N.Y.

Sandhu, R.S. and Pister, K.S., 1970. A variational principle for linear, coupled field problems in continuum mechanics. Int. J. Eng. Sci., 8: 989–997.

Sandhu, R.S., Wolfe, E., and Shaw, H.C., 1989. Dynamic response of saturated soils using three-field formulation. Soil Dynamics Earthquake Eng., 8:

Sandhu, R.S. and Hong, S.J.(1987. Dynamics of fluid saturated soils–variational formulation. Int. J. Num. Analy. Meth. Geomech., 11: 241–255.

Santos, J.E., 1986. Elastic wave propagation in fluid-saturated porous media, I: The existence and uniqueness theorems. Math. Model. Num. Analy., 20: 113–128.

Santos, J.E., Orena, E.J., 1986. Elastic wave propagation in fluid-saturated porous media, II: The Galerkin procedures. Math. Model. Num. Analy., 20: 129–139.

Santos, J.E., Corbero, J.M., and Douglas, J., 1990a. Static and dynamic behaviour of a porous solid. J. Acoust. Soc. Am., 87: 1428–1438.

Santos, J.E., Douglas, J., Corbero, J.M., and Lovera, O.M., 1990b. A model for wave propagation in a porous medium saturated by a two-phase fluid. J. Acoust. Soc. Am., 87: 1439–1448.

Santos, J.E., Corbero, J.M., Ravazzoli, C.L., and Hensley, J.L., 1992. Reflection and transmission coefficients in fluid-saturated porous media. J. Acoust. Soc. Am., 91: 1911–1923.

Sawicki, A. and Morland, L.W., 1985. Pore pressure generation in a saturated sand layer subjected to a cyclic horizontal acceleration at its base. J. Mech. Phys. Solids, 33: 545–559.

Schmidt, E.J., 1988. Wideband acoustic response of fluid-saturated porous rocks: Theory and preliminary results using wave guided samples. J. Acoust. Soc. Am., 83: 2027–2024.

Schuurman, I.E., 1966. The compressibility of an air/water mixture and a theoretical relation between the air and water pressures. Geotechnique, 16: 269–281.

Schwartz, L.M., 1984. Acoustic properties of porous systems: Microscopic description. In: D.L.

Johnson and P.N. Sen (Editors), Physics and Chemistry of Porous Media. Am. Inst. Phys., Vol. 107, pp. 105–118.

Scott, P.H. and Rose, W., 1953. An explanation of the Yuster effect. J. Petr. Technol., 5: 19–20.

Scott, R.F., 1986. Solidification and consolidation of a liquefied sand column. Soils and Foundations (Japan), 26: 23–31.

Seed, H.B., Martin, P.P., and Lysmer, H., 1976. Pore water pressure changes during soil liquefaction. J. Geotech. Engng., ASCE, 102: 323–346.

Seed, H.B. and Rahman, M.S., 1978. Wave induced pore pressure in relation to ocean floor stability of cohesionless soils. Marine Geotechnology, 3.

Seed, H.B. and Idriss, I.M., 1982. On the importance of dissipation effects in evaluating pore pressure changes due to cyclic loading. In: G.N. Pande and O.C. Zienkiewicz (Editors), Soil Mechanics—Transient and Cyclic Loads. Wiley, Somerset, N.J., pp. 53–70.

Sharma, M.D. and Gogna, M.L., 1991a. Propagation of Love waves in an initially stressed medium consisting of a slow elastic layer lying over a liquid-saturated porous half-space. J. Acoust. Soc. Am., 89: 2584–2588.

Sharma, M.D. and Gogna, M.L., 1991b. Wave propagation in anisotropic liquid-saturated porous solids. J. Acoust. Soc. Am., 90: 1068–1073.

Shukla, A. and Zhu, Y., 1988. Influence of the microstructure of granular media on wave propagation and dynamic load transfer. J. Wave-Material Interaction, 3: 249–265.

Siddharthan, R., 1987. Wave-induced displacements in seafloor sand. Int. J. Num. Analy. Meth. Geomech., 11: 155–170.

Slattery, J.C., 1967. Flow of viscoelastic fluids through porous media. AIChE J., 14: 1066–1071.

Sleath, J.F.A., 1970. Wave induced pressures in beds of sand. J. Hydraul. Div., ASCE, 96: 367–378.

Smith, D.T., 1974. Acoustic and mechanical loading of marine sediments. In: L. Hampton (Editor), Physics of Sound in Marine Sediments. Plenum, New York, N.Y., pp. 41–61.

Smith, P.G. and Greenkorn, R.A., 1972. Theory of acoustical wave propagation in porous media. J. Acoust. Soc. Am., 52: 247–253.

Smith, P.G., Greenkorn, R.A., and Barile, R.G., 1974a. Infrasonic response characteristics of gas and liquid porous media. J. Acoust. Soc. Am., 56: 781–788.

Smith, P.G., Greenkorn, R.A., and Barile, R.G., 1974b. Theory of transient pressure response of fluid filled porous media. J. Acoust. Soc. Am., 56: 789–795.

Spooner, J.A., 1971. Unsteady Inertial Effects in Fluid Flow Through Porous Media. Ph.D. Thesis, Univ. of Wisconsin, Madison, W.I.

Stoll, R.D., 1974. Acoustic waves in saturated sediments. In: L. Hampton (Editor), Physics of Sound in Marine Sediments. Plenum, New York, N.Y., pp. 19–39.

Stoll, R.D., 1977. Acoustic waves in ocean sediments. Geophysics, 42: 715–725.

Stoll, R.D., 1979. Experimental studies of attenuation in sediments. J. Acoust. Soc. Am., 66: 1152–1160.

Stoll, R.D., 1980. Theoretical aspects of sound transmission in sediments. J. Acoust. Soc. Am., 68: 1341–1350.

Stoll, R.D. and Bryan, G.M., 1970. Wave attenuation in saturated sediments. J. Acoust. Soc. Am., 47: 1440–1447.

Stoll, R.D. and Kan, T.K., 1981. Reflection of acoustic waves at a water-sediment interface. J. Acoust. Soc. Am., 70: 149–156.

Streeter, V.L., Wylie, E.B., and Richart, F.E., 1974. Soil motion computations by characteristics method. J. Geotech. Engng., ASCE, 100: 247–263.

Sun, F., Banks, P., and Peng, H., 1993. Wave propagation theory in anisotropic periodically layered fluid-saturated porous media., J. Acoust. Soc. Am., 93: 1277–1285.

Tajuddin, M., 1984. Rayleigh waves in a poroelastic half-space. J. Acoust. Soc. Am., 75: 682–684.

Tajuddin, M. and Moiz, A.A., 1984. Rayleigh waves on a convex cylindrical poroelastic surface Part II. J. Acoust. Soc. Am., 76: 1252–1254.

Tajuddin, M. and Ahmed, S.I., 1991. Dynamic interaction of a poroelastic layer and a half space. J. Acoust. Soc. Am., 89: 1169–1175.

Tiller, F.M., 1975. Compressible cake filtration. In: K.J. Ives (Editors), The Scientific Basis of Filtration. NATO/ASI Series No. 2, Noordhoff-Leyden, The Netherlands, pp. 315–397.

Tuncay, K. and Corapcioglu, M.Y., 1996a. Wave propagation in fractured porous media. Transport in Porous Media, 23: 237–258.

Tuncay, K. and Corapcioglu, M.Y., 1996b. Body waves in fractured porous media saturated by two immiscible newtonian fluids. Transport in Porous Media, 23: 259–273.

Turgut, A. and Yamamoto, T., 1990. Measurements of acoustic wave velocities and attenuation in marine sediments. J. Acoust. Soc. Am., 87: 2376–2383.

Valanis, K.C., 1971. A theory of viscoplasticity without a yield surface. Arch. of Mech., 23: 517–555.

Valanis, K.C., and Read, H.E., 1982. A New endochronic plasticity model for soils. In: G.N. Pande and O.C. Zienkiewicz (Editors), Soil Mechanics and Cyclic Loads. Wiley, Somerset, N.J., pp. 375–417.

van der Grinten, J.G.M., Van Dongen, M.E.H., and Van der Kogel, H., 1985. A shock-tube technique for studying pore pressure propagation in a dry and water saturated porous medium. J. Appl. Phys., 58: 2937–2942.

van der Grinten, J.G.M., Smits, M.A., Van der Kogel, H., and Van Dongen, M.E.H., 1987a. Shock induced wave propagation in and reflection from a porous column partially saturated with water. In: H. Gronig (Etitor), Proc. 6th Int. Symp. Shock Tubes and Waves. VCH, pp. 357–362.

van der Grinten, J.G.M., van Dorgen, M.E.H., and van der Kogel, H., 1987b. Strain and pore pressure propagation in a water-saturated porous medium. J. App. Phys., 62: 4682–4687.

van Genuchten, M. Th., 1980. A closed form equation for predicting the hydraulic coductivity of unsaturated soils. Soil Sci. Soc. Am. J., 44: 892–898.

Vardoulakis, I., 1987. Compression induced liquefaction of water saturated granular media. In: C.S. Desai (Editor), Constitutive Laws for Engineering Materials. Elsevier, New York, N.Y., pp. 647–656.

Vardoulakis, I. and Beskos, D.E., 1986. Dynamic behavior of nerly saturated porous media. Mech. Matls., 5: 87–108.

Verruijt, A., 1969. Elastic storage of aquifers. In: R.J.M. DeWeist (Editor), Flow Through Porous Media. Academic Press, New York, N.Y., pp. 331–376.

Verruijt, A., 1982. Approximations to cyclic pore pressures caused by sea waves in a poroelastic half-plane. In: G.N. Pande and Zienkiewicz (Editors), Soil Mechanics—Transient and Cyclic Loads. Wiley, Somerset, N.J., pp. 37–51.

Verruijt, A., 1984. The theory of consolidation. In: J. Bear and M.Y. Corapcioglu (Editors), Fundamentals of Transport Phenomena in Porous Media. Martinus Nijhoff, Dordrecht, The Netherlands, pp. 349–368.

Weng, X. and Yew, C.H., 1990. The leaky Rayleigh wave and Scholte wave at an interface between water and porous sea ice. J. Acoust. Soc. Am., 87: 2481–2488.

Whitaker, S., 1967. Diffusion and dispersion in porous media. AIChE J., 13: 420–427.

White, J.E., 1975. Computed seismic speeds and attenuation in rocks with partial gas saturation. Geophysics, 40: 224–232.

Wiggert, D.C. and Wylie, E.B., 1976. Numerical predictions of two-dimensional transient groundwater flow by the method of characteristics. Water Resour. Res., 12: 971–977.

Wijesinghe, A.M. and Kingsbury, H.B., 1979. On the dynamic behaviour of poroelastic materials. J. Acoust. Soc. Am., 65: 90–95.

Wijesinghe, A.M. and Kingsbury, H.B., 1980. Response to dynamic surface pressure distributions. J. Geotech. Engng., ASCE, 106: 1–15.

Wilson, R.K. and Aifantis, E.C., 1982. On the theory of consolidation with double porosity. Int. J. Eng. Sci., 22: 1009–1035.

Wilson, R.K. and Aifantis, E.C., 1984. A double porosity model for acoustic wave propagation in fractured-porous rock. Int. J. Eng. Sci., 22: 1209–1217.

Wu, K., Xue, Q., and Adler, L., 1990. Reflection and transmission of elastic waves from a fluid-saturated porous solid boundary. J. Acoust. Soc. Am., 87: 2349–2358.

Wylie, E.B., 1976. Transient aquifer flows by characteristics method. J. Hyd. Div., ASCE, 102: 293–305.

Wyllie, M.R.J., Gardner, G.H.F., and Gregory, A.R., 1962. Studies of elastic wave attenuation in porous media. Geophysics, 27: 569.

Yamamoto, T., Koning, H.L., Sellmeijer, H., and Van Hijum, E., 1978. On the response of a poro-elastic bed to water waves. J. Fluid Mech., 87(1): 192–206.

Yamamoto, T. and Schuckman, B., 1984. Experiments and theory of wave-soil interactions. J. Eng. Mech., ASCE, 110: 95–112.

Yamamoto, T. and Takahashi, S., 1983. Physical modeling of sea-seabed interactions. J. Eng. Mech., ASCE, 109: 54–72.

Yew, C.H. and Jogi, P.N., 1976. Study of wave motions in fluid-saturated porous rocks. J. Acoust. Soc. Am., 60: 2–8.

Yin, C.S., Batzle, M.I., and Smith, B.J., 1992. Effects of partial liquid/gas saturation on extensional wave attenuation in berea sandstone. Geophys. Res. Lett., 19: 1399–1402.

Yuster, S.T., 1951. Theoretical considerations of multiphase flow in idealized capillary system. Proc. Third World Petr. Cong., The Hauge, 2: 436–445.

Zhu, X. and McMechan, G.A., 1991. Numerical simulation of seismic responses of poroelastic reservoirs using Biot theory. Geophysics, 56: 328–339.

Zienkiewicz, O.C., 1982. Basic formulation of static and dynamic behaviour of soil and other porous media: In: J.B. Martins (Editors), Numerical Methods in Geomechanics. Reidel, Dordrecht, The Netherlands, pp. 39–55.

Zienkiewicz, O.C., Chang, C.T., and Hinton, E., 1978. Nonlinear seismic response and liquefaction. Int. J. Num. Analy. Meth. Geomech., 2: 381–404.

Zienkiewicz, O.C, Chang, C.T., and Battess, P., 1980. Drained, undrained, consolidating, and dynamic behaviour assumptions in soils, Limits of validity. Geotechnique, 30: 385–395.

Zienkiewicz, O.C., Leung, K.H., Hinton, E., and Chang, C.T., 1982a. Liquefaction and permanent deformation under dynamic conditions. Numerical solution and constitutive relations. In G.N. Pande and O.C. Zienkieqicz (Editors), Soil Mechanics and Cyclic Loads, Wiley, Somerset, N.J., pp. 71–103.

Zienkiewicz, O.C., Leung, K.H., and Hinton, E., 1982b. Earthquake response behaviour of soils with drainage. Univ. College of Swansea, Inst. for Num. Meth. in Engng. Rep. C/R/404/82.

Zienkiewicz, O.C. and Bettess, P., 1982c. Soils and other saturated media under transient, dynamic conditions: General formulation and the validity of various simplifying assumptions. In: G.N. Pande and O.C. Zienkiewicz (Editors), Soil Mechanics – Transient and Cyclic Loads. Wiley, Somerset, N.J., pp. 1–16.

Zienkiewicz, O.C. and Shiomi, T. 1984. Dynamic behaviour of saturated porous media, the generalized Biot formulation and its numerical solution. Int. J. Num. Analy. Meth. Geomech., 8: 71–96.

Zolotarjew, P.P. and Nikolaevskij, V.N., 1965. Propagation of stress and pore pressure discontinuities in water saturated soil. Izvestija Akademii Nauk. Mechanika, No. 1 (in Russian), 191–196.

Zwikker, C. and Kosten, C.W., 1949 Sound absorbing materials. Elsevier, New York, N.Y.